280907695X

REFERENCE ONLY

UNIVERSITY OF LONDON THESIS

Degree PhD Year 2006 Name of Author KATAOKA SORENSEN, Kenny

COPYRIGHT

This is a thesis accepted for a Higher Degree of the University of London. It is an unpublished typescript and the copyright is held by the author. All persons consulting the thesis must read and abide by the Copyright Declaration below.

COPYRIGHT DECLARATION

I recognise that the copyright of the above-described thesis rests with the author and that no quotation from it or information derived from it may be published without the prior written consent of the author.

LOAN

Theses may not be lent to individuals, but the University Library may lend a copy to approved libraries within the United Kingdom, for consultation solely on the premises of those libraries. Application should be made to: The Theses Section, University of London Library, Senate House, Malet Street, London WC1E 7HU.

REPRODUCTION

University of London theses may not be reproduced without explicit written permission from the University of London Library. Enquiries should be addressed to the Theses Section of the Library. Regulations concerning reproduction vary according to the date of acceptance of the thesis and are listed below as guidelines.

A. Before 1962. Permission granted only upon the prior written consent of the author. (The University Library will provide addresses where possible).

B. 1962 - 1974. In many cases the author has agreed to permit copying upon completion of a Copyright Declaration.

C. 1975 - 1988. Most theses may be copied upon completion of a Copyright Declaration.

D. 1989 onwards. Most theses may be copied.

This thesis comes within category D.

☐ This copy has been deposited in the Library of UCL

☐ This copy has been deposited in the University of London Library, Senate House, Malet Street, London WC1E 7HU.

Influence of Viscosity and Ageing on the Behaviour of Clays

by

Kenny Kataoka Sorensen

A thesis submitted to the University of London
for the degree of Doctor of Philosophy

Department of Civil and Environmental Engineering
University College London

August 2006

UMI Number: U593447

All rights reserved

INFORMATION TO ALL USERS
The quality of this reproduction is dependent upon the quality of the copy submitted.

In the unlikely event that the author did not send a complete manuscript
and there are missing pages, these will be noted. Also, if material had to be removed,
a note will indicate the deletion.

UMI U593447
Published by ProQuest LLC 2013. Copyright in the Dissertation held by the Author.
Microform Edition © ProQuest LLC.
All rights reserved. This work is protected against
unauthorized copying under Title 17, United States Code.

ProQuest LLC
789 East Eisenhower Parkway
P.O. Box 1346
Ann Arbor, MI 48106-1346

DECLARATION

I, Kenny Kataoka Sorensen, confirm that the work presented in this thesis is my own. Where information has been derived from other sources, I confirm that this has been indicated in the thesis.

August 2006

ACKNOWLEDGEMENTS

This Ph.D. thesis is the outcome of several years of hard but exciting and interesting research work. It would never have been possible for me to finish this if it had not been for the support from numerous people. Unfortunately I will not be able to mention all of them individually but I would like to thank some in particular.

Firstly, I would like to express my gratitude to my supervisor, Dr. Beatrice Baudet. Without her never-ending encouragement, support and guidance, I would never have finished this research project.

I would also like to give special recognition to Ove Arup & Partners International Ltd. for their support and particularly to Dr. Brian Simpson for his advice and inspiration on developing the BRICK model. I admire his enthusiasm and knowledge in the field of soil mechanics.

I am very thankful to the research staff at the Department of Soil Mechanics at Imperial College of Science, whom I have consulted many times during my research to obtain advice on the experimental testing. Particularly Dr. Matthew Coop for his guidance and help with the experimental testing at the start of the research. Imperial College also provided the rotary cores of undisturbed London Clay without which this research would never have been finalised.

The tests on cement-mixed kaolin were performed at the Institute of Industrial Science, University of Tokyo, Japan in collaboration with Mr. Nobuhiro Komoto under the guidance of Professor Fumio Tatsuoka and Dr. Junichi Koseki. I am very grateful for their hospitality during the study visit. The visit significantly widened my understanding of the time-dependent behaviour of clays and I particularly gained a lot from Professor Fumio Tatsuoka's many years of experience in this field. I highly appreciate the funding provided by the Royal Academy of Engineering, the University College London Graduate School and the Department of Civil Engineering, University of Tokyo which enabled the study visit to Tokyo.

At University College London the technical assistance from the technicians, in particular Mr. John Ford and Mr. Paul Mennell, on the development of testing equipment has been invaluable. I am grateful to Dr. Paul Greening and Ph.D. student Mr. Joao Rio for their advice on the use and interpretation of bender elements. The collaboration with Mr. Joao Rio on making the bender elements and our numerous discussions about their behaviour has been very enjoyable and a great help to me.

My thanks also go to all PhD students and staff at the Department of Civil and Environmental Engineering at University College London, who all contributed to a pleasant research environment.

The research was made possible through funding from an EPSRC Cooperation Award in Science and Engineering (CASE) in collaboration with the geotechnical division of Ove Arup & Partners International Ltd. in London.

Finally, I am very grateful to my family for their ever-present support and love which is keeping me strong and has kept me going throughout the research. I am also indebted to my lovely fiancée Jeanette, who has stood by my side and provided love, support and encouragement when I needed it most. I truly admire her patience. This thesis is dedicated to her.

ABSTRACT

With the aim to achieve a better understanding of the time-dependent behaviour of clays, particularly stiff natural clays, a critical review of literature and a program of laboratory testing have been carried out as part of this research work. With emphasis on examining the effects of viscosity and ageing, a series of advanced triaxial and oedometer tests were conducted, which have added significant data to the existing database of results and addressed important "grey areas" highlighted from the literature review. The performed experimental studies included;

a) An examination of the influence of ageing and global axial strain rate on the vertical elastic shear stiffness of kaolin and reconstituted London Clay in one-dimensional and isotropic compression test combined with bender element testing.

b) Characterisation of the influence of strain rate and strain acceleration on the monotonic stress-strain behaviour of reconstituted London Clay from a complex series of triaxial compression and extension tests.

c) An examination of the influence of structure, both natural and artificial, on the strain rate dependent behaviour of London Clay and artificially cemented kaolin in triaxial compression tests, in addition to an investigation of the influence of ageing (in this case curing of the cement) on the monotonic behaviour of cement-mixed kaolin.

Based on the literature review and findings from the performed experimental studies a framework for the conceptual time-dependent behaviour of natural clays was formulated with the underlying intention to characterise parameters that could eventually be used in a model for natural clays. Finally, on the basis of proposed conceptual behaviour a preliminary numerical study was carried out examining the implementation of general viscous behaviour into the advanced BRICK model of soil behaviour.

KEYWORDS: clays; fabric/structure of soils; laboratory tests; time dependence

TABLE OF CONTENT

SYMBOLS AND ABBREVIATIONS

Symbol

A	material parameter, a function of strain (BRICK model)
A	current cross-sectional area of sample
A	non-dimensional soil parameter
A_0	initial cross-sectional area of sample at beginning of test
$A_{\dot{\varepsilon}_{a,ref}}$	non-dimensional soil parameter given by reference axial strain rate
A_f	material constant (BRICK model)
A_f	final cross-sectional area of sample at end of test
B	pore pressure coefficient
c	material constant (BRICK model)
C_c	compression index
CF	clay fraction
C_α	coefficient of secondary consolidation
e	void ratio
E'	drained tangent Young's modulus
E'_0	very small strain Young's modulus / elastic Young's modulus
e_0	initial void ratio / void ratio at start of compression
e_i	void ratio at start of shearing
E_u	undrained tangent Young's modulus
E_u	undrained Young's modulus
F	force acting through load cell in triaxial apparatus
F_{dwh}	load from dead weight hanger in oedometer apparatus
F_p	load applied through loading piston in oedometer apparatus
G'	drained shear modulus
$G'^{elastic-after}_0$	elastic shear modulus after a step change in strain rate
$G'^{elastic-before}_0$	elastic shear modulus before a step change in strain rate
$G'^{total-after}_0$	measured total shear modulus immediately after a step change in strain rate
$G'^{total-before}_0$	measured total shear modulus before a step change in strain rate
$G_{0(e,\dot{\varepsilon}_{a,ref})}$	elastic shear modulus estimated at the current void ratio at a reference strain rate
$G_{0(p',\dot{\varepsilon}_{a,ref})}$	elastic shear modulus estimated at the current mean effective stress at a reference strain rate
$G_{0(VH)}$	elastic shear modulus - vertical direction and horizontal polarisation
G_{cement}	specific gravity of cement solids
G_{max}, G_0	very small strain shear modulus / elastic shear modulus
$G_{max,1000}$	elastic shear modulus measured 1000 min after initiation of creep
G_s	specific gravity of solids
G_t	tangent shear modulus

G_u	undrained shear modulus
G_{VH}, G_{HV}, G_{HH}	elastic shear modulus in different directions from bender element tests
H_0	initial height of sample at beginning of test
H_f	final height of sample at end of test
I_G	coefficient of shear modulus increase with time
K_0	coefficient of earth pressure at rest
L	length of shear wave travel path through sample
m	creep parameter
m, m'	non-dimensional soil parameters
$m_{T,0}$	initial total initial weight of the sample at beginning of test
N	extrapolated specific volume on NCL* at p′=1 kPa
n, n'	non-dimensional soil parameters
N_e	extrapolated void ratio on the NCL* at p′=1 kPa
N_G	normalised increase in shear modulus with time
N_G^*	(new) creep time coefficient
OCR	overconsolidation ratio
p'	mean effective stress
p'_0	overburden pressure
p'_c	actual maximum experienced preconsolidation pressure
p'_e	equivalent pressure on the NCL* at current void ratio of soil
PI	plasticity index
p_r	reference pressure
q	deviator stress
q_{ref}	reference deviator stress level on CRS stress-strain curve defined by lowest applied rate of strain
$q_{u,peak}$	undrained peak strength
R	lever arm ratio in oedometer apparatus
R_{α_0}	rate parameter
r^2	coefficient of correlation
t	relative time
T	travel time of shear wave propagating through sample
t_a	first point of deflection
t_b	first point of reversal
t_c	first point of inflection
t_{ref}	reference time
u	pore water pressure
u_{avr}	average pore water pressure assumed in sample
u_{base}	pore water pressure measured at the base of the cell
v	specific volume
V, V_T	total volume of sample
V_0	initial sample volume
V_s	volume of solids

V_s	velocity of shear wave propagating through sample
V_V	volume of voids
w	water content of sample
w_0	initial water content of sample at beginning of test
w_{dw}	total dead weight on hanger in oedometer apparatus
w_f	final water content of sample at end of test
w_L	liquid limit
w_p	plastic limit
w_{sat}	water content of sample after saturation
$\Delta q_{persistent}$	persistent stress jump after a step change in strain rate
$\Delta q_{total\ immediate}$	total immediate stress jump after a step change in strain rate
ΔV_{sat}	volume of water flowing into the sample during saturation
α_0	global rate coefficient – normalised increase in shear modulus with increasing strain rate
β	rate parameter quantifying the increase in undrained shear with an increase in strain rate
β	viscous material constant defining the change in string length (BRICK model) in relation to the ratio of strain rate change
β^*	viscous material constant defining the change in initial volumetric strain $\varepsilon_{v,0}$ (BRICK model) in relation to the ratio of strain rate change
$\dot{\varepsilon}$	strain rate in unspecified direction
$\dot{\varepsilon}_a$	axial/vertical strain rate in oedometer and triaxial cells
$\dot{\varepsilon}_{a,after}$	axial strain rate after a step change in strain rate
$\dot{\varepsilon}_{a,before}$	axial strain rate before a step change in strain rate
$\dot{\varepsilon}_{a,creep}$	axial creep strain rate
$\dot{\varepsilon}_{a,ref}$	reference axial strain rate
$\dot{\varepsilon}_n$	neutral strain rate (BRICK model)
$\dot{\varepsilon}_r$	radial strain rate
$\dot{\varepsilon}_r$	reference strain rate (BRICK model)
$\dot{\varepsilon}_s$	shear strain rate
$\dot{\varepsilon}_v$	volumetric strain rate
$\dot{\varepsilon}_{v,r}$	reference volumetric strain rate (BRICK model)
ε^e	elastic strain in unspecified direction
ε^p	(visco)plastic strain in unspecified direction
ε^t	total measured strain in unspecified direction
ε_a	axial/vertical strain in oedometer and triaxial cells
ε_{EL}	linear elastic limit strain
ε_r	radial strain
ε_s	shear strain
$\varepsilon_s^{elastic-after}$	elastic component of measured shear strain after a step change in strain rate

$\varepsilon_s^{elastic-before}$	elastic component of measured shear strain before a step change in strain rate
$\varepsilon_s^{plastic-after}$	plastic component of measured shear strain after a step change in strain rate
$\varepsilon_s^{plastic-before}$	plastic component of measured shear strain before a step change in strain rate
$\varepsilon_s^{total-after}$	measured total shear strain immediately after a step change in strain rate
$\varepsilon_s^{total-before}$	measured total shear strain before a step change in strain rate
ε_v	volumetric strain
$\varepsilon_{v,0}$	initial volumetric strain (BRICK model)
$\varepsilon_{v,f}$	final volumetric strain at end of test
ϕ'_{cs}	critical state angle of shearing resistance
ϕ'_{peak}	peak angle of shearing resistance
ι	elastic compression modulus (BRICK model)
κ	swelling modulus (BRICK model)
λ	compression index
ν'	Poisson's ratio
θ	angle of rotation of strain path
θ'	angle of rotation of stress path
ρ	total density of soil
ρ_w	density of water
σ'_a	effective axial stress
σ'_i	effective principal stress
σ'_r	effective radial stress
σ'_v	effective vertical stress
σ_a	total axial stress
σ_i	total principal stress
σ_r	total radial stress, confining pressure in triaxial tests
σ_v	total vertical stress

Abbreviation

1D	one-dimensional
C	fixed effective stress creep
cmk	cement-mixed kaolin
CRS	constant rate of strain
CRS*	constant rate of stress
CS	critical state
CSL	critical state line
CSL*	intrinsic critical state line
d.	drained
EOP	end of primary consolidation
IC	isotropic compression

IS	isotropic swelling
k	kaolin
LBS	local boundary surface
LC	London Clay
NC	normally consolidated
NCL	normal compression Line
NCL*	intrinsic normal compression Line
OC	overconsolidated
pwp	pore water pressure
r, recon.	reconstituted
RHP	rapid hardening Portland (cement)
RL	reloading
RSRC	ratio of strain rate change
SBS	state boundary surface
SL	string length (BRICK model)
SL	step-loaded
SL_r	reference string length (BRICK model)
SR	fixed strain stress relaxation
SRS	step-wise change in rate of strain
SRS*	step-wise change in rate of stress
TC	triaxial compression
TE	triaxial extension
TESRA	temporary effect of strain rate and strain acceleration
u.d.	undrained
UL	unloading
undist.	undisturbed
Y1	sub yield surface characterising a change from linear elastic to non-linear elastic behaviour
Y2	yield surface characterising a change from elastic to elasto-plastic behaviour
Y3	boundary surface characterising gross yield of the sample

CHAPTER 1 INTRODUCTION

This thesis entitled "*Influence of Viscosity and Ageing on the Behaviour of Clays*" presents the outcome of a research project carried out by the author at the Department of Civil and Environmental Engineering, University College London (UCL), UK in the period November 2002 to August 2006 in partial fulfilment of the University of London degree of Doctorate in Philosophy (Ph.D.) in the area of Soil Mechanics. The research project was made possible through collaboration between UCL and the geotechnical division of the engineering consulting company Ove Arup and Partners Ltd. in London (Arup Geotechnics) with financial support from an EPSRC Cooperation Award in Science and Engineering (CASE). Primary supervision of the research project was undertaken by Dr. Beatrice Baudet (UCL), while subsidiary supervision was carried out by Dr. Brian Simpson (Arup Geotechnics), Dr. Heleni Pantelidou (Arup Geotechnics) and Dr. Trevor Dunstan (UCL).

1.1 BACKGROUND

In recent years numerous sophisticated non-linear elasto-plastic models have been developed on the basis of recent advances in the characterisation of soil behaviour in the very small strain region ($<10^{-4}$ %). This has lead to a considerable improvement in the predictions of ground movement around typical engineering structures in comparison to predictions made by simple Mohr-Coulomb elasto-plastic models (e.g. Simpson, 1992b, Simpson 2002 and Stallebrass and Taylor, 1997). Yet, in some cases the use of advanced non-linear elasto-plastic constitutive models is still found to give inadequate predictions of the ground movements. A recent study by Kanapathipillai (1996) in collaboration with Arup Geotechnics examined the ground movement associated with the excavation of the Heathrow Express trial tunnel, West London, through a stratum of stiff heavily overconsolidated London Clay. The study suggested that time-effects such as ageing or creep might be one of the primary causes for the significant difference observed between the actual measured surface settlement profile and the profile predicted from finite element modelling using the advanced non-linear elasto-plastic constitutive BRICK model of soil behaviour (Simpson, 1992;Simpson, 1992). This however does not come as a surprise, since it has long been accepted that the time-dependency of soil behaviour plays an important role for predicting the short- and long-term performance of geotechnical structures. Therefore, with the aim to improve the accuracy of ground movement predictions, this research project was initiated by Arup Geotechnics, who expressed interest in modelling the influence of ageing and viscosity on the monotonic behaviour of natural stiff clays, like London Clay.

Recent findings from laboratory soil element testing have highlighted that the time-dependency of soils is more complex than initially thought (Tatsuoka et al., 2000). In particular the response to strain rate changes is found to be different for different soils, so that granular

materials, weak rocks and soft clays all have different time-dependent behaviours. Little is currently known of the factors that cause these differences, and only limited data is available on the time-dependent behaviour of stiff clays, particularly on stiff natural clays such as London Clay. The objectives of this research project, as presented in the following section, were formed on the basis of the above issues.

1.2 AIM AND OBJECTIVES

With the aim to implement ageing and viscous effects on soil behaviour into an existing advanced constitutive model, the key objectives of the research work were formulated as follows:

- To achieve a better understanding of the time-dependent behaviour of clays, particularly stiff natural clays, through critical review of literature and a program of laboratory testing. With emphasis on examining the effects of viscosity and ageing, the laboratory testing would add to the existing database of results and address important "grey areas" highlighted from the literature review.
- To develop a framework of conceptual time-dependent behaviour of clays on the basis of the first objective with the underlying intention to characterise parameters that could eventually be used in a model for natural clays.

1.3 METHODOLOGY

In addition to a detailed review of published and unpublished literature and communications with leading researchers in the field which highlighted a lack of data, particularly for stiff natural clays, the first objective was addressed via a series of experimental studies. Through an extensive programme of laboratory soil element tests, carried out using advanced triaxial and oedometer equipment, phenomena associated with ageing and viscosity have been characterised and their separate and coupled influence on the monotonic behaviour of clays has been investigated in detail. Aspects of ageing such as thixotropy, bonding and cementation has been examined in addition to aspects of viscous behaviour including stress relaxation, creep, strain rate dependency and effect of strain acceleration. Generally the phenomena of viscosity and ageing have been investigated at a macroscopic scale in the laboratory soil element tests. It has been outside the scope of the thesis to characterise the micro-mechanism associated with the observed macroscopic behaviour. Testing was made possible over a wide strain range in shearing through the development of two advanced triaxial apparatuses, in which highly accurate local strain gauges and a shear wave transmission system were incorporated, thereby enabling static and dynamic probes in the very small strain region ($<10^{-4}$ %). To expand the investigation, an advanced oedometer apparatus also incorporating a shear wave transmission system was developed, thereby making it possible to measure the dynamic shear modulus under one-dimensional conditions up to high applied loads (<5 MPa effective stress). The time-

dependent behaviours of two different clays have been investigated; the natural stiff London Clay in both its intact and reconstituted states and the commercially available kaolin clay, which has been tested in its pure state and mixed with a small quantity of cement to create artificial bonding. More specifically, the laboratory testing can be separated into four main studies, which are found to complement each other very well. A brief outline of the scope of each experimental study is given below:

I. Examination of the influence of ageing and global axial strain rate (as measured on the sample boundaries) on the vertical elastic shear modulus $G_{VH\text{-}max}$ determined from dynamic probes using a shear wave transmission system. Nominally drained one-dimensional oedometer compression tests and isotropic compression tests in the triaxial cell were carried out, in which the global axial strain rate was changed step-wise and prolonged periods of creep were introduced. Normally consolidated reconstituted samples of kaolin and London Clay were studied and compared.

II. Examination of the influence of axial and shear strain acceleration on the stress-strain behaviour in the small strain region in both drained and undrained triaxial compression and extension tests on normally consolidated reconstituted London Clay. Static stress path probes and strain path probes were performed, at different stress states and different ratios of applied axial strain rate to the current axial creep rate, to obtain three distinctly different situations characterised by; significant acceleration, insignificant acceleration or significant deceleration of the axial and shear strains.

III. An investigation into and comparison of the viscous behaviours of stiff heavily overconsolidated undisturbed London Clay and its reconstituted counterpart in normally consolidated and overconsolidated states. Drained and undrained triaxial compression tests were carried out, in which the axial strain rate was changed step-wise to characterise the viscous behaviours in both the pre- and post-failure regions. The comparison of the viscous behaviour of reconstituted and undisturbed London Clay highlighted the influence of natural structure including mechanical overconsolidation on the viscous behaviour.

IV. An investigation into the viscous and cementation effects in drained triaxial compression of cement-mixed kaolin. The axial strain rate was changed step-wise to characterise the viscous behaviour and samples where tested under different accumulated curing times to examine the effect of ageing (in this case curing of the cement). Small unload-reload cycles were performed to determine the small strain stiffness at different stages during testing. A comparison with the observed viscous behaviour of pure kaolin in the literature highlighted the influence of artificial cementation on the viscous behaviour of cement-mixed kaolin.

Based on the literature review and experimental findings from the performed studies, a framework for the conceptual time-dependent behaviour of natural clays has been proposed to address the second key objective. On the basis of this, a limited numerical study has been

carried out, in which the possibility for implementing general viscous behaviour of clays into an existing advanced constitutive soil model was investigated. Despite the fact that the aim of the research work was to implement ageing and viscosity into an existing advanced constitutive model, this has been outside the scope of this research.

1.4 LAYOUT OF THE THESIS

This thesis consists of eight chapters in total. The introduction to the performed research project is given in this chapter (Chapter 1), while the remainder of the thesis is structured as follows:

Chapter 2 presents an extensive review of the literature with regards to the observed time-dependent behaviour of clays in laboratory testing. The main focus is on the effects of viscosity and ageing, two of the primary causes for time-dependent behaviour observed in short term laboratory testing and in the ground on an engineering time-scale upon disturbance. Additionally, a brief review of the general pre-failure deformation characteristics of structured and non-structured clays is included in this chapter, as this is essential for the understanding and successful interpretation of observed time-effects.

Chapter 3 details the experimental testing programme employed in this study, including a description of testing materials, testing equipment, general testing procedures and the theoretical framework. In this chapter the selection of testing materials is explained, and the origin, mineralogy and geotechnical characteristics of the chosen materials are described. In addition to a general description of the testing apparatuses and instrumentation used in the research, the development and modifications made to the testing apparatuses are explained. The description of general testing procedures comprises a description of sample preparation, sample setup and a general overview of testing procedures. Detailed descriptions of the testing procedures are on the other hand given in the following chapters, Chapters 4-6, which also present the findings from the experimental work. The last part of Chapter 3 is a description of the theoretical framework used in this study. This includes details of the data analysis, interpretation methods and applied corrections to the raw data.

Chapter 4 is the first of three chapters on the experimental work. It examines the influence of global strain rate and ageing on the elastic shear stiffness of reconstituted clays, determined using dynamic probes, as observed in laboratory tests under one-dimensional and isotropic loading conditions on reconstituted kaolin and reconstituted London Clay. The presented results are discussed and compared to available data from the literature. On the basis of the findings a new set of parameters are proposed to quantify the influence of strain rate and creep on the elastic shear modulus.

Chapter 5 presents the outcome of a detailed experimental study on the viscous behaviour of reconstituted London Clay, as observed under general triaxial testing conditions. The influence of strain rate and strain acceleration on the monotonic stress-strain behaviour is examined and the presented results are discussed and compared to available data from the

literature. On the basis of the observed behaviour, conceptual viscous behaviour of normally consolidated reconstituted London Clay is proposed.

Chapter 6 presents an experimental investigation into the coupling of viscous and ageing effects in clays. The influence of structure, both natural and artificial, on the strain rate dependent behaviour of clay is examined in triaxial compression tests on London Clay and artificially cemented kaolin. Furthermore, the influence of ageing (in this case curing of the cement) on the monotonic behaviour of cement-mixed kaolin is investigated. The presented results are discussed and compared to available data from the literature, and on the basis of the observed behaviour, conceptual viscous behaviour of intact London Clay is proposed. Furthermore a preliminary framework is suggested, where the viscous behaviour of soil can be explained by the nature of its micro-structure.

Chapter 7 discusses the implementation of general viscous behaviour into the advanced constitutive BRICK model of soil behaviour on the basis of the literature review and the proposed conceptual behaviour of London Clay described in Chapters 5 and 6. The outcome of this preliminary study includes the introduction of a limited number of new parameters and a proposed set of relatively simple modifications to the existing model, which will extend its capabilities to include the simulation of general observed viscous behaviour of soils. The study is preceded by a brief description of the BRICK model of soil behaviour.

Finally, Chapter 8 concludes on the research work. A summary of the findings and conclusions from the performed research work is presented, and recommendations and suggestions for future research are given at the end.

CHAPTER 2 OBSERVED TIME-DEPENDENT BEHAVIOUR OF CLAYS

2.1 INTRODUCTION

This chapter gives a review of the published literature concerning the time-dependent behaviour of saturated clays with water contents generally below the liquid limit. The behaviours of granular soils and rocks are outside the scope of this thesis, however examples of the time-dependent behaviour of sands, gravels and soft rocks are included where these help to illustrate the special features of the clay behaviour. Soil behaviour is affected by factors other than and simultaneous to time effects, for example natural structure or anisotropy. Section 2.2 gives a brief review of the general pre-failure deformation behaviour of clays and the influence of structure in natural and artificially cemented clays, which will be relevant to this study. The time-dependent behaviour of soils is usually divided into viscous and ageing effects; while Section 2.3 concentrates on published research on viscous effects such as creep and strain rate effects, Section 2.4 reviews observed ageing effects on soil behaviour.

2.1.1 Background

The time-dependent behaviour of soils has been studied since the 1950's, when particular attention was given to soft clay. The significant time-delayed deformation behaviour of soft clay was addressed in the 1960's with application to the prediction of the long-term settlement of foundations on soft ground as highlighted for example by Bjerrum (1967) in the seventh Rankine lecture. Hence, numerous studies have previously investigated the creep characteristics of soft clays. Another aspect of time-dependent behaviour that also received considerable attention has been the time-dependent structuration in clays, in particular in connection to very sensitive clays, so-called quick clays. Skempton & Northey (1952), Mitchell (1960) and Bjerrum (1967) among others investigated and discussed the effect of leaching and thixotropy as possible explanations for the observed sensitivity of soft marine clays.

A large amount of data on the two areas of time-dependent deformation and time-dependent structuration has been gathered over the years, and in 1997 Mitchell and co-authors made an extensive review of observed time effects in soils (Mitchell et al., 1997). They concluded that viscous effects give rise to predictable patterns, which are essentially the same for all soils. Nevertheless, a few years later Tatsuoka et al. (2000) presented research work carried out in the late 1990's, which appeared to show that soils of varying nature exhibit very different viscous effects in triaxial compression tests, and that the patterns were more complex than previously thought. The need for a general constitutive soil model that could successfully simulate the combined effects of viscosity, structuration and destructuration was also

highlighted (Tatsuoka et al., 2000). To the knowledge of the author, as of today, such a model still has not been developed and published.

In soil mechanics time effects still remain an area where further research is needed to get a better understanding of the observed complex phenomena associated with time and deformation rate and their influence on the overall behaviour of the soil. The literature review carried out as part of this study will be presented in the following sections, where the main aspects of time effects observed primarily in clays, will be reported and discussed.

2.1.2 Classification of common time-effects

From the literature review it has become evident that some confusion of terminology has occurred in the past. Nevertheless, today most researchers appear to agree that aspects of the time-dependent behaviour of soils such as volumetric creep, deviatoric creep, creep rupture, stress relaxation and strain rate effects are all linked and can be grouped into what can be called viscous effects. The viscous effects observed in soils are primarily believed to be a result of sliding at interparticle contacts and associated particle rearrangements, with the presence or absence of water having only a minor influence (Mitchell, 1976). The term "viscosity" has been taken from the behaviour of liquids and gasses, where an increase in viscosity of the material gives higher resistance to flow at a given shear stress. Hence, viscosity is defined as the ratio of shear stress to shear rate. If the term is extended to soils then sands can be said to be more viscous than clays, because they give higher resistance to shearing at given shear rate. However, in contrast, the viscous effect, which can be quantified, for example by the magnitude of creep strains at fixed stress or the increase in shear stress due to an increase in strain rate, is greater for clays compared to granular materials. A material such as clay which is characterised by reducing viscosity with increasing shear rates can be classified as a pseudoplastic fluid.

Viscous effects cannot explain all observed time effects in soils. Other aspects include time-dependent structuration from physico-chemical processes such as thixotropy, bonding and cementation. The term thixotropy has been used in literature to describe a "process of softening, caused by remoulding, followed by a time-dependent return to the original, harder state" (Burgers & Scott Blair, 1948). Thixotropy is essentially a reversible effect, which Skempton & Northey (1952) suggested to result "from the gradual rearrangement of the particles, under the action of bonding forces, into positions of increasing mechanical stability". In this study it is suggested that thixotropy, bonding and cementation of the soil, which have in common that they do not require any interaction with the surrounding environment and may not necessarily lead to any significant changes in the intrinsic properties of the soil (significant cementation will be an exception), are classified as the inherent ageing effects. Time-dependent changes to the soil structure may also arise from weathering, chemical changes in pore water from external sources (e.g. leaching), heat- and pressure-induced changes to the soil structure. These effects could suitably be classified as environmental ageing effects, since they all have in common that they

require interaction with the surrounding environment and as such lead to changes in the soil composition and most likely to changes in the intrinsic properties of the soil as well (as in the case for leaching).

One of the main reasons for confusion and misuse of terminology in the literature is that the viscous effects often give rise to an apparent structuration. Apparent structuration is generally observed upon loading after a drained creep period where an increase in stiffness, yield stress and undrained shear strength is seen as a result. It will be shown later that these phenomena can be explained by the viscous effect and it is therefore not always a simple matter to distinguish between viscous effects and true ageing effects.

In this study the common time-effects have been classified as given in Table 2-1. The literature review will concentrate on the time-dependent behaviour of clays arising from the viscous effects and the inherent ageing effects. Despite the fact that the environmental ageing effects are likely to contribute significantly to the observed ageing effects in natural clays, an investigation of these effects is outside the scope of this thesis, the reason being that the environmental ageing effects are very difficult to reproduce in the laboratory and that they are almost impossible to control and separate from each other in-situ.

2.2 PRE-FAILURE DEFORMATION CHARACTERISTICS OF CLAYS

In order to identify and quantify the influence of viscosity and ageing on the behaviour of clays it is necessary to understand the mechanical behaviour, which arises solely due to changes in the state of the soil and which is independent of time and rate of strain. The following sections describe selected aspects of advanced pre-failure deformation characteristics of clays which will be relevant to this study.

2.2.1 Non-linear stress-strain shearing behaviour

It is generally accepted that the pre-failure stress-strain shearing behaviour of soils is highly non-linear. At small strains the stiffness is relatively high, while at large strains near failure the stiffness is low. The stiffness degradation with strain is often idealised as an S-shaped curve (Atkinson, 2000), as illustrated in Figure 2-1. Characterisation of the non-linear behaviour has predominantly been made through advanced laboratory soil element testing. However, only in recent years has the resolution of local strain gauges for use in soil element testing become accurate enough to resolve the very small strains (<0.0001 %). This makes it possible to unify the results from the dynamic testing methods, which inherently are at very small strains, with those of the static testing methods, enabling characterisation of the stiffness from the very small strains to the very large strains. The ground surrounding engineering structures will typically be subjected to strains ranging from small (<0.01 %) to large (>1 %), and the non-linear behaviour is therefore of high importance in routine design as recognized among others by Atkinson (2000) in the 40th Rankine Lecture. It should be mentioned that the general representation of stiffness degradation, as illustrated in Figure 2-1, is based on the assumption that the soil is sheared at a constant rate of stress or constant rate of strain, without experiencing any significant strain acceleration. Additionally, it is general practice to let the sample rest before start of shearing in order to minimize the influence of creep strains on the initial stiffness measurement (Clayton & Heymann, 2001; Jardine, 1994).

By performing repeated loading and unloading probes with increasing strain magnitudes the recent use of high resolution local strain gauges has revealed that generally for all soils the stress-strain behaviour at very small strains (typically below 0.0001 % to 0.001 %) appears to be linear elastic with a constant high stiffness value and fully recoverable strains upon unloading. With further straining in the small strain region (0.0001 % to 0.01 %), the cyclic loops gradually show increasing hysteretic behaviour, while strains to a large degree still remain fully recoverable. However, as straining proceeds beyond the small strain region (>0.01 %) and the state approaches failure, plastic non-recoverable straining progressively becomes more dominant.

2.2.2 Concept of kinematic sub-yield surfaces

Because of non-linearity, the simple elasto-plastic framework commonly used in the past in ultimate limit state type analyses does not represent well the pre-failure deformation characteristics of soils. In recent decades several new concepts of pre-failure deformation behaviour have been proposed to better represent the observed elasto-plastic behaviour from the very small strains to the very large. Multiple kinematic yield surfaces have been proposed, for example the widely referred to concept of kinematic Y_1 and Y_2 sub-yield surfaces proposed by Jardine (1992). Another more unique concept of multiple yield surfaces in strain-space was proposed by Simpson (1992), which has been incorporated into the BRICK model as described further in Section 7.1.1.

The simplified scheme of pre-failure behaviour as proposed by Jardine (1992), is illustrated in Figure 2-2. The concept was originally based on laboratory tests on reconstituted, low plasticity, Magnus till, but it has found broad acceptance and appears to fit a wide range of other clays as well, for example undisturbed soft Bothkennar clay (Smith, 1992) and undisturbed stiff London Clay (Gasparre, 2005). Within the scheme, the current stress state is surrounded by two kinematic sub-yield surfaces Y_1 and Y_2, while the large scale yield surface or local State Boundary Surface (LSB) for undrained stress paths is termed the Y_3 locus. Once the Y_1 and Y_2 yield surfaces are reached these will be dragged along with the current stress point and can change shape and size. Generally, large strains are required to reach and move the Y_3 locus. Within the Y_1 surface the behaviour is linear elastic, once the Y_1 surface is reached the behaviour becomes hysteretic, but strains are fully recoverable, and once the boundary of the Y_2 surface is reached the behaviour is non-linear elasto-plastic, with increasing plastic behaviour developing towards the Y_3 locus. However, after yield a sharp change in the stress path direction may cause the stress point to re-enter the Y_1 surface and elastic behaviour will be experienced again. The boundary of the Y_1 surface can be identified from the deviation of the initial linear stress-strain relationship (e.g. in q-ε_s plane), while the boundary of the Y2 surface is recognised by a sharp shift in the direction of the strain increment vector in the plane of shear strain against volumetric strain in drained tests or from the deviation of the initial linear relationship between undrained pore water response and e.g. deviator stress.

2.2.3 Elastic shear stiffness

The elastic shear stiffness, G_{max} (or G_0) of soil is the maximum shear stiffness obtained from either dynamic testing methods such as bender element testing or resonant column testing or from static stress-strain measurements in the very small strain region using high resolution local strain gauges. G_{max} is commonly termed the very small strain shear stiffness, because its range is usually found to be only that of the very small strains in monotonic loading tests carried out at constant rate of strain or stress, as described in Sections 2.2.1 and 2.2.2 above. This term is however rather misleading since the maximum (elastic) stiffness may be measured and observed

at any level of strain, as shown from dynamic testing (Viggiani & Atkinson, 1995) or from monotonic loading tests, where the strain rate is changed step-wise, as will be shown in Section 2.3.2. Therefore, the term elastic shear stiffness is considered to be more appropriate and will be used in the rest of the thesis.

Numerous factors have been found to affect the magnitude of the soil shear stiffness including the elastic shear stiffness. These include soil composition, soil fabric, chemical alterations, soil density, stress/strain history, current state, possibly recent stress history, drainage and strain rates (Jardine, 1992). The range of the linear elastic zone has also been found to vary for different soils, with softer soils such as soft reconstituted clays generally showing smaller ranges than stronger soils, such as cemented soils or natural highly structured clays. The elastic limit is typically found to be in the region of 0.001 % strain for soft clays and around an order or two higher for artificially cemented soils and soft rocks (Jardine, 1992). It has also been found that for a given soil the linear elastic Y_1 boundary surface may grow in size as a result of overconsolidation or ageing among other factors and the surface will usually change shape as a result of both inherent and induced anisotropy (Jardine, 1992).

The value of G_{max} is useful in characterising the non-linear behaviour of soils and hence has become an important parameter in routine design (Atkinson, 2000). Several empirical expressions have been proposed in the past to determine the value of the elastic shear stiffness as a function of the current state and stress history. In the pioneering work done by Hardin, G_{max} was expressed in terms of three state parameters; mean effective stress, p', void ratio, e and overconsolidation ratio (Hardin & Black, 1969). Within the critical state framework the interrelationships between the state parameters allow to simplify the function, and for isotropic stress states the elastic shear stiffness of clays can be determined from either two of the three state parameters, making one of the parameters redundant (Houlsby & Wroth, 1991; Viggiani & Atkinson, 1995). Viggiani & Atkinson (1995) proposed the following relationship based on a number of laboratory triaxial compression and extension tests on reconstituted clays, where G_{max} in the vertical plane was determined from bender element testing;

$$\frac{G_{\max}}{p_a} = A\left(\frac{p'}{p_a}\right)^n R_0^m \tag{2.1}$$

Where p_a is a reference pressure to make the expression dimensionally consistent, A, n and m are positive constants, while R_0 is the overconsolidation ratio, which is given by;

$$R_0 = \frac{p'_p}{p'} \tag{2.2}$$

p'_p is the preconsolidation pressure, which is found from the intersection between the swelling line going through the current state point and the normal compression line in v-p' plane. Viggiani and Atkinson also found Equation (2.1) to be valid for reconstituted normally consolidated kaolin at anisotropic stress states not close to failure.

A few years later Rampello et al. (1997) published the results of similar triaxial tests carried out to investigate further the influence of stress induced anisotropy in reconstituted Vallericca Clay. In contrast to the previous findings by Viggiani & Atkinson (1995) they observed higher values of G_{max} in the vertical plane for anisotropically compressed samples compared to isotropically consolidated samples measured at the same p'. This indicated that G_{max} could not simply be determined by two out of the three state parameters e, p' and R_0. Despite observations that G_{max} for normally consolidated states appeared to plot close to a single straight line in v-log G_{max} plane independently of the stress ratio, as seen from Figure 2-3, Rampello et al. argued that the elastic shear stiffness was likely to be influenced by both void ratio and strain history, but their results appear too ambiguous to support this.

Several studies, which have utilised bender elements to determine the elastic shear stiffness, have confirmed the linear relationships between e and log G_{max} and between log G_{max} and log p' for various clays, e.g. kaolin, NC reconstituted London Clay and intact London Clay (Jovicic & Coop, 1998), kaolin and a number of different reconstituted natural clays (Lohani et al., 2001). Typical results obtained from one-dimensional compression and swelling of Minato Mirai area clay (Lohani et al., 2001) are shown in Figure 2-4. The line given by the normally consolidated states in log G_{max}-log σ'_v plane has been termed G'-G' (Figure 2-4b), swelling lines are seen to be straight and they extend out to the left from the G'-G' line. Similarly to the observations by Rampello et al. (1997), Lohani et al. (2001) also observed a semi-logarithmic relationship between void ratio and G_{max} for normally consolidated states, refer to Figure 2-4c. The swelling lines are again seen to be straight and they extend out to the left from the line G"-G" defined by the normally consolidated states. Based on their results Lohani et al. (2001) proposed to extend the State Boundary (SB) concept to include G_{max} as a third axis, whereby the SB normal compression line would plot as a single straight line in e-log p'-log G_{max} space. The volume of possible (overconsolidated) states could then be found beneath the SB line, as illustrated in Figure 2-5. From the observed behaviour it can be deducted that at the same effective stress state a given soil in an overconsolidated state will have a higher elastic shear stiffness than when in an normally consolidated state, while on the other hand at the same void ratio the overconsolidated soil will show a lower elastic stiffness than the normally consolidated soil.

2.2.4 Effect of recent stress history

In addition to the geological stress history, several researchers have in the last two decades focused on the effects of recent stress history in order to better match the measured in-situ behaviour with that reproduced in the laboratory. However, in the past years there have been several contrasting findings concerning the effects of recent stress or strain history, which appear to have come about due to both different test procedures and possibly also different behaviours of the tested soils. For example Atkinson et al. (1990) highlighted the significant effects of approach path angle on the stiffness degradation curve in drained triaxial tests on reconstituted London Clay (refer to Figure 2-6), while Clayton & Heymann (2001) in contrast found that recent stress history neither affected the very small strain stiffness nor the stiffness at intermediate strains in undrained triaxial probes on undisturbed soft Bothkennar clay.

Recent research by Gasparre (2005) was carried out to further clarify the influence of different test procedures on recent stress history effects. The tests were specifically designed to clarify the influence of the different test procedures used in the studies by Atkinson et al. (1990) and Clayton & Heymann (2001). The influences of approach path angle, creep time and approach path lengths were investigated. Undisturbed samples of London Clay were taken to isotropic stress states followed by undrained stress probes in extension and compression. The test programme is shown in Figure 2-7 to Figure 2-9. Three sets of tests were carried out. Each set of tests consisted of two samples with approach paths in opposite direction along a p' constant line, which were sheared along the same outgoing stress path. To investigate the influence of the approach path lengths, the approach paths were either short or long. The short approach paths were kept within the Y_2 locus (approximately ±10 kPa), while the long approach paths were in the order of 100 kPa. Finally, creep was either allowed or not before the start of each stress probe. When creep was allowed, the samples were allowed to rest under constant effective stress for a few days, while for comparison stress probes were also conducted after a limited creep time of 3 hours. In the case where creep was allowed the results indicate that the stiffness was only influenced by the approach path angle if the approach paths had been long enough to cause significant straining. For the long approach path probes it was observed that the elastic stiffness was approximately the same for the two different approach paths angles, while the stiffness was indicated to degrade more rapidly for the probe which continued in the same direction as the approach path. In the case where only limited creep was allowed and the approach path length was short, the stiffness response at intermediate strains was seen to be lower for the probe which continued in the same direction as the approach path, while the influence on the elastic stiffness was ambiguous. Hence, for short approach path lengths creep was found to remove the effect of recent stress history, while this was not the case for longer approach path lengths.

The research by Gasparre (2005) may indicate that the approach paths used by Clayton & Heymann (2001), which were around 10 kPa, were not long enough to cause significant plastic

straining. However, there is also the possibility that a difference in observed behaviour can be explained by inherent differences in the tested soils. A stiffer soil like London Clay, which Gasparre (2005) tested, may be better at retaining the effects of recent stress history compared to a soft soil like Bothkennar clay, which Clayton & Heymann (2001) tested. Research reported by Tatsuoka et al. (2000) appears to support the idea that in some clays (possibly softer clays) the effects of recent stress history are more readily erased by a short period of creep, even in cases where the approach path has caused significant straining. In the study a series of undrained triaxial tests was performed on normally consolidated reconstituted Fujinomori clay, which showed that short term creep could remove the effects of different compression paths on the small strain behaviour in subsequent loading paths. In the study a number of samples were taken to the same anisotropic stress state A, through different compression stress paths, as shown in Figure 2-10. Samples 14, 16 and 28, all compressed along different paths to stress state A, experienced 2 days of drained creep at stress state A, followed by undrained triaxial compression to failure. Samples 8 and 9, on the other hand, were also compressed along different paths to stress state A and then subsequently sheared to failure from stress state A without experiencing a rest period. As seen from Figure 2-10a, samples 14, 16 and 28, which experienced a rest period before shearing, all showed similar high stiffness behaviour and almost identical stress paths at small strains despite having been subjected to very different compression paths. In contrast, samples 8 and 9, which did not rest at stress state A, showed distinctly different shearing paths as a result of their different compression histories, as seen from Figure 2-10b.

To summarise, in studies where the influence of creep strains have been minimized by allowing a period of creep, recent stress history effects at very small to small strains may have been fully or partially overshadowed by the influence of the imposed creep period. If on the other hand a rest period has not been allowed for, then the influence of creep strains seems to significantly obscure the measured stiffness at both very small and intermediate strains. Both sets of results are in agreement with statements made by Jardine (1992) that the kinematic sub-yield surfaces appear to have the ability to either grow in size and/or reposition around the current stress point as a result of creep. The question of the effects of recent stress history is still up for debate and results so far suggest that drastically different methods of testing are required to investigate the influence of recent stress history at the very small to small strains.

2.2.5 Naturally and artificially structured clays

a Classification of structure

The term "micro-structure" refers to the combination of micro-fabric (arrangement of particles) and interparticle bonding and/or cementation in the soil specimen or soil mass, while "macro-structure" covers the presence or lack of soil characteristics such as bedding, fissures, inhomogeneities and shear-surfaces. Hence, all soils, no matter what state they are in, have

components of both micro-structure and macro-structure. The term "structure" on the other hand is a relative measure, which in soil mechanics context generally is used to describe the components of the micro and macro-structure of the natural intact soil or artificially cemented soil, which are removed upon reconstitution (Coop et al., 1995) and the detrimental effect of this on the strength envelope. A reconstituted soil is therefore often referred to as being in a non-structured or destructured state, while the intact material is often referred to as being in a structured state or metastable state. In natural sedimentary soils, structure is commonly classified into sedimentation structure and post-sedimentation structure (Cotecchia & Chandler, 2000). Sedimentation structure is affected by the depositional conditions such as water salinity, temperature and current, which in some cases can give rise to a very open card house like structure that is likely to collapse upon further loading (Soga & Mitchell, 1996). Post-sedimentation structure on the other hand is developed as a result of inherent and environmental ageing processes such as thixotropy, cementing, weathering, leaching etc. in addition to mechanical unloading and reloading from processes such as erosion and deposition. The "metastable" structure which is broken down with straining is usually attributed to relative weak cementation and bonding between the particles.

b Critical state framework for structured clays

Numerous studies of the effects of structure on the behaviour of natural soils and artificially cemented soils are reported in the literature. Based on the general findings several frameworks have been proposed in an attempt to unify the behaviour of structured soils (Burland, 1990; Cotecchia & Chandler, 2000; Leroueil & Vaughan, 1990; Shibuya, 2000).

Leroueil & Vaughan (1990) described the general effects of structure, which were found to be common for a wide range of soils including soft and stiff clays, granular soils and residual soils. In general, the presence of structure in a soil increases its strength and the size of its gross yield surface, allowing the (natural) structured soil to exist in states outside the permissible space defined by the instrinsic State Boundary Surface (SBS) of the reconstituted soil. When compressed or sheared the natural soil will reach its natural boundary surface (Burland, 1990) and further loading will result in break down of structure, which will move the intact state towards the destructured state. This behaviour is evidenced from e.g. one-dimensional compression and undrained shearing of soft natural Bothkennar clay (Smith et al., 1992) as seen in Figure 2-11 and Figure 2-12. The one-dimensional compression path of the natural samples of Bothkennar clay was observed to move outside the intrinsic compression curve (ICC) defined by the reconstituted material. After gross yield the natural soil collapsed towards the ICC. Similarly, in undrained shearing the state paths of the intact samples of Bothkennar clay lied well outside the intrinsic SBS. After peak there was a rapid loss of strength due to destructuration and the state moved towards the intrinsic critical state.

c Assessing the degree of structure

Several ways of assessing the degree of structure have been proposed in the literature. For natural clays the proportion of the intact strength which is lost due to reconstitution can be quantified by the sensitivity, S_t, which Terzaghi (1944) defined as

$$S_t = \frac{S_u}{S_u^*} \tag{2.3}$$

where S_u is the undrained strength of the natural clay and S_u^* is the undrained strength of the reconstituted clay at the same water content. The sensitivity has been widely used as a measure of soil structure in clays, although it is likely to be affected by the possible destructuration which may take place due to straining in the pre-failure region. In contrast Leroueil & Vaughan (1990) suggested that the level of structure is most easily considered by comparing the stress-void ratio states of the natural soil with those of the reconstituted soil. This idea was adopted by Soga & Mitchell (1996), who proposed the use of a metastability index (*MI*) to measure the level of structure in natural structured soils. The index is expressed as the difference between the liquidity index, LI_p of a given soil at the preconsolidation pressure and the liquidity index LI_0 of the fully destructured soil at the same effective pressure:

$$MI = LI_p - LI_0 \tag{2.4}$$

The concept is illustrated in Figure 2-13. The metastability index is likely to be affected by destructuration prior to gross yield. In addition, Shibuya (2000) later argued that *MI* suffered from being affected by rate of straining and that the yield pressure and hence *MI* was not sensitive enough to reflect changes in structure during short periods of ageing. The undrained shear strength is also likely to be affected by strain rate, as shown later in Section 2.3.2a. Based on oedometer compression tests on various natural soft and reconstituted clays supplemented with bender element tests, it was observed that the elastic stiffness, G_{max} shows a more systematic and sensitive response to changes in structure than the yield pressure (see Section 2.3.1c below). Shibuya (2000) generally observed that structure gave rise to a higher G_{max} in the natural structured soil compared to the reconstituted soil at the same void ratio. Since G_{max} was not believed to be influenced by rate of straining, an alternative metastability index, $MI(G_{max})^e$ was therefore proposed as follows;

$$MI(G_{max})^e = \left(e - e^{\beta^* - \beta^*}\right)_{current\ G_{max}} \tag{2.5}$$

where $e - e^{\beta^* - \beta^*}$ is the difference in void ratio between the current void ratio, e of the structured soil and the void ratio, $e^{\beta^* - \beta^*}$, of the reconstituted soil taken at the same current elastic shear stiffness, G_{max}. The reduction in $MI(G_{max})^e$ with increasing stress level in oedometer compression of Ariake clay is illustrated in Figure 2-14. In contrast to *MI*, which is only used to assess the level of structure in the intact state, the use of $MI(G_{max})^e$ allows assessment of both the intact natural structure and the progressive destructuration that takes places with loading post gross yield.

2.3 VISCOUS EFFECTS IN CLAYS

The viscous behaviour in clays is commonly investigated by performing laboratory tests such as creep tests, stress relaxation tests, Constant Rate of Strain (CRS) tests or Step-wise change in Rate of Strain (SRS) tests. These test methods and the observed viscous behaviour of clays will be reviewed in the following sections.

2.3.1 Creep and stress relaxation

a Characterising creep and stress relaxation

Creep is the process in which the soil deforms with time at a rate controlled by the viscous resistance of the soil structure. It is generally observed that the magnitude of the viscous resistance appears to decrease with increasing plasticity, increasing water content and increasing stress level. However, the characteristics of creep behaviour are qualitatively similar for all types of soils irrespectively of grain size, mineralogy, degree of saturation and degree and type of soil structure (Mitchell et al., 1997). Creep tests are defined as tests performed under constant effective stress conditions, but keeping effective stress conditions is not always easy to achieve. For example in undrained constant stress triaxial creep tests, possible changes in the pore water pressure will result in changes in the effective stress conditions. Also in drained triaxial tests the stress conditions are not kept constant if the load is not continuously corrected for the changes in the cross-sectional area of the sample. An extensive review of creep behaviour of soils have been carried out by Feda (1992).

The creep process is commonly characterised by three separate stages; primary, secondary, and tertiary as illustrated in Figure 2-15. The primary stage, also called primary consolidation, is largely associated with the dissipation of excess pore water pressures. During the primary stage the strain rate decreases rapidly with time. After the end of primary consolidation (EOP), deformation continues at a reduced rate, which is associated with pure creep of the soil skeleton rather than consolidation of the soil mass. In the secondary stage, also called secondary compression, there is a steady evolution of creep strains with time. Finally, in creep tests where the stress state is close to failure a tertiary stage may appear in which an acceleration in creep rate is observed. The tertiary stage eventually leads to failure, also commonly known as creep rupture. It has been suggested that creep rupture may be a result of progressive failure of interparticle bonds and associated reduction in effective stress caused by increases in water content or pore water pressure (Mitchell et al., 1997). The phenomenon of creep rupture will not be observed in one-dimensional compression or isotropic compression tests. It should however be pointed out that the characteristics of creep behaviour described above are associated with deformations occurring after loading stages. Creep behaviour after a significant unloading stage will initially be influenced by creep "recovery" (Almeida & Marques, 2003; Li et al., 2003), where the creep strains are negative and therefore give rise to

additional swelling, but may reverse to positive creep i.e. compression after a period of time (den Hann & van den Berg, 2001).

Another special case of viscous behaviour is the phenomenon of stress relaxation, which is closely linked to the process of creep. Stress relaxation is defined as a time-dependent change in stress at constant deformation. In the literature, only very little has been reported on the characteristics of stress relaxation. In general the patterns of stress relaxation appear to be similar to those observed for creep deformation for states not close to failure (Lacerda & Houston, 1973). A relationship between creep at fixed stress state and stress relaxation has been suggested by Tatsuoka (2003a) and Leroueil & Marques (1996), and is described below. If we assume that a change in the current stress σ in a given direction is uniquely linked to a change in the current elastic strain ε^e in the same direction via the elastic stiffness modulus E_{max}, and that the measured total strain rate $\dot{\varepsilon}^t$ is the sum of the rate of elastic strains $\dot{\varepsilon}^e$ and the rate of the time-dependent (visco)plastic strains $\dot{\varepsilon}^p$ we have;

$$E_{max} = \frac{\Delta\sigma}{\Delta\varepsilon^e} \tag{2.6}$$

$$\dot{\varepsilon}^t = \dot{\varepsilon}^e + \dot{\varepsilon}^p \tag{2.7}$$

In a creep test the stress is constant, thus $\dot{\varepsilon}^e = 0$ and $\dot{\varepsilon}_t = \dot{\varepsilon}^p$. In a stress relaxation test the total strain is constant and it follows that $\dot{\varepsilon}^t = 0$ and $\dot{\varepsilon}^e = -\dot{\varepsilon}^p$. Therefore, if $\dot{\varepsilon}^p$ is positive as is usually the case after a loading stage, $\dot{\varepsilon}^e$ will be negative and during stress relaxation both ε^e and σ will reduce. It can be deducted that the rate of reduction in stress during stress relaxation is directly linked to the creep potential of the sample at the same state.

In the following the creep behaviour of clays that has been reported in literature will be examined and the effects of creep on the yield locus, state paths and the current elastic soil stiffness will be discussed.

b Observed creep behaviour

During secondary compression, where there is a steady evolution of creep strains, the relationship between creep strain and logarithm of time can often be approximated as linear. Figure 2-16 shows the axial creep strain plotted against the logarithm of time from drained triaxial creep tests on undisturbed London Clay performed at various deviatoric stress levels (Bishop, 1966). For each stress level the relationship between creep strain and logarithm of time is observed to be approximately linear after the first day for times up to about 200 days, while an increase in stress level has the effect of shifting the lines vertically upwards. For engineering purposes the compressibility of the soil with time during secondary compression can be quantified by the secondary compression index (or coefficient of secondary compression), C_α which is either expressed in terms of the relative change in void ratio Δe or the relative change in strain $\Delta\varepsilon$;

$$C_{\alpha} = \frac{\Delta e}{\Delta \log t} \tag{2.8}$$

$$C_{\alpha\varepsilon} = \frac{\Delta \varepsilon}{\Delta \log t} \tag{2.9}$$

The value of C_{α}, which is generally determined from one-dimensional compression tests, is found to be highly dependent on the stress level in relation to the preconsolidation pressure. However, a comprehensive study carried out by Mesri & Castro (1987) showed that for a wide range of soils the value of $C_{\alpha\varepsilon}$ was approximately proportional to the compression index $C_{c\varepsilon}$ independently of stress level, where;

$$C_{c\varepsilon} = \frac{\Delta \varepsilon_a}{\Delta \log \sigma_v} \tag{2.10}$$

For inorganic soft clays it was suggested;

$$\frac{C_{\alpha\varepsilon}}{C_{c\varepsilon}} = 0.04 \pm 0.01 \tag{2.11}$$

While slightly higher values were reported for organic soft clays.

However, in many cases the true relationship between the creep strain and logarithm of time may deviate significantly from the assumed linear relationship and instead show tendencies of either continuously increasing or decreasing gradients, as illustrated in Figure 2-17 which shows creep data from triaxial compression tests on various clays (Mitchell et al., 1997). Nevertheless, the creep behaviour of soils can generally be characterised by a linear relationship between the logarithm of creep rate and logarithm of time (Tavenas et al., 1978; Vaid & Campanella, 1977). Figure 2-18, shows the drained triaxial creep data from Bishop (1966) replotted by Mitchell et al. (1997). It can be observed that the logarithm of creep rate decreases linearly with increases in the logarithm of time. With an increase in deviator stress the lines shift vertically upwards, while the slope of the relationships appears to be independent of stress level. To characterise the creep behaviour Singh & Mitchell (1968) defined the parameter m as the slope of the straight lines in the $\log\dot{\varepsilon}$ - $\log t$ diagram, where;

$$m = -\frac{\Delta \log \dot{\varepsilon}}{\Delta \log t} \tag{2.12}$$

The special case where $m=1$ corresponds to a constant value of C_{α}.

The creep behaviour described above is associated with secondary compression, where creep strains develop steadily and the stress state is not approaching failure. This behaviour is characteristic for creep tests at isotropic stress states or anisotropic stress states far from the peak strength envelope. If on the other hand, creep is observed at states close to the peak strength envelope, the increase in pore pressures in undrained conditions or reduction in volume in drained conditions may eventually bring the sample to failure. The onset of failure is indicated by a deviation from the linear relationship between the logarithm of creep rate and logarithm of time and a subsequent increase in creep rate is observed. This is shown in Figure

2-16, where the drained triaxial creep test carried out at the highest deviator stress fails after 2 days. It has been suggested that creep rupture may be linked to the residual strength of heavily overconsolidated clays (Bishop, 1966)[1]. However, in contrast Vaid & Campanella (1977) later reported on results from undrained triaxial constant stress creep tests on a sensitive undisturbed soft marine clay (Haney clay), which suggested the existence of an upper yield stress below which creep rupture would not occur, as shown in Figure 2-19. The upper yield stress was shown to correspond to the minimum undrained strength observed at very slow straining. For stress levels above the yield stress the time taken to rupture was directly linked to the applied stress, while for applied stresses below the yield stress the samples showed a continuously decreasing creep rate. It was also shown that samples failed during creep due to the build-up of pore water pressures and that the effective strength had not changed. Similar behaviour has been observed in undrained tests on Saint-Jean-Vianney clay, which is also a sensitive marine clay (Vaid et al., 1979). Based on triaxial tests on undisturbed St. Alban clay, Tavenas & Leroueil (1977) additionally suggested that creep rupture would only occur if the stress state in the q-p' plane was located in the region between the critical state strength line and the peak strength envelope.

c Influence of creep on the yield locus and subsequent state paths

From creep observations of soft clays in one-dimensional compression Bjerrum (1967) proposed the concept of isochrones (*latin: same time*) or time lines. The time lines plot as parallel curves in e-log σ'_v plane and represent the equilibrium void ratios for specific times of sustained loading at various stress levels. The concept is illustrated in Figure 2-20. It was shown that under sustained stress the void ratio reduces with time as a result of creep (denoted delayed compression) and that this process results in an increase in the yield pressure or apparent preconsolidation pressure, p_c (quasi-overconsolidation). This means that if a normally consolidated sample is allowed to creep for a period of time and then subsequently loaded, the sample will be able to sustain a load in excess of the preconsolidation pressure without causing significant volumetric changes. The undrained shear strength was also found to increase as a result of drained creep, which could be explained solely by the reduction in void ratio. A few years later Arulanandan et al. (1971) reported on results from undrained triaxial creep tests on San Francisco Bay mud at different stress levels. Results of the tests were replotted by Leroueil & Marques (1996) to show that the isochrone concept proposed by Bjerrum in one-dimensional compression could be extended to the entire yield surface in triaxial stress space (Figure 2-21). From the figure it can be seen that the entire yield envelope in stress space progressively moves towards smaller stresses with time, while maintaining the same shape. The early concept of isochrones has later been replaced by the concept of Constant Rate of Strain (CRS) curves,

[1] The results presented by (Bishop, 1966) should be taken with some caution, since the control of constant effective stress conditions could not have been very accurate with the spring-loaded system they used.

which is found to describe the influence of viscosity on the stress-strain behaviour of soils in more general terms, and will be described in Section 2.3.2a.

Tavenas et al. (1978) carried out a more general study of the volumetric and axial creep behaviour using drained and undrained triaxial tests on undisturbed lightly overconsolidated St. Alban clay. The volumetric creep behaviour is shown in Figure 2-22. A series of creep tests were carried out along the lines 0 to 5 shown in the figure at stress states that move progressively closer to the State Boundary Surface. The yield pressures were deduced from the volumetric compression at given volumetric creep rates. The stress states at which the samples are found to yield at the same volumetric creep rates, were then connected to give the yield envelopes for the given volumetric strain rates. It can be seen that the outer yield envelope reduces in size with a reduction in volumetric strain rate, while the shape of the yield envelope is maintained. Tavenas et al. (1978) also found that generally creep can be characterised by a linear reduction in logarithm of strain rate with logarithm of time in accordance with Singh & Mitchell (1968) findings. The parameter *m* for St. Alban clay was found to be around 0.7-0.8 for both volumetric and axial creep. Based on these findings a general model of the effect of time on the yield envelopes was proposed, as illustrated in Figure 2-23. The soil is assumed to be preloaded to state B on the Y_0 yield envelope, then the soil rests at stress state B for a period of time, which results in an expansion of the yield envelope to the "aged" Y_1 envelope. Based on this concept, creep rupture will only be observed if the stress state is moved to region I or IV above the failure line and outside the Y_0 yield envelope. During a creep test the Y_0 yield envelope corresponds to the lower limit of the yield envelopes for very slow rates of straining. Hence if the stress state is inside the Y_0 yield envelope, creep rupture will not occur even if the state is above the failure line. The findings by Vaid & Campanella (1977) concerning creep rupture, described in Section 2.3.1b above, are in agreement with this concept.

As suggested by the isochrone concept in one-dimensional compression, subsequent loading after a creep period will result in an initial stiff response. Figure 2-24 shows a typical constant rate of strain oedometer test on reconstituted Fujinomori clay, where the sample was loaded at the original strain rate after a period of drained creep (Tatsuoka, 2003b). It can be seen that the initial stiff response was followed by gradual yield after which the state path rejoined the normal compression line defined by the original strain rate. Some studies reported in the literature have observed the state path to temporarily overshoot the normal compression line when reloading was initiated after a creep period. This behaviour could be attributed to either inherent ageing effects or temporary effects of strain rate changes as reported later in Section 2.3.2b. However, generally with large straining the state path will rejoin the normal compression line. Similar behaviour is also usually observed when shearing is interrupted by a period of creep. Figure 2-25 shows a typical example from undrained triaxial tests on undisturbed Vallerica clay (Tatsuoka et al., 2000). It can be seen that creep strains developed under sustained deviator stresses, while on subsequent loading an initial stiff response was seen

in both the q-ε_s and q-p' planes. After gradual yield the state path then rejoined the original curve, which is a characteristic of pure viscous behaviour. If inherent ageing effects had played a role during creep, then the subsequent state path would yield above the original curve and show persistent effects of structure with continuing straining. The state path would not rejoin the original curve unless significant straining caused it to destructure. General effects of ageing will be reported in more details in Section 2.4.

d Influence of creep on the current elastic shear modulus

Several studies have been undertaken to investigate the influence of creep time on the elastic shear modulus G_{max} using dynamic tests such as resonant column or bender element tests (Anderson & Stoke, 1978; Lo Presti et al., 1996; Lohani et al., 2001). In most of these studies an observed increase in G_{max} during creep has been largely attributed to ageing effects, but there is conflicting evidence that the observed increase could be due to viscous effects only.

Figure 2-26 shows a typical plot of the changes in G_{max} and sample height with time during drained creep (Anderson & Stoke, 1978). In the diagram G_{max} and the change in sample height are plotted against the logarithm of time. In this case a sample of Ball kaolinite was step loaded and kept under constant isotropic confining pressure for up to 7 days with drainage allowed. The elastic shear modulus was derived from resonant column test. It can be observed that during primary consolidation the elastic shear modulus initially increased slowly and then showed a rapid increase towards the end of primary consolidation (EOP). After EOP, when pore water pressures had dissipated, the deformation was governed solely by the creep behaviour and the elastic shear modulus was observed to increase linearly with the logarithm of time. The increase in G_{max} during secondary compression was seen to be significantly in excess of what could be expected from the reduction in void ratio, which was suggested to primarily be a result of "strengthening of physical-chemical bonds" (Anderson & Stoke, 1978). To describe the long-term effect of creep on the elastic shear modulus, a coefficient of shear modulus increase with time, I_G was proposed as follows;

$$I_G = \frac{\Delta G_{max}}{\log\left(\frac{t_2}{t_1}\right)} \tag{2.13}$$

where ΔG_{max} is the change in elastic shear modulus from time t_1 to time t_2 after EOP. To remove the influence of confining pressure the normalised increase in shear modulus with time, N_G was defined as;

$$N_G = \frac{I_G}{G_{max,1000}} \tag{2.14}$$

where $G_{max,1000}$ is the elastic shear modulus measured 1000 min after initiation of creep (which must be after EOP). The value of N_G was found to be between 2-40 % for a wide range of undisturbed clays. Generally, soft clays appeared to show higher values than stiff clays (or sands).

Lohani et al. (2001) carried out drained creep tests for periods up to 15 days on two reconstituted clays of marine origin; very high plasticity Tokyo Bay, Minato Mirai Clay and low plasticity Shikoku Clay. The samples were loaded in one-dimensional compression and temporarily subjected to sustained loading at different stress levels. The elastic shear modulus was determined from bender element testing. It was observed, similarly to the previous findings by Anderson & Stoke (1978) that the elastic shear modulus increased with time by an amount which was in excess of what could be explained by the reduction in void ratio. Figure 2-4 shows the relationship between void ratio, vertical effective stress and elastic shear modulus for three samples of Minato Mirai Clay subjected to a combination of one-dimensional compression, unloading-reloading paths and sustained creep loading for 7 days at 90 kPa and 300 kPa vertical effective stress. As explained in Section 2.2.3 the normally consolidated states are found to plot on linear lines in all three diagrams; e-log σ'_v, log G_{max}-log σ'_v and e-log G_{max}, while the overconsolidated states plot on straight lines extending out to the left from the state boundary (SB) lines. In the three diagrams the SB lines have been termed *G-G, G'-G'* and *G''-G''* respectively. The *G''-G''* SB line in the e-log G_{max} diagram have also been denoted the intrinsic G_{max} line (IGL). It can be seen that the state during creep moves into structure permitted space to the right of IGL in the e-log G_{max} diagram. The increased rate of increase in G_{max} against void ratio during creep was therefore suggested to be due to ageing effects. In the log G_{max}-log σ'_v diagram the state during creep is seen to move vertically upwards corresponding to a sudden increase in G_{max} at constant pressure. Creep in the standard e-log σ'_v diagram is shown as a reduction in void ratio at constant stress, which in contrast to the e-log G_{max} diagram shows the state to move inside the SB surface. Hence the effect of creep could misleadingly be assumed similar to the effect of mechanical overconsolidation if only the e-log σ'_v relationship was considered. However, as shown from the e-log G_{max} diagram, there are clear differences in the effects of creep and overconsolidation in terms of elastic shear modulus. In subsequent loading after a creep period the state is then seen to rejoin the SB lines. Despite the apparent structuration effects on the elastic shear modulus, the yield pressure was not observed to exceed the normal compression line, which indicates that no significant ageing effects had taken place during creep.

Other studies have similarly observed an excess increase in G_{max} during creep, which was attributed to ageing, while at the same time creep was not seen to affect the yield envelope or the effective shear strength envelope when the sample was subsequently loaded. This was for example seen in oedometer tests on reconstituted samples of NSF clay subjected to 2 weeks of drained creep (Shibuya, 2000). Even creep tests on the inactive kaolin clay have shown this behaviour, even though kaolin would be expected to show insignificant structuration effects with time (Anderson & Stoke, 1978; Rammah et al., 2004). These conflicting findings lead to think that the observed increase in G_{max} during creep may be due to viscous effects rather than

ageing effects. Experimental evidence obtained during this research tends to support this latter statement, as will be shown in Chapter 4.

2.3.2 Strain rate effects

Constant Rate of Strain (CRS) tests are generally employed to look at the effect of strain rate on soil behaviour. In a CRS test the nominal compression rate (such as the vertical strain rate in oedometer tests or the axial strain rate in triaxial tests) is kept constant throughout the test. The behaviour at different constant rates of straining are then compared. In order to reduce testing time and remove the possible effect of sample variability Richardson & Whitman (1963) proposed a method, where during a single test step-wise change in the rate of strain (SRS) is performed in order to investigate the immediate strain rate effects. Curves for given strain rates could be obtained by interpolation between portions of curves. However, it was pointed out that step-changed curves did not agree completely with continues CRS curves. Figure 2-27 illustrates CRS and SRS test paths. In the following sections the observed effects of strain rate obtained on various different clays using CRS or SRS tests will be reported.

a A unique stress-strain-strain rate relationship

Until the late 1990's most work on strain rate-dependent behaviour of soils had concentrated on soft clays and it was generally found that most soft clays appeared to behave in an isotach (*latin: same rate*) manner. In the isotach concept the stress state during both creep and shearing is uniquely defined by the current strain and its rate (Leroueil et al., 1985; Vaid & Campanella, 1977). It is however more rigorous to state that the current stress is a unique function of plastic strain and its rate, since immediately after strain rate changes the strain rate is largely affected by elastic strains (Tatsuoka, 2003a). In addition, Tatsuoka (2003a) found the behaviour to deviate during cyclic loading, and added that the isotach behaviour is only valid for the case of monotonic loading. One of the special features of isotach behaviour, which will be illustrated below, is that the effects of strain rate changes are persistent.

Several studies reported in the literature have investigated the strain rate dependency of one-dimensional and isotropic compression curves for soft clays (Leroueil et al., 1985; Tatsuoka et al., 2001). Typically, post yield, a linear relationship between void ratio and effective stress is observed for a given constant strain rate. An increase in strain rate will shift the normal compression curve to the right and hence for a given void ratio the soil will be able to sustain a higher pressure. The rate-dependent one-dimensional compression behaviour of Batiscan clay, a natural sensitive clay from Canada, is shown in Figure 2-28 with data from both CRS and SRS tests (Leroueil et al., 1985). It can be seen that the strain rate influences both the normal compression curve and the yield pressure (apparent pre-consolidation pressure), and there appears to be a unique normal compression curve for a given strain rate, independent of strain history. An increase in strain rate shifts the compression curve to the right and results in an increase in yield pressure. It should be noticed that the compression behaviour of the sample

compressed at the slowest vertical strain rate of $1.69 \cdot 10^{-8}$ s^{-1} significantly deviates from the otherwise unique relationship observed at higher strain rates. Leroueil et al. (1985) interpreted this as ageing effects that are allowed to occur when the applied strain rate is slow enough. The influence of ageing on the stiffness and yield locus will be reviewed in detail in Section 2.4.2a. After analysing the data in Figure 2-28 further, Leroueil et al. (1985) suggested a unique stress-strain-strain rate relationship and showed that the plotted strain rate curves could be normalised with respect to the yield pressure σ'_y measured at the corresponding strain rate. This would then imply that the ratio of effective stresses measured at two different strain rates would be constant, and that the CRS curves would be parallel in e-log σ'_v plane. Soga & Mitchell (1996) gathered published data from one-dimensional compression tests for a selection of normally consolidated or slightly overconsolidated clays, amongst other the data from Leroueil et al. (1985), and showed that the logarithm of the 'apparent' pre-consolidation pressure (=yield pressure), generally increases linearly with an increase in logarithm of strain rate. The yield stress was found to increase about 10-20 % per log cycle increase in strain rate for the tested clays, refer to Figure 2-29.

Vaid & Campanella (1977) performed CRS and SRS undrained triaxial compression tests on the undisturbed soft marine Haney clay. The undrained strength was found to reduce with a reduction in strain rate and it was indicated that there might be a lower bound strain rate below which further reduction in strain rate would not result in any further reduction in undrained strength. The lower bound undrained strength was said to be equal to the upper yield stress, below which creep rupture did not occur (see Section 2.3.1b). After comparing data obtained from different types of tests (constant stress creep, constant load creep, constant rate of loading shear tests and step creep) Vaid & Campanella (1977) suggested the existence of a unique stress-strain-strain rate relationship independent of test type. Figure 2-30 shows the unique stress-strain relationship for a given constant strain rate with data points collected from different tests. The unique relationship was observed both pre-peak and post-peak and hence it was indicated that both creep behaviour and creep rupture were directly related to and could be predicted by the CRS shearing curves. Soga & Mitchell (1996) and Graham et al. (1983) found the rate dependency of the undrained strength to show similar linear characteristics and be of similar magnitude to the rate dependency of the yield stress in one-dimensional compression described above.

Figure 2-31 shows the influence of step changes in strain rate on the stress-strain behaviour and stress path of reconstituted normally consolidated kaolin in undrained triaxial compression (Tatsuoka et al., 2002). Strain rate dependency is seen in both the stress-strain relationship and in the effective stress paths and separate CRS curves are indicated up until and including peak. Immediately after an increase in strain rate the stress-strain path or stress-path is seen to jump upwards and show an initial stiff response. Then pronounced yielding is observed and the path joins a unique stress-strain curve or stress path above the original curve defined by

the lower strain rate. If the strain rate is reduced back to the original strain rate then a downwards stress jump is observed after which the path rejoins the original curve defined by the lower strain rate. The paths in both stress-strain and stress space are indicated to be uniquely defined by the strain rate and the effects of strain rate changes are observed to be persistent, which is a characteristic of isotach behaviour. Not only is the undrained stress path influenced by strain rate, generally, the entire yield envelope of OC and NC clays is found to be rate-dependent, as was reported by several researchers for a range of clays (Graham et al., 1983; Leroueil & Marques, 1996; Tavenas et al., 1978; Vaid & Campanella, 1977). On the other hand the critical state failure line is found to be strain rate independent for most soils. Leroueil & Marques (1996) also reported that the effective angle of shearing resistance at peak strength was more or less independent of strain rate (possibly a slight reduction may be observed with reducing strain rate) and could therefore conclude that an observed reduction in undrained strength of both NC and OC clays with reducing strain rate was due to creep driven pore pressure changes. Several others, including Soga & Mitchell (1996) and Vaid & Campanella (1977), have come to similar conclusions.

Isotach behaviour has also been indicated in soils other than soft clays. For example Tatsuoka et al. (2000) presented results from drained TC tests on a sedimentary soft sandstone and on a sedimentary mudstone, which indicated isotach behaviour until peak. Komoto et al. (2003) also found undisturbed samples of stiff plastic Kitan and Oimachi clays to show isotach characteristics. From the observed behaviour in literature it appears that most soft clays in both undisturbed and reconstituted states, undisturbed natural stiff clays and cases of soft rock all show isotach viscous behaviour, where the stress is uniquely defined by the plastic strain and strain rate in monotonic loading independently of strain history. The isotach behaviour has been observed both in one-dimensional and triaxial compression, drained and undrained. While the yield envelope appears to be rate-dependent, the effective peak strength envelope and the critical state on the other hand are found to be rate-independent. In the late 1990's several new aspects of time-dependent behaviour were highlighted, especially tests on sands, gravels, cemented soils and some stiff natural clays showed behaviour which did not conform to the isotach concept. From the literature review it has however become apparent that studies of viscous effects in stiff natural clays are not exhaustive. The present study attempts to bring further knowledge on the viscous behaviour of very stiff undisturbed clay. In the next section, examples of observed viscous behaviour, which does not conform to the isotach concept, will be presented. The viscous behaviour of granular soils has been included to highlight the similarities with the special non-isotach behaviour of clays.

b Temporary effect of strain rate changes

In order to establish a unified framework for naturally structured soils it is essential to perform repeatable tests on well controlled materials. Several researchers have been using cement-mixed soils to simulate structured soils. Kongsukprasert & Tatsuoka (2003b) performed SRS drained

triaxial compression tests on cement-mixed gravel. They observed that pre-peak strength, the behaviour showed distinct isotach characteristics, while post-peak the behaviour changed dramatically. They found that post-peak the change in deviator stress due to a change in strain rate is not persistent, but instead the viscous effect appears to decay with strain to a unique curve which is strain rate independent. This viscous feature, which is only observed upon strain rate changes, was termed TESRA (Temporary Effect of Strain Rate and strain Acceleration) by Tatsuoka et al. (2002). In recent years Tatsuoka and co-authors have shown that the (pure) TESRA behaviour appears to be a characteristic of common clean sands over the full shearing range from start of loading until failure (Tatsuoka et al., 2000; Tatsuoka et al., 2002). Figure 2-32 shows an example of the viscous behaviour of Hostun sand in triaxial compression tests, which is typical of clean sands. From the data there appears to be a unique persistent CRS stress-strain curve which is independent of strain rate. Upon a change in strain rate, the initial stress-strain response is seen to significantly overshoot or undershoot the CRS path, but with continuing straining the path returns to the unique CRS curve. Despite the apparent lack of viscous effects on the CRS curves significant creep and stress relaxation effects have been observed in plain strain compression tests on e.g. Toyoura sand (Di Benedetto et al., 2002).

To investigate viscous effects in stiff Fukakusa clay, Oka et al. (2003) carried out a series of undrained triaxial compression tests on both normally consolidated and overconsolidated reconstituted samples. The stress-strain path and effective stress path for normally consolidated (NC) samples are shown in Figure 2-33, and for overconsolidated (OC) samples in Figure 2-34. The strain rate was changed step-wise during the tests to investigate the immediate and persistent viscous effects. Looking at the results from the NC samples in Figure 2-33, it can be observed that at low stress levels the effect of strain rate changes on the stress-strain relationship appears to be persistent and the viscous behaviour can be defined as isotach. Then at higher stress levels effects of strain rate changes become temporary with overshooting and undershooting of the persistent CRS curves, a feature which appears to become more and more apparent as failure was approached. However, in contrast to what has been seen for clean sands the path upon strain rate change did not decay completely to a single unique CRS curve, instead some of the viscous effect was still persistent after large straining. Furthermore, the persistent CRS curves are seen to separate and appear to show a unique stress-strain relationship for a given strain rate. A similar pattern is observed for the effective stress path. In addition, the permanent CRS effective stress paths appear to approach a unique critical state line, the observed difference in undrained strength of the NC samples being due to a difference in accumulated pore water pressures. However, it can also be seen that if the strain rate is changed after reaching the critical state, then the stress path temporarily either overshoots or undershoots the critical state line. The results for OC samples generally show similar behaviour (see Figure 2-34). Temporary overshooting and undershooting of the permanent CRS curves are observed upon strain rate changes and the stress paths are seen to approach a unique critical state line,

indicating that the effective angle of shearing resistance at critical state is independent of strain rate. The tests carried out by Oka et al. (2003) extended the work done on Fukakusa clay much earlier at the same university by Akai et al. (1975). Akai and co-authors however only tested undrained NC reconstituted samples and did not vary the strain rate step-wise during individual tests. Based on the observed CRS paths they suggested the existence of a unique stress-strain-strain rate relationship, which indicates that the persistent strain rate curves found by Oka et al. (2003) also are unique and independent of strain history.

Viscous soil behaviour characterised by a combination of temporary and persistent viscous effect have also been observed in drained triaxial compression (TC) of very dense Chiba gravel, drained TC of cement-mixed sand and undrained TC of reconstituted NC stiff Fujinomori clay (Tatsuoka et al., 2000). Similarly, behaviour was also observed for reconstituted samples of Kitan and Oimachi clays (Komoto et al., 2003), despite these showing isotach behaviour in undisturbed states as reported in Section 2.3.2a. Generally, in soils which show a combination of temporary and persistent viscous effects, the temporary effects are seen to increase with straining. This behaviour has been has been termed General TESRA behaviour (Tatsuoka et al., 2002).

Tables 2-2 to 2-4 list the observed viscous behaviours in a wide range of structured and non-structured soils. Observed viscous behaviour in triaxial compression of sands, gravels, cement-mixed soils and reconstituted stiff clays are listed in Table 2-2, observed viscous behaviour in triaxial compression of reconstituted and undisturbed soft clays, soft rocks and undisturbed stiff clays are listed in Table 2-3, while the observed viscous behaviour in one-dimensional and isotropic compression for different clays are listed in Table 2-4. From the literature review, it has become apparent that viscous effects in clays (and granular soils) are more complex than originally thought. Recent research has highlighted new interesting aspects of the viscous behaviour of soils. It appears that the viscous behaviour of soils in general can be divided into the three categories; Isotach behaviour, (pure) TESRA behaviour and General TESRA behaviour, as suggested by Tatsuoka et al. (2002). The characteristics of each category and the soils which demonstrate this type of behaviour are summarised in Table 2-5.

Based on an extensive number of tests looking at the viscous characteristics of various soils including sands, gravels, clays and soft rocks, Tatsuoka (2006) recently made a preliminary summary of the various factors, which appeared to influence the viscous behaviour of the tested geomaterials, as shown in Table 2-6. Influencing factors included: particle shape (large particles only), grading characteristics, particle size, strength of inter-particle bonding, strain level and stability of inter-particle contact points. A change in each of the given factors, while keeping all other factors unchanged, appeared to have the ability to alter the viscous behaviour between Isotach, TESRA and intermediate behaviour (a fourth type of viscous behaviour termed 'positive and negative' which only has been indicated from recent tests on

granular soils is not considered here). Tatsuoka (2006) made no further attempt to explain why the viscous behaviours of soils are influenced in this way.

c Quantifying the general viscous effect

As mentioned in Section 2.3.2a above, Soga & Mitchell (1996) generally found a linear relationship between the logarithm of the undrained shear strength and the logarithm of axial strain rate for various soils reported in the literature. They therefore proposed to quantify the increase in undrained shear strength with an increase in strain rate by the rate parameter β, given by;

$$\frac{q_f}{q_{f(ref)}} = \left(\frac{\dot{\varepsilon}_1}{\dot{\varepsilon}_{1(ref)}} \right)^{\beta} \tag{2.15}$$

Where q_f is the deviator stress at failure for a given strain rate $\dot{\varepsilon}_1$ while $q_{f(ref)}$ is a reference strength for the corresponding reference strain rate $\dot{\varepsilon}_{1(ref)}$. The constant β was found to be in the range 0.02 to 0.07 for a selection of normally or slightly overconsolidated clays reported in the literature, corresponding to about 5 % to 17 % increase in undrained strength per log cycle increase in strain rate. A more general quantification of the rate dependency of soils has been proposed by Di Benedetto et al. (2002) and Tatsuoka et al. (2003). They observed in triaxial compression and extension tests on a wide range of non-cemented soils including sands, gravels and soft and stiff clays that for the same ratio of shear strain rate change $\frac{(\dot{\gamma}^{ir})_{after}}{(\dot{\gamma}^{ir})_{before}}$ the immediate change in the vertical effect pressure $\Delta\sigma'_v$ is proportional to vertical the effective pressure σ'_v before the strain rate change (the definition of the stress jump is illustrated in Figure 2-35). Hence, a rate-sensitivity coefficient β was proposed (different to the rate parameter used by Soga & Mitchell, 1996 above), which could suitably quantify the viscous property of most types of soils;

$$\frac{\Delta\sigma'_v}{\sigma'_v} = \beta \cdot \log\left(\frac{(\dot{\gamma}^{ir})_{after}}{(\dot{\gamma}^{ir})_{before}} \right) \tag{2.16}$$

Where the plastic "irreversible" shear strain is defined as $\gamma^{ir} = \varepsilon_v^{ir} - \varepsilon_h^{ir}$, the difference in vertical and longitudinal irreversible strain. Typically, in triaxial compression the (total) axial strain rate gives a good approximation to the plastic shear strain rate, as the proportion of elastic strains is limited post yield and the radial strain rate will minor. Results from drained triaxial compression tests on reconstituted NC Fujinomori clay, shown in Figure 2-36a, illustrate the linear relationship between the vertical stress increment and the stress level for different ratio of axial strain rate change, while Figure 2-36b shows the obtained linear relationship between the relative change in vertical stress and the ratio of axial strain rate change before and after a step change in rate (Acosta-Martinez et al., 2003). Tatsuoka et al. (2003) also showed that the rate

dependency of the vertical effective stress increased in proportion to the current horizontal confining pressure σ'_h, hence Equation (2.16) was normalised by σ'_h to give;

$$\frac{\Delta R}{R} = \beta \cdot \log\left(\frac{(\dot{\gamma}^{ir})_{after}}{(\dot{\gamma}^{ir})_{before}}\right) \tag{2.17}$$

Where $R = \frac{\sigma'_v}{\sigma'_h}$.

Kongsukprasert (2003) found the change in deviator stress to be more relevant than the change in vertical effective stress when quantifying the viscous property of cemented Chiba gravel in triaxial compression tests. Figure 2-37 shows the jump in deviator stress, Δq, against the current stress, q, for a number of different ratios of strain rate changes both normalised by a reference pressure, p_a=*100kPa*. It can be seen from the plot that for each ratio of strain rate change there is a linear relationship between Δq and q. The lines for constant ratio of strain rate change do not intersect the origin, but instead join at a common point on the negative side of the origin. The relation between Δq and q was expressed as;

$$\frac{\Delta q / p_a}{q + q_0 / p_a} = \beta \cdot \log\left(\frac{(\dot{\varepsilon}_v)_{after}}{(\dot{\varepsilon}_v)_{before}}\right) \tag{2.18}$$

Where $-q_0$ is the common intersection point on the $\Delta q=0$ axis, and $\frac{(\dot{\varepsilon}_v)_{after}}{(\dot{\varepsilon}_v)_{before}}$ is the ratio of vertical strain rate change, which in triaxial compression of stiff soils will be of similar magnitude to $\frac{(\dot{\gamma}^{ir})_{after}}{(\dot{\gamma}^{ir})_{before}}$ (Kongsukprasert, 2003). It can be deducted that Equation (2.18) will only be consistent with Equation (2.16), which is generally valid for non-cemented soil, in cases where the confining pressure is constant and q_0 is found to be equal to σ'_h. This however appears not to be the case with cemented Chiba gravel. Nevertheless, values for the rate-sensitivity coefficient β found for cemented and non-cemented soils using Equation (2.18) or (2.17) are comparable. It is noted that Equation 2.16 to 2.18 all predict viscous effect at very small strains at start of shearing.

Tatsuoka et al. (2005) found the rate-sensitivity coefficients to range between 0.02 and 0.08 (corresponding to 2 % to 8 % increase in vertical effective stress per log cycle increase in strain rate) for a large number of different non-cemented soils including dense and loose sands and gravels, dry and saturated soils, and reconstituted and undisturbed clays. The general observed trends for reconstituted clays were of increasing rate-sensitivity with higher degree of saturation and higher plasticity. The influence of structure and geological age on the rate sensitivity of undisturbed and reconstituted samples of stiff plastic Pleistocene Kitan and Oimachi clays have been investigated by Komoto et al. (2003) in drained triaxial compression tests. Figure 2-38 shows representative plots of the rate sensitivity (in terms of $\Delta R/R$ against the

ratio of the vertical plastic strain rates before and after a step change) of undisturbed and reconstituted samples of Kitan clay from two different sampling depths and geological ages of 0.33 million years and 1.7 million years. The results show that the β values (i.e. the gradients of the plotted best fit lines) of undisturbed samples are significantly smaller than the values obtained for the reconstituted counterparts and it is indicated that this difference increases with an increase in the geological age of the samples. In addition, the results indicate that the β value of the undisturbed samples generally decreases with an increase in the geological age. The influence of structure has also been investigated by others. Soga & Mitchell (1996) found, in contrast to Komoto et al. (2003) that the rate-dependency of various normally consolidated clays became more pronounced as the metastability increased, while Leroueil et al. (1996) indicated that the strain rate effects observed in one-dimensional compression of young artificially sedimented Jonquière clay were of similar magnitude to those observed in naturally aged (and thus much older) clays.

d Effect of strain rate on soil stiffness

It seems to be generally accepted that the very small strain stiffness or elastic stiffness is independent of strain rate and only dependent on soil state (Lo Presti et al., 1996;Shibuya et al., 1996;Tatsuoka et al., 2000). Figure 2-39a shows the influence of strain rate on the stress-strain relationship of reconstituted normally consolidated NSF-clay in undrained triaxial compression tests at small strains (Shibuya et al., 1996). While Figure 2-39b shows the variation in the elastic limit strain, $(\varepsilon_a)_{EL}$ (A=1) with strain rate for the same tests. As a result of increasing strain rate the yield stress and corresponding elastic limit strain are seen to increase, while the initial gradient of the curve (i.e. elastic stiffness) does not appear to be affected by the imposed strain rates. The results suggest that the small strain elastic shear stiffness is independent of strain rate over the range 0.01 %/min to 1.4 %/min, equal to 0.7 %/hr to 84 %/hr, and that there is a linear relationship between the logarithm of strain rate and the logarithm of elastic limit strain $(\varepsilon_a)_{EL}$. Lo Presti et al. (1996) stated that due to the viscosity of the soil, strain rate dependency of the secant stiffness will generally be observed. Similarly cyclic loading tests reported by Matešic & Vucetic (2003) and Vucetic & Tabata (2003), in the small to large strain range, show the secant stiffness of clays to increase with an increase in strain rate, while the secant stiffness of sand does not appear to be affected by strain rate. The observed behaviour ties in with the observed TESRA and Isotach behaviour of sands and soft clays respectively in monotonic loading.

2.4 INHERENT AGEING EFFECTS IN CLAYS

In most cases, ageing effects are coupled with viscous effects, since generally ageing is a function of time and the rate of deformation usually is as well. An appreciation of both phenomena is therefore crucial in order to understand and separate their effects. As shown in Section 2.3, viscous effects will often give rise to apparent ageing effects, such as the observed increase in the sub yield surface and undrained strength after a period of drained creep. Many studies found in the literature confuse these apparent ageing effects with real ageing effects such as thixotropy, bonding and cementation, which give rise to a true increase in the effective strength of the soil. The main reason for this confusion is that most studies of ageing during drained creep have not normalised their results with respect to the void ratio changes that occur under the sustained stress. Numerous studies therefore show effects of drained creep which cannot be attributed solely to ageing, for example in studies of the influence of drained creep on the subsequent undrained shearing behaviour of reconstituted Magnus clay (Jardine, 1985), reconstituted black cotton soil and kaolinite (Allam & Sridharan, 1979), reconstituted Fujinomori clay (Tatsuoka et al., 2000) and Osaka Bay Clay (Tanaka et al., 2003). In the following sections, general observed inherent ageing effects in clays at water contents below the liquid limit are summarised. This study concentrates on inherent ageing in natural clays, nonetheless for comparison the observed ageing effects in clay slurries, commercial clays and artificially cemented soils have also been included. It should be made clear that the literature review highlights that not all clays show significant ageing effects. Clay mineralogy, organic content, degree of disturbance and water content are some of the factors which appear to influence the ageing effects on strength and stiffness, as will be reported in the following.

2.4.1 Influence of ageing on strength envelopes

a Reconstituted clay slurries

Several studies have reported an increase in undrained and drained shear strength due to thixotropic hardening in clays reconstituted at high water content (Tang & Tsuchida, 1999; Skempton & Northey, 1952; Zreik et al., 1998a; Zreik et al., 1998b). Clays reconstituted at high water content are often referred to as clay slurries, clay suspensions or clay-water systems. These soils are commonly tested at very low stress levels and the water contents are subsequently very high and hence often exceed the liquid limit. As mentioned before the term thixotropy describes a "process of softening, caused by remoulding, followed by a time-dependent return to the original, harder state" (Burger & Scott Blair, 1948). Thixotropy is essentially a reversible effect, which Skempton & Northey (1952) suggested to be a result of "the gradual rearrangement of the particles, under the action of bonding forces, into positions of increasing mechanical stability".

Skempton & Northey (1952) defined the thixotropic regain as the difference between the undrained shear strength $(s_u)_t$ at time t after reconstitution and the undrained shear strength of sample $(s_u)_r$ immediately after reconstitution at the same water content. The acquired sensitivity S_t at time t was defined as;

$$S_t = \frac{(s_u)_t}{(s_u)_r} \tag{2.19}$$

After comparing the thixotropic regain (measured using a laboratory vane apparatus) in a number of reconstituted moderately and extra sensitive clays at water contents near the liquid limit it was concluded that the full undisturbed strength and sensitivity were only likely to be regained in moderately sensitive clays due to thixotropy, while it seemed most unlikely in sensitive and extra-sensitive clays. Further testing suggested that leaching could partially explain the extra sensitivity measured in some natural clays. However, as shown in Figure 2-40 the acquired sensitivity was found to reduce significantly with a reduction in water content. The results indicated that thixotropic regain will be insignificant in soils at water contents near the plastic limit. Tang & Tsuchida (1999) referred to test by Mitachi et al. (1987) on Ohnegai clay that similarly indicated insignificant thixotropic regain at higher stress levels and hence lower void ratios. While at low pressures and high water contents, tests on several clay slurries showed a significant increase in shear strength with time, even after correcting for the reduction in void ratio. Generally, the corrected shear strength (measured using a vane apparatus) was found to increase linearly with the logarithm of time. Several studies have also investigated the influence of water content on the thixotropic regain in compacted clays (Mitchell, 1960; Seed & Chan, 1959 after Braja, 1985). However, because of the inherent uncertainties about the uniformity of the pore water pressures in the compacted samples, these results cannot be relied upon to be representative of natural clay behaviour.

b Natural clays

It appears as though thixotropic hardening will not be significant in natural clays at typical foundation stress levels (defined as $p'_0 = 50$ kPa to 1000 kPa) or in natural overconsolidated clays, like London Clay, since these generally have water contents near the plastic limit. The insignificant thixotropic hardening observed at low water contents ties in with the suggestion by Skempton & Northey (1952) that thixotropy is due to the gradual rearrangement of the particles, which is expected to be restricted at low void ratios. Furthermore, heavily overconsolidated clays rarely show a high degree of sensitivity since the mechanical overconsolidation typically results in a break down of the sedimentation structure (Skempton & Northey, 1952). Therefore, in natural clays observed inherent ageing effects appear primarily to be associated with gradual bonding and cementation of the soil structure. In a general review of marine clays and fossiliferous soils Locat et al. (2003) found that secondary consolidation is not a significant natural process responsible for structuration of natural soils, but it may be very significant as a result of human intervention. The main structuration in sediments comes from phenomena such

as cementation (chemical, cold cementation, clay bonding) or aching of particles. The following studies found in the literature all indicate inherent ageing effects, which cannot solely be explained by viscous effects.

Generally inherent ageing results in an expansion of the entire state boundary surface as indicated by an increase in the yield stress in isotropic and one-dimensional compression test or an increase in the effective angle of peak strength in triaxial compression tests. Therefore, if a sample experiences significant ageing effects during a prolonged period of rest, then when loading is resumed at the original strain rate the subsequent state paths are observed to move into structure permitted space outside the bounding surface as determined by the unaged soil (Allman & Atkinson, 1992; Burland, 1990; Skempton & Northey, 1952; Smith, 1992; Zreik et al., 1998b). Yet, several studies have indicated the effective critical state angle of shearing resistance not to be influenced by ageing effects, which most likely can be explained by the significant destructuration that occurs because of the large strains involved in reaching the steady state conditions (Smith, 1992; Vaid & Campanella, 1977).

Tatsuoka et al. (2000) reported on undrained triaxial compression tests on NC reconstituted Fujinomori clay after Momoya (1998), which investigated the effects of undrained creep. Figure 2-41 shows the result of two samples of Fujinomori clay which were isotropically consolidated under the same conditions. Sample 8 was sheared continuously to failure in undrained compression at a constant rate of vertical strain (ε'_v=*0.05 %/min*). Sample 13 was also sheared in undrained compression at a constant strain rate, but at stress state A the sample experienced a period of undrained creep for 1 day before continuing undrained shearing to failure. It can be seen that the stress state gradually moved to the left during undrained creep because of increases in pore water pressure. When subsequent loading was initiated after creep, a high stiffness zone was observed around the current stress point. The sample then yielded and followed a stress-strain path and stress path noticeably above the paths of sample 8. At failure, a noticeable increase in the undrained shear strength was observed for the sample which had experienced creep. Since volume changes were absent during creep and rate effects did not play a role, the observed increase in strength could be attributed to inherent ageing effects. It is however quite difficult to deduct from the two tests whether the critical state angle of shearing resistance was affected by the limited ageing period or not. There is some indication that sample 13 showed slightly stiffer behaviour prior to creep, with a stress path located slightly above the stress path of sample 8. Therefore, sample variability may explain part of the observed increase in undrained strength after creep. Figure 2-42 shows that samples of the same Fujinomori clay subjected to drained creep for 2 days showed comparable increases in undrained strength due to ageing after normalising with respect to the changes in void ratio.

Similar increase in undrained shear strength from undrained creep has been reported in triaxial compression tests on undisturbed samples of Haney clay (Vaid & Campanella, 1977). Figure 2-43 shows the stress-strain paths for samples I, II and III. Sample I was sheared

continuously after isotropic compression, while samples II and III were subjected to undrained creep at two different deviator stress levels for 20.000 minutes (13.8 days) before being sheared to failure. Besides the significant increase in undrained shear strength observed as a result of ageing effects, the results illustrate that creep at higher deviator stress levels gives rise to greater increase in undrained strength and furthermore shows more brittle behaviour. The failure strain however appears not to be influenced by the ageing effects. Jardine (1985) also found an increase in brittleness and a significant increase in undrained strength in triaxial compression tests on reconstituted Magnus clay after sustained periods of drained creep up to 20 days (see Figure 2-44). However, the observed increase in undrained strength could partially be attributed to the reduction in void ratio and hence in this case the actual increase due to ageing effects cannot be estimated.

Tang & Tsuchida (1999) estimated the undrained shear strength gain due to ageing effect by subtracting the effect of volumetric compression (viscous effect) from the shear strength increase actually observed as a result of drained creep at isotropic stress state. The increase in undrained shear strength Δs_u (corrected for changes in void ratio) with ageing time t at isotropic stress state under a given overburden pressure p_0 was found to follow a relationship given by;

$$\frac{\frac{\Delta s_u}{p_0}}{\Delta \log t} = c \tag{2.20}$$

in which the constant c quantifies the rate of increase in undrained shear strength with ageing time. Equation (2.20) suggests a linear increase in strength with the logarithm of ageing time. Tang & Tsuchida (1999) successfully applied Equation (2.20) to test data on reconstituted Ariake clay (Yasuhara & Ue 1983), Okayama clay (Ue et al. 1997) and Hayakita clay (Mitachi et al. 1987), and found the rate of shear strength gain, c, to be in the order of 0.013 to 0.023. A linear relationship between strength increase and ageing time have also been suggested in tests on undisturbed Haney clay (Vaid & Campanella, 1977). However, as mentioned in Section 2.4.1a above Tang & Tsuchida (1999) had also found from test data on Ohnegai clay that ageing effect can be insignificant in some clays at higher stress levels.

c Artificially cemented clays

Studies of artificially cemented soils are generally carried out with the purpose of characterising a method of ground improvement. Nevertheless, the studies found in the literature suggest that many of the characteristics associated with inherent ageing in natural soils are reproduced when artificially cemented soils are cured. Studies on artificial cementation in granular soils are commonly found, while artificial cementation of clays has been studied to a lesser extent. Cementation of the soil structure is usually achieved by either flushing a solution of cementing agents through the sample after setup, or by mixing the cementing agent directly with the dry or saturated soil before creating a reconstituted sample. The flushing technique is only feasible with porous materials such as sands and gravels, while cement-mixing in dry or saturated states

is typically used with clays which have a low permeability. Common cement agents include gypsum, quick lime, Portland cement and calcite. For most types of cementing agents, the presence of water is necessary in order to start the chemical reaction that gradually leads to the creation of strong cementation at interparticle contacts. In the case of Portland cement, when contact is made with water, hydration of the cement paste takes place and the strength of the cement increases progressively with curing time. In addition to the growth of strong interparticle cementation bonds, heat development and absorption of pore water occurs as a result of the cement hydration.

Horpibulsuk et al. (2003) tested samples of Ariake clay mixed with ordinary Portland cement at percentages of the dry weight varying between 5 % and 25 %. The samples were prepared in split moulds at different water contents above the liquid limit of the pure clay and the slurries were left to cure under atmospheric pressure for periods up to 170 days. The unconfined compressive strength was used as a measure of the increase in strength with curing time. Figure 2-45 shows the strength increase plotted against the curing time for the samples of Ariake clay along with collected data from similar tests on marine clays from Thailand (data from Udin, 1994 and Bergado et al., 1999) and Indian inland clay (data from Nagaraj, 1994). The following linear relationship between normalised strength and the logarithm of curing time was suggested.

$$\frac{q_D}{q_{28}} = 0.038 + 0.218 \ln D \qquad \text{for } LI=1.0\text{-}2.5 \tag{2.21}$$

in which q_D is the strength after D days of curing, and q_{28} is the 28-day strength used for normalising the results. The normalisation appears to remove most of the effects of difference in clay type, clay water content and cement content. But the normalised results still show significant scatter. Similar linear relationship between strength increase and curing time has been observed in unconfined compressive tests on cement-mixed kaolin (Komoto, 2004) and in drained triaxial compression tests on cement-mixed granular soils (Horpibulsuk et al., 2003; Kongsukprasert & Tatsuoka, 2003a; Lohani et al., 2003), both for curing at isotropic stress states and curing at anisotropic stress states.

Komoto, 2004 performed consolidated drained (CD) triaxial tests on cement-mixed kaolin in order to investigate the influence of curing time and curing stress state on the drained shear strength. Generally, 50x100 mm samples were prepared from dry-mixing kaolin powder with 3 % rapid hardening Portland cement. Samples were then preconsolidated in a split-mould followed by saturation in the triaxial cell. Figure 2-46 shows the relationship between deviator stress and axial strain for samples saturated and cured under an isotropic confining pressure of σ'_c=100 kPa for curing times varying between 1 day and 45 days. Figure 2-47 shows the evolution of volumetric strains for the same tests. The general observed trend is an increase in stiffness, peak strength and brittleness and a slight reduction in failure strain with increasing curing time. Despite significant influence of curing time on the peak strength, the critical state

strength at large strains appear to be independent of curing time. Only the sample cured for 45 days show a large strain strength, which is significantly above the critical state strength plateau observed for the other tests. This may be because the sample had not reached a steady state, as indicated from Figure 2-47, where it can be seen that the volumetric strains are still reducing at a relative high rate at large axial strains. Figure 2-48 shows that the scatter in the results makes it difficult to deduct a unique relationship between the measured peak strengths and curing times. A second test series was carried out in which the influence of the curing stress state was investigated. The samples were first compressed dry under an isotropic confining pressure of 100 kPa and then sheared by drained triaxial compression to a deviator stress level of either 0 kPa, 50 kPa, 100 kPa or 150 kPa. Each sample was then saturated and cured for 48 hrs at the respective stress level. After curing the samples were sheared in drained triaxial compression to large strains beyond failure. Figure 2-49 shows the deviator stress against axial strains for all the samples. It can be seen that the effect of increasing curing deviator stress level is a marked increase in the stiffness at small strains. There is also some indication that the peak strength increases with increasing curing deviator stress level, however this trend is not so clear from the results.

2.4.2 Influence of ageing on the elastic shear stiffness and yield envelopes

a One-dimensional and isotropic compression of natural clays

Test results from one-dimensional and isotropic compression on clays typically show similar effects of ageing. After an ageing period with associated creep at constant stress state, or stress relaxation at fixed strain, the initial reloading response is seen to be very stiff (as was illustrated in Figure 2-11 for a naturally aged clay). This initial response is the combined effect of the viscous property due a sudden change in strain rate, and the structure formation resulting from ageing. With continuing straining the reloading curve gradually yields and is seen to overshoot the intrinsic compression curve (ICC) for same strain rate as it reaches a yield point outside the previous state boundary surface (SBS). Then, typically, as the stresses continue to increase, destructuration forces the compression curve back towards the unaged ICC, making the compression line initially steeper than the ICC (Burland, 1990; Lohani et al., 2001). In some cases where strong bonds are created due to ageing, a persistent effect of ageing is seen on the compression curve even at high pressures post yield.

Significant ageing effect on the one-dimensional compression curve has been observed among others by (Perret 1995) in tests on artificially sedimented Jonquière clay, as shown in Figure 2-50a from Leroueil et al. (1996). In the test, a sample was subjected to drained creep for 120 days under an applied effective stress of 10 kPa before being loaded again. It can be seen that the yield pressure after ageing is significantly greater than what could be expected from the reduction in void ratio. Measurements of G_0 from bender element tests similarly indicated significant structuration during creep, as shown in Figure 2-50b. However, both the

compression curve and the G_0 measurements indicate that the created structure is broken down at higher stress levels. Tatsuoka et al. (2000) reported on tests on Fujinomori clay (after Momoya, 1998), which additionally confirmed an increase in stiffness during creep from static measurement. The values for the initial constraint modulus M_0, defined for a vertical strain of 0.001 % from the restart of loading, were obtained for different periods of ageing up to 30 days (Figure 2-51b). The compression curve after drained creep of 30 days, which is shown in Figure 2-51a, also indicates ageing effects on the yield pressure.

In order to investigate further ageing effects in one-dimensional compression of artificially sedimented Jonquière clay, Leroueil et al. (1996) performed a series of oedometer compression tests consisting of conventional 24-hrs load step compression tests along with CRS compression tests at two different strain rates of $1.27 \cdot 10^{-5}$ s^{-1} (4.6 %/hr) and $1.00 \cdot 10^{-7}$ s^{-1} (0.036 %/hr). The strain rate at the end of the loading period in the conventional 24hrs loading tests was found to be close to 10^{-7} s^{-1}. Hence, if the compression behaviour was only affected by viscous effects, the compression curve for the conventional 24hrs compression tests should coincide with the CRS curve for the strain rate of 10^{-7} s^{-1}. However, as seen from Figure 2-52, this was not the case. The test for the slowest CRS test shows much stiffer compression behaviour than what would be expected from the viscous behaviour. It can be seen that the compression curve for the slowest strain rate is located above the higher strain rate curve and the curve for the conventional 24hrs compression test. The behaviour can be explained by the progressive structuration (ageing), which takes place at low strain rates ($<10^{-7}$ s^{-1}). As seen, the ageing effects overshadow the effects of strain rate. While, when the clay is rapidly loaded, as in the case of the CRS tests with a strain rate of 1.27×10^{-5} s^{-1}, structure has no time to develop. On the other hand, in the conventional 24-hrs step-loading test, structure, which could have developed during one loading step, was destroyed when loading was applied in the subsequent step. Based on the findings, it was concluded that structuration should be related to the combined effect of time and strain rate.

Similar ageing effects at low strain rates have also been observed by in one-dimensional tests on Bothkennar clay (Tatsuoka, 2000; data from Khansari, 1993) and in tests on Batiscan clay and St. Alban clay (Leroueil et al., 1985). Generally, the results suggests that ageing effects observed during slow loading are similar to those developed during prolonged periods of rest e.g. during creep or stress relaxation. Despite evidence of ageing in artificially sedimented Jonquière clay, Leroueil et al. (1996) reported on findings from literature which showed that ageing effect were not significant in all clays. In long-term oedometer compression tests performed by (Perret et al., 1995) it was observed that a natural sample of Saguenay Fjord clay with low organic content showed significant ageing effects on the strength, while another sample of Saguenay Fjord clay of same geological origin, but with a higher organic content showed insignificant ageing effects. Leroueil et al. (1985) also did not observed any significant ageing effects in slow CRS compression tests on Berthierville clay.

b Triaxial compression of natural clays

The effects of ageing on the stiffness and yield envelopes, which were found in data from oedometer compression tests, as reported above, have been confirmed in general terms in triaxial compression tests. Only limited studies are found in the literature, but generally it is observed that ageing during a period of rest has the effect of simultaneously increasing the gross yield surface and the magnitude of the stiffness at very small to small strains for reconstituted samples. Some findings also support an increase in the size of the sub-yield surfaces due to ageing. In contrast, for undisturbed samples the effects of ageing appear not to influence the elastic stiffness. Allman & Atkinson (1992) examined the effects of ageing after one-dimensional compression on the subsequent drained shearing behaviour of reconstituted Bothkennar clay. Figure 2-53 compares the stress paths normalised with respect to void ratio for four samples with different stress-time histories. All samples were one-dimensionally compressed to p'=200 kPa. Sample B49 was sheared immediately after drained compression, while sample B33 experienced drained creep for 20 hrs and sample B70 experienced drained creep for 200 hrs prior to shearing to failure. A fourth sample B55 was unloaded to a lightly overconsolidated state before shearing. From the figure, it can be seen that the samples that were subjected to a creep period showed initial high stiffness at the start of loading with near vertical stress paths, similar to the behaviour of the lightly overconsolidated sample. This was in contrast to sample B49, which showed a soft response at the start of shearing immediately after the drained one-dimensional compression. Figure 2-54 indicates that the shear stiffness at small to large strains increases with ageing time during drained creep. It is likely that the low stiffness observed for sample B49 has been influenced by significant creep strains remaining after one-dimensional compression. The initial stiff behaviour of samples B33 and B49 could be explained by the viscous effect due to an increase in the strain rate upon reloading. In fact only sample B70, which was aged for 200 hrs, indicated an increase in the gross yield surface due to ageing. Sample B33 on the other hand yields and thereafter follows the state boundary surface of the unaged sample B49. Based on these observations it was concluded that the effect of creep for short periods of ageing was equivalent to overconsolidation (Allman & Atkinson, 1992). This conclusion is however misleading, as there is evidence that overconsolidation and creep or ageing influence soil behaviour in different ways – Firstly, if ageing effects were significant (as indicated for sample B70), then creep would give rise to an increase in the gross yield surface, while overconsolidation or creep without ageing effects would not. Without ageing effects the creep effects or viscous effects could be said to be similar to overconsolidation. However, creep effects will not be equivalent to overconsolidation in all aspects as reported in Section 2.3.1d, where it was shown that in terms of G_0–e relationship then creep is distinctly different from overconsolidation (Lohani et al., 2001).

Mukabi & Tatsuoka (1999) investigated the influence of ageing at the final reconsolidation stress state on the subsequent undrained triaxial shearing path in tests on three

different nominally undisturbed samples of stiff natural clays. From the findings, it was concluded that ageing within the gross yield locus (Y_3) of the undisturbed soil did not give rise to any significant changes in the very small strain elastic stiffness, while on the other hand the linear elastic range (Y_1) and the linearity of the stress-strain behaviour at intermediate strains increased with ageing. Figure 2-55 shows the undrained stress paths and stiffness degradation curves for two samples of undisturbed Osaka Bay Clay aged for one day (ST) and ten days (LT) respectively at the final reconsolidation stress state. Both samples exhibit initial stiff behaviour, but the sample, which was aged the longest (LT) showed a significantly greater linear elastic range and more linear stress-strain behaviour at intermediate strains. A systematic increase in the linear elastic range was also found in tests on undisturbed reconsolidated OAP clay for ageing periods up to 41 days. In contrast to these findings Santagata et al. (2005) indicated a significant increase in the elastic stiffness of reconstituted normally consolidated Boston blue clay after 11 days of ageing at K_0 state when subsequently shearing the samples in undrained triaxial compression. To explain the difference in behaviour Mukabi & Tatsuoka (1999) suggested that the degree of sample disturbance dictated the effect of ageing. Because undisturbed samples had already aged for a long time in the field, these would not show any significant effect of short-term ageing if the stress state was kept within the yield surface, while reconstituted samples or samples, which were not truly undisturbed would show noticeable effects of ageing.

From the literature review it is found that artificially cemented clays show similar effect of curing time to the effects of ageing observed in natural clays. Generally, an increase is observed in the linear elastic range, the elastic shear modulus, the linearity of the stress-strain behaviour and the effective peak angle of shearing resistance with increasing curing time in triaxial tests (Komoto, 2004; Sugai et al., 2003; Tatsuoka et al., 2000).

2.5 TABLES AND FIGURES FOR CHAPTER 2

Table 2-1 Classification of common time effects (modified after Kongsukprasert & Tatsuoka, 2003)

Phenomenon		**Micro-mechanisms**
Viscous effect		creep, stress relaxation, strain rate effects, apparent structuration from creep
Ageing effect	-Inherent- (no external influence)	thixotropy, bonding, cementation etc.
	-Environmental- (external influence)	weathering, chemical changes to pore water (e.g. leaching), heat- and pressure-induced changes to the soil structure etc.

Table 2-2 Observed viscous behaviour in triaxial compression for sands, gravels, cement-mixed soils and reconstituted clays

Soil name	Description	PI	Observed viscous behaviour		
			Isotach	Combined TESRA* and Isotach	Pure TESRA*
Hostun[2]	Quartz rich sub-angular, poor-graded medium sized sand		-	-	until peak
Toyoura sand[2]			-	-	until peak
Chiba gravel[2]	Very dense, crushed sandstone		-	pre-peak and post-peak	-
Metramo silty sand[2]	Dense, crushed granite, fines content 16%	14	-	pre-peak?	post-peak
Cement-mixed sand[2]	4% cement		-	pre-peak and post-peak	post-peak?
Cement-mixed gravel[3]	Chiba gravel mixed with 2.5% cement		pre-peak	-	post-peak
Cement-mixed kaolin[8]	3% RHP cement		?	?	post-peak
Lower Mississippi River Valley clay[4]	Reconsituted slightly organic back-swamp alluvial deposit	38	possibly at low stresses	evidence at higher stresses pre-peak	possibly at peak state
Fukakusa clay[5]	Reconstituted, NC and OC Pleistocene marine clay	27	at low stresses	high stresses pre-peak and post-peak	-
Fujinomori clay[2]	Reconstituted, NC	33	at low stresses	high stresses pre-peak and post-peak	-
Kitan clay[6]	Reconstituted, Pleistocene	22-62	at low stresses	intermediate stresses pre-peak	high stresses and peak state
Kitan clay[6]	Reconstituted – aged for one year	22-62	at low stresses	intermediate stresses pre-peak	high stresses and peak state
Oimachi clay[7]	Reconstituted, Pleistocene	20	at low stresses (<3% strain)	?	?
London Clay[8]	Reconsituted, NC	37	at low stresses	intermediate stresses pre-peak	high stresses and peak state
London Clay[8]	Reconsituted, OC	37	at low stresses	high stresses pre-peak and post-peak	-

*TESRA: Temporary effect of strain rate and strain acceleration (Tatsuoka et al., 2002)

[2] (Tatsuoka et al., 2000)
[3] (Kongsukprasert & Tatsuoka, 2003b)
[4] (Richardson & Whitman, 1963)
[5] (Oka et al., 2003)
[6] (Komoto, 2004)
[7] (Komoto et al., 2003)
[8] This study

Table 2-3 Observed viscous behaviour in triaxial compression for reconstituted and undisturbed soft clays, soft rocks and undisturbed stiff clays

Soil name	Description	PI	Observed viscous behaviour		
			Isotach	Combined TESRA and Isotach	Pure TESRA
St. Alban clay[9]	Undisturbed, OC	17-23	until peak	-	-
Haney clay[10]	Undisturbed sensitive marine, NC	18	until peak	-	-
Vallerica clay[11]	Undisturbed stiff marine clay, OC	26	at low stresses	possibly at high stresses pre-peak and post-peak	-
Belfast clay[12]	Undisturbed organic estuarine, lightly OC	50-70	pre peak and post peak	-	-
Winnipeg clay[12]	Undisturbed plastic lacustrine, lightly OC	35-55	pre peak and post peak	-	-
Kaolin clay[13]	Reconstituted, NC	42	until peak	-	-
Kazusa sedimentary rock[11]	Rotary core sedimentary soft sand/silt stone	-	until peak	-	-
Kitan clay[14]	Undisturbed, stiff, Pleistocene	22-62	until peak	-	-
Oimachi clay[15]	Undisturbed, stiff, Pleistocene	20	at low stresses (<3% strain)	?	?
London Clay[16]	Undisturbed, stiff, heavily OC	37	pre peak and post peak	-	-

Table 2-4 Observed viscous behaviour in one-dimensional and isotropic compression for different clays

Soil name	Description	PI	Observed viscous behaviour		
			Isotach	Combined TESRA and Isotach	Pure TESRA
Batiscan clay[17]	Sensitive natural	21	1D compression	-	-
Fujinomori clay[18]	Reconstituted, NC	33		-	-
Oimachi clay[18]	Reconstituted, Pleistocene	20		-	-
Kitan clay[18]	Undisturbed, stiff, Pleistocene	22-62		-	-
London Clay[16]	Reconstituted, NC	37	Isotropic compression	-	-

[9] (Tavenas et al., 1978)
[10] (Vaid & Campanella, 1977)
[11] (Tatsuoka et al., 2000)
[12] (Graham et al., 1983)
[13] (Tatsuoka et al., 2002)
[14] (Komoto, 2004)
[15] (Komoto et al., 2003)
[16] This study
[17] (Leroueil et al., 1996)
[18] (Acosta-Martinez et al., 2003)

Table 2-5 Viscous characteristics of soils

Phenomenon	Viscous characteristics	Observed in
Isotach	• Separate CRS curves • Unique relationship between stress, plastic strain and its rate independently of strain history • Persistent effect of strain rate changes	• Soft clays (undisturbed and reconstituted) • Some soft rocks • Undisturbed stiff natural clays
(pure) TESRA	• Non-persistent temporary effect of strain rate changes • Overshooting and undershooting of the persistent CRS curve after changes in strain rate and subsequent decay towards a single unique CRS curve	• Clean sands
General TESRA	• Increasing TESRA effect with increasing strain • In the case of clays the TESRA effect is not observed at low stress levels, only at higher stress levels does the TESRA effect become increasingly apparent	• Cemented soils • Some dense gravels • Dense silty sands • Reconstituted stiff natural clays.

Table 2-6 Factors influencing the viscous behaviour of soils (after Tatsuoka, 2006)

Viscosity type (θ) / Influencing factors	Isotach (θ=1) → TESRA (θ=0) → Positive & negative (θ<0)
Particle shape (stiff particles)	More angular → More round
Grading characteristics	More uniformly graded → More poorly graded
Particle size (saturated)	Smaller (*clay*) → Larger (*sand/gravel*)
Particle crushability	More crushable ?? → Less crushable ??
Inter-particle bonding	Stronger → Weaker → Null (*rock/cement-mixed soil*) (*unbound granular materials*)
Strain level	Smaller strain → Larger strain (in particular, post-peak)
Inter-particle contact point	More stable (more cohesive & larger co-ordination numbers) → Less stable (less cohesive & smaller co-ordination number)

- *Creep deformation* - *Deformation by cyclic loading*	*Larger → Smaller* *Smaller → Larger*

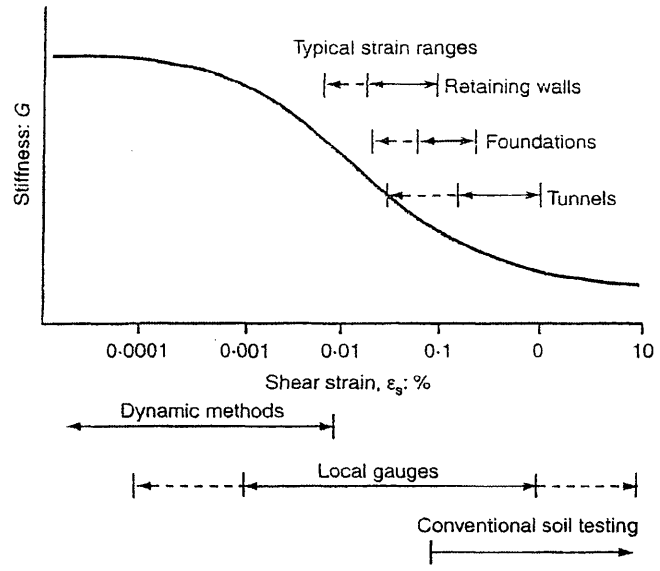

Figure 2-1 Characteristic stiffness-strain behaviour of soils with typical strain ranges for laboratory tests and structures (Atkinson, 2000)

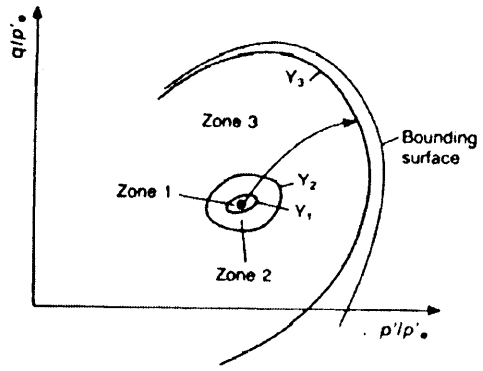

Figure 2-2 Schematic diagram of kinematic sub-yield surfaces (Jardine, 1992)

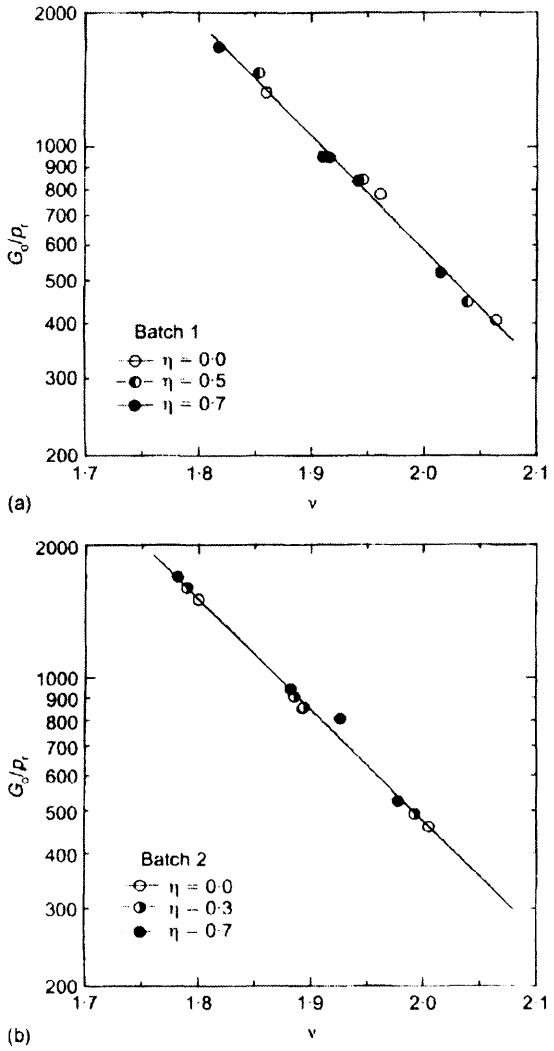

Figure 2-3 Small-strain shear modulus against specific volume for Vallericca Clay at NC states under different stress ratios, η (a) batch 1, (b) batch 2 (Rampello et al., 1997)

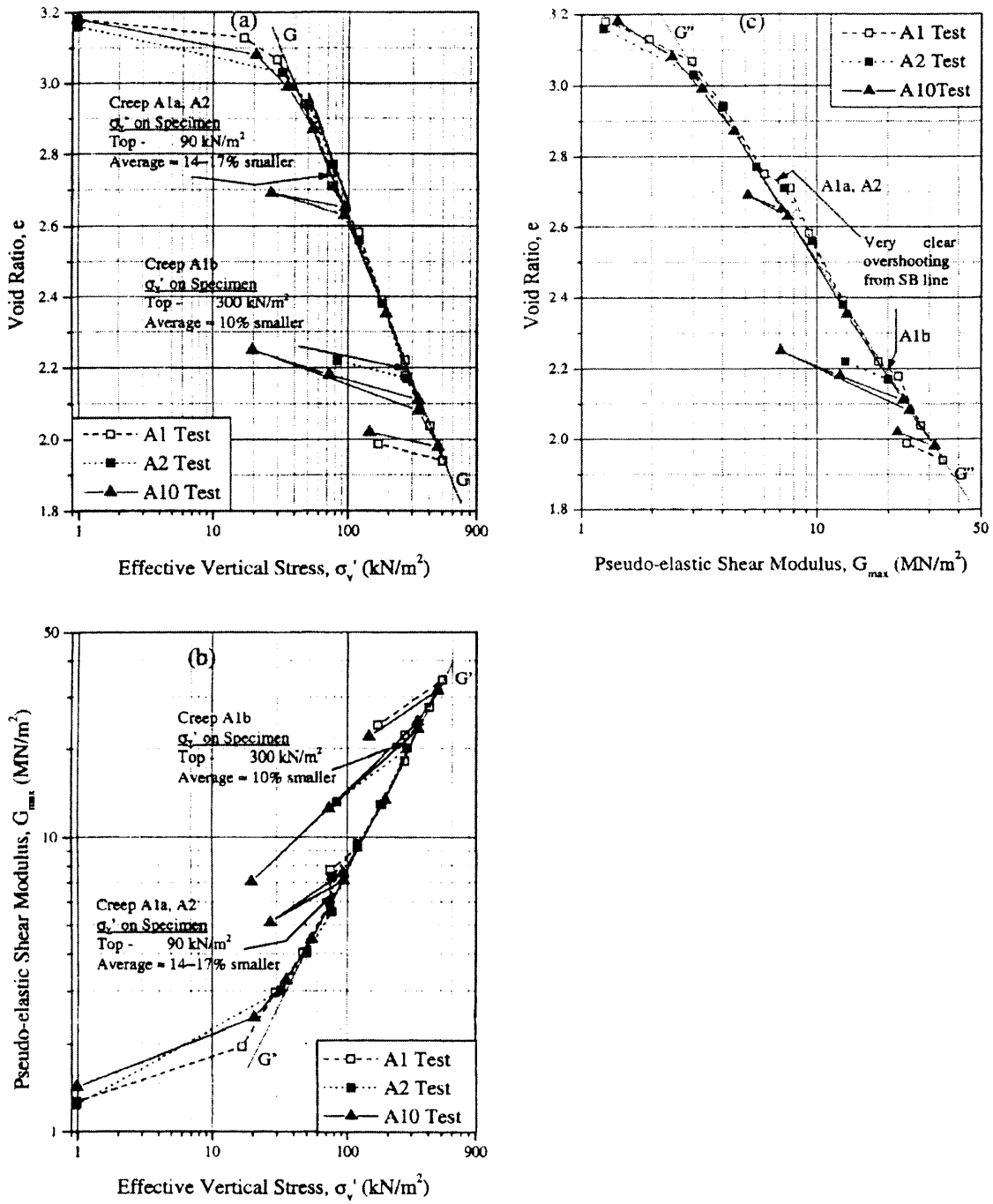

Figure 2-4 (a) e-log σ'_v, (b) log G_{max}-log σ'_v, and (c) e-log G_{max} plots for Minato Mirai area clay in NC and OC states (Lohani et al., 2001)

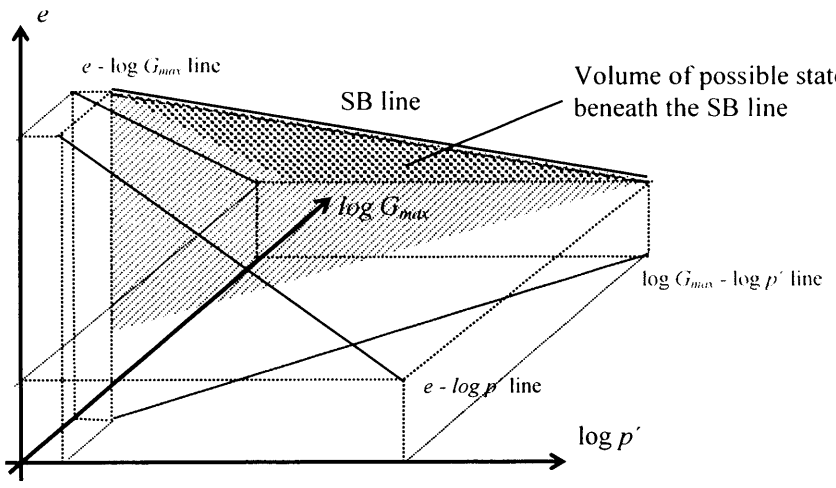

Figure 2-5 State Boundary Concept in e-log p'-log G_{max} space (interpreted from Lohani, et al., 2001)

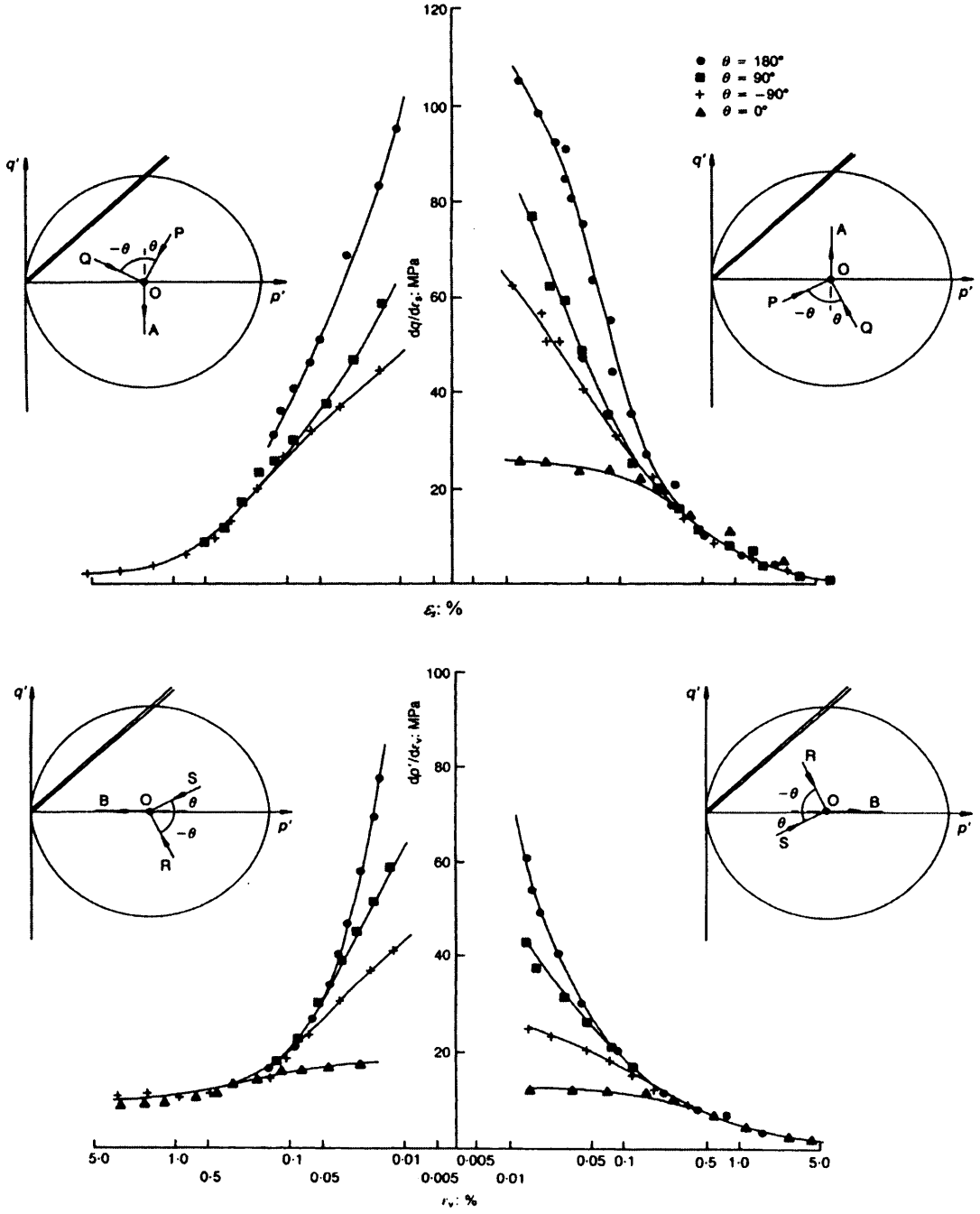

Figure 2-6 Influence of recent stress history on stiffness degradation curves in TC tests on reconstituted London Clay (Atkinson et al., 1990)

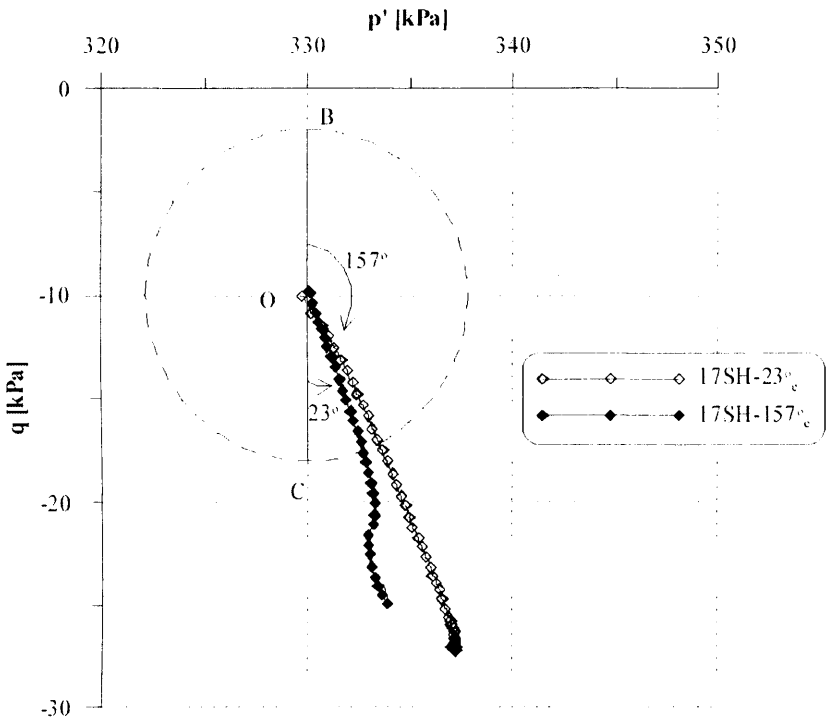

Figure 2-7 Short approach stress paths (BO and CO) and shear probes for sample 17SH - creep allowed (Gasparre, 2005)

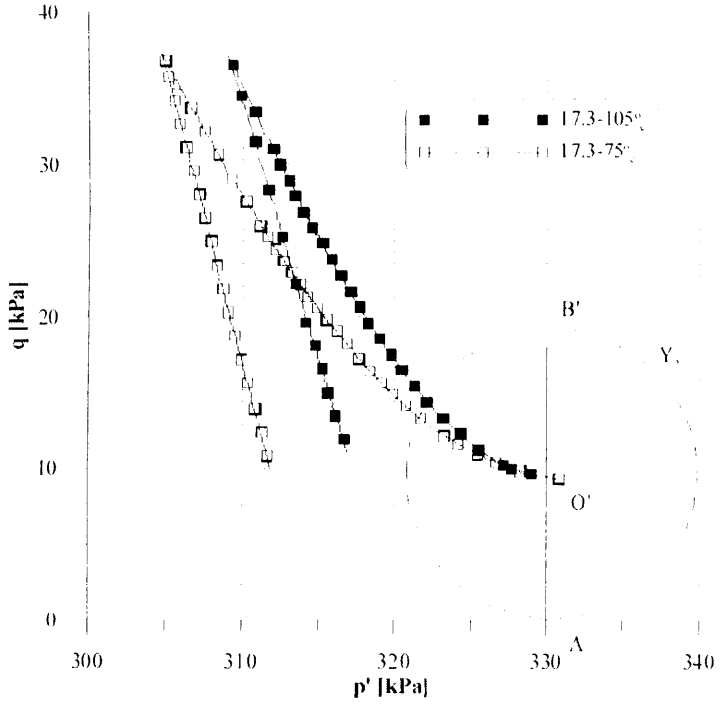

Figure 2-8 Short approach stress paths (AO' and B'O') and shear probes for sample 17.3SH - creep not allowed (Gasparre, 2005)

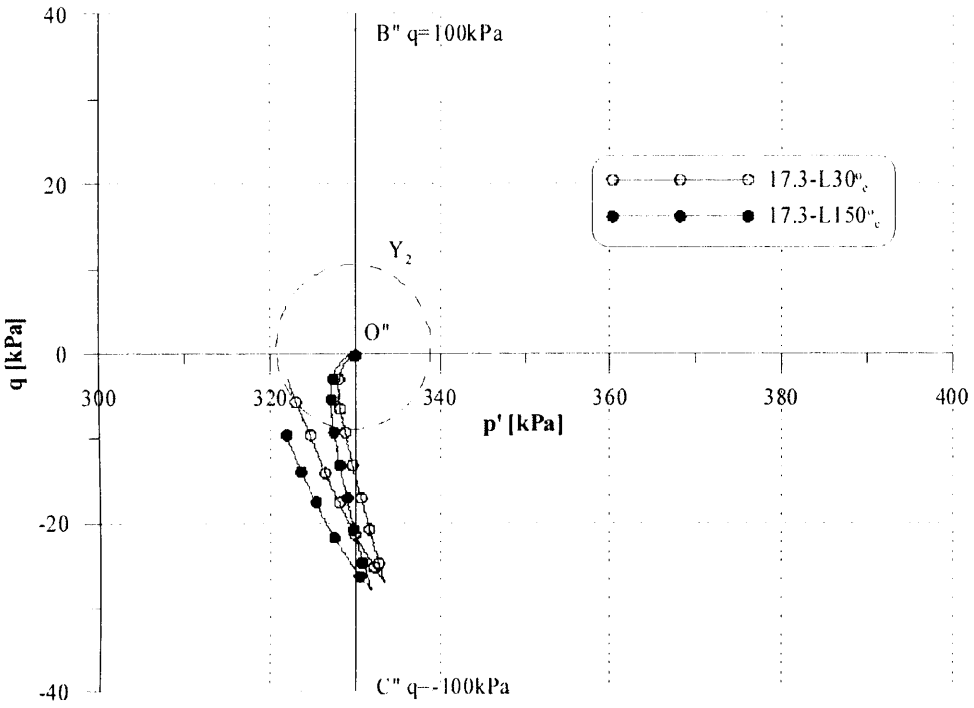

Figure 2-9 Long approach stress paths (B"O" and C"O") and shear probes for sample 17.3L - creep allowed (Gasparre, 2005)

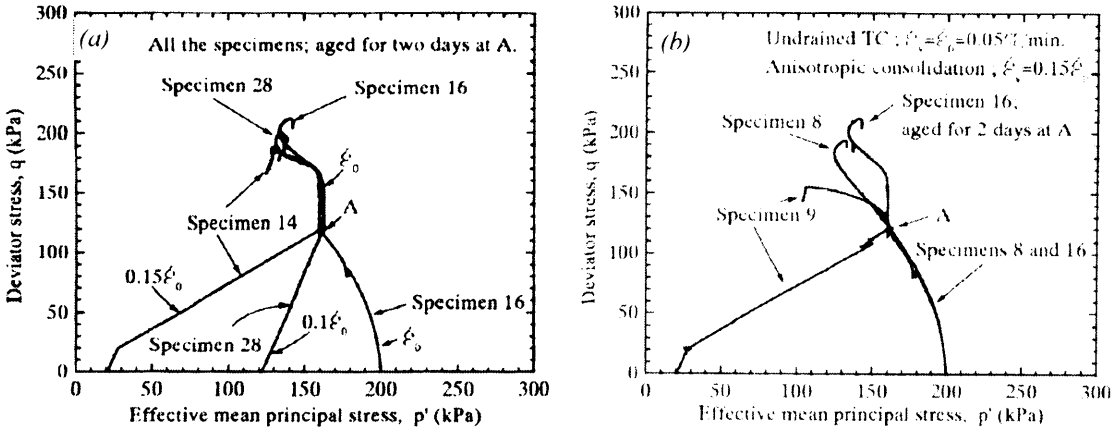

Figure 2-10 Effective stress paths showing the effect of compression history and drained creep at stress state A on subsequent undrained TC behaviour of NC Fujinomori Clay (Tatsuoka et al., 2000)

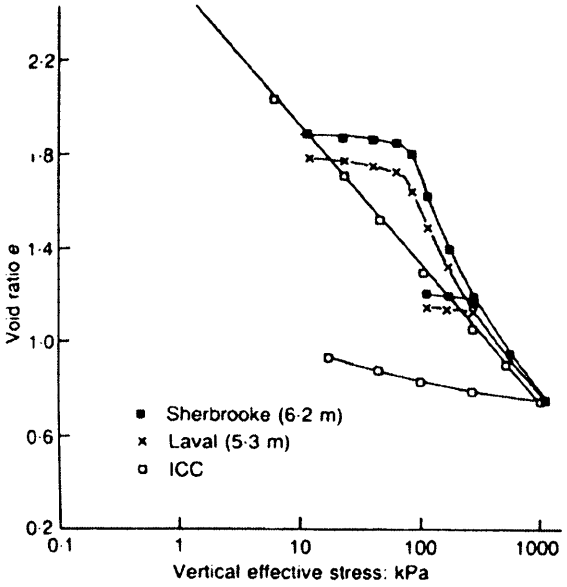

Figure 2-11 Influence of natural structure on the one-dimensional compression behaviour of Bothkennar clay (Smith et al., 1992)

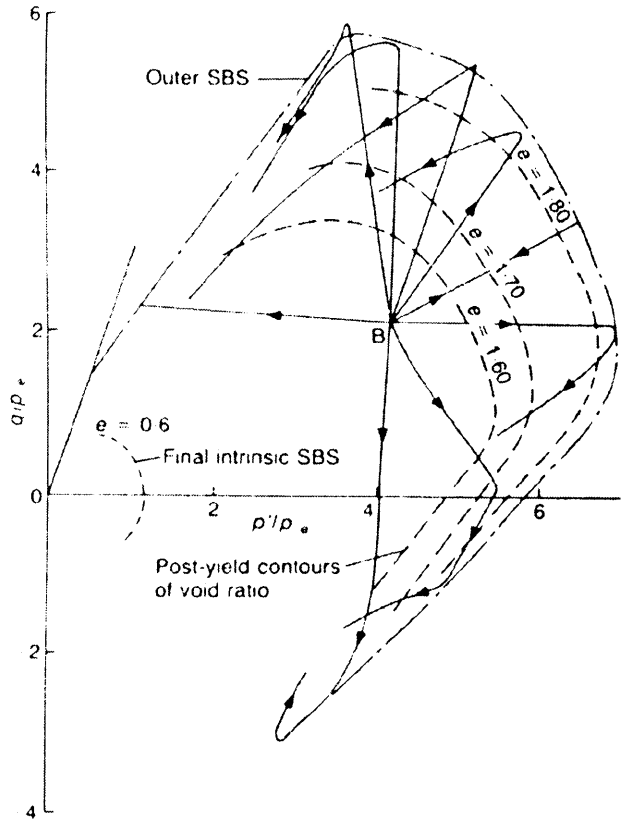

Figure 2-12 Degradation of structure during shearing of Bothkennar clay (Smith et al., 1992)

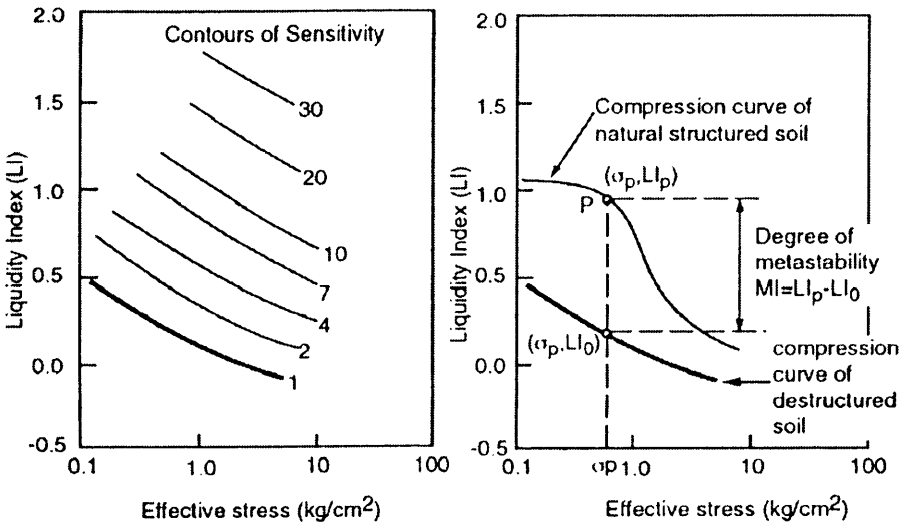

(a)A general liquidity index-effective stress-sensitivity relationship of sensitivity clays (after Houston&Mitchell (1968))

(b) Definition of Metastability index (*MI*)

Figure 2-13 Concept of metastability index (MI) in structured clays (Soga & Mitchell, 1996)

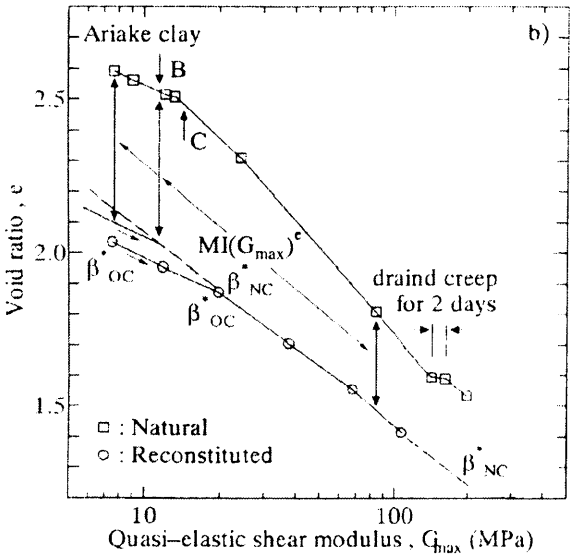

Figure 2-14 Assessing structure in natural Ariake clay using the alternative metastability index, $MI(G_{max})^c$ (Shibuya, 2000)

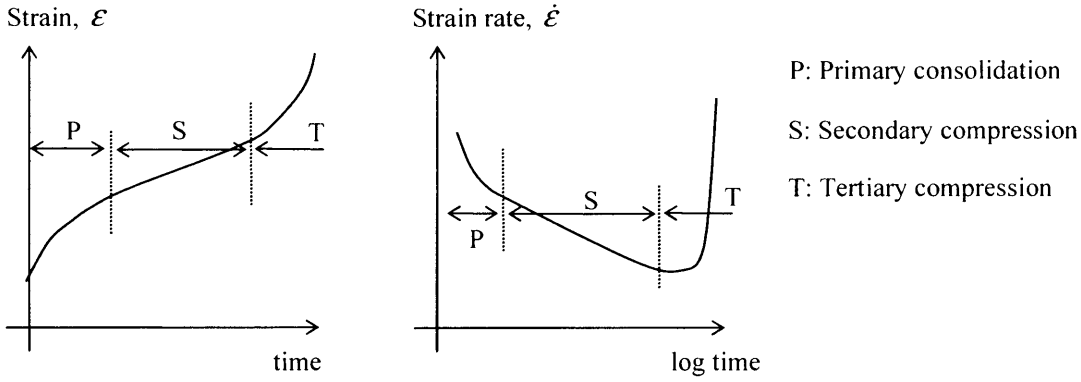

Figure 2-15 Illustration of creep characteristics

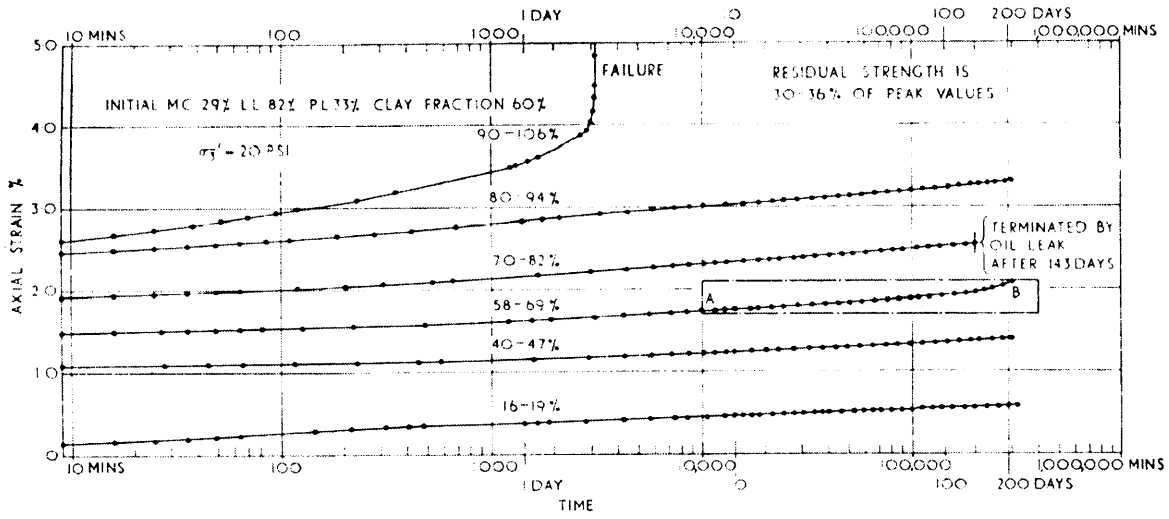

Figure 2-16 Influence of deviator stress in drained triaxial creep tests on undisturbed London Clay (Bishop, 1966)

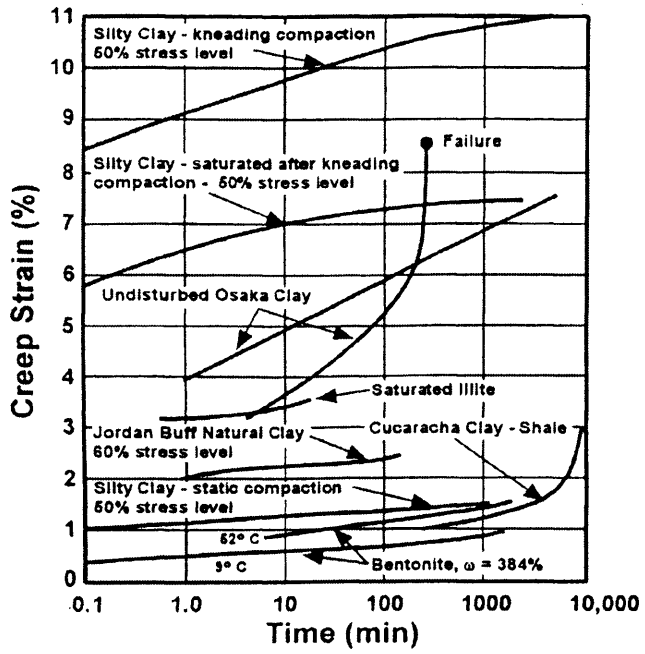

Figure 2-17 General creep characteristics (Mitchell et al., 1997)

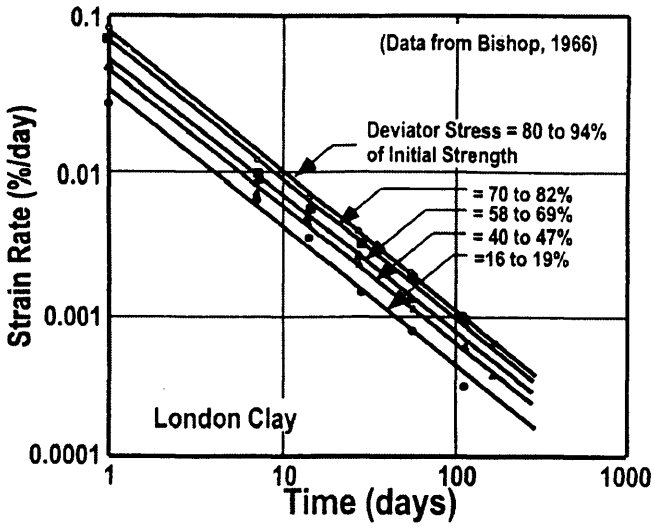

Figure 2-18 Strain rate vs. time relationships during drained triaxial creep of London Clay (Mitchell et al., 1997, replotted data from Bishop, 1966)

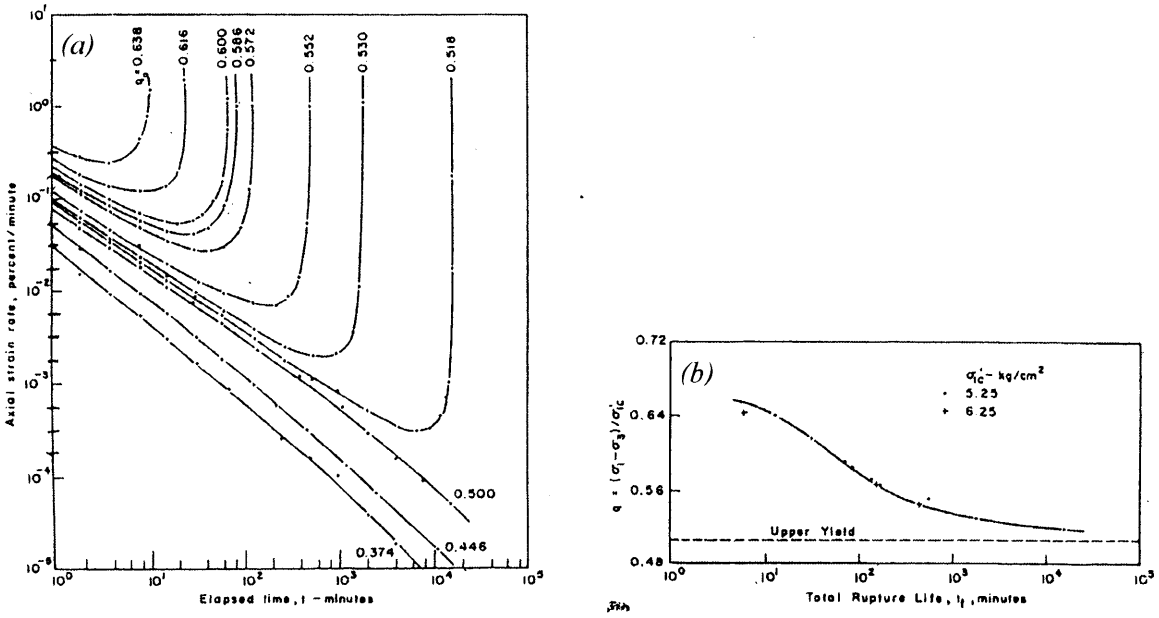

Figure 2-19 (a) Variation of creep rate with time in constant stress creep and (b) influence of deviator stress level on the rupture life in undrained triaxial compression of undisturbed Haney clay (Vaid & Campanella, 1977)

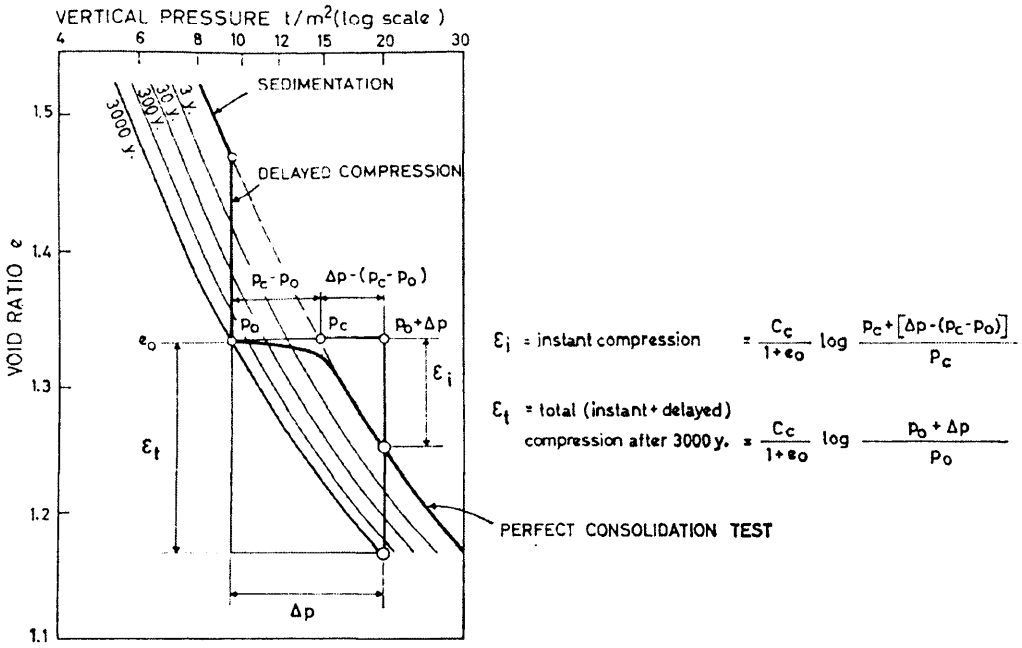

Figure 2-20 Concept of isochrones "time lines" in one-dimensinal compression of soft clays (Bjerrum, 1967)

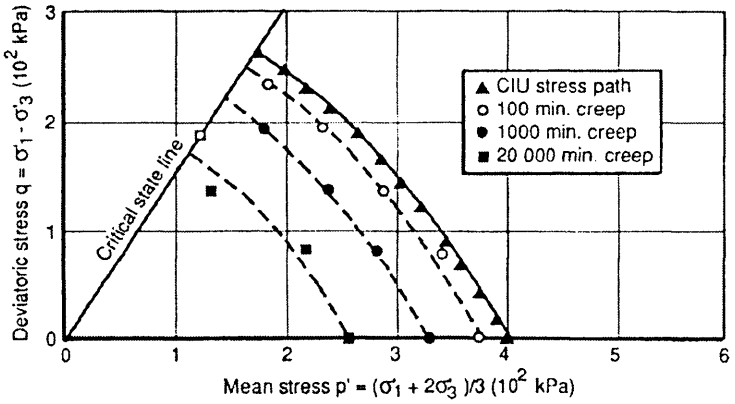

Figure 2-21 Influence of creep time on the yield envelope in triaxial stress space in tests on San Francisco Bay mud (Leroueil & Marques, 1996; data from Arulanandan et al., 1971)

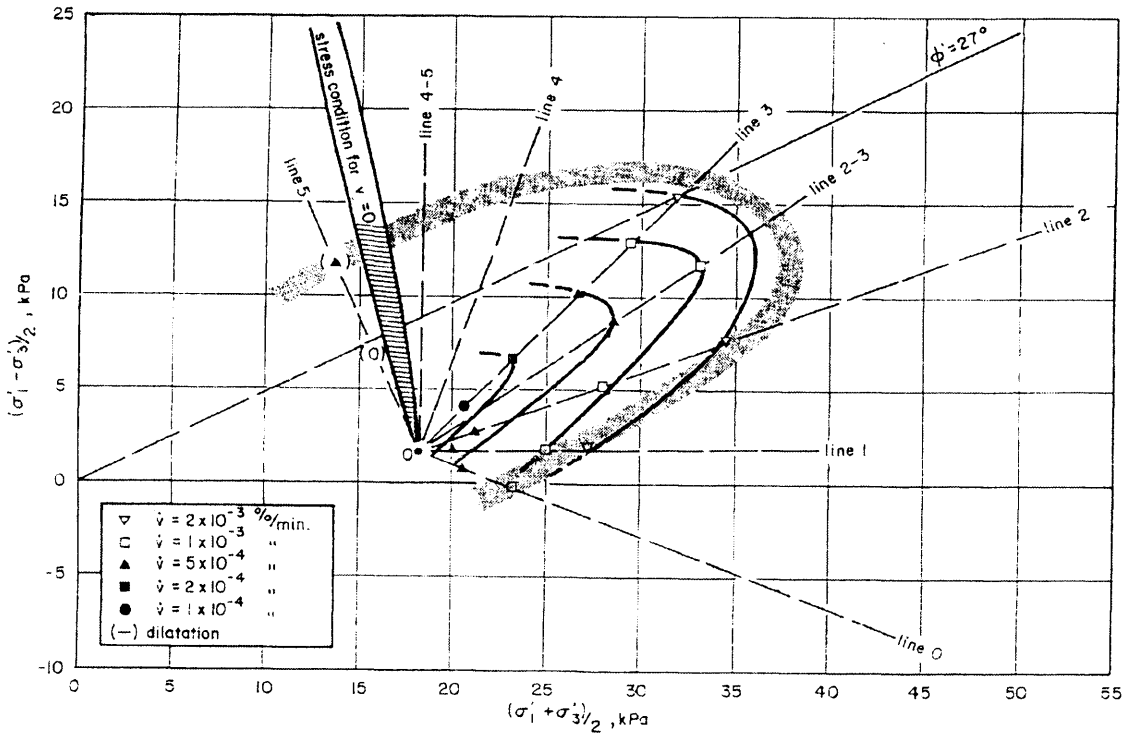

Figure 2-22 Influence of volumetric creep rate on the limit state curve from drained triaxial tests on undisturbed lightly overconsolidated St. Alban clay (Tavenas et al., 1978)

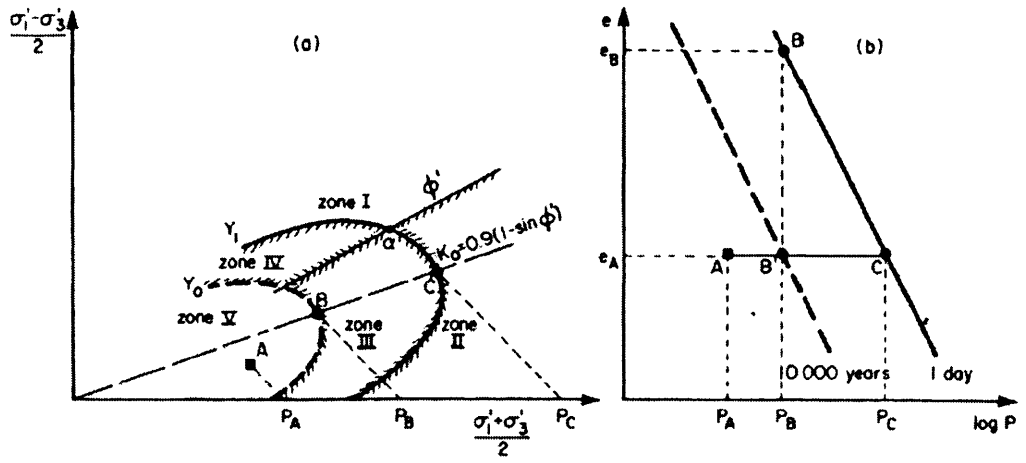

Figure 2-23 Proposed general model of the effects of time on the yield envelope of clays (Tavenas & Leroueil, 1977)

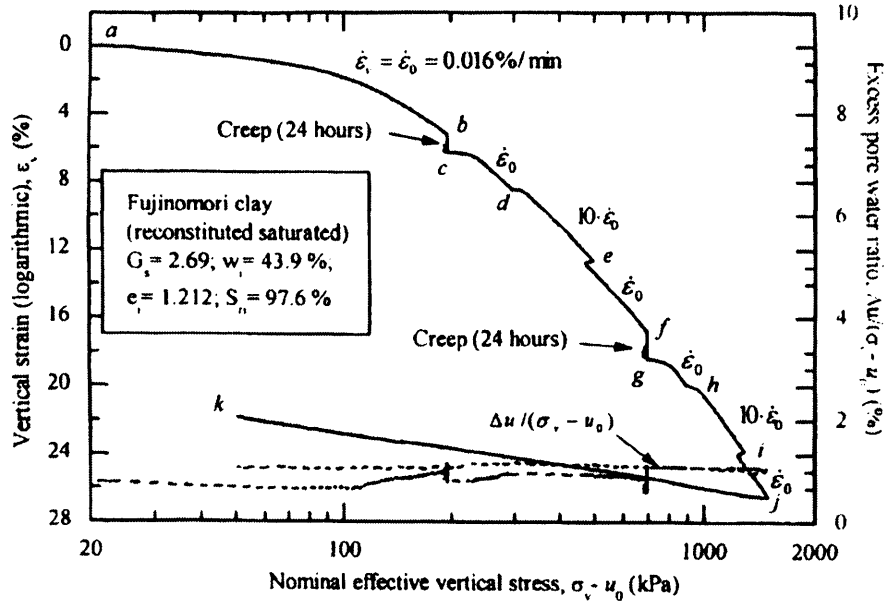

Figure 2-24 Influence of drained creep on subsequent one-dimensional compression behaviour in CRS oedometer tests on reconstituted Fujinomori clay (Tatsuoka, 2003b)

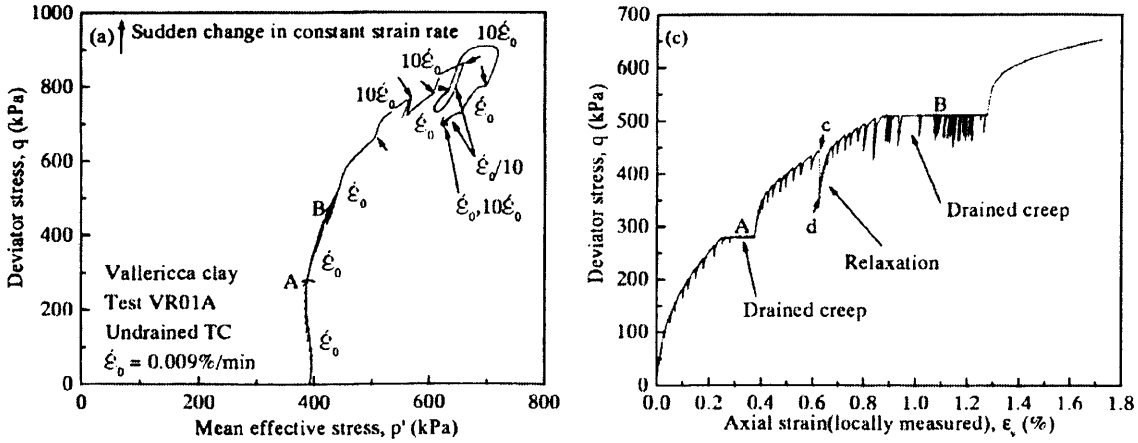

Figure 2-25 Influence of drained creep on subsequent undrained shearing behaviour in triaxial compression of undisturbed Vallerica clay (Tatsuoka et al., 2000; after Santucci de Magistris 1998)

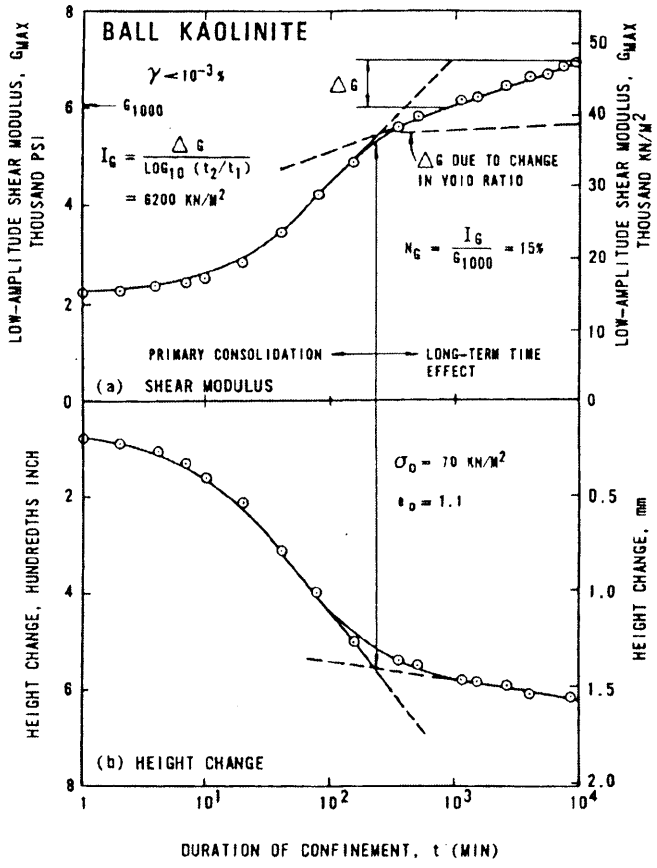

Figure 2-26 Observed change in elastic shear modulus with time during drained creep (Anderson & Stoke, 1978)

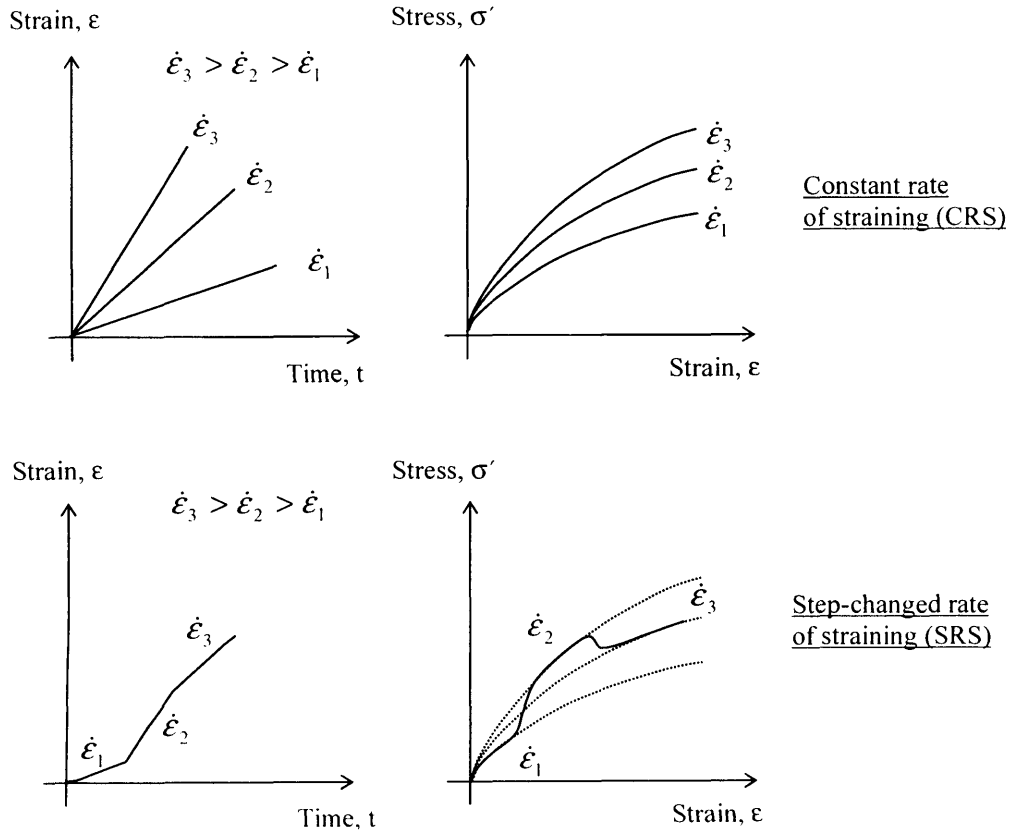

Figure 2-27 CRS and SRS tests test paths in triaxial compression

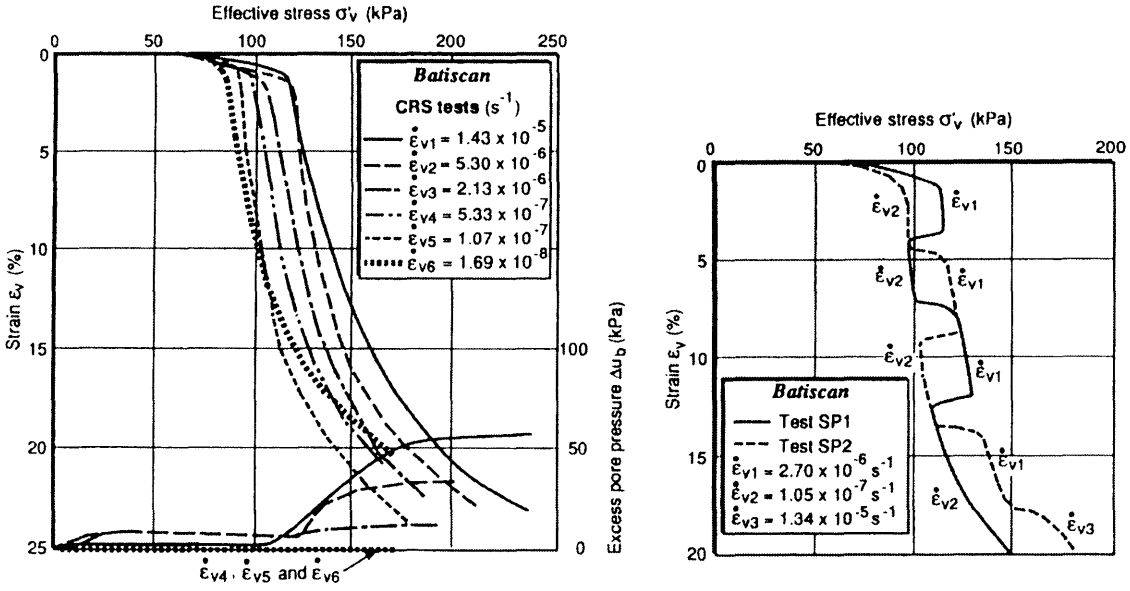

Figure 2-28 Typical CRS and SRS oedometer tests on Batiscan clay (Leroueil et al., 1985)

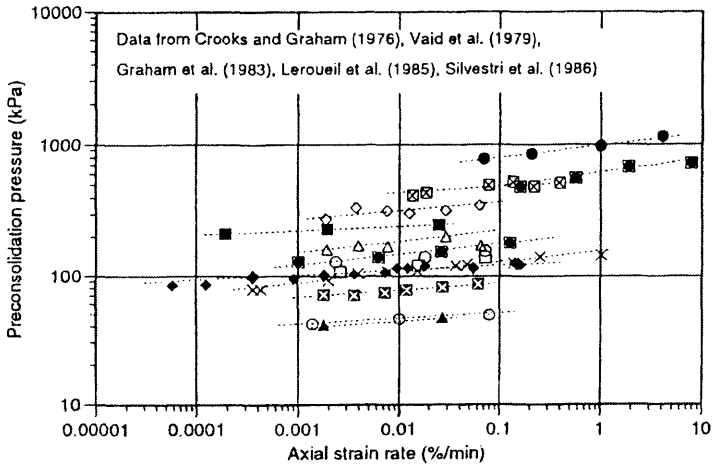

Figure 2-29 Rate dependency of pre-consolidation pressure determined from one-dimensional compression tests for normally consolidated or slightly overconsolidated soft clays (Soga & Mitchell, 1996).

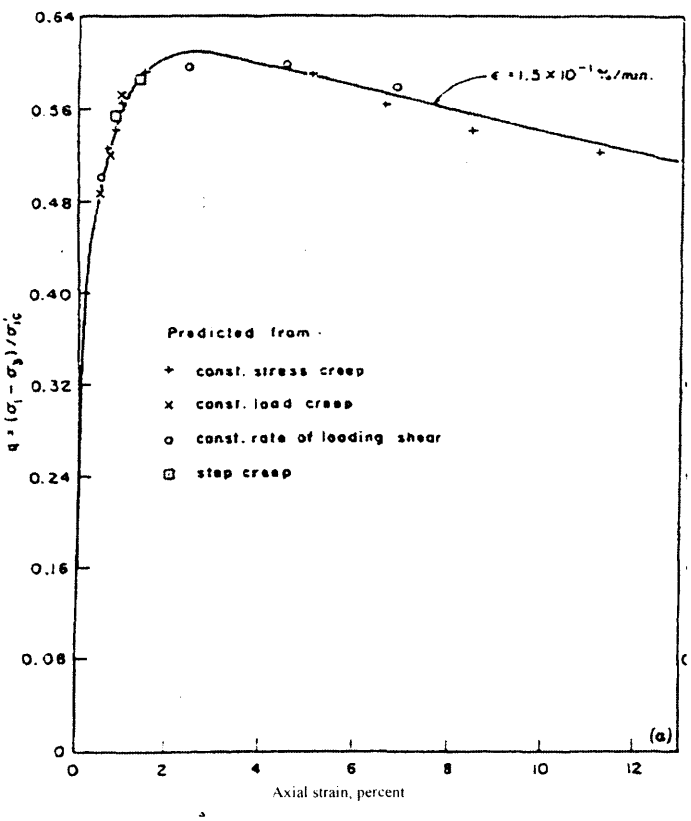

Figure 2-30 Unique stress-strain-strain rate relationship in triaxial compression tests on undisturbed Haney clay (Vaid & Campanella, 1977)

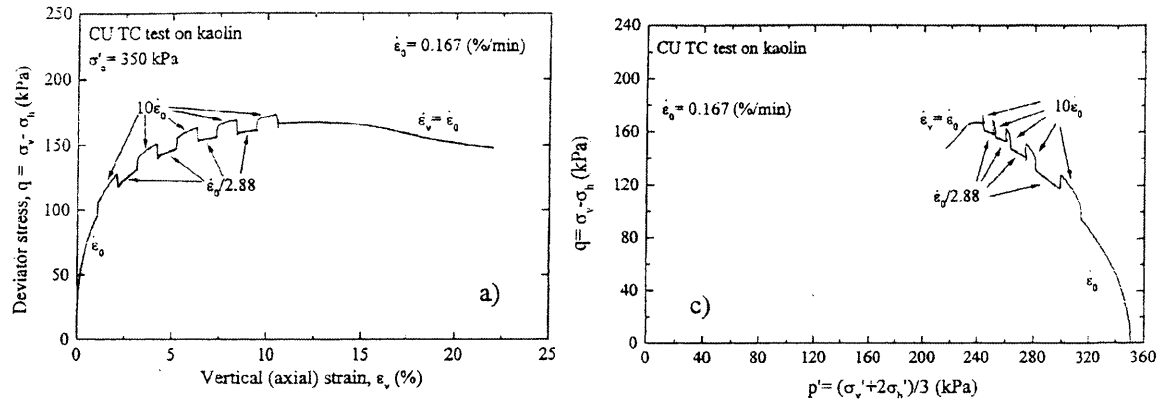

Figure 2-31 Isotach behaviour observed in CU TC tests on reconstituted NC kaolin (Tatsuoka et al., 2002)

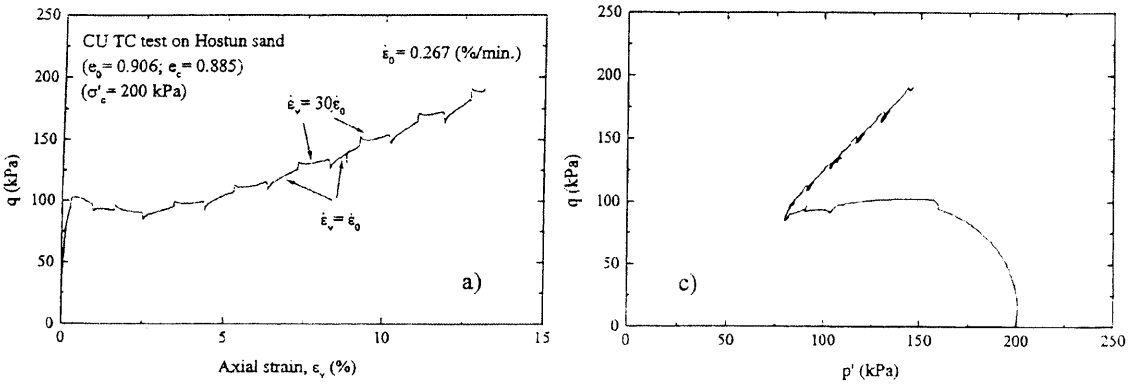

Figure 2-32 Pure TESRA behaviour observed in CU TC tests Hostun sand (Tatsuoka et al., 2002)

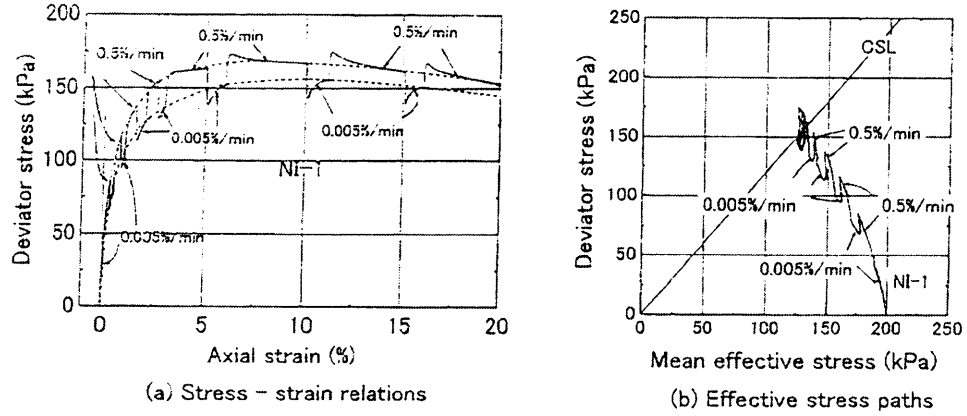

Figure 2-33 General TESRA behaviour observed in CU TC tests on NC reconstituted Fukakusa clay (Oka et al., 2003)

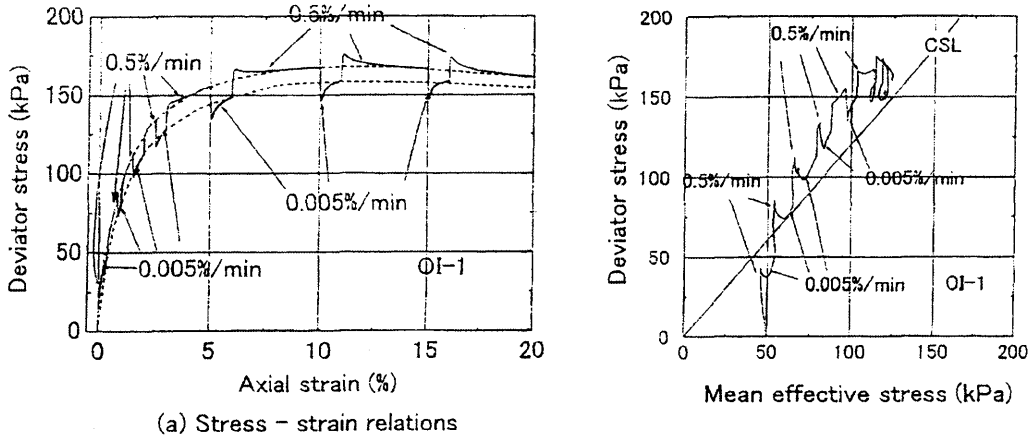

Figure 2-34 General TESRA behaviour observed in CU TC tests on OC reconstituted Fukakusa clay (Oka et al., 2003)

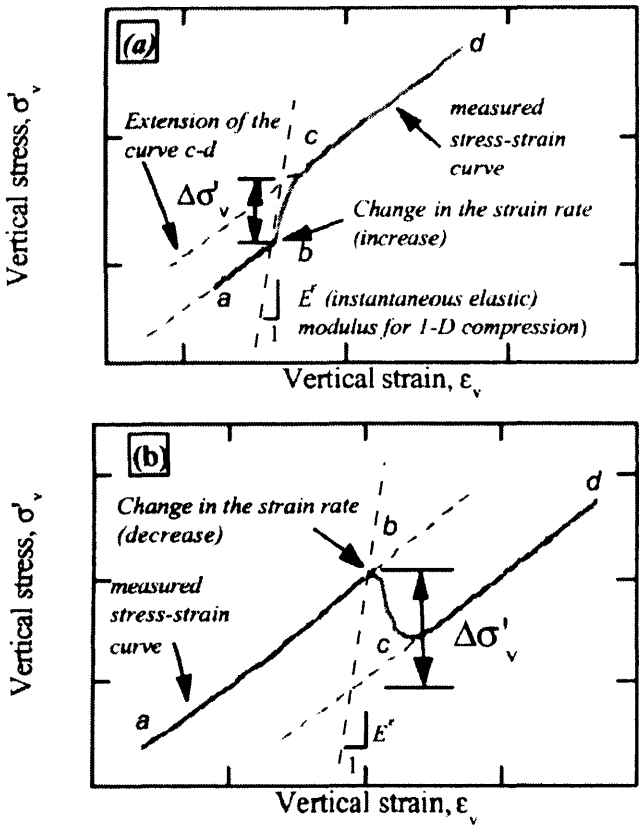

Figure 2-35 Definition of stress change immediately after a significant change in axial strain rate (Acosta-Martinez et al., 2003)

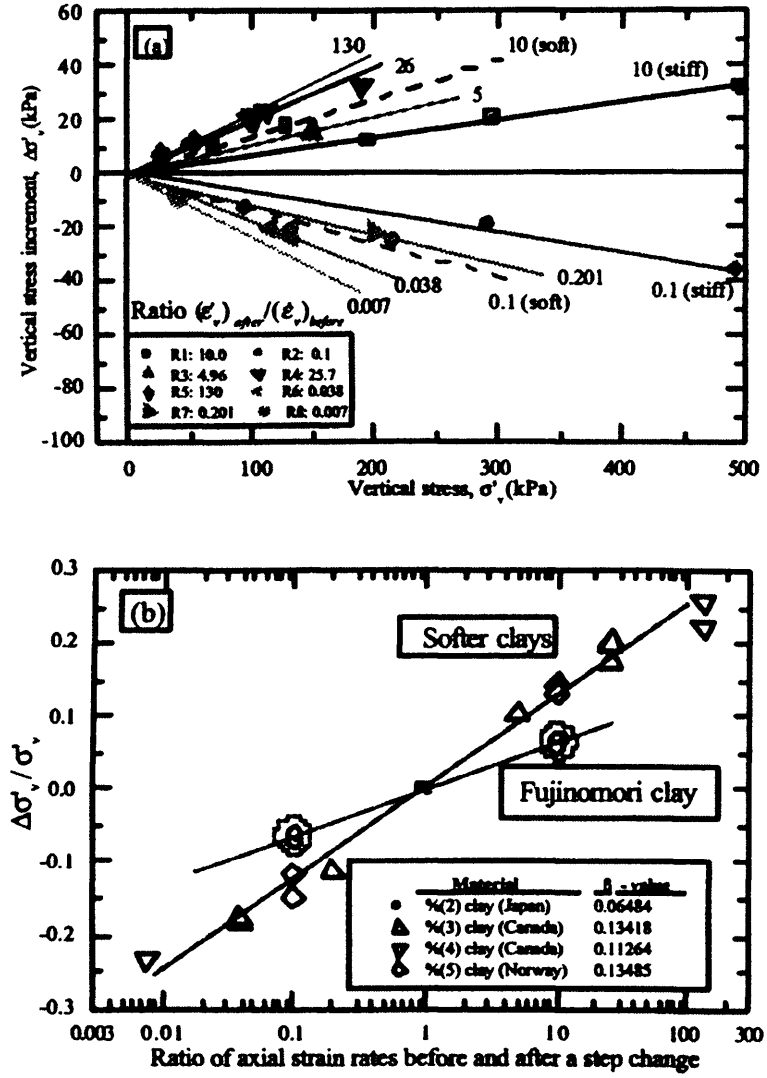

Figure 2-36 Relationship between vertical stress increment and stress level for different ratios of strain rates before and after a strain rate change in triaxial compression tests on reconstituted Fujinomori clay (Acosta-Martinez et al., 2003)

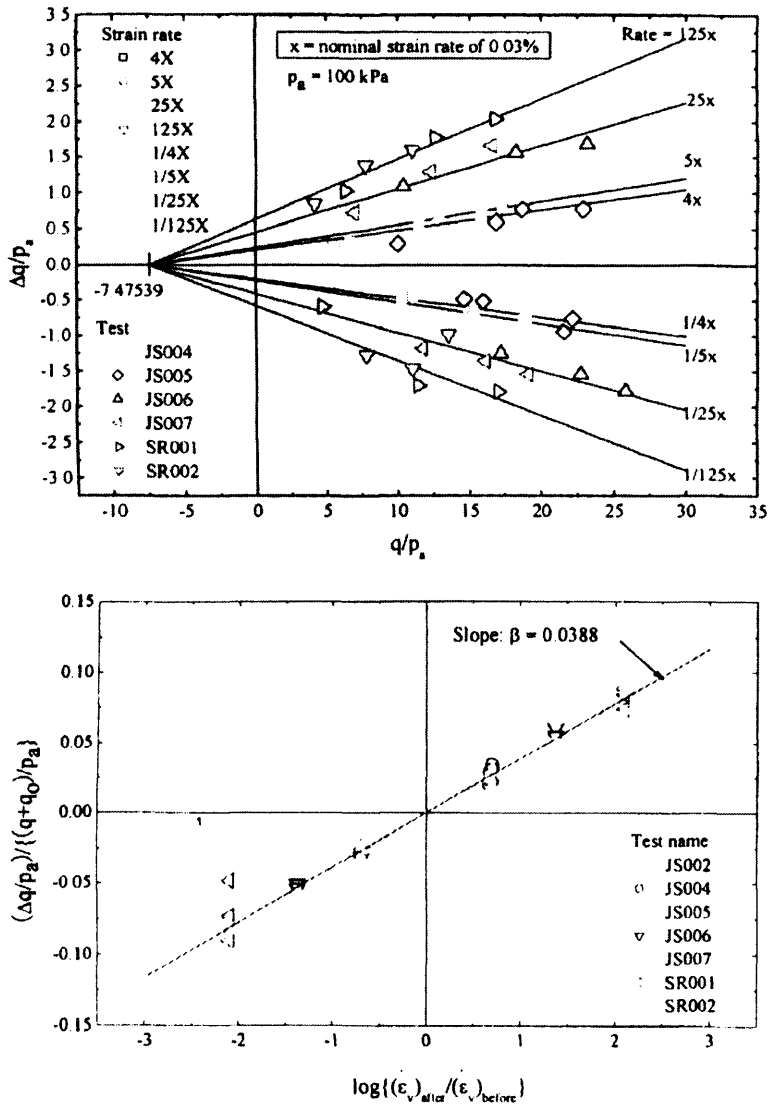

Figure 2-37 Relationship between change in deviator stress and current deviator stress for different ratios of strain rates before and after a strain rate change in triaxial compression tests on cement-mixed Chiba gravel (Kongsukprasert, 2003)

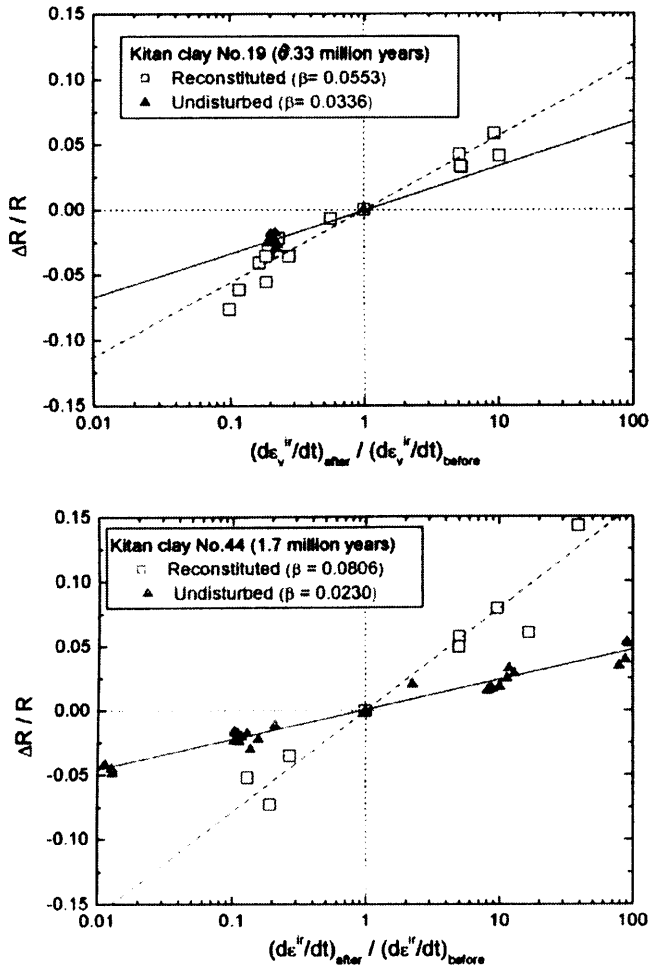

Figure 2-38 Comparison of strain rate effects in triaxial compression tests on reconstituted and undisturbed samples of Kitan clay with different geological ages (a) 0.33million years and (b) 1.7million years (Komoto et al., 2003)

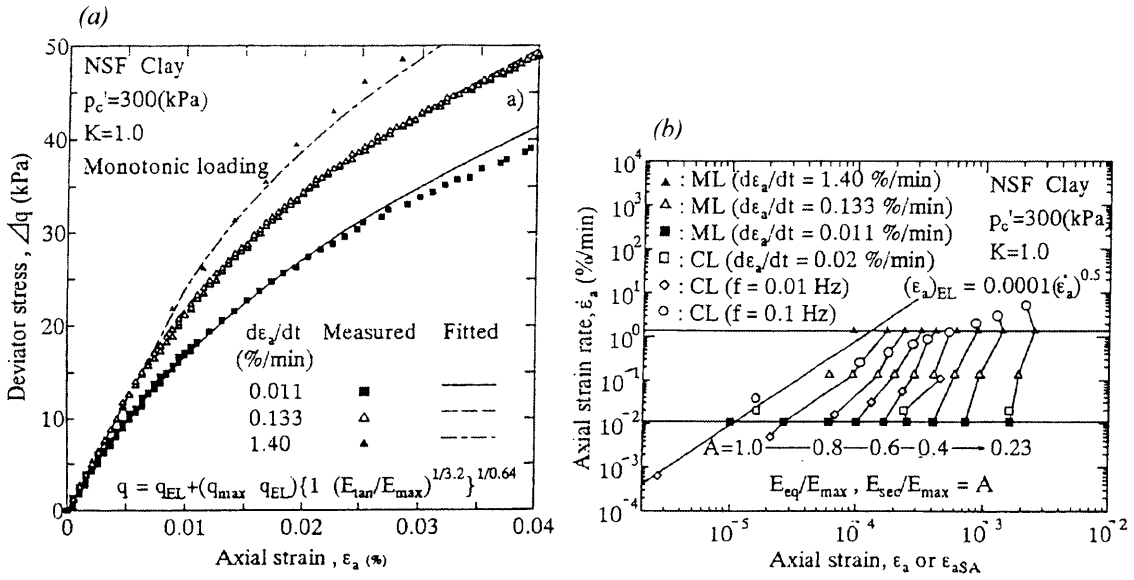

Figure 2-39 Effect of strain rate on stress-strain relationship in undrained TC test on NSF-clay (Shibuya et al., 1996)

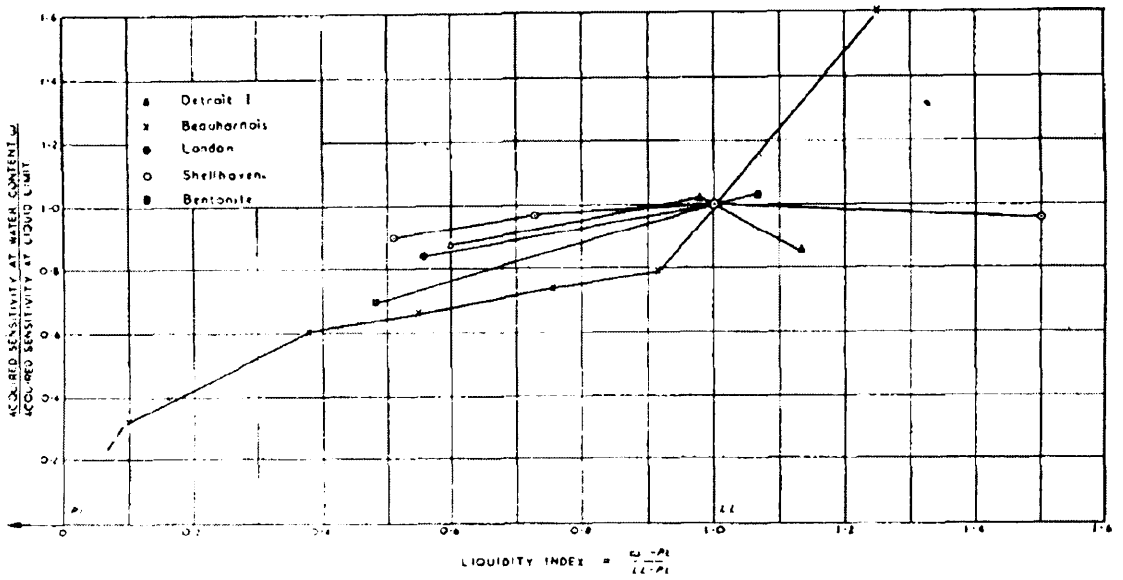

Figure 2-40 Relationship between acquired sensitivity and water content of reconstituted London samples (Skempton & Northey, 1952)

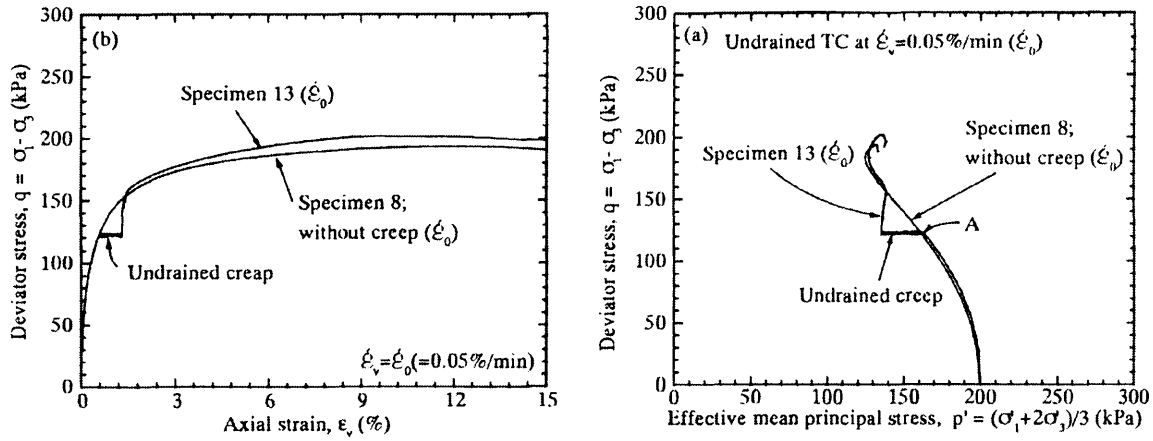

Figure 2-41 Influence of undrained creep on subsequent stress-strain behaviour in undrained triaxial compression of Fujinomori clay (Tatsuoka et al., 2000; after Momoya 1998)

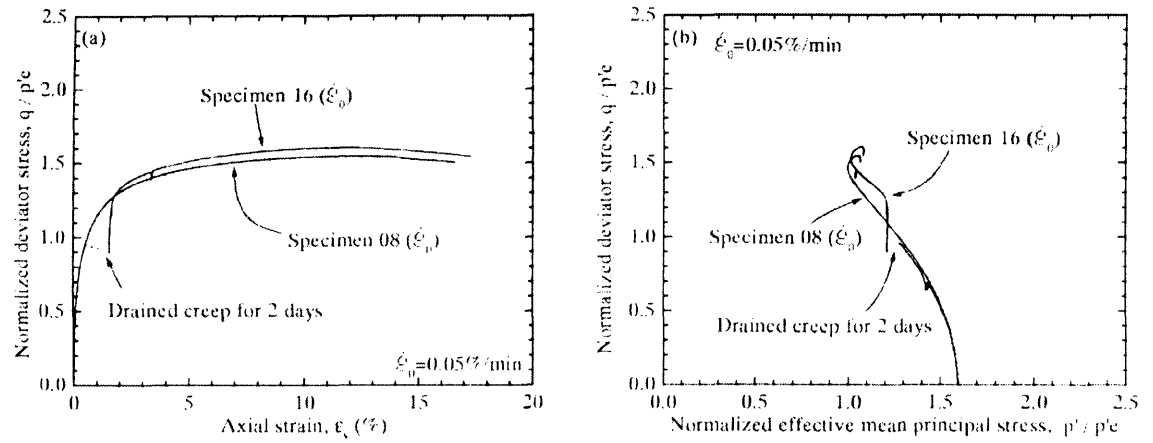

Figure 2-42 Influence of drained creep on subsequent stress-strain behaviour in undrained triaxial compression of Fujinomori clay (Tatsuoka et al., 2000; after Momoya 1998)

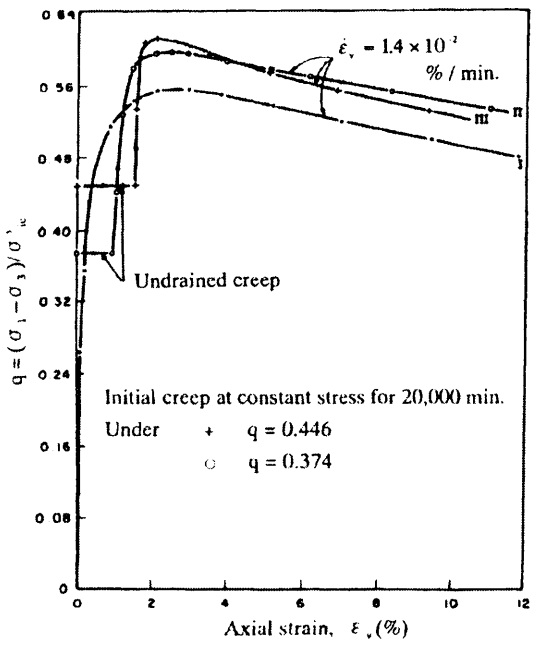

Figure 2-43 Influence of undrained creep and deviatoric stress level on subsequent stress-strain behaviour in triaxial compression of undisturbed samples of Haney clay (Vaid & Campanella, 1977)

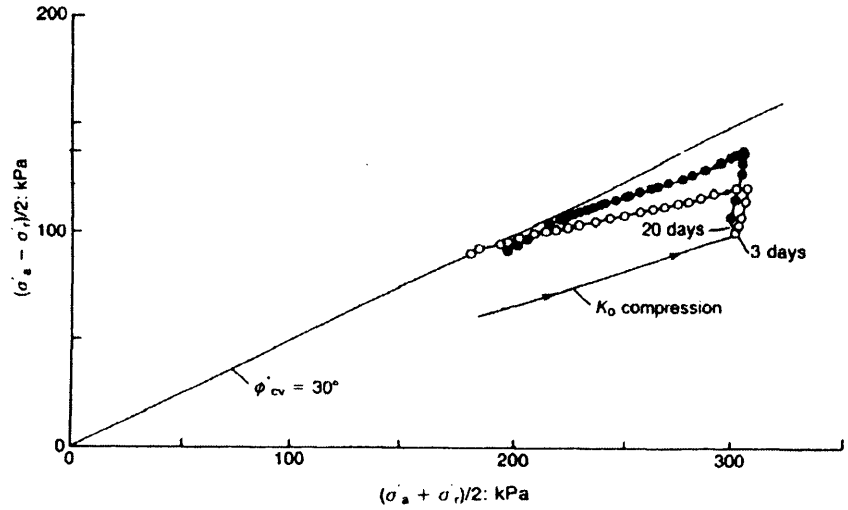

Figure 2-44 Influence of drained creep on subsequent undrained stress path in triaxial compression of reconstituted Magnus clay (Burland, 1990; after Jardine, 1985)

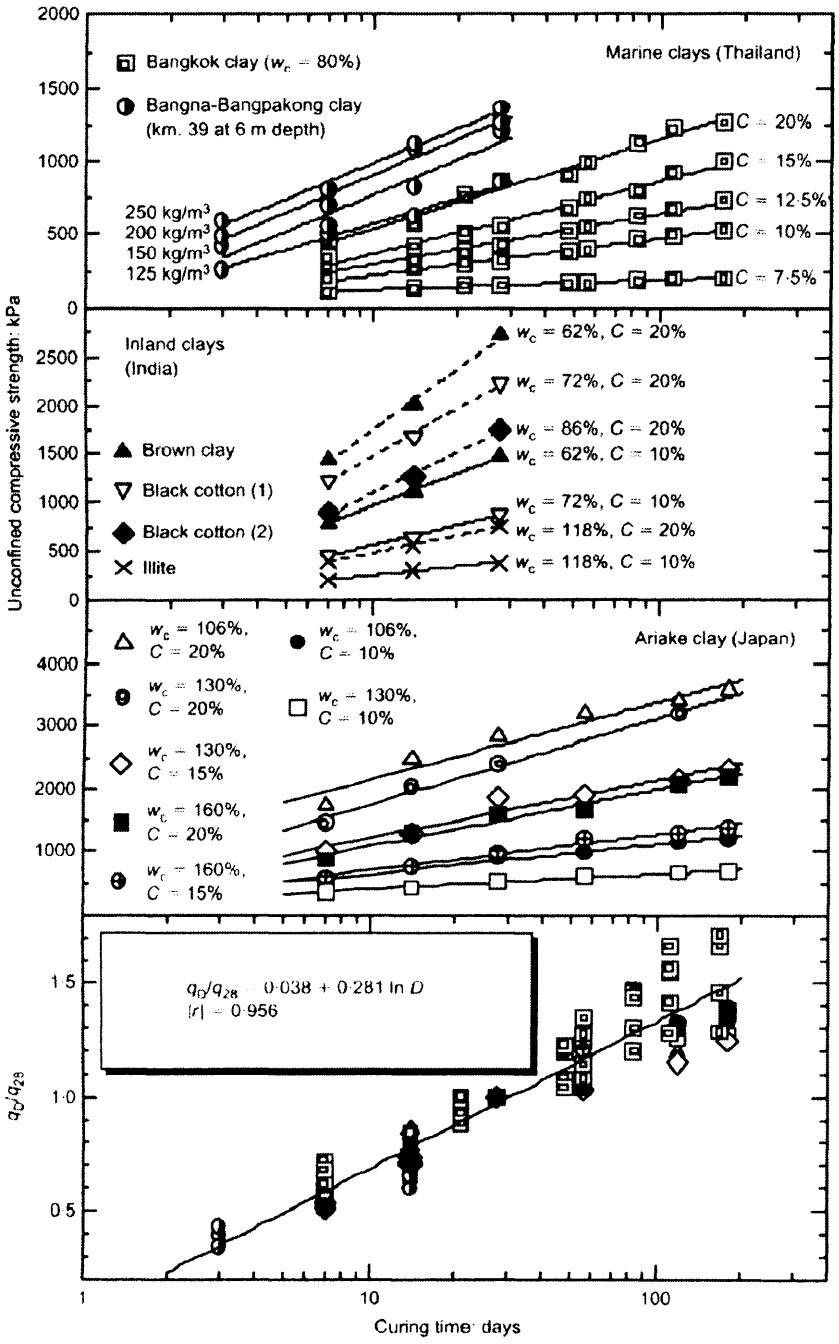

Figure 2-45 Relationship between curing time and unconfined compressive strength in tests on several cement-mixed clays at various water and cement contents (Horpibulsuk et al., 2003)

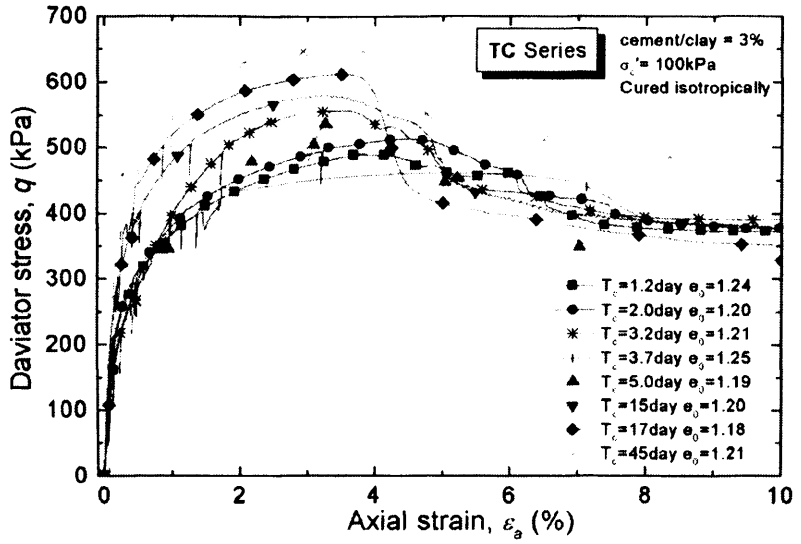

Figure 2-46 Influence of curing time at isotropic stress state on the stress-strain relationship in drained triaxial compression of cement-mixed kaolin (Komoto, 2004)

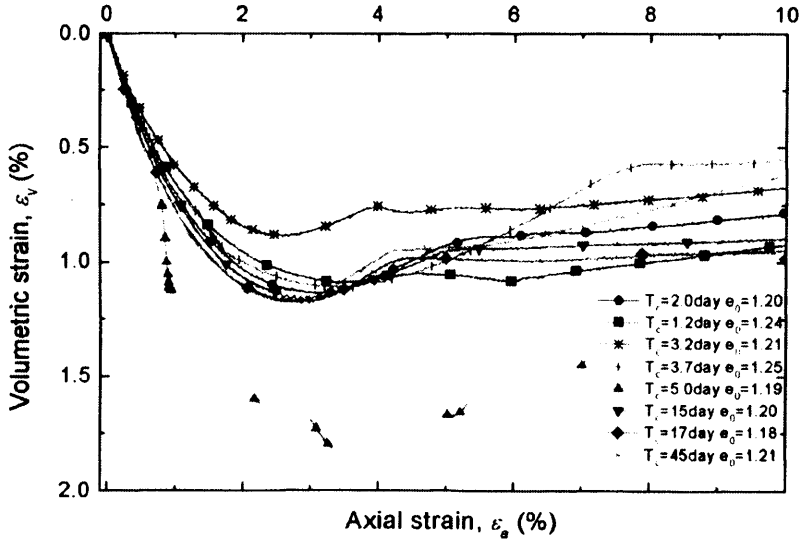

Figure 2-47 Influence of curing time at isotropic stress state on the volumetric compression in drained triaxial compression of cement-mixed kaolin (Komoto, 2004)

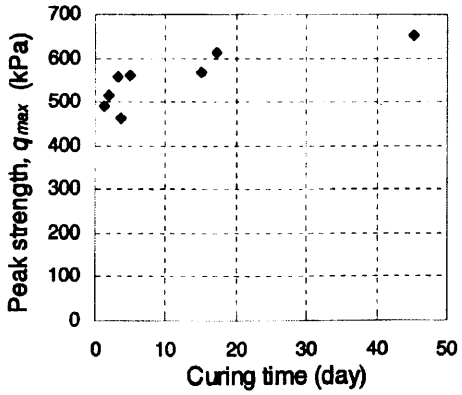

Figure 2-48 Relationship between peak strength and curing time at isotropic stress state in drained triaxial compression of cement-mixed kaolin (Komoto, 2004)

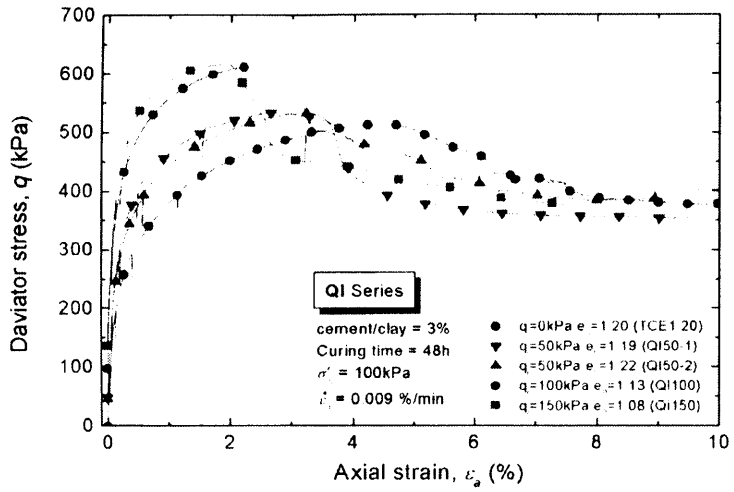

Figure 2-49 Influence of curing stress state on the stress-strain relationship in drained triaxial compression of cement-mixed kaolin (Komoto, 2004)

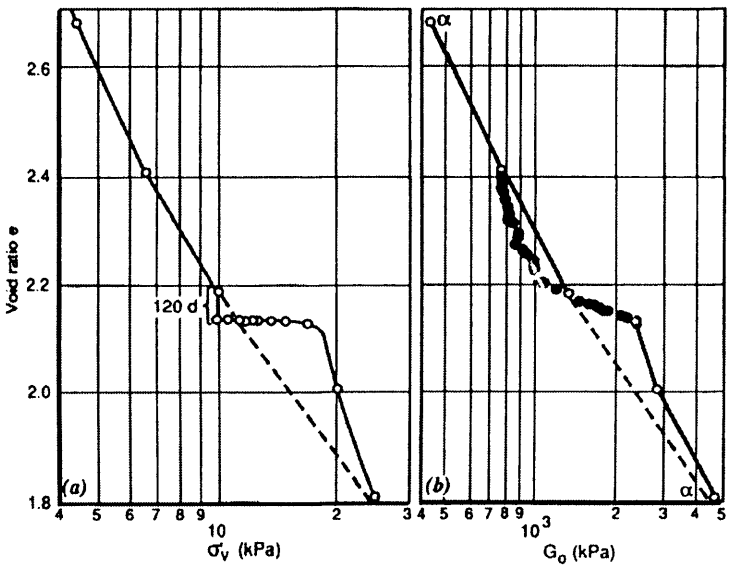

Figure 2-50 Influence of drained creep on (a) one-dimensional compression behaviour and (b) elastic shear stiffness in tests on artificially sedimented Jonquière clay (Leroueil et al., 1996; after Perret et al., 1995)

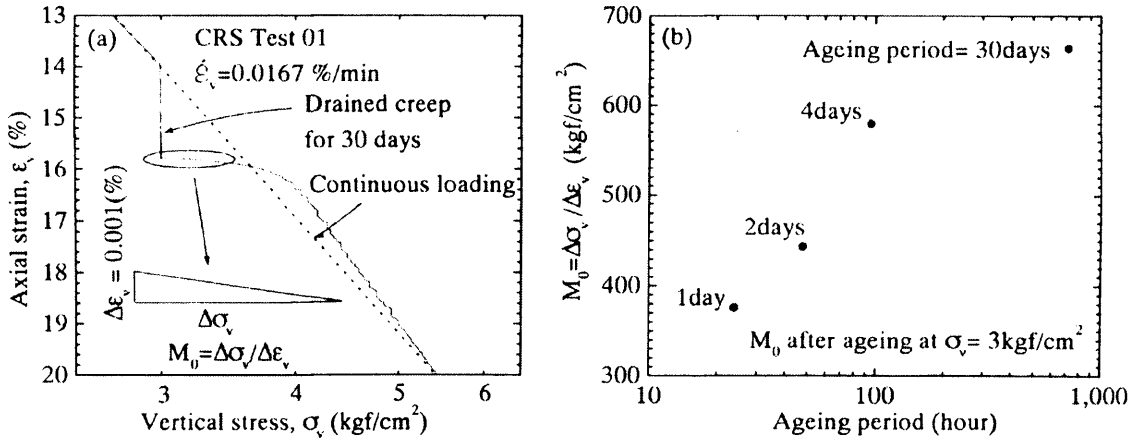

Figure 2-51 Influence of drained creep on the compression behaviour of reconstituted Fujinomori clay and change in initial constraint modulus M_0 for different ageing periods (Tatsuoka et al., 2000; after Momoya, 1998)

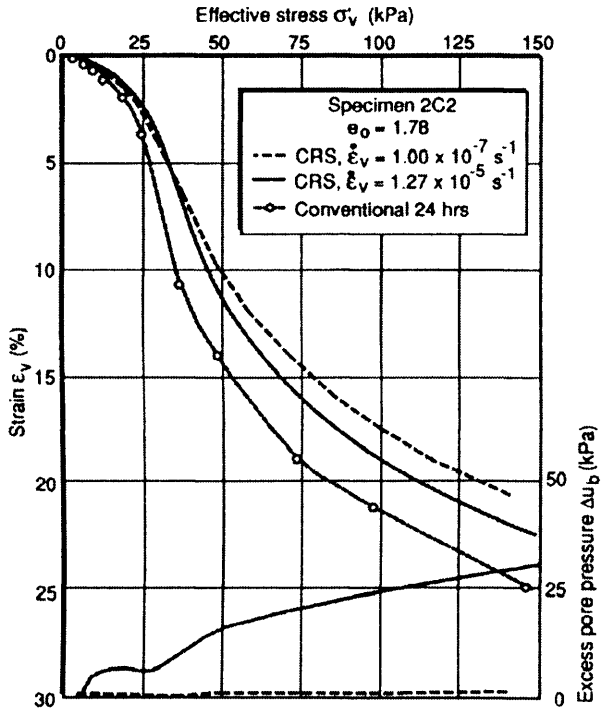

Figure 2-52 Effect of slow rate of straining on the one-dimensional compression behaviour of artificially sedimented Jonquière clay (Leroueil et al., 1996)

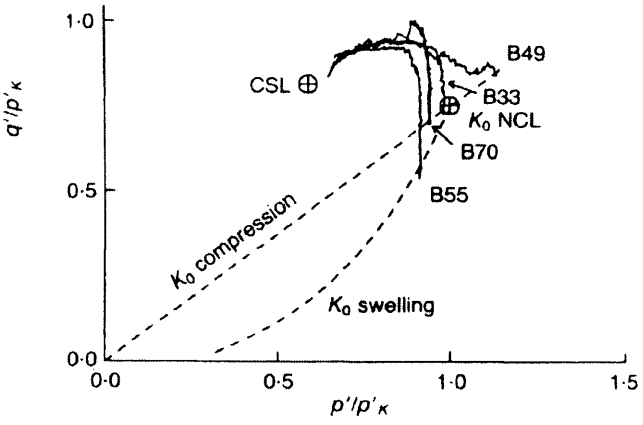

Figure 2-53 Influence of drained creep after one-dimensional compression on the subsequent drained triaxial compression behaviour of reconstituted Bothkennar clay (Allman & Atkinson, 1992)

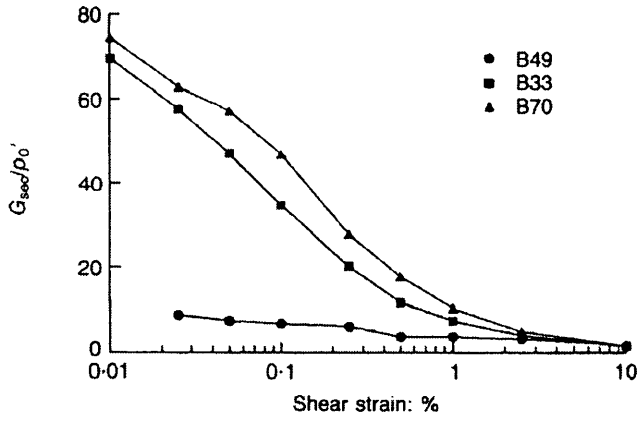

Figure 2-54 Influence of drained creep after one-dimensional compression on stiffness degradation in subsequent drained triaxial compression of reconstituted Bothkennar clay (Allman & Atkinson, 1992)

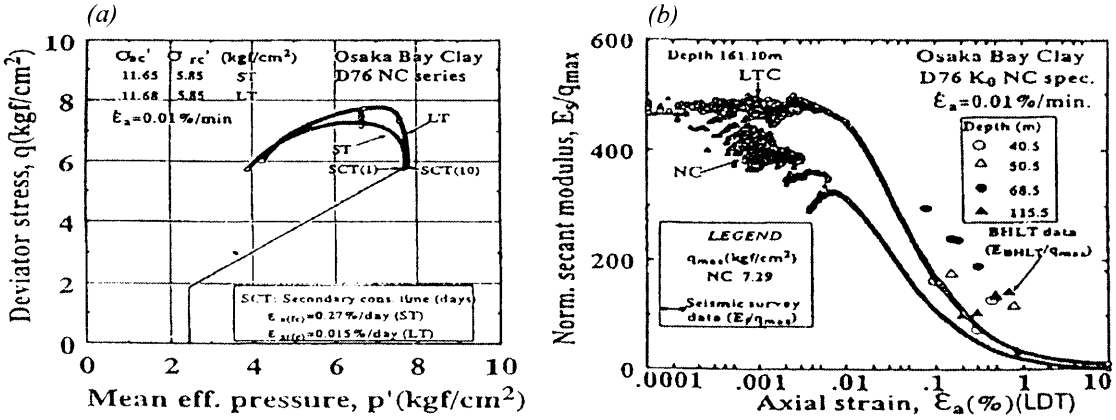

Figure 2-55 Influence of ageing at final reconsolidation stress state on (a) undrained stress path and (b) stiffness degradation curve in triaxial compression of undisturbed Osaka Bay Clay (Mukabi & Tatsuoka, 1999)

CHAPTER 3 EXPERIMENTAL TESTING PROGRAMME

3.1 INTRODUCTION

This chapter describes the experimental testing program in detail. In Section 3.2 the selection of testing materials is explained and the basic geotechnical and geological characteristics of the chosen materials are described. Advanced laboratory soil element testing equipment have been used to obtain high quality results and the equipment setup and any special modifications made to the equipment to suit the research objectives are described in Section 3.3. The following section, Section 3.4, explains the testing procedures which comprise a combination of standard and unconventional testing procedures employed to investigate the time-dependent behaviour of clays. Finally, Section 3.5 accounts for the theoretical framework relating to each testing apparatus including a description of any corrections made to the results and possible significant sources of errors are highlighted and discussed.

3.2 TESTING MATERIALS

As explained in the introduction in Chapter 1, the purpose of the experimental work was to investigate the viscous and inherent ageing effects in clays. The effects of structure on the viscous and ageing behaviour could be examined by studying both a structured and a non-structured clay - London Clay was specifically chosen to determine the viscous and ageing effects in an undisturbed natural structured firm clay and its reconstituted counterpart, thus highlighting the effect of natural structure on the viscous behaviour. Additionally, the influence of cementation on the viscous behaviour was observed in artificially cemented (TA) kaolin clay. On the other hand, the viscous behaviour of a reconstituted insensitive clay without the possible influence of bonding and cementation was studied in pure (speswhite) kaolin clay, which can generally be considered inactive. All the materials were tested saturated and their viscous behaviours were generally characterised at water contents below the liquid limit. Samples of the artificially cemented kaolin were tested in the Koseki laboratory at the Institute of Industrial Science (IIS), University of Tokyo, Japan while samples of pure kaolin and London Clay were tested in the soils research laboratory at UCL. The geotechnical properties and general monotonic behaviour of kaolin and London Clay have been heavily researched in the past and the basic geological and geotechnical characteristics of the used materials are described in more detail below.

3.2.1 Speswhite kaolin

Speswhite kaolin is an inorganic low plasticity clay, which is extracted from weathered granite in southwest England and is commercially available. Kaolin primarily consists of kaolinite

particles, which generally can be considered inactive under neutral PH pore water conditions (Morris, 2003), meaning that time-dependent bonding or cementation is not expected to take place when the material is tested in its pure form. The clay is characterised by a relatively high permeability compared to many natural clays with a high clay content, which has the benefit of significantly reducing the time required to test the material under drained conditions. Kaolin was generally seen as an ideal material for studying viscous effects without the influence of ageing effects. Geotechnical index properties of Speswhite kaolin are given in Table 3-1.

3.2.2 Cement mixed TA kaolin

To reproduce cementation effects similar to what is typically observed over many years in natural clays, artificially cemented clay was produced by mixing TA kaolin clay with a small quantity (3% by weight) of Rapid Hardening Portland (RHP) cement[1]. TA kaolin is a regional kaolin clay produced in Japan with similar characteristics to Speswhite kaolin. In this artificially cemented clay the interrelationship between viscous and cementation effects are more easily studied. The particular type of cement was chosen to achieve a rapid hydration with the majority of the strength increase seen within a couple of days. The geotechnical index properties of TA Kaolin are given in Table 3-1 and the characteristics of the RHP cement are given in Table 3-2.

3.2.3 London Clay from Heathrow Terminal 5 site (T5)

Natural London Clay was chosen because of its presence and influence on many foundation structures in the greater London region. Additionally, ageing and viscous effects in high plasticity, low sensitive stiff clays, such as London Clay, have not been investigated rigorously in the past.

High quality 100 mm wax-sealed rotary cores of London Clay were obtained via Imperial College from the Terminal 5 (T5) ground investigation at Heathrow airport, west London. The cores were taken from a depth of 13.95-15.45 m below ground level, corresponding to the geological $B_{2(b)}$-sub-unit (Gasparre, 2005), at a location where the ground profile comprises 52 m of London Clay overlain by 6 m of Terrace gravel. The water table was located approximately 1.5 m above the base of the Terrace gravel and a hydrostatic pore water pressure profile was generally found within the London Clay. London Clay was deposited under marine conditions in the Eocene period, around 30 million years ago. Uplift and erosion have subsequently removed overlying deposits and large parts of the London Clay itself. In the most recent event Terrace gravel was deposited on top of the eroded London Clay sediments. The likely maximum past overburden pressure 30 m above the base of the London Clay was estimated by Skempton & Henkel (1957) to be approximately 2.2 MPa, corresponding to around 2 MPa at the depth the rotary cores were obtained from.

---

[1] Produced by Sumitomo Osaka Cement, Japan (http://www.soc.co.jp/cement/shohin/cm2.html)

Clay minerals present in London Clay are illite (mica group) and to a lesser extend kaolinite (kaolin group) and smectite (montmorillonite group). Secondary non-clay minerals such as quartz (silicate) and pyrite (non-silicate, e.g. occurring as pyrotised fossil shells) are also commonly found (Perrin, 1971). If pyrite is oxidised for example as a result of weathering this will give rise to crystals of gypsum (Marshall, 1975). In this study, fractures of pyrotised fossil shells up to 20 mm in length were found in the cores, however as explained in Section 3.4.3b, the tested specimens were cut from homogenous parts of the cores.

In undisturbed state London Clay can be characterised as a very stiff and heavily overconsolidated clay of high plasticity and low sensitivity with a macro-fabric that is characterised by the presence of fissures. The geotechnical index properties of London Clay from the geological $B_{2(b)}$-sub-unit are given in Table 3-1. In contrast to push-in thick walled tube sampling, rotary coring is generally expected to cause only minimal disturbance to the natural structured clay. It is known that as the anisotropic stress conditions are relieved when the soil is extracted from the ground some disturbance of the soil structure is inevitable (Hight et al., 1992; Leroueil & Vaughan, 1990; Lo Presti et al., 1999). However, given that the London Clay is of low sensitivity and for simplicity, in this thesis the rotary-cored samples will be considered to be undisturbed. In a study recently carried out by Gasparre (2005) it has been shown that shearing along pre-existing fissures in specimens of undisturbed London Clay will lead to a reduction in the effective peak strength to a level, which is comparable to the reconstituted strength. Nevertheless, when care was taken in sample preparation and small 38 mm samples were tested it was found that the presence of fissures typically did not influence the intact behaviour. In the study by Gasparre (2005) it was furthermore indicated that weathering extending to a depth of 15 m below ground level at the T5 site might have affected the soil composition and natural structure of the weathered London Clay.

3.3 TEST EQUIPMENT

The viscous and ageing effects in the selected clays have been investigated using modified one-dimensional oedometer and advanced triaxial testing equipment. To supplement the static testing methods, dynamic testing using bender elements was introduced in some of the test cells. As described in more detail in Section 3.3.1e below, using bender elements a shear wave can be transmitted through the soil and from the determined velocity of propagation the elastic shear stiffness of the soil can be estimated using simple elastic theory. Generally, static testing methods are useful in assessing the soil behaviour over a large continuous strain range, while dynamic testing is useful in assessing the very small strain stiffness response at a given state without causing any significant disturbance to the soil specimen. The oedometer cell was mainly used because of its simplicity and its applicability to one-dimensional field scenarios such as time-dependent settlement after natural deposition or settlement of ground loaded under large rafts or platforms. On the other hand, the triaxial cell was used to investigate the time-dependent soil behaviour under more general axi-symmetric stress-strain conditions. The triaxial cell allows for a greater control of boundary conditions and furthermore can significantly improve the accuracy of stress-strain measurements. Triaxial testing equipment with high resolution local strain instrumentation was found to be essential in studying time effects, as viscous and ageing effects firstly can be relatively small and secondly difficult to separate from each other and from effects arising due to changes in state. The use of bender elements was also found to be invaluable in determining the influence of ageing on the very small strain shear stiffness.

In the following, the test equipment will be described in detail. Special attention has been given to modifications made to the equipment to suit the objectives of the study and to the use of advanced instrumentation to allow for accurate measurements of soil behaviour. A separate section will be dedicated to the dynamic testing system using bender elements, which have been incorporated into both the (UCL) oedometer cell and one of the (UCL) triaxial cells.

3.3.1 (UCL) Oedometer testing system

The (UCL) oedometer apparatus is very unique and was designed by the author in collaboration with UCL technicians. It comprises a multipurpose loading-frame and modified Wykeham Farrance oedometer cell fitted with bender elements for shear wave transmission. The setup of the oedometer testing system is shown in Figure 3-1 and the layout of the oedometer cell is shown schematically in Figure 3-2.

a Test cell

The soil sample is confined laterally in a standard 75 mm diameter size oedometer cell, which has been modified to allow for initial sample heights up to 40 mm. Features, which have been

retained from the original Wykeham Farrance cell, are a fixed rigid confining ring and one-way top drainage with base pore water pressure measurement both through porous stones. Filter paper was generally used to avoid clogging up the porous stones, which has the downside of slightly increasing the compliance of the apparatus.

b Loading system

The cell was fitted into a combined loading frame consisting of a standard Wykeham Farrance constant strain rate machine Model T56 (1 ton capacity) and a standard oedometer lever arm and dead weight hanger (ratio 1:11). The idea behind this unusual design was to allow both constant rates of straining and constant total vertical stress creep stages to be performed in the same tests using available standard equipment. The constant strain rate machine is driven by a motorised 25 speed gearbox, which can raise the loading ram at deformation rates between 0.00122 mm/min and 0.381 mm/min depending on the gear setting.

c Instrumentation

The vertical movement of the top cap was recorded by means of an accurate dial gauge and a high resolution miniature LVDT of the type RDP-D5/200H with an unguided armature. Both have a 10 mm range and were placed on opposing sides of the top cap. When testing reconstituted materials starting from a slurry state the initial vertical deformation was found to be very significant and hence during testing both the dial gauge and LVDT had to be adjusted once or twice to cope with the full range of vertical deformation. In addition to load applied by dead weights any vertical pressure applied through the loading ram was measured by a 2 ton load cell (N.C.B./M.R.E. type 403) placed between the loading frame and the top cap. The pore water pressure was measured using a Wykeham Farrance pressure transducer (type WF17600) fitted to a transducer block at the base outlet. Characteristics of the used transducers in the oedometer apparatus have been listed in Table 3-3.

d Signal conditioning and data acquisition

Datalogging of the transducers was introduced in this study to allow for continuous recording of stresses and strains, as this would be beneficial in long-term testing in terms of time saved and quality/quantity of readings. A PC based data-logger (PICO ADC-16) was obtained, which simply and economically made high-resolution data-logging possible. The enclosed windows compatible PICO software recorder allowed for manual adjustment of the frequency of readings and real-time monitoring of selected transducer voltages or derived engineering parameters. During testing collected data were copied and pasted into a spreadsheet for further analysis.

Signal conditioning by amplification of the transducer output signals was applied to the LVDT and load cell. The miniature LVDT was connected to an RDP D7M amplifier, while the load cell signal was conditioned using an in-house made amplifier with built-in digital meter. In addition to amplification of transducer output signals, a considerable improvement in resolution

was achieved by means of earthing. This was done for each transducer by grounding one of the signal channels to increase the relative output on the other channel. This procedure led to a significant reduction in the experienced noise. Moreover, strategic arrangement of transducer cables away from mains voltage sources also helped to reduce noise levels.

e Dynamic testing system

In order to measure changes in the vertical elastic shear modulus of the tested clays during compression, the standard oedometer cell was fitted with (UCL) bender elements. The bender elements, described in detail in Section 3.3.3, were fitted into the top cap and base of the cell (Figure 3-6 shows a photo of the bender elements incorporated into the top cap and base pedestal, which is also shown schematically in Figure 3-2). This configuration allowed shear wave transmission along the vertical axis of the sample with a horizontal polarisation and hence made it possible to determine the vertical shear modulus, G_{VH}. The bender elements generally protruded 2 mm into the sample at either end, meaning that the vertical distance between the tips was only about 16 mm at the start of compression in the original 20 mm high oedometer cell. This combined with the high compressibility of the tested reconstituted clays meant that the cell had to be modified from the standard 20 mm height to 40 mm height to allow for a greater working range of the bender element testing. An initial test series on reconstituted kaolin confirmed that in the standard 20 mm cell the distance between transmitting and receiving bender elements quickly became too short under increasing stresses, which clearly resulted in erroneous stiffness measurements.

f Calibration of transducers

The calibration of the load cell was made in two steps; first, the load cell and in-house digital meter were calibrated against a pneumatic Denison loading system with a resolution of 0.04 kN over the full working range of the load cell. Then the amplified output from the digital meter was captured by the data-logger and calibrated against the digital meter reading (resolution of 0.02 kN) using the manually adjusted loading ram to supply the pressure. Calibration of the pore pressure transducer was done in similar steps. First, a digital pressure meter of the type WF17900 was calibrated for minimum and maximum pressure with the pressure transducer attached. The known maximum pressure of approximately 999 kPa was obtained by pressurising a small oil-water interface chamber (oil pot) by applying dead weights to the 'friction less' loading piston (diameter of 14.5 mm) that penetrated the chamber. The loading piston was rotated gently to minimize the friction. Following calibration of the digital meter, the non-amplified voltage output from the pore pressure transducer was captured by the data-logger and calibrated against the reading from the digital meter (resolution of 1 kPa) over the full working range of the transducer using a variable hydraulic pressure. Using a purpose made mount to hold the miniature LVDT the travel of the LVDT armature was varied using a Baty dial gauge with a resolution of 0.002mm. The amplified output from the LVDT as recorded by

the data-logger was then calibrated against the accurate dial gauge readings of the armature travel. Calibration data for all the transducers in the oedometer apparatus are given in Table 3-4.

3.3.2 (UCL) Triaxial testing systems

Two computer controlled hydraulic triaxial testing systems have been used at UCL. Both triaxial systems allow fully computer controlled stress paths to be carried out at controlled rate of strain or controlled rate of stress. The general setup of the triaxial systems is shown schematically in Figure 3-3. Triaxial testing system no. 1 was acquired from the Geotechnical Research Group at City University, who also designed the system. To suit the objectives of this study Triaxial system no. 1 was subsequently subjected to a few modifications, which included the introduction of high-resolution miniature local LVDTs to improve the accuracy of strain measurements in the small strain region. All the triaxial compression and extension tests on reconstituted and undisturbed specimen of London Clay were carried out using this system. The setup of Triaxial system no. 1 is shown in Figure 3-4. The other triaxial system used at UCL, Triaxial system no. 2, was acquired from the UK Transport Research Laboratory and similarly to Triaxial system no. 1 was designed by the Geotechnical Research Group at City University. The main modification to Triaxial system no. 2 involved the incorporation of bender elements, as described in Section 3.3.2i below. In contrast to Triaxial system no. 1, Triaxial system no. 2 came with a set of local Hall Effect transducers. There was therefore little incentive to improve the strain measurements further, despite lower resolutions of the Hall Effect transducers compared to the resolution of the miniature local LVDTs. Triaxial system no. 2 was used to perform isotropic compression tests on reconstituted London Clay and kaolin with simultaneous bender element testing. Details of the specimen setup with bender elements in Triaxial system no. 2 are shown schematically in Figure 3-5. The basic features of the two triaxial systems are the same, while the main differences primarily concern details in the pressure regulation, local strain instrumentation and data acquisition as described in the following sections.

a Test cells

The triaxial cells are similar in design to the original hydraulically operated stress path cell designed by Bishop & Wesley (1975) (refer to Figure 3-3). Each cell consists of a water filled main chamber for applying a uniform radial confining pressure to the sample. The cylindrical sample is placed on a pedestal inside the cell and is separated from the cell water by a thin membrane. A hydraulically activated loading piston applies the axial force to the base of the sample, which in turn reacts against a submersible load cell fixed at the top. The cell accommodates a 38mm sample fitted with local strain gauges. Drainage was permitted through the base pedestal only, while for measurement of pore water flow and for the purpose of saturation, the drainage line was connected to a combined volume gauge and back-pressure system. The drainage line from the base pedestal consist of short thin stiff tubing in order to

minimize the compressibility of the drainage system, which could significantly influence the pore water pressure response.

b Loading systems

In both triaxial systems, the hydraulic pressure system consists of a constant air pressure source, computer-controlled air pressure controllers and use of air-water interfaces to achieve the regulation of the back-pressure, ram pressure and cell pressure. The main air pressure was supplied by a vane-compressor, which was set to maintain a continuous pressure between 800 kPa to 950 kPa. In each system, three air pressure controllers is used to give three independent pressure sources used for the cell pressure, axial ram pressure and back-pressure. Each pressure controller is adjusted on an individual basis using feedback loops from the load cell and the pressure transducers connected to the cell water and the sample pore water respectively. Triaxial systems no. 1 and no. 2. are slightly different when it comes to pressure regulation. Triaxial systems no. 1 makes use of accurate multi-stage pressure controllers attached to stepper motors; where each steps of the motor corresponds to a change in pressure of about 0.4 kPa. In contrast, the pressures in Triaxial systems no. 2 are regulated by electropneumatic controllers (Watson Smith type 101XA), which convert a voltage signal input into a proportional pneumatic output pressure. The pressure controllers have the advantage of showing higher accuracy and they are not at risk of sudden losses in pressures should the power supply fail temporarily.

In Triaxial system no. 1 the cell chamber was filled with water directly from the mains water supply, while a Wykeham Farrance (model 13000) bladder type air-water interface was connected to the pressure line. The bladder type air-water interface was used in order to minimize dissolved air in the cell water, as dissolved air may penetrate the thin membrane surrounding the sample (Head, 1998). In contrast, in Triaxial system no. 2 the cell chamber was connected to a large Wykeham Farrance direct air-water interface with a capacity large enough to fill the cell with water and subsequently pressurise it. The latter system may have experienced a minor problem with dissolved air in the cell water. In both triaxial testing systems, Imperial College type volume gauges were used as drainage reservoirs, which double as sealed air-water interfaces for regulating the pore/back-pressures. Again, a sealed air-water interface was used in order to minimize dissolved air in the drainage lines, which could lead to an erroneous pore pressure response. On the other hand, a small direct air-water interface was used for the ram pressure, as there is no risk of dissolved air migrating to the sample. Air in the ram pressure line is however likely to have affected the accuracy of the movement of the ram and hence the axial deformation of the sample.

In addition to the main pressure system, the piston movement in both triaxial apparatuses was regulated using an accurate constant rate of strain pump, which was connected directly to the ram pressure line. The secondary displacement system consists of a bishop ram driven by a small stepper motor with a 1:125 reduction through a gearbox. The stepper-motor was regulated by a so-called clicker box, which switches on and off at manually controllable

intervals from 1 s to 40 s corresponding to rates of axial straining of about 0.003 %/hr to 0.12 %/hr. However, since bedding errors and presence of dissolved air in the ram pressure line, as mentioned above, will influence the accuracy of the constant rate of straining displacement system, the recorded local strain rates were found to fluctuate and vary from the nominal rates.

c Top cap connection

For testing undisturbed samples the used connection between load cell and top cap consisted of a half ball and coned seating on the top cap. This connection type allows free rotation and sliding between loading ram and the top cap. For stiff undisturbed samples, which may not be perfectly aligned initially, this setup is necessary in order to avoid significant stress non-uniformities at the top of the sample. However, the connection does not allow extension tests to be performed. On the other hand, when testing initial soft reconstituted samples a suction-cap and flat connection between top cap and load cell was used. This rigid connection forces the top of the sample to align horizontally during compression, but the stress non-uniformities experienced after reaching the preconsolidation pressure will be minor as the tested samples initially were relatively soft. When using the suction-cap both compression and extension tests can be performed. The use of a suction-cap is particularly important for capturing the small-strain behaviour, as the load cell is connected to the sample prior to shearing and thereby initial disturbance is minimized. For all sample types, the connection between top cap and sample was flat and rough, which would have given rise to end restraints and stress non-uniformities at the sample ends. However, the 2:1 height to diameter ratio of the sample means that the stress non-uniformities at the sample ends should not have affected the stresses in the centre part of the sample significantly (Head, 1998).

d Instrumentation – general

Both triaxial apparatuses featured the same basic instrumentation, details of which are listed in Tables 3-5 and 3-7. Pore water flow was measured using an Imperial College type volume gauge with a LVDT displacement transducer attached (RDP type LDC with spring return armature). The gauge has a 50 cc capacity, which corresponds to 25 mm travel of the LVDT. For measuring axial strains each of the triaxial cells featured a single external LVDT displacement transducer (same type as the volume gauge LVDT), which was supplemented with more accurate local strain instrumentation as described in the following sections below. For measurement of the axial force internal submersible load cells, Wykeham Farrance type STALC3, were used in both triaxial cells. The capacity of the load cells in Triaxial system no. 1 and 2 cells were 5 kN and 3 kN respectively. The cell pressure was measured by a pressure transducer (Wykeham Farrance type WF17060) connected directly to the base of the cell chamber. While the measurement of pore/back-pressure occurred through short thin stiff tubing connecting the top of the base pedestal to an external transducer block with a second pressure

transducer attached (again WF type WF17060). As noted earlier, the use of short thin stiff tubing minimizes the compressibility of the pore water system.

e Small strain local instrumentation – Triaxial system no. 1

External strain measurements are prone to errors, which can be summarised as seating, bedding and alignment errors of the sample, top cap and base porous stone (Head, 1998). Additionally, external strain measurements will be affected by system compliance and strain non-uniformity due to end restrains. To overcome the majority of these errors, local strain measurements were taken over the middle 2/3 of the sample as recommended by Baldi, Hight & Thomas (1986). The local strain measurements were achieved by using high-resolution submersible miniature local LVDTs attached directly to the membrane surrounding the soil sample. Two axial miniature LVDTs were placed diametrically opposite on the sample to cancel out strain non-uniformities. A third miniature LVDT was incorporated into a radial strain belt attached around the centre of the sample to be able to determine shear strains and volumetric changes at small strains for comparison with the pore water flow (Figure 3-13). The transducer body of each local axial LVDT was mounted onto the top part of the sample simply by gluing the mounts directly onto the membrane, while the armature extends downwards and rests on a flat surface mount glued onto the lower part of the sample. The floating type setup has been described by Cuccovillo & Coop (1997). As recommended, the two mounts for each transducer were initially mounted about 50 mm apart, corresponding to 2/3 of the sample length. The lightweight radial strain belt, which was glued directly onto the centre part of the sample, has been designed as a single-hinge free-hanging aluminium belt based on a similar design by Jotisankasa (2003). It should be noted that because of the hinge type design, the effective capacity of the radial displacement transducer was reduced from 10 mm to about 4 mm radial displacement, which is acceptable due to the smaller radial dimension of the sample.

All three miniature LVDTs were slightly modified versions of the standard RDP D5/200W transducer, which have a 10mm linear range and a very high resolution allowing measurement of strains in the order of 10^{-4} % depending on setup. The modifications of the standard model included right-angle connection and short cable outer sleeve for greater flexibility in the restricted cell space, as recommended by Coop, 2004. In addition, for each of the axial LVDTs the unguided armature had its threads removed and a through bubby bore was made in the transducer body to give the armature unrestricted travel even after large strains. Due to the shortening of the cable outer sleeve the manufacturer reduced the operating pressure from 35 bar to 20 bar. The characteristics of the local LVDTs used in triaxial system no. 1 are given in Table 3-5.

Yimsiri (2001) made a comprehensive review of some of the available local strain measurements systems for use in the triaxial apparatus. In this study, out of all commercially available displacement transducers, LVDTs were chosen because of their high resolution, robustness and linear calibration.

f Small strain local instrumentation – Triaxial system no. 2

Triaxial system no. 2 was purchased already equipped with a set of local Hall Effect transducers. The setup of the Hall Effect transducer for measurement of both axial and radial displacements was similar in principle to the setup of the floating type LVDTs. Two transducers oriented vertically on opposing sides of the sample were used for measuring axial displacement, while a third transducer was placed in a lightweight single-hinge type radial belt mounted at mid-height of the sample to measure radial strains (Figure 3-13). Glue was used to attach the lightweight mounts onto the membrane surrounding the sample. Similarly to the LVDTs, the Hall Effect transducers have the advantage of linear calibration, but in contrast have a significantly lower resolution. Clayton & Khatrush (1986) achieved a resolution in the order of 0.002 %, however in this study the resolution of the utilised Hall Effect transducers was found to be less, as mentioned in Section 3.3.2h below. The Hall Effect transducer type was developed at the University of Surrey (Clayton & Khatrush, 1986). It makes use of the Hall Effect, which results in a varying voltage output of a semiconductor plate depending on its position within a magnetic field. Each transducer consists of a mount holding the Hall Effect sensor, while another mount holds a small magnet, which is able to move relative to the sensor. The characteristics of the local LVDTs used in Triaxial system no. 2 are given in Table 3-7.

g Signal conditioning and data acquisition – Triaxial system no. 1

For data acquisition and control of pressures in the Triaxial system no. 1 a spectra micro-ms measurement system was used in connection with a Pentium processor PC. The spectra box (model SBL-11) was manufactured by Intercole System Ltd. and features 32+ input channels, internal Instrumentation Amplifier, auto calibration, auto ranging and programmable integration. A triaxial control software written in Q-Basic™ code and developed over several years by Matthew Coop was used for calibration and monitoring of transducers, control of stress paths and recording of data. Before reaching the spectra box, signal conditioning of transducer output signals plays a very import role when highly accurate results are necessary. Special attention was therefore paid to the voltage supply, amplification of output signals and earthing of cables. Since the LVDT output signal is proportional to the excitation voltage, it is beneficial to have as high as possible excitation with as little as possible fluctuation in order to increase the resolution. A single Farnell stabilised voltage supply (type L30) was used to excite all the transducers with 9.90 V, which is close to the 10 V capacity of the spectra box and the transducers.

Output signals from all transducer, but the pressure transducers, were amplified before reaching the spectra box. The two external displacement transducers (axial displacement and volume gauge), which are not restricted by the limited cell space, were both of the RDP LDC type with built in amplification. On the other hand, the load cell and local displacement transducers, which were placed inside the cell under pressure, required external amplification to improve their resolution. The load cell was connected to a RDP S7DC amplifier, while the three

local LVDTs were connected to separate RDP S7AC amplifiers before reaching the spectra box. For the external amplifiers the amplification was manually adjusted so the output signal was amplified as much as possible without reaching saturation of the amplifier within the linear range of the transducers. The accuracy of the miniature local LVDT's at the start of shearing was further improved by earthing transducer cables, using stabilised voltage supply, amplifying of the output signal and using a method proposed by Cuccovillo & Coop (1997). This method consists of adjusting the amplifiers zero potentiometer to set the transducers at their electrical zero, which allows the datalogger to operate in its most sensitive range. The datalogger was also programmed to perform long integration of the data, which helped to filter out noise. A resolution of the miniature LVDTs of about 0.0002 % strain was typically achieved in the testing in the small strain region.

h Signal conditioning and data acquisition – Triaxial system no. 2

For data acquisition and control of pressures in Triaxial system no. 2 a 486 processor PC with a multifunction interface/data-logger card was used. The interface card (Alpha PC Super card from CIL) features 8 input channels (16 bit resolution) for logging of transducers, 4 output channels (16bit resolution) for control of the electro-pneumatic transducers and programmable digital filter and amplification. Similarly to Triaxial system no. 1 a triaxial control software written in Q-Basic™ code and developed over several years by Matthew Coop was used for calibration and monitoring of transducers, control of stress paths and recording of data. Apart from the load cell, which was connected to a RDP S7DC amplifier, none of the other transducers, including the local Hall Effect strain gauges, were subjected to amplification before reaching the interface card. The transducers were excited with 9.90 V, which is close to the 10 V capacity of the data-logger card and the transducers. Since no particular care was taken to improve the earthing and signal conditioning of the Hall Effect transducers, the resolution of these was observed to be around 0.005%, which was similar to the resolution of the external LVDTs and about 1.5 orders of magnitude worse than what was achieved from the miniature LVDTs in Triaxial system no. 1. However, since triaxial system no. 2 was only used for isotropic compression tests a high resolution of the measured strains was not necessary.

i Dynamic testing system – Triaxial system no. 2

Bender elements were incorporated into Triaxial system no. 2 in order to get a quick and non-intrusive dynamic testing method of measuring the changes in the elastic shear modulus, which could supplement the static stiffness measurements obtained at larger strains using the local Hall Effect transducers. A pair of (UCL) bender elements was fitted into the top cap and base pedestal respectively as shown in Figure 3-6. This configuration allowed shear wave transmission along the length of the sample and hence made it possible to determine the vertical shear modulus, G_{VH}. The bender elements generally protruded 2mm into the sample at either end.

j Calibration of transducers

The load cells were calibrated using dead weights over their initial linear range up to a pressure of 0.5kN. Limitations of the dead weight loading meant that the transducers were not calibrated over their full linear range. However, since the greatest accuracy was usually required at the beginning of shearing the possible reduction in accuracy at high deviatoric stresses was not considered significant. Both the cell pressure and pore pressure transducers were calibrated against a pre-calibrated pressure transducer attached to a Wykeham Farrance digital pressure meter (refer to section 3.3.1f for calibration of the digital meter). Calibration was done in the triaxial cell by substituting the pressure transducers one at a time with the pre-calibrated transducer. By allowing a direct flow of water from the cell chamber to the drainage system, the remaining pressure transducer could then be calibrated over its full range using the cell pressure system.

The external LDVTs were calibrated in a purpose made mount against a micrometer with a resolution of 0.01 mm, while the Hall Effect transducers and miniature LVDTs were calibrated against a Baty dial gauge with a resolution of 0.002 mm. A cylindrical aluminium dummy sample with diameters ranging from 36 mm to 40 mm in steps of 1mm was used as a calibration-tool for the radial strain belts. All strain transducers were calibrated over their full working range. As a special procedure, each of the local LVDTs was adjusted before calibration on its respective amplifier to an easily achievable reference state. The reference state for each transducer was chosen as the state without any armature inside the transducer body with the output signal adjusted to its electrical zero. Finally, calibration of the volume gauges in both triaxial systems were carried out against the volumetric flow from a manual operated Bishop ram, which in turn had been calibrated against a burette with a resolution of 0.02 mL. Calibration data for all the transducers in the two triaxial systems are given in Tables 3-6 and 3-8.

3.3.3 (UCL) Shear wave transmission system

Piezoceramic bender elements have been used in soil testing for decades since the method was first introduced by Shirley & Hampton (1977). The use of bender elements provide a quick, simple and non-disturbing procedure for determining the very small strain elastic shear modulus of a soil sample by means of shear wave transmission and measurement of the shear wave velocity between a transmitting and a receiving element. In-house made bender elements were produced in collaboration with UCL Ph.D. research student Joao Rio and incorporated into the base pedestal and top cap of the modified oedometer cell and Triaxial testing system no. 2 at UCL. The general setup of the bender element testing system for use in both the oedometer cell and triaxial cell is shown schematically in Figure 3-7. This consists of a pulse (function) generator, a transmitting and a receiving bender element protruding into two opposing ends of

the sample, a data-logger and signal-conditioning unit and a PC with the data-logging software. Each of the used components is described in the following.

a Concept of the bender element method

A bender element comprises a piezoceramic plate, which has a polarised crystal structure. If the element is subjected to a deflection the crystal structure develops an electric moment which can be measured as a voltage output and equally if the element is subjected to an electric moment from a voltage input the crystal structure will deflect (Morgan Electro Ceramics, 2003). The idea behind the bender element technique is to excite an element, which protrudes into one end of the soil sample, using a pulse generator, to create a small transverse deflection of the element. As a result a shear wave is created, which will propagate through the sample perpendicular to the movement of the tip of the element. A second bender element, which protrudes into the opposite end of the sample, will deflect and generate a small voltage due to the motion of the incoming wave. The transmitted and received wave signals can be traced using an oscilloscope and an estimate of travel time between the two elements and hence velocity of propagation can be made. The elastic shear stiffness of the soil is then simply related to the velocity of the propagating shear wave and the current total density of the sample, as given in Section 3.5.5. In practice, it may be difficult to determine the exact arrival time of the sent signals, since the signal have been distorted as result of the propagation through the sample and because of the influence of for example signal noise, as explained further in Section 3.3.3d below. For these reasons, a reliable and objective method for determining the arrival time of the shear wave is still being discussed today.

b Design of (UCL) bender elements

Both the transmitting and receiving in-house made bender elements consist of a 10x6x0.6 mm series bimorph element[2]. The series bimorph element consists of two thin piezoelectric ceramic plates separated by a non-conducting layer (for further details refer to Morgan Electro Ceramics, 2003). To create the bender element a shielded 2-wire cable was connected to the bimorph element by soldering a wire to either side of the element. Then the bimorph flexing element was coated with a thin layer of stiff and brittle epoxy resin[3] to avoid ingress of water and to improve its durability. A photo of a free single bender element is shown in Figure 3-6. The base of the series element was generally fixed into the top cap or base pedestal, such that the effective length of the element was about 8 mm and the tip of the element protruded approximately 2 mm into the sample. A soft silicone rubber[4] was used to fill the void along the length of the element

[2] Piezoelectric ceramic grade PXE 5, supplied by Morgan Electro Ceramics

[3] Epoxy coating from Vosschemie; 2-part Glosscoat consisting of a hardener and a high gloss coating resin

[4] 2-part Moldsil silicon rubber supplied by W.P. Notcutt Ltd

inside the top cap or base pedestal so that the element was not restrained from moving. In order to promote easy replacement, each of the bender elements, apart from the bender element used in the top cap in the triaxial cell, was cast into a brass confining-ring, which was sealed in place using an o-ring. Since the bender elements were very brittle and appeared to deteriorate with time when in contact with water, this special feature was incorporated to be able to quickly and easily replace the deteriorated elements. The incorporation of bender elements into the oedoemeter cell and triaxial cell is illustrated in schematic diagrams in Figure 3-2 and Figure 3-5, while Figure 3-6 shows photos of the actual positioning of the bender elements in the top caps and base pedestals.

c Pulse generation, data acquisition and signal conditioning

The use of pulse signals is under certain testing conditions essential for determining the correct travel time of the transmitted shear wave, as discussed in Section 4.2.2. To excite the transmitting bender element, a programmable TTi function generator (TTi TG1010) was used in the majority of the tests. Compared to a simple standard function generator, which only allows continuous wave forms to be sent, the TTi function generator has the advantage of being able to generate a wide range of signals, including; continuous harmonic sinusoid signal, single sinusoid pulse, multiple sinusoid pulses and sinusoid frequency sweep. A high resolution 2-channel Pico data-logger (ADC-212) connected up to a PC was used to capture the transmitted and received signals from the bender elements. The generated signal was fed simultaneously to both the transmitting element and to the data-logger, while the received signal was obtained directly from the receiving element. The accompanying PicoScope™ PC software was used as an oscilloscope to display and capture the signals in time domain and as a linear spectrum analyser to show the frequency content of the signals. Digital filtering, amplification and averaging of data were enabled in the software to reduce the experienced noise.

d Standard bender element testing techniques and methods of interpretation

Despite several attempts by other researchers to standardise the bender element testing technique, no reliable method has yet been determined, which can be said to be applicable to all types of soils, testing conditions and testing equipment.

By testing samples of varying lengths Viggiani & Atkinson (1995) demonstrated that the tip-to-tip distance between the transmitting and receiving elements corresponded to the effective travel distance of the propagating shear wave. This assumption has usually been adapted in published research, and is also adapted in this study. However, the main problem associated with bender element testing does not concern the slight uncertainty about the travel distance. Instead, it primarily concerns the determination of the shear wave travel time, which is made difficult because of observed discrepancies in waveforms between the transmitted and received signals. These discrepancies arise due to several factors such as electrical noise, irregular dispersion and boundary reflection of signals, resonance of soil-element system, imperfect

translation of element to soil movements and imperfect translation of electric signal to element deflection and vice versa. Moreover, since the deflection of the transmitting bender element generates a wave with components of both shear and compression, the compression components, which travel at a velocity greater than the generated shear wave, may obscure the initial trace of the received signal when the main shear wave arrives. This is the so-called near-field effect (Arroyo et al., 2003). Generally, in the literature four different methods have been suggested for the determination of travel time. These are the three traditional time domain methods; first arrival, travel time between characteristic points and cross-correlation of the sent and received signals, and additionally the phase-delay method in frequency domain. In Section 4.2.2 these different methods are explained and a comparison is carried out in order to find a suitable method, which would give consistent results.

3.3.4 (IIS) Triaxial testing system

The (IIS) triaxial testing system was used as part of a six-week study visit at the Institute of Industrial Science (IIS), University of Tokyo, Japan. It comprised a triaxial apparatus with a manually regulated hydraulic cell pressure and back-pressure system and a computer controlled mechanical axial loading system which was devised at IIS. The system made it possible to perform shearing under constant confining pressure at very accurately controlled rate of axial strain or controlled rate of deviator stress. A photo of the triaxial testing system setup is shown in Figure 3-8, and a schematic layout is illustrated in Figure 3-9. In the following a basic description of the (IIS) triaxial testing system will be given. A more detailed description of the loading system, instrumentation, signal conditioning, data acquisition and calibration can be found in (Komoto, 2004).

a Test cell

Three similar triaxial cells were used. Each cell consisted of an inner frame and an outer Perspex chamber with a capacity of 1000 kPa. The inner frame left enough space to accommodate an internal load cell and allowed testing of 50 mm diameter cylindrical samples. Both the top cap and base pedestal were connected to drainage leads, which gave the choice of two-way drainage or combined one-way drainage and pore water pressure measurement. The sample drained directly to an external twin-burette volume change unit (25 mL capacity) connected to a back-pressure system.

b Loading system

The effective cell pressure, being the differential pressure between the pore/back-pressure system and the cell pressure system, was regulated using a twin-air-pressure-controller. The twin-air-pressure-controller was made up of two Pneumatic Precision Regulators (Fairchild model 10) combined in such a way that the first air pressure controller was used to keep a constant differential pressure between the cell pressure line and the back-pressure line, while the

second air pressure controller adjusted the total output pressure on both output pressure lines. The cell chamber worked as a direct air-water interface for the cell pressure, while the twin-burette volume gauge doubled as a direct air-water interface for the back-pressure system. To apply an axial pressure the triaxial cell was placed in a loading frame and the cell piston was connected to a motor-driven mechanical axial loading system described in (Komoto 2004). The system, which makes use of a servomotor, has virtually zero backlash when reversing the loading direction and it was therefore particularly suited for carrying out small unload-reload probing paths. Furthermore, the servo motor benefits from a large operating range, which made it possible to change the strain rate about three orders of magnitude from about 10^{-5} to 10^{-2} mm/min. Constant rate of stress or strain was accurately controlled via a PC installed control card using feedback from the internal load cell or external displacement transducer. The top cap connection in all three cells consisted of a flat rough connection with the sample and a fixed rigid connection to the internal load cell.

c Instrumentation

For measuring axial strain all three cells were fitted with an external combined dial gauge and electronic displacement transducer (type NEC 9E08-D1-20) with a 20 mm range, which measured the relative movement of the axial loading piston to the cell frame. Additionally, to minimize the influence of system compliance (especially from the deflection of the internal load cell) one cell had a single internal proximity transducer with a 2 mm range fitted. The transducer body was fixed to the inner frame and measured the relative displacement of the target metal plate, which was placed between the internal load cell and the top cap (refer to Figure 3-9). Volume change of the sample was measured using a low capacity differential pressure transducer connected to the twin-burette volume change unit. The effective cell pressure, being the differential pressure between the pore/back-pressure and the cell pressure was measured using a high capacity (up to 600 kPa) differential pressure transducer connected to the cell pressure line and the drainage system. The axial load was recorded using both an external load cell (2.0 kN capacity, not shown in Figure 3-9) and internal load cell (4.9 kN capacity). The use of an internal load cell generally eliminates any problems arising due to friction between piston and cell bush, however the performed tests indicated the friction loss to be minimal as the readings from the two load cells were found to compare well. It should be mentioned that during testing the water level in the cell chamber was generally kept just below the top of the internal load cell in order to avoid problems with the internal dry connections used for the proximity transducer and load cell.

d Signal conditioning and data acquisition

A PC with two internal interface/datalogger cards was used to record data from the transducers and to control the axial loading system. Input data from the transducers was acquired using a

high resolution 16 bit A/D card (CONTEC AD16-16(PCI)E), while the output control signal to the mechanical axial loading system was sent via a 12 bit D/A output card (CONTEC DA12-4(PCI)). Only the transducer signals from the internal load cell and internal proximity transducer were amplified and conditioned before reaching the A/D interface card. Amplification and filtering of the signals was done in two separate conditioning units (both San-ei Strain Amplifier model 6M81).

e Calibration of transducers

Calibration of the transducers was carried out prior to testing by N. Komoto, a Master student whom the author collaborated with during the study visit. Details of the calibration can be found in (Komoto, 2004).

3.4 TESTING PROCEDURES

3.4.1 General

The performed oedometer and triaxial tests principally followed a similar set of testing procedures, which consisted of pre-test checks of the testing equipment, sample preparation, sample set-up in the cell followed by a number of test stages where the soil behaviour was observed. Triaxial testing however significantly differentiates from standard oedometer testing in the performed test stages by having a saturation stage prior to compression and allowing more general stress paths to be carried out, which could eventually bring the sample to failure. Figure 3-10 shows a flowchart for the general testing procedures followed in the performed oedometer and triaxial tests and the testing procedures are described in more detail in the following sections.

3.4.2 (UCL) Oedometer tests on reconstituted speswhite kaolin and London Clay samples

a Pre-checks, sample preparation and set-up

Before sample preparation was commenced, preparation of the testing equipment was carried out. This involved de-airing the upper and lower porous discs by means of vacuum, filling the drainage system with tap water and bleeding the transducer block to ensure that the drainage system was free of air. All transducers were checked and the load cell and pore water pressure transducers were re-zeroed prior to setting up the sample in the cell. Before the start of each test a steel dummy sample with a known height was inserted into the cell with the top cap applied to obtain a reference reading from the dial gauge and LVDT. The actual sample height during testing could then be obtained from the relative difference between the reference reading and the current reading from either the dial gauge or LVDT.

Oedometer tests were carried out on both reconstituted kaolin and reconstituted London Clay samples. The kaolin samples were reconstituted at a water content of about 1.3 times the Liquid Limit (w_L~65%) by hand mixing dry kaolin powder with tap water. The London Clay samples on the other hand were reconstituted by wetting-up trimmings from the undisturbed rotary core samples with tap water and thoroughly mixing until a homogenous slurry was obtained at a water content of about 1.6 times the Liquid Limit (w_L~65%). Following preparation, the reconstituted clay slurries were transferred to the oedometer cell, making the best effort not to trap excessive amounts of air in the samples. The consistency of the reconstituted London Clay slurry made it possible to pour it directly into the cell, while the reconstituted kaolin had to be transferred to the cell in multiple layers using a spatula. The top cap and hanger were then applied (equivalent of 8 kPa) and samples were left overnight to stabilise before further compression was initiated. The dial gauge and LVDT were mounted soon after the top cap was placed, and initial readings were commenced.

b Test stages

The oedometer loading system developed at UCL made it possible to perform a combination of loading stages, which included

- One-dimensional compression and swelling at a constant rate of strain (CRS).
- Step change in rate of strain during both compression and swelling (SRS) to observe viscous strain rate effects.
- Step loading and step unloading with observation of excess pore water pressure dissipation (SL).
- Rest periods at intermediate stages during compression or swelling with either fixed axial strain (stress relaxation - SR) or fixed load creep (C) to observe viscous effects and possible ageing effects.

Depending on what was investigated, each test was performed with a combination of several of the above loading stages, which all had the purpose of investigating viscous and ageing effects on the one-dimensional compression and swelling behaviour. In CRS tests the minimum strain rate allowed by the loading machine was around $2.3 \cdot 10^{-7}$ s^{-1} =0.08 %/hr, and in SRS tests the strain rate was changed step-wise by a factor of 5 or a multiple of 5 up to a factor of 125.

In tests on both kaolin and London Clay the strain rates used in CRS tests were all too fast to allow fully drained conditions and hence excess pore water pressures were observed to build up during all of the performed tests. Therefore, initially after the commencement of a rest period, a combined effect of excess pore water pressure dissipation and creep was observed. Only after the pore water pressure had reached zero could the effect of creep be observed on its own. Rest periods of up to one month were maintained in some of the tests to observe viscous effects and possible effects of ageing. In addition to the static loading tests, bender element tests were carried out at suitable intervals during compression, swelling and resting in order to determine the changes in the elastic shear modulus. The bender element testing procedures are explained in Section 4.2.2, while further details of the static test procedures used in individual oedometer tests are given in Section 4.3 and 4.4, which describe the individual studies.

c Data acquisition, data monitoring and data post-processing

Real-time monitoring of axial displacement, total vertical stress and pore water pressure in numerical format was carried out using the PICO recorder software. The change in behaviour was additionally monitored in graphical format as the recorded data was continuously plotted against elapsed time. Generally, the frequency of data recording was adjusted periodically to reflect the rates of change in the monitored parameters. During stages of high rates of change, the frequency of recording was increased to a maximum of one reading every 2 seconds, while the frequency of recording during long-term creep stages was decreased to a minimum of one reading every 2 hours. The recorded data were continuously stored on the computers hard drive. The data were progressively transferred to an EXCEL™ spreadsheet for further analysis and for

a more in-depth monitoring of stress-strain behaviour. As the performed tests did not follow any standard testing procedures, the in-depth monitoring of stress-strain behaviour was essential for the progressive planning and control of the tests.

3.4.3 (UCL) Triaxial tests on reconstituted speswhite kaolin and reconstituted and undisturbed London Clay

The (UCL) triaxial cells were primarily used to tests both undisturbed and reconstituted samples of London Clay. However, a single sample of reconstituted kaolin was also tested in Triaxial cell no. 2 under isotropic stress conditions, as described in detail in Section 4.5.

a Pre-checks of testing equipment

To ensure that the drainage and pore water pressure systems were free of air, the porous discs were de-aired under vacuum, the systems were bled and the tubes were flushed with de-aired tap water. Prior to testing the complete system was also checked for leakages, cable connections were checked and noise on transducer signals was monitored, especially for the local transducers. Depending on the planned test stages, it was ensured that the volume gauge, the hydraulic loading piston and the bishop ram were positioned to allow enough free travel in both directions. If needed the amplifiers for the local LVDTs were adjusted back to their reference state, which was the point at which the transducers signals were at their electrical zero without the armatures inside the transducer bodies. This was done to ensure that the correct linear ranges of the LVDTs were known before start of testing. Finally, immediately before testing the pore pressure and cell pressure transducers were re-zeroed with the water level in the cell located just above the pedestal.

b Sample preparation

The sample preparation for each sample type is distinctly different and is described in more detail below.

Undisturbed samples

Two nominally undisturbed samples of London Clay (denoted S1LC and S2LC) were cut vertically from the centre of two short 100 mm diameter wax-sealed rotary cores taken in succession from a depth of 13.95-15.45 m below ground level at the T5 site. The specimens were to be cut to a nominal 38 mm in diameter and 76 mm in length. To ensure minimal disturbance to the sample, the following procedures were followed: after removing the cling film and wax layer, the core ends were cut parallel with a wire saw leaving a core of roughly 100 mm in length. The circumference of the core was then rapidly, but carefully, trimmed in layers using a wire saw, down to roughly 50mm in diameter leaving the specimen with a hexagonal shape. Finally, the coarsely trimmed specimen was transferred to a soil lathe, where the specimen was finely trimmed with a special made trimming knife to give it a circular shape

with a diameter of approximately 38 mm. Due to previous experience the soil lathe was surrounded by damp cloth which helped to avoid opening of fissures during trimming due to loss of moisture from the samples. Additionally, to prevent opening of fissures a low vertical pressure was maintained on the sample in the soil lathe during the trimming procedure. After trimming the lateral circumference, the sample was placed in a split mould and cut to approximately 76 mm in length. Extra care was taken to achieve flat and horizontally parallel ends, which is particularly important for stiff soils to avoid stress non-uniformities at the sample ends when the sample is loaded axially. The coarse trimming took about 10 minutes, while the fine trimming took about 15 minutes. After trimming, the samples were weighted in the split mould and the average dimensions of the samples were determined using a Vernier calibre. Some of the end-trimmings were collected and used for determining the moisture content by oven drying.

Generally, the clay cores were seen to be very homogeneous, but on a few occasions, fractures of pyritised shells up to 20 mm in length were found. Where pyritised shells were found these were removed carefully from the core and the specimens were cut from the remaining homogeneous part of the core.

Reconstituted samples

Two separate batches of reconstituted London Clay were created by wetting up and thoroughly mixing the trimmings from the undisturbed rotary core samples with tap water until a homogenous slurry was obtained at a water content of about 1.6 times the Liquid Limit (w_L~65%), which made the clay slurry very liquid and easy to pour. Deairing of tap water/pore water was not found to be essential for obtaining a high degree of saturation due to the saturation procedures employed, as explained in Section 3.4.3d below. The first batch used the trimming around the first intact sample, while the second batch used the trimming around the second intact sample. Each cylindrical specimen was then created by pouring the reconstituted clay slurry into a tall floating ring consolidometer with an inner diameter of 38 mm (illustrated schematically in Figure 3-11), where the slurry was pre-compressed and consolidated to make the sample strong enough to handle. The vertical pressure on the sample was increased in steps up to 90 kPa ($p'_c \approx 70$ kPa) over the first few days, where after the sample was left to consolidate fully for a minimum of 10 days to make it sufficiently strong to handle. A single overconsolidated sample was created by preconsolidation under an effective vertical pressure of about 1500 kPa ($p'_c \approx 1100$ kPa) in the consolidometer. This meant that at the start of shearing, with p'=300 kPa, the soil had an overconsolidation ratio, defined as the ratio of the actual maximum preconsolidation pressure p'_c over the current mean effective stress p', of about 4 (assuming a K_0 value of 0.64). After pre-compression in the consolidometer, the samples were extruded into a split mould, where they were cut to about 76 mm in length. Similarly to the undisturbed samples the reconstituted samples were then weighted in the split mould and the

average dimensions of the samples were determined using a Vernier calibre before the samples were setup in the triaxial cell. The end-trimmings were collected and used for determining the moisture content by oven drying.

The single sample of kaolin was reconstituted at a water content of about 1.3 times the Liquid Limit (w_L~65%) by hand mixing dry kaolin powder with tap water and following preconsolidated in the consolidometer under an effective vertical stress of 90 kPa, similar to the reconstituted specimens of London Clay. However, due to the higher permeability of the kaolin compared to the London Clay the consolidation time was reduced to less than a day.

c Sample set-up

After preparation, each sample was rapidly transferred to the base pedestal of the triaxial cell, where the sample was placed on a de-aired saturated porous disc covered with filter paper. During set-up, the drainage valve was closed to avoid water being sucked up by the sample from the back-pressure system. The top cap was then applied and vertical side drains were adhered to the sample before the rubber membrane was placed over the sample using a suction mould. The filter papers were pre-wetted and excess water removed immediately before use, while the membrane was pre-soaked for 24 hrs before setting up to avoid removing water from the sample upon contact. Two o-rings were used at either end to seal the sample from the cell water. The time taken from the extrusion of reconstituted samples or after final trimming of the undisturbed samples to a sealed position on the pedestal was about 10 minutes, which was considered rapid enough to avoid significant swelling or a significant loss of moisture in the samples.

Finally, the mounts for the local strain gauges were glued onto the membrane using "super glue"[5] and the edges of the mounts were further attached with "EVO-stik Impact adhesive". The flexible adhesive from the "EVO-stik" prevented the mounts from falling off at large strains, where the brittle "super glue" in many cases gave in due to bulging or single plane slip. The radial strain belt was fixed at mid-height and the two axial strain gauges were positioned on opposing sides of the sample with the upper and lower mounts placed approximately 50 mm apart. To ensure that the strain gauges ended up within their linear range during shearing, all of the strain gauges were initially positioned mid-range for undisturbed samples and at the beginning of travel for reconstituted samples, since these would experience significant compression before shearing. The sample setup with local LVDTs in Triaxial cell no. 1 and setup with local Hall Effect transducers in Triaxial cell no. 2 are shown in Figures 3-13 and 3-14. After finalising the sample set-up procedure, the cell chamber was sealed to the base and the cell was filled with tap water.

[5] "Super glue" is based on cyanoacrylate

d Saturation

Generally, the degree of saturation was checked using Skempton's B-value (Skempton, 1954), which is a measure of the undrained pore water pressure response (Δu) to a change in the confining pressure ($\Delta\sigma_r$);

$$B = \frac{\Delta u}{\Delta \sigma_r} \tag{3.1}$$

A stress increase of 50 kPa followed by a stress reduction by the same amount was typically used. For soft normally consolidated clays like reconstituted London Clay, B-values above 0.99 typically indicate full saturation, while for very stiff soils like undisturbed samples of London Clay B-values can be as low as 0.90 under fully saturated conditions, primarily as a result of the compressibility of the drainage system (Head, 1998).

Reconstituted samples

The B-values for the reconstituted samples of London Clay after preconsolidation in the consolidometer were consistently found to be around 0.87-0.90, which indicated a lack of full saturation. The samples were therefore initially saturated by the application of a back-pressure to force air bubbles into solution and at the same time by allowing a free flow of water into the sample. As a general procedure, the back-pressure and the cell pressure were increased simultaneously at a rate of 100 kPa/hr while keeping an effective stress of 10 kPa at all times. The back-pressure was raised to 300 kPa and the samples were then left overnight under high back-pressure and low effective stress to allow further flow of water into the sample. Typically, after 16 hours the volumetric flow into the sample was deemed insignificant and the B-value was checked again. After saturation, the reconstituted London Clay samples typically gave B-values close to 1, which indicated a satisfactory degree of saturation. During the remaining stages of the tests, the back-pressure level was maintained at 300 kPa under drained conditions to avoid the dissolved air coming out of solution again. The change in sample volume during saturation, as measured by the local strain gauges, was observed to be insignificant. This confirms that the flow of water into the sample during saturation simply replaced the air voids. Generally, similar procedures were used for the sample of kaolin.

Undisturbed samples

For simplicity, the heavily overconsolidated undisturbed samples of London Clay were subjected to combined isotropic compression and elevation of the back-pressure, since the main interest was placed in the shearing behaviour. After setup, the samples were rapidly compressed to an isotropic effective pressure of about 300 kPa, with an applied back-pressure of 300 kPa to improve saturation, the samples were then left to stabilise for up to 6 days. The volume change as measured by the local strain gauges during this procedure was minor. The B-values were

generally around 0.7 to 0.8 after the stabilisation period, which appeared to indicate a lack of full saturation, but it may also partly reflect the compressibility of the drainage system. If the tested samples were not fully saturated this would have influenced the pore water pressure response in the undrained test to some degree, while the results of the drained test would have been less affected.

e General testing

In the (UCL) triaxial tests several unconventional testing procedures were carried out in the test stages in order to investigate strain rate effects and influence of creep under drained and undrained conditions. After the initial saturation stage all samples were subjected to a combination of test stages which depended on the nature of the investigation. Only general testing procedures are described in this section, while further details are given in Chapters 4, 5 and 6, which report on the different studies.

Performed test stages included (carried out in no particular order);

- Isotropic compression and swelling at constant rate of confining stress (CRS*) or step-wise change in the rate of confining stress (SRS*).
- Drained or undrained shearing in extension or compression with step-wise change in strain rate (SRS).
- Resting stages at fixed axial strain (stress relaxation, SR) or fixed effective stress creep (C).

Isotropic compression was generally carried out under computer-controlled constant rates of confining stress which were slow enough to allow fully drained conditions. For the soft reconstituted samples the maximum rate of compression used was 3 kPa/hr. In tests where step changes in stress rate were performed to investigate the viscous behaviour during isotropic compression, the rates were changed by factors up to 10. Bender element testing was carried out at interval in Triaxial testing system no. 2 in addition to the static testing methods during all test stages of isotropic compression to determine the changes in elastic shear modulus. Section 4.2.2 gives details of the bender element testing procedures.

Shearing was performed under either fully drained or undrained conditions. Sufficient slow strain rates were chosen to avoid pore water pressure build up during the drained tests, while slightly higher strain rates were used in the undrained tests, where pore water pressure equalisation had to be considered. Generally, simple monotonic axial loading and unloading paths were performed with the confining pressure kept constant at the level reached in isotropic compression (generally σ_r= 600 kPa). In contrast to the isotropic compression, rather than using computer controlled shearing paths, shearing was carried out using the manually regulated motor-driven constant rate of strain pump. This was done in order to achieve a more accurate control of the imposed strain rates. Nevertheless, because of the compliance of the system, which also affected the external strain measurements as mentioned in Section 3.3.2e, the strain

rates experienced locally in the centre part of the sample differed from the nominal imposed rates.

f Data acquisition, data monitoring and data post processing

Continuous monitoring of calibrated and derived parameters from the transducer readings was carried out using the triaxial control program. In addition to monitoring the derived stress state in terms of deviator stress and mean effective stress, the monitored and recorded parameters were; axial stress, pore water pressure, radial confining stress, external axial strain, volumetric strain from pore water flow and calculated radial strain, local axial strains and local radial strain. The frequency of data recording was adjusted periodically to reflect the rates of change in the monitored parameters. During stages of high rates of change, the frequency of recording was increased to a maximum of one reading every 10 seconds, while the frequency of recording during long-term resting stages was decreased to a minimum of one reading every 2 hours. The maximum frequency of readings was primarily influenced by the processor speed and the specified long length of integration in the data-logger. During testing, the recorded data was continuously printed on paper and periodically stored onto a floppy disc. From the floppy disc, the data were progressively transferred to an EXCEL™ spreadsheet on a more powerful computer for further analysis and for monitoring of stress-strain behaviour.

3.4.4 (IIS) Triaxial tests on cement-mixed TA kaolin

The following testing procedures described below were adopted from Komoto (2004) with whom the author collaborated during a study visit in 2003 at IIS, Japan. Generally, samples were prepared and pre-compacted dry, then they were saturated at isotropic stress state at which point the hydration and curing of the cement commenced to create strong inter-particle cementation bonds. The samples were then subjected to a shearing program which investigated viscous and cementation effects.

a Pre-checks and initial setting up

Generally, a few days prior to testing the kaolin powder was oven-dried to remove any moisture, while the used cement was stored at room temperature. To supply the sample and drainage system with de-aired water, the water in the air-water interface chambers was de-aired by applying a vacuum to the chambers for more than 24 hrs. Then, just before testing, any water was removed from the drainage lines and porous discs by using an airgun, to avoid premature hydration of the cement. In order to determine the actual sample height when inserted into the cell, a dummy sample of 100 mm height was temporarily inserted into the inner frame, the top cap and loading piston were connected and the piston length outside the frame could then be recorded.

b Sample preparation and setting up

Approximately 250 g of kaolin were mixed thoroughly in a standard kitchen blender with 3 % cement. The soil-cement mix was then compacted by hand force into a split mould of 50 mm internal diameter in approximately 6-7 layers, using a metal rod and a thin OHP sheet as lining to ease removal of the sample after compaction. The lightly compacted sample in the mould was subsequently transferred to a bellofram-piston, where the sample was compressed further under a steady pressure. A high pressure of about 600 kPa was needed to make the dry density of the sample high enough to avoid a significant volume reduction upon saturation. Following compaction, the sample was strong enough to handle. The sample was then removed from the split mould, its dry weight was determined and the average diameter was measured using a Vernier calibre. The sample was placed on the pedestal in the inner frame along with top and bottom porous discs and filter papers. Using a suction mould the pre-cut membrane and radial filter paper were put around the sample and the membrane was sealed around the pedestal and top cap using 1cm wide elastic bands cut from spare parts of a membrane. After the sample had connected to the top cap and loading piston the initial sample height could be determined from measuring the piston length outside the frame.

c Saturation

Once the sample was in place, the outer cell chamber was tightened around the inner frame and filled with tap water to just above the top cap. A suction of about 90 kPa was then applied to both the top and bottom drainage lines for about 30 minutes to remove air from the sample. After dry recompression the sample height was determined and the sample was then slowly saturated by connecting an air-water interface with de-aired water under 90 kPa suction to the top and bottom drainage and placing it about 0.7 m above the cell. As the sample gradually saturated, the suction was gradually reduced in the air-water interface and the cell pressure was simultaneously increased to keep the effective isotropic stress at 100 kPa. Visual saturation was achieved in about 30 minutes, after which the cell pressure was increased to 300 kPa and the back-pressure was increased to 200 kPa manually, keeping the effective isotropic stress at 100 kPa. To outbalance the lack of cell pressure over the area of the piston, dead weights were added on top of the piston. After an hour, the rate of compression was observed to be minor. The process of saturation is shown in Figure 3-14.

In order to measure the sample dimensions after saturation, 90 kPa suction was temporarily applied to the drainage system, the cell pressure was reduced to 0 kPa and the outer cell was removed to allow direct measurements of the sample diameter using a Vernier calibre. Then the cell pressure was returned to 300 kPa and the back-pressure was returned to 200 kPa, at which point the degree of saturation was checked. A single undrained excursion of 50 kPa increase in cell pressure was applied to determine the B-value. Approximately two hours after start of saturation and start of curing the sample was ready for shearing. The above procedure,

which involves saturation at isotropic stress conditions, was followed for the majority of the tested samples. However, a couple of samples were saturated under a deviator stress. In these cases, dead weights were used to step load the sample to the required deviator stress, before the saturation took place.

d Setup prior to shearing

Before the start of shearing the triaxial control and monitoring software were engaged, the calibration factors were checked and the pre-determined shearing program was loaded. In the shearing program, constant rate of strain or constant rate of stress control was specified at desired rates over a number of desired intervals in strain or stress. To engage the axial loading system, the cell was transferred to the motor driven loading frame and the internal load cell and displacement transducers were connected to the data-logger. Then the top and bottom drainage were connected up to the back pressurised volume gauge to monitor the volume change, and the cell pressure line and back-pressure lines were connected to the differential pressure gauge to monitor the "effective cell pressure". At all times care was taken not to trap air in the water pressure lines. The remaining instrumentation, being the dial gauge and gap sensor (if present), were fixed and adjusted. Finally, all strain gauges were re-zeroed, the computer controlled motor servo system was switched on and the computer controlled shearing program was engaged.

e Shearing and creep stages

In the (IIS) triaxial tests, several unconventional test stages were performed in order to investigate viscous and cementation effects under drained conditions. Generally, depending on the nature of investigation, one or several of the following test stages were performed in each test. Only general testing procedures are described in this section, while further details are given in Section 6.2 which report on the study on cement-mixed kaolin.

The performed test stages included:

- Initial curing at isotropic or anisotropic stress state, as described in Section c above.
- Shearing in compression at constant rate of strain (CRS).
- Shearing in compression with step-wise change in strain rate (SRS).
- Small unload-reload cycles during shearing to determine the small strain stiffness.
- Resting stages with fixed effective stress creep (C).

Shearing was generally carried out under drained conditions with two-way drainage and no measurement of pore water pressure. However, to investigate if full drainage was generally achieved, one sample was sheared allowing only bottom drainage, while pore water pressure measurements were taken from the top of the sample. This test confirmed that full drainage could generally be assumed. Generally, simple monotonic axial loading and unloading paths were performed with the effective confining pressure kept constant (generally σ'_r= 100 kPa). Constant rate of straining was carried out at rates varying between 0.078 %/hr and 2.6 %/hr,

while in tests where step changes in strain rate were performed to investigate viscous effects, the rates were changed step-wise by factors between 4 and 33. Additionally, several small unload-reload cycles with a magnitude of about 0.02 % change in axial strain were performed during shearing to assess the small strain stiffness properties of the sample. For some of the tests with a creep stage planned under constant deviator stress, the following special testing procedure was carried out. After reaching the creep stress, the load piston was temporarily clamped in place. The cell was then taken out of the loading frame, dead weights were added on top of the piston to give the wanted deviator stress and the clamp was then released. This was done to free up the loading frame for use with either of the two other cells. After the creep stage, the piston was once again temporarily clamped in place, the dead weights were removed and the cell was transferred to the loading frame. Once in the loading frame the given deviator stress was applied and the clamp could then be released after which the shearing program resumed. Creep stages were maintained at different deviator stresses close to the failure stress for periods with varying length up to 9 days.

f Data acquisition, data monitoring and data post processing

A triaxial control program developed at the University of Tokyo was used for continuous monitoring of calibrated and derived parameters from the transducer readings in both numerical and graphical format. Both transducer output voltages and derived parameter such as total stresses, effective stresses and strains were recorded and continuously stored in separate files on the computer's hard drive. It was generally only possible to adjust the frequency of recording at the beginning of each stage of the test, which meant that a huge amount of data was collected to ensure a high enough sampling rate when the rates of change in stress were high, for example at the start of shearing or after step changes in strain rate. The frequency of recording used was up to a maximum of one reading every 5 seconds. After testing, the recorded data were transferred to an EXCEL™ spreadsheet for further analysis.

3.5 THEORETICAL FRAMEWORK

3.5.1 Generally on the determination of effective stresses and void ratio

In both the oedometer and triaxial cell the stress-strain conditions are at all times assumed to be axi-symmetric and the principle of effective stresses is applied, since testing was carried out on nominally fully saturated samples. Hence, the two effective principal stresses, σ'_1 and σ'_2, can be derived from;

$$\sigma'_i = \sigma_i - u_{avr} \quad , i = 1, 2 \tag{3.2}$$

where σ_i, represents total principal stresses and u_{avr} is the average pore water pressure in the sample. In the (UCL) oedometer cell the total vertical stress is the only principal stress known, while the triaxial cell allows determination of both total axial and radial stresses. In both apparatuses measurements of pore water pressure allows effective stresses to be derived. In the oedometer cell however the two principal strains are determinable (the radial strain always being equal to zero), while in the triaxial cell the same is only possible if a radial strain belt is used, as in the case of the (UCL) triaxial cells. Without the measurement of radial strains, only the axial strains are known, as in the case of the (IIS) triaxial cell.

Generally, the current void ratio in the sample, e, is derived from the initial void ratio, e_0, and the volumetric strain, ε_v

$$e = e_0 - (1 + e_0) \cdot \varepsilon_v \tag{3.3}$$

It is usual practise to derive the initial void ratio at the start of compression from the average of one or several values found from the following four methods:

I. From initial water content, w_0, assuming full saturation;

$$e_0 = w_0 \cdot G_s \tag{3.4}$$

where G_s is the specific gravity of the solids. The accuracy of this method heavily relies on having close to full saturation, which for undisturbed stiff triaxial samples of London clay and oedometer samples was found to be difficult to achieve.

II. From initial dimensions and initial solid weight;

$$e_0 = \frac{V_v}{V_s} = \frac{V_T}{V_s} - 1 = H_0 \cdot A_0 \cdot \frac{G_s \cdot \rho_w}{\frac{m_{T,0}}{w_0 + 1}} - 1 \tag{3.5}$$

where V_T, V_v and V_s are the initial total volume, volume of voids and volume of solids respectively, H_0 and A_0 are the initial height and area of the sample respectively, while ρ_w is the density of water and $m_{T,0}$ is the total initial weight of the sample. The accuracy of this method relies on accurate determination of the initial total sample volume, which has proven difficult to obtain for the hand trimmed undisturbed samples of London Clay.

III. From final water content, w_f, at the end of testing assuming full saturation;

$$e_f = w_f \cdot G_s = e_0 - (1 + e_0) \cdot \varepsilon_{v,f} \tag{3.6}$$

where $\varepsilon_{v,f}$ is the final volumetric strain. This method relies on quick removal of the sample from the lower porous discs after complete unloading and dissipation of excess pore water pressures, to avoid further swelling and ingress of water. The final water content is determined from either part or the whole of the extracted sample by the method of oven drying.

IV. From final dimensions and initial solid weight;

$$e_f = H_f \cdot A_f \cdot \frac{\frac{G_s \cdot \rho_w}{m_{T,0}}}{w_0 + 1} - 1 = e_0 - (1 + e_0) \cdot \varepsilon_{v,f} \tag{3.7}$$

where H_f and A_f are the final measured height and area of the sample. For reconstituted samples in both the oedometer and triaxial cell this method was generally found to be too unreliable, primarily because the softness of the sample after complete unloading and swelling made it very difficult to obtain an accurate measure of sample height. Moreover, due to barrelling and possible single plane slip, the average cross-sectional area of the triaxial sample was also very difficult to determine accurately.

3.5.2 Specific for (UCL) oedometer tests

a Determination of void ratio

In the oedometer the initial sample height and diameter were determined from the inner dimensions of the confining ring, and the initial total weight of the sample was determined from the weight of the soil gone into preparing the sample. The initial water content was generally determined from part of the remaining soil used in the sample preparation by the method of oven drying. Despite an expected low initial saturation, the initial void ratio determined from initial dimensions and initial solid weight was found to correspond very well with the void ratio determined from initial water content assuming full saturation (usually within 0.02). Slightly more discrepancy was found if the initial void ratio was back-calculated from the final water content (difference was typically between 0.02 and 0.10). In the analysis, the main interest lies in the post-yield compression behaviour at higher stresses. It has therefore been chosen to use the void ratio back-calculated from the final water content as given in Equation (3.6), which also appeared to give the most consistent results between individual tests. During the tests, the change in void ratio has been determined from the measured volumetric change of the sample.

b Determination of stresses and strains

In the oedometer test, a flat cylindrical sample is compressed by applying a total vertical stress, σ_v, at the top of the sample. The rigid confining ring prevents the sample from deforming in the lateral directions and compression is therefore only one-dimensional. The total vertical stress acting at the top of the sample was derived from the sum of the load, F_{dwh}, transferred to the top

cap from the dead weight hanger via the 11:1 ratio lever arm, and the load, F_p, applied directly via the loading piston as measured by the load cell;

$$\sigma_v = \frac{F_{dwh} + F_p}{A} = \frac{(w_{dw} \cdot R) + F_p}{A} \tag{3.8}$$

where w_{dw} is the total dead weight on the hanger, R is the lever arm ratio and A is the cross-sectional area of the sample.

In the (UCL) oedometer cell, the top cap worked as the only drainage boundary, while pore water pressure was measured at the base. In the further analysis the average pore water pressure has, as a good approximation, been assumed to be equal to half of the measured pressure at the base;

$$u_{avr} = \frac{u_{base}}{2} \tag{3.9}$$

This assumption may have lead to a slight overestimation of the effective stresses, because of the curved nature of the actual pore water pressure profile through the sample, as illustrated in Figure 3-15.

Unfortunately, it has not been possible to introduce lateral stress measurements in the oedometer, which would have enabled determination of the complete stress state of the sample in terms of deviatoric stress, q, and mean effective stress, p'. The stress state will therefore be characterised only by the vertical effective stress, σ'_v, and the corresponding vertical (axial) strain, ε_a. It should be noted that since radial straining was prevented, the cross-sectional area stayed constant and the volumetric strain, ε_v therefore equals the axial strain.

$$\varepsilon_v = \varepsilon_a \tag{3.10}$$

c Sources of error and corrections of results

Since, the (UCL) Oedometer apparatus had not incorporated a back-pressure system, full saturation of the sample was practically impossible to achieve during testing. A lack of full saturation and possible presence of air in the drainage system would both result in erroneous measurements of the pore water pressure response in partially drained conditions in the oedometer, which meant that the theory of effective stress was strictly only valid when the pore water pressures throughout the sample equalled the atmospheric pressure.

Though side friction from the confining ring is believed to have had a significant influence in the *40 mm* oedometer cell, it has not been possible to correct for this, since it was not measured. With a fixed rigid confining ring, all of the developed side friction would have acted against the applied vertical stress and would hence have lead to a concentration of load at the edges of the sample. The sample would therefore experience an average effective stress, which would be less than what is assumed in the analysis. Using both bottom and top load cells Lohani et al. (2001) showed that the average effective stress in a sample of clay of 40 mm height to be typically 10-17 % smaller than the stress applied at the top, due to side friction.

However, the small height to diameter ratio of the confining ring means that stress non-uniformities would only have been significant right at the edges, while they would be insignificant in the majority of the sample. No correction has been applied to compensate for the compliance of the loading system. The vertical deformation may therefore be slightly overestimated at the start of the test, however as large deformation took place as the sample consolidated under increasing pressures, the errors associated with the compliance are likely to be negligible over the majority of the tested stress range.

3.5.3 Specific for (UCL) triaxial tests

a Determination of void ratio

In the (UCL) triaxial tests, the initial sample diameter and height of each undisturbed sample were determined from direct measurements using a Vernier calibre, while the diameter of reconstituted samples was determined from the inner diameter of the consolidometer. The initial total weight of the sample was measured in the split mould. In the triaxial tests, where the sample was initially saturated by increasing the back-pressure and allowing a flow of water into the sample, the water content before compression and after saturation is given by;

$$w_{sat} = w_0 + \Delta w = w_0 + \left(\frac{\Delta V_{sat} \cdot \rho_w}{\frac{m_{T,0}}{w_0 + 1}} \right) \tag{3.11}$$

where Δw is the increase in water content stemming from the measured volume of water flowing into the sample during saturation, ΔV_{sat}. The initial void ratio after saturation can then be determined from;

$$e_0 = w_{sat} \cdot G_s \tag{3.12}$$

However, for the reconstituted samples the initial void ratio, e_0, after saturation and at the start of compression has generally been determined from the calculated dimensions after saturation and the initial solid weight as given by Equation (3.5), which gives void ratios very close to those determined using Equation (3.12). The calculated saturation was therefore generally 1.0. The void ratio at the start of shearing was then determined from the flow of water out of the sample during compression. For the undisturbed samples, despite the measured B-values after saturation and recompression were generally quite low and trimming of the samples gave some uncertainties in the initial measured dimensions, the initial void ratio at start of shearing was based on either the initial dimensions of the sample or the initial water content depending on which showed the most realistic values.

b Determination of stresses, strains and stiffness

In the triaxial cell, a cylindrical sample with a height to diameter ratio of 2:1 is separated from the cell water by a thin membrane. The cell pressure applies an all-round total radial pressure, σ_r,

on the sample, while the total axial pressure, σ_a, is equal to the sum of the cell pressure and the pressure supplied by the loading piston, as measured by the internal load cell.

$$\sigma_a = \sigma_r + \frac{F}{A} \tag{3.13}$$

where A is the current effective cross-sectional sample area over which the force, F, acts through the load cell. Since radial drains were used on the sample, the pore water pressure in the sample is assumed to be uniformly distributed in the longitudinal direction at all times and the average pore water pressure is assumed equal to the pressure measured through the base outlet.

$$u_{avr} = u_{base} \tag{3.14}$$

For axi-symmetric stress-strain conditions in the triaxial cell, stresses are expressed in terms of the deviator stress, q and the mean effective stress, p', which are given by

$$q = \sigma_a - \sigma_r = \sigma'_a - \sigma'_r \tag{3.15}$$

$$p' = \frac{1}{3}(\sigma_a + 2\sigma_r) - u_{avr} = \frac{1}{3}(\sigma'_a + 2\sigma'_r) \tag{3.16}$$

where σ'_a and σ'_r are the axial and radial effective stresses acting on the sample. Deformation is expressed in terms of the corresponding deviatoric strain, ε_s, and volumetric strain, ε_v. The deviatoric strain is defined as;

$$\varepsilon_s = \frac{2(\varepsilon_a - \varepsilon_r)}{3} \tag{3.17}$$

where ε_a and ε_r are the local axial strain and radial strains respectively. While the volumetric strain is found directly from the flow of water from the sample as recorded by the volume gauge;

$$\varepsilon_v = -\frac{\Delta V}{V_0} \tag{3.18}$$

where V_0 is the initial total sample volume and ΔV is the volume change measured by the volume gauge. The volumetric strain can also be determined from the local axial and radial strains assuming the sample keeps it cylindrical shape during deformation;

$$\varepsilon_v = \varepsilon_a + 2\varepsilon_r \tag{3.19}$$

However, this assumption is only valid at smaller strains, where the effect of bulging is insignificant. Nevertheless, upon strain rate changes at small to large strains the immediate volumetric response calculated from the local strains is believed to be more accurate than the measurements from the volume gauge, primarily because air in the drainage system could give rise to a slow response in the measurement of pore water flow.

The soil stiffness will generally be expressed in terms of the shear modulus, G′;

$$G' = G_u = \frac{\Delta q}{3\Delta\varepsilon_s} \tag{3.20}$$

however in cases where the radial strain measurements are deemed unreliable the soil stiffness will be expressed in terms of the effective Young's modulus, E′ for drained conditions;

$$E' = \frac{\Delta\sigma'_a}{\Delta\varepsilon_a} \tag{3.21}$$

and undrained Young's modulus E_u for undrained conditions;

$$E_u = \frac{\Delta\sigma_a}{\Delta\varepsilon_a} \tag{3.22}$$

c Sources of error and corrections of results

It was not considered necessary to make any corrections to the axial load measurements. Firstly, the use of internal load cell eliminated the effect of friction between piston and cell bush, while corrections for membrane flexibility and side drain were not applied, as these were considered insignificant during shearing. For a 38 mm diameter sample Head (1998) estimated the correction in deviator stress due to side drains to be approximately 0.5 kPa for every 0.1 % strain up to 2 % and then to remain constant at roughly 10 kPa. The membrane correction due to barrelling was suggested to be approximately 0.1 kPa for every 1 % strain, which is insignificant. The compliance of the loading system was checked using a hard rock dummy sample and found to be in the order of 0.0005 %/kPa increase in the axial pressure. The results are generally not affected by the compliance, since local strain measurements have been utilised at small strains.

The cross-sectional area of the sample has been corrected for barrelling assuming the sample deforms as a right cylinder. The area correction is given by;

For drained conditions:
$$A = A_0 \frac{(1-\varepsilon_v)}{(1-\varepsilon_a)} \tag{3.23}$$

For undrained conditions:
$$A = \frac{A_0}{(1-\varepsilon_a)} \tag{3.24}$$

The undisturbed overconsolidated samples were additionally influenced by the development of shear bands, which had an increasing significance post-peak. However, no area correction has been made for single-plane slip, and hence the deviator stress could possibly be underestimated post-peak. The normally consolidated reconstituted samples were not affected due to their strain-hardening behaviour.

The drainage system showed significant volumetric compression during saturation when the back-pressure was raised, primarily because of the presence of air. Hence, before the start of each test, the volumetric compression of the drainage system was checked and a correction has been applied to the measured volumetric strain during saturation. The correction was generally found to be in the order of $\Delta\varepsilon_v = -0.001\%$ *per kPa* increase in the back-pressure for Triaxial cell no. 1, while the correction was found to be about an order of magnitude higher for Triaxial cell no. 2.

Local measurement of strain is preferred when high precision is required in the very small strain range, mainly because the effects of seating errors, alignment errors, bedding errors and

compliance of the loading system can be avoided. Bedding errors were expected to be most pronounced in tests on undisturbed samples, where non-perfect trimming of the sample ends has had an influence. Bedding errors at the start of shearing should have been minor for reconstituted samples, which had already experienced isotropic compression to high strains. For reconstituted samples at higher strains near failure the barrelling of the sample typically affected the local axial strain gauges too much and generally the external strain measurements were then preferred. For undisturbed samples, the development of slip planes at peak stress state significantly affected the local strain measurements, which then became unreliable. The external strain measurements were less affected and these were relied upon for characterising the post-peak stress-strain behaviour.

3.5.4 Specific for (IIS) triaxial tests

a Determination of void ratio

In the (IIS) triaxial test the initial sample diameter and height of each sample prior to compression were determined from direct measurements using a Vernier calibre after initial saturation. The initial void ratio, e_0, after saturation and at the start of compression was determined from the calculated dimensions after saturation and the initial solid weight. Due mainly to the nature of sample preparation, full saturation was not possible to achieve and hence volumetric strains measured in the tests are not believed to be very accurate. Therefore, the change in voids ratio during the tests cannot be determined accurately either.

b Determination of stresses and strains

The effective stresses and strains in the (IIS) triaxial cell are determined in the same way as mentioned in Section 3.5.3b for the (UCL) triaxial cell with the only difference that in the (IIS) Triaxial apparatus only external axial deformation and volume change are measured. This means that the radial strains and hence the deviatoric strains has to be derived from the external volumetric and axial strains. However, since radial strains are limited in the stiff cemented soil the axial strain is believed to give a good representation of the deviatoric strain. Consequently, in this analysis the deviator stress is plotted against the axial strain and the soil stiffness will be expressed in terms of the effective Young's modulus, E′.

c Sources of error and corrections of results

For the same reasons as mentioned in Section 3.5.3c for the (UCL) triaxial testing, no corrections have been made for side drains and membrane flexibility. The system compliance was not checked in the (IIS) triaxial cell, for this reason the reported external axial strains will be slightly overestimated, meaning that the determined small strain stiffness may be underestimated. Additionally, no correction has been applied for the compressibility of the drainage system. The use of an internal load cell eliminated the effect of friction between piston and cell bush and no further corrections have been applied to the measurement of axial force.

For all test the cross-sectional area of the sample has been corrected for the effect of barrelling due to axial compression, which however will not be very significant due to the relatively high stiffness and brittleness of the cemented clay samples. Area correction for single plane slip conditions has not been applied.

The performed tests may have experienced problems with dissolved air in the cell water and drainage systems, since the used air-water interface systems were not sealed from the air. Air in the drainage system may have given rise to unreliable volume change measurements in the performed drained tests and these have generally not been relied upon. Similarly, dissolved air in the cell water may readily have penetrated the membrane surrounding the sample, however as the tests were generally performed under drained conditions this should not have affected the results significantly.

3.5.5 Bender element tests

a Determination of elastic shear modulus

Using the techniques and interpretation methods described in Section 4.2.2. the velocity of the transmitted shear wave propagating though the soil is determined. The elastic shear stiffness of the soil, G_{max} (or G_0) is then simply related to the velocity of the propagating shear wave, V_s, by;

$$G_{\max} = \rho V_s^2 = \rho\left(\frac{L}{T}\right)^2 \tag{3.25}$$

where L is the tip-to-tip travel distance, T is the travel time and ρ is the total density of the soil, given by;

$$\rho = \rho_w\left(\frac{G_s + e}{1+e}\right) \tag{3.26}$$

where ρ_w is the density of water. (Dyvik & Madshus, 1985) estimated the maximum shear strain associated with bender element tests to be less than 10^{-3} %, and the determined shear modulus is therefore believed to be the maximum elastic shear stiffness of the soil structure, which is associated with very small strains (Atkinson, 2000). (Rio, 2005) on the other hand showed, using a laser velocitymeter, the maximum movement of the tip of the bender element in free air to be in the order of 40 μm. If similar magnitude of movement is experienced when the bender element is placed within the soil sample, than the radial strain at the bender element tip would be in the order of $2 \cdot 10^{-1}$ % for a 38mm diameter sample, which is well outside the expected elastic range. However, the maximum movement experienced within the soil is expected to rapidly attenuate as the shear wave propagates through the sample. The attenuation of the shear wave amplitude is among other factors the reason why the measured output signal voltage is seen to be 2 to 3 orders of magnitude smaller than the voltage of the input signal, as illustrated from the results in Chapter 4.

3.6 TABLES AND FIGURES FOR CHAPTER 3

Table 3-1 Geotechnical index properties of testing materials

Material	w_p [%]	w_L [%]	PI [%]	G_s [g/cm^3]	CF [%]
Speswhite Kaolin[6]	35	65	30	2.68	~100
TA Kaolin[7]	21	46	25	2.68	~100
London Clay[8] average	28	65	37	(2.65-2.76) 2.73	54

Table 3-2 Properties of Rapid Hardening Portland cement (after Tennis, 1998)

G_{cement} [g/cm^3]	Initial setting time [hr-min]	Percent of 28-day strength			
		1 day	3 day	7 day	28 day
3.13	1-55	47	69	83	100

Table 3-3 Characteristics of (UCL) oedometer transducers and signal conditioning

Transducer	Type	Capacity	Resolution	Excitation [V]	Signal output range [V]
Dial gauge	WF John Bull	10 [mm]	0.002 [mm]	-	-
LVDT	RDP D5/200H	10 [mm]	0.001[mm]	5	-1.45 to 1.45[a]
Load cell	N.C.B./M.R.E. type 403	20 [kN]	1 [kPa]	10	0 to 0.2[a]
Pore pressure transducer	WF17060	1000 [kPa]	1 [kPa]	10	0 to 0.1

[a] Amplified

Table 3-4 Calibration factors for (UCL) oedometer transducers

Transducer	Calibration factor	Coefficient of correlation r^2
LVDT	-0.003545 [mm/mV]	0.99991
Load cell	-0.0977 [kN/mV]	0.99999
Pore pressure transducer	-9.87 [kPa/mV]	0.99999

[6] After Atkinson et al. (1987)

[7] After Komoto (2004)

[8] After Gasparre (2005) for geological sub-unit $B_{2(b)}$, obtained at T5 site

Table 3-5 Characteristics of transducers and signal conditioning used in (UCL) Triaxial system no. 1

Tranducer	Type	Capacity	Resolution	Excitation [V]	Signal output range [V]
External axial LVDT	RDP LDC500A	25 [mm]	4 [μm] 0.005 [%] strain	9.90	-2.2 to 2.2 [a]
Volume gauge LVDT	RDP LDC500A	25 [mm] 50 [cm^3]	4 [μm] 0.005 [%] strain	9.90	-2.2 to 2.2 [a]
Local axial LVDT 1	RDP D5/200WRA	10 [mm]	0.16 [μm] 0.0002 [%] strain	9.90	-3.3 to 4.5 [b]
Local axial LVDT 2	RDP D5/200WRA	10 [mm]	0.16 [μm] 0.0002 [%] strain	9.90	-3.2 to 4.4 [b]
Local radial LVDT	RDP D5/200WRA	10 [mm][1] 3.8 [mm][2]	0.16 [μm] 0.0002 [%] strain	9.90	-3.4 to 4.2 [b]
Internal load cell	WF STALC3	5 [kN]	0.1 [kPa]	9.90	0 to 3.0 [b]
Cell pressure transducer	WF17060	1000 [kPa]	0.1 [kPa]	9.90	0 to 0.1
Pore pressure transducer	WF17060	1000 [kPa]	0.1 [kPa]	9.90	0 to 0.1

[a] built-in amplification, [b] amplified with separate amplifier before reaching spectra box, [1] direct LVDT capacity, [2] radial belt effective capacity

Table 3-6 Calibration factors for transducers in (UCL) Triaxial system no. 1

Tranducer	Calibration factor	Coefficient of correlation r^2
External axial LVDT	175.6 [mm/mV]	0.99998
Volume gauge LVDT	-99.20 [cc/mV]	0.99994
Local axial LVDT 1	804.9 [mm/mV]	0.99997
Local axial LVDT 2	828.0 [mm/mV]	0.99994
Local radial LVDT belt	1994 [mm/mV]	0.996 [a] (0.99994) [b]
Internal load cell	608.2 [kPa/mV]	0.99999
Cell pressure transducer	0.1019 [kPa/mV]	0.99999
Pore pressure transducer	-0.09951 [kPa/mV]	0.99999

[a] calibration of radial belt using dummy sample

[b] direct calibration of LVDT

Table 3-7 Characteristics of transducers and signal conditioning used in (UCL) Triaxial system no. 2

Transducer	Type	Capacity	Resolution	Excitation [V]	Signal output range [kbits]
External axial LVDT	RDP LDC500A	25 [mm]	4 [μm] 0.005 [%] strain	9.90	-8.0 to 6.5 [a]
Volume gauge LVDT	RDP LDC500A	25 [mm] 50 [cm^3]	4 [μm] 0.005 [%] strain	9.90	-7.0 to 7.0 [a]
Axial Hall Effect transducer 1	Cambridge type	5 [mm]	4 [μm] 0.005 [%] strain	9.90	-2.1 to 2.4
Axial Hall Effect transducer 2	Cambridge type	5 [mm]	4 [μm] 0.005 [%] strain	9.90	-2.1 to 2.4
Radial Hall Effect transducer	Cambridge type	5 [mm][1] 2.4 [mm][2]	4 [μm] 0.005 [%] strain	9.90	-2.1 to 2.4
Internal load cell	WF STALC3	3 [kN]	0.1 [kPa]	9.90	0 to 3.0 [b]
Cell pressure transducer	WF17060	1000 [kPa]	0.1 [kPa]	9.90	0 to 0.1
Pore pressure transducer	WF17060	1000 [kPa]	0.1 [kPa]	9.90	0 to 0.1

[a] built-in amplification, [b] amplified with separate amplifier before reaching the PC interface datalogger card, [1] direct Hall Effect transducer capacity, [2] radial belt effective capacity

Table 3-8 Calibration factors for transducers in (UCL) Triaxial system no. 2

Transducer	Calibration factor	Coefficient of correlation r^2
External axial LVDT	-584.1 [mm/bit]	0.99997
Volume gauge LVDT	-309.8 [cc/bit]	0.9998
Axial Hall Effect transducer 1	-826.5 [mm/bit]	0.99997
Axial Hall Effect transducer 2	-847.3 [mm/bit]	0.9997
Radial Hall Effect transducer belt	-1858.5 [mm/bit]	0.99994 [a]
Internal load cell	-1969.1 [kPa/bit]	0.99999
Cell pressure transducer	-0.3269 [kPa/bit]	0.99994
Pore pressure transducer	-0.3265 [kPa/bit]	0.99998

[a] calibration of radial belt using dummy sample

Table 3-9 Characteristics of (IIS) transducers

Transducer	Type	Capacity	Excitation [V]
External axial displacement transducer	NEC 9E08-D1-20	20 [mm]	10.0
Proximity transducer	in-house made	2 [mm]	10.0
Low capacity differential transducer for volume change	FFF36WB	50 [cm^3]	10.0
External load cell	?	2.0 [kN]	10.0
Internal load cell	in-house made	4.9 [kN]	10.0
High capacity differential transducer for effective cell pressure	FFF36WB	600 [kPa]	10.0

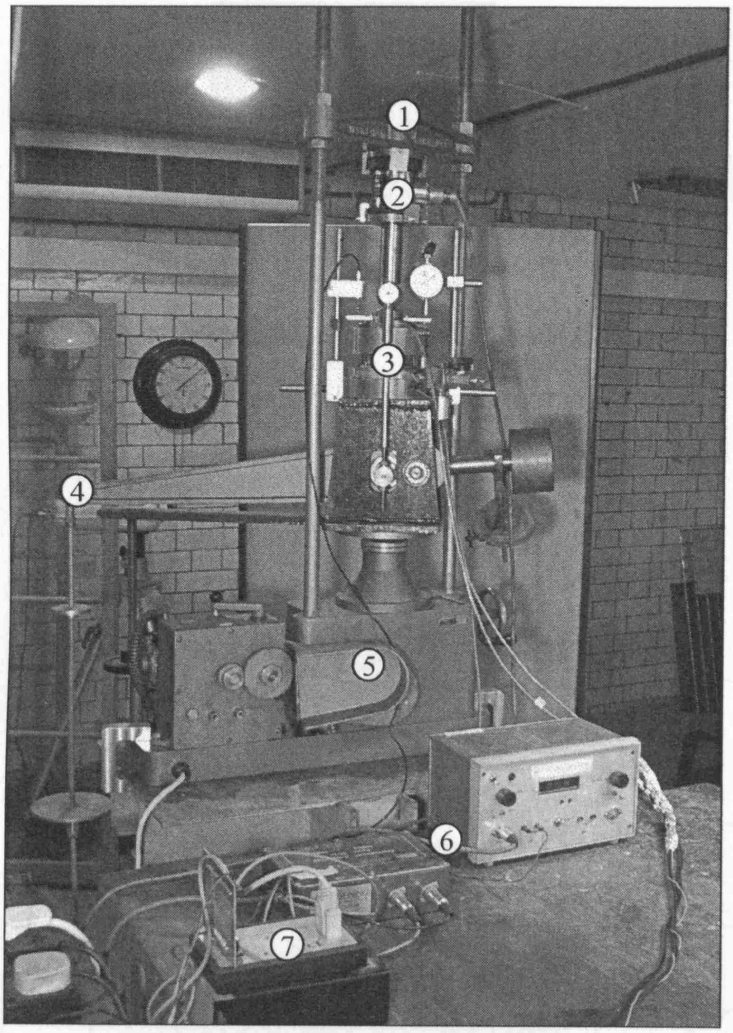

(1) Load frame

(2) Load cell

(3) Oedometer cell

(4) Lever arm and dead weight hanger

(5) CRS loading machine

(6) Amplifiers for LVDT and load cell

(7) Pico datalogger

Figure 3-1 (UCL) oedometer testing system setup

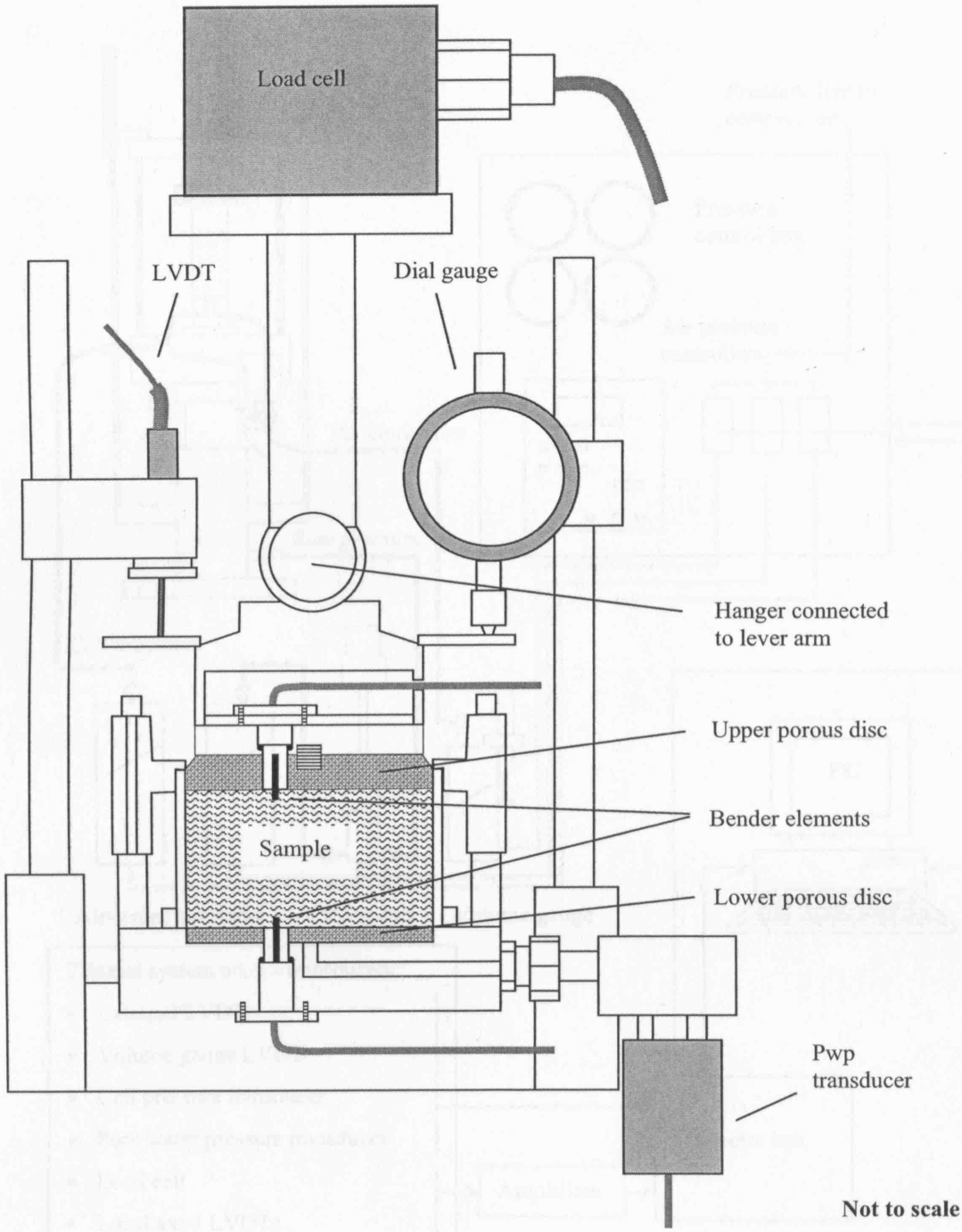

Figure 3-2 Schematic layout of (UCL) oedometer cell

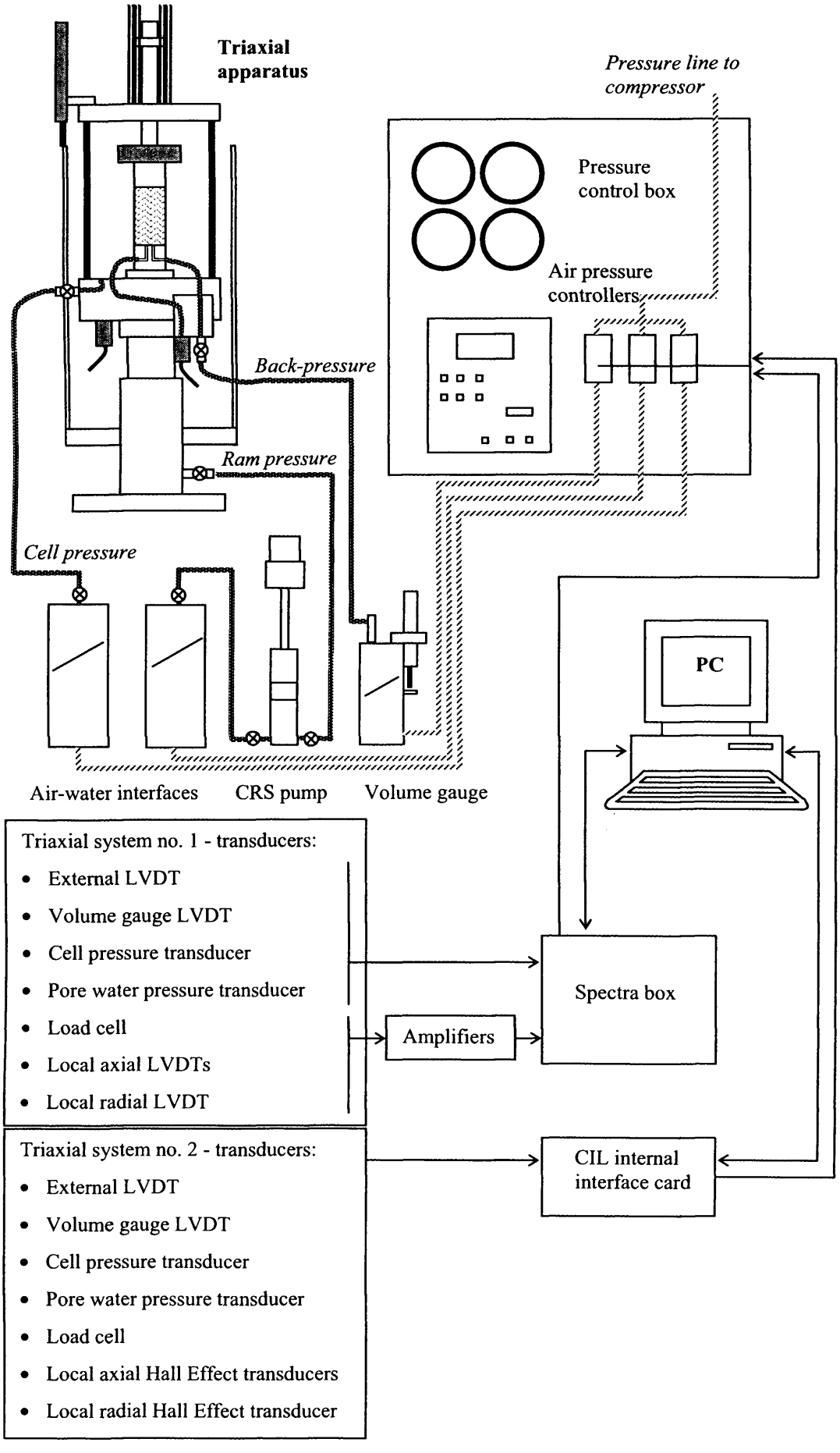

Figure 3-3 Schematic layout of (UCL) triaxial testing systems

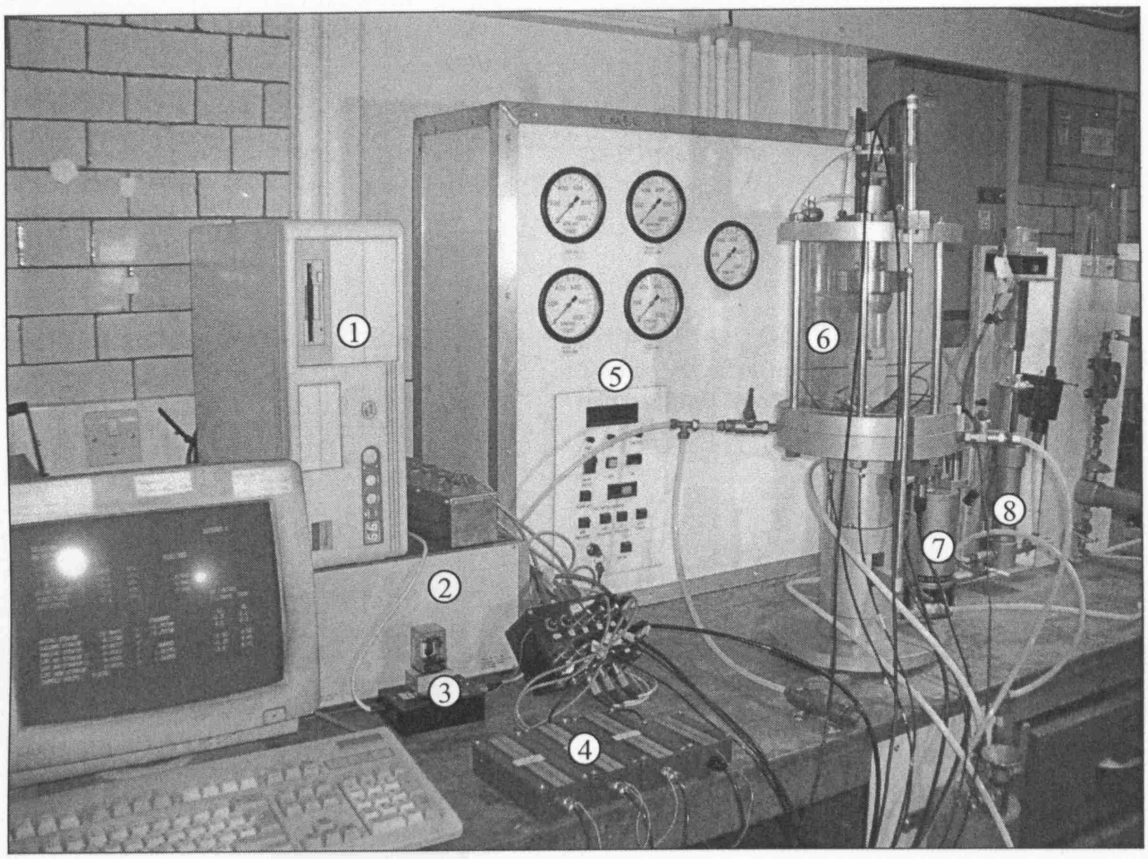

(1) PC

(2) Spectra datalogger box

(3) Clicker-box

(4) Amplifiers for local LVDTs and internal load cell

(5) Pressure control box

(6) Triaxial cell

(7) Volume gauge

(8) CRS pump

Figure 3-4 (UCL) triaxial system setup

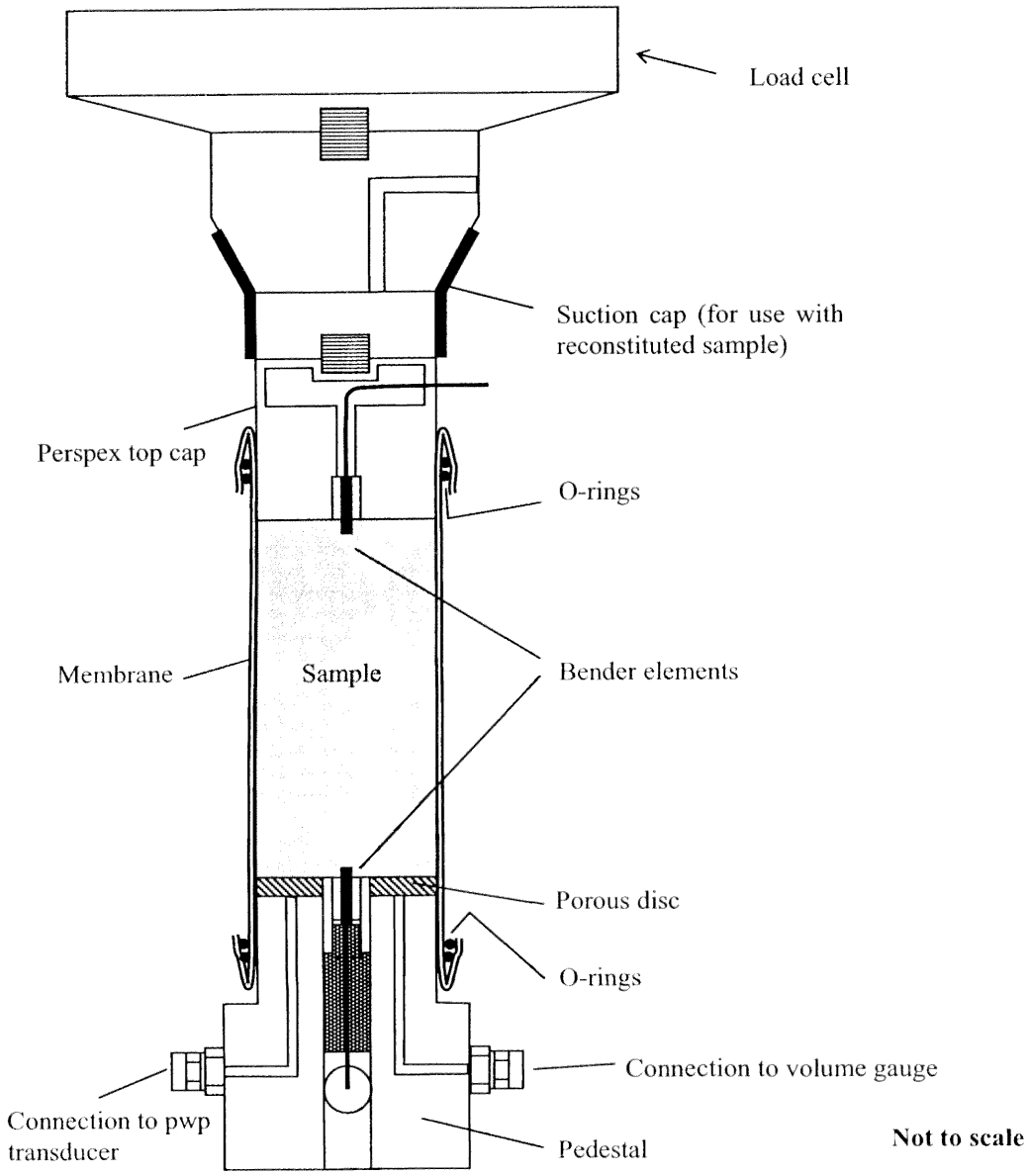

Figure 3-5 Schematic representation of sample setup in (UCL) Triaxial cell no. 2

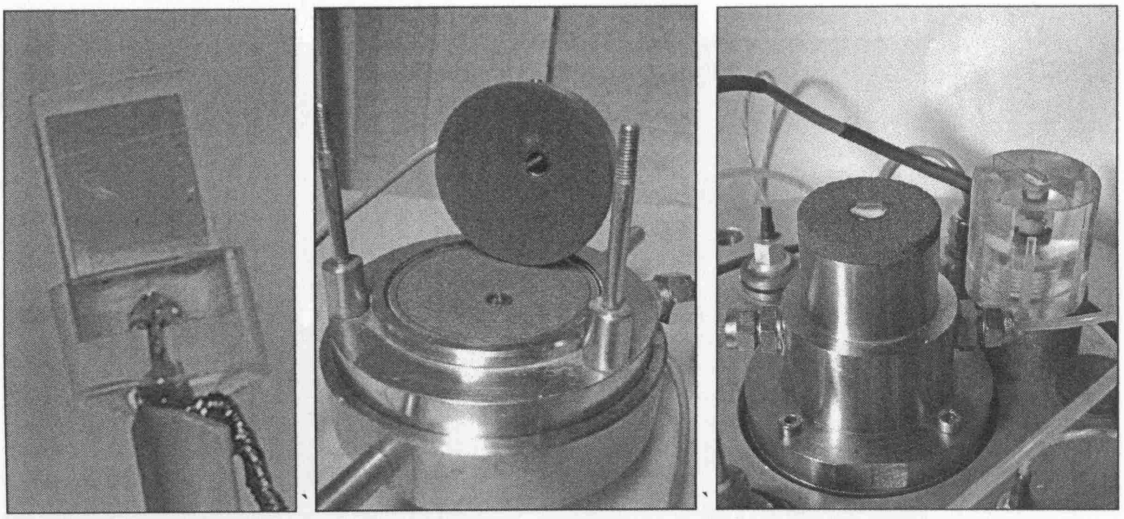

a) Free single (UCL) bender element

b) Bender element setup in (UCL) oedometer cell

c) Bender element setup in (UCL) Triaxial cell no. 2

Figure 3-6 Details of (UCL) bender elements

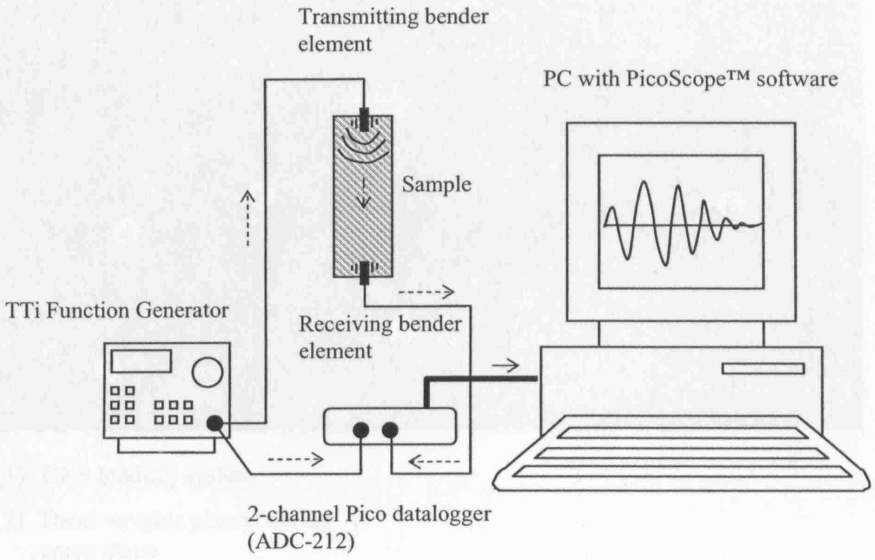

Figure 3-7 Schematic layout of (UCL) bender element testing system

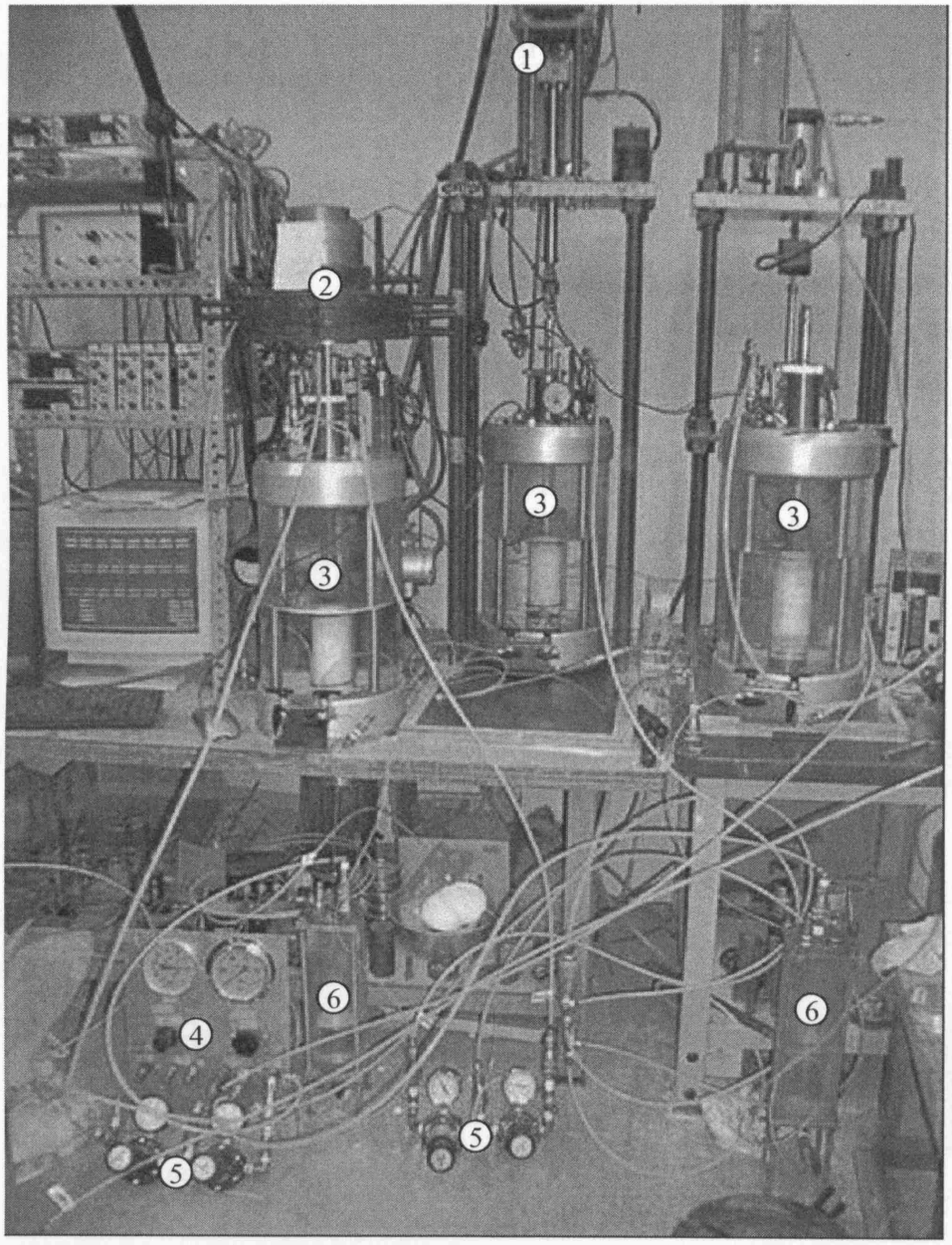

(1) CRS loading system

(2) Dead weights placed during creep stage

(3) Triaxial cell

(4) Vacuum supply regulator

(5) Twin-air-pressure-controllers

(6) Air-water interface

Figure 3-8 (IIS) triaxial system setup

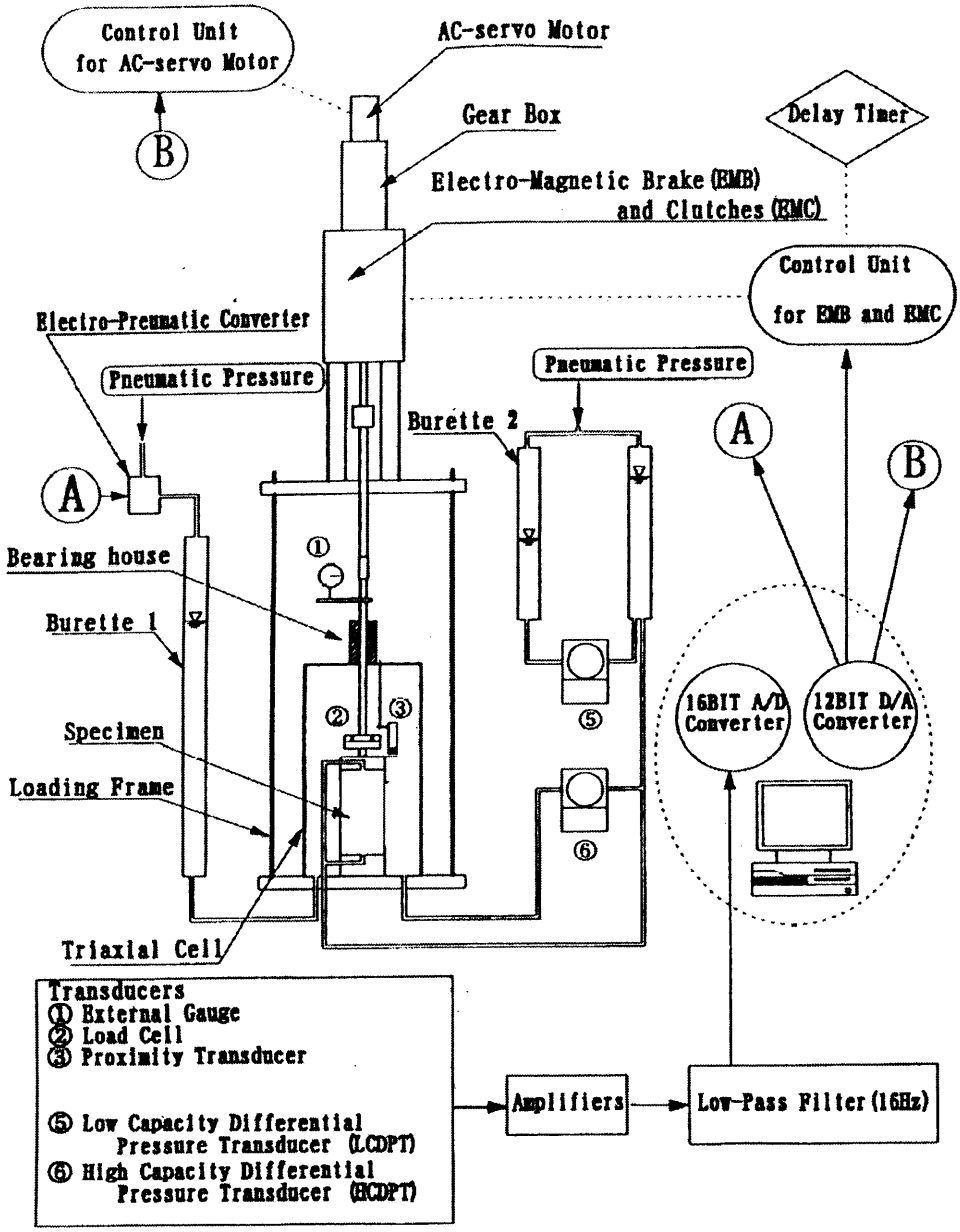

Figure 3-9 Schematic layout of (IIS) triaxial testing system (modified after Santucci de Magistris et al., 1998)

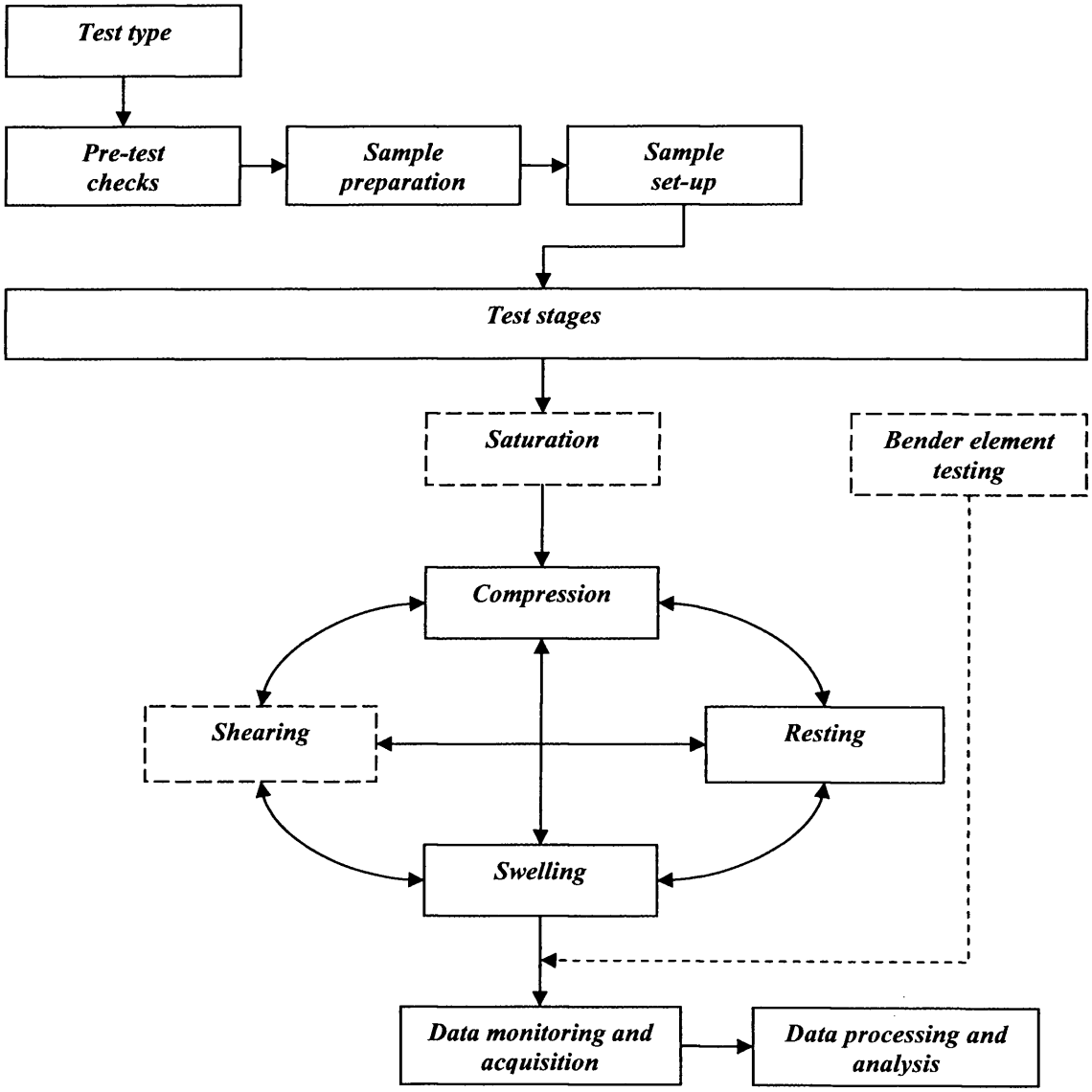

Figure 3-10 Flowchart for general testing procedures used in one-dimensional and triaxial testing

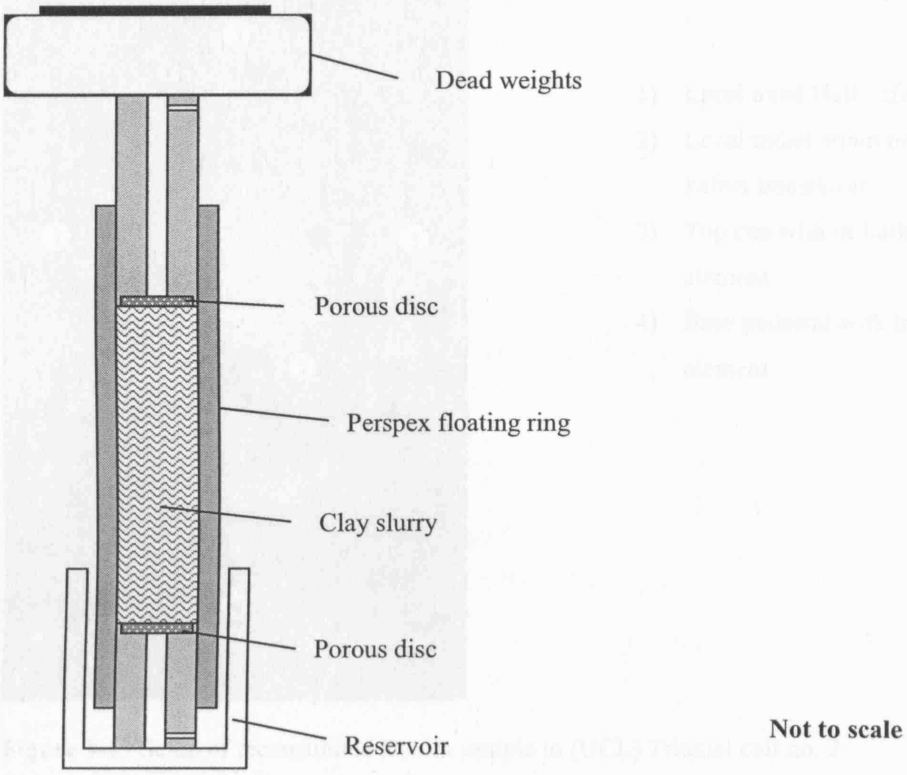

Figure 3-11 Schematic illustration of floating ring consolidometer

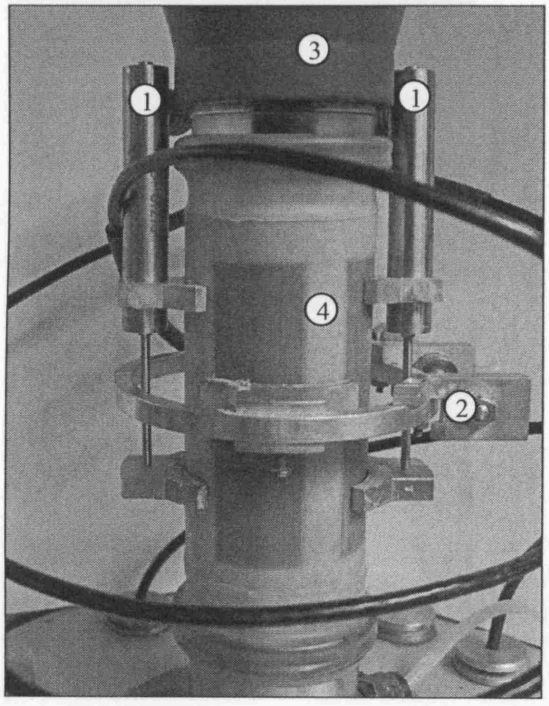

(1) Local axial LVDTs
(2) Local radial strain belt
(3) Suction cap
(4) Side drains

Figure 3-12 Setup of reconstituted London Clay sample in (UCL) Triaxial cell no. 1

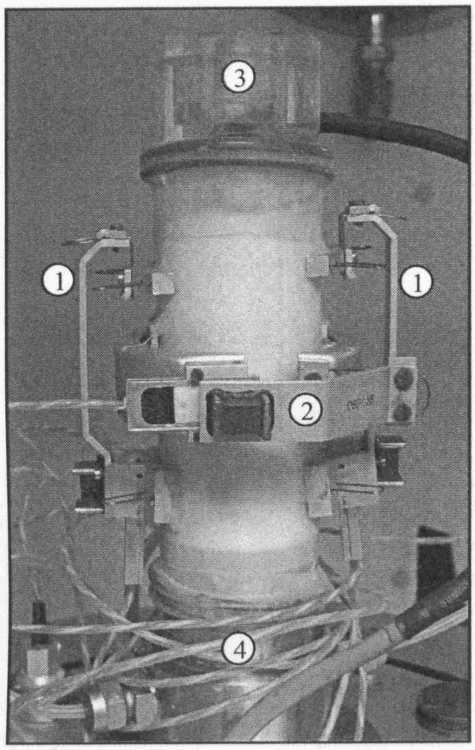

1) Local axial Hall Effect transducers
2) Local radial strain belt with Hall Effect transducer
3) Top cap with in-built bender element
4) Base pedestal with in-built bender element

Figure 3-13 Setup of reconstituted Kaolin sample in (UCL) Triaxial cell no. 2

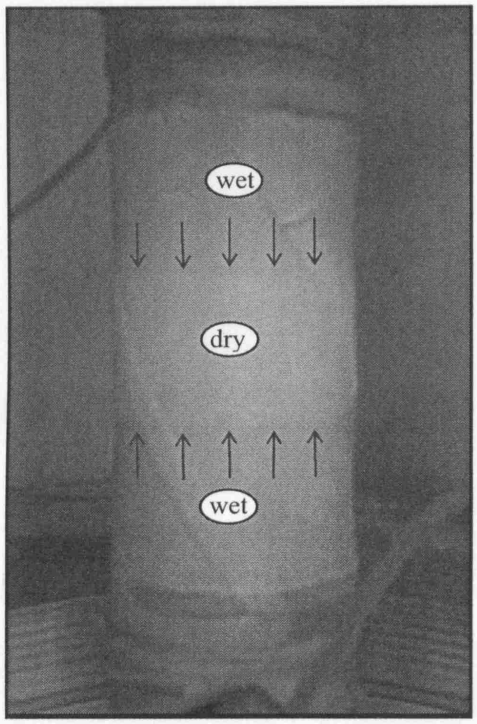

↓ direction of water flow

Figure 3-14 Saturation of cement-mixed kaolin sample in (IIS) triaxial cell

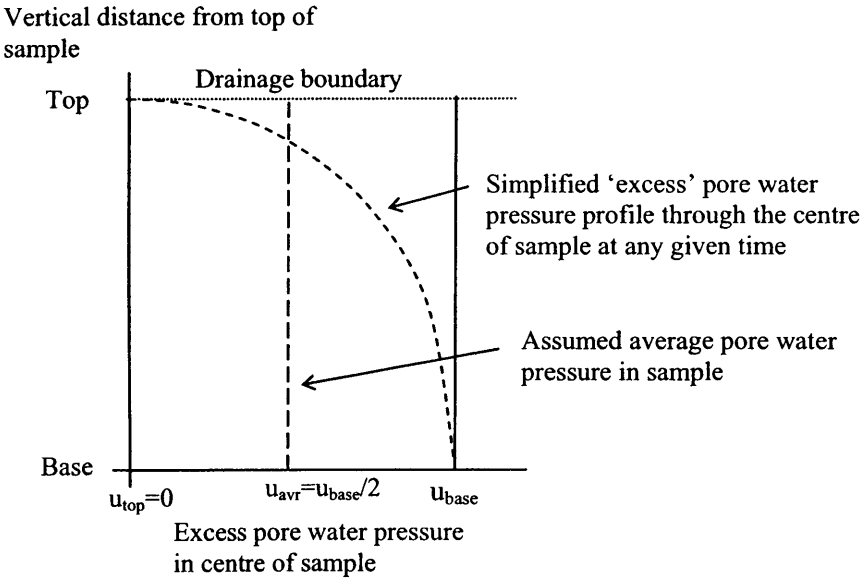

Figure 3-15 Illustrating the simplified pore water pressure profile through the centre of an oedometer sample

CHAPTER 4 INVESTIGATION OF ELASTIC SHEAR STIFFNESS AND ITS RELATION TO GLOBAL STRAIN RATE AND AGEING

4.1 INTRODUCTION

This chapter describes part of the experimental research work, focusing on three complementary series of monotonic one-dimensional and isotropic compression tests on specimens of reconstituted kaolin and London Clay, which were carried out to investigate the influence of global axial strain rate and ageing on the elastic shear stiffness determined from bender element testing. It should be clarified that the global axial strain rate has been defined as the monotonic rate at which the entire sample deforms in a given direction due to the imposed boundary conditions. The global axial strain rate should not be confused with the local cyclic strain rate imposed by the transmitted shear wave in bender element tests, which varies with the frequency of the transmitted signal. In the following axial strain rates will refer to the global axial strain rates unless otherwise specified.

This chapter has been structured as follows: Section 4.2 explores the interpretation of bender element results, while the following three sections report on the findings from the performed laboratory tests. Section 4.3 reports on the influence of axial strain rate on the elastic shear stiffness determined from bender element tests in one-dimensional compression of kaolin. Changes in the elastic shear stiffness during consolidation, swelling and creep in one-dimensional compression of reconstituted London Clay are presented in Section 4.4, while the effects of stress rate and creep on the elastic shear stiffness in isotropic compression of kaolin and reconstituted London Clay are reported in Section 4.5. The findings are finally brought together, discussed and compared to previous research in Section 4.6. Details of the geomaterials, testing equipment, general testing procedures and data analysis were given in Chapter 3.

4.2 BENDER ELEMENT TESTING

As mentioned in Section 3.3.3d correct interpretation of the bender element tests has been and is still discussed heavily among researchers. Despite several suggestions made in the past there appears to be no general consensus about a reliable and objective interpretation method to obtain an estimate of the travel time of the transmitted shear wave. In this study bender elements that were fabricated by the author were utilised. The characteristics of the transmitted and received signals will be explained in the following, and in order to find a suitable method for determining the travel time, different methods of interpretation are investigated and compared. As explained in Section 3.5.5a the velocity of the propagating shear wave can be determined from the estimate of travel time and the assumed tip-to-tip travel distance (Viggiani & Atkinson,

1995). From the shear wave velocity an estimate of the shear modulus of the soil can be obtained using Equation 3.25.

4.2.1 Characteristics of (UCL) bender elements

a Test setup

In both the oedometer and the triaxial cell, the transmitting bender element was fitted in the top cap, while the receiving element was fitted in the bottom pedestal as described in Sections 3.3.1e and 3.3.2i. This setup allowed transmission of a shear wave through the soil in the vertical direction with a horizontal polarisation, and hence the elastic shear stiffness $G_{0(VH)}$ could be derived from the estimated shear wave velocity. Since bender elements were not fitted in the horizontal direction, no estimate has been made of G_{HV} and G_{HH} in the performed tests. During isotropic triaxial compression the inherent anisotropy resulting from sample preparation and preconsolidation is likely to remain to very high pressures and within the tested stress range $G_{0(VH)}$ cannot be expected to match G_{HV} and G_{HH}. In the one-dimensional oedometer tests the anisotropic stress and stiffness conditions would be even more pronounced.

In order to reduce the noise level and prevent excessive crosstalk between the transmitted and received signals it was found necessary to earth the cable which transmitted the received signal to the Pico datalogger. Figure 4-1 shows the beneficial effect of grounding on the received signal (from test S1k). It can be observed that without proper grounding the observed noise and crosstalk will completely obscure the received signal and hence make accurate estimation of travel time very difficult. To confirm that no other travel paths existed but the path through the sample, alternative travel paths through a stiffer medium were checked by performing bender element tests in the oedometer and triaxial cells filled with water. The tests confirmed that no signal was received by the receiving bender element.

b Transmitted signal

In all tests a ±10V sinusoid signal was sent to the transmitting bender element using the function generator. The sinusoid signal is generally preferred because of its more narrow frequency content compared to e.g. a square signal (Viggiani & Atkinson, 1995). The influence of the sent wave form was investigated by carrying out tests with different numbers and frequencies of the sent pulses. The nominal frequency was generally varied between 1 kHz and 50 kHz, while a range of signals were transmitted, which included single pulse, multiple pulses, continuous signal and semi continuous signals (basically a continuous signal with a monitored start)[1]. Additionally, the TTi function generator (described in Section 3.3.4d) allowed a frequency sweep signal to be sent, which could be analysed by the automatic computerised spectrum

[1] A semi-continuous signal can successfully be produced using a simple function generator, which would normally only allow continuous signals to be sent, by commencing monitoring before flicking the function generator quickly on.

analyser ABETS (Greening et al., 2003) and used to estimate the travel time using the phase-delay method, as described in Section 4.2.2c below.

It should be mentioned that previous research using a laser velocity-meter pointed at a bender element tip has indicated that the unrestricted movement of the transmitting element in air does not correspond exactly to the wave form of the sent signal (Lings & Greening, 2001). It was shown that the first peak amplitude of the tip deflection was much lower than what could be expected from the sent signal, as illustrated in Figure 4-2. Since the shear wave transmitted to the soil will reflect the actual tip motion, the received signal can also be expected to show similar distortion. This has been generally confirmed in the literature and in the tests described here, as shown in Section 4.2.1c below.

c Characteristics of received signal

Observations made in the literature and from this study indicate that the quality, amplitude and wave-form of the received bender element signal is influenced by many factors; most importantly the wave-form of the transmitted signal, but also the influence of soil-element coupling, sample geometry, sample boundary conditions and soil characteristics such as mineralogy, structure and density. A so-called near-field effect may arise from the compression component of the transmitted wave, which travels at a velocity significantly faster than the shear wave. The near-field effect is found to be more significant at lower frequencies and for shorter distances between the transmitting and receiving bender elements (Arroyo et al., 2003). In cases where a significant near-field effect is present the earlier arrival of the compression components of the transmitted wave is observed to cause an initial deflection of the received signal before the arrival of the actual shear wave (Jovicic et al., 1996).

Quality of bender element testing in oedometer and triaxial cells

In this study the bender elements in the triaxial cell were found to give much clearer received signals compared to the bender elements in the oedometer cell. The reason for this difference was most likely due to the difference in boundary conditions and sample size. The shorter travel distance in the oedometer may have given rise to significant near-field effects and the stainless steel confining ring could have introduced disturbing signals from reflected waves and short-circuiting of the travel paths through the metal. Moreover and more interestingly, samples of reconstituted London Clay appeared to give clearer received signals than reconstituted samples of kaolin when both soils where tested in the oedometer cell. The reason for this difference is more difficult to explain, but could have arisen from a more homogenous nature of the macro-fabric of the London clay, which was reconstituted a water content of approximately 1.6 times the liquid limit compared to the kaolin samples, which were reconstituted at water contents roughly 1.3-1.4 times the liquid limit. The initial slightly more liquid nature of the London clay sample would have resulted in an improved soil to element coupling in both ends of the sample and a more uniform dispersion of the transmitted shear wave. It is unknown whether soil

mineralogy could have had a significant influence. Nevertheless, in the triaxial cell both soils performed equally well and gave both very clear received signals.

Secondary phase lag

In order to determine the accurate shear wave velocity through the sample, it is essential to estimate any significant secondary phase lag, which may be present in the testing system. Among other factors, secondary phase lag may result from the conversion of electrical signal to a physical movement in the transmitting element, conversion of physical movement to electrical signal in the receiving element and soil-element coupling at both ends. The differential delay in the transmission of electrical signals through cables and computation time in the pico datalogger and PC software is believed to be negligible. By setting up the transmitting and receiving bender elements in direct contact in air, an estimate could be obtained of the secondary phase lag resulting from the conversion of physical movement to electrical signal and visa versa. Figure 4-3 illustrates the determination of time lag, while Figure 4-4 shows the estimated time lag for different frequencies. In Figure 4-3 the polarisation of the transmitting and receiving bender elements is observed to be opposite, which was how the bender elements generally were set up. The plot in Figure 4-4 shows that the time lag based on first arrival was approximately 5μs independently of the transmitted frequency, for frequencies between 2 kHz and 13 kHz. The resonant frequency of the bender element to bender element system was 8.1 kHz. Since it is unknown whether the phase lag will be constant under increasing confining pressures, the shear wave velocity has for this reason not been corrected for the estimated minor phase lag. The error in the estimated travel time, due to time lag, is expected to be most significant at higher stress levels, when the travel time is shorter.

The following representative figures in Section 4.2 are all obtained from one-dimensional compression of sample S01oeds4 of reconstituted London Clay at a vertical effective stress of 590 kPa, where nothing else is mentioned.

Characteristic of multiple pulse signal

Figure 4-5 shows the characteristic of the received signal when a multiple pulse sinusoid wave is transmitted through the oedometer sample. The sent signal, shown in Figure 4-5a in a plot of magnitude against relative time, was varied between 1 and 10 periods and the frequency of the transmitted signals was 35.4 kHz equal to the resonant frequency of the soil-bender element system. The received signals for the different number of transmitted pulses are shown in terms of magnitude against relative time in the remaining five graphs in the figure (Figure 4-5b to f). The following characteristic features of the received signals shown in Figure 4-5 can be observed. Generally, it can be observed that the transmitted signal experiences a high degree of attenuation due to its passage through the sample. When transmitting a ±10 V amplitude signal, the received signal has an amplitude of around 1/3000 of this, as seen from the figures. As mentioned above the actual transmitted signal is likely to be very different from the intended

constant amplitude signal, which was produced by the function generator. In accordance with the expectations the received signal reflects the distorted transmitted shear wave and generally it is observed that the amplitude of the received signal increases over the first five to six cycles and then stays constant (refer to plot showing the received signal for 10 pulses in Figure 4-5b). The constant plateau reached after the first few cycles corresponds to the amplitude obtained had a continuous sinusoid signal been transmitted. However, it seems unlikely that the transmitting element, if unrestricted, would not reach a steady dynamic state earlier than indicated by the received signal. The observed phenomenon is therefore believed to be caused by the relative large mass of the sample, which requires more cycles to reach a steady state of vibration.

Another characteristic feature observed in the received signal is the gradual attenuation of the signal after the fully transmitted signal has been received. From the plots it can be seen that the received signals attenuate fully over about five to six cycles, which is believed to reflect the inertia of the mass of the sample and the bender elements themselves. The similarity between the attenuation period and the period required to reach a steady state at the beginning may have been a coincidence, but it could also indicate that it is primarily the mass of the sample, which controls both phenomena.

Resonant frequency

The frequency of the transmitted signal was found to have a significant influence on the amplitude and wave-form of the received signal. Generally, for a given state, the sample-bender element system was found to resonate at given frequencies. At the dominant resonant frequency the amplitude of the received signal was observed to reach an absolute maximum and the system could be assumed to be resonating in the dominant mode of vibration. At other frequencies, local maxima in the amplitude was observed, which could be assumed to correspond to less dominant modes of vibration. The signal transmitted in Figure 4-5 had a frequency of 35.4 kHz, which corresponded to the dominant resonant frequency, as shown from the frequency spectrum in Figure 4-6 obtained using the automatic spectrum analyser ABETS, developed by Paul Greening. A local maximum can also be observed at around 15 kHz. At the dominant resonant frequency, the sample-bender element system is not forced to vibrate at a frequency other than the natural frequency of the system, and hence the frequency of the received signal is observed to be the same as the transmitted frequency and more characteristically the attenuated signal remains at the same frequency, as seen from Figure 4-5.

Generally, in the performed isotropic and one-dimensional compression tests the resonant frequency of the soil-bender element system is found to increase systematically with increasing stress level or density of the sample. Figure 4-7a shows a typical plot of the measured increase in resonant frequency with increasing stress level for a sample of preconsolidated kaolin subjected to isotropic compression in the triaxial cell from 0 kPa to 500 kPa (sample S1k).

While Figure 4-7b shows the associated reduction in estimated travel time plotted against the determined resonant frequency. It is generally observed that for a given stress interval the phase difference between the sent and received signals appears be constant, which gives a unique relationship between the resonant frequency and the travel time. As the stress level increases a jump in the phase difference is observed along with a jump in the measured resonant frequencies. It is possible that this behaviour is linked to a sudden change in the mode of vibration and associated resonant frequency.

Influence of frequency of transmitted signal

Figure 4-8 illustrates what the received signal looks like when the transmitted signal has a frequency significantly different to the dominant resonant frequency of 35.4 kHz. In the example shown, a 4 pulse sinusoid wave was transmitted at 20 kHz. It can be observed that the shape of the received pulse was significantly different to the transmitted pulse. Slight distortion occurs in the initial part of the received signal, but the frequency of the first 4 cycles of the received pulse, corresponding to the transmitted number of pulses, is seen to be close to the transmitted frequency of 20 kHz. In contrast, for the subsequent cycles of the received pulse, which are associated with the damping of the shear motion rather than the direct transmission of a shear wave, the frequency of the received signal is seen to increase and is found to be close to the dominant resonant frequency of 35.4 kHz. This illustrates that the damping motion of the soil-bender element system is controlled by its dominant resonant frequency independently of the transmitted frequency. Hence if a single pulse sinusoid wave is transmitted at a frequency other than the resonant frequency then the shear wave will be subjected to a transformation when passing through the sample, and the shapes of the sent and received signals will therefore not correspond exactly. Only at the resonant frequency does the transmitted signal retain its shape. On the other hand if the number of sent pulses is large, then the system is gradually forced to vibrate at the frequency of the sent signal. Nevertheless, as soon as the sent signal ceases, the natural frequency of the system quickly gains control of the movement.

4.2.2 Estimating travel time from bender element testing

Generally, in the literature four different methods have been suggested for the determination of travel time. These are the three traditional time domain methods; first arrival, travel time between characteristic points and cross-correlation, and additionally the phase-delay method in frequency domain. In this study all methods, apart from the cross-correlation method, have been used and compared in order to find a suitable method, which would give consistent results.

a First arrival method

Typically the first arrival method is used in connection with a transmitted single sinusoid pulse, nevertheless as long as the transmitted and received signals have monitored beginnings, multiple pulses and semi-continuous sinusoid signals can also successfully be used. Using this

method, the travel time of the transmitted shear wave is generally taken as the time between the start of the transmitted signal and the assumed first arrival of the shear wave at the receiving bender element. In the literature some researchers take the first point of deflection (t_a) as the arrival time of the shear wave (Abbiss, 1981), while other researchers use the first point of reversal (t_b) of the received signal because of the assumed influence of near-field effects (Viggiani & Atkinson, 1995). In this study the first point of inflection (t_c), which lies in between t_a and t_b, was generally found to give the most consistent travel times with travel times estimated from other reliable methods, as will be shown in the following. The three interpretation methods are illustrated in Figure 4-9. However, at higher resonant frequencies in the triaxial cell, where the near-field effect is insignificant, the first point of deflection and the first point of inflection will give travel times close to each other, and either method of interpretation is satisfactory. On the other hand, in tests where significant near-field effects or noise in the signals are present, the first arrival point can generally be very difficult to determine. Figure 4-10 shows an example of the difficulties in determining the first arrival point for a bender element test carried out in the oedometer apparatus.

In theory the elastic shear stiffness and hence shear wave velocity and travel time through an infinite elastic medium should be independent of the frequency of the transmitted shear wave. To investigate if this theory holds true for a finite sample, Figure 4-11 shows a typical plot of the influence of the transmitted frequency on the determined first arrival time using the first point of inflection. Single pulse sinusoids were transmitted with frequencies ranging between 6 and 50 kHz, and as before the dominant resonant frequency was around 35.4 kHz. It can be seen that the travel time estimated using the first arrival method showed a slight reduction (about 11%) with increasing frequency at lower frequencies, while beyond the resonant frequency the travel time was more or less independent of frequency.

b Correlation between characteristic points

Because of the uncertainties in determining the first arrival when significant near field effects are present, several researchers have suggested that the travel time can be estimated more reliably from the measured time between corresponding characteristics points on the sent and received signals, such as peaks or troughs. However, as Jovicic et al. (1996) among other researchers have pointed out, this method will only be reliable when the sent and received signals have similar shapes. To achieve similar shapes of the sent and received signals, the frequency of the transmitted signal should generally be equal to the dominant resonant frequency of the sample-bender element system, as shown previously. Otherwise, transmitting a continuous signal will also give rise to similar sent and received signals, however the travel time between corresponding peaks in the continuous signals is highly influenced by the frequency of the transmitted signal, as shown from Figure 4-11. It can be seen from the figure that only at the resonant frequency does the method of correlation between characteristic points on continuous signals agree with the first arrival method using the first point of inflection. The use of the

correlation method should therefore be used with caution, if the resonant frequency cannot be determined accurately. Despite this, the determination of travel time between two corresponding peaks is in many cases simpler than finding the first arrival. This method is therefore considered the most reliable out of all of the compared methods.

Any difficulties in using the method of correlation between characteristic points will lie in finding the corresponding peaks or troughs. In the case of soft reconstituted samples loaded from high void ratios, this is however a fairly easy matter. For soft samples the resonant frequency is initially low and the time difference between adjacent peaks in the received signal is large. Therefore, using the first arrival method as a first estimate, one can quickly locate the corresponding peaks or troughs, which gives a travel time close to the estimated time, as illustrated in Figure 4-12. As the sample is then compressed and the resonant frequency and the travel time gradually changes, it is possible to track the corresponding peaks. If at any time uncertainty arises over the correct choice of peaks or troughs, it can be checked by the first arrival method or from an estimate of travel time using phase-delay methods, as described in the following.

Another possibility is to find the corresponding peaks or troughs by transmitting a multiple pulse signal, as suggested by Jovicic et al. (1996) among others. In this study a four-pulse sinusoid signal was routinely transmitted at the resonant frequency and the trace of the sent and the received signals was saved for later comparison. Figure 4-13 illustrates such a trace for a four-pulse signal sent at the resonant frequency of 35.4 kHz. On the figure the travel times obtained using the first arrival methods are reported for comparison. It is observed that because of slight distortion the travel time estimated from the first couple of peaks is slightly higher than the travel time estimated from the corresponding fourth peaks. The peak to peak travel time is found to agree closely with the travel time estimated at the first point of inflection. To avoid the small error associated with the distortion of the initial received signal, in this study the travel time was estimated from the corresponding peaks or troughs in the continuous signal or from the corresponding fourth peaks in the multiple pulse signal.

c Phase delay method

In the phase-delay method the travel time is determined as the gradient of the linear interpolation of the relative phase between sent and received signals plotted against the frequency of the signal, as has been suggested by Viggiani & Atkinson (1995). A continuous signal is used to find the frequencies where the sent and received signals are in and out of phase, and from these so-called π-points a graph of relative phase against frequency can be plotted. However, the automatic computerised spectrum analyser ABETS (Greening et al. (2003) makes it possible to obtain the complete diagram of relative phase against frequency less onerously from a transmitted frequency sweep signal. In this study both the π-point method and ABETS were compared against each other and against the time domain methods. When using ABETS the TTi function generator was used to transmit a frequency sweep with a bandwidth of 1-50

kHz. Figure 4-14 shows an example of the phase diagram obtained using ABETS and the π-point method. As shown in the figure the gradient of the complete phase-diagram from ABETS varies significantly with frequency and hence a certain degree of subjectivity will be introduced when choosing a suitable interval for determining the travel time. The π-points obtained for frequencies between 27 kHz and 58 kHz are seen to agree well with the obtained phase-diagram from ABETS. The travel times determined from the moving gradient of the phase-diagram over an interval of about 10 data points (about 2 kHz) from ABETS and between each adjacent pair of π-points have been plotted against the frequency in Figure 4-15 alongside the travel time obtained from the first arrival method (first point of inflection) and the travel time obtained at the resonant frequency using the peak-to-peak correlation method. The plot shows that the estimated travel time from the phase-delay method is highly dependent on frequency, however around the resonant frequency the travel time varies only little. Generally, the phase-delay methods appear to overestimate the travel time compared to the time obtained from the first arrival method or peak-to-peak correlation method.

In the light of the above comparison, the method of correlation between characteristic peaks or troughs at the resonant frequency using a continuous signal has been deemed the most suitable because of its reliability and simplicity. Hence, in the following analysis the elastic shear stiffness has been derived from the estimated travel time using this method. As will be seen from the following results the chosen method of interpretation gives very consistent results, which emphasizes the reliability of the interpretation.

4.3 EFFECT OF STRAIN RATE ON THE ONE-DIMENSIONAL COMPRESSION OF KAOLIN

4.3.1 Purpose and overview of tests

This section presents results obtained from four advanced oedometer tests on reconstituted kaolin, which were carried out to investigate the effect of strain rate on the compression behaviour and elastic shear modulus. The elastic shear modulus was determined from dynamic shear wave measurements using bender elements. The tests were performed in the period 23rd February to 2nd October 2004 in the geotechnical research laboratory at UCL. Details of the conducted oedometer tests have been summarised in Table 4-1.

4.3.2 Special testing procedures

An initial test series performed on 20 mm high samples showed that the distance between the transmitting and receiving bender elements quickly became to short at relatively low stress levels, which consequently resulted in erroneous stiffness measurements. The oedometer cell was then modified to take 40 mm high samples (refer to Section 3.3.1e), which solved that problem. Data-logging was also added so that overnight interruption in stress-strain readings did not occur. In the test series discussed below all samples were initially about 40 mm high and 75 mm in diameter. All samples were reconstituted at a water content of about 1.3-1.4 times the Liquid Limit by hand-mixing dry kaolin powder with tap water. The mixture was subsequently transferred to the oedometer cell, making the best effort not to trap excessive amounts of air in the sample. Then the top cap and hanger were applied (equivalent to 8 kPa vertical total stress) and samples were left overnight to stabilise before a constant rate of straining (CRS) test or step change in rate of straining (SRS) was initiated.

Samples S02oeds3, S03oeds3 and S04oeds3 were compressed with step changes in the vertical (axial) strain rate, to investigate the immediate and persistent effects of strain rate changes on the compression behaviour. The nominal vertical strain rate $\dot{\varepsilon}_a$ was varied step-wise by a factor of up to 125, ranging between 2.3×10^{-7} s^{-1} (=0.083 %/hr) and 3×10^{-5} s^{-1} (=10.8 %/hr). Additionally, stress relaxation and constant total vertical stress creep/pore water dissipation were introduced at different stages to complete the investigation, for periods up to four days. Finally, sample S03oeds3 was unloaded after compression, while samples S02oeds3 and S04oeds3 experienced an unload-reload cycle before being fully unloaded. For comparison sample S01oeds3 was compressed at continuous high CRS followed by unloading. In the tests performed on samples S01oeds3, S03oeds3 and S04oeds3, bender element tests were carried out at regular intervals to investigate the effect of the various loading conditions and history on the elastic shear modulus. Significant excess pore water pressure build-up was expected and observed at most of the higher strain rates and hence the effective stress conditions governed the

compression behaviour of the samples. In the following, results for samples S03oeds3 and S04oeds3 are presented. Discussion and comparison with the isotropic compression tests are found at the end of this chapter in Section 4.6.2.

4.3.3 Effect of strain rate on the compression behaviour of reconstituted kaolin

Figure 4-16 shows the one-dimensional compression curves obtained for samples S03oeds3 and S04oeds3. The plot indicates that the general CRS virgin compression path is linear in e-log σ'_v plane over most of the tested stress range, from small (~6 kPa) to high stress levels (~5000 kPa), i.e. an exponential increase in stress with reducing void ratio. Values of the compression index C_c (=$\Delta e/\Delta \log \sigma'_v$) for all the tests are listed in Table 4-3. The unloading path also appears to be linear in e-log σ'_v plane, while the reloading path shows signs of hysteresis. Up to 8 kPa effective stress, the compression path is a result of excess pore water pressure dissipation under constant total load from the top cap. At 8 kPa when the pore water pressure was zero, the samples experienced constant effective stress drained creep for about 15 hrs. Both during pore water pressure dissipation and drained creep the rate of vertical straining reduced. At the point of first reading the strain rate was about 10^{-5} s^{-1}, reducing by about three orders of magnitude to 10^{-8} s^{-1} at the end of creep. At the end of the initial creep stage both samples consistently ended up at a void ratio around 1.72-1.76. After the creep stage the samples were compressed with step-wise change in the vertical strain rate.

Figures 4-17 and 4-18 show the influence of step-wise change in strain rate on the compression behaviour of samples S03oeds3 and S04oeds3 respectively in single logarithmic scale (e-log σ'_v) and natural scale (e-σ'_v). Two different strain rates were used for sample S03oeds3, and four different strain rate for sample S04oeds3. Looking at the compression of sample S04oeds3, the initial stress measurements upon starting the CRS compression appear to be excessively high. This was caused by additional friction from the guide pins, and was resolved from about 100kPa onwards. It can be seen from the plots that strain rate changes, despite being small, have an effect at both low and high stress levels. However, in single logarithmic scale the strain rate changes appear to have a diminishing effect at increasing stress levels, while in natural scales it can be seen that the effect is persistent even at the highest stress level. When increasing the strain rate the initial response is seen to be very stiff (e.g. Figure 4-17b), the soil then yields and follows a path above the lower strain rate path. When the strain rate is reduced back to the previous rate, the path appears to rejoin the extrapolated path for that rate. Figure 4-17 indicates that after a decrease in strain rate the initial path temporarily undershoots the permanent path and similarly temporarily overshoots the path after an increase in strain rate. The overshooting and undershooting appear to be most pronounced at low stress levels, and are also observed after stress relaxation and creep stages. A more detailed look at the data indicates that the stress jump increases with increasing ratio of strain rate change (Figure 4-18b), while the results are slightly ambiguous concerning the influence of initial strain rate.

However, the results could indicate that the stress jump is more or less proportional to the logarithm of strain rate ratio independently of initial strain rate. Moreover, the stress jump appears to increase with stress level for the same initial strain rate and ratio of strain rate change (Figure 4-17b). The influence of strain rate on the accumulated pore water pressure during compression is shown in Figures 4-19 and 4-20. It is observed that significant pore water pressures accumulated during compression at the highest strain rates. As explained in Section 3.5.2b an assumption had to be made concerning the average pore water pressure in the sample, which may have resulted in a slight overestimation of the effective stresses.

4.3.4 Effect of strain rate on the G_0-σ'_v relationship for reconstituted kaolin

Figure 4-21 and 4-22 show the influence of step-wise change in strain rate on the elastic shear modulus plotted against effective vertical stress relationship for samples S03oeds3 and S03oeds4 respectively in double logarithmic and natural scales (data below σ'_v=100 kPa have been excluded for sample S03oeds4). Generally, the results show that for a given strain rate the logarithm of the elastic shear modulus is proportional to the logarithm of the stress level (linear relationship on double logarithmic scale). Figure 4-22 shows that the unloading and reloading paths are separated, that both are linear in double log scales and that they plot above the virgin compression line with lower gradients. The gradient for the reloading path is slightly lower than the gradient for the unloading paths until the state is back on the virgin compression line, where a sudden increase in gradient is seen. From the plot it can be deducted that a sample in a normally consolidated state will always have a lower elastic shear modulus than what can be obtained at any overconsolidated state at the same stress level.

Figures 4-17 and 4-18 showed that upon an increase in strain rate the stress level initially increases rapidly with little change in void ratio. At the same time, G_0 is surprisingly seen to reduce, as for example seen from Figure 4-21a for sample S03oeds3 when increasing the strain rate back to 0.43 %/hr after the stress relaxation stage at around σ'_v=45 kPa. When the compression path subsequently yields at around σ'_v=80 kPa (Figure 4-17a) so appears the G_0-σ'_v relationship to do as well and G_0 starts increasing again (Figure 4-21a). For two given constant rates of strain the higher strain rate response plots beneath the lower strain rate line, as seen from Figure 4-21a. Hence, it is indicated that a normally consolidated sample compressed at a high strain rate will have a lower value of the elastic shear modulus for a given stress level than a sample compressed at low strain rate. In double logarithmic scale the constant rate of strain lines are seen to approach each other at high stress level, while in natural scale the separation of the curves appears to be persistent, similarly to what was observed for the compression curves.

From the test data from sample S03oeds3, where the strain rate is changed step-wise between $\dot{\varepsilon}_a$ and $25\dot{\varepsilon}_a$, the percentage increase in G_0 is found to be about 46 % when the strain rate is reduced at low stress level (10kPa) compared to an increase of about 7 % at high stress

level (5000kPa). Hence, the effect of strain rate changes on the elastic shear modulus appears to be most significant low stress levels (percentage wise). The increase in G_0 observed as a result of gradual changes in strain rate during the stress relaxation stage at around σ'_v=45 kPa for sample S03oeds3 appears to be of comparable magnitude to changes observed as a result of step-wise change in strain rate (Figure 4-21a).

4.3.5 Effect of strain rate on the e-G_0 relationship for reconstituted kaolin

Figures 4-23 and 4-24 show the influence of step-wise change in strain rate on the elastic shear modulus against void ratio relationship for samples S03oeds3 and S04oeds3 respectively in single logarithmic and natural scales (for sample S04oeds3 data below σ'_v=100 kPa have been excluded due the previously mentioned errors). Figure 4-25 gives details of the e-log G_0 behaviour during stress relaxation and immediately after when constant rate of straining is initiated.

Generally, the results show that for a given strain rate the elastic shear modulus increases exponentially with reducing void ratio (linear relationship in e-log G_0 plot), similarly to the relationship between stress level and void ratio. The unloading and reloading paths are almost identical and both also appear to be linear in the plot of e against log G_0. The unloading path plots below the virgin compression line with a significantly lower gradient, from which it can be deducted that a sample in a normally consolidated state will always have a higher elastic shear modulus than what can be obtained at any overconsolidated state at the same void ratio. Upon an increase in strain rate G_0 initially reduces, where after it is seen to increase again with reducing void ratio in a linear manner on single logarithmic scale. Upon a strain rate reduction the rate of increase in G_0 with void ratio increases significantly and then gradually reduces back to a rate close to the initial rate. For two given constant rates of strain the higher strain rate response plots below the lower strain rate line, as seen from Figures 4-23a and 4-24a. Hence, it is indicated that a normally consolidated sample compressed at high strain rate will have a lower value of the elastic shear modulus for a given void ratio than a sample compressed at low strain rate. On single logarithmic scale the constant rate of strain lines are seen to approach each other at high stress level, while in natural scale the separation of the curves appears to increase with reducing void ratio. Figure 4-25 shows details of the stress relaxation stage at around σ'_v=45 kPa for sample S03oeds3. It is observed that during stress relaxation G_0 increases at constant void ratio and slightly reducing stress level. After commencing compression at the original high strain rate, G_0 is observed to initially reduce, then the G_0-e state is seen to return to the constant strain rate line given by the high strain rate. Changes in G_0 observed as a result of gradual changes in strain (plastic) rate during the 14-hrs stress relaxation stage appear to be of comparable magnitude to changes observed as a result of a step-wise change in strain rate by a factor of 25 (Figure 4-23a). Further analysis and discussion of the results is given in Section 4.6, where the behaviour will also be compared to the observed behaviour in the literature.

4.3.6 Normalised behaviour

Because of the non-parallel nature of the constant strain rate relationships observed in plots of G_0 against σ'_v and e against G_0 normalisation proves very difficult. The effect of strain rate changes on the elastic shear stiffness is seen to reduce with increasing stress level or reducing void ratio, hence it is not possible to normalise the results in a simple way so the effects of either state or strain rate are completely removed.

4.4 CONSOLIDATION, SWELLING AND CREEP CHARACTERISTICS IN ONE-DIMENSIONAL COMPRESSION OF RECONSTITUTED LONDON CLAY

4.4.1 Purpose and overview of tests

In addition to the above described SRS and CRS oedometer tests on kaolin, a single step-loaded oedometer test on reconstituted London Clay (sample S01oeds4) was conducted in order to investigate the influence of strain rate changes on the elastic shear modulus in more detail during consolidation, creep and stress relaxation. The test was carried out using the modified 40 mm oedometer cell fitted with bender elements in the top cap and the base pedestal, which allowed the elastic shear modulus in the vertical direction to be determined from dynamic shear wave measurements. The test was performed in the period 18th February to 24th June 2005 in the geotechnical research laboratory at UCL. Details of the conducted oedometer test have been summarised in Table 4-1.

4.4.2 Special testing procedures

The sample of London Clay was reconstituted at a water content of approximately 1.6 times the Liquid Limit by hand mixing trimmings from the rotary core sample with tap water until a homogenous liquid paste was obtained. The mixture was poured into the oedometer cell, making the best effort not to trap excessive amounts of air in the sample. The initial dimensions of the sample were about 40 mm in height and 75 mm in diameter. Then top cap and hanger were applied (equivalent to 3 kPa vertical total stress) and the sample was left overnight to stabilise before step-loading was initiated. Consolidation, creep and stress relaxation were investigated as follows. The sample was step-loaded to 785 kPa by adding dead weights to the hanger on the lever arm (1:11 ratio) in six increments: 0-1-2-4-8-16-32 kg corresponding to 3-28-52-101-199-394-785 kPa total vertical stress at the top of the sample (including weight from top cap and hanger). Generally, after each new load step the sample was left to consolidate for about 24 hrs during which most of the excess pore water pressures dissipated. After the last load increment the sample experienced a prolonged creep period for 30 days after the end of primary consolidation (EOP) in order to investigate the characteristics of pure creep. Following this rest period the sample was compressed further under the slowest constant rate of vertical strain allowed by the loading frame, which was nominally $\dot{\varepsilon}_a$=2.3×10^{-7} s^{-1} (=0.083 %/hr). As the vertical effective stress reached about 2000kPa, the top cap was fixed in position and the sample experienced stress relaxation over approximately 4 days.

Finally, the sample was unloaded to 785 kPa under a nominal constant rate of strain of $\dot{\varepsilon}_a$=-2.3×10^{-7} s^{-1} (again slowest allowed) and then fully unloaded in steps of about 100 kPa total stress; 785-687-590-492-370-248-128-3 kPa. After each unloading step the sample was generally left to swell under fixed total stress for about one to two days during which the

majority of the negative pore water pressures (suction) were relieved. In two unloading stages however, swelling and subsequent creep was allowed for up to about 5 weeks to investigate swelling and creep characteristics. During all stages of loading and unloading the elastic shear modulus G_0 was determined from bender element testing at suitable intervals to investigate the effect of strain rate and ageing on the elastic shear stiffness.

4.4.3 Compression behaviour observed during step and CRS loading of reconstituted London Clay

Figure 4-26 shows the compression in e-log σ'_v plane resulting from the combined step loading and CRS compression. Immediately after each positive load increment the effective stress compression path is seen to jump straight to the right (a→b on the graph), which primarily can be attributed to the slow response of the pore water pressure transducer and therefore does not reflect the actual effective stress conditions. As the response of the pressure transducer gradually starts to reflect the sudden increase in pore water pressure, the effective stress path moves back towards the actual effective stress conditions (b→c on the graph), which can be assumed to have been reached when the effective stress path reverses again (point c on the graph). The point of reversal will in the following be referred to as the 'second reversal point'. The effective stress compression path then moves down as the sample consolidates and excess pore water pressures dissipate (c→d on the graph). The consolidation curves for each load increment, the corresponding pore water pressure dissipation curves and the plots of axial strain rate reduction against time are shown in Figures 4-27, 4-28 and 4-29 respectively. From the plots it can be seen that independently of stress level the end of primary consolidation (EOP) was reached about 24 hrs (=1440 min) after each load increment at which point the vertical strain rate had reduced to around 4×10^{-8} s^{-1} (=0.014 %/hr). In comparison, the strain rates measured immediately after applied load increment and at the second reversal point were generally around 4×10^{-5} s^{-1} (=14.4 %/hr) and 4×10^{-6} s^{-1} (=1.44 %/hr) respectively. The creep behaviour observed post EOP after the last load increment at σ'_v=785 kPa can be characterised by a near-linear reduction in void ratio with logarithm of time with a coefficient of secondary compression $C_\alpha = \Delta e / \Delta \log t = 0.016$ (Figure 4-27). The behaviour can also be characterised by a logarithmic linear reduction in strain rate with time with the value of $m = \Delta \log \dot{\varepsilon}_a / \Delta \log t$ being close to 1 (Figure 4-29).

In Figure 4-26 an approximately straight normal compression line (NCL) can be obtained in the plot of e against log σ'_v by connecting EOP points from each consolidation path. This suggests that the strain rates obtained at EOP are of similar magnitude in agreement with the findings. This was further supported by the value of the compression index C_c (=$\Delta e/\Delta$log σ'_v), given in Table 4-3, which is found to be in close agreement with the C_c values found for reconstituted London Clay in constant rate of compression. Similarly, a constant rate of strain NCL is obtained from the second reversal points, which is parallel to the NCL given by the EOP

points, but due to strain rate effects lies above it. Because of the progressive reduction in strain rate during consolidation it is noticed that the individual consolidation paths do not follow a given NCL, instead the paths progressively move towards underlying NCLs defined by lower strain rates. This behaviour is similar to the behaviour observed during pure creep, with the difference that the stress state during creep is fixed. When commencing CRS compression after the last load step at a nominal vertical strain rate of $\dot{\varepsilon}_a = 2.3\times10^{-7}$ s^{-1} (=0.083 %/hr), an initial stiff response is observed due to the sudden increase in strain rate. The CRS compression path then yields and follows a path, which in conformity with the applied strain rate lies parallel and in between the two NCLs defined by the characteristic points on the consolidation paths.

It should be mentioned that the excess pore water pressure gradually increases during CRS compression since the rate of straining is too fast for complete consolidation to take place. Nevertheless, as the strain rate is lower than the characteristic strain rate of 4×10^{-6} s^{-1} (=1.44 %/hr) associated with second reversal point, the pore water pressure response is believed to be reliable. At the highest vertical effective stress of around 2000 kPa the sample experienced fixed strain stress relaxation for about 4 days (5700 min) at which point the excess pore water pressures, which had accumulated during CRS compression, had fully dissipated, as shown from Figure 4-30. It can be seen from the plot, which shows the reduction in stress level and pore water pressure with time after the start of stress relaxation, that the stress relaxation in contrast to the dissipation of excess pore water pressures continued after EOP and similarly to the observed creep behaviour was characterised by a linear reduction in stress with logarithmic increase in time post EOP.

4.4.4 Swelling behaviour observed during step and CRS unloading of reconstituted London Clay

In addition to the compression paths Figure 4-26 shows the swelling behaviour in the e-log σ'_v plane resulting from the combined step and CRS unloading. After the stress relaxation stage the sample was unloaded to 785 kPa total vertical stress at a nominal constant rate of vertical strain of $\dot{\varepsilon}_a = -2.3\times10^{-7}$ s^{-1} (-0.083 %/hr) followed by a fixed total stress swelling and creep period for about 38 days. Figure 4-31 shows the relief of negative pore water pressure (suction) with time during this period of rest, while the corresponding swelling curve in terms of void ratio changes with time is shown in Figure 4-32. A significant build up of negative pore water pressure was expected after the relative rapid unloading. However, most likely because of the limitations of the pore water pressure transducer the maximum suction measured was only around -22 kPa, which may not reflect the actual suction experienced in the sample. Nevertheless, the general trend of suction relief with time is clear from Figure 4-31. It is observed that equilibrium in pore water pressure (apparent offset of 5 kPa) was reached after about 9000 min (~6.3 days), which was notably longer than the consolidation time required to reach EOP during step loading stages. In contrast, the volumetric changes showed a different picture; up until about 9000 min the

sample was observed to swell as result of the relief of suction pressures and the associated movement of water into the sample. However, after equilibrium was reached in the pore water pressure, the void ratio changes were seen to reverse and positive volumetric creep strains then slowly developed with time. The coefficient of secondary compression was estimated to be C_α~0.0085 at the later stages, which is significantly lower than the value reported above at the same stress level during virgin compression. After 38 days of rest the net change in void ratio is observed to be negative, despite the initial tendency to swell.

Similar behaviour can be observed from the subsequent step unloading stages, as shown in Figures 4-33 and 4-34. For the first three step reductions in stress the sample was left to swell until the pore water pressures had equalised, while the subsequent swelling stages at lower pressures were all stopped before the pore water pressures had time to equalise and before any tendencies of strain reversals were observed. The point of strain reversal at the highest stresses is slightly ambiguous, but there are some indications that the vertical strain reverses after about 2100 min (1.5 days) after unloading to a total stress of 492 kPa, while after unloading to 590 kPa total stress the vertical strain appeared to reverse after about 18 days. The observed reversal of volumetric strains after unloading confirms findings made by e.g. (den Hann & van den Berg, 2001) and (Almeida & Marques, 2003), as reported in the literature review.

4.4.5 Effect of consolidation, swelling and creep on the elastic shear stiffness G_0 of reconstituted London Clay

The change in G_0 with time during consolidation and creep after each step increment in load is shown in Figure 4-35. During consolidation and creep after step loading G_0 is observed to increase consistently with time; an approximately linear relationship between G_0 and logarithm of time is indicated pre EOP (<1440 min). The behaviour in terms of G_0 change with logarithm of time after the last load increment (to σ_v=785 kPa) indicates a reduction in gradient at EOP; post EOP the linear relationship between G_0 and logarithm of time continues. It can also be observed that as a general trend the change in G_0 with time during consolidation increases consistently with increasing stress level, as indicated by the increase in gradients of the linear relationships between G_0 and logarithm of time. Additionally the figure shows the change in G_0 with time during stress relaxation at the highest stress state and during fixed total stress swelling and subsequent creep after CRS unloading to 785 kPa and after step unloading from 687 kPa to 590 kPa. A similar linear increase in G_0 with logarithm of time was found during stress relaxation at the highest stress level. Again there are some indications of a change in gradient at EOP. In contrast the plot shows that after CRS unloading to 785 kPa G_0 initially reduced with time until about 9200 min, at which point the suction had been fully relieved and the vertical strains reversed, and then G_0 appears to increase rapidly on logarithmic scale during the subsequent positive creep. During swelling and subsequent creep after step unloading from 687 kPa to 590 kPa G_0 is observed to remain more or less constant at times between 2000 min (1.4

days) and 50.000 min (35 days). A slight reduction in G_0 is indicated, which tie in with the minor expansion of the sample and the relative small changes in rate of straining with time.

As suggested by (Anderson & Stoke, 1978) the increase in G_0 with time during creep can be quantified using the coefficient $I_G = \frac{\Delta G_{max}}{\log\left(\frac{t_2}{t_1}\right)}$ or the normalised coefficient $N_G = \frac{I_G}{G_{max,1000}}$ (refer to Section 2.3.1d). The coefficients I_G and N_G have been used to quantify the changes in G_0 after each step load and during stress relaxation. For most of the loading stages, data were only obtained until EOP, hence the obtained values of I_G and N_G will not reflect the pure creep behaviour. It will however be possible to illustrate the influence of stress level. The values of the coefficients are listed in Table 4-3. Figures 4-36 and 4-37 show the influence of the average vertical effective stress level on the coefficients I_G and N_G respectively. I_G is observed to increase in a bilinear manner, showing an initial rapid increase until a stress level of about 180 kPa and then a slower but steady increase at higher stresses. Despite being normalised for some of the effect of stress level, N_G on the other hand reduces rapidly with increasing stress level from a value of 37% at 92 kPa to a value of 6% at 1900 kPa. The significant change in N_G with stress level clearly indicates that the true creep behaviour has not been characterised, instead the high values of N_G, particularly at low stress levels, reflect the changes in G_0 due to consolidation and the associated changes in void ratio, stress level and rapid changes in strain rate.

4.4.6 Effect of consolidation, swelling and creep on the G_0-σ'_v relationship for reconstituted London Clay

Figure 4-38 shows the logarithm of G_0 plotted against the logarithm of σ'_v during the various loading and unloading stages. The first G_0 measured after each load step corresponds to the point where the pore water pressure becomes reliable, i.e. the second reversal point on the compression path (point c in Figure 4-26). It can be observed that the initial points after each step load all fall on a straight line in log G_0-log σ'_v plane, which can be assumed to correspond to a strain rate of about 4×10^{-6} s^{-1} (=1.44 %/hr). This line defines a lower bound trend line for the observed increase in G_0 with σ'_v. During consolidation and creep after each step load, the increase in G_0 with σ'_v is seen to be significantly greater than what can be expected from the general trend of G_0 increase with σ'_v as derived from all the load stages. This behaviour is similar to the observed behaviour of the compression paths, which could be explained by the influence of a reducing strain rates. During consolidation and creep the strain rate progressively reduces as shown in Figure 4-29 and hence the σ'_v-G_0 state progressively moves outwards from the CRS line defined by the initial points at a strain rate of about 4×10^{-6} s^{-1} (=1.44 %/hr). The EOP points, which roughly correspond to a strain rate of 4×10^{-8} s^{-1} (=0.014 %/hr) are seen to fall close around a straight line, which lies parallel and above the line given by the initial points after each step load at the higher strain rate. Similar to what was observed on the compression

paths, during CRS compression at an intermediate strain rate σ'_v-G_0 states fall between the straight lines given by the characteristic points at higher and lower strain rates. During stress relaxation at the highest stress level (σ'_v ~1900 kPa) the shift in the σ'_v-G_0 state from the initial point to EOP is similar to that observed during consolidation after step loading, and the EOP point at the end of stress relaxation fall close to the CRS line given by the EOP points from step loading. Because there is no change in void ratio during stress relaxation, this indicates that the change in void ratio is of minor importance to the changes in σ'_v-G_0 state with time and that the controlling factor is simply 'ageing' time or the associated reduction in rate of plastic strain during consolidation and creep after step loading or during stress relaxation. In Section 4.5.7 this is investigated further.

From Figure 4-38 it can be observed that the swelling path deviates significantly from the compression path in log G_0-log σ'_v plane. Despite differences in strain rate states, the general trends are observed to be a linear relationship between the logarithm of G_0 and the logarithm of σ'_v with a gradient that is significantly lower than the gradient of the relationship obtained in compression. This behaviour is similar to what was observed from the one-dimensional compression tests on kaolin as described in Section 4.3.4, and similar to what has been observed in the literature, for example as shown in Figure 2-4b. The effect of strain rate in the unloading regime is not possible to deduct from the limited data points.

4.4.7 Effect of consolidation, swelling and creep on the e-G_0 relationship for reconstituted London Clay

Figure 4-39 shows the corresponding relationship between void ratio and the logarithm of G_0 during the various loading and unloading stages. Despite more scatter in the obtained data points the general trends are similar to those observed in log G_0-log σ'_v plane. During periods of rest and related reduction in the rate of plastic strain after step loading and during stress relaxation the e-G_0 state progressively moves outwards to the right of the linear lower bound e-log G_0 relationship given by the initial data points at higher strain rates. A linear relationship between e and the logarithm of G_0 is also indicated in the unloading regime from step unloading. The gradient of the swelling line is seen to be significantly lower than the compression line. This behaviour is similar to what was observed from the one-dimensional compression tests on kaolin as described in Section 4.3.5, and similar to what has been observed in the literature, for example as shown in Figure 2-4c.

4.5 EFFECT OF STRESS RATE AND CREEP ON THE ISOTROPIC COMPRESSION OF RECONSTITUTED KAOLIN AND LONDON CLAY

4.5.1 Purpose and overview of tests

Due to the aforementioned uncertainties about the true stress conditions in the oedometer tests, a series of three additional tests was conducted in the triaxial apparatus, where the stress conditions could be controlled and determined more easily. For this purpose Triaxial cell no.2 at UCL had been fitted with a pair of bender elements in the top cap and base pedestal to allow for measurement of G_0 in the vertical direction. The test series consisted of isotropic compression tests with step-wise change in rate of stress (SRS*) on one sample of reconstituted kaolin (S1k) and two samples of reconstituted London Clay (S2LCrB1 and S2LCrB2). The tests were carried out to confirm the previously observed behaviour under one-dimensional conditions and to investigate in more details the interrelationship between ageing, global strain rate and elastic shear modulus during SRS* isotropic compression and during prolonged periods of creep. The tests were performed in the period 25th March 2005 to 13th December 2005 in the geotechnical research laboratory at UCL. Details of the conducted triaxial tests are summarised in Table 4-2.

4.5.2 Special testing procedures

The tested samples of kaolin and reconstituted London Clay were prepared by preconsolidation to nominal 90 kPa vertical effective stress (corresponding to $p'_c \approx 70$ kPa, assuming a K_0 value of 0.64) as described in Section 3.4.3b. After set-up and the initial saturation stage all three samples were isotropically compressed in Triaxial cell no. 2, while maintaining the back pressure at 300 kPa. In order to increase the reliability of the tests the load cell was not connected to the top cap during the compression stage. As a result the external strain gauge was not in use and only internal strain measurements using the Hall Effect gauges were relied upon in addition to the external volume gauge. Isotropic compression was carried out with step changes in the confining stress rate and at different stages during the individual tests prolonged periods of creep were additionally introduced for up to one month. The nominal stress rates used were 0.3 kPa/hr, 1 kPa/hr (only pre-yield) and 3 kPa/hr in tests on reconstituted London Clay and 0.1 kPa/hr, 1.0 kPa/hr and 5 kPa/hr in the test on reconstituted kaolin. The control of stress rate rather than strain rate resulted in slight variations in the strain rates during stages of otherwise constant stress rate. This however appears not to have affected the results significantly, as seen from the presented data in the following. Since measurements of pore water pressure were not taken during compression the fastest stress rates were assumed to permit fully drained conditions. However, findings in Section 5.2.3 indicated that some build-up of positive pore water pressures could be expected in reconstituted London Clay samples during isotropic compression at a rate of 3 kPa/hr. The kaolin specimen on the other hand was shown

to require significantly shorter consolidation time and hence the build-up of positive pore water pressure is expected to have been insignificant even at the fastest compression rate of 5 kPa/hr.

It should be noted that due to technical problems both tests on reconstituted London Clay were prematurely terminated during a creep stage, sample S2LCrB2 at p'=132 kPa and S2LCrB1 at p'=300 kPa. The test on sample S1k of reconstituted kaolin was taken to about 500kPa effective stress, at which point both the cell pressure and the local strain gauge measurements had reached their limits. As in the one-dimensional compression tests the vertical elastic shear stiffness G_0 was determined from bender element testing at suitable intervals during all stages of isotropic compression and creep.

4.5.3 Characteristics of SRS* compression and creep behaviour

The effects of stress rate and creep on the isotropic compression behaviour of the two specimens of reconstituted London Clay (samples S2LCrB1 and S2LCrB2) are shown in Figures 4-40 and 4-41 respectively, while Figure 4-42 shows the behaviour of the reconstituted specimen of kaolin (sample S1k). The void ratio considered has been calculated from the local strain measurements, which were found to compare well with the volume gauge measurements as illustrated in Figure 4-43. The initial void ratio of the London Clay samples was determined to be around 1.29-1.33, while the initial void ratio of the kaolin sample was somewhat higher at 1.52. The marked difference in initial void ratio between the reconstituted kaolin and London Clay samples highlights the higher compressibility of the reconstituted London Clay. At the start of isotropic compression the behaviour of the two tested clays is similar. The initial compression behaviour is seen to be relatively stiff due to the preconsolidation. Each compression path then gradually yields and joins the respective normal compression line at mean effective stresses around 50-80 kPa, which correspond well with the estimated preconsolidation pressure of about $p'_c \approx 70$ kPa. In each test the NCL for fixed stress rate is observed to be approximately linear in e-ln p' plane, which indicates that the variations in strain rate over the tested stress intervals were only minor. Average values of the compressibility indexes $\lambda = \Delta e / \Delta \ln p'$ and C_c ($= \Delta e / \Delta \log \sigma_v'$) are listed in Table 4-3 together with values found from the oedometer tests. λ was found to be in the order of 0.178 (C_c= 0.41) to 0.221 (C_c= 0.51) for reconstituted London Clay and 0.178 (C_c= 0.41) for reconstituted kaolin. The λ value of 0.221 (C_c= 0.51) for reconstituted London Clay is similar to what has been estimated from the oedometer test in Section 4.4.3, but it is significantly higher than the average value of λ=0.182 found from the isotropic compression tests, which utilised the more accurate LVDTs to measure local strains, as reported in Section 5.2.3. It should be noted that the e-ln p' plot for sample S2LCrB2 (Figure 4-41) indicates an outwards shift in the normal compression line around p'=90 kPa. Both the volume gauge and the local radial strain measurement show this behaviour, while the local axial strain measurements do not. It therefore appears that it may have been caused by the radial strain belt preventing radial movement. For samples S2LCrB1 and

S2LCrB2 of reconstituted London Clay the strain rates associated with the imposed rates of confining stress were around 0.06-0.07 %/hr and 0.006-0.007 %/hr for stress rates of 3 kPa/hr and 0.3 kPa/hr respectively (Figure 4-44 and Figure 4-45). In the test on sample S2LCrB1 the strain rate reduces slightly towards the highest stress levels to around 0.03 %/hr for an imposed stress rate of 3 kPa/hr. During isotropic compression of the kaolin sample the associated strain rates at low stress levels were about 0.1 %/hr, 0.01 %/hr and 0.002 %/hr for stress rates of 5 kPa/hr, 1 kPa/hr and 0.1 kPa/hr respectively (Figure 4-46). Towards the highest stress levels the strain rates were observed to reduce to about 50% of their initial values.

The compression curves for the two samples of reconstituted London Clay show a clear effect of stress rate. When the stress rate is reduced by a factor of 10 from 3 kPa/hr to 0.3 kPa/hr, the compression path shifts downwards and subsequently appears to follow a path below and parallel to the NCL given by the higher stress rate. When the stress rate is increased back to the original higher rate, the compression path is observed to rejoin the NCL given by the higher stress rate. Some signs of undershooting and overshooting are observed. The limited stress range and limited number of changes in stress rate however makes it difficult to confirm the apparent parallel nature of the normal compression lines. The influence of stress rate on the compression curve of reconstituted kaolin is in contrast ambiguous (Figure 4-42a), which may in part be due to a greater variation in the strain rates. The effect of stress rate change becomes clearer when the compression path is plotted on natural scales (Figure 4-42b). Here it is seen that the curves for stress rates of 5 kPa/hr and 1 kPa/hr separate. The results for the slowest stress rate of 0.1 kPa/hr deviate from the general trends, which may be due to fluctuations in the transducer readings. Undershooting and overshooting are evident immediately after stress rate changes.

In all three tests fixed confining stress creep stages were imposed at different stress levels. In the tests on reconstituted London Clay, sample S2LCrB1 experienced a creep period for about 4 weeks at a stress level of p'=300 kPa, while sample S2LCrB2 experienced a creep period of about 3 weeks at p'=132 kPa. In both tests the fixed stress creep was initiated from a stress rate of 3 kPa/hr. During compression of the reconstituted kaolin specimen (sample S1k) four short-term stages of creep were imposed with varying length of up to 4 days at different stress levels. Creep was initiated from a stress rate of 5 kPa/hr at mean effective stresses of 30 kPa, 70 kPa and 262 kPa and from a stress rate of 1 kPa/hr at p'=500 kPa. The creep curves in Δe-log t plane are plotted in Figures 4-47 to 4-49 for the three samples respectively and the corresponding reductions in axial strain rate with time during creep are plotted on double logarithmic scales in Figures 4-50 to 4-52. For sample S1k data from four creep stages have been plotted. The creep behaviour in theses stages, apart from the creep stage at p'=500 kPa, can be characterised by an approximately linear reduction in the void ratio (or linear increase in the axial creep strain) with the logarithm of creep time after short initial transition period. This is also reflected in the logarithmic linear relationship between the axial strain rate and the creep

time, which in these cases plots with a gradient close to m=1 (refer to Section 2.3.1b). For the creep stage at p'=500 kPa, on the other hand the creep behaviour in Δe-log t plane (Figure 4-49) is seen to be more non-linear and the gradient of the curve in log $\dot{\varepsilon}_a$ -log t plane is estimated to be around m=0.6 (Figure 4-52). The transition period for the kaolin sample is generally observed to be around 1 hr (60 min), while for the samples of reconstituted London Clay the transition period is much higher at around 24 hrs (1440 min). For two samples of reconstituted London Clay it is observed that there is a rapid change in the gradient of the Δe-log t relationship during the initial transition period (Figure 4-47 and Figure 4-48). Despite that is was assumed that the tests were performed fully drained, the nature of the transition period for the samples of reconstituted London Clay indicate that it may be due to the dissipation of excess pore water pressures, which have accumulated under the highest rate of stress/strain.

Values of the coefficient of secondary compression C_α=$\Delta e/\Delta \log t$ for each creep stage are listed in Table 4-3. C_α is found be 0.0048 and 0.0052 for the two samples of reconstituted London Clay, while for the kaolin sample values of C_α are found to vary between 0.0043 and 0.0053 for the three creep stages that commenced from the same rate of compression of 5 kPa/hr. In contrast the creep stage that commenced from a lower rate of compression of 1 kPa/hr at p'=500 kPa gave a significantly lower C_α value of 0.00073. This however is likely to be due to the initial slower strain rate. Generally the values of C_α are indicated to reduce with increasing stress level for a given clay as shown in Figure 4-53, where the values of C_α obtained from the three samples have been plotted against the stress level at which the creep was taking place. From the plot it can additionally be observed that a given stress level the samples of reconstituted London Clay generally show a slightly higher degree of deformation during creep compared to the sample of kaolin.

4.5.4 Effect of creep on the elastic shear stiffness G_0

The changes in G_0 with time during the creep stages for all three tests are shown in Figures 4-54 to 4-56. It is observed that the data points in all cases fall close to straight lines in the plots of G_0 against log t. From the plots the coefficients I_G and N_G have been derived and summarised in Table 4-3. The two samples of reconstituted London Clay gave I_G values of 2200 kN/m^2 and 5100 kN/m^2 and N_G values of 0.10 and 0.11 for stress levels of p'=132 kPa (S2LCrB2) and p'=300 kPa (S2LCrB1) respectively. While the kaolin sample gave I_G values between 1700 kN/m^2 and 7000 kN/m^2, and N_G values between 0.08 and 0.09 for the three creep stages commencing from an initial stress rate of 5 kPa/hr. In contrast the creep stage that commenced from a lower rate of compression of 1 kPa/hr at p'=500 kPa gave an I_G value of 8700 kN/m^2 and relative low N_G value of 0.06. In all cases the normalisation appears to have removed most of the effect of stress level on the stiffness increase during creep. However, as can be seen the normalisation does not appear to take account of the effect of the initial stress rate. The N_G value,

which quantifies the relative increase in stiffness with time during creep, is generally seen to be greater for reconstituted London Clay compared to that of reconstituted kaolin.

4.5.5 Effect of stress rate and creep on the G_0-p' relationship

Figures 4-57 to 4-59 show the influence of stress rate and creep on the relationship between the elastic shear stiffness G_0 and the mean effective stress p' for each individual test. The consistency of the obtained results have generally been found to be very high as seen from Figure 4-60, where the data from the two tests on reconstituted London Clay have been plotted together in a plot of G_0 against p'. It is generally observed that for normally consolidated states at a given fixed stress rate the data points fall close to straight lines in the double logarithmic plots of G_0 against p'. Hence, the relationship between G_0 and p' at constant stress rate (or strain rate) can be described by a power function in the form:

$$\frac{G_0}{p_r} = A \cdot \left(\frac{p'}{p_r} \right)^n \tag{4.1}$$

as proposed by (Viggiani & Atkinson, 1995), where p_r is a reference pressure used to make the equation dimensionally consistent, and A and n are positive constants. Table 4-4 lists the estimated values of the non-dimensional soil parameters A and n for the three samples, obtained from the best fit lines through the data points (post yield only) at the given stress rates. The reference pressure p_r was taken as 1 kPa for simplicity. The linear nature of the lines for fixed stress rate again confirms that the variation in strain rate was only of minor magnitude over most of the tested stress intervals. However, for the sample of kaolin (S1k) the reduction in strain rate is observed to influence the results at the highest stresses towards the end of the test. Nevertheless, in all tests the trends are clear. The lines for different stress rates are seen to separate and generally appear to lie parallel. A reduction in stress rate has the effect of shifting the line upwards. The behaviour for overconsolidated states at low stresses clearly deviates from the logarithmic linear relationships observed post yield. Similar to the findings from the literature and the conducted one-dimensional tests, G_0 is generally observed to increase with overconsolidation ratio at a given p'. As a result the logarithmic increase in G_0 with logarithmic increases in p' at low stresses is much lower than what can be observed at higher stresses beyond the preconsolidation pressure. It is very interesting to note that the increases in elastic stiffness observed as a result of reductions in the imposed stress rate are seen to be very significant and are of comparable magnitude to the increases observed during periods of fixed effective stress creep for up to one month. This was also indicated from the one-dimensional tests, but the trends are much clearer in the isotropic compression tests due a smaller scatter in the results.

A closer look at the results for the test on kaolin (sample S1k) reveals that the immediate effect of a stress rate increase is a noticeable reduction in the elastic stiffness. For example at around p'=70 kPa the stress rate is increased to 5 kPa/hr after a short creep period. In this case

the elastic stiffness is initially observed to reduce with increasing mean effective stress until the p'-G_0 state reaches the constant stress rate line defined by the stress rate of 5 kPa/hr. At this point there is a marked change of direction in the p'-G_0 path and the elastic stiffness starts to increase again with increasing mean effective stress. Immediately after a stress rate increase the void ratio reduces slightly and the effective stress increases. An increase in the elastic stiffness would be expected based on the changes in state of the soil, yet this is not observed and the initial reduction in G_0 after a stress rate increase therefore cannot be explained by changes in the state. Similarly, the immediate increase in G_0 after a stress rate reduction cannot be explained by changes in the state of the soil. In Section 4.6 ageing, destructuration and strain rate are discussed as possible explanations for the observed behaviour.

4.5.6 Effect of stress rate and creep on e-G_0 relationship

In Figures 4-61 to 4-63 the results for each of the three tests are shown as void ratio e plotted against the measured elastic shear stiffness G_0. The influence of changing stress rates and periods of creep in these plots are observed to be similar to what was observed in the plots of elastic stiffness against mean effective stress. It is seen that the data points for normally consolidated states at a given fixed stress rate fall close to straight lines in the plots of e against logarithm of G_0. Hence, the relationship between G_0 and e at constant stress rate can be described by an exponential relationship in the form:

$$\frac{G_0}{p_r} = A' \cdot \exp^{-n' \cdot e} \tag{4.2}$$

Where the reference pressure p_r was introduced to make the equation dimensionally consist. p_r was taken as 1 kPa for simplicity. Table 4-5 lists the estimated values of the non-dimensional soil parameters A' and n' for the three samples. The values were obtained from the best fit lines through the data points (post yield only) at the given stress rates. Lines for different stress rates clearly separate and appear to lie parallel. A reduction in stress rate has the effect of shifting the line upwards. The initial data points at low stresses, for overconsolidated states, are seen to deviate from the linear relationships obtained post yield at normally consolidated states. For the test on kaolin (sample S1k) the results at the highest stresses under a fixed stress rate of 1 kPa/hr are seen to gradually plot further to the right of the nominal constant stress line, which may possibly be explained by the gradual variation in strain rate even during constant stress rate test. For compression of sample S2LCrB2 of reconstituted London it is observed that after having compressed the sample at 0.3 kPa/hr, the data points obtained at a rate of 3.0 kPa/hr appear to plot above the constant stress rate line defined by the initial results obtained under the same high stress rate. The reason for this deviation may be found in the possible prevention of radial strains by the radial strain belt, which was indicated after the first stage at high stress rate in Figure 4-41. The consistency of the results is otherwise good as seen from Figure 4-64, where the results from the two tests on kaolin have been plotted together in the plot of e against G_0.

From the test on kaolin (sample S1k) it can be observed that the immediate effect of a stress rate increase is a reduction in the elastic shear stiffness, despite a continuous reduction in void ratio. This is similar to what was observed in the G_0-p' plot. When the G_0-e state reaches the constant stress rate line defined by the higher stress rate the elastic shear stiffness then starts increasing again. It is also generally observed in the e-G_0 plot that the increase in elastic shear stiffness due to reductions in stress rate is of comparable magnitude to the increase in elastic stiffness observed with time during fixed effective stress creep for periods up to one month. The results show slightly more scatter in the G_0-e plot compared to the scatter in the G_0-p' plot, reflecting the fact that stress measurements are more reliable and that the determination of volumetric changes from the local strain measurements might have been slightly in error. The results however makes it clear that the observed changes in elastic shear stiffness after changes in stress/strain rate cannot entirely (in fact far from) be explained by the experienced changes in state, i.e. changes in mean effective stress or more importantly void ratio. In the section below the test data have been normalised to take account of the increase in mean effective stress and decrease in void ratio during compression, highlighting the direct influence of strain rate and ageing on the elastic shear stiffness.

4.5.7 Normalised behaviour

To investigate if either the influence of strain rate or ageing could explain the observed changes in the elastic shear stiffness during creep and constant rate of compression, the elastic shear stiffness was normalised to remove effects of stress and void ratio. To achieve this, the elastic shear stiffness G_0 was normalised with respect to the elastic shear stiffness $G_{0(p',\dot{\varepsilon}_{a,ref})}$ estimated at the current mean effective stress at a reference strain rate. The reference strain rate was chosen as the strain rate associated with the maximum imposed stress rate. In the two tests on reconstituted London Clay the reference rate was 0.07 %/hr, corresponding to a reference stress rate of 3 kPa/hr and for the test on reconstituted kaolin the reference strain rate was 0.1 %/hr, corresponding to the reference stress rate of 5 kPa/hr. Hence the normalised elastic shear stiffness $G_0 / G_{0(p',\dot{\varepsilon}_{a,ref})}$ represents the relative offset in state from the logarithmic linear compression line defined by the reference strain rate (or stress rate) in the plot of G_0 against p'. During stages of fixed effective stress creep $G_{0(p',\dot{\varepsilon}_{a,ref})}$ remains constant, while during compression $G_{0(p',\dot{\varepsilon}_{a,ref})}$ is a function of the mean effective stress. In each test the relationship between $G_{0(p',\dot{\varepsilon}_{a,ref})}$ and p' was obtained from the best fit line through the data points (post yield only) at the given reference stress rate, as shown previously. The elastic shear stiffness could in similar manner be normalised with respect to the elastic shear stiffness obtained at a reference strain rate at the current void ratio. In this case the reference stiffness $G_{0(e,\dot{\varepsilon}_{a,ref})}$ would increase slightly during stages of fixed effective stress creep. The effect of this would however be minor

and the two normalisation procedures would generally yield comparable results due to the unique linear relationship that exist between $\log p'$ and e at a given fixed strain rate.

a Effect of ageing time on the elastic shear stiffness G_0

Figures 4-65 to 4-67 show the normalised shear stiffness $G_0 / G_{0(p',\dot{\varepsilon}_{a,ref})}$ plotted against the logarithm of relative time (in minutes) for the three samples in order to highlight the effect of time (hence ageing) on the elastic shear stiffness. The data points are plotted from both creep stages and stages of constant rate of stress compression. However, pre-yield results immediately after stress rate increases have been excluded, since the predominant elastic behaviour would obscure the results. The relative time has been defined as the extra time required to reach the current stress level at the current stress rate compared to the time required if the sample was compressed at the corresponding reference stress rate after each step-wise change in constant rate of stress. Hence, in the case of compression of sample S1k of reconstituted kaolin, where the corresponding reference stress rate was 5 kPa/hr, after a reduction in the stress rate from 5 kPa/hr to 1 kPa/hr the relative time increased by four hours for every 5 kPa increase in mean effective stress. During creep stages the mean effective stress was constant and hence the relative time corresponds to the actual creep time. The relative time could also be defined by using the reference strain rate rather than the reference stress rate. This would however only make a minor difference to the plotted results.

The results for reconstituted London Clay (Figures 4-65 and 4-66) show some scatter. The results obtained at the corresponding reference stress rate of 3 kPa/hr would generally plot around a time of zero, which is not reflected well on a logarithmic scale. The results obtained at a rate of 3 kPa/hr have therefore all been plotted for illustration purposes at a relative time of 1 min. The values of the normalised elastic shear stiffness are found to range between 0.98-1.05 in the two tests. Results obtained during compression at the stress rate of 0.3 kPa/hr, i.e. one log cycle reduction in stress rate (or strain rate) from the reference rate, show a clear non-linear relationship between the normalised elastic shear stiffness and the logarithm of relative time. The normalised elastic shear stiffness appears to reach an upper bound plateau at a value around 1.12-1.13 for both sample S2LCrB2 and sample S2LCrB1 after relative times of roughly 1000 min and 5000 min respectively. During creep a linear increase in the normalised elastic shear stiffness against the logarithm of relative time is on the other hand observed, which simply reflect the previously shown linear relationship between elastic shear stiffness and logarithm of creep time.

The observed behaviour is confirmed in the test on reconstituted kaolin (Figure 4-67), in which the results are more extensive. The four creep stages show the expected linear increase in normalised stiffness, while the results for constant rate of stress compression at 1 kPa/hr and 0.1 kPa/hr show distinct non-linear behaviour in time domain. During compression at 0.1 kPa/hr the normalised elastic shear stiffness appears to reach an upper bound plateau at a value of around 1.20 after a relative time of roughly 4000 min. In contrast, the normalised elastic shear

stiffness shows no tendency to reach an upper bound limit during compression at the stress rate of 1 kPa/hr. This may be explained by the observed reduction in strain rate at higher stress levels during the otherwise constant rate of stress. The values of the normalised elastic shear stiffness for the corresponding reference stress rate of 5 kPa/hr are found to range between 0.97 and 1.04. As explained above, for illustration purposes these data have all been plotted at a relative time of 1 min. From all the three tests it can be generally observed that there is no unique relationship between relative time and the increase in the normalised elastic shear stiffness. Hence, it does not seem likely that the observed increase in elastic shear stiffness both during creep and after step-wise reductions in the stress (or strain rate) can be explained by ageing.

b Effect of global axial strain rate on the elastic shear stiffness G_0

To investigate the influence of strain rate the normalised elastic shear stiffness has been plotted against the logarithm of local axial strain rate for each of the three tests in Figures 4-68 to 4-70 respectively. Results are plotted for both fixed effective stress creep stages and for stages of constant rate of stress. Pre-yield results including results at low stresses in the overconsolidated region, have been excluded for the same reason as mentioned above. The average axial strain rate during each creep stage has been obtained from the relationship with creep time given by the best fit line through the data points shown previously in Figures 4-50 to 4-52. This was done in order to smooth the data and avoid interference from the significant observed (cyclic) fluctuations in strain rate during creep resulting from fluctuations in the Hall effect transducer readings. As described above, for creep stages linear relationships have been found both between logarithm of the axial strain rate and logarithm of creep time and between G_0 and the logarithm of creep time. Hence, it comes as no surprise that the creep data from all three tests is observed also to fall close to straight lines in the plots of the normalised elastic shear stiffness against the logarithm of axial strain rate. The general trend during creep is seen to be a continuous reduction in strain rate coupled with an increase in the elastic shear stiffness with time. Despite the scatter due to the fact the test were stress-controlled rather than strain – controlled, a look at the data from all three tests reveals a clear effect of strain rate on the normalised elastic shear stiffness. It is also observed that the normalised elastic shear stiffness increases consistently with the imposed step reductions in the strain rate.

In the test on sample S1k of kaolin (Figure 4-70) the normalised elastic shear stiffness, as per definition, is found to be around 1.0 for data points taken close to the reference axial strain rates of 0.1 %/hr, which generally corresponded to a stress rate of 5 kPa/hr. A step reduction in the stress rate to 1 kPa/hr, was found to be associated with a gradual reduction in axial strain rate of approximately one log cycle to 0.01 %/hr and a corresponding gradual increase in the normalised elastic shear stiffness to a value of around 1.12. A further reduction in stress rate to 0.1 kPa/hr, was associated with a gradual reduction in axial strain rate to about 0.002 %/hr and a corresponding gradual increase in the normalised elastic shear stiffness to a value around 1.19.

Despite some scatter, all the data fall in a narrow defined band. For example at an axial strain rate of 0.01%/hr the normalised elastic shear stiffness G_0 is found to vary in the interval between 1.07 to 1.14, corresponding to a deviation of 3-4 % from a mean of 1.11. From the data a general trend emerges; for each individual test all the data for constant stress rate compression and data taken during stages of fixed effective stress creep appear to define a unique linear relationship between the normalised elastic shear stiffness and the logarithm of the axial strain rate, which can be described in the form:

$$\frac{G_0}{G_{0(p',\dot{\varepsilon}_{a,ref})}} = 1 - \alpha_0 \cdot \log \dot{\varepsilon}_a \tag{4.3}$$

The value $-\alpha_0$ is the slope of the trend "line" and hence the coefficient α_0 represents the increase in the normalised elastic shear stiffness per log cycle reduction in the axial strain rate. Since the gradient of the trend "line" is found to be approximately constant the global rate coefficient α_0 appears to be independent of stress rate, strain rate, state and creep time. Interestingly the α_0 value is found to be approximately 12 % in tests on both reconstituted London Clay and reconstituted kaolin, which may indicate that the coefficient is not significantly affected by clay mineralogy, but more data is needed to confirm this. Data for all three tests are compared in Figure 4-71. In order to compare tests with different reference strain rates the normalised elastic shear stiffness have been plotted against the logarithm of strain rate normalised with respect to the reference strain rate, thus highlighting the effect of changes in strain rate rather than absolute values of strain rate. A unique linear relationship between normalised elastic shear stiffness and logarithm of the normalised strain rate is apparent from the plot, despite that data is plotted for samples of both reconstituted London Clay and kaolin. The relationship can be expressed as follows;

$$\frac{G_0}{G_{0(p',\dot{\varepsilon}_{a,ref})}} = 1 - \alpha_0 \cdot \log\left(\frac{\dot{\varepsilon}_a}{\dot{\varepsilon}_{a,ref}}\right) \tag{4.4}$$

The uniqueness of the relationship between the normalised elastic shear stiffness and the normalised axial strain rate, which include data from both constant stress rate compression and fixed effective stress creep, strongly suggests that the increase in elastic shear stiffness observed during periods of rest and after step reductions in strain rate or stress rate can simply be explained by viscous strain rate effects rather than ageing effects. Its is quickly realised that a similar unique relationship between the normalised elastic shear stiffness and the stress rate cannot be obtained, since the creep data in contrast to the constant stress rate data would generally plot at zero stress rate.

It is proposed that the influence of state and strain rate on the elastic shear stiffness can be expressed in the following general form;

$$\frac{G_0}{p_r} = A_{\dot{\varepsilon}_{a,ref}} \left(\frac{p'}{p_r} \right)^n R_{\alpha_0} \tag{4.5}$$

Where $A_{\dot{\varepsilon}_{a,ref}}$ is a non-dimensional soil parameter obtained from the constant strain rate line defined by the reference axial strain rate $\dot{\varepsilon}_{a,ref}$, while the influence of strain rate is quantified by the rate parameter R_{α_0}, given by

$$R_{\alpha_0} = 1 - \alpha_0 \cdot \log\left(\frac{\dot{\varepsilon}_a}{\dot{\varepsilon}_{a,ref}} \right) \tag{4.6}$$

In order to validate the hypothesis on the soil behaviour's dependency on strain rate, the elastic shear stiffness has been normalised with respect to the rate parameter R_{α_0} for each of the three performed isotropic compression tests to remove the influence of strain rate, and plotted against the mean effective stress and void ratio respectively. The normalised plots are shown in Figures 4-72 to 4-77. It can be seen from the plots of $\log\left(G_0 / R_{\alpha_0}\right)$ against $\log p'$ and $\log\left(G_0 / R_{\alpha_0}\right)$ against e that the normalisation has removed most of the effect of strain rate and unique relationships are suggested. The normalisation is seen to work especially well in the plots of $\log\left(G_0 / R_{\alpha_0}\right)$ against $\log p'$, while larger scatter is observed in the plots against void ratio, possibly due to errors in estimating void ratio, as mentioned before.

4.6 DISCUSSION

4.6.1 Generally on the reliability of the presented results

The sources of errors in the described one-dimensional and isotropic compression tests have the potential to be significant and could have affected the determination of all the used variables, such as stresses, strains, creep time and travel time of the bender element shear waves and their derivatives, which include void ratio, strain rates and elastic shear stiffness. However as has been shown from the presented results, the overall consistency of the data especially in the isotropic compression tests and the clarity of the observed trends indicate reliable results with only little or insignificant influences of uncontrollable disturbing factors.

Factors which may especially have affected the results from the isotropic triaxial compression tests include the build up of pore water pressure (not monitored) under high rates of strain under the assumed drained conditions and inaccurate local strain measurements, which would have affected the determination of strain rates and void ratio. Inaccuracies in the determination of local strains could have been caused by non-cylindrical distortion of the sample and fluctuation in the temperature. Nevertheless, the general parallel nature of constant stress rate lines indicates that the actual variations in the strain rates and the gradual build up of pore water pressures at high stress rates were small and hence had only minor observed effects on the overall results. Local inaccuracies in the results were however observed as mentioned previously in each of the tests. In addition to this it should be mentioned that for sample S1k of reconstituted kaolin a significant drift in the pore water pressure transducer readings (positive direction) at the end of the test was indicated by the external pressure gauge. This error in the pore water pressure readings may in part explain the gradual shift in the data away from the constant stress rate lines as observed in the plot of G_0 against p' at the highest stresses (Figure 4-59). However, the consistency of the data in Figure 4-70 generally indicates that the observed shift in the plot of G_0 against p' at the highest stresses is primarily caused by a gradual reduction in strain rate under the constant stress rate.

The reliability of the results from the one-dimensional oedometer compression tests is not as great as the reliability of the results obtained in the isotropic triaxial compression tests. This can mainly be attributed to the differences in the testing systems. In contrast to the triaxial cell the total stress conditions were not fully known in the oedometer cell, because of the lack of radial stress measurements and the influence of vertical friction from the confining ring. Moreover, the determined effective stress conditions may be in error due to the assumption made concerning the average pore water pressure in the sample. The determination of vertical strains and changes in void ratio would have been slightly influenced by tilting of the top cap, however the errors associated with this are generally small as indicated by the measured strain rates. As will be discussed in the Section 4.6.2 below, the one-dimensional compression tests on

kaolin show a behaviour which is different to what has been otherwise observed. It is possible that part of this deviation may be explained by the uncertainties in the effective stress conditions.

The reliability and accuracy of the bender element results are generally believed to be very good in the triaxial tests, while in the oedometer tests the boundary conditions of the cell and the relatively small distance between the receiving and transmitting elements may have led to inaccurate estimations of the elastic shear stiffness. In the isotropic triaxial compression tests the small scatter in the results, for the observed relationship between the elastic shear stiffness and void ratio or mean effective stress, highlight that the chosen objective method of interpretation gives rise to very reliable and very consistent results. The highest accuracy of the results was obtained in isotropic compression of sample S2LCrB1 of reconstituted London Clay, where the best fit lines through the data points of e against G_0 and G_0 against p' at the highest stress rate of 3 kPa/hr showed R^2 values of 0.9998 and 0.99995 respectively, as listed in Tables 4-4 and 4-5. In the isotropic compression test on kaolin (sample S1k) the number of data points was greater and the accuracy was seen to reduce slightly. While in the one-dimensional oedometer compression tests the accuracy of the derived elastic shear stiffness was seen to be further reduced, which could possibly be connected to the abovementioned boundary conditions.

4.6.2 Comparing the effect of strain rate on elastic shear stiffness in one-dimensional compression with the effects observed in isotropic compression

From the isotropic triaxial compression tests and one-dimensional oedometer compression tests it was found that for a given constant rate of strain the logarithm of the elastic shear modulus was to a good approximation proportional to both the void ratio and the logarithm of the mean effective stress or the logarithm of vertical effective stress. In Figures 4-78 and 4-79 the behaviour in isotropic and one-dimensional compression tests on kaolin are compared in plots of ln G_0 against ln p' and e against ln G_0 respectively. The best fit lines through the data have been plotted from two representative tests; the isotropic compression test on sample S1k and the one-dimensional compression test on sample S03oeds3. A constant K_0 value of 0.69 has been assumed to determine p' from the oedometer test. It can be seen from the plots that the values of elastic shear stiffness generally are predicted to be lower in the one-dimensional compression test compared to the isotropic compression test over the tested stress interval. The difference is seen to increase with increasing stress level or reducing void ratio. Hence, in the plot of ln G_0 against ln p' the slopes of the constant strain rate lines appear steeper for the isotropic compression test compared to the one-dimensional compression test, while in the plot e against ln G_0 it is the other way around. It is expected that the observed offset in stiffness measurements between the isotropic and one-dimensional compression tests is due in part to the influence of different sample dimensions and confinement conditions and in part due to the overestimation of stresses in the oedometer test. It can furthermore be observed that the CRS lines obtained from the one-dimensional SRS compression tests on kaolin clearly approached each other with

increasing stress level in the plots of e against ln G_0 and ln G_0 against ln p'. This differs from the parallel nature of the CRS lines obtained in isotropic compression.

The relatively small difference between the limited stress range up to 500 kPa in the isotropic compression tests compared to the higher stress range up to 4000 kPa in oedometer tests, does not seem to be able to explain the difference in behaviour between the two types of tests. As mentioned above, one explanation could be that the uncertainty in stress conditions in the CRS oedometer test on kaolin has influenced the results. Both the side friction and the anisotropic K_0 stress conditions may have shown considerable variations with increasing stress level and strain rates. The plot of ln G_0 against ln σ'_v can therefore not be expected to be similar to the more relevant plot of ln G_0 against ln p', as assumed by using a constant K_0 value. Even so, erroneous stress conditions cannot explain the deviation in behaviour also observed in the plot of e against ln G_0. It may be more likely that the boundary conditions and the gradually reducing distance between the bender elements in the oedometer cell with increasing stress level have resulted in a gradual increasing underestimation of the elastic shear stiffness. The underestimation of the elastic shear stiffness may have affected the results at the slowest strain rate most. Generally, it can be said that the results obtained from the isotropic compression tests are most reliable. Hence, in the following comparison with literature only results from isotropic compression tests are used. In isotropic compression the behaviours of kaolin and reconstituted London Clay are seen to be similar. Both materials show clear effects of strain rate, with parallel relationships obtained for different strain rates in plots of e against ln p', e against ln G_0 and ln G_0 against ln p'. This is shown schematically in Figure 4-80.

4.6.3 Comparison of isotropic compression results with available data from the literature

The general linear relationships observed in plots of e against ln p', e against ln G_0 and ln G_0 against ln p' for both reconstituted kaolin and reconstituted London Clay have been confirmed in several previous studies found in the literature on various clays (Jovicic & Coop, 1998; Lohani et al., 2001; Rampello et al., 1997; Viggiani & Atkinson, 1995). The obtained relationships between ln G_0 and ln p' and e against ln G_0 for reconstituted kaolin in the isotropic compression test on sample S1k are compared to available data from the literature in Figures 4-81 and 4-82, while the relationships between ln G_0 and ln p' and e against ln G_0 obtained for reconstituted London Clay in the representative isotropic compression test on sample S2LCrB1 are compared to available data from the literature in Figures 4-83 and 4-84. Similarly to this study, in the previous studies the elastic shear stiffness has in all cases been obtained from bender element tests with shear waves transmitted in the vertical direction.

From Figure 4-81 it can be seen that the data obtained from three different studies in the literature for reconstituted kaolin generally fall close to the linear relationship found in this study between ln G_0 and ln p' at the slowest stress rate of 1 kPa/hr. The slope of the constant stress rate lines obtained in this study is however slightly higher than that found by others. The

elastic shear stiffness measured at the fastest stress rate of 5 kPa/hr is noticeable lower than the values obtained in the literature. The close agreement between the data from this study at the slowest strain rate and the data obtained in the literature confirm that the chosen method of interpretation of the bender element tests is satisfactory. Unfortunately none of the studies found in the literature have reported on the used strain rates. This would have helped to clarify if the data from previous studies plot close to the slowest strain rate line by coincidence or because the used strain rates were close to 1 kPa/hr. The close agreement between the different studies also highlights the commercial nature of speswhite kaolin, which makes it possible to compare data of practically identical materials. In the plot of e against ln G_0, shown in Figure 4-82, the constant strain rates lines have been compared to data obtained from one-dimensional compression reported by Lohani et al. (2001). It is observed the slopes of the post yield lines are similar, however the elastic shear stiffness at a given void ratio is seen to be significantly lower in one-dimensional tests compared to the values obtained in this study in isotropic compression. Part of this offset may be explained by the offset between the isotropic and one-dimensional compression lines in the plot of e against p' due to anisotropy. However, different interpretation methods and different boundary conditions are most likely the primary causes for the observed differences also observed in this study and mentioned before (refer to Figure 4-79).

When comparing results from tests on reconstituted London Clay it is a different matter, mainly because mineralogy, grain size distribution and soil properties in general of London Clay may vary significantly if the tested specimens have been obtained from different geological sub-units (Gasparre, 2005). A good comparison with literature data is therefore not expected. The relationships between ln G_0 and ln p' obtained in this study in compression of sample S2LCrB1 of reconstituted London Clay at two different strain rates have been compared to data obtained from isotropic compression tests on specimens of both reconstituted and undisturbed London Clay in studies by Viggiani & Atkinson (1995) and Jovicic & Coop (1998), as shown in Figure 4-83. It can be observed that both the magnitude of the elastic shear stiffness at a given stress state and the slope of the lines found in this study for reconstituted London Clay do not compare well with those reported by Viggiani & Atkinson (1995) over the same stress interval. The data points for reconstituted states reported by Jovicic & Coop (1998) have been obtained at high pressures. If the lines found in this study are extrapolated to similar high pressures, it is seen that the data compare fairly well, in terms of magnitude of the elastic shear stiffness at given stress level. The slopes of the lines for intact natural specimens (heavily overconsolidated) reported in the literature compare well with the gradient observed in the overconsolidated region at stresses below the preconsolidation pressure in compression of sample S2LCrB1. Only data from Jovicic & Coop (1998) were available for comparison in terms of void ratio against elastic shear stiffness, as shown in Figure 4-84. The slopes of the lines compare reasonably well, however the elastic shear stiffness reported by Jovicic & Coop (1998) at a given void ratio appears to be significantly higher, which does not tie in with the

observations made in the plot of ln G_0 against ln p'. As mentioned above the primary reason for the observed differences in the compared studies is believed to be due to inherent differences in the tested samples. Different methods used to interpret the bender element tests may also have had a minor influence. The comparison is even more approximate given the strain rates for the tests available from the literature are not known.

4.6.4 General discussion on normalisation and normalised behaviour

In the performed one-dimensional and isotropic compression tests the variables are many, which makes normalising difficult. Apart from the two common state parameters, void ratio and mean effective stress, the influence of global strain rate and creep time have been considered to explain the elastic shear stiffness. Additionally, at pressures below the preconsolidation pressure there will be an influence of the overconsolidation ratio. Therefore, as a first step to remove the influence of OCR in the normalisation procedure, data for stress levels below the preconsolidation pressure have simply been excluded. For a given strain rate and stress ratio a unique relationship is generally found between e, ln p' and ln G_0 (Rampello et al., 1997). The value of G_0 has therefore been normalised to remove the effects of e and p' by normalising with respect to a reference G_0 determined at a reference strain rate at the current mean effective stress. The influence of the imposed global strain rate and creep time could then be investigated without the influence of other variables. In the initial investigation of the variation in the normalised G_0 with strain rate it was observed that pre-yield results (approximately within the Y2 surface) obtained immediately after stress rate increases did not correlate well with the rest of the post yield results. The predominant elastic behaviour in the pre-yield region could explain this and it became apparent that the variation in the normalised G_0 value would only correlate well with the plastic strain rate. Hence, pre-yield results were excluded from the normalised data. However, results immediately after strain rate reductions have been included since these generally remain within the plastic region.

4.6.5 General discussion on the influence of ageing and viscosity on the elastic shear stiffness

As mentioned in the literature review several previous studies on various clays suggest that the extraordinary increase in G_0 observed during creep, in excess of what could be explained by the reduction in void ratio, could be attributed to structuration phenomena such as bonding. In tests on reconstituted kaolin clay, Lohani et al. (2001) and Anderson & Stoke (1978) also attributed the extraordinary increase in G_0 observed during creep to structuration effects. This was believed despite that kaolinite, which makes up the majority of kaolin clay, is generally considered inactive and therefore is not likely to generate significant interparticle bonds. Structuration effects observed on the elastic shear stiffness also conflict with the general lack of structuration effects observed on the yield stress and effective strength envelope in kaolin and some other clays after creep, as reported by e.g. Lohani et al. (2001). Many studies found in the

literature do not consider the changes in void ratio occurring during periods of drained creep and erroneously attribute the observed increase in the yield surface or effective strength to structuration effects. Another interesting point made by Prof. Tatsuoka (Tatsuoka, 2003c) is that generally upon initiation of a constant stress creep period an immediate deviation in the e-G_0 relationship is observed. If structuration was to be the cause, a deviation would not have been expected immediately. Instead structuration effects would only be noticeable after some time, at a point when the strain rate has reduced to a slow enough rate. This argumentation is supported by the findings in the study on artificially sedimented Jonquière clay (Leroueil et al., 1996), as reported in the literature review in Section 2.4.2a, for which it was found that structuration effects on the one-dimensional compression path were only observed at very slow strain rates.

The results presented in this study on reconstituted kaolin and reconstituted London Clay generally indicate that the changes in the elastic shear stiffness observed during pore water dissipation, creep, stress relaxation and as a results of strain rate changes in both one-dimensional and isotropic compression can be attributed to the combined effect of a change in state and a change in the plastic strain rate rather than time dependent "inherent" ageing effects. In the one-dimensional oedometer compression tests there were significant uncertainties about the actual all-round stress conditions. Rampello et al. (1997) observed an influence of stress ratio η on G_0 for the same stress level in tests on reconstituted Vallericca clay, nevertheless G_0 appeared to be uniquely linked to e independently of stress ratio for normally consolidated states. Hence, it appears as though a gradual change in stress ratio, i.e. K_0 conditions, cannot explain the influence of strain rate observed in the one-dimensional compression tests. Similarly, uncertainties about the pore water pressure in both the oedometer and triaxial compression tests cannot explain the effects of strain rate observed in the e-G_0 relationship.

It is interesting to find that reconstituted London Clay, which in natural state shows signs of metastable structure from bonding and cementation (Gasparre, 2005), does not appear to be significantly influenced by ageing effects for short term periods up to one month. In this study a lot of evidence has been presented against the presence of significant short-term ageing effects in natural and commercial clays. Despite this some studies found in the literature report on increases in the very small strain stiffness, yield surface and effective strength envelope with time, which cannot be explained by viscous effects e.g. one-dimensional compression of artificially sedimented Jonquière clay at very slow strain rates (Leroueil et al., 1996) and in triaxial compression of Fujinomori clay after short creep periods of 2 days (Tatsuoka et al., 2000). It is possible that reconstituted London Clay tested in the laboratory may show signs of "inherent" ageing effects in the long term (years). Nevertheless, the majority of structuration effects observed in natural London Clay are expected to be attributed to post sedimentation "environmental" ageing effects such as leaching, weathering and other changes to the pore water chemistry due to external factors. Hence, "inherent" ageing effects may contribute relatively little to the overall structure.

4.6.6 New proposed parameters to quantify the influence of strain rate and creep time on the elastic shear stiffness

The two coefficients I_G and N_G proposed by Anderson & Stoke (1978) to quantify the increase in G_0 with time during creep have been widely used in the studies reported in the literature. The two coefficients are expressed as;

$$I_G = \frac{\Delta G_0}{\Delta \log t} \text{ and } N_G = \frac{I_G}{G_{0,1000}}$$

In order to remove effects of stress level Anderson & Stoke (1978) suggested to normalise I_G with respect to an arbitrary value of G_0 taken at reference time of 1000 min, which should be after the end of primary consolidation. Presumably to have a more reliable reference state other researchers have instead chosen to normalise with respect to a G_0 value taken at EOP. Hence any uncertainties in the origin of creep time are avoided. Both methods of normalisation however have their limitations. Normalisation with respect to a G_0 value taken at the EOP requires the creep stage to be initiated from a state of excess pore water pressure, which may not necessarily be the case in compression at slow rates of strain. Additionally, the EOP point may depend on drainage conditions and sample size, and the corresponding strain rates may therefore not be of similar magnitude. On the other hand using an arbitrary G_0 value taken at a reference time of 1000 min, as originally suggested, also gives rise to some problems. Firstly the normalisation requires that the sample has fully consolidated within 1000 min, which can be a problem for step loading of a very low permeable soil like London Clay. Secondly, the G_0 value obtained at a reference time of 1000 min will for the same soil at the same state be affected by whether the creep stage commences from a state pre- or post-EOP. The magnitude of the accumulated pore water pressure before commencing the creep stage may also influence the results.

In this study a unique relationship between the normalised elastic shear stiffness and the plastic strain rate was suggested for a given clay. In Section 4.5.7 the general increase in G_0 with reduction in strain rate normalised with respect to G_0 taken a the current mean effective stress at a reference strain rate was quantified using the global rate coefficient, which can be expressed as;

$$\alpha_0 = -\frac{\Delta\left(G_0 / G_{0(p',\dot{\varepsilon}_{a,ref})}\right)}{\Delta \log \dot{\varepsilon}_a} \tag{4.7}$$

The global strain rate coefficient bares resemblance to the cyclic rate coefficient $\alpha(\gamma)$, which was suggested by Lo Presti et al. (1996) to quantify the general strain rate dependency of the shear modulus in cyclic loading;

$$\alpha(\gamma)=\frac{\Delta G_0(\gamma)}{\Delta(\log\gamma)\cdot G(\gamma,\dot{\gamma}_{ref})} \tag{4.8}$$

The suggested unique relationship given by Equation (4.7) applies generally for isotropic compression of the two tested clays and appears to be valid for both positive and negative step-wise changes in strain rate, positive and negative gradual changes in strain rate and negative changes in strain rate during creep. It should be noted that it would generally be more correct to only consider the plastic component of the global strain rate and by doing so the suggested relationship will also predict the increase in G_0 as a result of gradual reductions in the plastic strain rate during stress relaxation. The findings suggest that during creep the changes in G_0 are controlled by changes in strain rate rather than ageing effects with time. A new creep time coefficient N_G^* is therefore proposed to quantify the increase in G_0 with time during stages of fixed effective stress creep in a more objective manner. The new coefficient is given by,

$$N_G^* = \frac{\Delta\left(G_0 / G_{0(p',\dot{\varepsilon}_{ref})}\right)}{\Delta\log t} \tag{4.9}$$

Where $G_{0(p',\varepsilon_{a,ref})}$ is the elastic shear stiffness found at the current mean effective stress at a reference strain rate, $\dot{\varepsilon}_{a,ref}$. In Figure 4-85 values of N_G^* and corresponding values of N_G are compared. The values of N_G^* were obtained at the reference strain rate of 0.07 %/hr in the reported tests on reconstituted London Clay and 0.1 %/hr in tests on reconstituted kaolin. It can be seen that the new normalisation generally result in slightly higher values of N_G* compared to N_G, since the value of the reference stiffness $G_{0(p',\varepsilon_{a,ref})}$ generally is lower than the value of $G_{0,1000}$. Conveniently N_G^* can be related to the global rate coefficient α_0 and the creep coefficient $m=-\frac{\Delta\log\dot{\varepsilon}_a}{\Delta\log t}$ (Singh & Mitchell, 1968) in the following manner,

$$N_G^* = \alpha_0 \cdot m \tag{4.10}$$

Which is also shown from Figure 4-86, where the schematic influence of strain rate on the unique relationships between $G_0 / G_{0(p',\varepsilon_{a,ref})}$, $\dot{\varepsilon}_a / \dot{\varepsilon}_{a,ref}$ and t / t_{ref} is plotted. The findings in this study suggest that the value of α_0 is constant for a given soil and hence N_G^* will simply be proportional to the creep coefficient m. Values of N_G^* and m have been obtained from the creep stages in the three isotropic compression tests on reconstituted kaolin and reconstituted London Clay. These are listed in Table 4-3. In Figure 4-87 the values of N_G^* are plotted against values of m. All the data points are observed to fall reasonably close around a linear line, which goes through the origin and has a gradient corresponding to α_0=*0.12*. Despite reconstituted kaolin and reconstituted London Clay giving similar values of the global rate coefficient, different clays may be expected to have different values of α_0.

In contrast to the simple relationship between N_G^* and m, previous studies found in the literature have with mixed success tried to correlate the coefficient of increase in G_0 with time,

N_G with the coefficient of secondary consolidation, C_α. Most researchers indicate an increase in N_G with increasing C_α in tests on soft clays (Lo Presti et al., 1996; Lohani et al., 2001; Mesri & Castro, 1987), but some have reported a reduction in N_G with increasing C_α e.g. data from Lee et al. (1995) reported by Lo Presti et al. (1996). Generally in all the studies a considerable scatter in the correlation is seen. In this study the relationship between N_G and C_α for reconstituted kaolin and reconstituted London Clay is found to be ambiguous. Nonetheless, the data compare well with the general trend of the data reported by Lohani et al. (2001) and Lo Presti et al. (1996) for a wide range of soils including sands and clays, as shown in Figure 4-88. The data given by Lohani et al. (2001) however also indicate that for kaolin the relationship between N_G and C_α does not adhere to the general trend found for a wide range of soils. Hence, it is possible that the overall trend for different soils stems from the fact that the values of N_G and C_α both increase consistently with a reduction in for example grain size, rather than there being a direct relationship between N_G and C_α. The incoherent correlation between N_G and C_α, found for a given clay, can indeed be explained by a non existing relation between the elastic shear stiffness, ageing effects and deformation during creep, as highlighted in this study. The similar values of N_G found in this study and the studies reported in the literature indicate that the increase in G_0 observed during creep in the study by for example Lohani et al. (2001) and other researchers also can be attributed to strain rate effects rather than ageing effects.

4.7 TABLES AND FIGURES FOR CHAPTER 4

Table 4-1 Overview of one-dimensional oedometer compression tests with bender element testing

Sample no.	Material	Type	Nominal strain rates $\dot{\varepsilon}_a = 1.2\times10^{-6}$ s^{-1} = 0.43 %/hr	Test stages
S01oeds3	r. kaolin	CRS	$25\,\dot{\varepsilon}_a$	C, UL
S02oeds3#	r. kaolin	SRS	$25\,\dot{\varepsilon}_a$, $200\,\dot{\varepsilon}_a$	C, UL-RL-UL
S03oeds3	r. kaolin	SRS	$\dot{\varepsilon}_a$, $25\,\dot{\varepsilon}_a$	C, SR, UL
S04oeds3	r. kaolin	SRS	$\dot{\varepsilon}_a/5$, $\dot{\varepsilon}_a$, $5\,\dot{\varepsilon}_a$, $25\,\dot{\varepsilon}_a$	C, SR, UL-RL
S01oeds4	r. London Clay	SL, CRS	$\dot{\varepsilon}_a/5$	C, SR, UL

CRS: constant rate of straining, SRS: step change in rate of straining, SL: step-loaded, C: short-term creep stage, SR: short-term stress relaxation stage, UL: unloading, RL: reloading
Bender element testing omitted

Table 4-2 Overview of isotropic triaxial compression tests with bender element testing

Sample no.	Material	Type	Nominal stress rates [kPa/hr]	*B*-value after saturation	Void ratio after saturation	Test stages
S2LCrB1	r. London Clay	SRS*	0.3, 1.0, 3.0	0.98	1.29	C
S2LCrB2	r. London Clay	SRS*	0.3, 3.0	0.87	1.33	C
S1k	r. kaolin	SRS*	0.1, 1.0, 5.0	0.993	1.52	C

SRS*: step change in rate of stress, C: short-term creep stage

Table 4-3 Soil parameters

Sample no.	Material	λ	C_c	C_α	m	I_G	N_G	N_G*
S01oeds3	r. kaolin	-	0.37	-	-	-	-	-
S02oeds3	r. kaolin	-	0.40	-	-	-	-	-
S03oeds3	r. kaolin	-	0.37	-	-	-	-	-
S04oeds3	r. kaolin	-	0.40	-	-	-	-	-
S01oeds4	r. London Clay	-	0.51	0.016	1.0	2303-13677	0.06-0.37	-
S2LCrB1	r. London Clay	0.221	0.51	0.0048	1.0	5100	0.11	0.12
S2LCrB2	r. London Clay	0.178	0.41	0.0052	1.0	2200	0.10	0.11
S1k	r. kaolin	0.178	0.41	0.00073-0.0053	0.57-0.99	2700-8700	0.06-0.09	0.06-0.13

Table 4-4 Non-dimensional soil parameters A and n [#]

Sample no.	Material	Ref. stress rate [kPa/hr]	Ref. strain rate [%/hr]	A	n	r^2
S03oeds3 [$]	r. kaolin	-	10.8	481	0.625	0.9990
S03oeds3 [$]	r. kaolin	-	0.43	784	0.561	0.991
S2LCrB1	r. London Clay	3	0.07	302	0.873	0.9998
S2LCrB2	r. London Clay	3	0.07	546	0.741	0.991
S1k	r. kaolin	5	0.1	807	0.800	0.9990
S1k	r. kaolin	1	0.01	913	0.800	0.993

[#] $\frac{G_0}{p_r} = A \cdot \left(\frac{p'}{p_r} \right)^n$ (Viggiani & Atkinson, 1995). p_r = 1 kPa.

[$] p' has been estimated using a K_0 value of 0.69.

Table 4-5 Non-dimensional soil parameters A′ and n′ [#]

Sample no.	Material	Ref. stress rate [kPa/hr]	Ref. strain rate [%/hr]	A'	n'	r^2
S03oeds3	r. kaolin	-	10.8	2928	3.80	0.998
S03oeds3	r. kaolin	-	0.43	2572	3.54	0.990
S2LCrB1	r. London Clay	3 kPa/hr	0.07	1288	3.94	0.99995
S2LCrB2	r. London Clay	3 kPa/hr	0.07	1122	3.77	0.994
S1k	r. kaolin	5 kPa/hr	0.1	10436	4.48	0.9990
S1k	r. kaolin	1 kPa/hr	0.01	11210	4.48	0.98

[#] $\frac{G_0}{p_r} = A' \cdot \exp^{-n' \cdot e}$. p_r = 1 kPa.

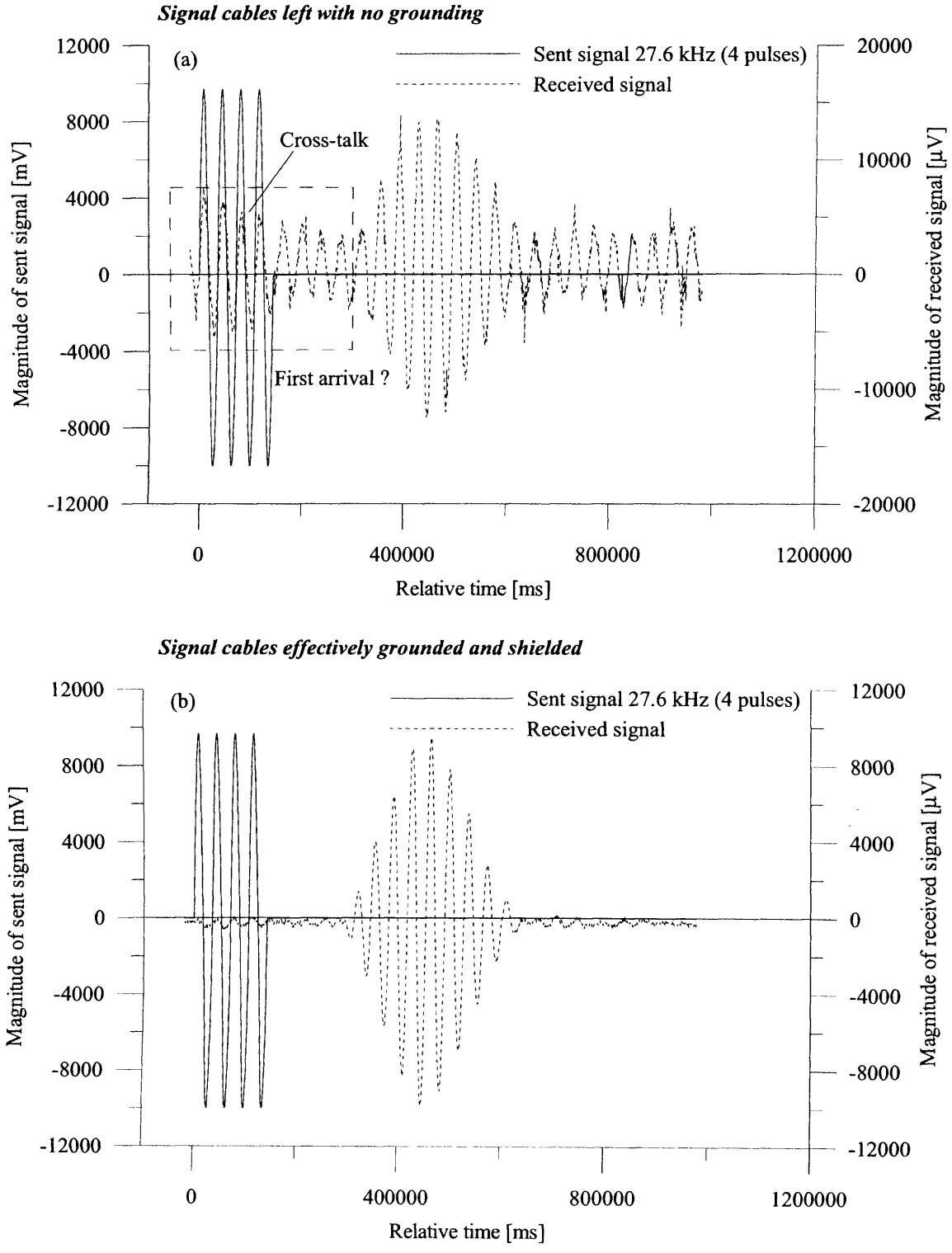

Figure 4-1 Beneficial effect of grounding signal cables

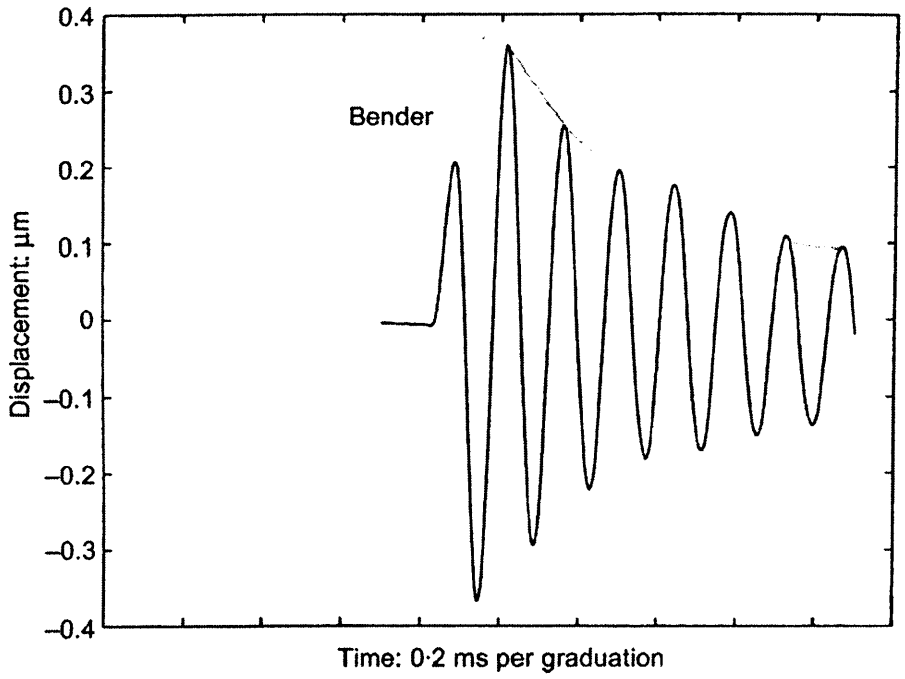

Figure 4-2 Unrestricted movement of bender element tip in air when transmitting a single sinusoid pulse, (modified after Lings & Greening, 2001)

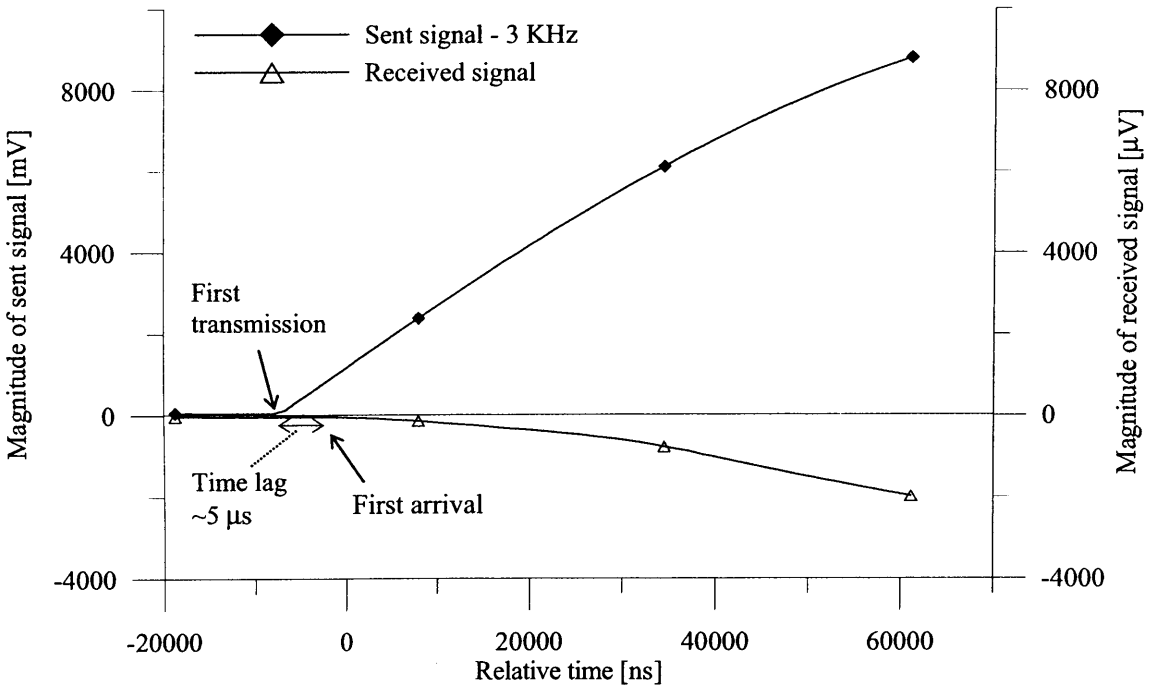

Figure 4-3 Determination of time lag for bender elements in direct tip to tip contact in air

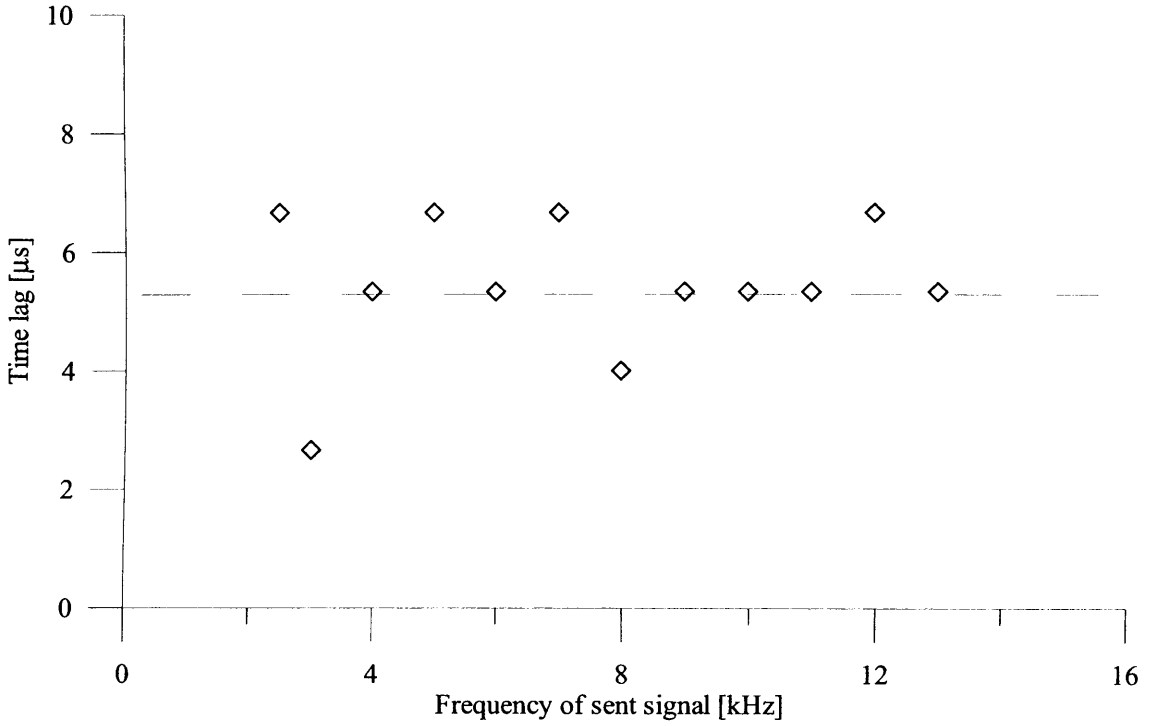

Figure 4-4 Influence of frequency of the transmitted bender element signal on the estimated time lag

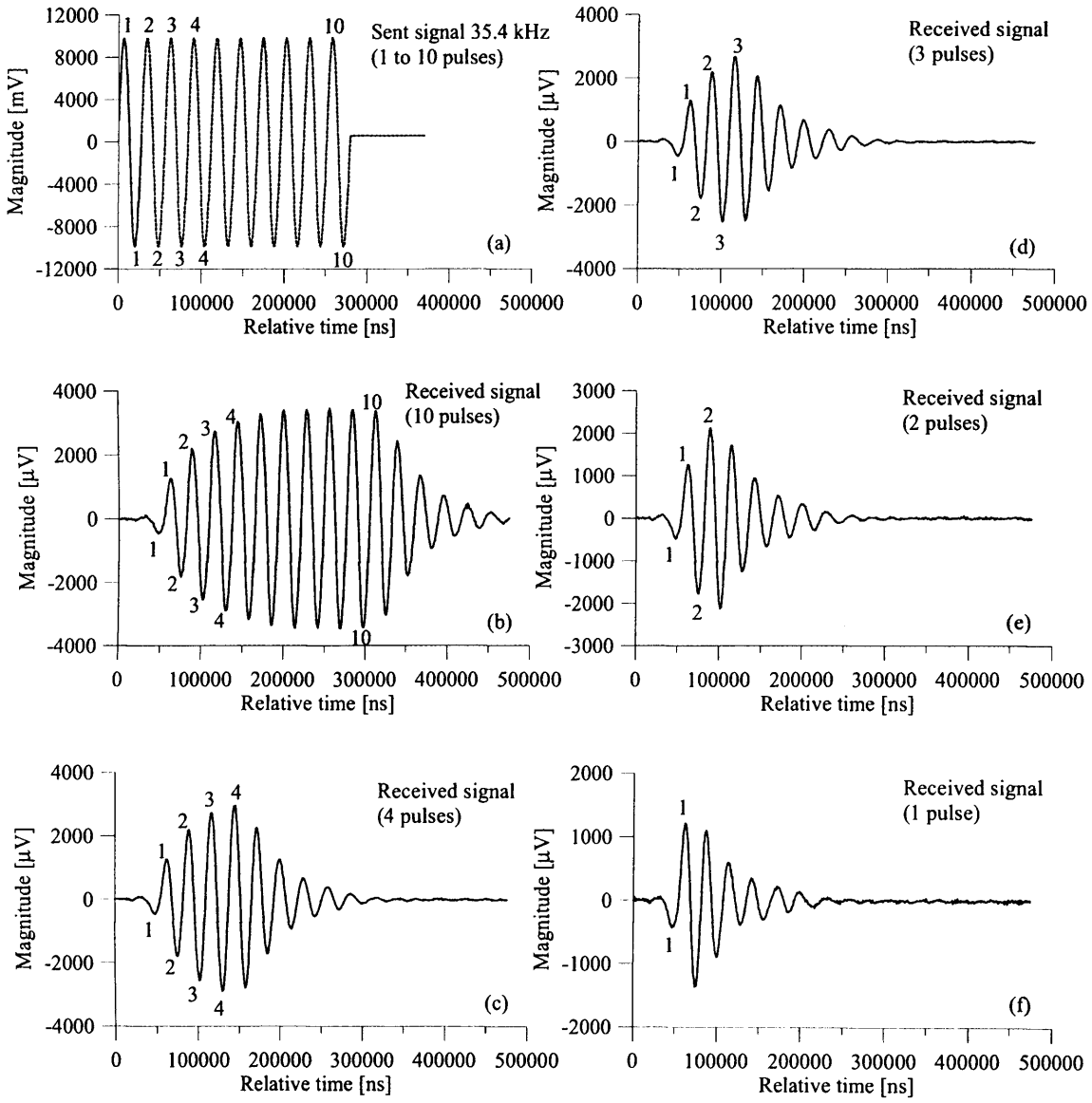

Figure 4-5 Characteristics of received bender element signals after transmission of multiple pulse sinusoid waves at the dominant resonant frequency in oedometer test on reconstituted London Clay

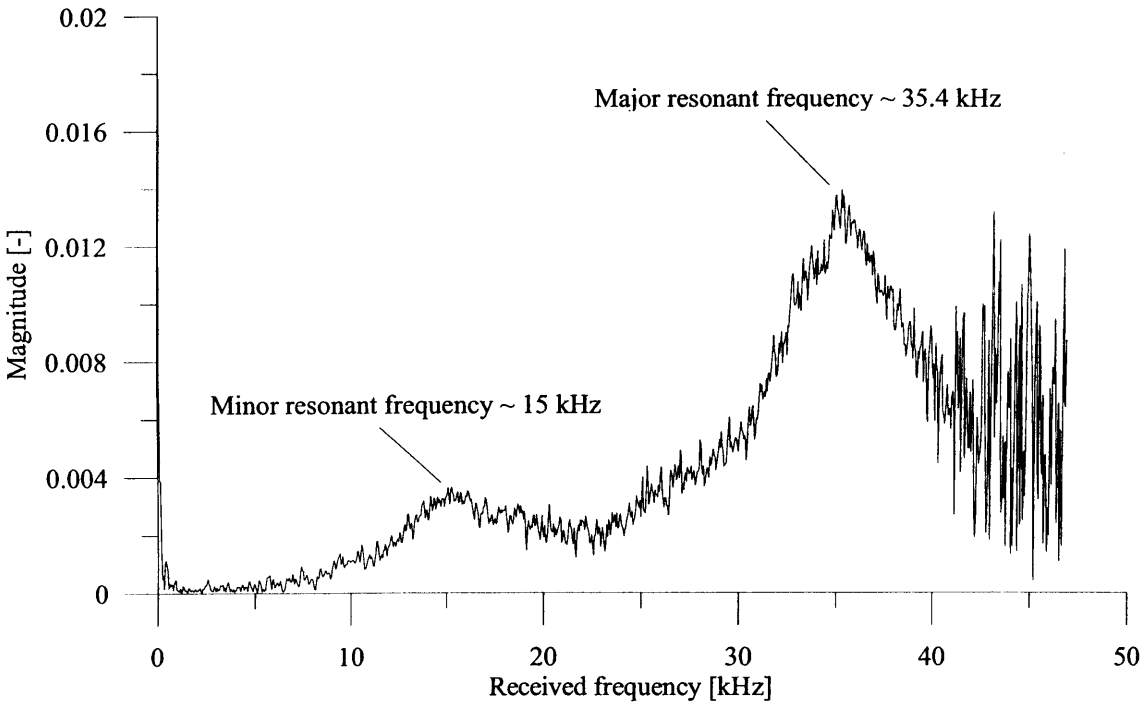

Figure 4-6 Frequency spectrum for sample of NC reconstituted London Clay in oedometer cell (σ'_v=590 kPa, Sample S01oeds4)

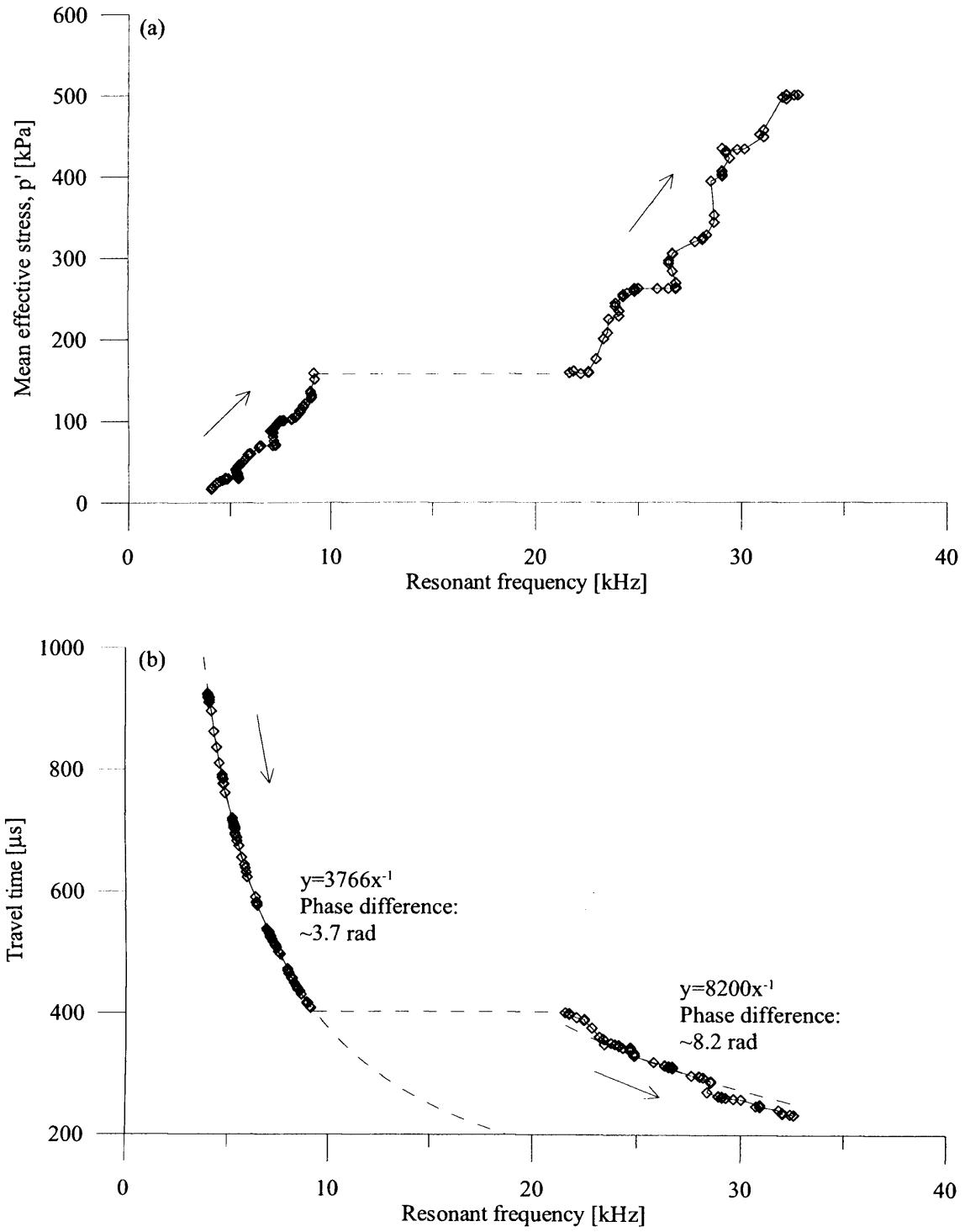

Figure 4-7 Relationship between dominant resonant frequency and (a) mean effective stress and (b) estimated travel time during isotropic compression of reconstituted kaolin (sample S1k)

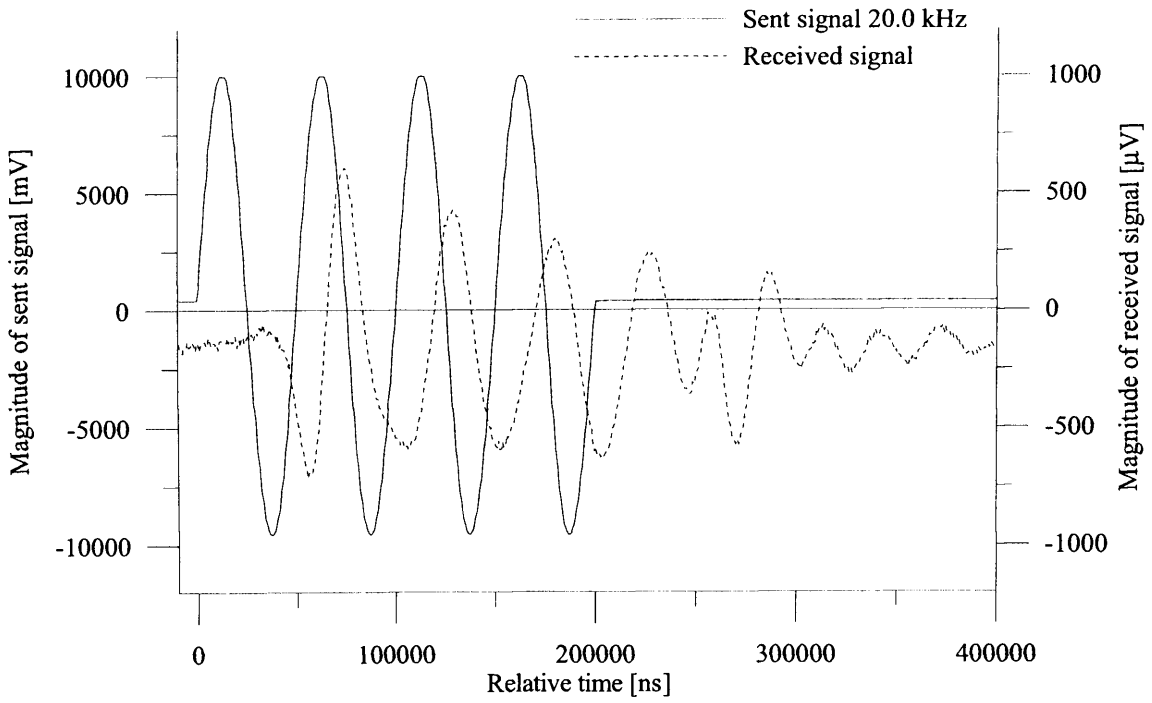

Figure 4-8 Characteristics of received bender element signal after transmitting a four-pulse sinusoid wave at a frequency lower than the dominant resonant frequency

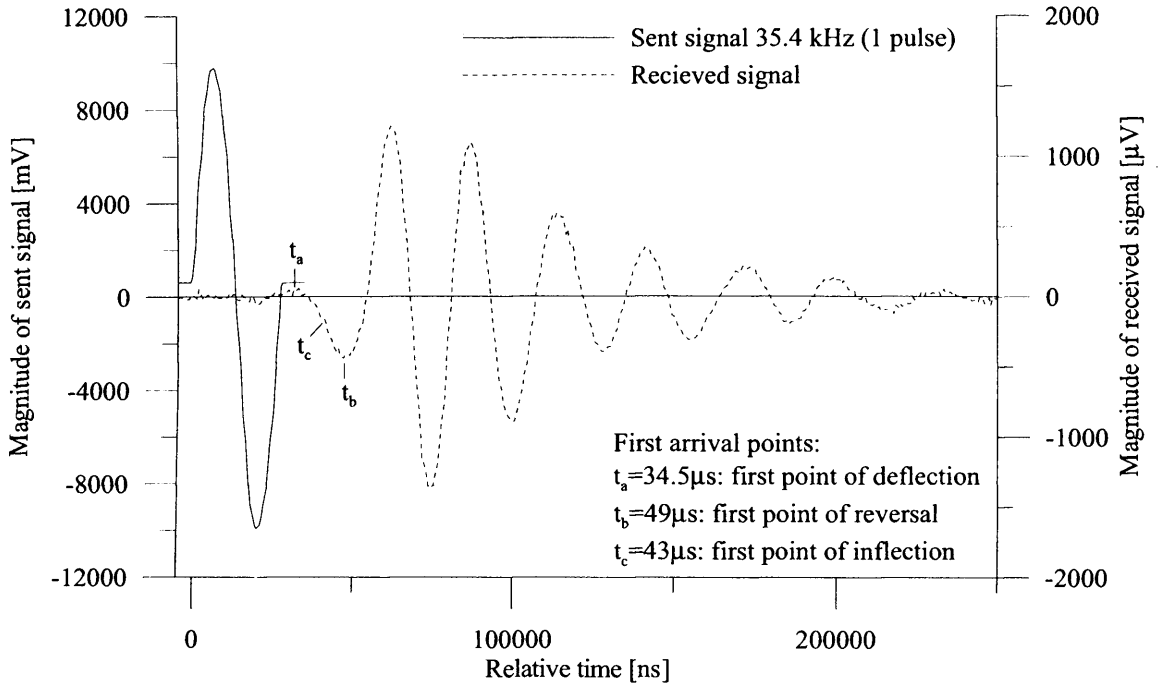

Figure 4-9 Estimating travel time of transmitted single pulse sinusoid wave through sample using first arrival method

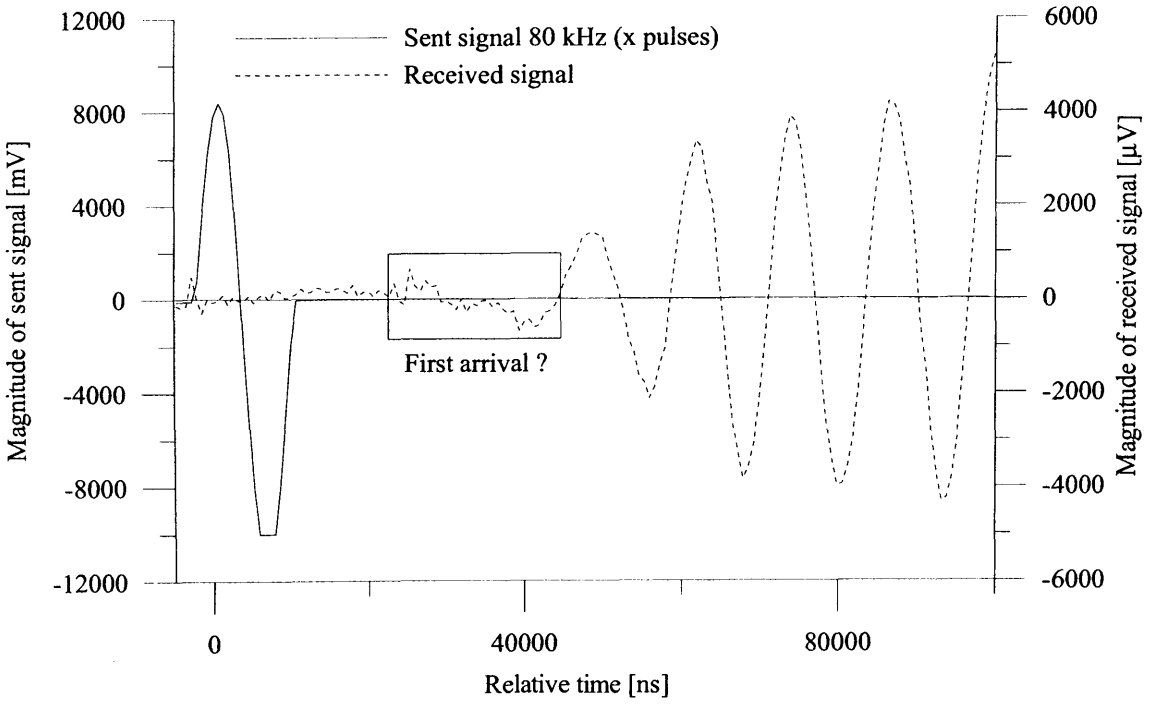

Figure 4-10 Illustrating difficulties in determining first arrival time due to detrimental influence of near-field effect and noise in the oedometer cell

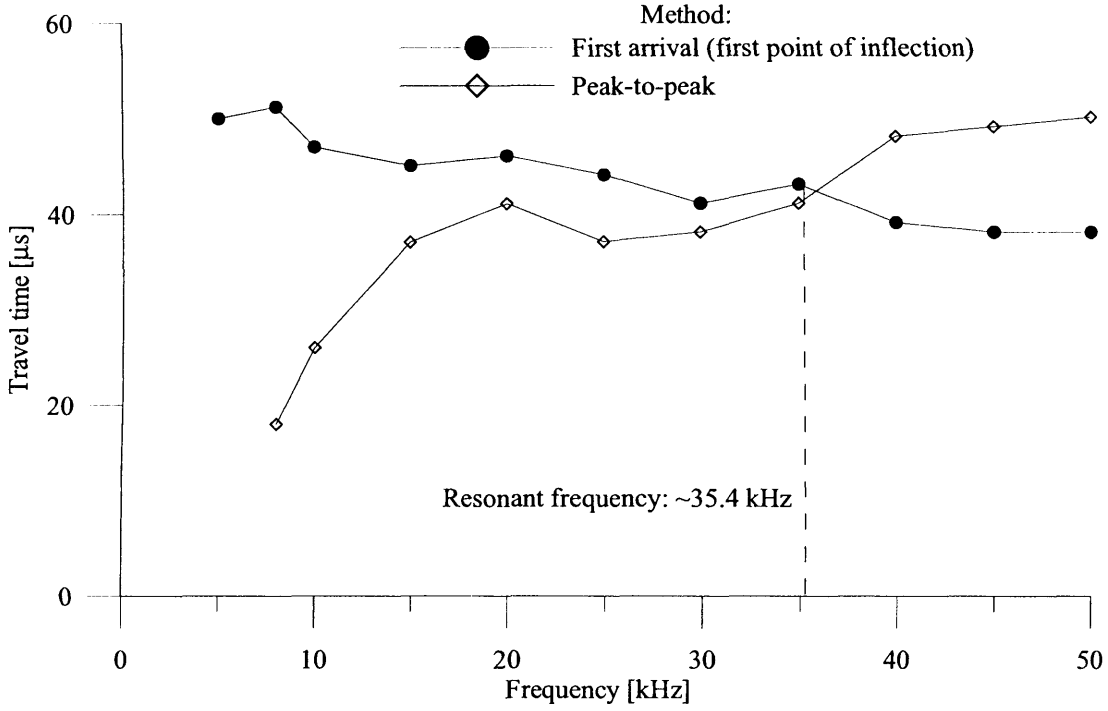

Figure 4-11 Influence of frequency of transmitted single pulse sinusoid wave on the estimated travel time using first arrival method and peak-to-peak correlation method

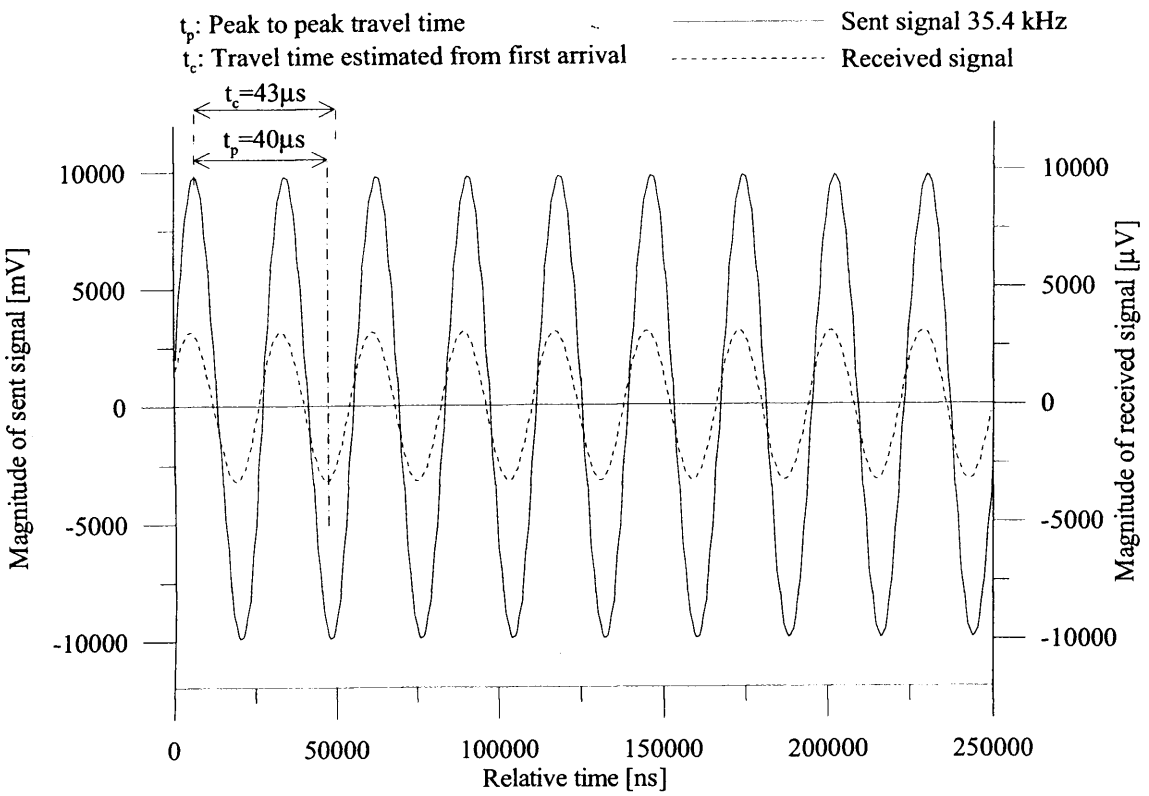

Figure 4-12 Estimating travel time of transmitted continuous sinusoid wave through sample using peak-to-peak correlation method

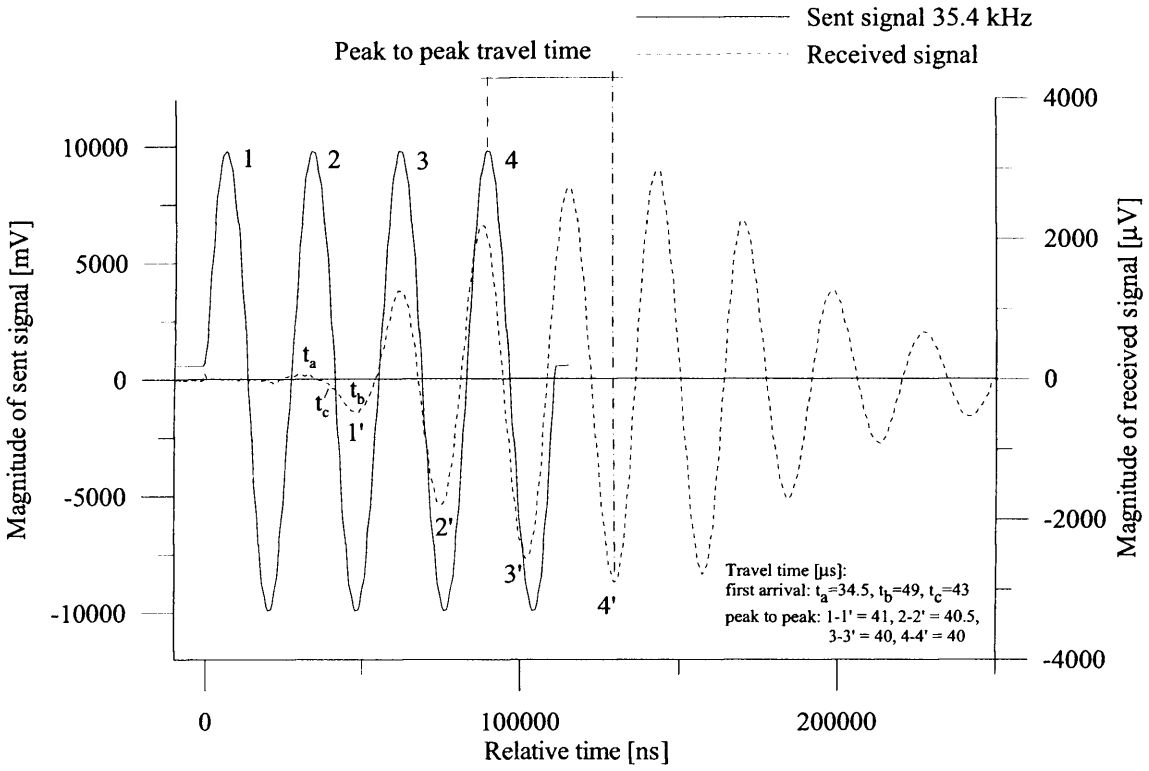

Figure 4-13 Estimating travel time of transmitted multiple pulse sinusoid wave through sample using peak-to-peak correlation method

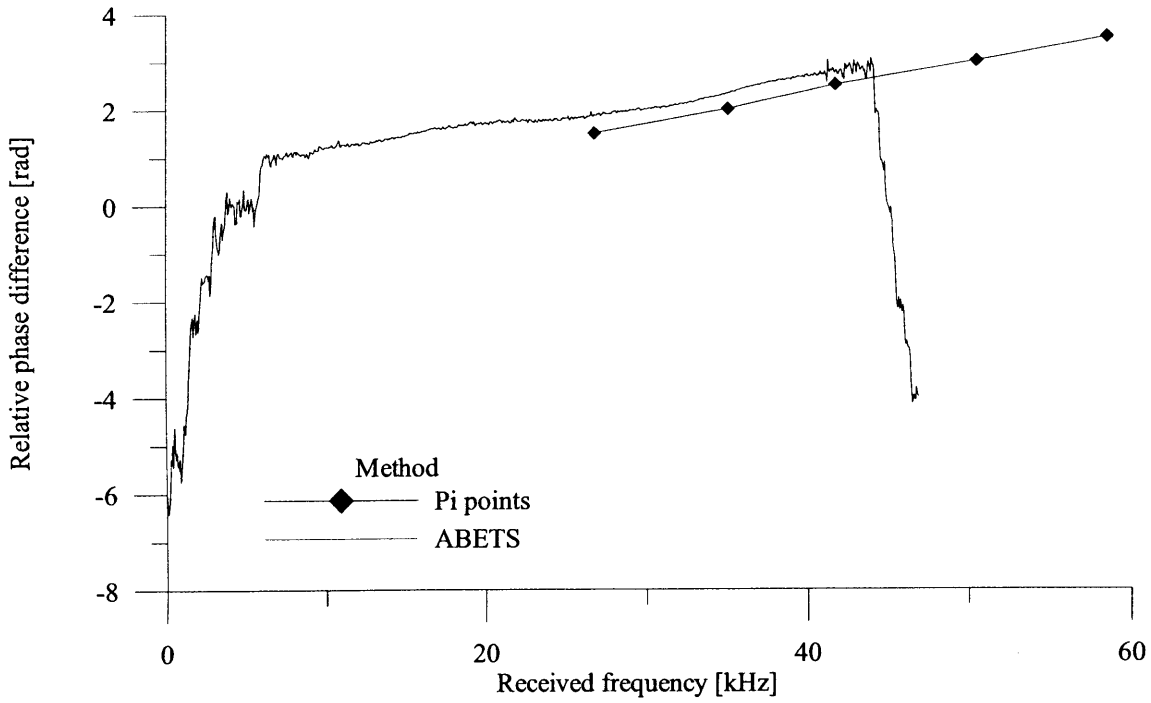

Figure 4-14 Phase diagram for obtained using ABETS and the π-point method

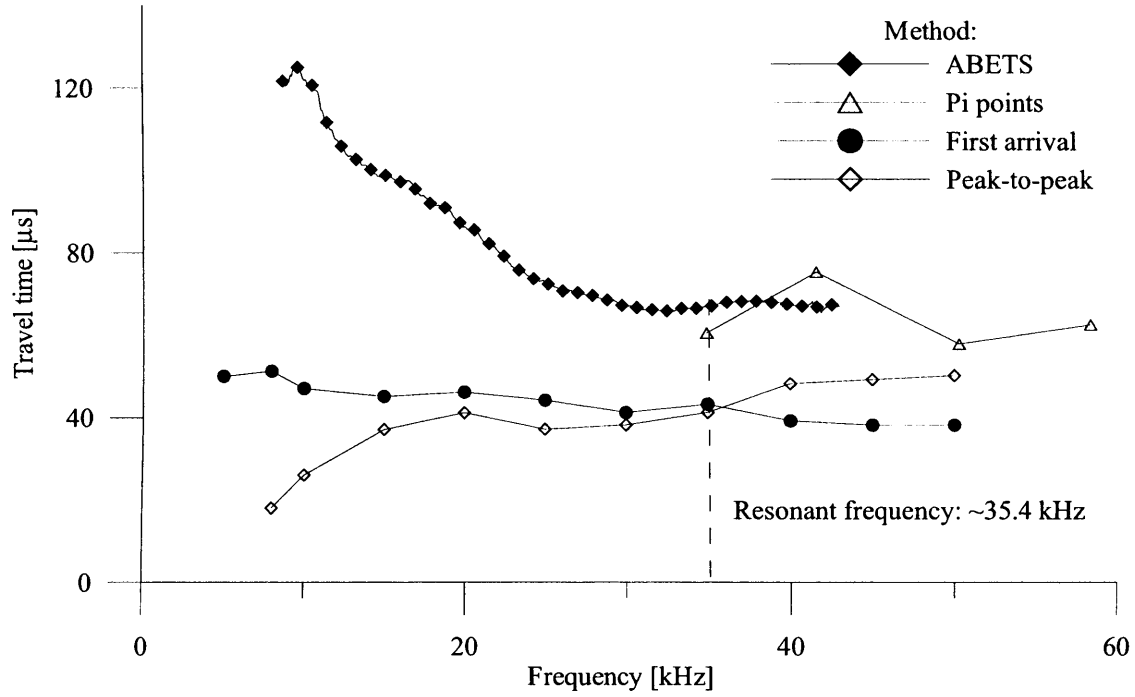

Figure 4-15 Comparing travel times determined from phase delay method with those obtained from time-domain method at a range of frequencies

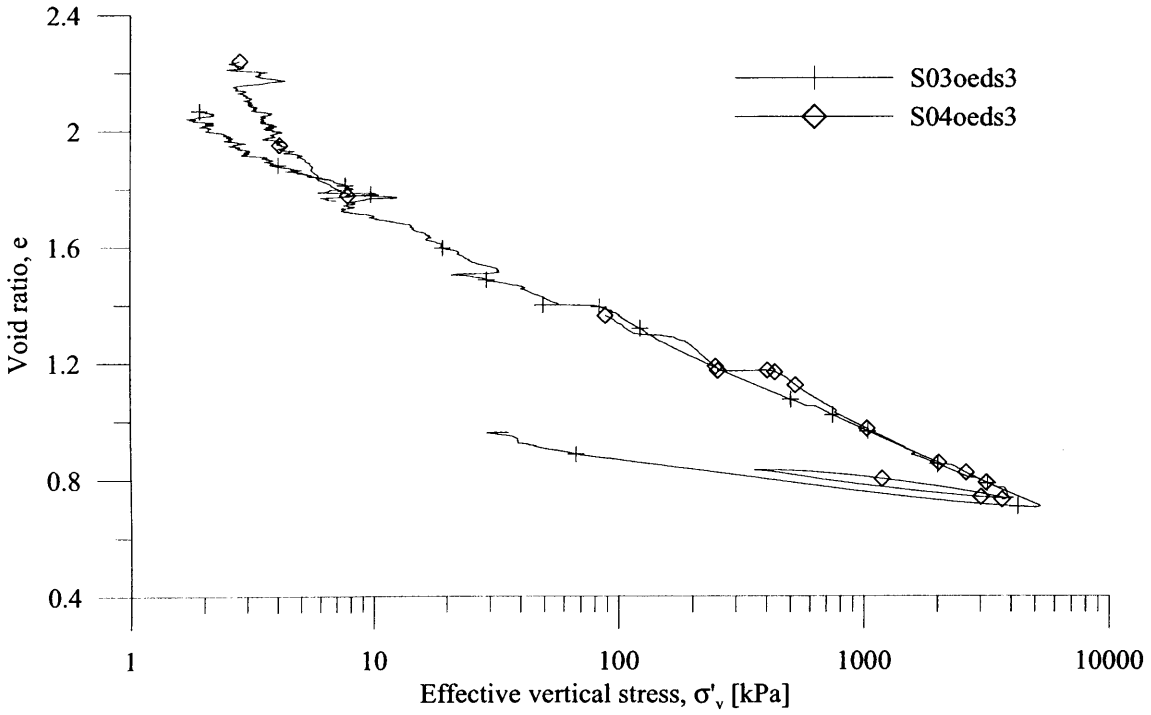

Figure 4-16 Representative one-dimensional compression curves for reconstituted kaolin

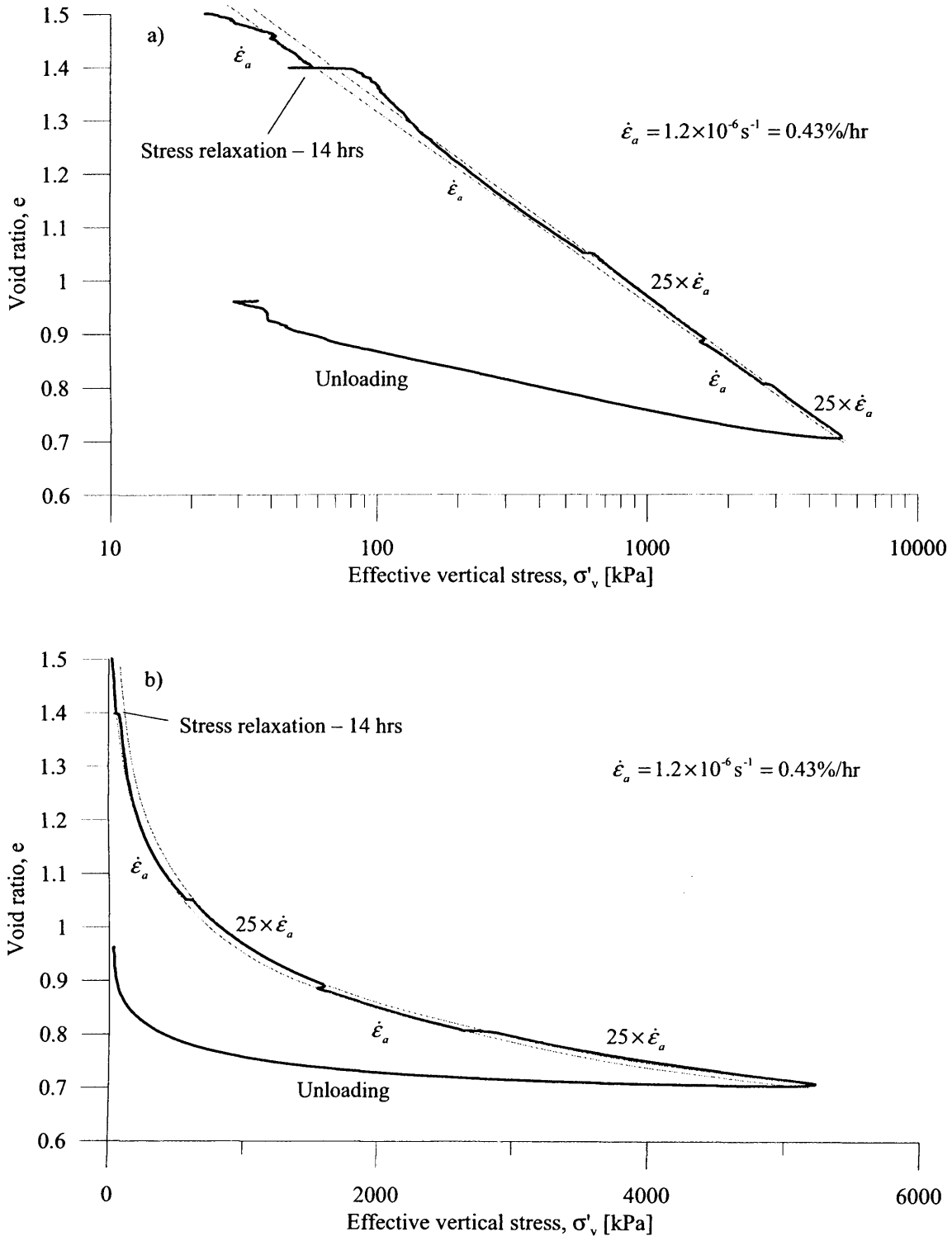

Figure 4-17 Influence of step-wise change in strain rate on the 1D compression curve of reconstituted kaolin sample S03oeds3, plotted in (a) single log scale and (b) natural scale

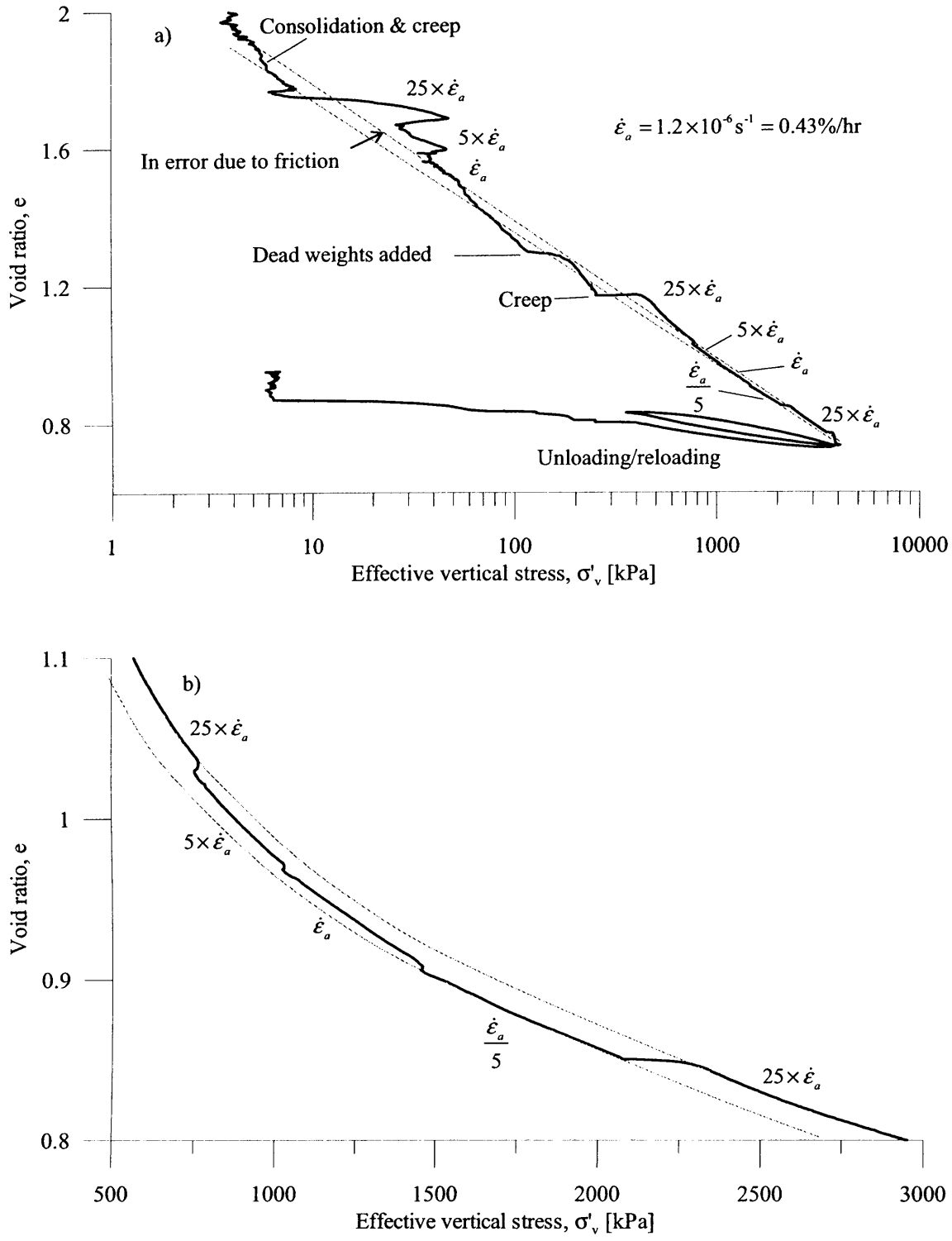

Figure 4-18 Influence of step-wise change in strain rate on the 1D compression curve of reconstituted kaolin sample S04oeds3, plotted in (a) single log scale and (b) natural scale

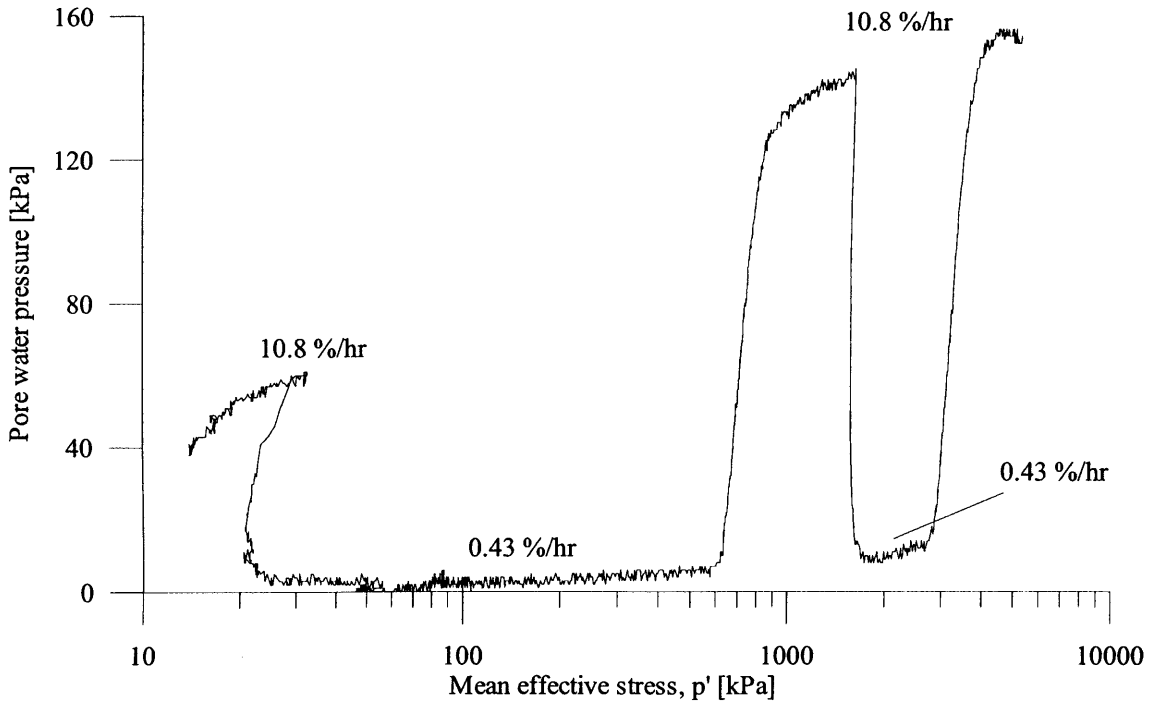

Figure 4-19 Accumulated pore water pressures during the 1D compression of reconstituted kaolin sample S03oeds3

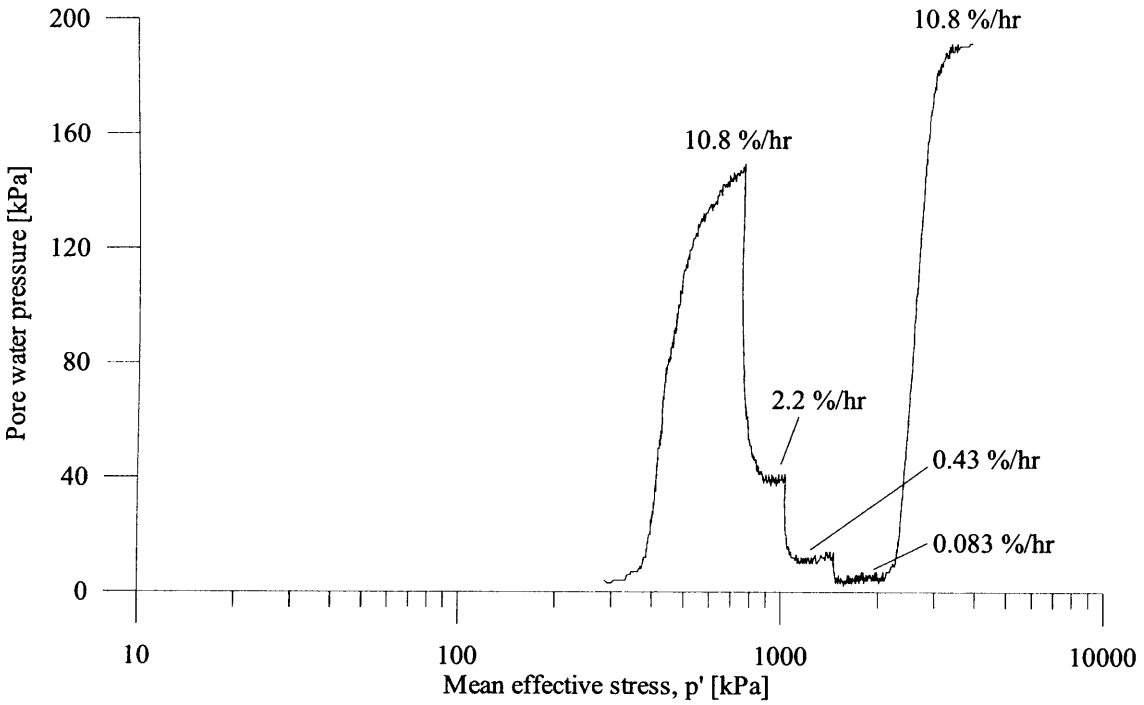

Figure 4-20 Accumulated pore water pressures during the 1D compression of reconstituted kaolin sample S04oeds3

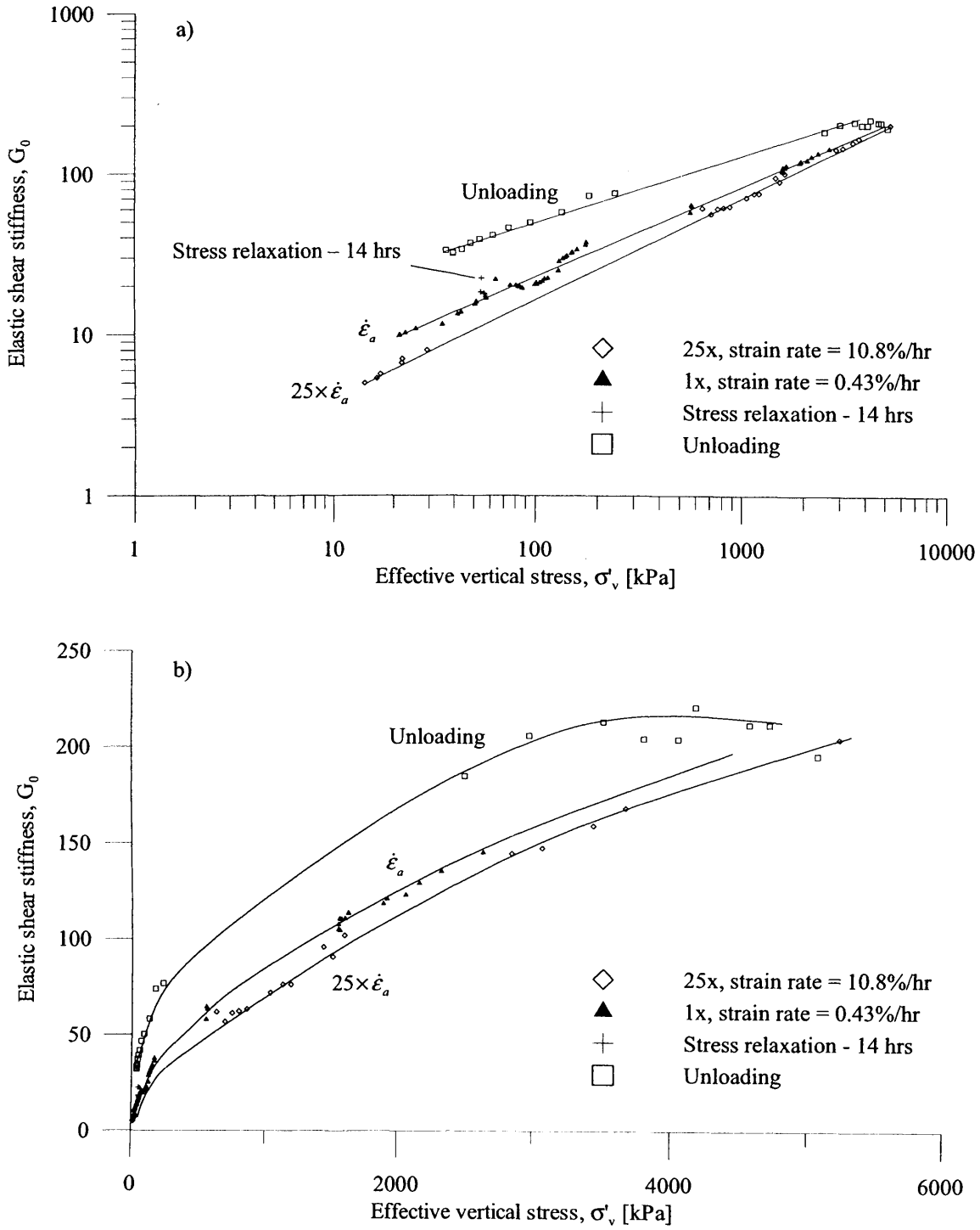

Figure 4-21 Influence of step-wise change in strain rate on the G_0-σ'_v relationship curve in 1D compression of reconstituted kaolin (sample S03oeds3), plotted in (a) double log scale and (b) natural scale

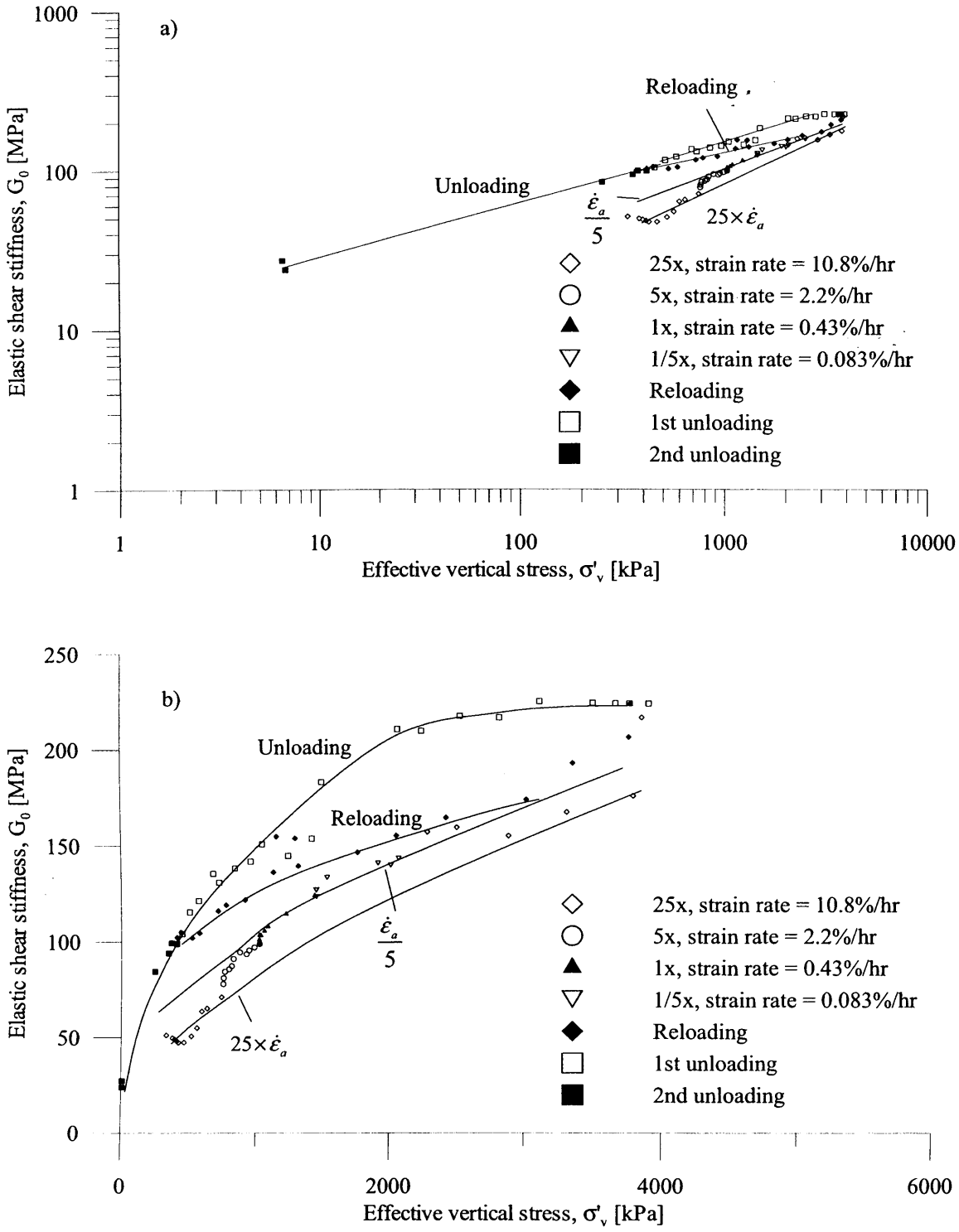

Figure 4-22 Influence of step-wise change in strain rate on the G_0-σ'_v relationship curve in 1D compression of reconstituted kaolin (sample S04oeds3), plotted in (a) double log scale and (b) natural scale

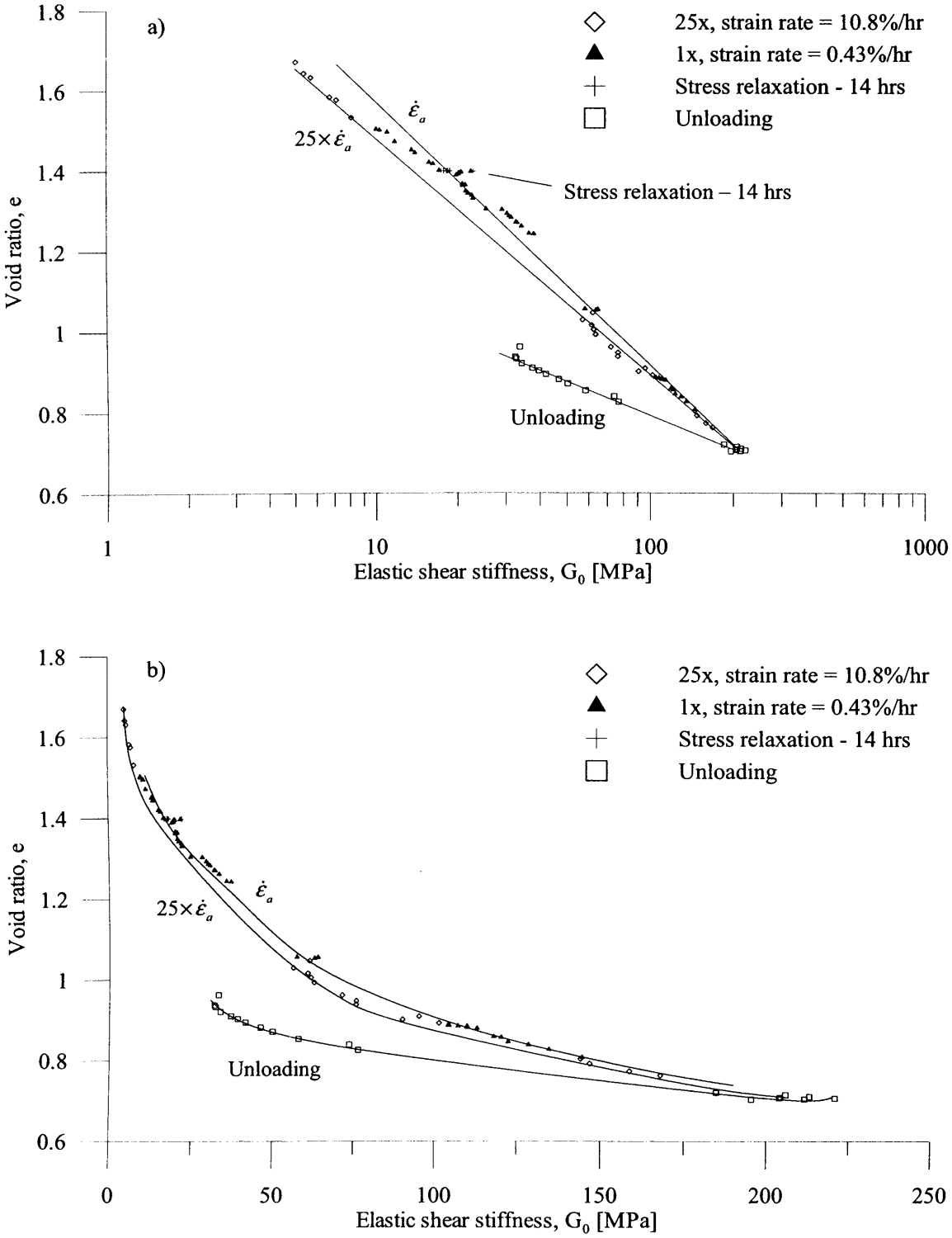

Figure 4-23 Influence of step-wise change in strain rate on the *e*-G_0 relationship curve for 1D compression of reconstituted kaolin (sample S03oeds3), plotted in (a) single log scale and (b) natural scale

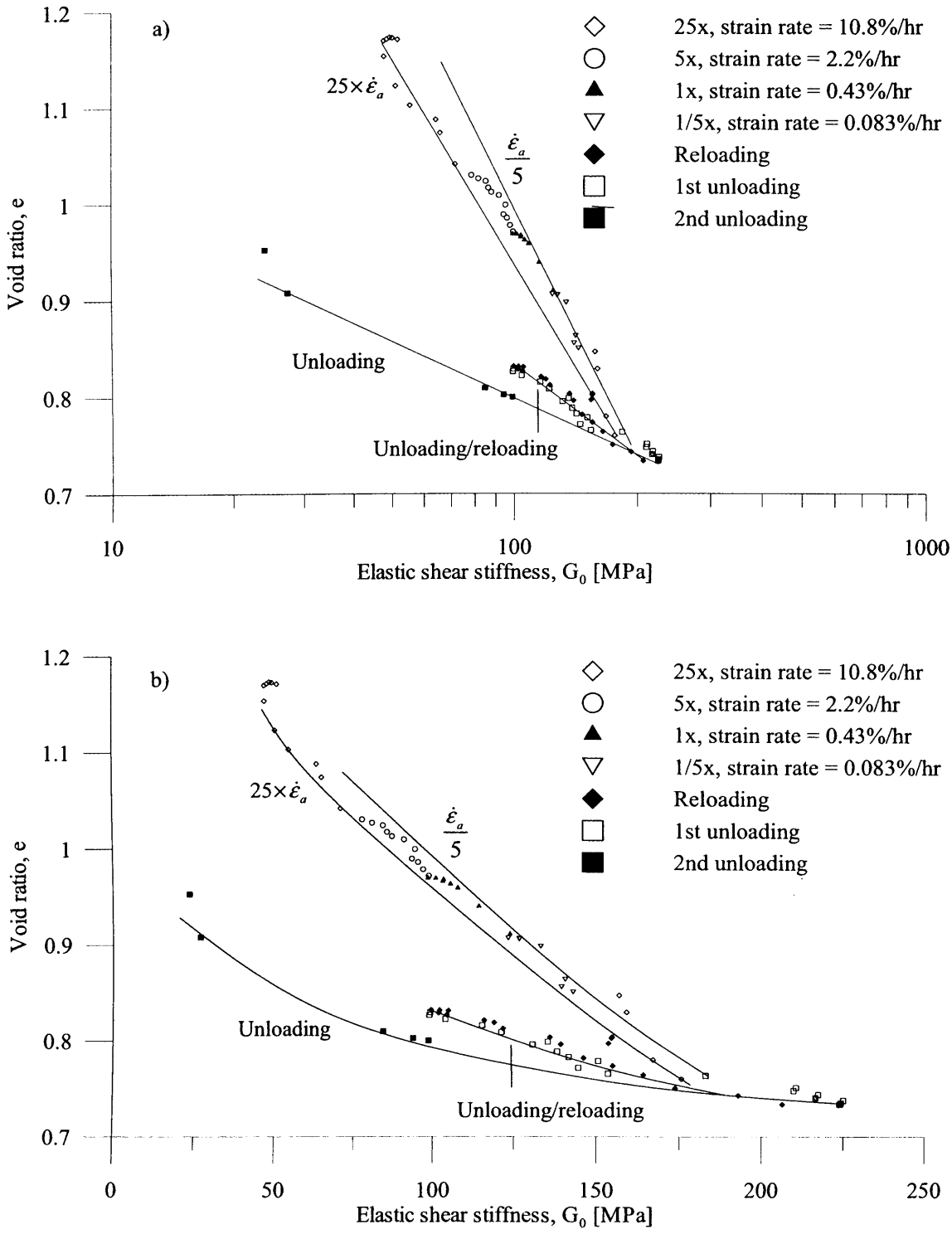

Figure 4-24 Influence of step-wise change in strain rate on the e-G_0 relationship curve for 1D compression of reconstituted kaolin (sample S04oeds3), plotted in (a) single log scale and (b) natural scale

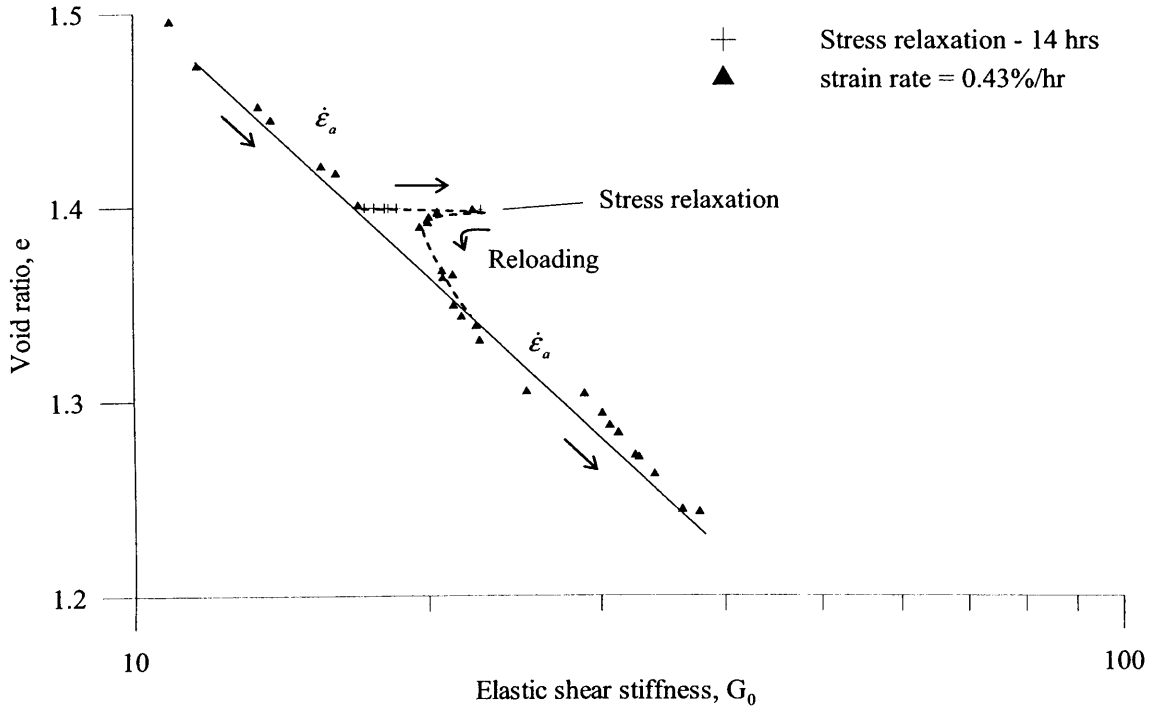

Figure 4-25 Details of stress relaxation in e-G_0 plot for 1D compression test of reconstituted kaolin (sample S03oeds3)

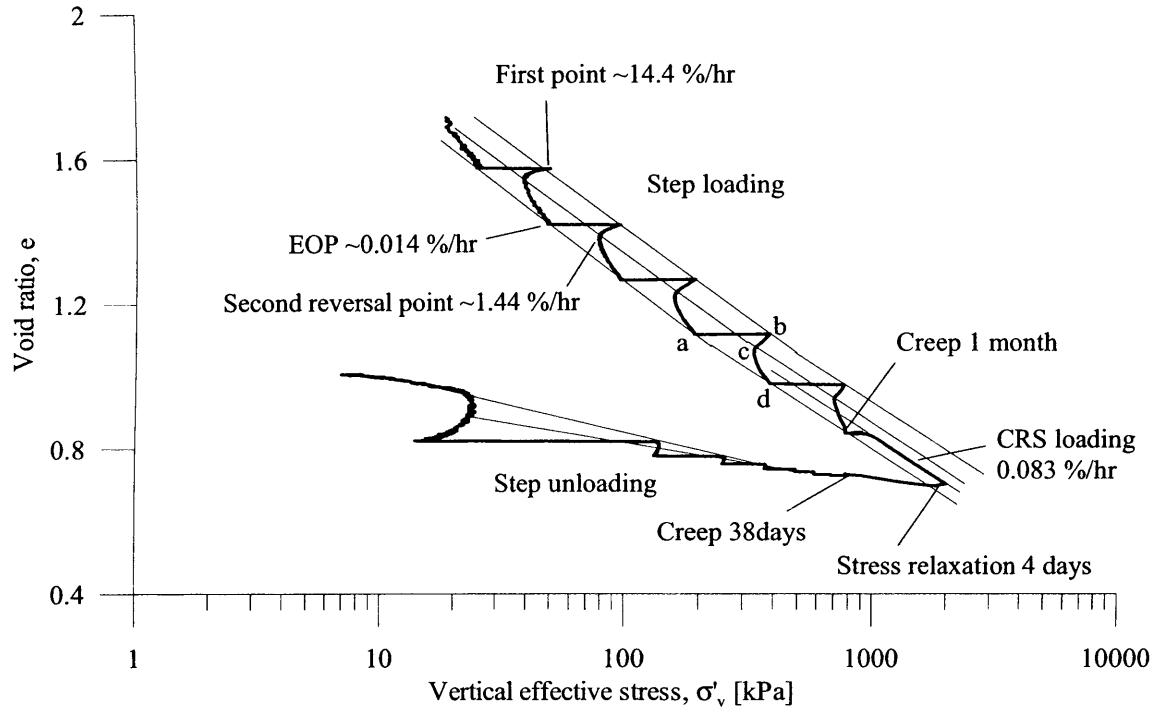

Figure 4-26 1D compression and swelling path resulting from step loading, step unloading and constant rate of strain compression/swelling in test on reconstituted London Clay (sample S01oeds4)

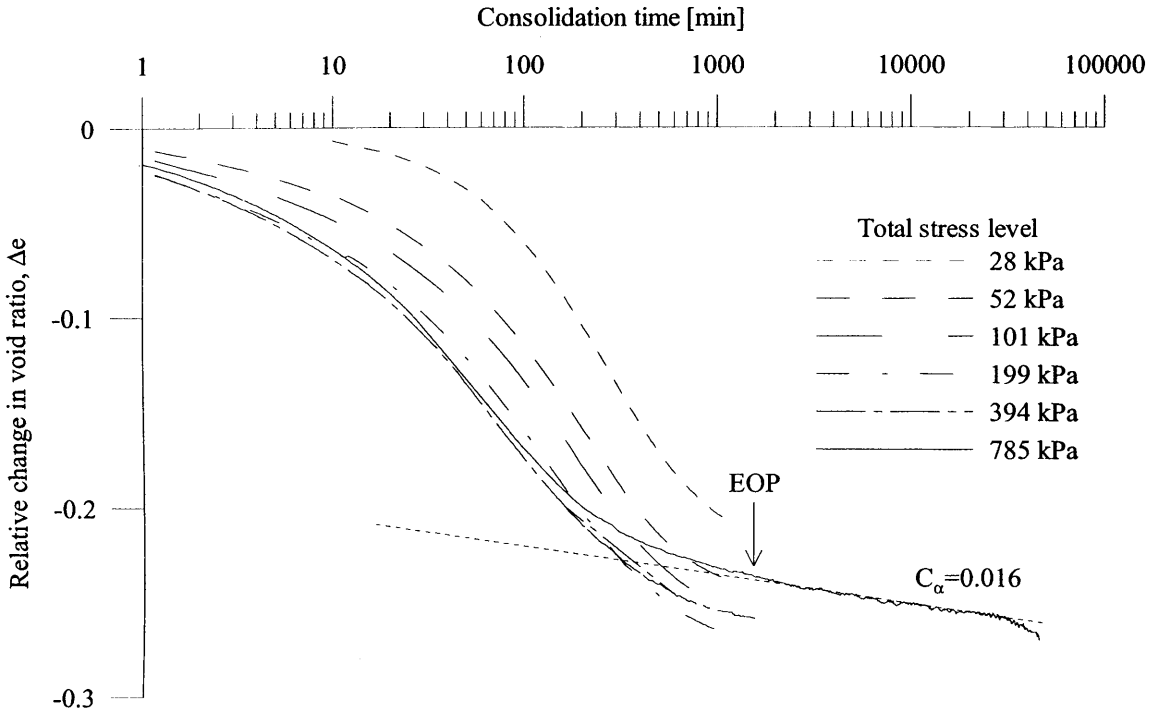

Figure 4-27 Constant total stress consolidation curves for each step load increment in 1D compression test on reconstituted London Clay (sample S01oeds4)

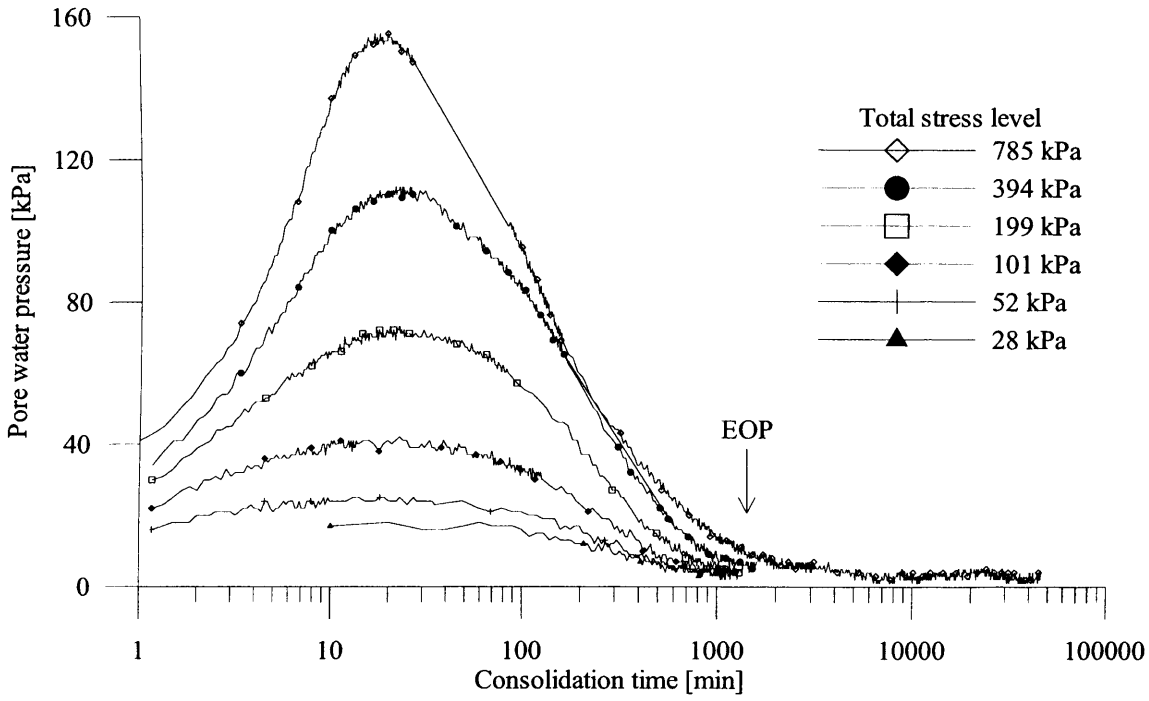

Figure 4-28 Pore water pressure dissipation curves for each step load increment in 1D compression test on reconstituted London Clay (sample S01oeds4)

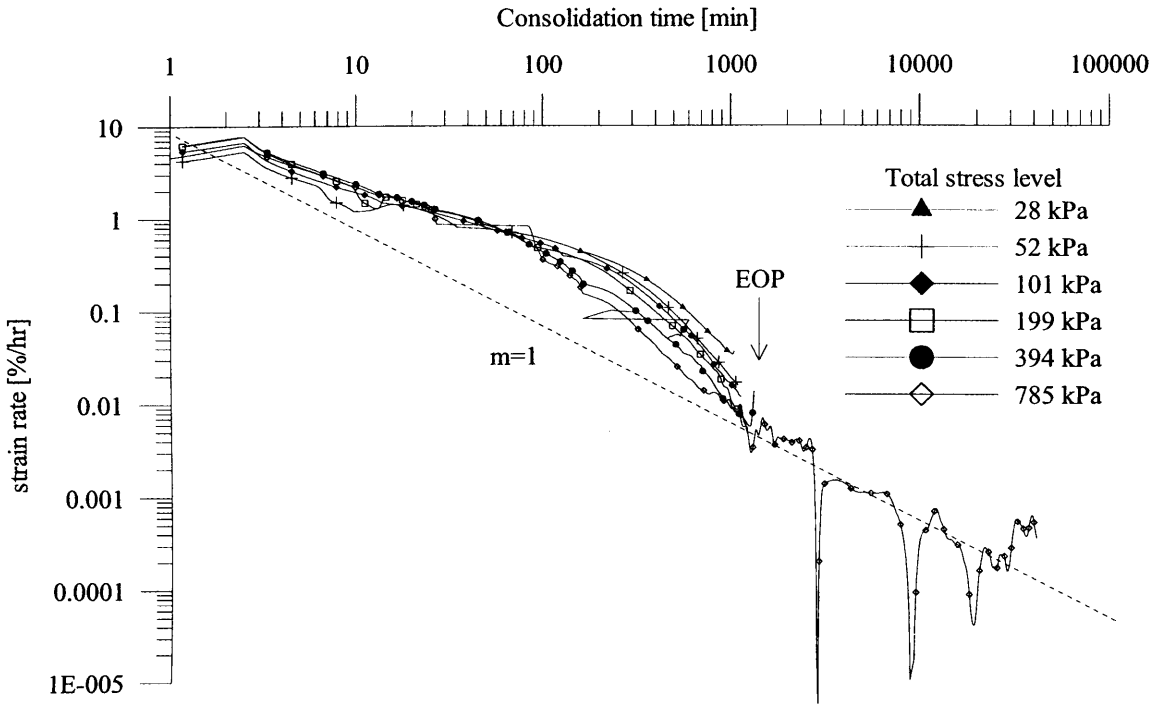

Figure 4-29 Axial strain rate reduction during consolidation for each step load increment in 1D compression test on reconstituted London Clay (sample S01oeds4)

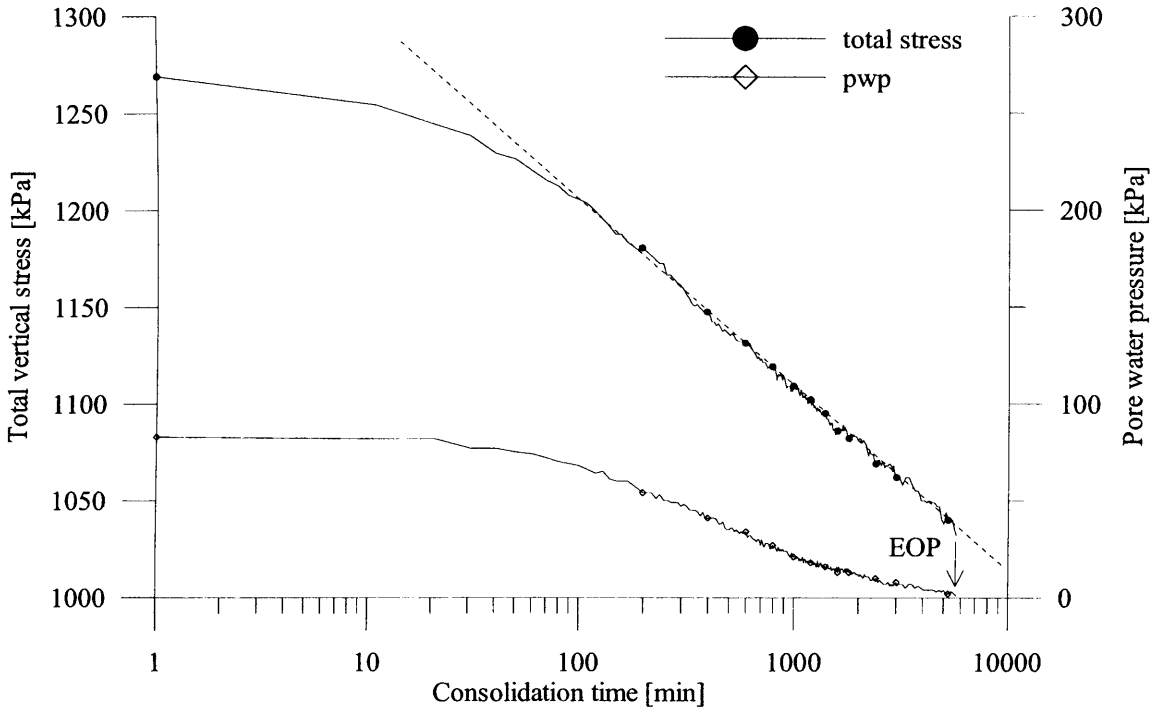

Figure 4-30 Stress relaxation and associated pore water dissipation after CRS compression in 1D compression of reconstituted London Clay (sample S01oeds4)

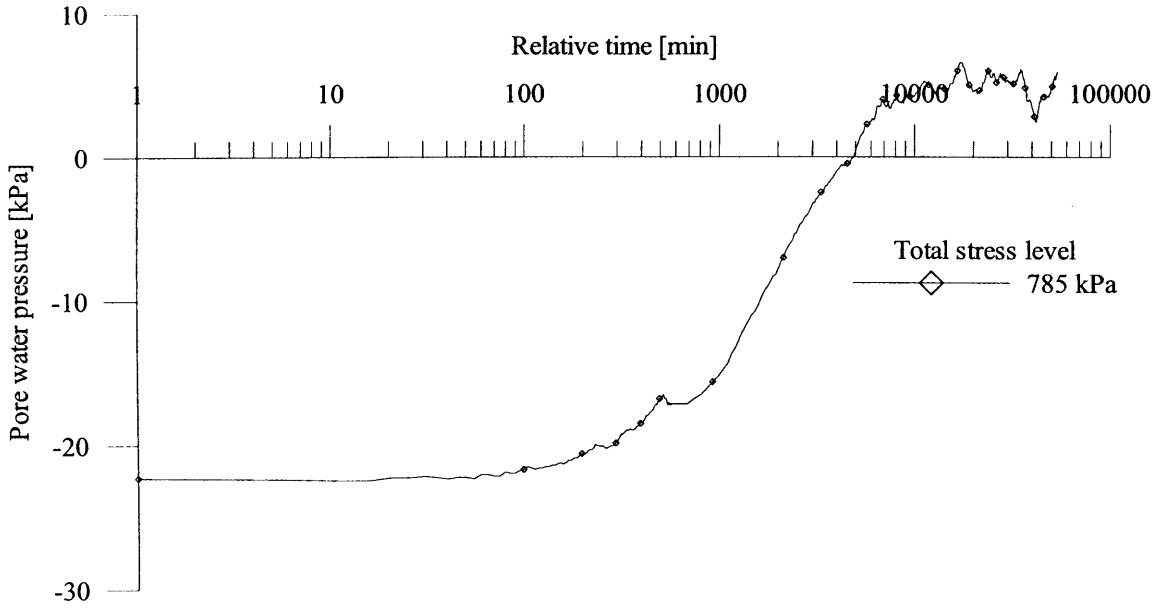

Figure 4-31 Relief of negative pore water pressures with time during constant total stress swelling after CRS unloading in 1D compression test on reconstituted London Clay (sample S01oeds4)

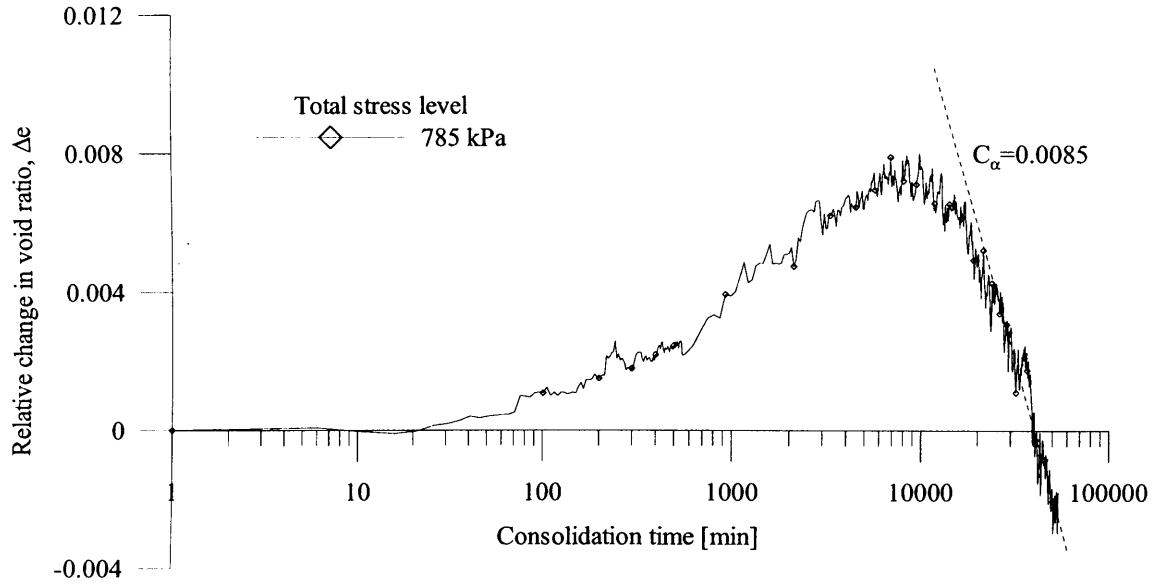

Figure 4-32 Constant total stress swelling curve after CRS unloading in 1D compression test on reconstituted London Clay (sample S01oeds4)

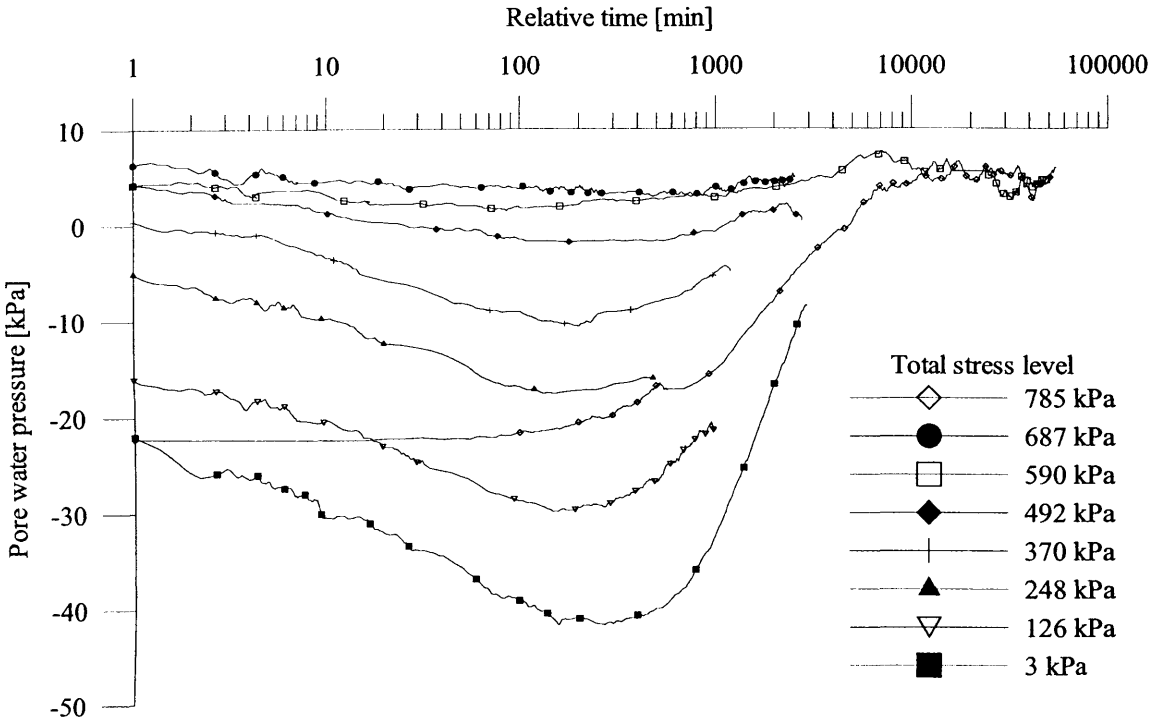

Figure 4-33 Relief of negative pore water pressures with time during constant total stress swelling for each step unload increment in 1D compression test on reconstituted London Clay (sample S01oeds4)

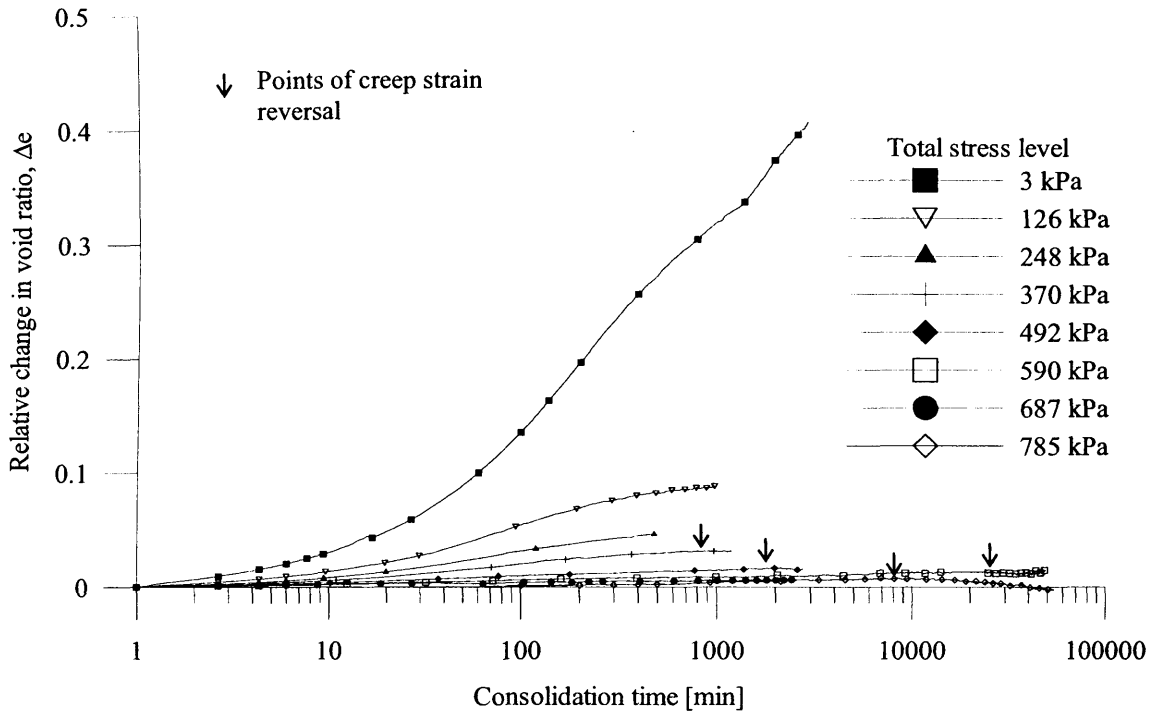

Figure 4-34 Constant total stress swelling curves for each step unload increment in 1D compression test on reconstituted London Clay (sample S01oeds4)

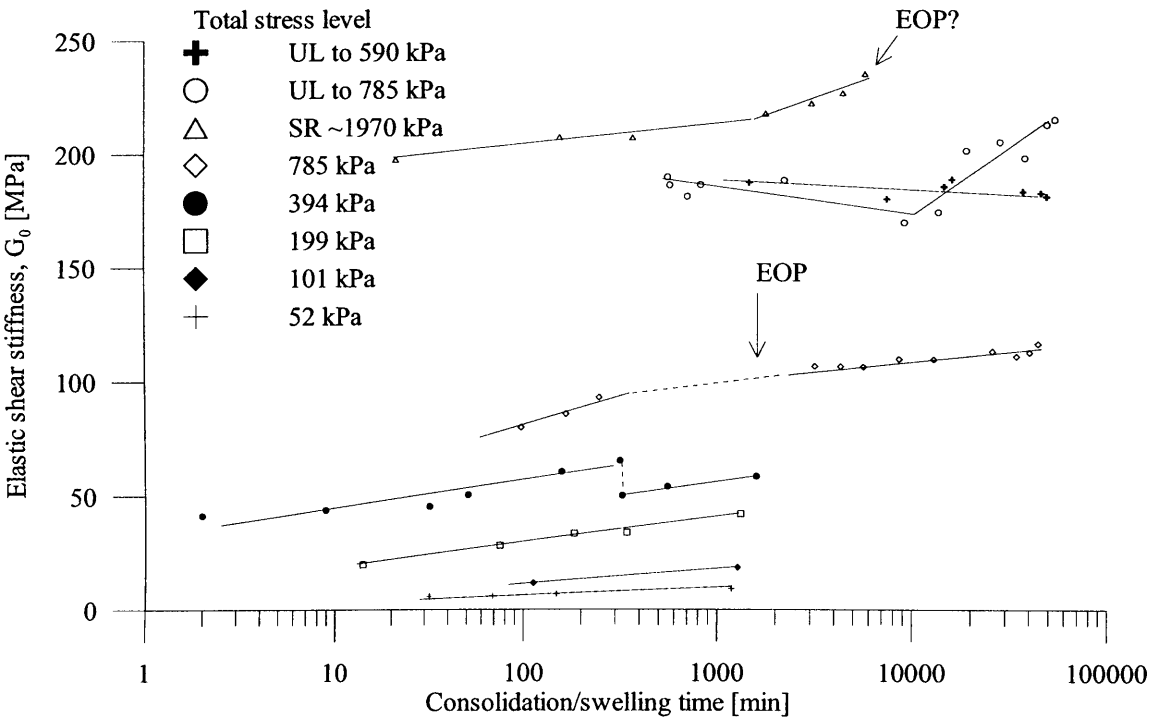

Figure 4-35 G_0 change with time during stages of constant total stress consolidation and creep for each step load increment in 1D compression test on reconstituted London Clay (sample S01oeds4)

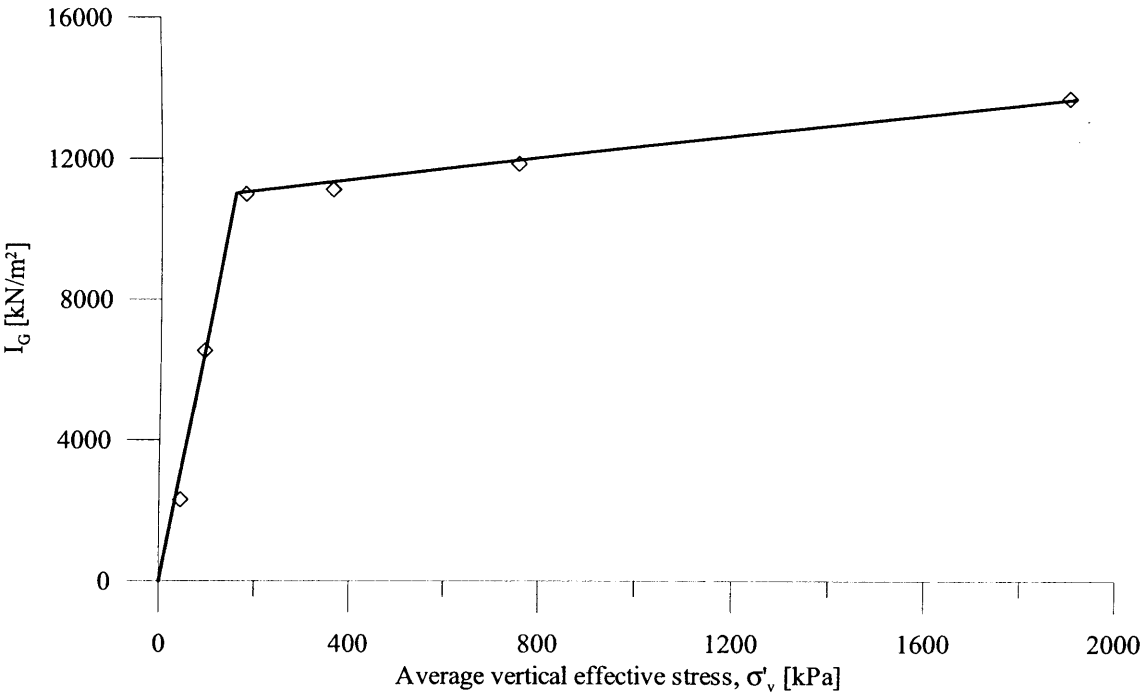

Figure 4-36 Influence of stress level on coefficient I_G in 1D compression test on reconstituted London Clay (sample S01oeds4)

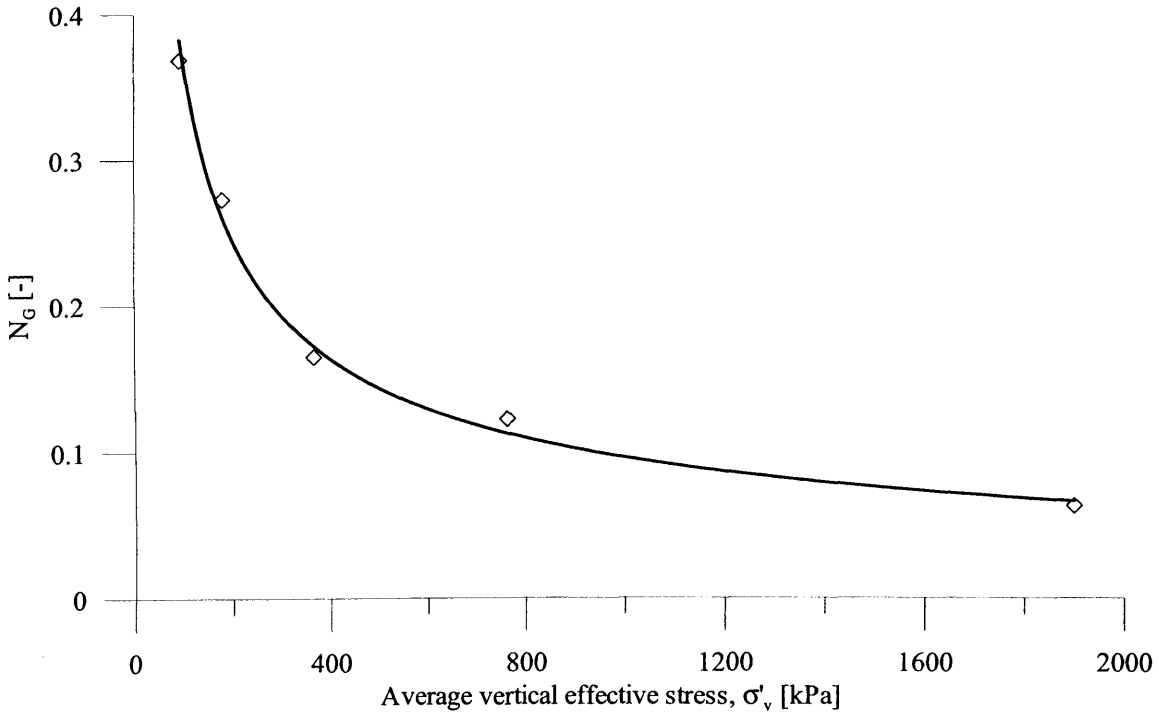

Figure 4-37 Influence of stress level on coefficient N_G in 1D compression test on reconstituted London Clay (sample S01oeds4)

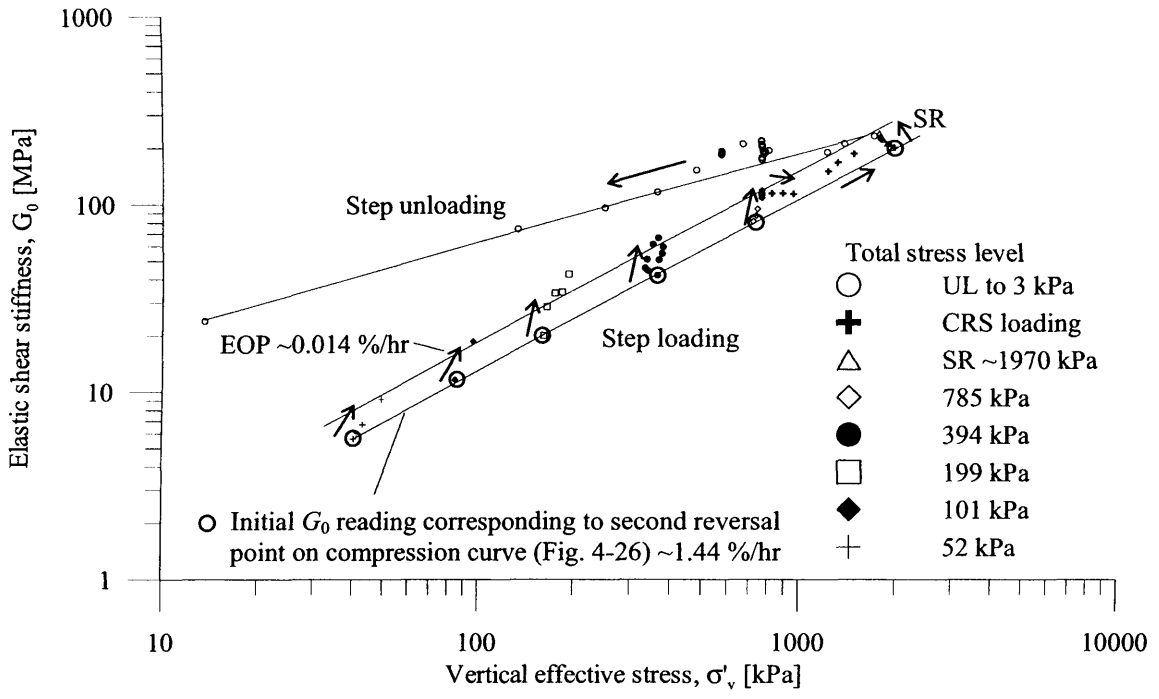

Figure 4-38 Relationship between G_0 and σ'_v for step loading, step unloading and constant rate of strain compression/swelling stages in 1D compression test on reconstituted London Clay (sample S01oeds4)

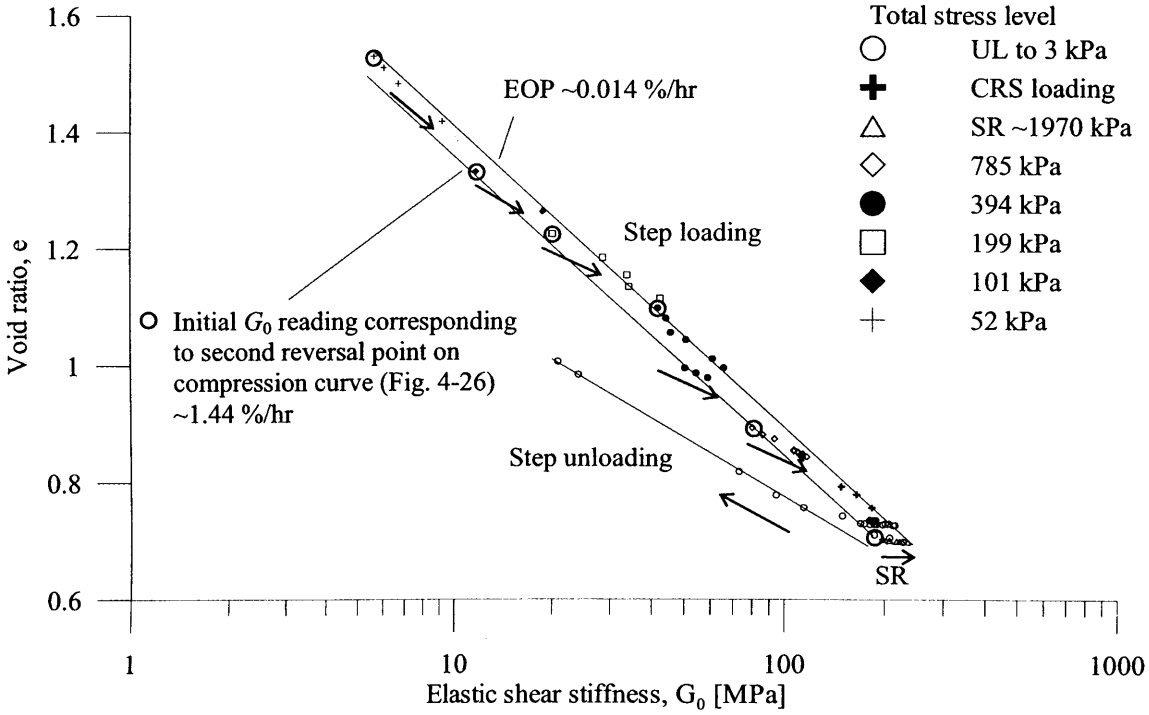

Figure 4-39 Relationship between e and G_0 for step loading, step unloading and constant rate of strain compression/swelling stages in 1D compression test on reconstituted London Clay (sample S01oeds4)

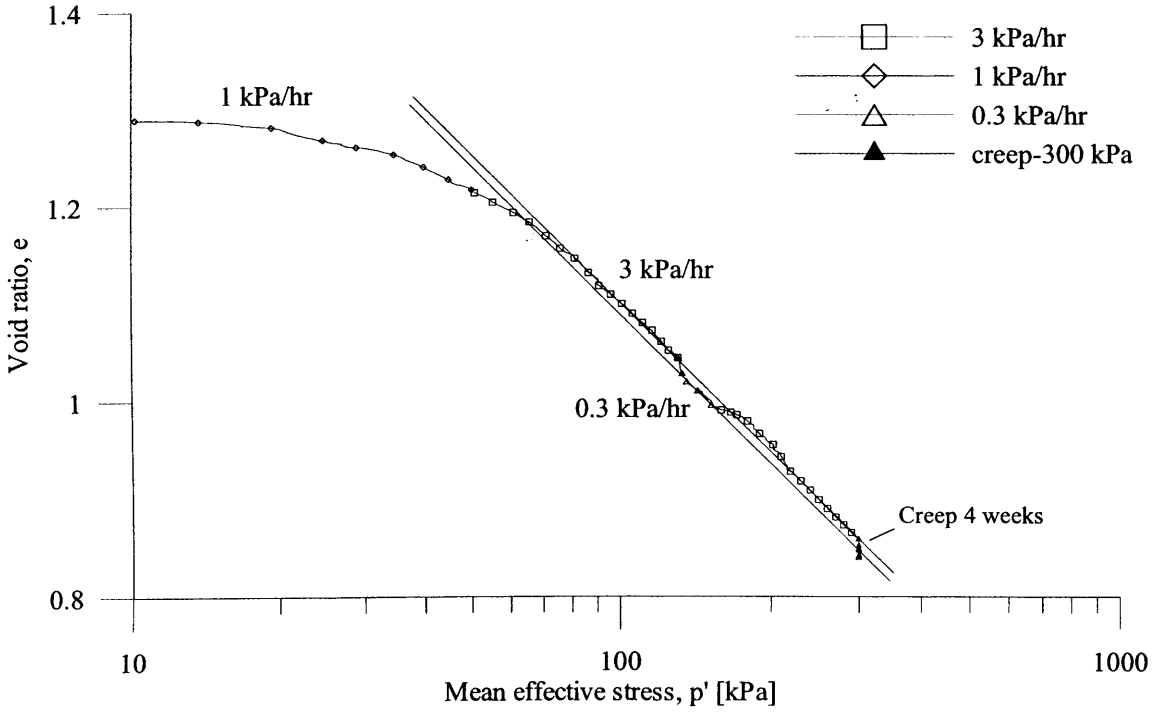

Figure 4-40 Influence of step-wise change in rate of stress and creep on the isotropic compression path of reconstituted London Clay (sample S2LCrB1)

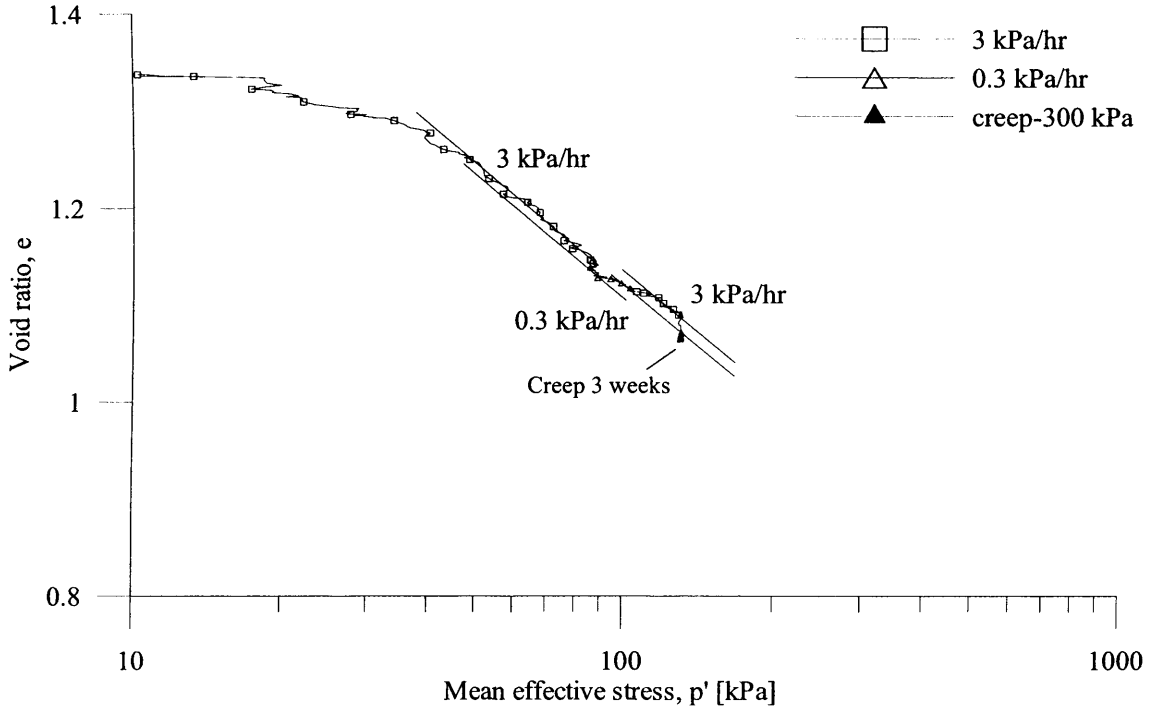

Figure 4-41 Influence of step-wise change in rate of stress and creep on the isotropic compression path of reconstituted London Clay (sample S2LCrB2)

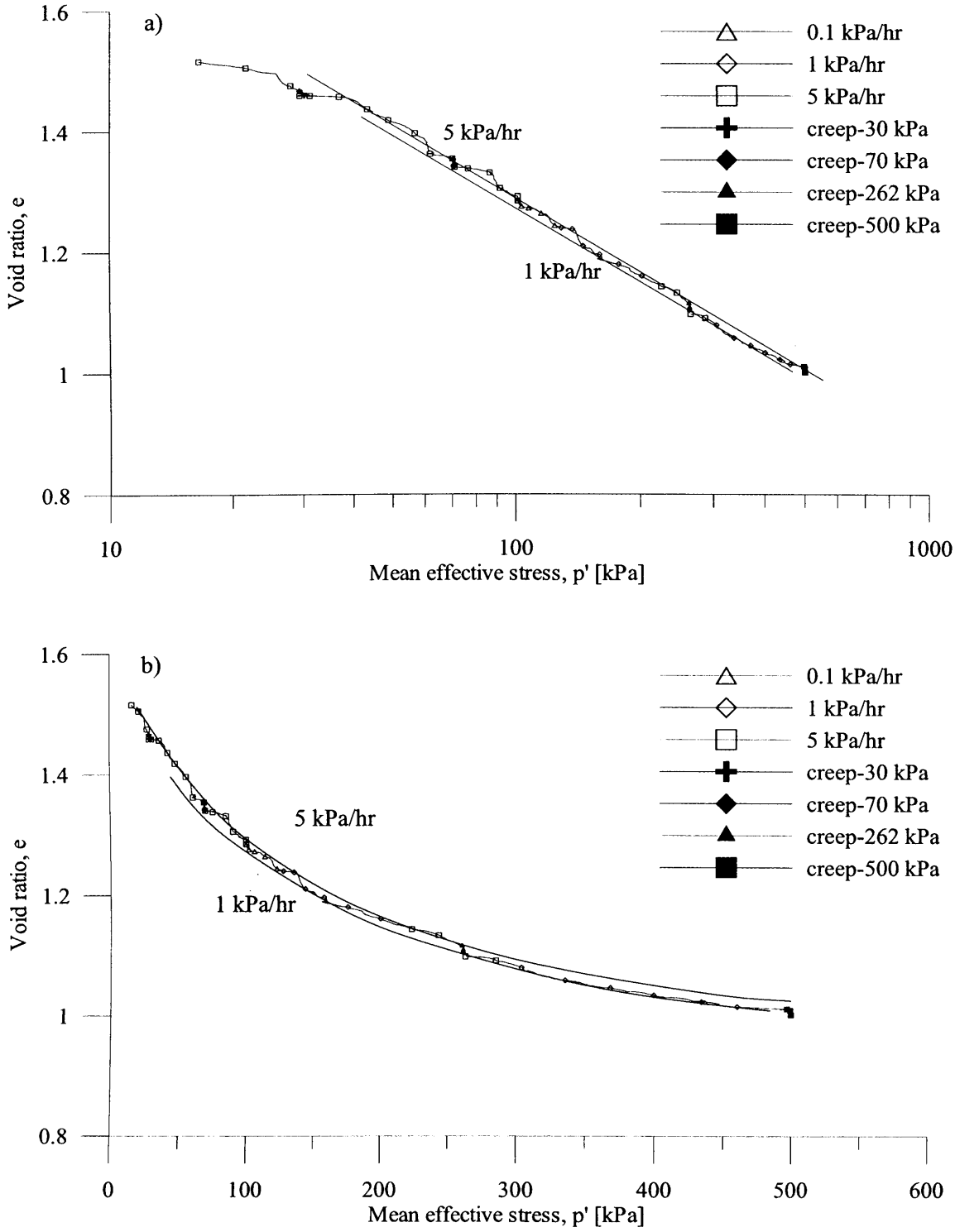

Figure 4-42 Influence of step-wise change in rate of stress and creep on the isotropic compression path of reconstituted kaolin (sample S1k), plotted in (a) single log scale and (b) natural scale

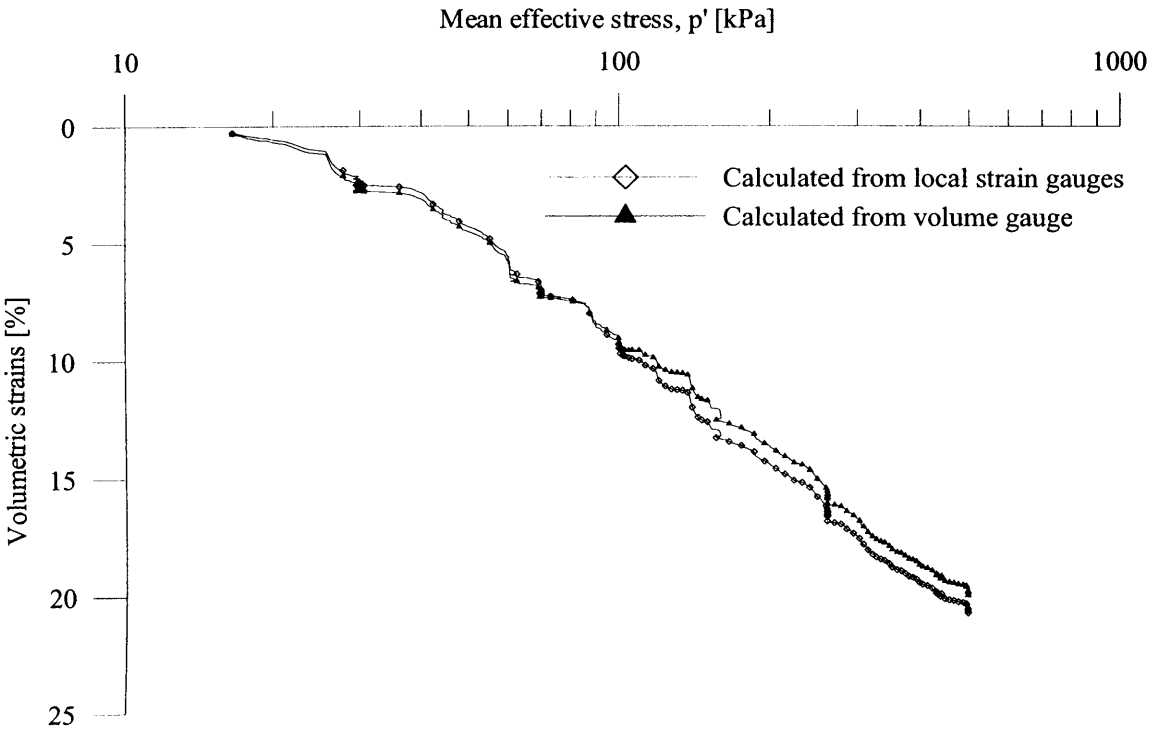

Figure 4-43 Comparing volumetric strains determined from volume gauge measurements with local strain gauge measurements in isotropic compression (sample S1k of reconstituted kaolin)

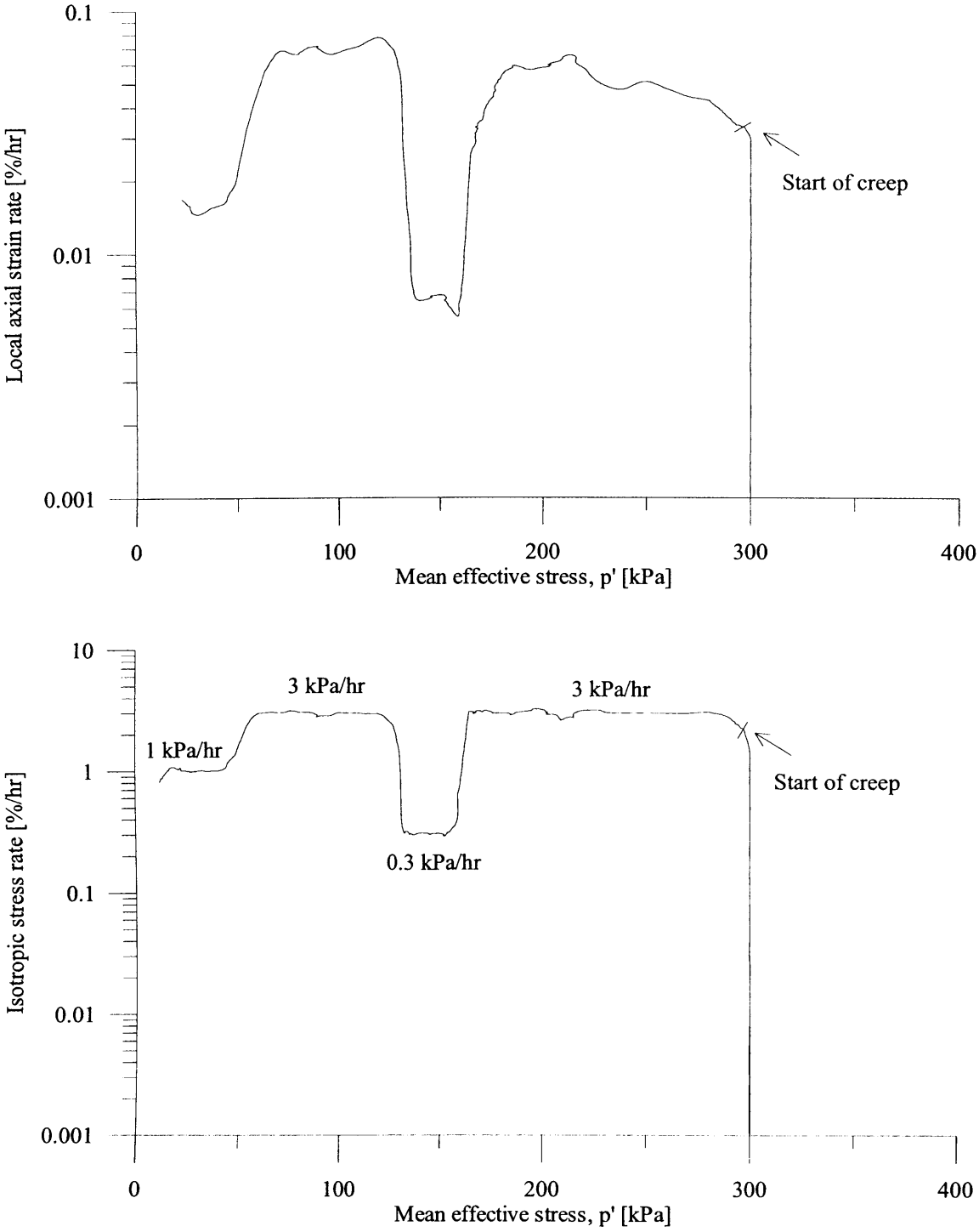

Figure 4-44 Axial strain rates and isotropic stress rates imposed in isotropic compression test on reconstituted London Clay (sample S2LCrB1)

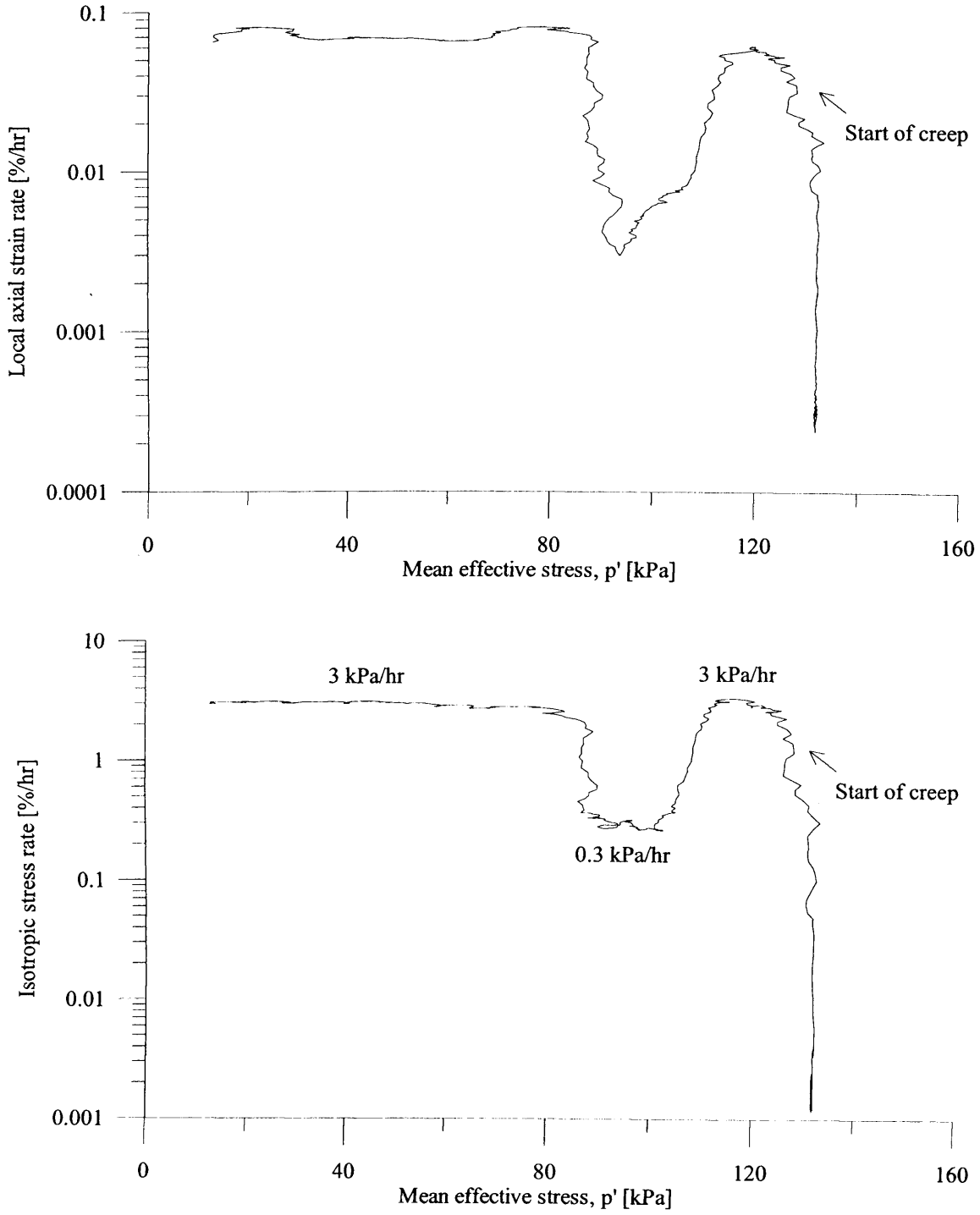

Figure 4-45 Axial strain rates and isotropic stress rates imposed in isotropic compression test on reconstituted London Clay (sample S2LCrB2)

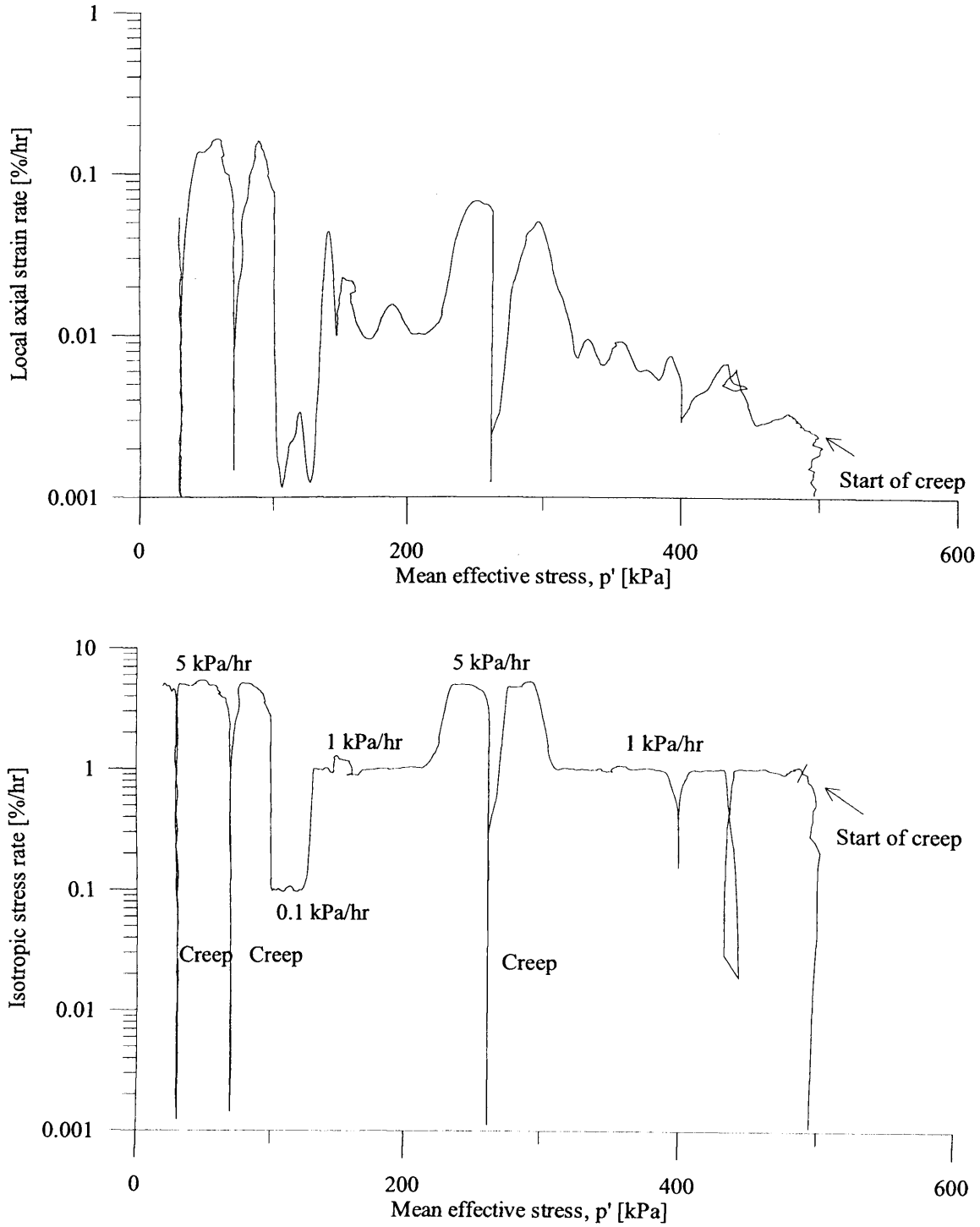

Figure 4-46 Axial strain rates and isotropic stress rates imposed in isotropic compression test on reconstituted kaolin (sample S1k)

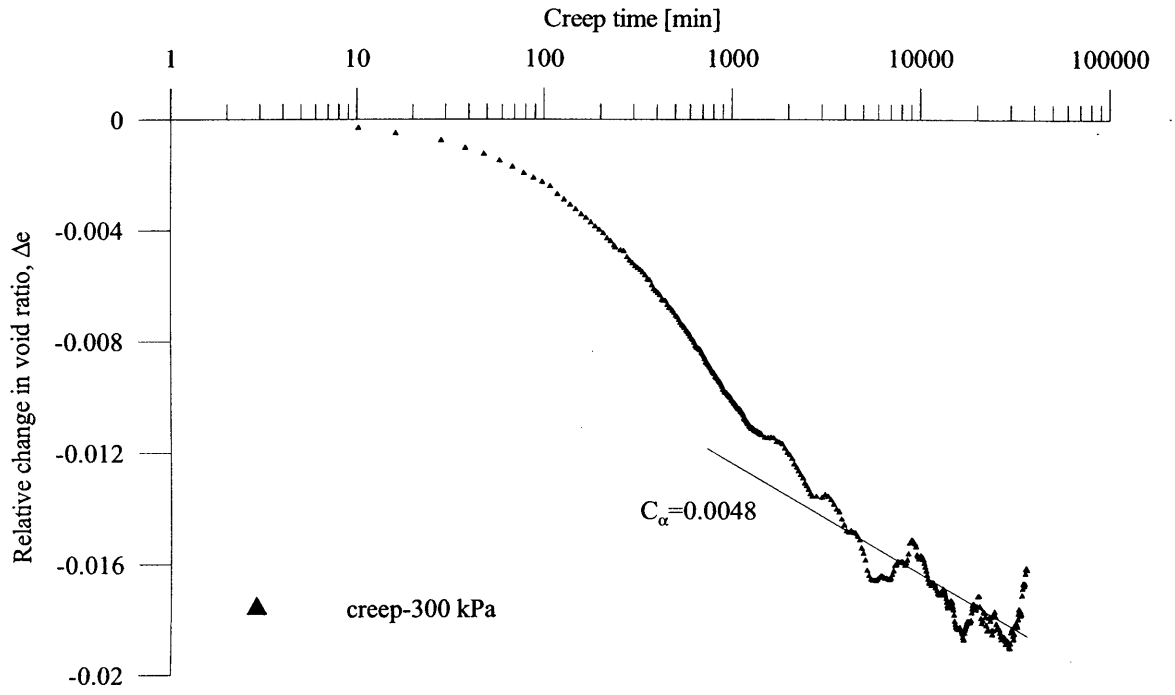

Figure 4-47 Variation in void ratio with time during isotropic creep for reconstituted London Clay (sample S2LCrB1)

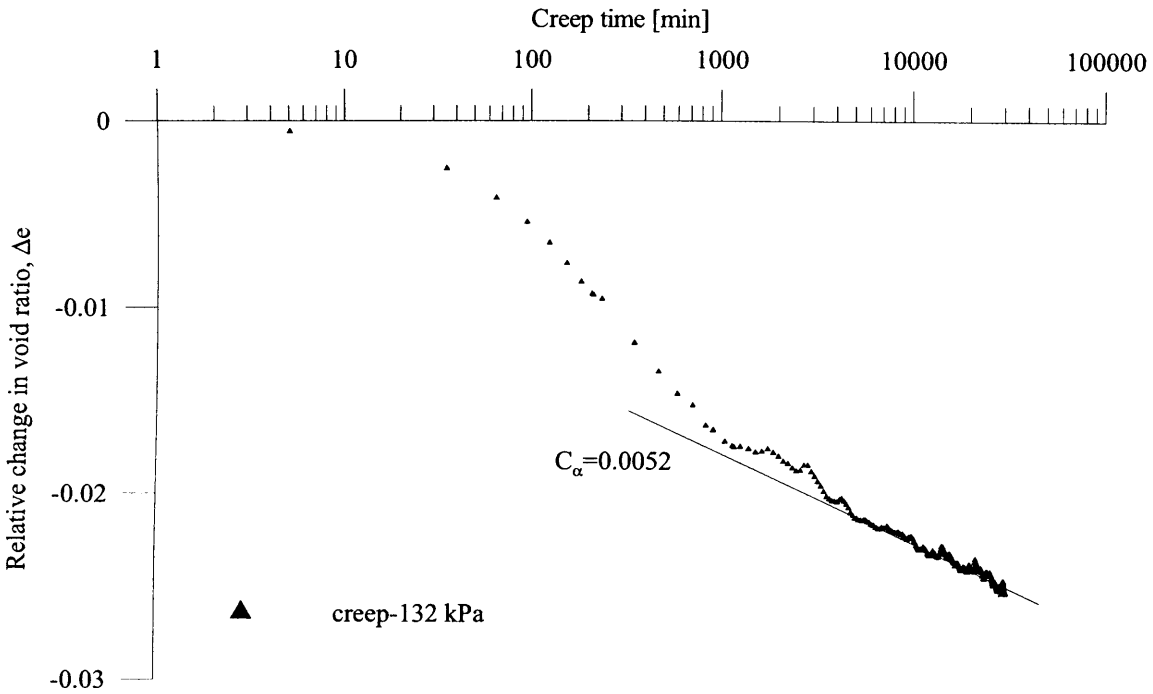

Figure 4-48 Variation in void ratio with time during isotropic creep for reconstituted London Clay (sample S2LCrB2)

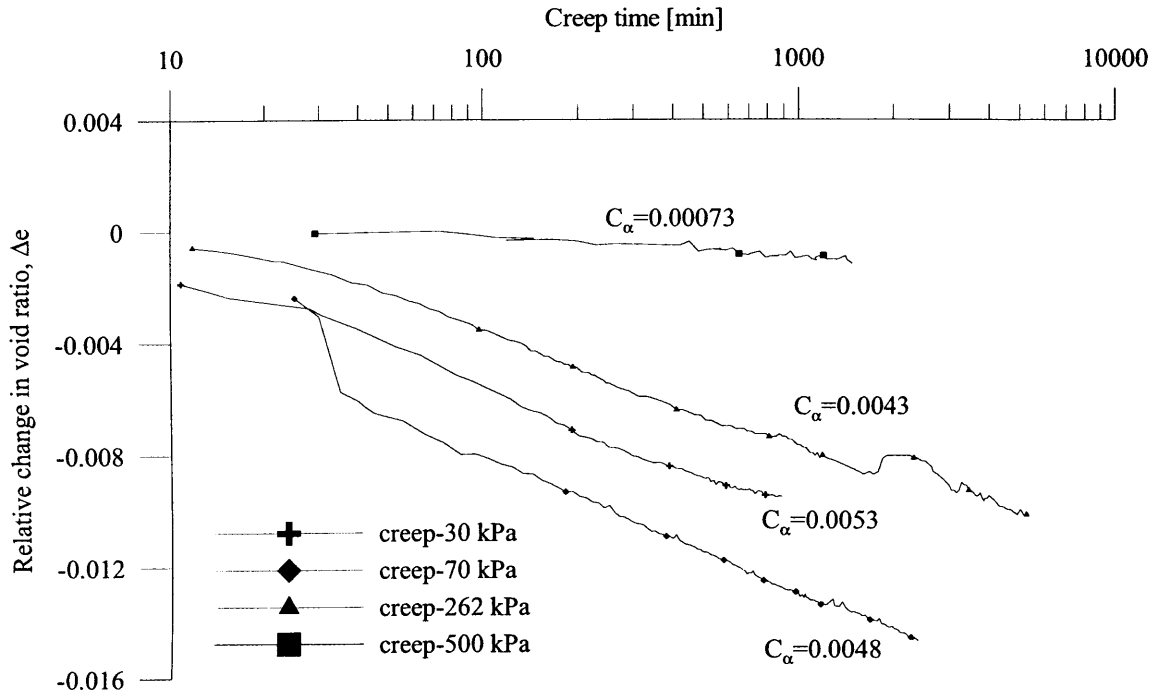

Figure 4-49 Variation in void ratio with time during isotropic creep for reconstituted kaolin (sample S1k)

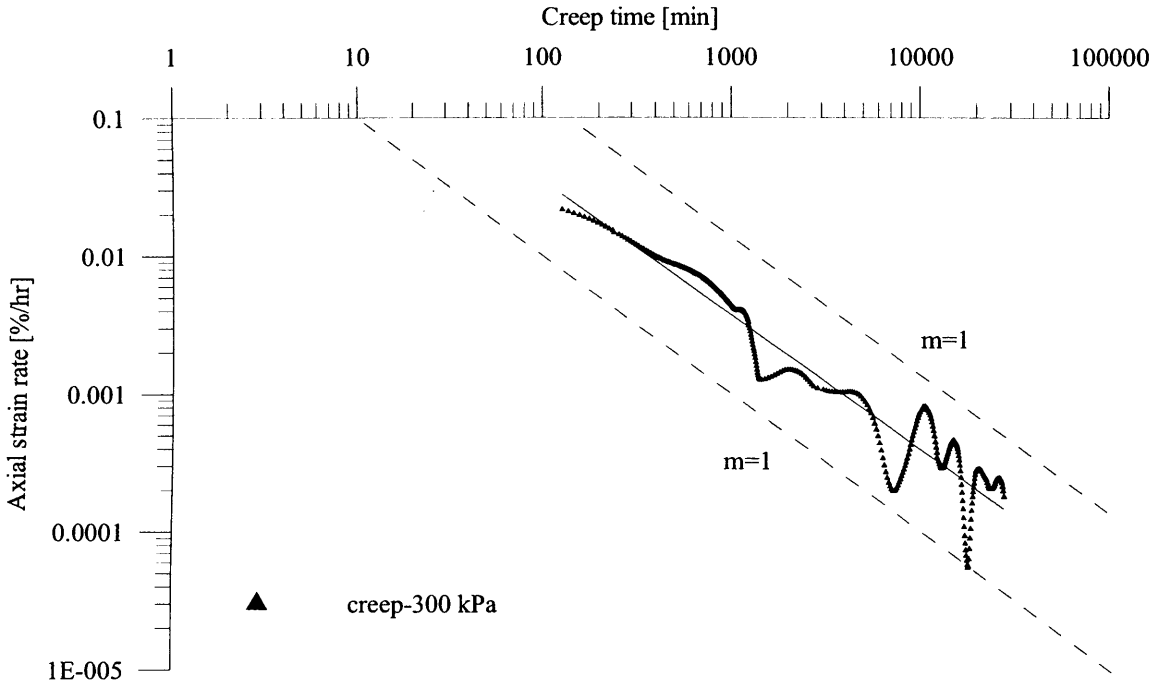

Figure 4-50 Variation in axial strain rate with time during isotropic creep for reconstituted London Clay (sample S2LCrB1)

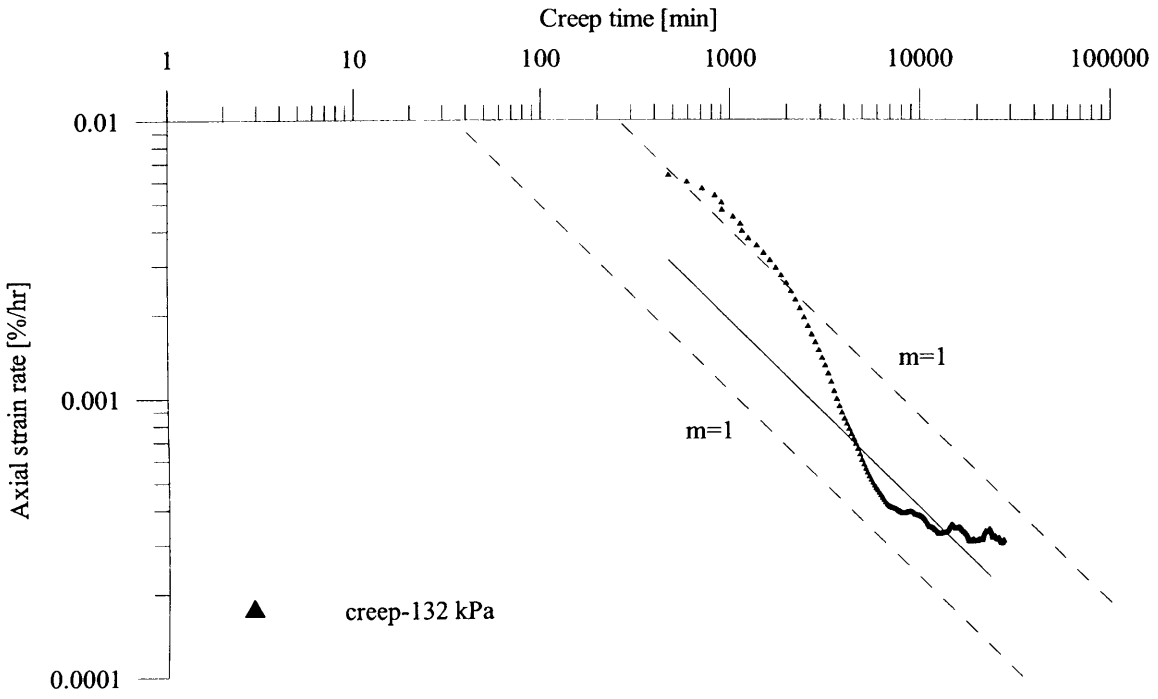

Figure 4-51 Variation in axial strain rate with time during isotropic creep for reconstituted London Clay (sample S2LCrB2)

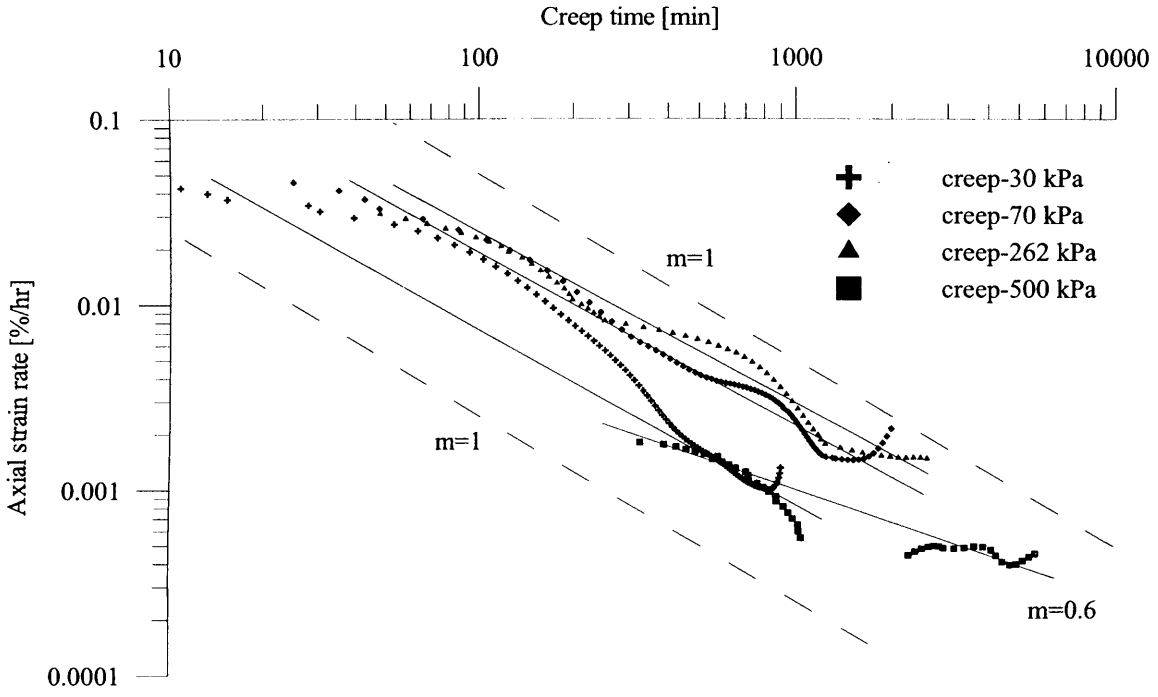

Figure 4-52 Variation in axial strain rate with time during isotropic creep for reconstituted kaolin (sample S1k)

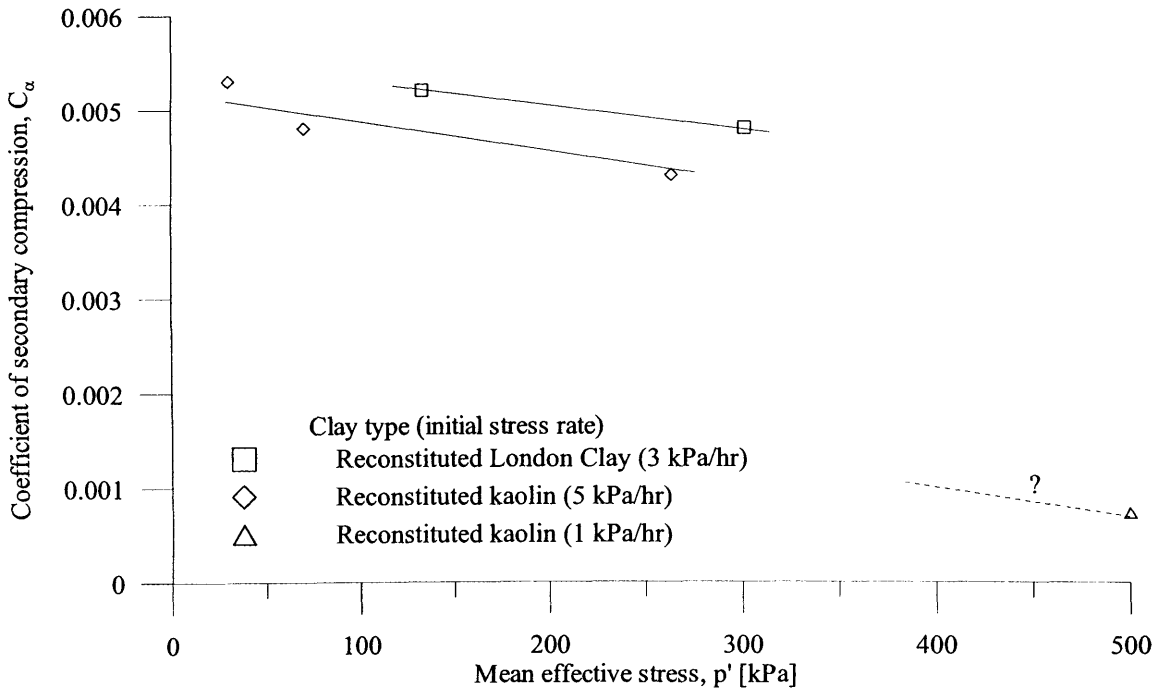

Figure 4-53 Variation in the coefficient of secondary compression, C_α with stress level in isotropic compression test on reconstituted kaolin and reconstituted London Clay (samples S2LCrB1, S2LCrB2 and S1k)

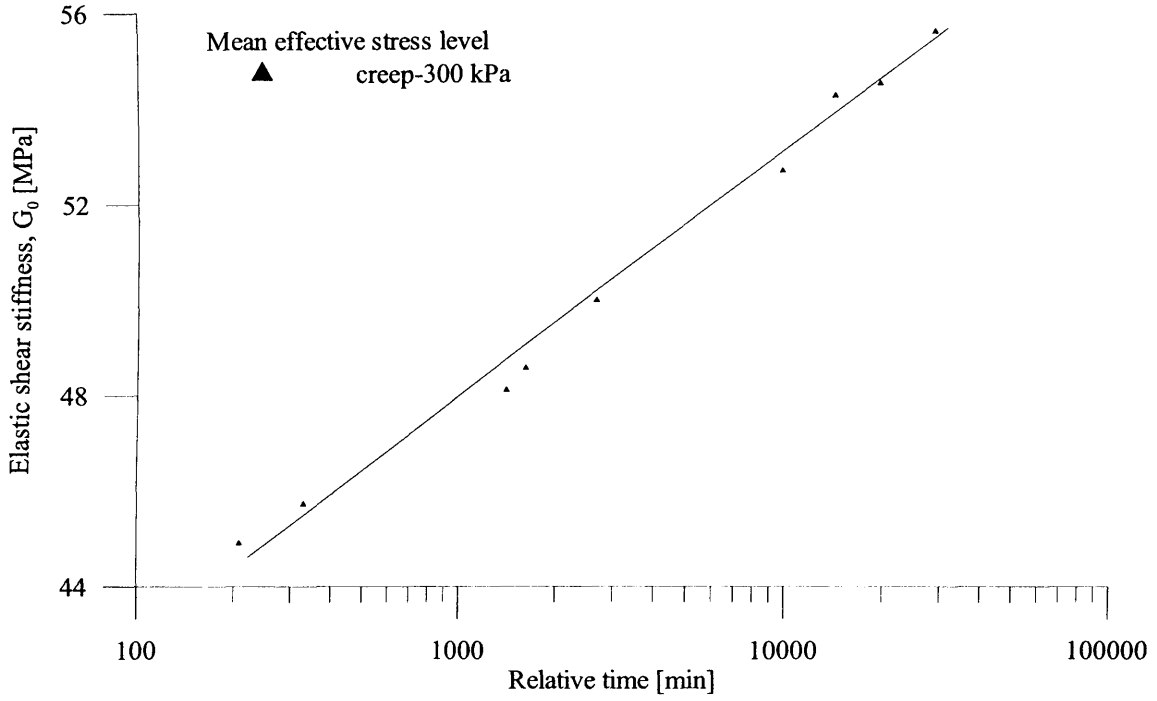

Figure 4-54 Increase in elastic shear stiffness with time during isotropic creep for reconstituted London Clay (sample S2LCrB1)

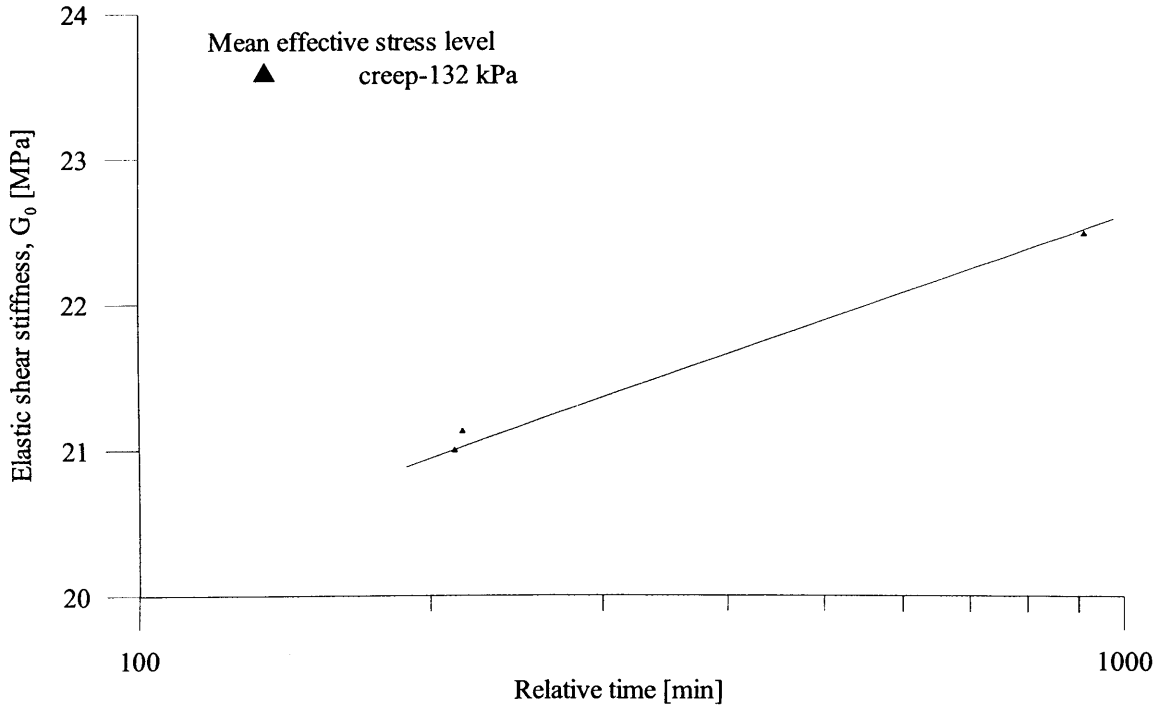

Figure 4-55 Increase in elastic shear stiffness with time during isotropic creep for reconstituted London Clay (sample S2LCrB2)

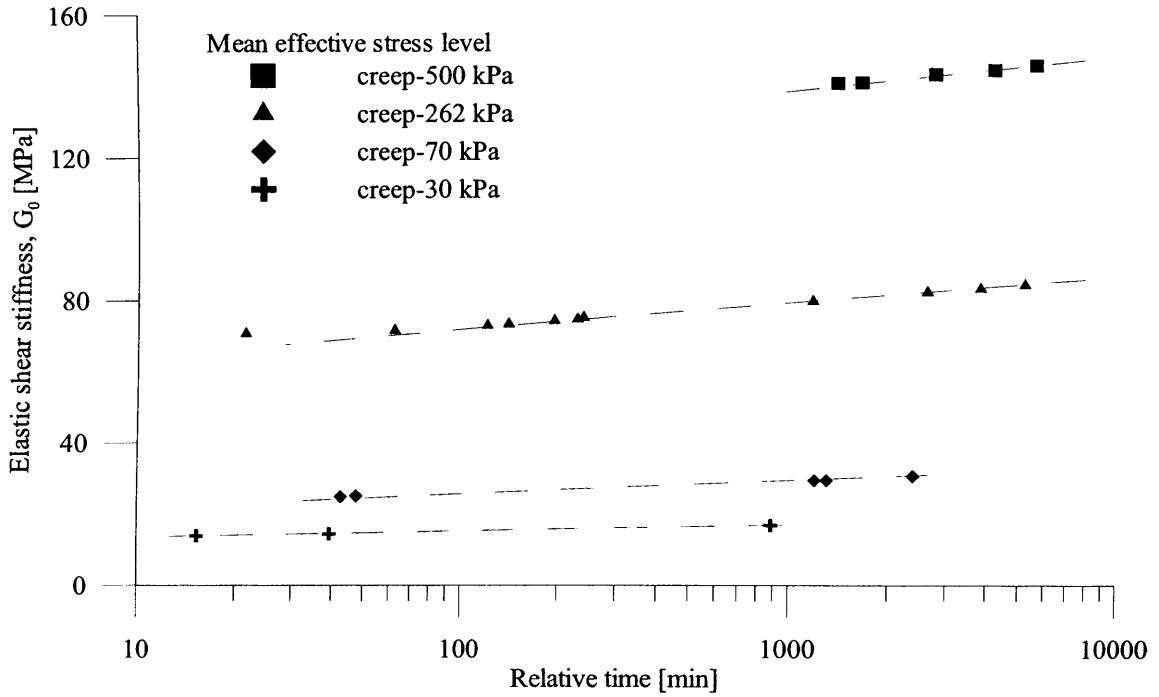

Figure 4-56 Increase in elastic shear stiffness with time during isotropic creep for reconstituted kaolin (sample S1k)

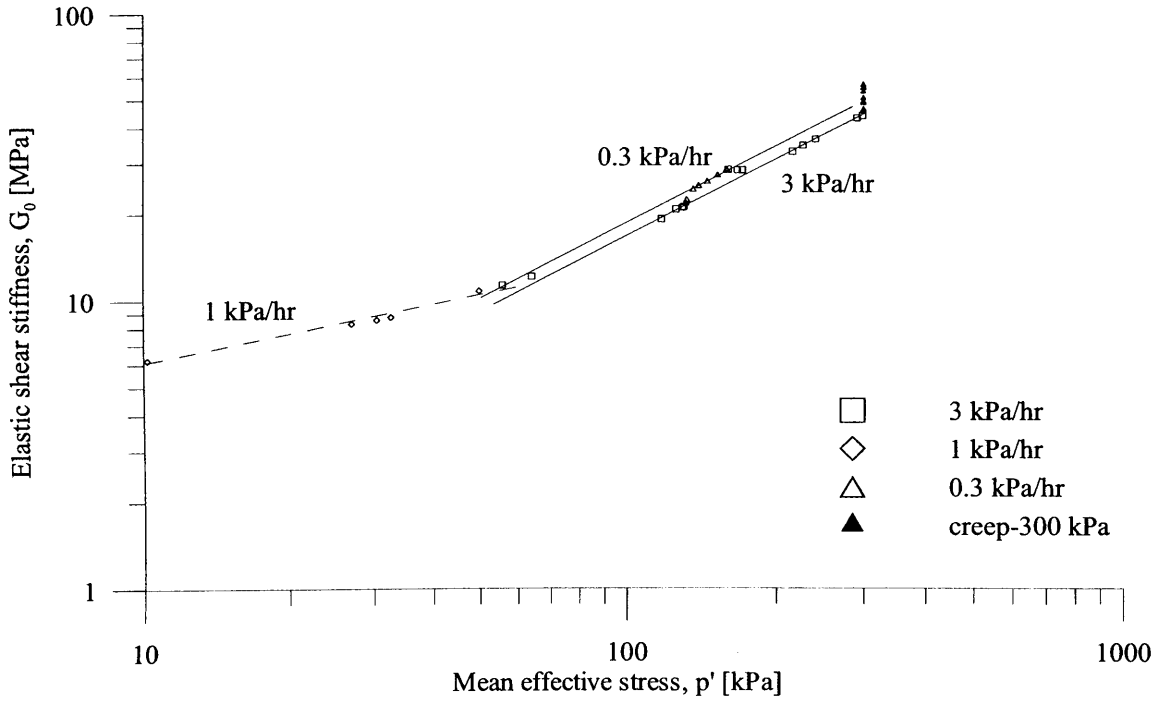

Figure 4-57 Influence of step-wise change in rate of stress and creep on the G_0-p' relationship curve during isotropic compression of reconstituted London Clay (sample S2LCrB1)

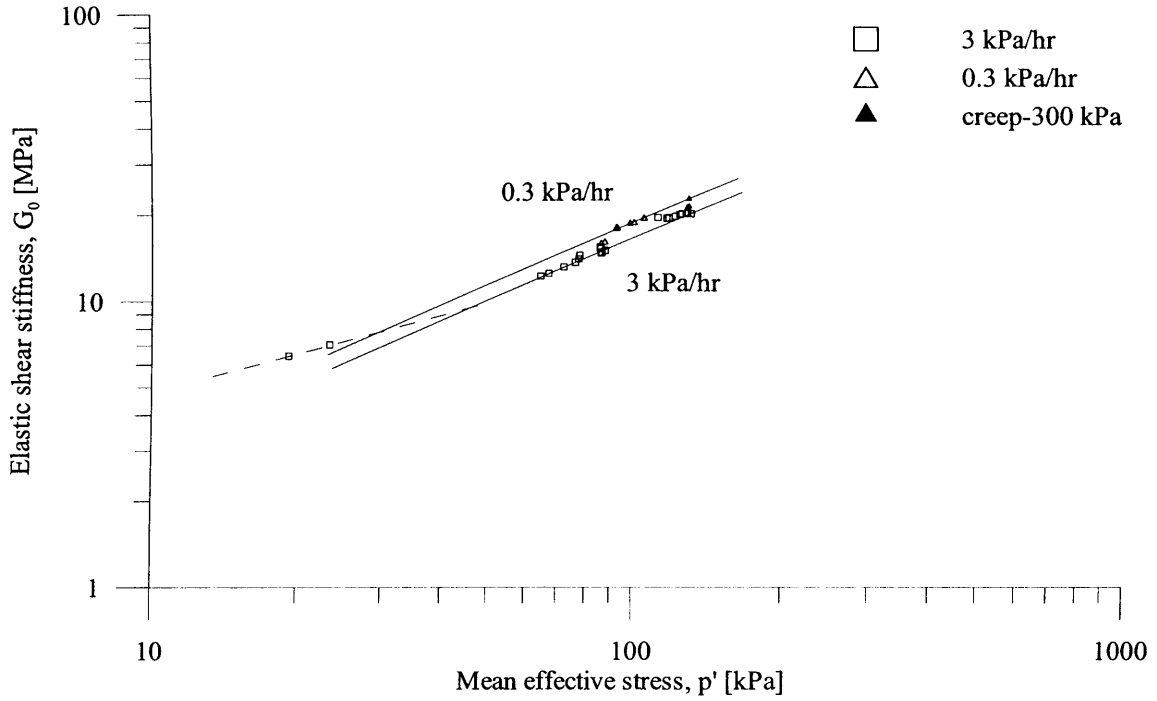

Figure 4-58 Influence of step-wise change in rate of stress and creep on the G_0-p' relationship curve during isotropic compression of reconstituted London Clay (sample S2LCrB2)

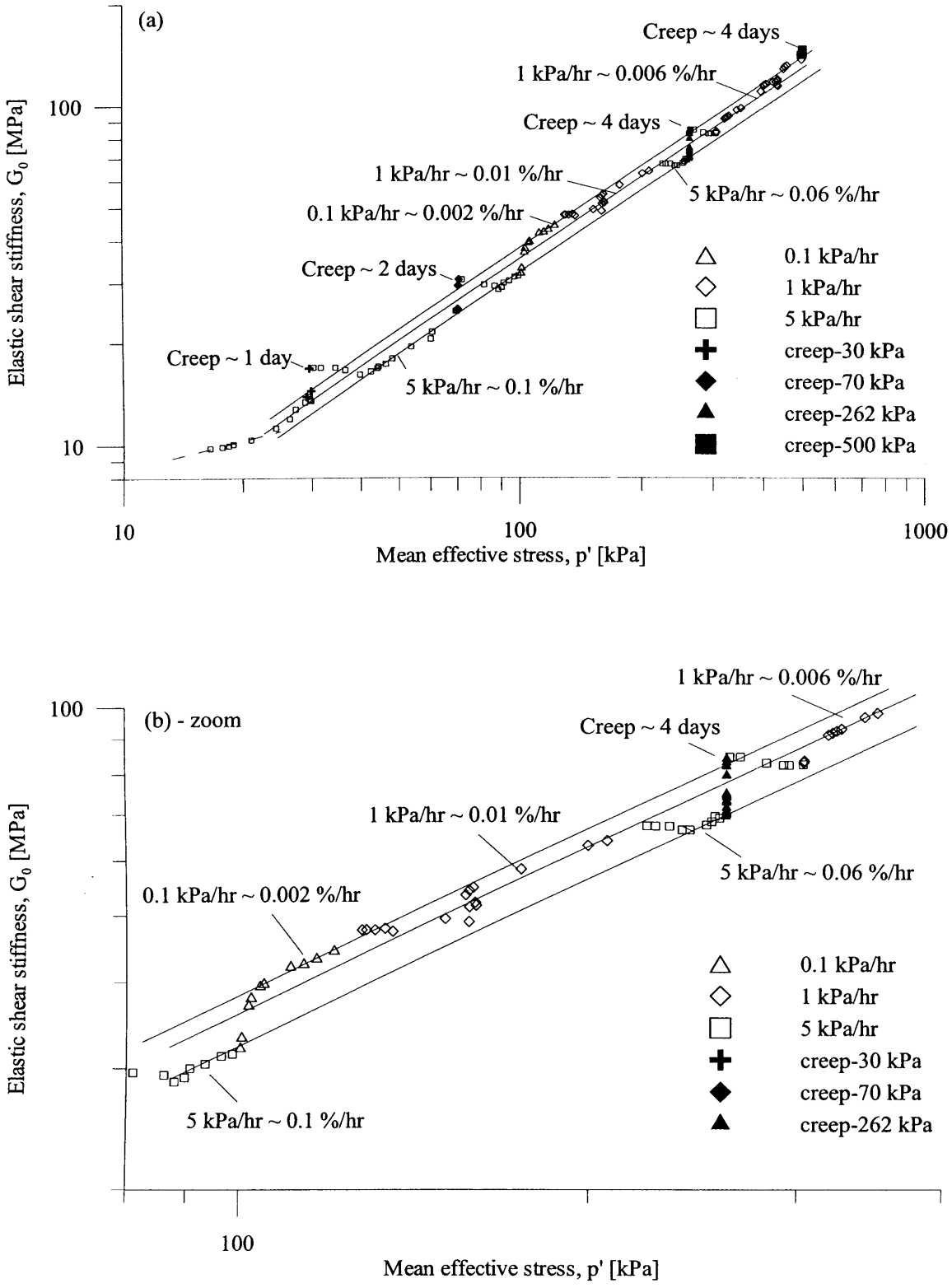

Figure 4-59 Influence of step-wise change in rate of stress and creep on the G_0-p' relationship curve during isotropic compression of reconstituted kaolin (sample S1k)

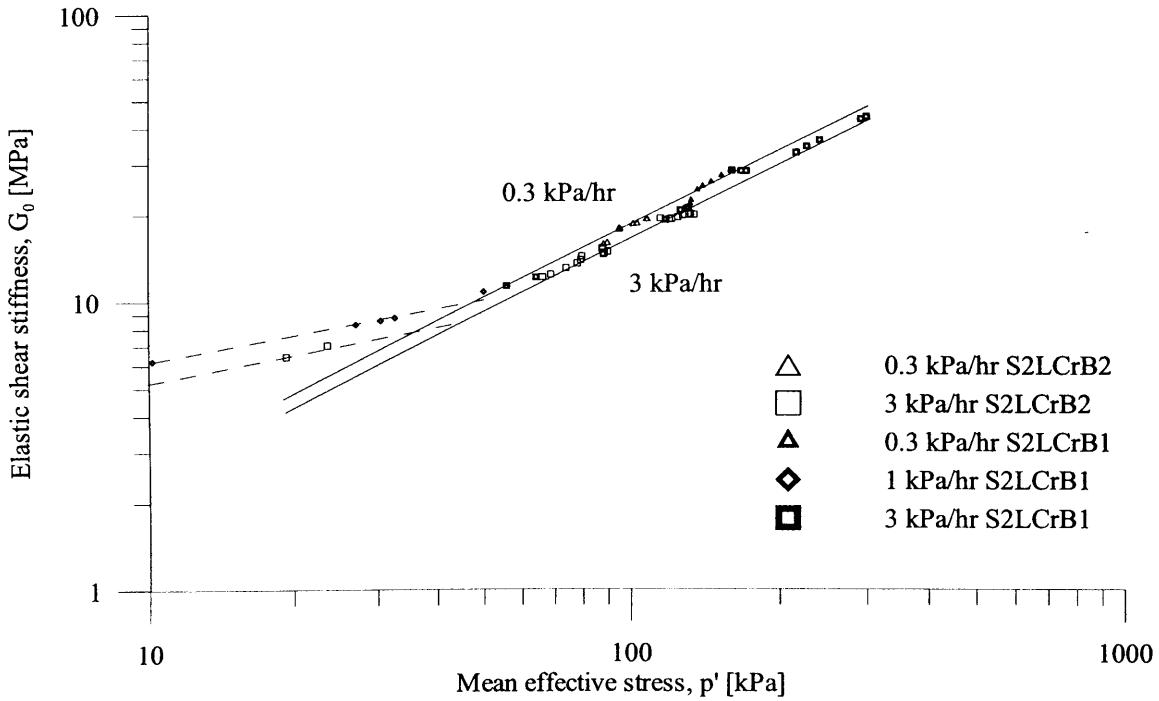

Figure 4-60 Consistency of G_0-p' relationship curves obtained for isotropic compression tests on two samples of reconstituted London Clay (samples S2LCrB1 and S2LCrB2)

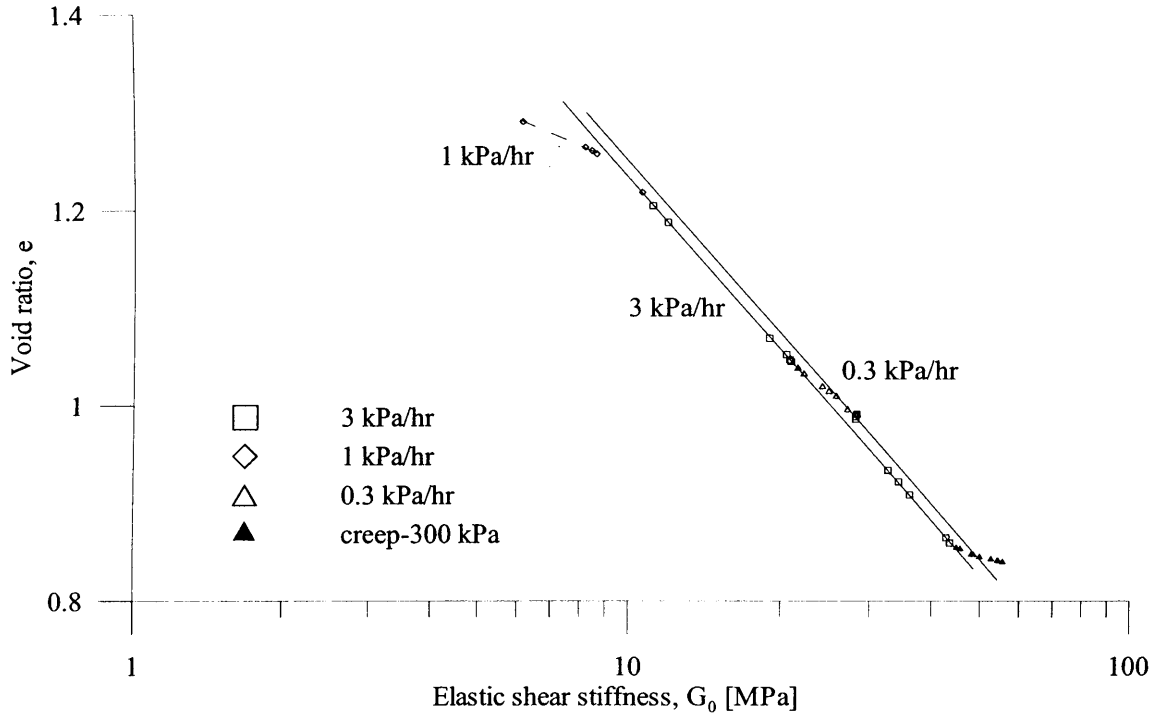

Figure 4-61 Influence of step-wise change in rate of stress and creep on the e-G_0 relationship curve during isotropic compression of reconstituted London Clay (sample S2LCrB1)

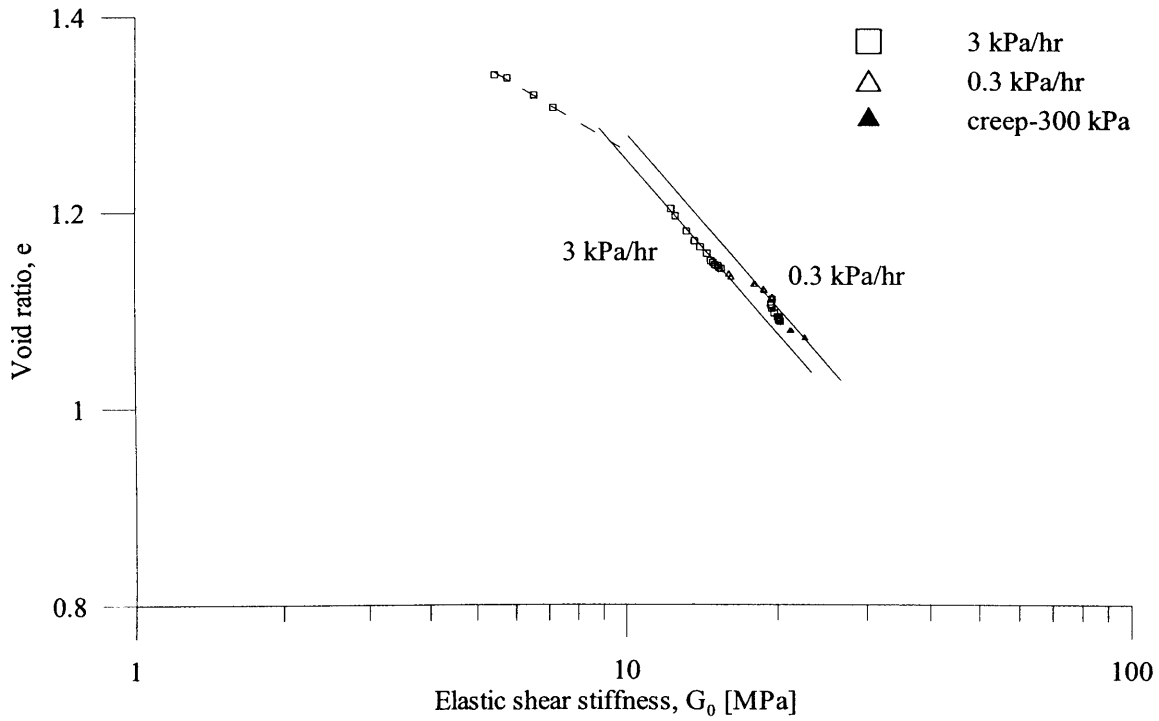

Figure 4-62 Influence of step-wise change in rate of stress and creep on the e-G_0 relationship curve during isotropic compression of reconstituted London Clay (sample S2LCrB2)

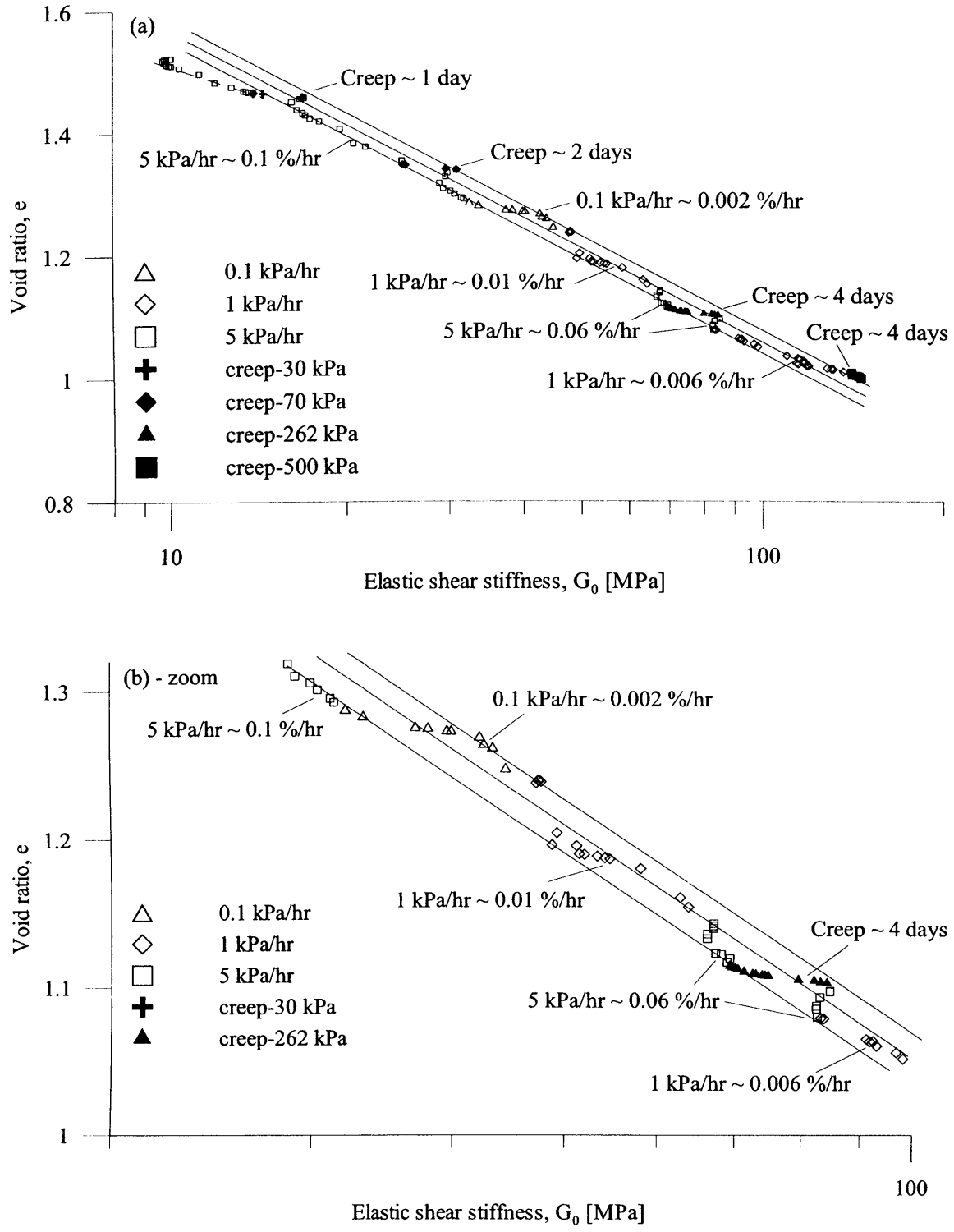

Figure 4-63 Influence of step-wise change in rate of stress and creep on the e-G_0 relationship curve during isotropic compression of reconstituted kaolin (sample S1k)

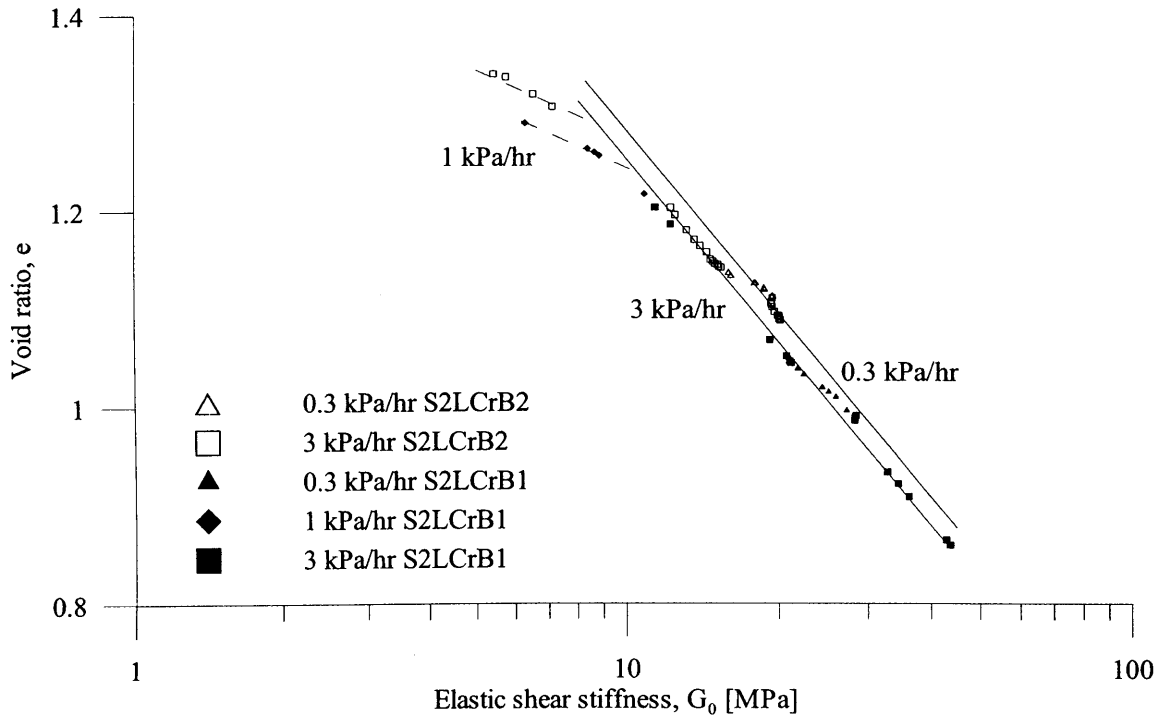

Figure 4-64 Consistency of e-G_0 relationship curves obtained for isotropic compression tests on two samples of reconstituted London Clay (samples S2LCrB1 and S2LCrB2)

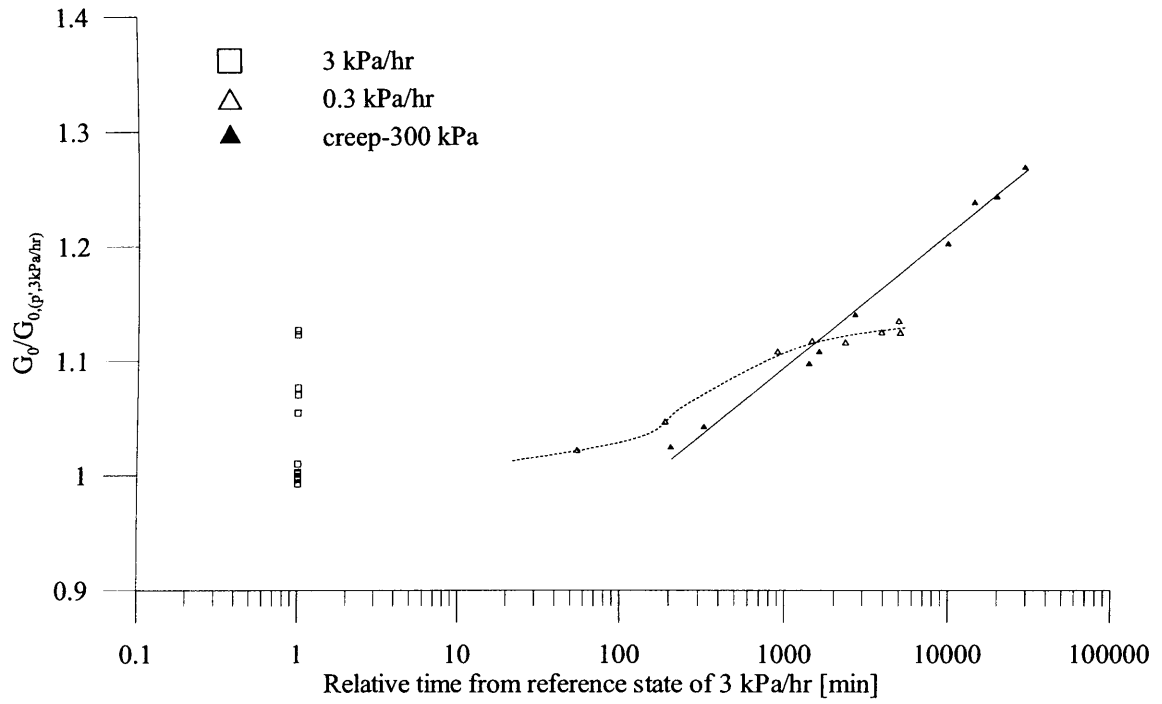

Figure 4-65 Plot of normalised elastic shear stiffness against time during SRS* isotropic compression and isotropic creep for reconstituted London Clay (sample S2LCrB1)

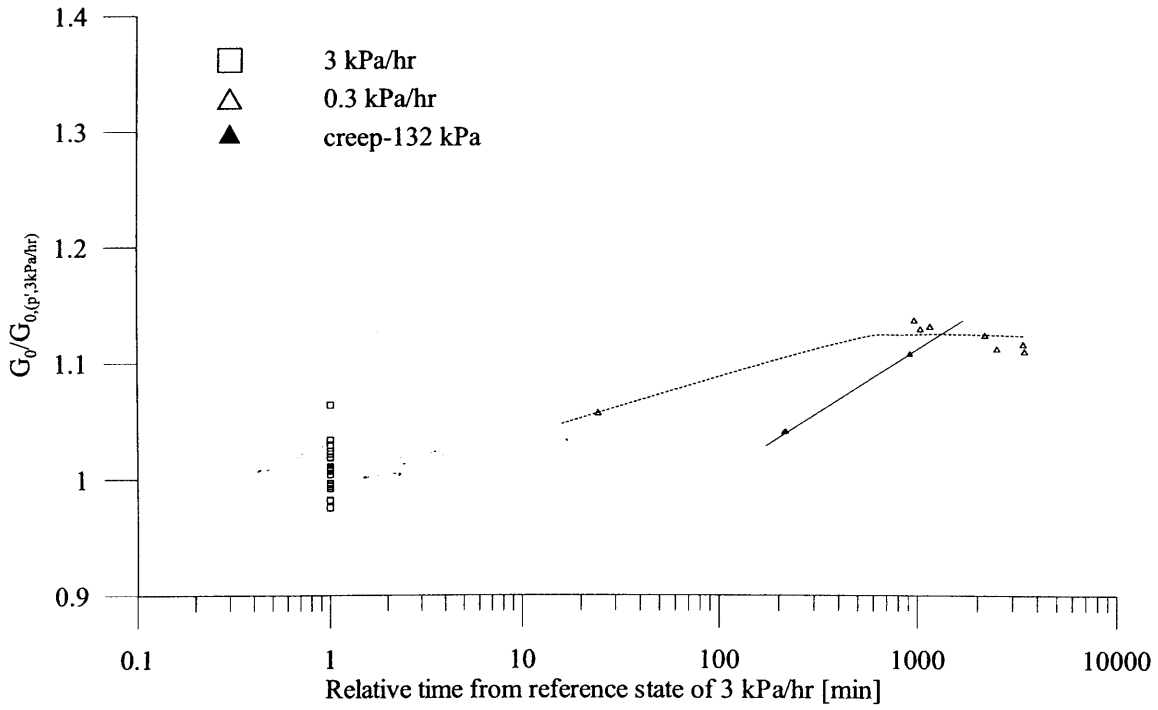

Figure 4-66 Plot of normalised elastic shear stiffness against time during SRS* isotropic compression and isotropic creep for reconstituted London Clay (sample S2LCrB2)

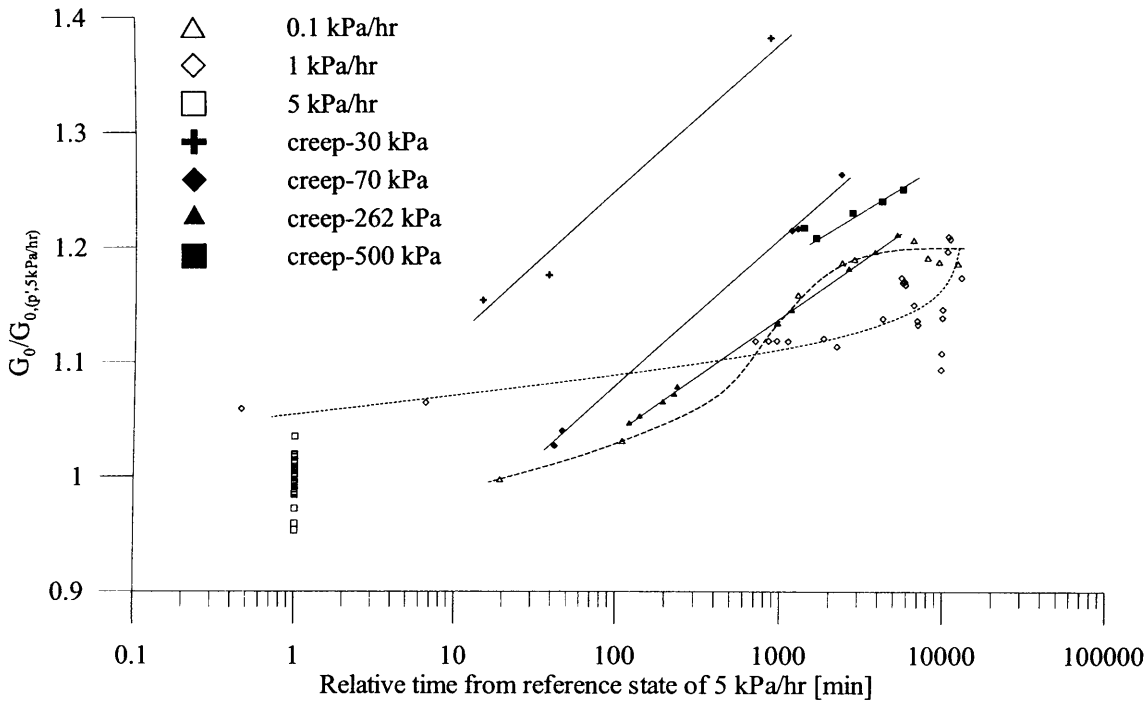

Figure 4-67 Plot of normalised elastic shear stiffness against time during SRS* isotropic compression and isotropic creep for reconstituted kaolin (sample S1k)

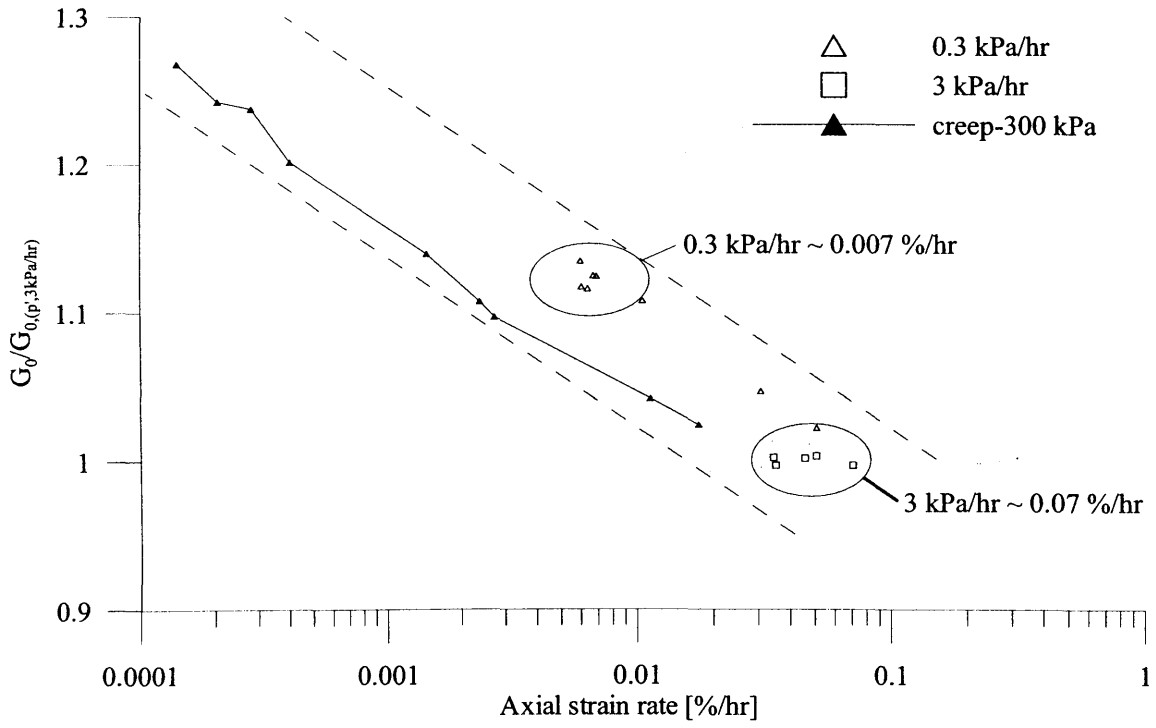

Figure 4-68 Plot of normalised elastic shear stiffness against strain rate during SRS* isotropic compression and isotropic creep for reconstituted London Clay (sample S2LCrB1)

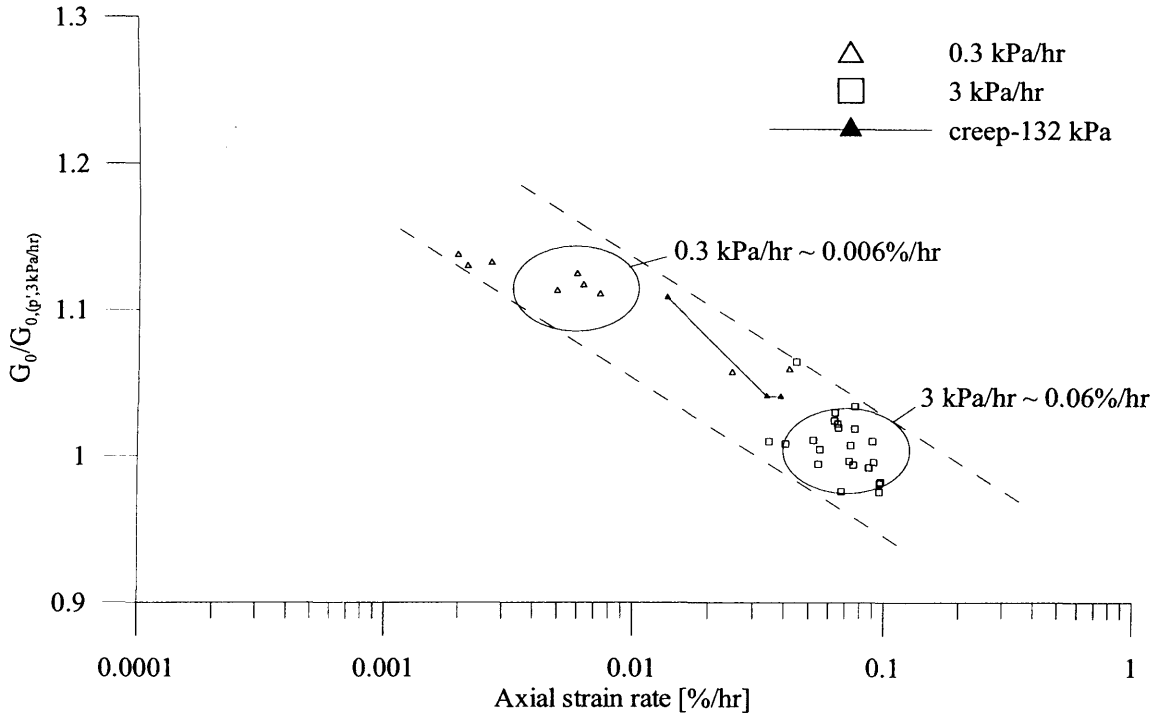

Figure 4-69 Plot of normalised elastic shear stiffness against strain rate during SRS* isotropic compression and isotropic creep for reconstituted London Clay (sample S2LCrB2)

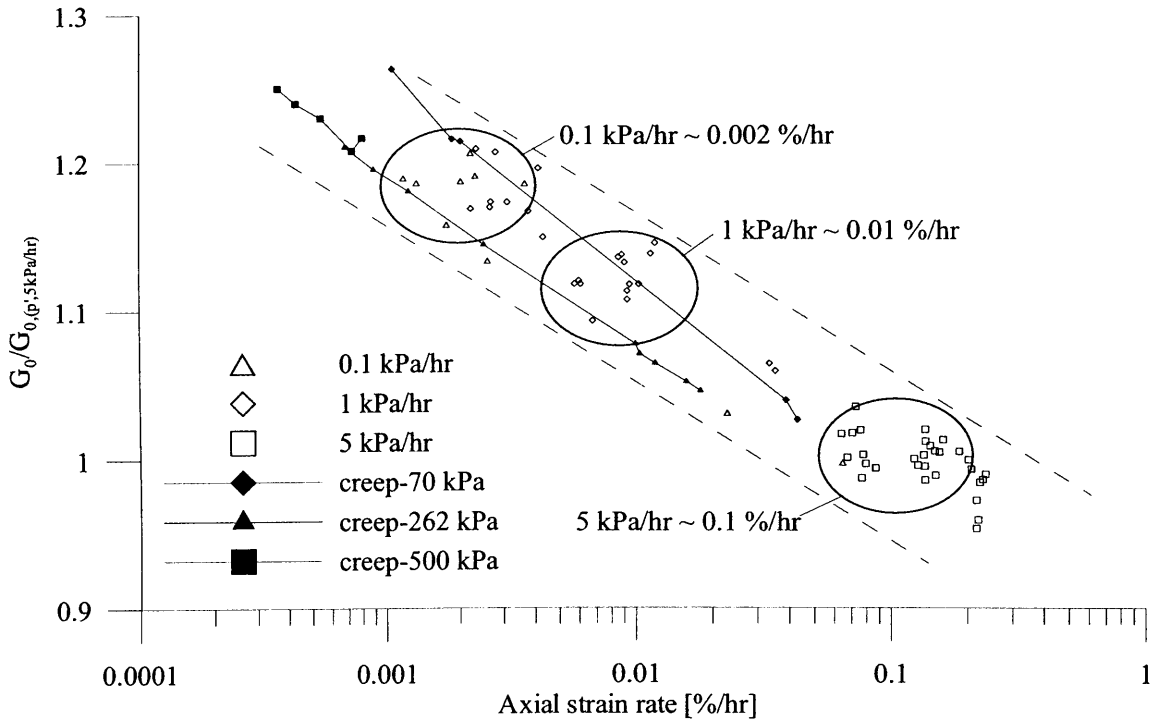

Figure 4-70 Plot of normalised elastic shear stiffness against strain rate during SRS* isotropic compression and isotropic creep for reconstituted kaolin (sample S1k)

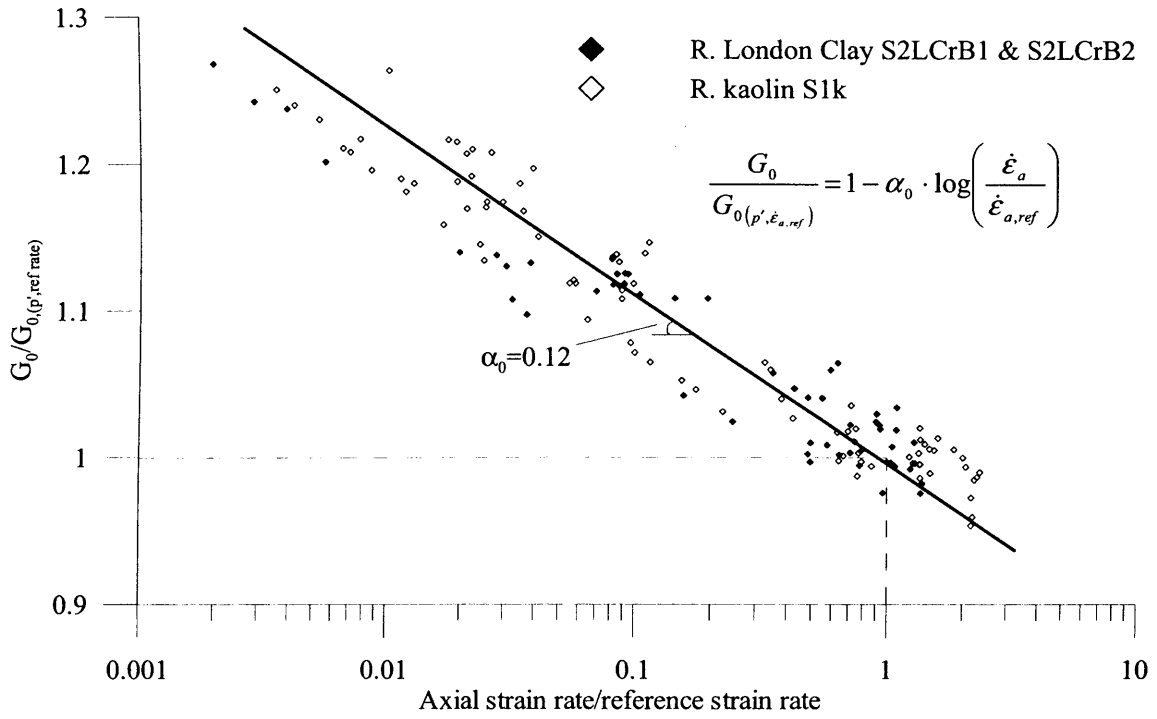

Figure 4-71 Comparison of normalised elastic shear stiffness against relative change in strain rate during SRS* isotropic compression and isotropic creep for reconstituted London Clay and kaolin (samples S2LCrB1, S2LCrB2 and S1k)

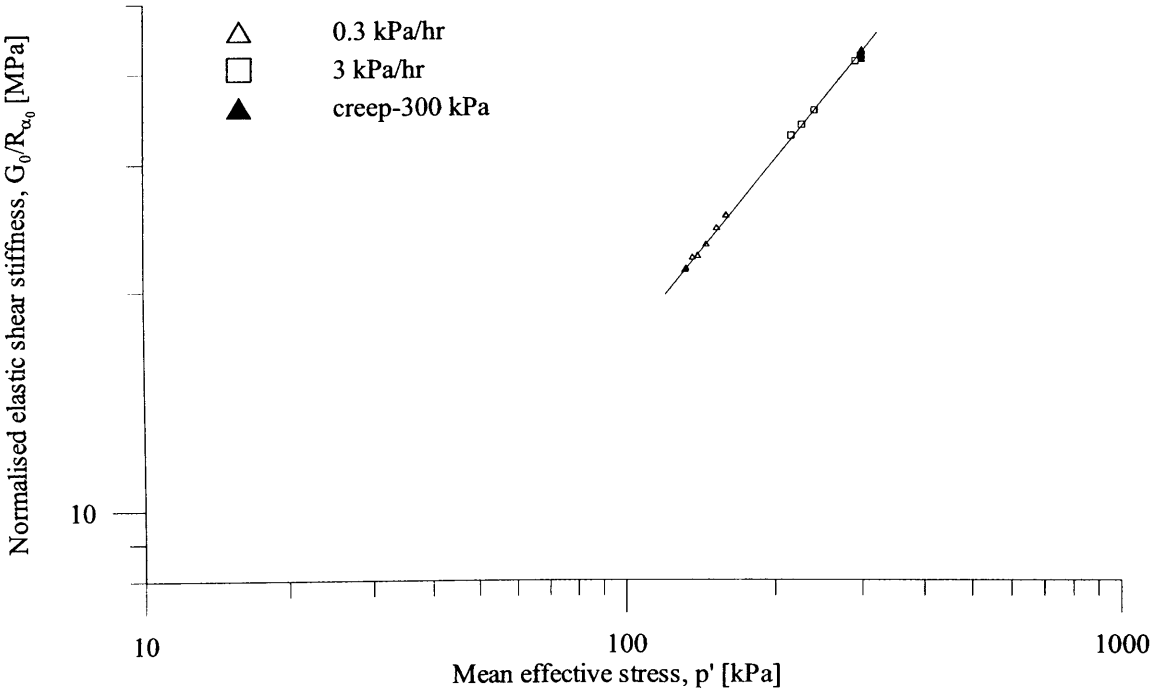

Figure 4-72 Relationship between elastic shear stiffness and mean effective stress, normalised to remove effects of strain rate in isotropic compression of reconstituted London Clay (S2LCrB1)

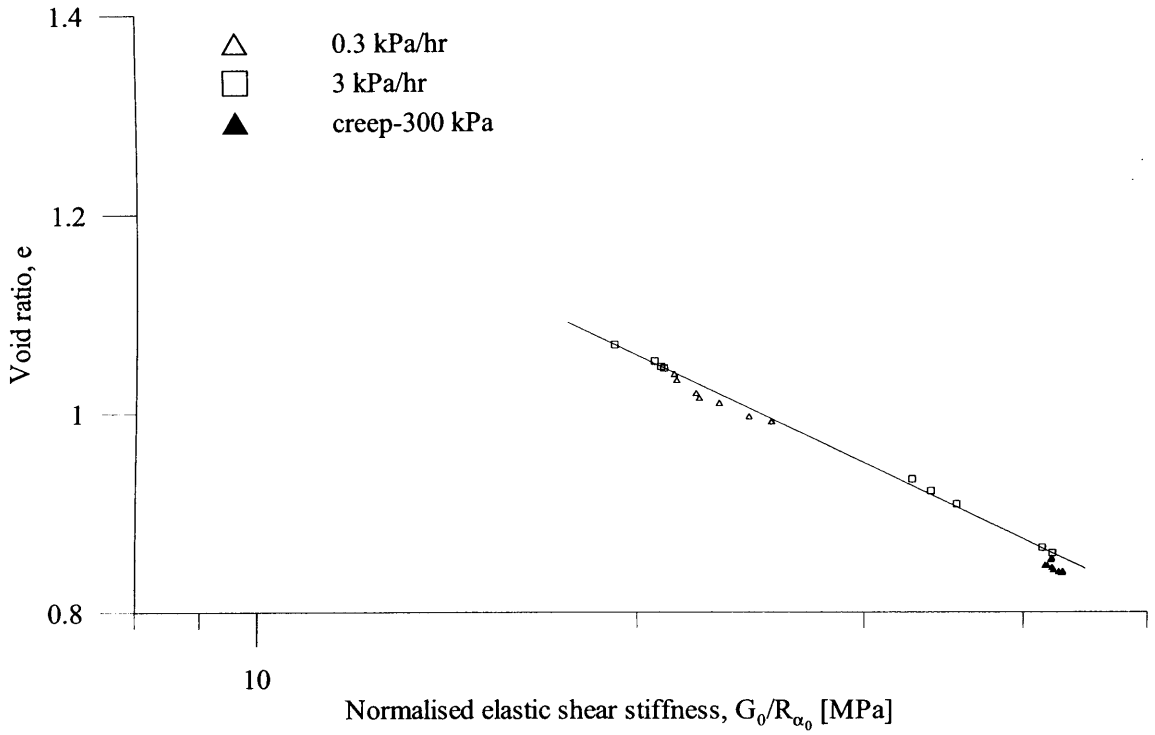

Figure 4-73 Relationship between elastic shear stiffness and void ratio, normalised to remove effects of strain rate in isotropic compression of reconstituted London Clay (S2LCrB1)

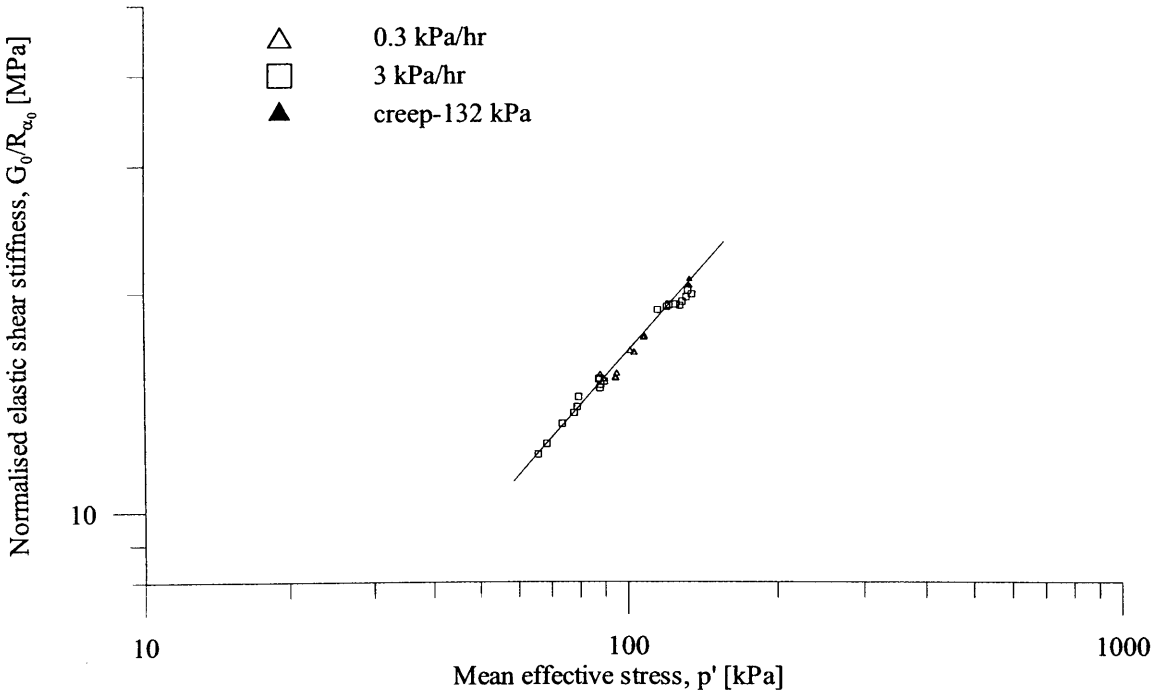

Figure 4-74 Relationship between elastic shear stiffness and mean effective stress, normalised to remove effects of strain rate in isotropic compression of reconstituted London Clay (S2LCrB2)

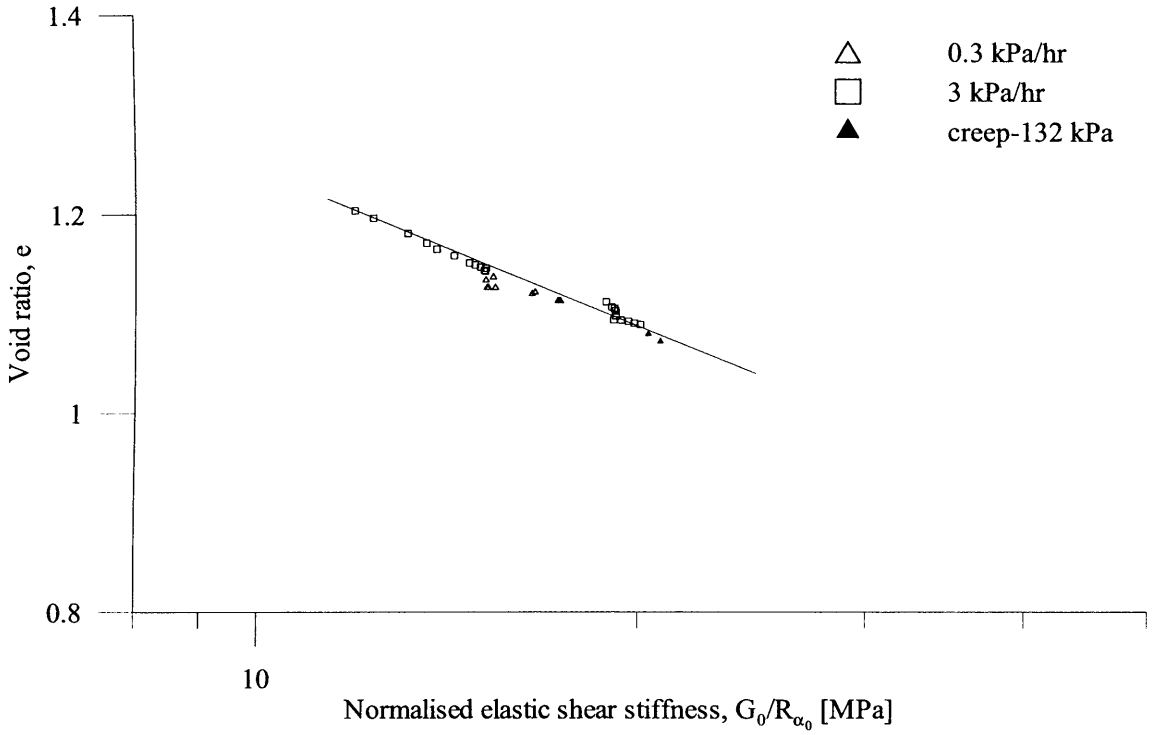

Figure 4-75 Relationship between elastic shear stiffness and void ratio, normalised to remove effects of strain rate in isotropic compression of reconstituted London Clay (S2LCrB2)

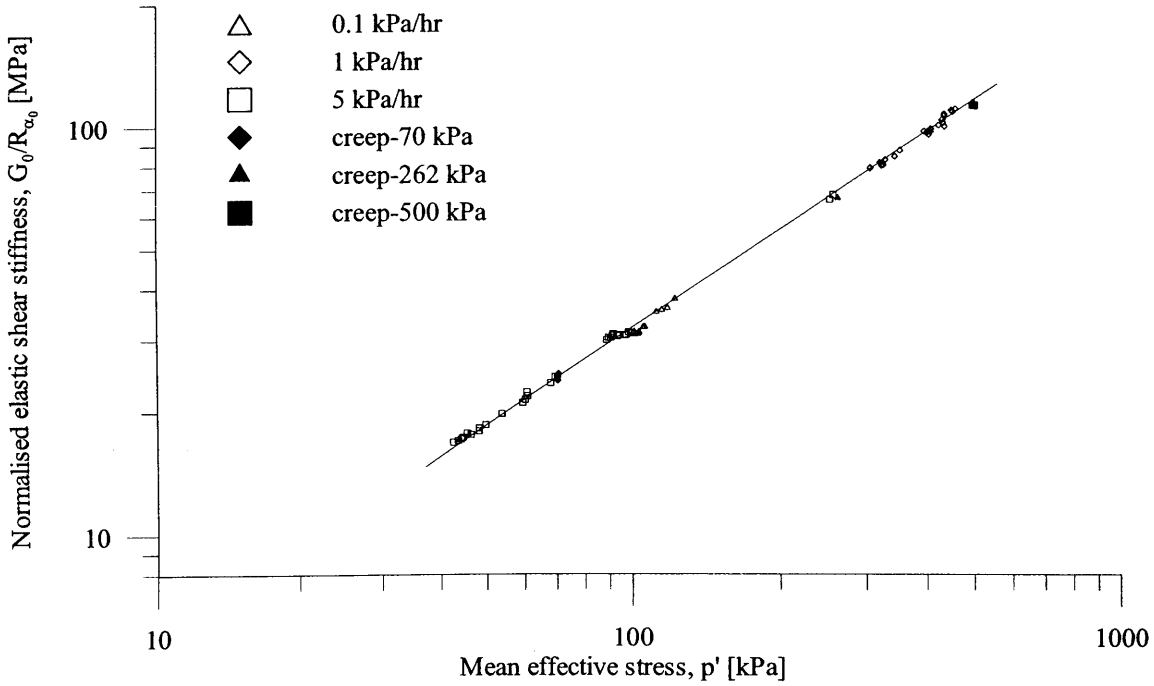

Figure 4-76 Relationship between elastic shear stiffness and mean effective stress, normalised to remove effects of strain rate in isotropic compression of reconstituted kaolin (S1k)

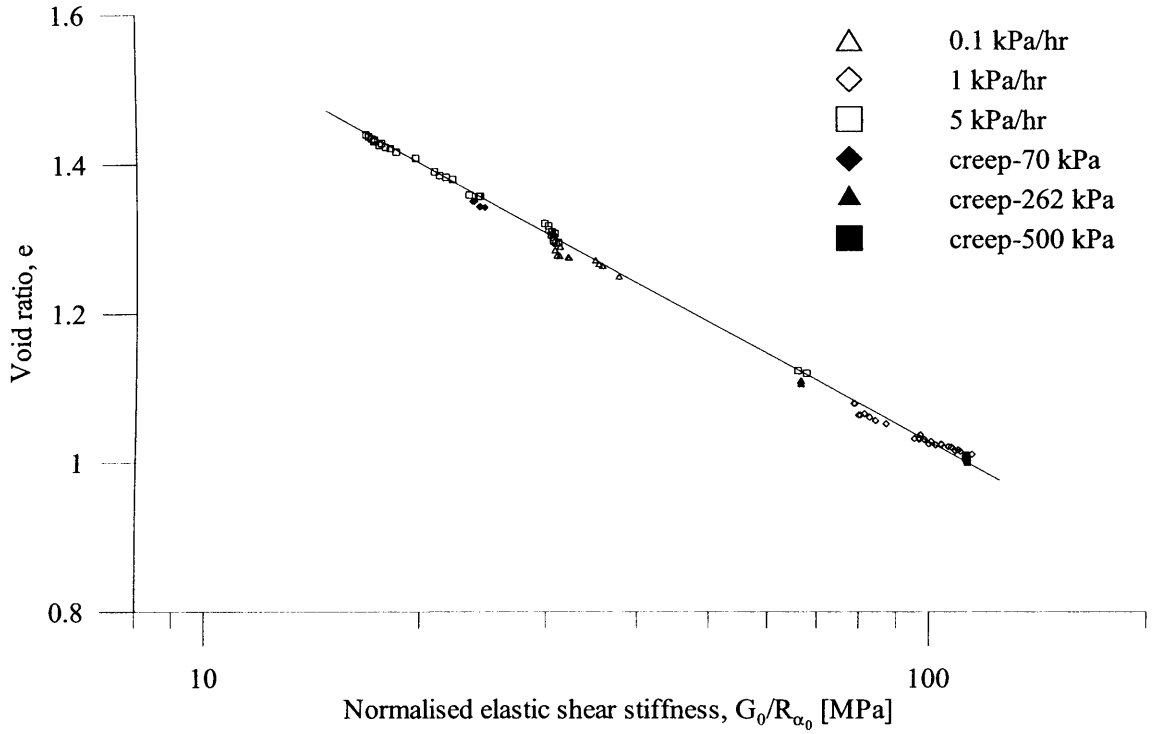

Figure 4-77 Relationship between elastic shear stiffness and void ratio, normalised to remove effects of strain rate in isotropic compression of reconstituted kaolin (S1k)

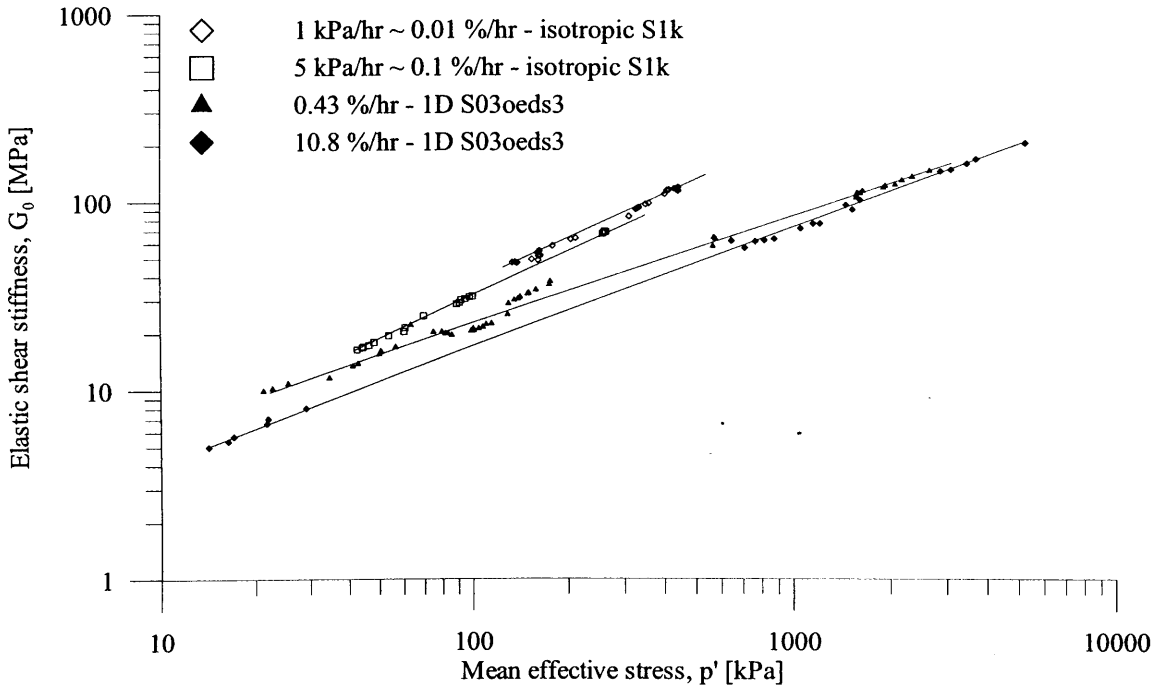

Figure 4-78 Comparison of ln G_0'-ln p′ relationship curves obtained in 1D compression and isotropic compression of reconstituted kaolin

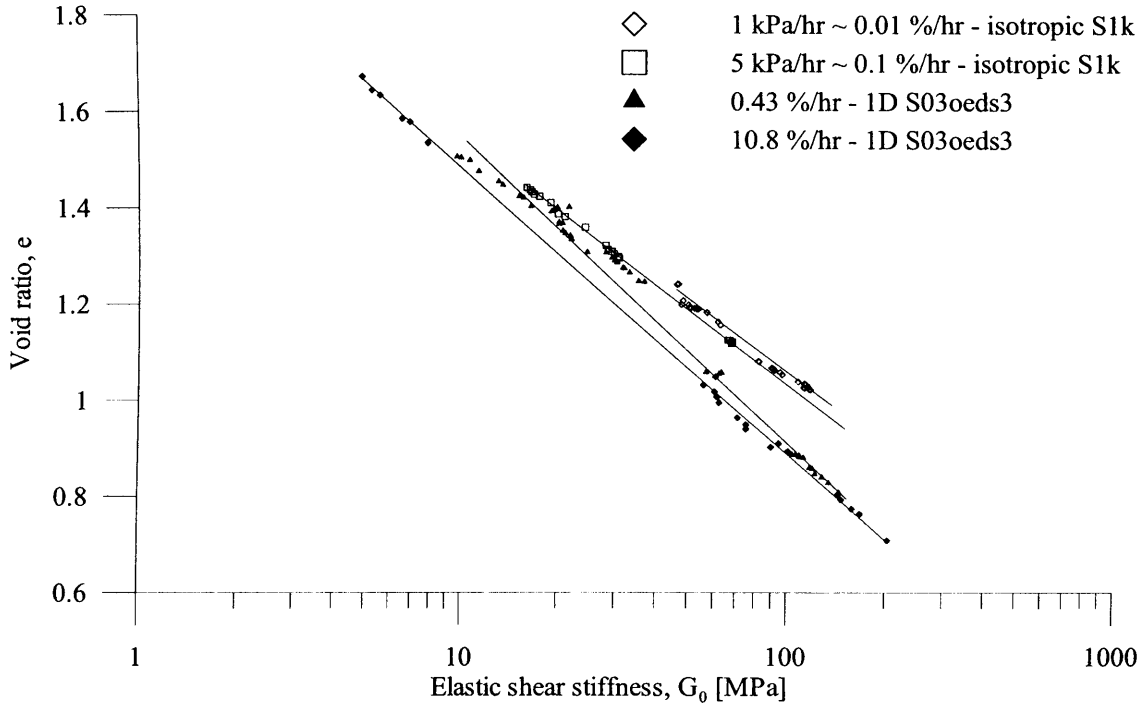

Figure 4-79 Comparison of e-ln G_0' relationship curves obtained in 1D compression and isotropic compression of reconstituted kaolin

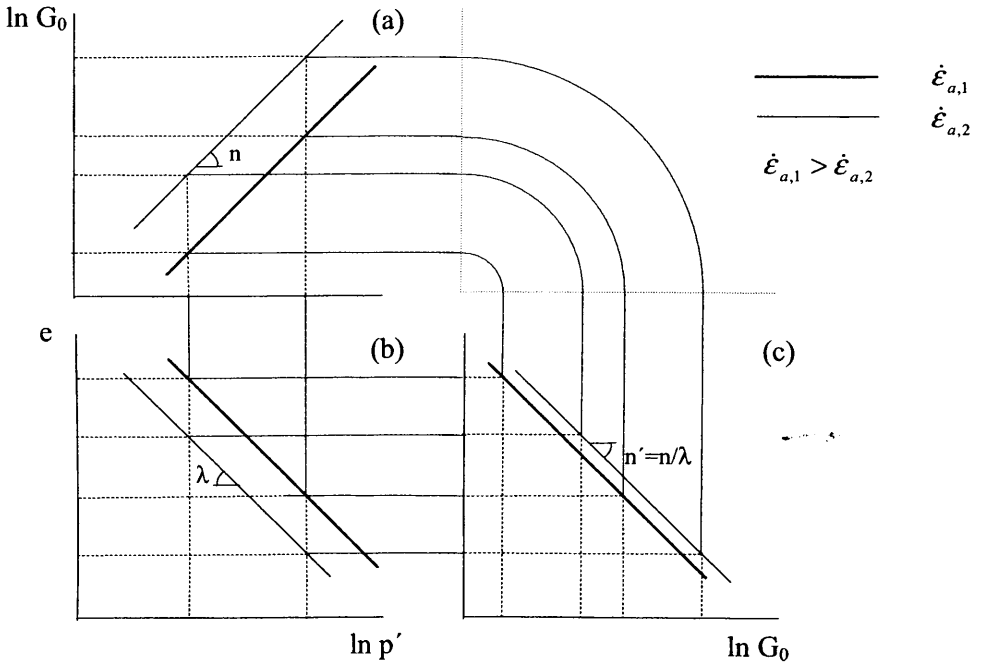

Figure 4-80 Schematic diagram showing the influence of strain rate on the e-ln p', ln G_0-ln p' and e-ln G_0' relationships in isotropic compression found for reconstituted kaolin and reconstituted London Clay

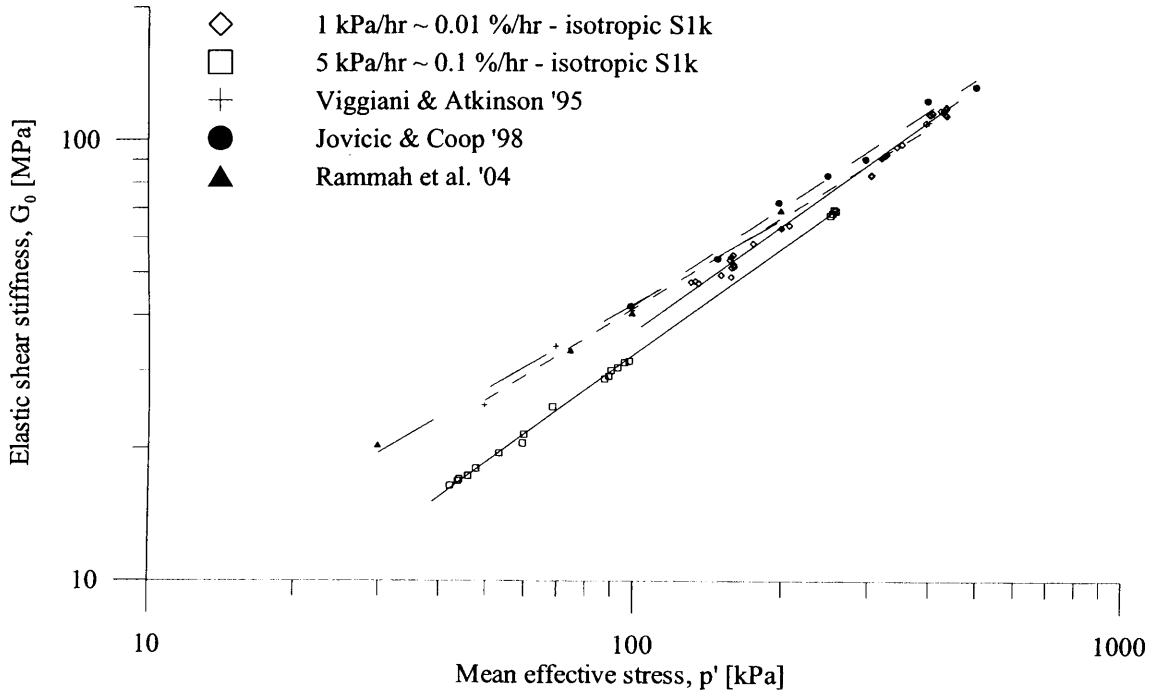

Figure 4-81 Comparison of G_0-p' relationship curves obtained in isotropic compression of reconstituted kaolin with available data from the literature

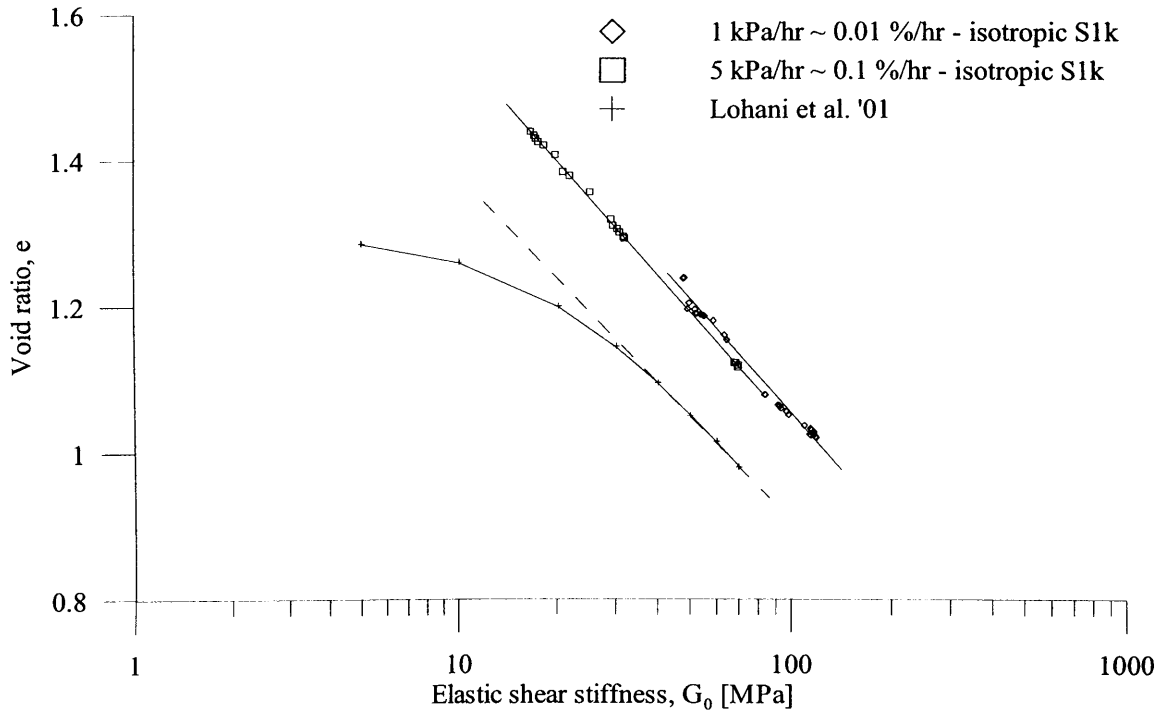

Figure 4-82 Comparison of e-G_0' relationship curves obtained in isotropic compression of reconstituted kaolin with available data from the literature

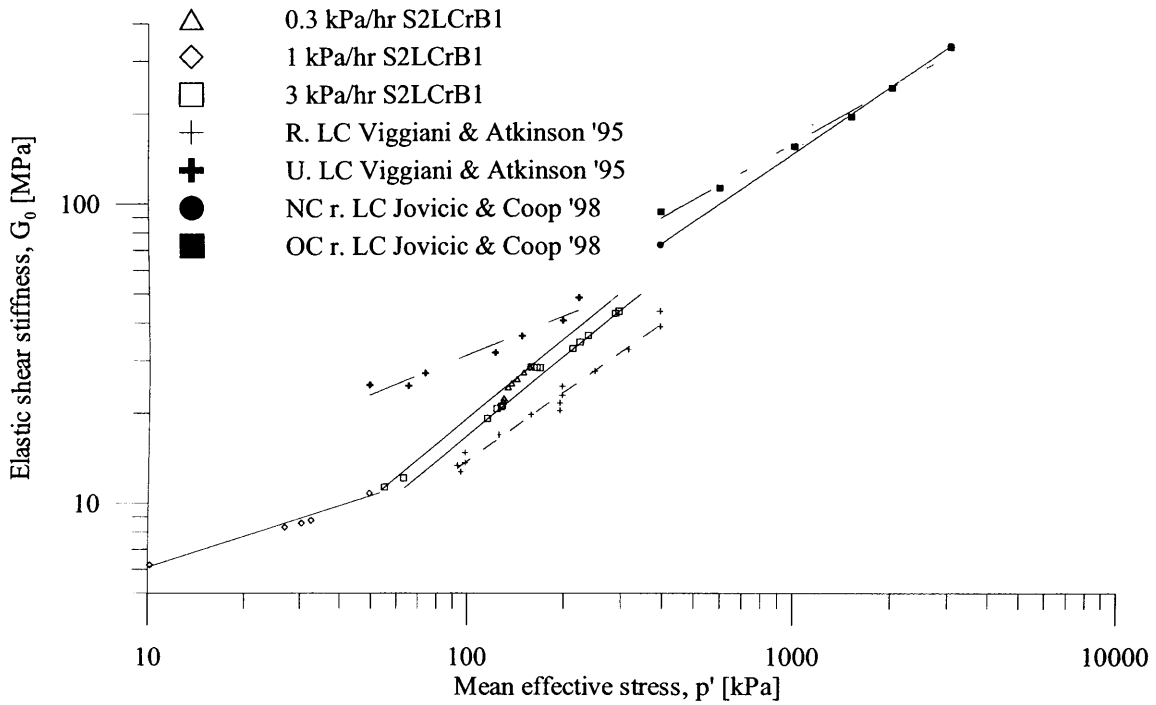

Figure 4-83 Comparison of G_0-p' relationship curves obtained in isotropic compression of reconstituted London Clay with available data from the literature

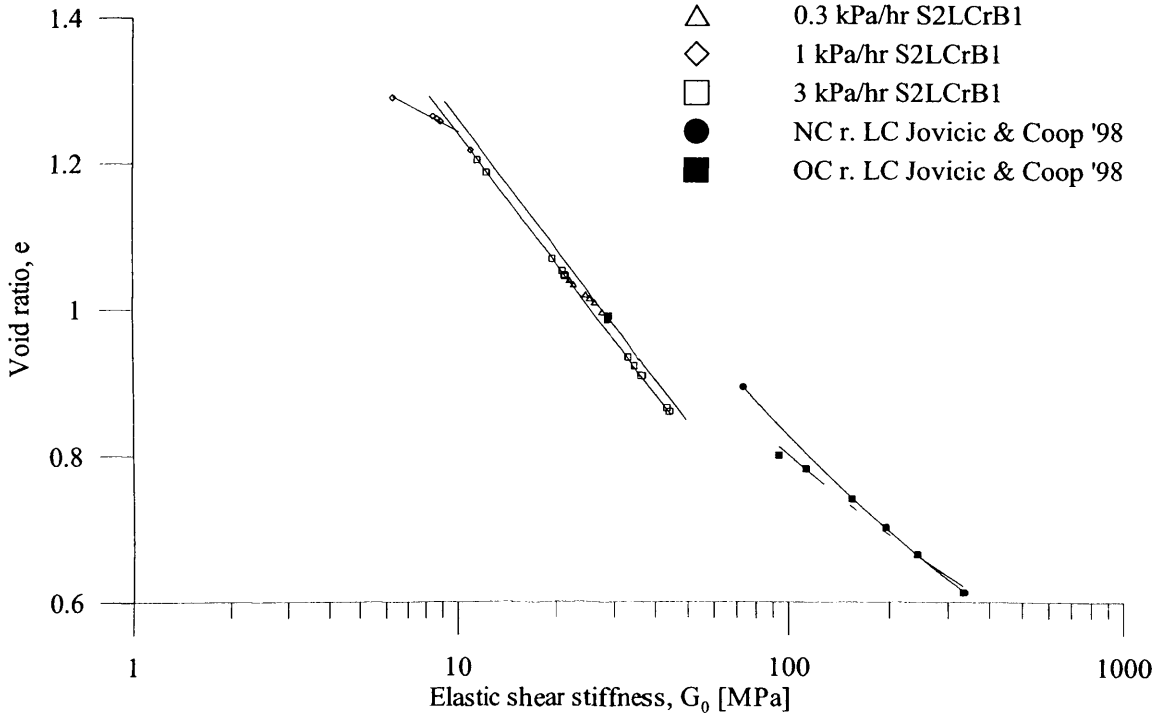

Figure 4-84 Comparison of e-G_0' relationship curves obtained in isotropic compression of reconstituted London Clay with available data from the literature

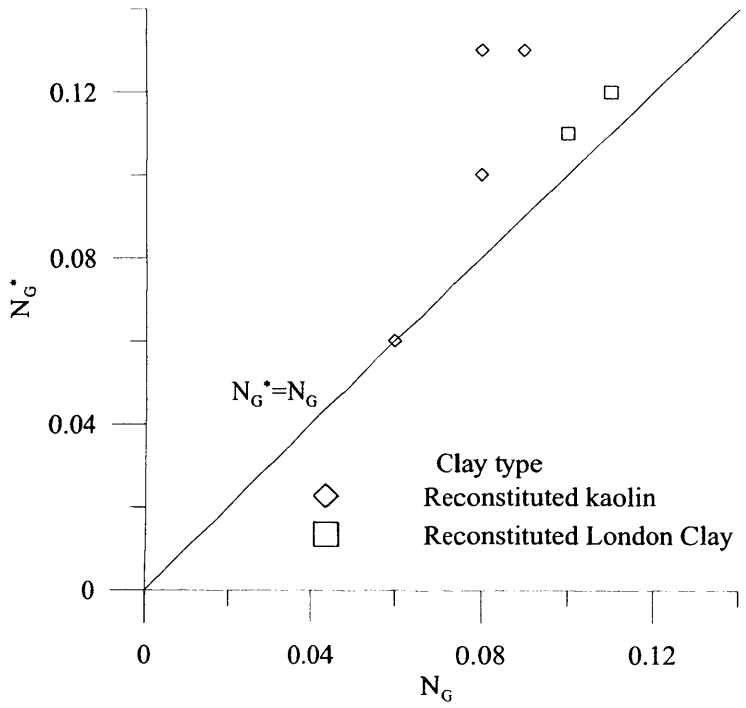

Figure 4-85 Comparison between obtained values of N_G^* and values of N_G from creep stages in isotropic compression of reconstituted London Clay and reconstituted kaolin

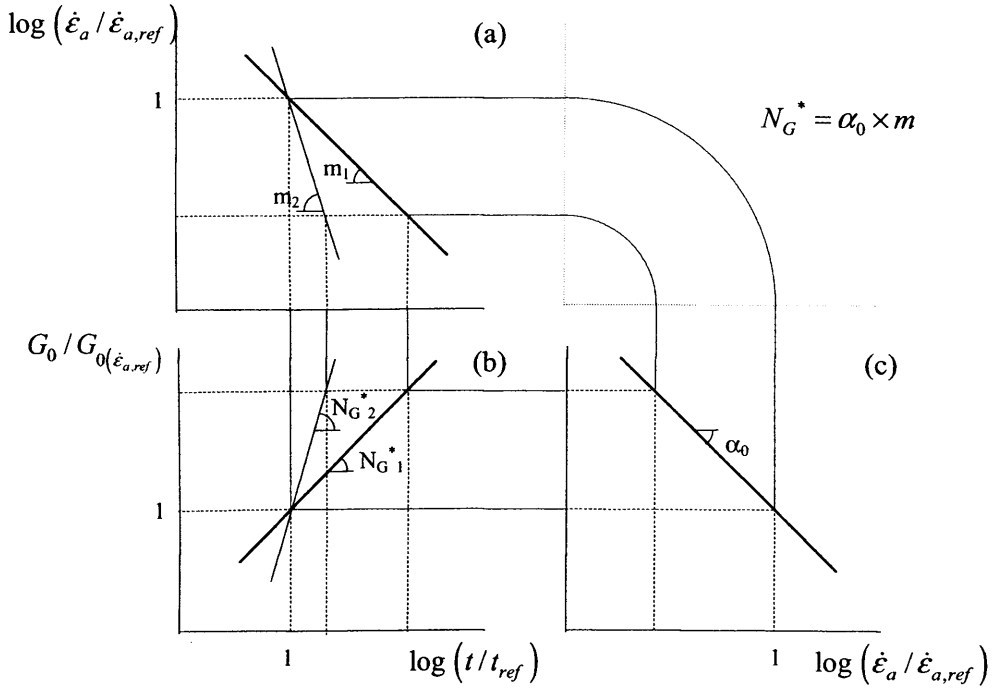

Figure 4-86 Schematic diagram showing the relationship between normalised elastic shear stiffness, normalised strain rate and normalised time during isotropic creep found for reconstituted kaolin and reconstituted London Clay

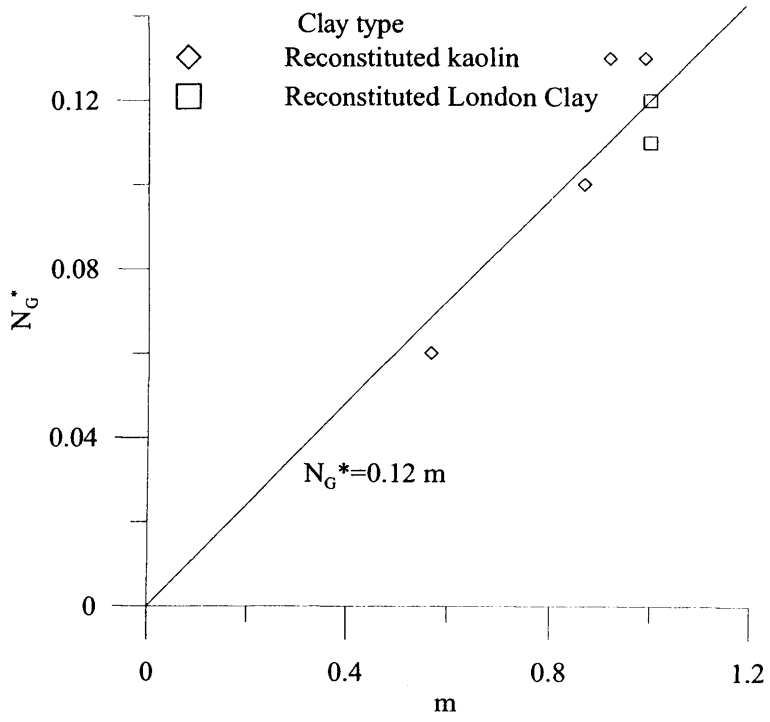

Figure 4-87 Relationship between coefficients N_G^* and m from creep stages in isotropic compression tests on reconstituted London Clay and reconstituted kaolin

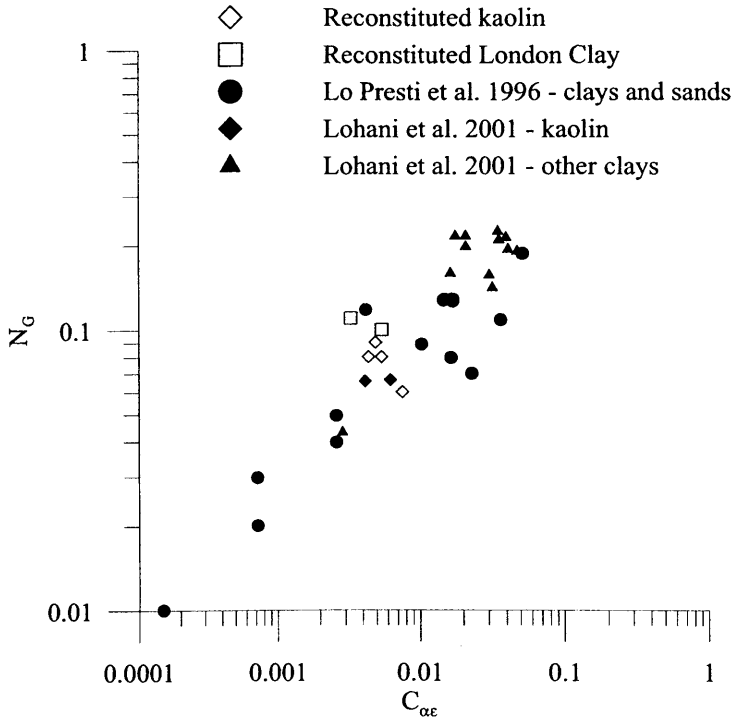

Figure 4-88 Relationship between coefficients N_G and C_α from creep stages in isotropic compression tests on reconstituted London Clay and reconstituted kaolin and comparison with data from literature

CHAPTER 5 VISCOUS BEHAVIOUR OF NORMALLY CONSOLIDATED RECONSTITUTED LONDON CLAY

5.1 INTRODUCTION

This chapter describes part of the experimental research work. The study comprised a series of monotonic isotropically consolidated triaxial compression and extension tests on specimens of normally consolidated reconstituted London Clay, which were carried out to investigate the viscous behaviour of a natural stiff clay in its reconstituted state. Section 5.2 below concentrates on the influence of axial strain rate changes on the isotropic compression behaviour and the general stress-strain shearing behaviour, while Section 5.3 takes a closer look at the influence of strain acceleration on the shear stiffness in the small strain region. The findings are finally discussed and compared to previous research in Section 5.4. Details of the geomaterial, testing equipment, general testing procedures and data analysis were given in Chapter 3.

5.2 INFLUENCE OF STRAIN RATE ON THE BEHAVIOUR OF NORMALLY CONSOLIDATED RECONSTITUTED LONDON CLAY

5.2.1 Purpose and overview of study

A series of triaxial tests was carried out with the main purpose to characterise the influence of step changes in axial strain rate on the triaxial compression behaviour of normally consolidated reconstituted London Clay. As a side study the influence of step-changes in the all-round isotropic stress rate (indirectly axial or volumetric strain rate) on the isotropic compression behaviour was investigated in a few tests. These results were used to complement the findings from the isotropic compression test series described in Section 4.5.3. The presented tests were performed in the period 22nd May 2004 to 9th August 2005 in the geotechnical research laboratory at UCL and details of the conducted triaxial tests have been summarised in Table 5-1 and Table 5-2. In Section 5.2.2 below the test methodology is described and the test results are presented in the following sections.

5.2.2 Special testing procedures

All the tested samples were prepared by reconstitution and preconsolidation ($p'_c \approx 70$ kPa, assuming a K_0 value of 0.64) of the natural London Clay as described in Section 3.4.3b. The samples were tested in Triaxial cell no. 1, which utilised highly accurate miniature LVDTs for local axial and radial strain measurements. Measured B-values and initial void ratios after saturation are given in Table 5-1. The determined degree of saturation was generally found to be close to 1 in all of the tested samples. In the tests, samples were consistently compressed to a mean effective stress of p′=300 kPa before shearing, apart from the test on sample S2LCrA4,

which had to be terminated at a lower stress level due to technical problems. Hence the samples could generally be assumed normally consolidated at the start of shearing. The all-round isotropic stress rate (i.e. rate of change in the confining pressure) was kept constant at a rate of 3 kPa/hr during isotropic compression, except for samples S2LCrA2 and S2LCrA4, which were isotropically compressed with step changes in the stress rate. In the test on sample S2LCrA2 the stress rate was varied between 1 kPa/hr and 3 kPa/hr, while the stress rate was varied by a factor of 10 between 0.03 kPa/hr, 0.3 kPa/hr and 3 kPa/hr in the test on sample S2LCrA4. The control of stress rate rather than strain rate resulted in slight variations in the axial strain rates during stages of otherwise constant stress rate. This however appears not to have affected the result significantly, as seen from the presented results in the following. After isotropic compression to p'=300 kPa, four samples (S1LCrA2-A3 and S2LCrA1-A2) were sheared in triaxial compression with step changes in the axial strain rate. One sample was sheared under undrained conditions (S1LCrA2), while the other samples were sheared nominally drained. In the drained triaxial compression tests the nominal axial strain rate was varied between 0.007 %/hr, 0.015 %/hr and 0.05 %/hr by a factor of up to 7, while in the undrained test the nominal axial strain rates used were significantly higher and varied between 0.05 %/hr, 0.2 %/hr and 0.9 %/hr by a factor of up to 18. The strain rates were chosen to allow full dissipation of pore pressures under drained conditions and full equalisation of pore water pressure under undrained conditions. This assumption has been supported by pore water pressure checks during both isotropic compression and drained shearing, as reported in the following. It should be mentioned that because of the slower strain rates used in the drained tests, these were very time consuming and technical problems occurred in all of the drained tests prior to samples reaching peak strengths. In the single undrained test (S1LCrA2) on the other hand the sample was taken to failure and subsequently experienced stress relaxation for 4 days.

To improve the accuracy of the miniature local LVDT's in Triaxial cell no. 1 further, the zero potentiometers on the amplifiers were on several occasions adjusted to set the transducers at their electrical zero, as described in Section 3.3.2g. This method was generally employed at the start of shearing in all of the tests and for test S2LCrA2 also on several occasions immediately before step increases in strain rate at large strains, where a high stiffness was expected and a higher resolution was desirable.

5.2.3 Effect of step-wise change in stress rate on isotropic compression behaviour

The influence of post-yield step changes in the stress rate during isotropic compression was investigated in Section 4.5.3. The two samples S2LCrB1 and S2LCrB2, which were tested in Triaxial cell no. 2, highlighted the significant influence of stress rate and indirectly strain rate experienced in reconstituted London Clay. Unique linear relationships between void ratio and the logarithm of mean effective stress were found for fixed stress rates post yield, which highlighted the rate dependency of the intrinsic isotropic normal compression line, NCL*. For

different constant stress rates the isotropic NCLs were indicated to lie parallel. However, it was difficult to confirm this trend since only two step changes in the stress rate were made in each of the two tests. The results from the tests on samples S2LCrA2 and S2LCrA4 have been used to complement and confirm the previous findings. In the test on sample S2LCrA2 the stress rate was varied between 1 and 3 kPa/hr in several steps, as shown in Figure 5-1. For the two stress rates unique NCLs are seen, which appear to lie parallel. In the test on sample S2LCrA4 on the other hand the stress rate was changed from 3 kPa/hr to 0.03 kPa/hr in two steps in order to investigate the influence of pore water pressure build-up under high rates of stress. Figure 5-2 shows the obtained compression curve. During testing the drainage valve was closed temporarily at different stages to check the build-up of pore water pressures under different compression rates. The recorded excess pore water pressures against time after closing the valve are shown in Figure 5-3. It should however be noted that the actual build-up of excess pore water pressures in the samples during testing would have been somewhat lower than indicated from the results, since the positive contribution from volumetric creep have not been excluded. The results indicate that excess pore water pressures corresponding to about 8 % of the total stress accumulated during compression at the highest stress rate of 3 kPa/hr, at a mean effective stress of 80 kPa. For the slower stress rate of 0.3 kPa/hr, the recorded excess pore water pressure build-up was about 3 % at p'=91 kPa, but was otherwise found to be insignificant for pressures above p'=96 kPa. From the compression curve in Figure 5-2 it is seen that the gradient of the NCL for the highest rate of stress of 3 kPa/hr appears to be slightly higher than the gradients of the NCLs obtained for the lower stress rates of 0.3 kPa/hr and 0.03 kPa/hr. The reason for this small deviation is likely to be the gradual build-up of excess pore water pressures under the highest rates of compression, which are not recorded and corrected for. Part of the offset between the two NCLs defined by stress rates of 3 kPa/hr and 0.3 kPa/hr is therefore also likely to be due to non-recorded pore water pressures. The compression curves defined by the two slowest stress rates of 0.3 kPa/hr and 0.03 kPa/hr, which are not affected by pore water pressure build-up, are however still seen to show a noticeably offset from each other and are moreover indicated to lie parallel.

The monotonic isotropic compression curves obtained from all the performed tests on reconstituted London Clay have been plotted together in Figure 5-4. These include CRS* and SRS* compression tests performed in both of the UCL Triaxial cells. Generally, good consistency is observed between the individual tests. Obtained values of the compression index, $\lambda=\Delta e/\Delta \ln p'$ for each compression curve in this test series are listed in Table 5-1. λ is found to vary between 0.165 and 0.195 with a mean of 0. 182 (corresponding to $C_c=\Delta e/\Delta \log \sigma'_v$=0.42). If the influence of pore water pressure is considered, as discussed above, the average value of λ may be slightly overestimated. Furthermore the value of λ obtained from constant stress rate NCLs will be somewhat higher than the λ value obtained from a constant strain rate NCL. Table 5-1 also lists the void ratios obtained after isotropic compression to p'=300 kPa. The values of e

at p'=300 kPa ranged between 0.81 and 0.92 with a mean of 0.88. The best-fit normal compression line, which does not consider the effect of strain rate, has been determined from the average value of λ and e at p'=300kPa. By back extrapolation, the void ratio at p'=1 kPa was found to be N_e=1.92, hence the isotropic NCL* for normally consolidated reconstituted London Clay can be formulated as;

$$e = N_e - \lambda \cdot \ln p' = 1.92 - 0.182 \cdot p' \tag{5.1}$$

or

$$v = N - \lambda \cdot \ln p' = 2.92 - 0.182 \cdot \ln p' \tag{5.2}$$

Where v=1+e is the specific volume, and N is the specific volume at p'=1 kPa. The best-fit isotropic NCL* given by Equation (5.1) have been used to normalise the subsequent drained shearing path of the reconstituted samples, as reported in the following. The isotropic NCL* have furthermore been used as a reference line to normalise both drained and undrained shearing paths of intact samples and overconsolidated samples of reconstituted London Clay, which have been reported in Section 6.3.

5.2.4 Effect of step-wise change in strain rate on shearing behaviour

Table 5-2 gives a brief overview of the four performed triaxial compression tests, in which samples were all sheared from an isotropic state at p'=300 kPa, as mentioned above. The tests were carried out with step changes in the axial strain rate to characterise the viscous behaviour of NC reconstituted London Clay; more specifically to investigate the influence of strain rate on the stress-strain shearing path, stress path, volumetric strains in drained tests and accumulation of pore water pressures in undrained conditions. The results from tests on samples S1LCrA2-A3 and S2LCrA1-A2 will be presented in the following. Generally, drained and undrained tests are found to show similar trends. The monotonic behaviour of NC reconstituted London Clay during shearing was found to be typical of that of a NC reconstituted clay. The samples generally bulged, showed strain hardening up to axial strains of about 9% and showed no signs of localisation of strains. Further straining may however have revealed minor strain softening (Gasparre, 2005).

a Effect of step-wise change in strain rate on stress-strain shearing path

Figure 5-5 shows the effect of axial strain rate changes on the drained shearing path for shear strains up to about 1.3% of sample S2LCrA2. In the test the nominal axial strain rate was changed step-wise between three different levels; $\dot{\varepsilon}_a/7, \dot{\varepsilon}_a/3, \dot{\varepsilon}_a$, where $\dot{\varepsilon}_a$ = 0.05 %/hr. The plot generally shows that when the strain rate is increased the sample builds up additional shearing resistance, initially showing a very stiff nearly elastic response. Then the soil gradually yields and follows a path above and similar to the lower strain rate path. If the strain rate is reduced back to the initial rate, the stress-strain paths drops down and appear to follow the original path. Over the tested strain interval the effect of strain rate changes appears to be persistent and unique stress-strain curves can be obtained for different constant axial strain rates, as shown by

the stippled lines. The CRS curves moreover appear to be parallel. This is the characteristics of so called Isotach viscous behaviour, as explained previously in the literature review. Similar isotach behaviour was observed in drained shearing of sample S2LCrA1 for shear strains up to about 0.5%. Contrasting behaviour was however observed in the third drained test on sample S1LCrA3. In this test the sample was taken to slightly higher shear strains of about 1.6%, as seen from the stress-strain curve in Figure 5-7. After step changes in axial strain rate by a factor of 7 at shear strains beyond 1.2% the stress-strain path appears to slightly overshoot or undershoot the extrapolated persistent curve given by the original strain rate. Hence it appears that the effect of strain rate becomes partly temporary at higher strains. During drained triaxial compression of sample S2LCrA2 the drainage valve was closed temporarily at different stages to check the build-up of pore water pressures under different axial strain rates. The recorded excess pore water pressures against time after closing the valve are shown in Figure 5-6. It should however be noted that the actual build-up of excess pore water pressures in the samples during testing would have been somewhat lower than indicated from the results, since the positive contribution from volumetric creep have not been excluded. The results indicate that insignificant excess pore water pressures generally accumulated during shearing. Under the highest applied axial strain rate of 0.05 %/hr the excess pore water pressure increased to about 2 % of the current mean effective stress at a mean effective stress of 327 kPa. The accumulation of excess pore water pressure was found to reduce even further at higher pressures and during shearing at slower rates of axial strain.

The observed behaviour in the three drained tests is confirmed in the undrained test on sample S1LCrA2, in which the sample was taken all the way to failure at an axial strain of about 9 % and subsequently experienced short-term stress relaxation. The stress-strain curve is shown in Figure 5-8 and the extrapolated persistent paths for the highest and lowest strain rates (factor of 18 in difference) are shown with stippled lines. Axial strains have in this case been used instead of shear strains due to errors in the local radial strain measurements. As before at low stress levels the behaviour is seemingly Isotach, then around an axial strain of 1% temporary effects of strain rate changes become noticeable. As the stresses increase and the sample approaches failure the temporary overshooting and undershooting of the persistent paths visibly become more pronounced. Generally, the overshooting or undershooting is seen to decay gradually with increasing strain at a rate which appears to decrease with increasing stress level towards failure. The persistent paths for the highest and lowest strain rates are seen to approach each other towards failure, indicating that the peak strength (=critical state strength) of reconstituted normally consolidated samples of London Clay are independent of the applied axial strain rate. Yet, at failure significant temporary effects of strain rate changes are still observed. In contrast to the persistent effects, Figure 5-9 indicates that the boundary curves for the temporary effects move further apart with increasing stresses towards failure. Another interesting observation can be made from the stress-strain curves in both drained and undrained

tests; generally the extrapolated persistent CRS paths appear to maintain a separation at the origin. In other words, even at the start of shearing at q=0 kPa and at very small strains the effect of strain rate changes is pronounced.

Strain rate changes are not only seen to influence the stress-strain shearing paths, but are also observed to influence the volumetric compression paths during shearing, as shown in Figure 5-10 and Figure 5-11 for the drained shearing of samples S1LCrA3 and S2LCrA2 respectively. At low stresses the effects of strain rate changes appear to be persistent, while temporary effects are indicated at higher stresses for sample S1LCrA3, similarly to what was observed on the stress-strain shearing paths. Additionally, on each plot the normal compression line for the respective test is shown as a reference. As expected, in each test the compression path during shearing is seen to gradually move away from the NCL towards a critical state line (CSL) on the left side of the NCL. It has not been possible to confirm from the drained compression paths whether the CSL is unique or strain rate dependent, since the drained tests were terminated prior to reaching a critical state. The strain rate dependency of the undrained stress path, shown in the following, however does indicate that the critical state line is unique both in stress plane and in general e-p'-q space.

b Effect of step-wise change in strain rate on stress path

Figure 5-12 shows the effect of axial strain rate changes on the undrained stress path in a plot of q against p' for sample S1LCrA2. The plot indicates that the influence of strain rate changes on the stress path is similar to what was observed on the stress-strain path; when the axial strain rate is changed step wise, the stress path jumps between CRS paths for the corresponding strain rates. The immediate response after a step increase in strain rate is seen to very stiff and possibly elastic as indicated by the nearly vertical stress paths. With increasing stress the stress path is seen to yield and gradually approach the persistent stress paths for the given strain rate. At low shear stresses the effect of strain rate changes is seen to be persistent, while at higher shear stresses towards failure temporary overshooting and undershooting of the persistent CRS paths are evident. Similar to what was seen for the stress-strain paths, the extrapolated persistent CRS paths appear not to intersect the initial stress point (p'=300 kPa, q=0 kPa) and the persistent CRS paths are also seen to approach a unique critical state point in terms of stresses. The temporary effects of strain rate changes are in contrast seen to increase with increasing stress level.

After reaching failure the sample experienced stress relaxation for 4 days, during which the deviator stress showed a significant reduction with only minor changes in the axial strain, as was seen from the stress-strain path in Figure 5-8. The stress path during stress relaxation is seen to initially show a reduction in both q and p', which corresponds quite well with the gradient of the stress paths seen immediately after step reductions in strain rate. Then after a while the stress relaxation path shows a marked shift in direction and subsequently appears to follow a nearly vertical stress path with little or no changes in p', similar to the gradient of the

stress path seen immediately after step increases in strain rate. It appears that this change in behaviour can be associated with a change from actual stress relaxation with fixed strain to elastic unloading with minor change in the axial strain. The stress path during elastic unloading will be very steep and be similar to the very stiff and nearly elastic response seen after step increases in axial strain rate. The point, at which the behaviour is seen to change, can be assumed to lie on the lower bound temporary strain rate curve, beyond which further reductions in strain rate have no effects, as illustrated in Figure 5-12.

The normalised stress paths for both drained and undrained tests are plotted in Figure 5-13. The stresses have been normalised with respect to the equivalent pressure, p'_e to remove effects of void ratio changes during drained shearing, where p'_e corresponds to the mean effective stress on the average isotropic NCL* given by Equation (5.1) at the current void ratio of the soil (Hvorslev, 1937). It can be seen from the plot that the normalised drained stress paths correspond quite well, but on the other hand deviate slightly from the undrained stress path. The steeper normalised drained stress paths may to some extent be a result of the possible overestimation of the compression index λ, as discussed above, due to the influence of pore water pressure build-up and because p'_e was derived from the average constant stress rate NCL* rather than a constant strain rate NCL*. It should be noted that the normalised stress paths are still seen to be affected by strain rate, because the normalisation does not consider the effect of strain rate on p'_e. For comparison the intrinsic local boundary surface LBS* and intrinsic critical state line CSL* (ϕ'_{cs}=21°) suggested by (Gasparre, 2005) for reconstituted London Clay (obtained from the T5 site, irrespectively of geological unit) have been indicated on the plot. The critical state angle of shearing resistance is seen to be of similar magnitude to that indicated by the failure state of sample S1LCrA2, however the location of the normalised LBS* and CSL* are different. From the tests on NC reconstituted London Clay it can however generally be deducted that the LBS* is strain rate dependent, while the critical state line in stress plane appears not to be.

c Effect of strain rate on the evolution of volumetric strains and accumulation of pore water pressures

Figure 5-14 shows the evolution of volumetric strain against axial strain in drained shearing of samples S1LCrA3 and S2LCrA1-A2. Volumetric strains have been determined from both the volume gauge measurements and derived from the local strain measurements. For comparison both methods have been plotted in the figure. Generally, the local strain measurements are likely to be more sensitive to small changes in the volume compared to the relative slow response of the volume gauge. However, as mentioned in Section 3.5.3c the accumulated volumetric strains estimated from the local strains will only be accurate at small strains due to barrelling of the sample during shearing. As expected, at intermediate and higher strains the local strains are generally seen to underestimate the volumetric deformation compared to the estimated volume

change from the flow of water out of the sample. The local strain measurements indicate that the volumetric deformation against axial strains is not influenced noticeably by the changes in axial strain rate. Immediately after axial strain rate changes nearly elastic behaviour was generally indicated from the stress-strain paths, which in theory should have translated into a temporary effect on the volumetric response. This however is not observed, as seen from the plot. It is indicated that the axial strain rate changes affect the volumetric strain and axial strain, which is approximately equal to the shear strain, equally, so that no effect of strain rate changes are observed in the plot of ε_v against ε_a. The observed ripples in the volume gauge response, seen for example during shearing of sample S1LCrA3, are believed to have been caused by temperature sensitivity of the volume gauge LVDT. Figure 5-15 on the other hand shows the evolution of pore water pressure against axial strain in undrained shearing of sample S1LCrA2. It can be seen that the evolution of persistent (i.e. after yield) pore water pressure with strain is not influenced by axial strain rate, similar to the volumetric response. However, unlike the volumetric response upon a change in strain rate a temporary overshooting or undershooting of the persistent pore water pressure response is observed, which can be assumed to be due to the initial stiff response of the soil skeleton.

d Effect of step-wise change in strain rate on the intermediate to large strain stiffness

As an example, the degradation of Young's modulus, E_u against axial strain during undrained shearing of sample S1LCrA2 is plotted in Figure 5-16. The stiffness degradation curve reflects the observed stress-strain response and the curve therefore also shows both temporary and persistent effects of strain rate changes. The extrapolated persistent stiffness degradation curves for the highest and lowest strain rates (factor of 18 in difference) are shown with stippled lines. Generally, post yield the stiffness is seen to show a significant temporary increase immediately after every step increase in axial strain rate. With increasing strains the stiffness then rapidly reduces back and appears to drop slightly below the persistent response predicted by the original slower strain rate. After step reductions in the axial strain rate, the opposite behaviour is observed; the stiffness initially shows a high negative value, after which the stiffness rapidly increase to values above the persistent response predicted by the original higher strain rate. Generally at intermediate to high strains the persistent stiffness degradation curve is seen to be affected by strain rate; the stiffness at a given strain is indicated to be slightly but noticeably higher for slower strain rates.

e Quantifying the viscous effects in shearing

It was described in Section 2.3.2c how several different methods of quantifying the viscous effect have been proposed in the literature. A similar but slightly modified method to that proposed by (Di Benedetto et al., 2002) has been used to quantify the effect of strain rate on the stress-strain shearing behaviour. The jump in deviator stress for a given reference deviator stress level has been used to quantify the effect of step changes in the strain rate. The reference stress

level has been obtained from the extrapolated persistent stress-strain curve for the slowest strain rate applied at the initial strain level before the step change in strain rate. As described above, step changes in the strain rate give rise to both temporary and persistent effects on the stress-strain curve for NC reconstituted London Clay at intermediate to high strains. The viscous stress jump at a given reference stress level for a given change in strain rate can therefore suitably be defined using the two following methods; (a) persistent stress jump, from persistent to persistent CRS curve (b) total immediate stress jump (=combined persistent and temporary effect), from persistent to temporary CRS curve. Hence, the difference between (a) and (b) is the temporary effect. The two different methods of quantifying the viscous effect have been defined in Figure 5-17. Using data from undrained shearing of sample S1LCrA2 as an example, the persistent and total immediate stress jump for fixed ratio of axial strain rate change of ±18 times have been plotted in Figure 5-18 against the reference stress level. As was shown from the extrapolated persistent and temporary stress-strain curves in Figure 5-8 and Figure 5-9, the persistent and temporary stress jumps after step changes in strain rate appear to be equal at low stress levels where the behaviour can be characterised as predominantly Isotach. At higher stresses on the other hand, the persistent stress jump gradually reduces with increasing stress level and tends to zero at failure, while the temporary stress jump increases gradually with increasing stress level. Interestingly, the total immediate stress jump in deviator stress is found to be constant with stress level for a given ratio of strain rate change. To investigate the influence of the ratio of strain rate change on the stress jump, the total immediate stress jumps for different ratios of strain rate changes, have been determined from all the tests on reconstituted samples of London Clay and plotted against the reference stress level in Figure 5-19. The stress jump is found to increase consistently with increasing ratios of strain rate change, while for a given ratio of strain rate change the total immediate stress jump appears to be constant with stress level. Moreover, strain rate effects in drained and undrained tests appear to be of similar magnitude. However, it is observed that the results for sample S1LCrA3 for a strain rate ratio of 7 times deviate from the other results. It is not clear why. In Figure 5-20 the average values of the total immediate stress jumps, determined from Figure 5-19, have been plotted against the corresponding ratio of strain rate change. The data suggest that there is a linear relationship between the stress jump and the logarithm of ratio of strain rate change.

The results are further discussed in Section 5.4.1, where the behaviour also will be compared to the observed behaviour in literature.

5.3 INFLUENCE OF STRAIN ACCELERATION ON THE STRESS-STRAIN RESPONSE IN TRIAXIAL COMPRESSION AND EXTENSION TESTS ON NORMALLY CONSOLIDATED RECONSTITUTED LONDON CLAY

5.3.1 Purpose and overview of study

Test results for triaxial compression on reconstituted London Clay shown in Section 5.2, highlighted that strain acceleration, resulting from step-increases in axial strain rate, gives rise to a temporary stiff response in the post yield region. This high stiffness is similar to the high stiffness response usually seen in the pre-yield region at the start of shearing in a standard test. A series of triaxial tests was carried out to investigate the influence of strain acceleration on the subsequent stress-shear strain response in more general terms, where the influence of strain acceleration was examined at various stress states and under different stress paths. The characteristics of strain acceleration were observed in both triaxial compression and extension. The behaviour was investigated at isotropic stress state and during shearing, within the pre-yield region at very small strains and also in the large strain post-yield region. Many of the triaxial tests presented in Section 5.2 above were planned to investigate both the influence of strain rate changes and strain acceleration in order to minimize testing time. Test results may therefore be repeated in the following, but different aspects of the results are concentrated on and the results will be interpreted in a different light. The presented tests were performed in the period 22nd May 2004 to 1st May 2005 in the geotechnical research laboratory at UCL and details of the conducted triaxial tests have been summarised in Table 5-1 to Table 5-5. In Section 5.3.2 below the test methodology is described and the test results are presented in the following sections.

5.3.2 Special testing procedures

All the tested samples were prepared by reconstitution and preconsolidation of the natural London Clay as described in Section 3.4.3b and tested in Triaxial cell no. 1. The test procedures described below are very complex as some samples have been used to investigate several aspects of the viscous behaviour. To aid in the understanding of the performed tests, the general test procedures have been illustrated in Figure 5-21, an overview of the investigation is found in Table 5-3, while details of the testing procedures and test results have been summarised in Table 5-4. Furthermore the performed stress probes have been illustrated in general terms in Table 5-5 along with the associated strain paths.

a Strain acceleration from isotropic stress state in triaxial compression

The testing procedures for samples S1LCrA2-A3 and S2LCrA1-A2 were partially described in Section 5.2.2 above and included isotropic compression to p'=300 kPa and subsequent shearing in triaxial compression with step changes in the axial strain rate. To investigate the influence of shear strain acceleration on the initial stiffness response at very small strains, the initial applied

axial strain rate was varied in each of the four tests in relation to the axial (creep) strain rate remaining after isotropic compression and optional creep period at the final isotropic state. Three different scenarios were investigated: a) acceleration of shear strains: the applied axial strain rate is greater than the axial creep rate remaining after isotropic compression and drained creep $\dot{\varepsilon}_a > \dot{\varepsilon}_{a,creep}$, b) insignificant acceleration of shear strains: the applied axial strain rate is equal to the axial creep rate $\dot{\varepsilon}_a = \dot{\varepsilon}_{a,creep}$ and c) deceleration of shear strains: the applied axial strain rate is lower than the axial creep rate $\dot{\varepsilon}_a < \dot{\varepsilon}_{a,creep}$. Sample S1LCrA2 was left to creep for approximately 3 hrs after isotropic compression to p'=300 kPa before undrained shearing was commenced. At the end of the creep period the axial strain rate had reduced to around 0.012 %/hr and as shearing was initiated with an applied axial strain rate of around 0.05 %/hr the shear strains and axial strains experienced acceleration with a ratio of axial strain rate change (RSRC: $\frac{\dot{\varepsilon}_{a,after}}{\dot{\varepsilon}_{a,before}}$) of about 4. In contrast samples S1LCrA3 and S2LCrA1 were sheared drained immediately after isotropic compression to p'=300 kPa by applying axial strain rates which were chosen to be slower than the axial strain rate imposed during the constant stress rate isotropic compression. In these cases a deceleration of axial strains was achieved. Sample S1LCrA3 was sheared with an applied axial strain rate of 0.012 %/hr, giving an RSRC of about 1/2, while sample S2LCrA1 was sheared with an applied axial strain rate of 0.006 %/hr, giving an RSRC of about 1/10. The last of the four samples (S2LCrA2) was sheared drained after a short creep period at isotropic stress state at an applied axial strain rate of 0.006 %/hr. The applied axial strain rate was chosen to be equal to the axial creep rate remaining after isotropic compression, giving an RSRC of 1 and thereby insignificant acceleration of both axial and shear strains could be assumed at the start of shearing.

To complement the drained triaxial compression tests an additional sample (S2LCrA3) was subjected to a set of complex test paths with short drained stress path probes from different isotropic stress states. Figure 5-22 shows a schematic diagram of the test paths. Sample S2LCrA3 was first isotropically compressed to p'=300 kPa, similarly to the other samples. After one day of creep at isotropic state, the sample was then subjected to two small unload-reload cycles in drained triaxial compression, reaching a maximum amplitude of q=5 kPa (stress probe a). The applied axial strain rates were ±0.006 %/hr, which gave an initial RSRC of about 4, i.e. the strains were accelerated.

It should be emphasised that in a standard triaxial test, the sample is allowed to rest before shearing in order to avoid an influence of creep strains on the initial stiffness response. In this test series, however, as samples were isotropically compressed in normally consolidated state, the shear strain rate was assumed to be negligible at start of shearing and the initial shear stiffness, G′ or G_u, was therefore not assumed to be influenced by the creep strains remaining after isotropic compression, unlike Young's modulus. Young's modulus, on the other hand

could be expected to reduce as a result of axial creep strains; the greater the ratio of axial creep strain rate to applied axial strain rate, the lower the measured Young's modulus would be. In the following sections, where possible, the results are therefore presented in terms of shear stiffness and shear strains.

b Strain acceleration from isotropic stress state in triaxial extension

As illustrated schematically in Figure 5-22 to investigate the influence of shear strain acceleration in extension as well, sample S2LCrA3 was swelled at a constant stress rate of -1 kPa/hr under isotropic stress conditions from the state at the end of probe a to p'=188 kPa at which point the axial strain rate had reduced to about -0.006 %/hr. Then immediately after swelling, with insignificant creep allowed, the sample was subjected to a short stress probe (b) in extension to q=-2 kPa at an initial applied axial strain rate equal to the creep rate remaining after isotropic swelling, giving an RSRC of 1. For comparison an acceleration path was also obtained in extension from isotropic stress state (stress probe c), which was achieved by unloading the sample back to isotropic stress state. Here the sample was left to creep for about 4.5 days and following sheared in extension to q=-8 kPa at an initial applied axial strain rate of -0.008 %/hr. At the end of the creep period the axial creep rate was about -0.0004 %/hr, which resulted in significant strain acceleration with a RSRC of 20. Before unloading back to isotropic stress state (stress probe d) the sample was left to creep for one day. To check repeatability the two stress probes in extension, one with insignificant acceleration of strains and the other with significant acceleration of strains, were repeated after performing a compression-swelling cycle between p'=188 kPa and p'=262 kPa under isotropic stress conditions at a stress rate of ±1 kPa/hr. The two new short stress probes (e and f) had RSRC of 1 and 20 respectively and were both sheared at an initial applied axial strain rate of -0.006 %/hr.

c Strain acceleration at very small to small shear strains

To investigate the influence of strain acceleration in the small strain region, as a result of step changes in strain rate, the axial strain rate was changed in a step-wise manner during stress probe f, in sample S2LCrA3, in both the pre-yield and post-yield region until q=-14 kPa. The axial strain rate was varied between three different rates; -0.01 %/hr, -0.021 %/hr and -0.042 %/hr. Similarly, the influence of strain acceleration was subsequently investigated in the small strain region in triaxial compression after letting the sample rest at isotropic stress state (p'=188 kPa) for 11 days (stress probe g). The axial strain rate was here changed step-wise between; 0.006 %/hr, ±0.015 %/hr and 0.023 %/hr. Stress probes f and g are also shown schematically in Figure 5-22.

d Strain acceleration at large strains

The influence of strain acceleration resulting from step changes in axial strain rate during drained and undrained shearing in the large strain post-yield region was highlighted in triaxial

compression of samples S1LCrA2-A3 and S2LCrA1-A2 (see Section 5.2 above). To supplement these findings, sample S2LCrA2 was additionally used to investigate the influence of strain acceleration after sudden changes in drainage conditions and associated changes in stress path. The test paths are illustrated in Figure 5-23. Sample S2LCrA2 was sheared drained to a stress level of around q=100 kPa at a final axial strain rate of 0.016 %/hr. At this point the drainage valve was closed and shearing subsequently continued at the same rate of axial strain, but now under undrained conditions. This resulted in a change in stress path direction, while maintaining an insignificant acceleration of strains. A short stress probe (a) (Δq=2 kPa) was then performed and the stress path was then brought back to the drained stress path again by opening the drainage valve, thereby allowing the dissipation of excess pore water pressures with further straining. A second stress probe (b) (Δq=4 kPa) was then carried out at q=103 kPa. Again the drainage valve was closed to shift to undrained conditions, but this time the axial strain rate was simultaneously increased to 0.05 %/hr, giving an RSRC of 3. This resulted in a change in stress path direction and an acceleration of strains. A third and final stress probe (c) was conducted after bringing the sample back to the drained stress path and unloading to q=82 kPa by means of stress relaxation. The drainage valve was again closed, at which point the axial strain rate had reduced to around -0.0002 %/hr and the applied strain rate was simultaneously increased to 0.014 %/hr to achieve a significant acceleration of strains.

5.3.3 Effect of strain acceleration from isotropic stress state on shear stiffness

This section reports on obtained results showing the influence of shear strain acceleration on the initial stress-strain response in triaxial compression and extension from an isotropic stress state.

a Strain acceleration from isotropic stress state in triaxial compression

Figure 5-24 compares the initial stress-strain response (in q-ε_s plane) of samples S2LCrA2 and S2LCrA3a in drained triaxial compression after isotropic compression to p'=300 kPa, while Figure 5-25 and Figure 5-26 show the associated variation in rates of axial, radial and shear strain with testing time in the two samples respectively. Sample S2LCrA2 was sheared at an initial average axial strain rate of 0.016 %/hr matching the axial creep rate remaining after the short creep period (2 hrs) at the isotropic stress state; hence the sample experienced an insignificant acceleration of axial strains. As the radial strain rate initially is equal to the axial strain rate and only reduces slowly with further straining, the acceleration of shear strains can be assumed insignificant at start of shearing (Figure 5-25). Sample S2LCrA3a, which had rested for a longer time (1 day) at the isotropic state, was in contrast subjected to an acceleration of shear strains as the applied axial strain rate of 0.006 %/hr was around 4 times greater than the axial and radial creep rate remaining after the creep period. It is seen from the stress-strain curves in Figure 5-24 that if the initial shearing rate is significantly greater than the creep rate, as in a standard test, the initial response is very stiff (S2LCrA3a). A similar stiff response

followed by gradual yielding is also observed when reloading after a short unload path, as strains here again are accelerated. If the initial axial shearing rate, on the other hand, equals the creep rate, then the soil is seen to yield immediately and there is no sign of a high stiffness developing (S2LCrA2). The results will not be affected by the fact that there is a difference between the applied axial strain rates of the two samples, since it is the relative change in strain rate which matters most.

The corresponding (secant) shear stiffness degradation curves for the reload path of sample S2LCrA3a and the initial shear path of sample S2LCrA2 are plotted in Figure 5-27. It is here seen that the maximum shear stiffness at very small strains is in the order of 65 MPa, when experiencing significant acceleration of strains, while the maximum shear stiffness, in marked contrast, was only 18 MPa for sample S2LCrA2, which experienced insignificant acceleration of strains. For comparison, the elastic shear modulus obtained in Section 4.5.5 using bender elements was found to be around 50 MPa at isotropic stress state p'=300 kPa under an applied axial strain rate of 0.006 %/hr. The discrepancy between the values obtained from dynamic and static testing may possibly be explained by slightly inaccurate radial strain measurements on sample S2LCrA3a, something which is also indicated from the unexpected hysteretic behaviour observed during the low amplitude unload-reload cycle at small strains. It is also possible that the elastic shear stiffness determined using bender elements may be somewhat in error due to incorrect interpretation methods, as discussed previously in Section 4.2.2.

Figure 5-28 shows the initial drained stress-strain response of sample S2LCrA1, while the associated variations in rates of axial, radial and shear strain are shown in Figure 5-29. In Figure 5-28 the stippled lines represent the persistent constant rate of strain (CRS) curves for the given axial strain rates. Sample S2LCrA1 was initially subjected to an applied axial strain rate smaller than the axial creep rate remaining after isotropic compression, hence a deceleration of axial strains took place. As a result of the deceleration of axial strains, the stress level is initially seen to reduce. However, unlike the response seen at larger strains, the reduction in stress level is also accompanied by a reduction in the shear strain. This can be explained by the radial creep strain rate, which after isotropic compression will be somewhat higher than the applied axial strain rate and hence give rise to a negative shear strain rate. At large strains in the post yield region, the radial creep strain rate is generally found to be of only minor magnitude and a deceleration of axial strains will therefore result in a corresponding deceleration of the shear strains. As a result the shear strain rate remains positive and the shear strains continue to accumulate, while the stress level temporarily reduces due to the step reduction in strain rate. This is for example seen from the stress-strain curve in Figure 5-28 at around 0.11 % shear strain, when the axial strain rate is reduced from 0.05 %/hr to 0.006 %/hr. In sample S2LCrA1 the initial axial strain rate of 0.006 %/hr was maintained until the response of the sample had stabilised. It is observed that the stress-strain path initially moves downwards to the left and then subsequently reverses and moves upwards to the right. At the point of reversal of the shear

strains, the radial creep strain rate had reduced to a level equal to the applied axial strain rate and the shear strain rate then becomes positive, as shown from Figure 5-29. Since, the deviator stress is controlled by the shear strain and its rate, the point of reversal of shear strains also marks the point at which the deviator stress reverses and starts increasing again. With further straining the radial strain rate gradually reduces towards zero, resulting in a gradual increase in the shear strain rate towards a level of 2/3 of the applied axial strain rate. The shear strain can therefore be expected to have experienced an insignificant acceleration and correspondingly the initial stiffness after reversal is seen to be very low.

The stress paths corresponding to isotropic compression (IC) followed by drained triaxial compression (TC) with either acceleration (RSRC>1, S2LCrA3a), insignificant acceleration (RSRC=1, S2LCrA2) or deceleration (RSRC<1, S2LCrA1) of shear strains are illustrated in Table 5-5. For both acceleration and insignificant acceleration after isotropic compression the drained stress paths sees an anti-clockwise rotation of θ=72 degrees (since $\Delta q/\Delta p'$=3), while for deceleration the stress path temporarily moves downwards. The associated strain paths are also illustrated in Table 5-5, while the actual strain paths have been plotted in Figure 5-30 in ε_s-ε_v plane. The strain path corresponding to an acceleration of shear strains is seen to show a sudden rotation after isotropic compression, while the strain path for insignificant acceleration of shear strains in contrast starts tangential to the volumetric strain axis (i.e. direction of the isotropic compression path) and then experiences a gradual rotation with an increasing ratio of shear strain to volumetric strain. After a deceleration in axial strains, the strain path initially moves downwards and then gradually rotates upwards. After intermediate shear strains (<0.4 %) the gradients of all of the strain paths are seen to approach the same value, which according to theory can be expected to be:

$$\frac{\Delta\varepsilon_s}{\Delta\varepsilon_v}=\frac{\frac{2}{3}(\Delta\varepsilon_a-\Delta\varepsilon_r)}{\Delta\varepsilon_a+2\Delta\varepsilon_r}=\frac{\frac{2}{3}(1+\nu')}{1-2\nu'} \tag{5.3}$$

Where Poisson's ratio, ν' is given as

$$\nu'=-\frac{\Delta\varepsilon_r}{\Delta\varepsilon_a} \tag{5.4}$$

In the drained triaxial compression tests, the radial strain rate quickly reduces to become very small. The gradient of the strain paths is therefore given by, $\frac{\Delta\varepsilon_s}{\Delta\varepsilon_v}=\frac{2}{3}$, corresponding to an angle of rotation of the strain path of θ'=34 degrees from horizontal (anti-clockwise). With further straining the strain path are expected to rotate gradually towards vertical as a critical state with negligible volume change is approached, however the short stress probes were not taken this far.

A single triaxial compression test was performed under undrained conditions on sample S1LCrA2, which was subjected to an initial acceleration of shear strains, with an RSRC of 4. Similar to the behaviour observed in drained triaxial compression of sample S2LCrA3a, the initial acceleration of strains gives rise to a very stiff response in sample S1LCrA2 that can be observed on both the stress-strain response (Figure 5-31) and seen from the near vertical stress path at start of shearing (Figure 5-32).

It is interesting to note that the extrapolated persistent CRS curves in both drained and undrained triaxial compression show clear separation at the origin and do not seem to join a single line. The persistent CRS curves moreover do not show a steep gradient (i.e. high stiffness) at small strains. In fact, for strain rates significantly greater or significantly lower than the creep rate at start of shearing the CRS curves seem not to intersect the origin. Only in the case where the initial strain rate is equal to the creep rate remaining after isotropic compression and the acceleration of strains therefore is insignificant, does the CRS curve intersect the origin, as exemplified by sample S2LCrA2 at an axial strain rate of 0.016 %/hr in Figure 5-24 and Figure 5-5.

b Strain acceleration from isotropic stress state in triaxial extension

In order to investigate the influence of significant acceleration on the initial stress-strain response in triaxial extension from isotropic stress state, it was necessary to swell the tested sample (S2LCrA3) under isotropic stress conditions to achieve a negative axial and radial strain rate. The initial negative axial and radial strain rate made it possible to perform triaxial extension tests without experiencing significant acceleration of axial strains, as the applied axial strain rate and the axial creep rate would in this case both have negative values. Figure 5-33 shows the stress-strain response for stress probes e and f of sample S2LCrA3, while Figure 5-34 and Figure 5-35 show the associated variation in rates of axial, radial and shear strain for the two stress probes respectively. Stress probe e was performed immediately after isotropic swelling to p'=188 kPa (OCR of 1.5) at an applied axial strain rate of -0.006 %/hr matching the axial creep rate obtained after isotropic swelling. Hence, stress probe e was assumed to have experienced insignificant acceleration of strains. Stress probe f on the other hand was performed after 2 days of creep at isotropic stress state (p'=188 kPa, OCR of 1.5) also at an applied axial strain rate of -0.006 %/hr, which however lead to a significant acceleration of strains, with a RSRC of around 20, due to the initial slow creep rate. Similarly to what was observed in triaxial compression, a stiff response is observed when accelerating the shear strains, both at start of shearing but also upon reloading and reversal of the stress path. Moreover, the sample shows a much softer response when experiencing insignificant acceleration of shear strains. Figure 5-34 however indicates that the shear strain rate at start of triaxial extension in stress probe e was not negligible. The soft response for insignificant acceleration of strains may therefore partially be a result of the remaining shear creep strains after isotropic swelling.

The corresponding (secant) shear stiffness degradation curves for stress probe f and the initial shear path of stress probe e are plotted in Figure 5-36. The maximum shear stiffness obtained for the acceleration path in triaxial extension is around 34 MPa, which is about twice the magnitude of the stiffness given when experiencing insignificant acceleration of strain.

The associated strain paths have been plotted in Figure 5-37 in ε_s-ε_v plane and have also been illustrated in general terms in Table 5-5. Similar to what was observed in triaxial compression, the strain path corresponding to an acceleration of shear strains is seen to show a sudden rotation at the start of shearing in extension, while the strain path for insignificant acceleration of shear strains on the other hand initially start tangential to the volumetric strain axis (i.e. direction of the isotropic swelling path) and then experiences a gradual rotation with an increasing ratio of shear strain to volumetric strain. Like in triaxial compression, the radial strain rate is found to be negligible in extension after creep in the small strain region (<0.1 % shear strain), the gradient of the acceleration strain path is therefore close to 2/3, while the gradient of the strain path for insignificant acceleration rapidly approaches 2/3 with further straining. The rotation of the strain path for insignificant acceleration is seen to be significantly faster in extension than what was observed in triaxial compression.

5.3.4 Effect of strain acceleration at very small to small shear strains

This section reports on obtained results showing the influence of strain acceleration on the stress-strain response in the very small strain (<10^{-4} %) to small strain (<0.01 %) region in triaxial compression and extension.

a Strain acceleration at very small to small shear strains in triaxial compression

Figure 5-38 shows the stress-strain path for stress probe g, which was performed in triaxial compression after 11 days of drained creep at isotropic stress state (p'=188 kPa, OCR of 1.5), while Figure 5-40 shows the corresponding (secant) shear stiffness degradation curve. The initial applied rate of axial strain of 0.015 %/hr gave an initial significant acceleration of strains, with an RSRC of around 75. Correspondingly, the initial response is seen to be very stiff, with the maximum shear stiffness at very small strains determined to be in the order of 59 MPa. As expected, due to the difference in stress level and OCR, the maximum stiffness for the acceleration path in triaxial compression at p'=188 kPa is seen to be slightly lower than the stiffness (65 MPa) found previously for the acceleration path in triaxial compression at p′=300 kPa. However, as previously, the obtained maximum shear stiffness from static testing is still seen to be significantly higher than what can be predicted from the bender elements results in Section 4.5.5. To investigate the influence of strain rate changes within the yield surface at very small strains, a short unload-reload cycle was performed between q=2.4 kPa and q=-0.3 kPa, and the axial strain rate was subsequently reduced from 0.015 %/hr to 0.006 %/hr at q=2 kPa (~ε_s=0.0008 %) on the reloading path. From the plot it is observed that the initial performed unload-reload loop shows minor hysteretic behaviour, as a result of the dominant

elastic behaviour at very small strains after the prolonged creep period at isotropic state. Interestingly, the step reduction in axial strain rate (strain deceleration) at q= 2kPa does not appear to affect the stress-strain path. This suggests that it is the relative change in plastic strain rate, which controls the acceleration behaviour, while changes in elastic strain rate are of minor importance. At q=3 kPa a brief (5 min) stress relaxation period with fixed axial strain does not result in a noticeable reduction in stress, which indicate that the behaviour is still predominantly elastic. As the axial strain rate subsequently is increased step-wise back to 0.015 %/hr at the same stress level, there is again little observed affect on the stress-strain response. Soon after however, the stress-strain curve shows signs of yielding at around q=3.5 kPa (ε_s=0.0017 %), yet it is only after further straining to around q=5 kPa (ε_s=0.0027 %) that clear yielding is seen on both the stress-strain curve and the stiffness degradation curve. Another brief (10 min) stress relaxation period at q=7 kPa gives rise to a noticeable reduction in stress level, indicating the presence of plastic strains. As the strain rate is increased again, a temporary stiff response may be observed. The step reduction in strain rate at around q=6 kPa, which is expected to be outside the yield surface, does not result in any reduction in stress level. This is somewhat peculiar.

b Strain acceleration at very small to small shear strains in triaxial extension

Figure 5-39 shows the complete stress-strain path for stress probe f, which was performed in triaxial extension after 2 days of drained creep at isotropic stress state (p'=188 kPa, OCR of 1.5), while Figure 5-40 compares the corresponding (secant) shear stiffness degradation curve with the curve obtained at the same stress level and OCR in triaxial compression. The initial part of the stress-strain path for stress probe f was seen previously in Figure 5-33. As reported in Section 5.3.3b above, the initial applied axial strain rate of -0.006 %/hr (increasing to an average of -0.01 %/hr with further straining) gave an initial significant acceleration of strains, with an RSRC of around 20. As a result the initial response is seen to be reasonably stiff, with the maximum shear stiffness at very small strains determined to be in the order of 34 MPa. If this value is compared to the stiffness determined for the acceleration path in triaxial compression at the same stress level and OCR, it is seen to be significantly lower. This is in contrast to expectations. Since shearing starts from the same isotropic stress state, the sample is not expected to behave softer in extension than in compression. It is therefore possible that the testing conditions and/or testing equipment may have influenced the results. Under the initial shearing rate of -0.01 %/hr, the sample appears to yield at around q=0 kPa (Δq=-2 kPa and ε_s=-0.0019 %), which is at about the same shear strain level as determined in compression. When the sample subsequently is subjected to a step increase in strain rate outside the yield surface, a temporary increase in the gradient of the stress-strain curve (tangent shear stiffness) is observed to a value of similar magnitude to the initial shear stiffness. The secant stiffness will however be relatively insensitive to these changes. Step increases in axial strain rate are seen at q=-2 kPa (ε_s=-0.0050 %) and q=-8.2 kPa (ε_s=-0.0143 %) for changes in axial strain rate from

-0.01 %/hr to -0.021 %/hr and from -0.01 %/hr to -0.042 %/hr respectively. Outside the yield surface, step reductions in axial strain rate are on the other hand seen to result in a temporary reduction in stress level and an apparent shift in the stress-strain curve towards a lower absolute value of the shear stress at a given shear strain. This is in agreement with what has been observed in triaxial compression at large strains.

5.3.5 Effect of strain acceleration at large shear strains

This section reports on obtained results showing the influence of strain acceleration on the stress-strain response in the post-yield region at large strains in triaxial compression. The influence of strain acceleration on the subsequent stress-strain response have been investigated in two situations; firstly, in standard drained or undrained triaxial compression tests where it is assumed that no changes occur in the drainage conditions at the point of strain acceleration, and secondly in the special situation where the point of strain acceleration coincides with a change from drained to undrained triaxial compression. The two situations are reported separately below.

a Strain acceleration at large shear strains with no change in drainage conditions

The influence of strain acceleration at large shear strains in drained and undrained triaxial compression was highlighted in Section 5.2.4 above. In both drained and undrained triaxial compression, significant strain acceleration as a result of a step increase in axial strain rate could generally be seen to be associated with a temporary very stiff response. This behaviour appeared to be independent of strain or stress level, as similar strain acceleration effects were observed at large strains post yield at the start of shearing and at critical state. The influence of strain acceleration on the stress-strain response, also appeared to be unaffected by the drainage conditions, as similar behaviour was observed in drained and undrained triaxial compression. In undrained triaxial compression, the temporary stiff response resulting from strain acceleration was also clearly reflected on the stress path.

In this section the influence of strain acceleration and the ratio of axial strain rate change (RSRC: $\frac{\dot{\varepsilon}_{a,after}}{\dot{\varepsilon}_{a,before}}$) on the subsequent stiffness response at large strains post yield will be investigated in more detail. Figure 5-41 shows the drained stress-strain path for sample S2LCrA2, also shown previously in Figure 5-5 and described in Section 5.2.4a. The sample experienced insignificant acceleration at the start of shearing from the isotropic stress state p'=300 kPa and during the subsequent drained triaxial compression the axial strain rate was changed in a step-wise manner between three different rates. By varying the axial strain rate between 0.007 %/hr, 0.016 %/hr and 0.05 %/hr, RSRCs of 1/3, 1/2, 2, 3 and 7 were obtained. Additionally, at the start of shearing where the sample experienced an insignificant acceleration of strains a RSRC of 1 was achieved. The shear stiffness degradation curves obtained after step changes in strain rate have been plotted in Figure 5-42 for six different values of the RSRC

obtained at different strain levels, as indicated on the stress-strain curve. In this case the stiffness degradation curves are plotted in terms of tangent shear stiffness against the relative shear strain.

The shear stiffness at small strains is found to increase consistently with the value of the RSRC in drained shearing of sample S2LCrA2. It should be noted that in a fully drained tests at any given time post yield the applied axial strain rate can be assumed equal to the axial creep rate (i.e. plastic strain rate) that will initially remain if loading were to suddenly stop, since the elastic strain rate is low post yield and dissipation of excess pore water pressures will be insignificant. The RSRC which is the ratio of applied axial strain rate to the previous axial strain rate therefore also reflects the expected proportion of the applied strain rate immediately after a strain rate change which is due to the axial creep rate. For increasing RSRC the influence of the creep rate reduces. Since the shear stiffness is seen to increase with the value of RSRC this therefore indicates that the measured shear stiffness is influenced by shear creep strains. For the highest value of the RSRC of 7, the small strain shear stiffness reaches a maximum of around 46 MPa, which is slightly lower than the elastic shear stiffness of 50 MPa determined using bender elements in Section 4.5.5 at the isotropic stress state, p'=300 kPa. For lower values of the RSRC (above 1) the small strain stiffness is seen to reduce quite significantly, as a result of the increasing influence of creep strains. Yet, the small strain tangent shear stiffness obtained immediately after strain acceleration is always significantly greater than the stiffness which would otherwise have been obtained if no changes had occurred in the axial strain rate, i.e. a RSRC of 1, both at start of shearing and at large strains.

For values of the RSRC below 1, deceleration of strains occur and as a result of the temporary reduction in stress level the shear stiffness will initially be negative. With further straining however, the stiffness returns to positive values. For both acceleration and deceleration of the shear strains resulting from step changes in strain rate, the shear stiffness is seen to return to the non-accelerated constant rate of strain stiffness response curve at around 0.1 % shear strain. Generally, the stress and strain paths in drained triaxial compression are not affected by strain acceleration, as the paths do not change direction. However, if deceleration of strains occurs then the stress path will temporarily be subjected to a 180 degree turn in direction. Despite, the sudden rotation in stress path after a deceleration of strains, the shear stiffness however do not increase significantly, as has been found in studies of recent stress history (e.g. Atkinson et al., 1990).

b Shear strain acceleration at large shear strains with change in drainage conditions

The influence of strain acceleration has been investigated in the special situation at large shear strains where the point of strain acceleration coincides with a change from drained to undrained triaxial compression. Hence, both the stress path and the strain path are forced to change direction at the point, whether or not a significant acceleration of strain is imposed. Figure 5-43 shows the three undrained stress probes experienced by sample S2LCrA2 along the drained

triaxial compression path commencing from the isotropic stress state p'=300 kPa. The first undrained stress probe (a) was performed with insignificant acceleration of the axial strain (RSRC=1) after loading to q=100 kPa, the second undrained stress probe (b) was then performed with an acceleration of the axial strain (RSRC=3) at q=102 kPa, while the third undrained stress probe (c) was performed with significant acceleration of axial strains (RSRC=infinite) after unloading along the drained triaxial path to q=82 kPa.

Similarly to what has been observed during undrained triaxial compression the undrained stress probes from initial drained triaxial compression show a marked effect of strain acceleration. The acceleration paths for stress probes b and c are observed to be significantly steeper than the stress path for stress probe a, which experienced insignificant acceleration of strains. This behaviour reflects the temporary stiff response of the sample when experiencing strain acceleration, which is associated with a reduction in the pore water pressure increase during undrained shearing. With further straining the initial accelerated paths are expected to yield and join the persistent CRS undrained stress path for the given applied strain rate, as illustrated in Figure 5-21. When the sample in contrast experiences insignificant strain acceleration at the start of the undrained stress probe a, the sample yields immediately and is expected to follow the CRS undrained stress path for the given applied strain rate.

In Figure 5-44 the stress-strain paths for the three undrained stress probes are compared to the uninterrupted drained triaxial compression stress-strain path followed prior to stress probe a, while the corresponding tangent shear stiffness degradation curves are shown in Figure 5-45. The acceleration probes are seen to show significantly higher stiffness than the non-accelerated probe and the drained triaxial compression path. For stress probe c the RSRC was infinitely large because the sample was unloaded prior to loading and the undrained shear stiffness is determined to be very high at around 57 MPa. The stiffness of the other acceleration stress probe (b) is seen to be significantly lower at around 30 MPa, which is likely to be explained by the influence of shear creep strains in the direction of loading. In contrast, the undrained shear stiffness of stress probe a, which did not experience an acceleration of strains, is found to be around 10 MPa, while the stiffness of the uninterrupted drained stress path at large strains is only around 2 MPa. The difference in stiffness between the undrained and drained stress paths without acceleration of strains cannot be explained by the difference in drainage conditions. It is therefore possible that the switch from drained to undrained drainage conditions may have given rise to some disturbance in the applied shear strain rates.

5.4 DISCUSSION

5.4.1 Consistency and reliability of presented results

Generally, consistent and repeatable strain rate dependent behaviour has been observed in isotropic compression and drained and undrained triaxial compression of NC reconstituted London Clay. Effects of strain acceleration behaviour were also observed to be consistent at isotropic stress states, in the very small strain pre-yield region and in the large strain post-yield region in both triaxial compression and triaxial extension. Observed differences in the very small strain shear stiffness in triaxial compression and triaxial extension appear to indicate an influence of the testing equipment rather than the actual response of the soil (see Section 5.3.4b). It is possible that inaccurate radial strain measurements may have caused this, but this cannot be concluded for certain. On the other hand, the apparent influence of the ratio of strain rate change on the measured shear stiffness after strain acceleration in triaxial compression may be explained by the influence of creep strains. This is discussed in Section 5.4.4 below.

Despite the fact that measurements of pore water pressure were not taken continuously during the drained shearing of specimens of reconstituted London Clay, it was assumed that the presented tests were fully drained. Similarly full equalisation of pore water pressures was assumed in undrained shearing. This was based on the findings that during the isotropic tests the pore water pressure only became significant for stress rates greater than 3 kPa/hr, corresponding to axial strain rates greater than approximately 0.1 %/hr. Gasparre (2005) similarly found negligible build-up of excess pore water pressure during isotropic compression at stress rates of 2-3 kPa/hr in tests on undisturbed and reconstituted 38 mm samples of London Clay. Furthermore, as reported in Section 5.2.4a, the check performed during drained shearing of sample S2LCrA2 indicated insignificant build-up of excess pore water pressure (<2 % of the current mean effective stress) under the highest applied rate of axial strain of 0.05 %/hr. The consistent strain rate independent nature of the measured pore water response in undrained tests and volumetric response in drained tests at strain rates varying by up to over one order of magnitude also supports these assumptions.

5.4.2 Comparing the observed monotonic behaviour of NC reconstituted London Clay with observed behaviour in the literature

The monotonic shearing behaviour of NC reconstituted London Clay is typical of that of an isotropically normally consolidated non-structured soft clay; the stress-strain response is ductile, the volumetric response is contractive and the sample generally shows signs of bulging rather than localization of the strains on a shear plane. It is clear from the observed behaviour that the process of reconstitution has removed all of the natural structure that may have been present in the intact natural samples. In Section 6.3.3 the stress-strain behaviour of intact natural samples of London Clay will be described and compared to the behaviour of the reconstituted samples in

order to investigate the influence of natural structure. Since the reconstituted London Clay reflects the inherent properties of the intact material, the monotonic behaviour of reconstituted London Clay, as described above, can therefore be used as suitable reference behaviour for the intact naturally structured samples.

The isotropic compression curves for a given constant strain rate for different reconstituted samples of London Clay were generally found to fall close to each other, defining a single unique intrinsic normal compression line NCL*. An average NCL* was given by Equation (5.2). In the literature several studies have similarly reported on the isotropic compression characteristics of reconstituted London Clay and the two parameters λ and N, which describe the NCL*, are easily obtained. However, a recent study by Gasparre (2005) showed that the NCL* of London Clay is not unique but varies significantly with the depth, depending on the geological unit from which the sample was obtained. The obtained compression parameters found in the literature may for this reason not always compare well with those determined in this study. Nevertheless, for samples obtained from the same site and geological unit ($B_{2(b)}$) as the samples tested in this study, Gasparre (2005) derived values of λ=0.168 (C_c~0.39) and N=2.95 (N_e=1.95) for the NCL* corresponding to a constant strain rate of 2-3 kPa/hr. The value of the compression index, λ is found to match the lower bound values determined in this study (refer to Table 5-1), which supports the suggestion that the average value of λ determined in this study may be slightly overestimated due to the build-up of excess pore water pressure. The value of N determined by Gasparre (2005) places the NCL* significantly higher than that found in this study in terms of void ratio, as shown in Figure 5-46. The reason for this is most likely due to the different methods used to calculate the initial void ratio after saturation. In Figure 5-13 the normalised undrained and drained stress paths were compared to the intrinsic local boundary surface, LBS*, and critical state, CS*, determined by Gasparre (2005). Since the critical state angle of shearing resistance is indicated to be of similar magnitude, the difference in the location of the CS* and LBS* is likely to be due to the differences in the location and gradient of the NCL*, as this will significantly affect the value of the equivalent pressure, p'_e used for normalisation.

5.4.3 General discussion on the influence of strain rate on the behaviour of NC reconstituted London Clay and comparison with observed behaviour in the literature

a Viscous characteristics

The test results obtained in this study show that the viscous behaviour of NC reconstituted London Clay during shearing is comparable to what has been observed in the literature for other NC reconstituted stiff natural clays, however with some differences. Like reconstituted Fukakusa clay (Oka et al., 2003), reconstituted Vallerrica Clay and reconstituted Fujinomori Clay (Tatsuoka et al., 2000) the viscous behaviour of NC reconstituted London Clay can be characterised by Isotach behaviour at low stresses and increasing TESRA behaviour towards

failure. However, at the failure state the viscous behaviour of the reconstituted London Clay samples was seen to be that of pure TESRA with no persistent effects of strain rate changes on either the stress-strain curve or the stress path. This behaviour differs from the behaviour of other reviewed reconstituted stiff natural clays, as none of these appears to have seen a gradual, but complete loss of the persistent viscous effect at peak state as seen for reconstituted London Clay. It is peculiar how NC reconstituted London Clay shows viscous behaviour, which initially at low stresses is similar to the observed Isotach behaviour of soft clays but then, in marked contrast, at high stresses near the failure state the viscous behaviour is of the TESRA type, similar to what is generally seen for clean sands. The reasons for this behaviour are possibly linked to changes in the micro-structure of the soil during shearing as discussed in Section 6.4.5. The conceptual influences of strain rate and strain rate changes on the stress-strain path and stress path of normally consolidated reconstituted London Clay have been illustrated in Figure 5-47 and Figure 5-48 for drained and undrained triaxial compression respectively, while the viscous behaviour normalised for void ratio is illustrated conceptually in Figure 5-49. In this case the normalisation of the stress parameters have been carried out with respect to the equivalent mean effective stress obtained at the current void ratio on the intrinsic isotropic NCL* corresponding to the chosen reference strain rate.

The viscous behaviour of NC reconstituted London Clay was quantified by the total immediate stress jump in deviator stress for a given ratio of strain rate change. In agreement with general observations reported in the literature, for a given stress level the viscous stress jump increases linearly with increase in the logarithm of the ratio of strain rate change. This means that at a given stress level the vertical distance between CRS stress-strain curves for e.g. axial strain rates of 0.5 %/hr and 0.05 %/hr will be of similar magnitude to the vertical distance between CRS curves for axial strain rates of 0.05 %/hr and 0.005 %/hr. However, in this study the total immediate stress jump was found to be more or less constant with stress level during shearing, unlike in other clays reported in the literature, which generally indicate a linear increase in the total immediate stress jump with increasing stress level (see for example results for Fujinomori clay and cement-mixed Chiba gravel in Figures 2-36 and 2-37). It is possible that the observed behaviour in previous reported research is different, because these studies have mainly been on clays and other soils which show predominant Isotach characteristics. In contrast reconstituted London Clay shows combined persistent and temporary effects and the total immediate viscous stress jump is therefore likely to have been affected by this. Interestingly, if the temporary boundary curves in the performed tests on London Clay are considered then the viscous effect, as quantified by the distance between the temporary boundary curves, is seen to increase consistently with stress level.

In Section 6.3 and 6.4.5 in the following chapter, it is attempted to explain the general observed viscous behaviour of soils by considering the influence of both macro- and micro-structure.

b Influence of strain rate on the yield envelopes

Results from the conducted triaxial compression tests on NC reconstituted London Clay indicate that the undrained yield envelope/Local Boundary Surface LBS* increases with an increase in the applied axial strain rate. The rate dependency of the LBS* suggests that the intrinsic state boundary surface (Roscoe-Rendulic surface) SBS* will show similar dependency on the strain rate, as was also indicated by the normalised drained stress paths. It was interesting to note that the extrapolated persistent CRS paths appeared to approach a common stress state at peak strength, while at the start of shearing a separation in both the stress-strain plot and in stress plane was maintained. It is therefore suggested that the yield envelope is significantly affected by the applied strain rate even at very small shear strains. This is consistent with the observed strain rate dependency of the isotropic NCL* (i.e. boundary surface), as it similarly predicts a strain rate dependency of the yield envelope and state boundary surface. From the undrained stress path in Figure 5-12 it can be seen that the offset along the x-axis, i.e. in the p′ direction, between the extrapolated persistent stress paths for the highest and lowest applied rate of strain at start of shearing is of similar magnitude to the predicted increase in yield pressure in isotropic compression had the strain rate been increased by the same amount (e.g. as seen from Figure 5-2). The observed viscous behaviour in shearing can therefore be said to be consistent with the observed viscous behaviour in isotropic compression and this suggests that the strain rate dependency of a single state boundary surface will encompass the viscous behaviour in both isotropic compression and shearing, as has been illustrated conceptually in Figure 5-48 and Figure 5-49. This agrees well with findings by Tavenas et al. (1978). As reported in the literature review in Section 2.3.1c, Tavenas and co-authors likewise found that the general creep behaviour at both isotropic and anisotropic stress states was consistent with a general expansion of the entire yield envelope with increasing strain rates.

c Influence of strain rate on the strength envelopes

The conducted tests suggest that the critical state strength (equal to peak strength) of NC reconstituted London Clay in undrained shearing is independent of the applied axial strain rate (see Figure 5-12). A unique strain rate independent critical state point in terms of e, q and p′ is therefore found, which may suggest that the entire critical state line in *e-q-p′* space is also unique and strain rate independent. Unfortunately it has not been possible to confirm this in drained shearing, as none of the drained triaxial compression tests were taken to failure. Interestingly, the experimental results on reconstituted London Clay show that after reaching a critical state at constant strain rate the soil may deviate from the critical state line if the strain is accelerated as a result of step changes in the strain rate or as a result of creep or stress relaxation periods. However when the rate of strain assumes a relatively constant value again the state will return to the critical state line with further straining, as shown conceptually in Figure 5-47, Figure 5-48 and Figure 5-49.

From the literature it appears that most studies similarly have found the critical state line in stress space to be unique and independent of strain rate. However, very little is reported about the uniqueness in terms of void ratio. If the critical state line is unique and independent of the strain rate then the critical state strength must attain the same value for samples sheared undrained at different rates from the same initial void ratio. In contrast to the findings in this study several studies in the literature report that the critical state strength in undrained shearing is dependent on the axial strain rate (increases with an increase in strain rate), while the critical state angle of shearing resistance is not. The strain rate dependency of the critical state strength is therefore explained by the creep generated pore water pressure at failure which typically is found to reduce with an increase in axial strain rate. These tests hence suggest that the critical state line cannot be unique in e-q-p' space, since for a given void ratio several failure states can be obtained in undrained shearing depending on the applied strain rate. Many of the reported tests (e.g. undrained triaxial compression tests on undisturbed Haney Clay, Vaid & Campanella 1977, refer to Figure 2-35) may have been terminated prior to reaching a true critical state and it is possible that the observed rate dependency of the undrained strength at large strains simply reflects the rate dependency of the state boundary surface rather than a rate dependency of the critical state.

d Strain rate effects at start of shearing

The indications that axial strain rate effects may be significant at the very start of shearing however appear to contradict the general perception of shearing behaviour of clays and other soils in the very small strain range. Numerous recent studies on advanced soil behaviour report on the elasto-plastic behaviour of soils in shearing, which generally can be characterised by perfectly elastic behaviour at very small strains followed by increasingly dominating plastic behaviour with increasing strains towards the failure state. In the elastic region strain rate effects are found to be negligible and for this reason CRS path for significantly different magnitudes of axial strain rate are always shown to pass though the origin, for example as was shown in Figures 2-30 and 2-33 in the literature review. Despite this when the stress dependency of the viscous stress jump in a single test is quantified, most studies usually indicate significant strain rate effects at q=0 kPa, as was seen e.g. in Figure 2-37. The observed discrepancies can be explained by the fact that in general test procedures samples are always allowed to rest before start of shearing to avoid an influence of creep strains. Samples sheared at different nominal axial strain rates will therefore all experience an initial significant increase in the strain rate, as the samples moves from a state of rest to a state of relatively high rate of strain. As shown in this study, the initial response should therefore be very stiff followed by gradual yield towards the persistent path for the given axial strain rate. Hence only after yield can the stress-strain response be assumed to correspond to the persistent response of the soil to the applied strain rate. The initial part of a standard shearing path can therefore not be said to characterise the soil response to a constant rate of axial strain, it is on the contrary a response to a step increase in the

axial strain rate. The conceptual influence of step changes in axial strain rate in the pre-yield and post yield regions at small strains in triaxial compression of NC reconstituted London Clay has been illustrated in Figure 5-50. While the influence of axial strain rate and step changes in axial strain rate on the stiffness response is shown conceptually in Figure 5-51. The observed behaviour at very small strains is discussed further in Sections 5.4.4 and 5.4.5 below in relation to the influence of the initial creep rate and strain acceleration.

5.4.4 General discussion on the influence of initial applied strain rate in relation to the creep rate

a Origin of constant rate of strain (CRS) curves in triaxial compression

One of the interesting findings highlighted from the results in this study, is the indication that only the CRS path corresponding to an axial strain rate equal to the final axial creep rate after isotropic compression (or extension), will intersect the origin. This is illustrated conceptually in Figure 5-52. The results show that if the initial applied axial strain rate $\dot{\varepsilon}_a$ is greater than the axial creep rate $\dot{\varepsilon}_{a,creep}$ remaining after isotropic compression then both the stress-strain path and stress path will show a temporary stiff response as the strains accelerate. This is then followed by gradual yield towards the corresponding CRS paths, which will be located above the origin, as shown in undrained triaxial compression of sample S1LCrA2 in Figure 5-31 and Figure 5-32. Similarly if the initial applied axial strain rate is lower than the axial creep rate at start of shearing then the strains initially decelerate and the sample subsequently stabilises on a CRS path, which fall below the origin (Figure 5-28). It can be hypothesized that CRS paths at different axial strain rates will only have same origin if they all are compressed to the same stress level and start at an applied axial strain rate equal to the axial creep rate remaining after isotropic compression. However, two different CRS path will correspond to two different initial void ratios, because to reach the same stress level in compression at different strain rates the final void ratios will generally be different. If on the other hand samples are compressed to the same void ratio at different strain rates and the applied axial strain rate corresponds to the axial creep rate, then the CRS paths will all start at different pressures.

There is also an uncertainty about the origin of shear strains. For example, usually shearing in triaxial compression from an isotropic stress state can be said to commence as soon as the deviator stress and hence the shear strain starts to increase. Nevertheless, for a sample which initially experiences a deceleration of strains and an associated drop in deviator stress, the shear strain may well be in the intermediate strain region before the deviator stress becomes positive again and triaxial compression starts, as shown in Figure 5-28. The relative difference between the applied strain rate and the initial creep rate has therefore an important influence on the predicted state path of the soil when sheared from isotropic stress state. This is however something, which is generally not considered in constitutive modelling.

b Influence of creep rate on the stiffness response after significant strain acceleration

The drained triaxial compression test on Sample S2LCrA2 highlighted that the maximum shear stiffness determined after a significant strain acceleration event reduced with an increase in the ratio of axial strain rate change, as a result of the influence of plastic creep strains. In the post yield region the applied axial strain rate before an acceleration event will be dominated by the plastic strain rate, while the contribution from the elastic strain rate will be minor. This is indicated from the results, which show that at shear strains above 0.1 % the steady state constant rate of strain shear stiffness was less than 2 % of the elastic shear stiffness. Therefore, as shearing generally was performed fully drained, the axial creep rate at any point during shearing can be assumed to correspond to the steady state axial strain rate, whether this is an applied axial strain rate or an actual axial creep rate after a period of rest. In order to investigate if the response after strain acceleration events is truly elastic, the measured maximum shear stiffness $G'_0{}^{total-after}$ for different ratios of strain rate change will be corrected for creep strains, as outlined in the following. For a unit change in stress the assumed elastic shear stiffness $G'_0{}^{elastic-after}$ after the strain acceleration event can be related to $G'_0{}^{total-after}$ as given by the following relationship:

$$\frac{G'_0{}^{elastic-after}}{G'_0{}^{total-after}} = \left(\frac{\Delta\varepsilon_s{}^{total-after}}{\Delta\varepsilon_s{}^{elastic-after}} \right) \quad \Rightarrow \quad G'_0{}^{elastic-after} = G'_0{}^{total-after} \left(\frac{\Delta\varepsilon_s{}^{total-after}}{\Delta\varepsilon_s{}^{elastic-after}} \right) \tag{5.5}$$

Where for a unit change in stress and time, the relative increase in the total strain $\Delta\varepsilon_s{}^{total-after}$ after the acceleration event can be derived from the ratio of shear strain rate change RSRC (assumed equal to the ratio of axial strain rate change) and the relative increase in total strain $\Delta\varepsilon_s{}^{total-before}$ before the acceleration event, as follows;

$$RSRC = \frac{\dot{\varepsilon}_s{}^{total-after}}{\dot{\varepsilon}_s{}^{total-before}} = \frac{\Delta\varepsilon_s{}^{total-after}}{\Delta\varepsilon_s{}^{total-before}} \quad \Rightarrow \quad \Delta\varepsilon_s{}^{total-after} = RSRC \cdot \Delta\varepsilon_s{}^{total-before} \tag{5.6}$$

While the relative increase in elastic strain $\Delta\varepsilon_s{}^{elastic-after}$ after the acceleration event is given by

$$\Delta\varepsilon_s{}^{elastic-after} = \Delta\varepsilon_s{}^{total-after} - \Delta\varepsilon_s{}^{plastic-after} \tag{5.7}$$

The relative increase in the plastic strain (per unit change in stress) immediately before and after the acceleration event can be considered to be equal, assuming that the plastic straining is initially unaffected by the strain acceleration event. Hence $\Delta\varepsilon_s{}^{plastic-after}$ can suitably be derived from the values of total shear stiffness $G'_0{}^{total-before}$ and elastic shear stiffness $G'_0{}^{elastic-before}$ before the event:

$$\begin{aligned} &\Delta\varepsilon_s{}^{plastic-after} = \Delta\varepsilon_s{}^{plastic-before} = \Delta\varepsilon_s{}^{total-before} - \Delta\varepsilon_s{}^{elastic-before} \quad \Rightarrow \\ &\Delta\varepsilon_s{}^{plastic-after} = \Delta\varepsilon_s{}^{total-before} - \frac{G'_0{}^{total-before}}{G'_0{}^{elastic-before}} \Delta\varepsilon_s{}^{total-before} \end{aligned} \tag{5.8}$$

By substituting Equations (5.7), (5.6) and (5.8) into Equation (5.5), the elastic shear stiffness after the acceleration event is given by:

$$G'^{\,elastic-after}_{0} = G'^{\,total-after}_{0}\left(\frac{RSRC}{RSRC-1+\frac{G'^{\,total-before}_{0}}{G'^{\,elastic-before}_{0}}}\right) \tag{5.9}$$

If the behaviour before the acceleration event is considered to be dominated by plastic strains, i.e. $G'^{\,total-before}_{0} << G'^{\,elastic-before}_{0}$, as would generally be the case in the post yield region equation (5.9) reduces to

$$G'^{\,elastic-after}_{0} = G'^{\,total-after}_{0}\left(\frac{RSRC}{RSRC-1}\right) \tag{5.10}$$

It can be assumed that the ratio of change in axial strain rate is approximately equal to the ratio of change in the shear strain rate. Therefore the measured maximum shear stiffness $G'^{\,total-after}_{0}$ after the acceleration event can be corrected by the value of the ratio of axial strain rate change RSRC to obtain a value of the shear stiffness, which reflects the elastic response after the acceleration event. The measured maximum shear stiffness for RSRC of 1, 2, 3 and 7 in triaxial compression of sample S2LCrA2 have been obtained from Figure 5-42 and plotted against the RSRC in Figure 5-53. A consistent increase in shear stiffness with an increase in RSRC is observed. With increasing RSRC, the influence of creep strains reduce and at high RSRC the shear stiffness is expected to approach a constant plateau, corresponding to the elastic shear stiffness. The measured shear stiffness has been corrected for creep strains according to equation (5.10) and is plotted in the same figure. (note that is not possible to correct the shear stiffness for a RSRC of 1). The correct shear stiffness seems to be independent of RSRC and strain levels, and forms an upper-bound value for the measured stiffness. The corrected shear stiffness is approximately 55 MPa, which compares well with the elastic shear stiffness of 50 MPa determined in Section 4.5.5 from bender element tests at isotropic stress state p'=300 kPa under an applied axial strain rate of 0.006 %/hr. Hence it is suggested that the acceleration of strains at large shear strains in the post yield region in triaxial compression give rise to an elastic response of the soil similarly to the elastic response seen at very small strains at the start of shearing.

Values of the measured maximum shear stiffness obtained from all the performed tests after acceleration events at isotropic stress state, at very small strains in the pre-yield region and at large strains in the post-yield region in both triaxial compression and extension have been tabulated in Table 5-4. Where possible these values have been corrected for creep strains and the corrected values of shear stiffness have been tabulated in Table 5-6 and plotted in Figure 5-54 against the level of mean effective stress. On the same plot the relationship between the elastic shear stiffness and mean effective stress is plotted, as determined in Section 4.5.5 from bender element tests during isotropic compression of reconstituted London Clay. The static values of shear stiffness corrected for creep strains are seen to show a large scatter but are otherwise found to compare reasonably well with the elastic shear stiffness determined from

dynamic testing. It is therefore suggested that strain acceleration will result in an elastic response of the soil which is not influenced by strain level, stress state nor stress (or strain) history. The elastic response may however be masked by the influence of creep strains, as highlighted from this study.

5.4.5 General discussion on the influence of strain acceleration on stiffness

a Influence of strain acceleration and recent stress and strain histories on stiffness response

A more detailed look at the results reveals some interesting findings with respect to the influence (or lack thereof) of recent stress history, strain history and direction of loading on the acceleration behaviour. The performed tests reveal that, in contrast to predictions from the concept of recent stress history (e.g. Atkinson et al., 1990), it is possible to have a significant rotation of both the stress path and the strain path without observing an associated increase in the shear stiffness, and vice versa; it is also possible to observe a significant increase in the shear stiffness without having an associated significant rotation of the stress path or strain path. A significant rotation of the stress path and/or the strain path without an associated increase in the shear stiffness was observed in the following cases: a) when changing to drained triaxial compression after isotropic compression and drained triaxial extension after isotropic swelling, with insignificant acceleration of shear strains at the point of stress path rotation (Section 5.3.3) b) whenever significant deceleration of the shear strains took place during drained or undrained triaxial compression, which resulted in a 180 degree reversal of the stress path (Section 5.3.5a) c) when changing from drained triaxial compression to undrained triaxial compression with insignificant acceleration of shear strains at the point of strain path rotation (Section 5.3.5b). On the other hand a significant increase in the shear stiffness without an associated rotation of the stress path or the strain path could be observed when accelerating the shear strains during drained and undrained triaxial compression.

The findings in this study generally suggest that a temporary elastic stiffness response only occurs if the sample experiences a temporary significant acceleration of shear strains, as illustrated in Figure 5-51. Therefore, if insignificant acceleration takes place, independently of stress history, strain history and loading direction, a high stiffness response will not be observed as the sample continues to yield. Instead the stiffness remains on the persistent CRS stiffness degradation curve, which is located significantly lower than the elastic shear stiffness and can be characterised by a gradual reduction in stiffness with straining towards the failure state and a noticeable reduction in stiffness at a given strain level with increases in the applied axial strain rate. For gradual changes in strain rate in the post-yield region, such as during constant stress rate shearing, the acceleration of strains can be assumed to be insignificant and the development of an elastic zone is therefore not seen. The study has furthermore indicated that the influence of strain acceleration is not only applicable to shearing behaviour, as acceleration of the volumetric

strains is found to have a comparable influence on the compression behaviour in isotropic compression or one-dimensional compression.

b Proposal of modified concept of kinematic yield surfaces

Based on the above discussion it is advanced that to model the behaviour of clays in a more accurate and general way the concept of kinematic yield surfaces, as suggested by Jardine (1992), should include strain rate dependency, with the size of the yield surfaces being dependent on the applied (plastic) strain rate and strain acceleration. In the concept of kinematic yield surface proposed by Jardine (1992), the stiff response observed after a rest period is generally modelled by imagining that the yield surfaces re-centre around the current stress point after creep. This way of modelling the behaviour will only be accurate if the applied strain rate after the rest period is significant greater than the creep rate. If on the other hand the applied strain rate is equal to the creep rate or significantly lower than the creep rate remaining after the rest period, then the concept cannot model the behaviour highlighted above. Instead, by considering strain rate dependent yield surfaces, then post-yield the engaged yield surfaces will shrink in size during a resting period as the (plastic) strain rate gradually reduces. If shearing continues at the current creep rate the sample will remain on the engaged yield surfaces, and the behaviour will be dominantly plastic as it was during shearing before the creep period at the original higher strain rate. On the other hand if shearing is resumed to a strain rate higher than the creep rate the yield surfaces will expand. As a result the current state point moves inside the previously engaged yield surfaces and a temporary elastic response will be seen with further straining. If the applied strain rate is lower than the creep rate, the yield surfaces will shrink in size and the stress will reduce until the corresponding smaller yield surface is reached. The modified concept of kinematic yield surfaces has been discussed further in Section in 7.1.2 in relation to the formulation of a similar concept for implementation into the advanced constitutive "BRICK" model (Simpson, 1992).

c Influence of strain acceleration on the elastic shear stiffness determined from shear wave propagation in bender element testing

The influence of strain rate and strain acceleration on the behaviour of reconstituted London Clay can be used to explain the observed global strain rate dependency of the elastic shear modulus determined from shear wave propagation in Chapter 4. The transmitted shear wave from the bender element propagates the sample in the vertical direction, but subjects the sample to rapid cyclic strains in the horizontal direction. As a result the radial strains are accelerated and the sample therefore responds almost perfectly elastically to the transmitted shear wave. This means that the shear wave travels at a speed, which is governed by the elastic properties of the soil structure, even if the sample is already yielding due to the action of global straining (i.e. straining due to the application of force to the sample boundaries). It is hypothesized that the observed reduction in the determined shear stiffness with increasing rate of global axial strain

can be explained by considering the strain rate dependency of the yield surfaces. When the global strain rate is increased during isotropic compression or shearing, the sample can be said to become more unstable, as the current state engages yield surfaces determined by higher strain rates. Hence, when the transmitted shear wave subjects the sample to rapid cyclic shear strains, even if these are not in the same direction as the predominant direction of global movement, the sample can be expected to respond slightly softer under higher global strain rates.

d The general representation of stiffness degradation

The non-linear behaviour of soils in shearing is widely accepted and the shear stiffness degradation with shear strain is commonly represented by an S-shaped curve with high stiffness at small strains, which rapidly degrade to a low stiffness near failure. The general representation of stiffness degradation, as illustrated in Figure 2-1, is based on the assumption that the soil is sheared at a constant stress or strain rate, without experiencing any significant acceleration of strains. Moreover, it is general practice to let the sample rest before shearing in order to minimize the influence of creep strains on the initial stiffness measurement (Clayton & Heymann, 2001). However, clearly these procedures contradict each other because it is not practically possible to avoid a significant acceleration in strains at the beginning of shearing, when the sample moves from a state of rest to a state of relatively high rate of movement. The findings in this study suggests that the well-known standard S-shaped stiffness degradation curve, which is commonly used in routine design, is not an inherent feature of the soil since it only represents the specific situation, where the soil experiences an initial significant acceleration of strains, which is not necessarily associated with a rotation of the stress path. In support of this Clayton (2004) noted that it is peculiar how different soils (such soft clays, stiff clays and granular soils, which have values of the very small strain stiffness several magnitudes apart), all show similar stiffness degradation curves. This strongly suggests that the very small strain stiffness is controlled by the structure of soil, while the degradation of stiffness with shear strains is predominantly not. As suggested above, it can be hypothesized that the initial elastic stiffness response (linear or not) observed in most standard triaxial tests on non-cemented clays is a result of strain acceleration only, while the subsequent degradation of stiffness is governed by the transition from a state of acceleration to a steady state with constant rate of straining.

5.5 TABLES AND FIGURES FOR CHAPTER 5

Table 5-1 Overview of isotropic compression tests on reconstituted London Clay

Sample no.	Type	Nominal stress rates [kPa/hr]	*B*-value after saturation	Void ratio, *e*		Compression index, λ ($=\Delta e/\Delta \ln p'$)
				After Saturation[$]	After compression to p'=300 kPa	
S1LCrA2	CRS*	3.0	0.984	1.29	0.89[#]	0.174
S1LCrA3	CRS*	3.0	0.999	1.29	0.88[#]	0.174
S1LCrA4	CRS*	3.0	0.996	1.28	0.89[#]	0.187
S2LCrA1	CRS*	3.0	0.994	1.32	0.88[#]	0.191
S2LCrA3	CRS*	3.0	0.993	1.32	0.81[$]	0.174-0.195
S2LCrA2	SRS*	1.0, 3.0	0.993	1.35	0.92[#]	0.191
S2LCrA4	SRS*	0.03, 0.3, 3.0	1.000	1.29	-	0.169-0.187
Average				1.31	0.88	0.182

[$] based on initial dimensions and volumetric deformation calculated from local strain measurements
[#] based on initial dimensions and volumetric deformation calculated from volume gauge measurements

Table 5-2 Overview of absolute nominal axial strain rates used in SRS triaxial compression and extension tests on reconstituted London Clay

Sample no.	Type	Nominal axial strain rates[#] $\dot{\varepsilon}_a$ = 0.05 %/hr
S1LCrA2	CiU	$\dot{\varepsilon}_a$,4$\dot{\varepsilon}_a$,18$\dot{\varepsilon}_a$
S1LCrA3	CiD	$\dot{\varepsilon}_a$/7,$\dot{\varepsilon}_a$
S2LCrA1	CiD	$\dot{\varepsilon}_a$/7,$\dot{\varepsilon}_a$
S2LCrA2	CiD	$\dot{\varepsilon}_a$/7,$\dot{\varepsilon}_a$/3,$\dot{\varepsilon}_a$
S2LCrA3	CiD	$\dot{\varepsilon}_a$/7,$\dot{\varepsilon}_a$/3,$\dot{\varepsilon}_a$

[#] actual applied axial strain rates may vary from the given nominal values

Table 5-3 Overview of strain acceleration procedures in triaxial testing of reconstituted London Clay

	Approach path:																				
	d. IC						d. IS			d. TC						u.d. TC			d. TE		
	Outgoing path:																				
Sample:	d. TC			u.d. TC			d. TE			d. TC			u.d. TC			u.d. TC			d. TE		
S1LC				A												A	N	D			
S2LC	A									A	N	D									
S2LCrA5				A												A	N	D			
S1LCrA2				A												A	N	D			
S1LCrA3			D							A	N	D									
S2LCrA1			D							A	N	D									
S2LCrA2		N								A	N	D	A	N							
S2LCrA3	A						A	N		A	N	D							A		D

d.: drained, u.d.: undrained, A: acceleration (step increase in axial strain rate), N: no acceleration (no change in axial strain rate), D: deceleration (step reduction in axial strain rate), IC: isotropic compression, IS: isotropic swelling, TC: triaxial compression, TE: triaxial extension

Table 5-4 Influence of strain acceleration on shear stiffness at very small strains in triaxial testing of reconstituted London Clay

Sample no.	AP	OP	AA θ (θ′) [deg]	iSR 10^{-3} [%/hr]	aSR 10^{-3} [%/hr]	RSRC [-]	p′ [kPa]	q [kPa]	ε_0 10^{-4} [%]	G'_0 $G_{u,0}$ [MPa]
S1LCrA2	IC	uTC	90 (90)	12	50	4	301	3	-	-
S1LCrA3	IC	TC	72 (29)	31	12	1/2	301	2	-	-
S2LCrA1	IC	TC	72 (31)	60	6	1/10	301	2	-	~12
S2LCrA2	IC	TC	72 (~0)	"12"	16	~1	300	-1	2	18
S2LCrA2	TC	TC	0 (0)	8	16	2	309	27	3	23
S2LCrA2	TC	TC	0 (0)	16	50	3	310	30	5	37
S2LCrA2	TC	TC	"180" (0)	50	16	1/3	314	42	(14) 1060	(-28) 3
S2LCrA2	TC	TC	"180" (0)	16	8	1/2	317	52	(12) 746	(-22) 4
S2LCrA2	TC	TC	0 (0)	7	50	7	319	57	9	46
S2LCrA2	TC	TC	"180" (0)	50	16	1/3	327	81	(13) 792	(-26) 2
S2LCrA2 a	TC	uTC	54 (52)	16	16	1	333	101	10	10
S2LCrA2 b	TC	uTC	29 (52)	16	50	3	333	104	5	30
S2LCrA2 c	TE	uTC	207 (232)	"-2"	14	∞	327	83	2	57
S2LCrA3 a	IC	TC	72 (32)	"1.5"	6	4	300	1	10	32
S2LCrA3 a	TE	TC	180 (139)	-6	6	∞	299	-2	6	65
S2LCrA3 b	IS	TE	72 (~0)	-6	-6	1	188	1	4	13
S2LCrA3 b	TE	TC	180 (180)	-6	6	∞	187	-2	2	29
S2LCrA3 c	TC	TE	180 (180)	"-0.4"	-8	~20	188	0	3	28
S2LCrA3 d	TE	TC	180 (180)	"-0.6"	8	∞	185	-8	2	32
S2LCrA3 e	IS	TE	72 (~0)	-6	-6	1	188	1	7	17
S2LCrA3 e	TE	TC	180 (180)	-6	6	∞	186	-5	3	27
S2LCrA3 f	TC	TE	180 (180)	"-0.3"	-6	20	187	2	5	34
S2LCrA3 g	TC	TC	0 (0)	"0.2"	15	75	188	0	5	59

AP: Approach stress path, OP: Outgoing stress path, IC: isotropic compression, IS: isotropic swelling, TC: triaxial compression, TE: triaxial extension, u: undrained (otherwise drained), AA: Approach angle (θ: angle between approach stress path and outgoing stress path, θ′: angle between approach strain path and outgoing strain path, anti-clockwise rotation), iSR: initial (axial) "creep"/strain rate, aSR: applied (axial) strain rate, RSRC: Ratio of strain rate change (RSRC=iSR/aSR), G'_0 and $G'_{u,0}$: first reliable maximum shear modulus (drained and undrained respectively) measured at the shear strain level, ε_0.

Table 5-5 Schematic illustration of performed stress and strain paths

AP	OP	RSRC	Stress path (q-p′ plane)	AA θ [deg]	Strain path (ε_s-ε_v plane)	AA θ′ [deg]
TC	TC	≥1		0		0
TE	TE	≥1		0		0
TC	TC	<1		"180"		0
TE	TE	<1		"180"		0
TC	TE	∞		180		≈180
TE	TC	∞		180		≈180
IC	TC	<1	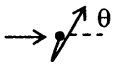	72	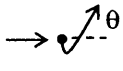	<90 (~34)
IC	TC	1 >1	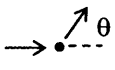	72	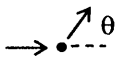	0 <90 (~34)
IS	TE	1 >1	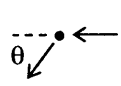	72	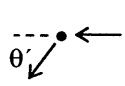	0 <90 (~34)
IC	uTC	>1	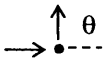	90	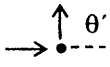	90
TC	uTC	≥1		<108		<56 (~56)
TE	uTC	>1		<288		<236 (~236)
uTC	uTC	<1 1 >1		<180 0 >270	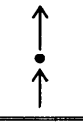	0

Table 5-6 Corrected very small strain shear stiffness in triaxial testing of reconstituted London Clay

Sample no.	AP	OP	RSRC [-]	p′ [kPa]	q [kPa]	ε_0 10^{-4} [%]	Measured G'_0 [MPa]	Corrected $G'^{\#}_0$ [MPa]
S2LCrA2	TC	TC	2	309	27	3	23	46
S2LCrA2	TC	TC	3	310	30	5	37	55
S2LCrA2	TC	TC	6	319	57	9	46	55
S2LCrA2 b	TC	uTC	3	333	104	5	30	45
S2LCrA2 c	TE	uTC	∞	327	83	2	57	57
S2LCrA3 a	IC	TC	4	300	1	10	32	43
S2LCrA3 a	TE	TC	∞	299	-2	6	65	65
S2LCrA3 b	TE	TC	∞	187	-2	2	29	29
S2LCrA3 c	TC	TE	~20	188	0	3	28	29
S2LCrA3 d	TE	TC	∞	185	-8	2	32	32
S2LCrA3 e	TE	TC	∞	186	-5	3	27	27
S2LCrA3 f	TC	TE	20	187	2	5	34	36
S2LCrA3 g	TC	TC	75	188	0	5	59	60

$^{\#}$ corrected for creep strains using equation (5.10)

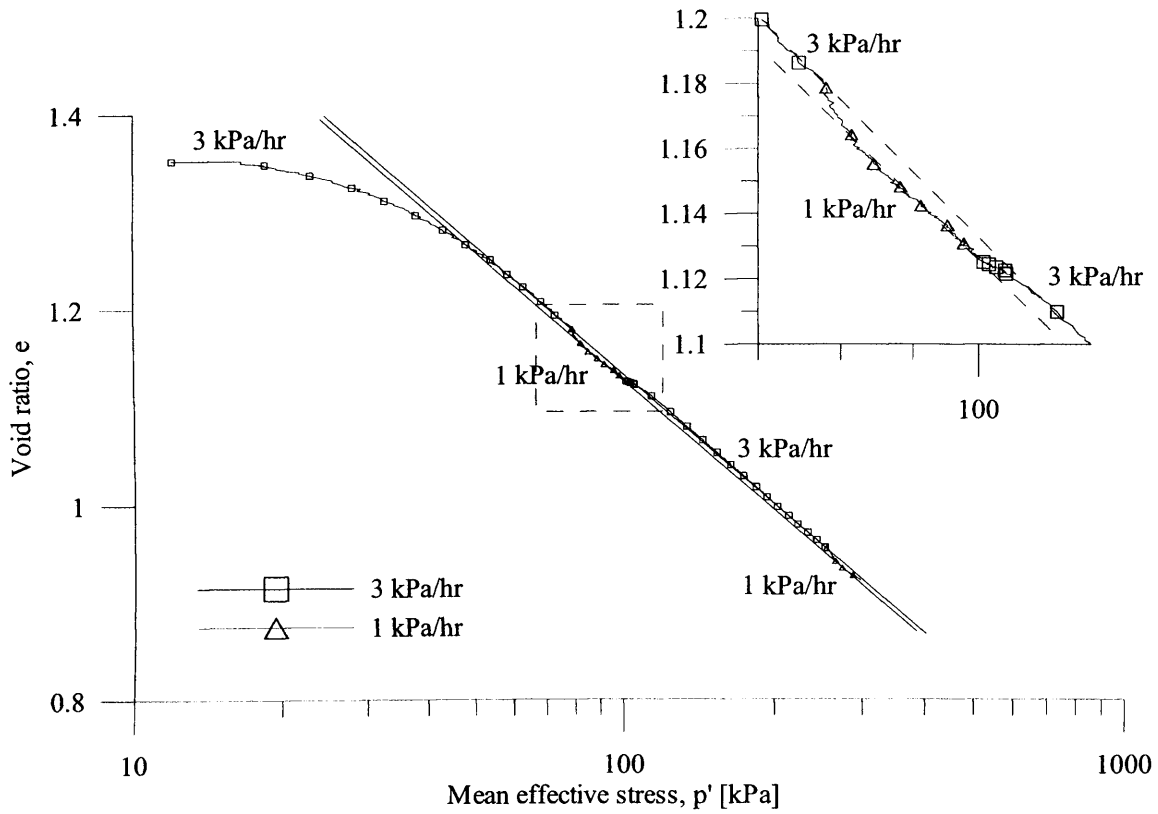

Figure 5-1 SRS* isotropic compression curve on NC reconstituted London Clay (S2LCrA2)

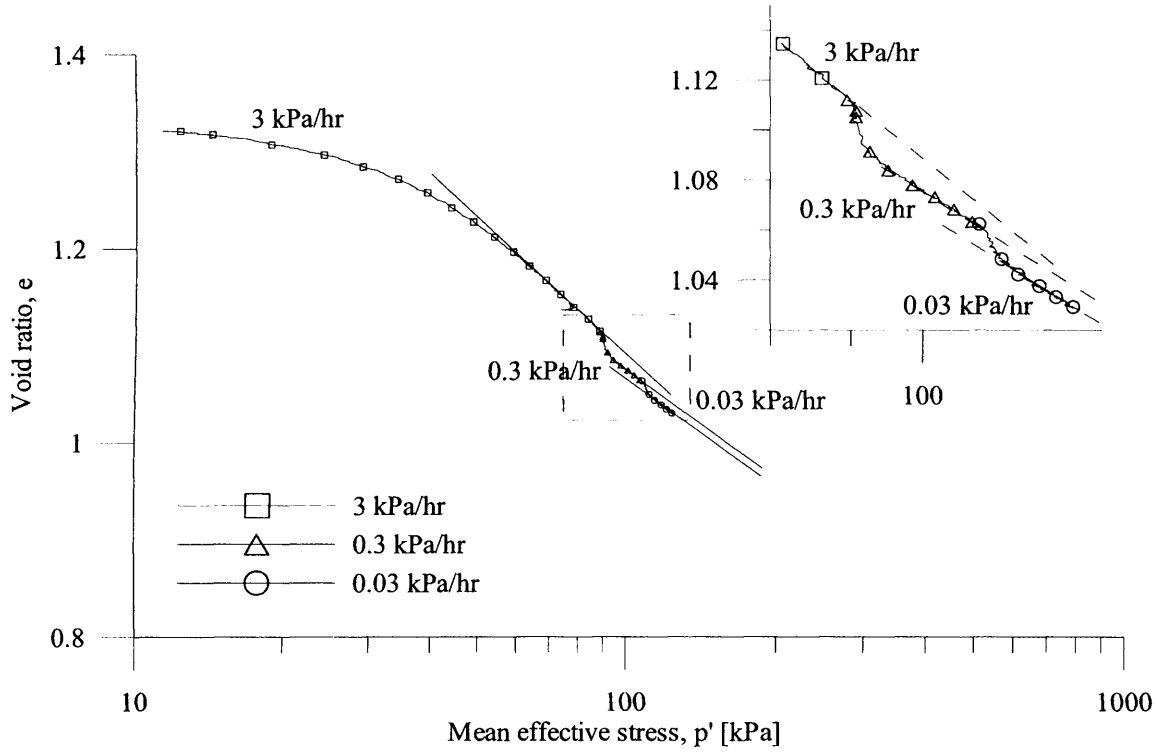

Figure 5-2 SRS* isotropic compression curve on NC reconstituted London Clay (S2LCrA4)

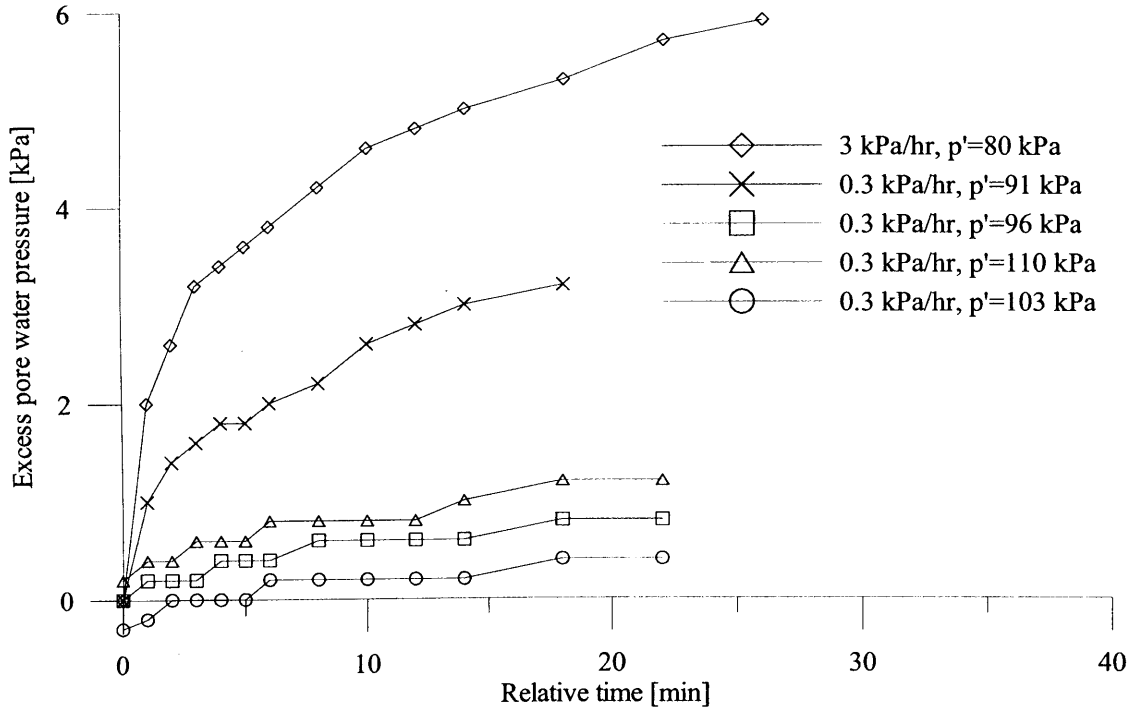

Figure 5-3 Build-up of excess pore water pressure during isotropic compression of NC reconstituted London Clay (S2LCrA4)

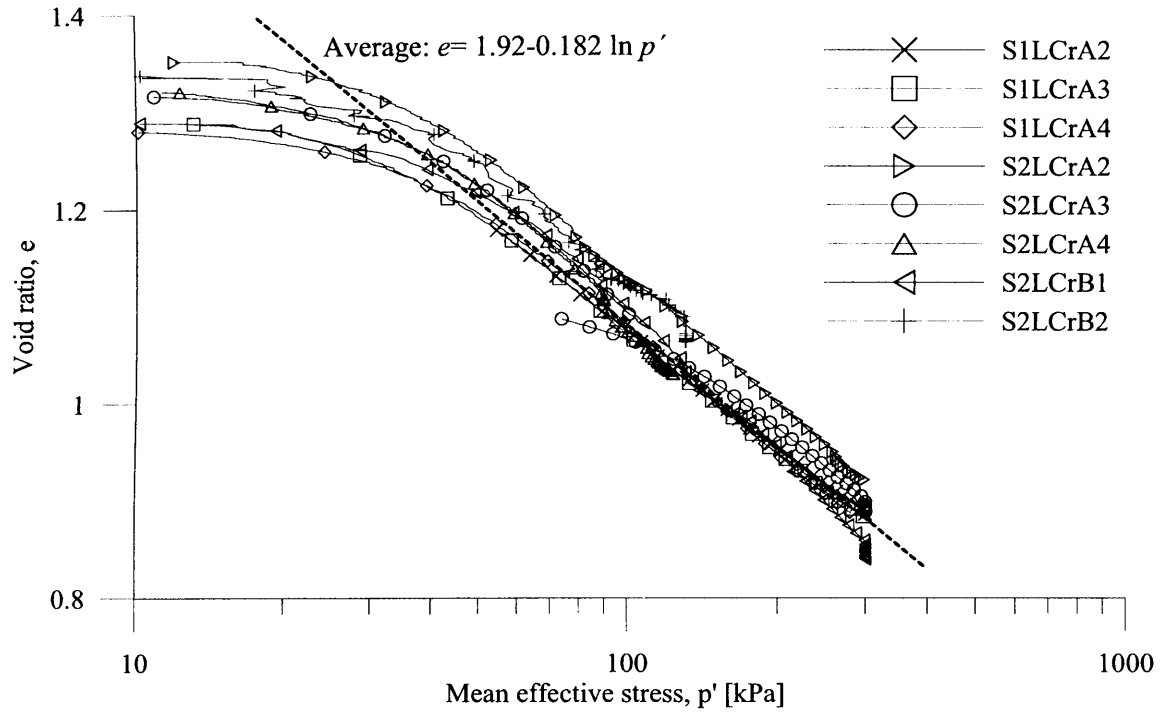

Figure 5-4 CRS* and SRS* isotropic compression curves on NC reconstituted London Clay

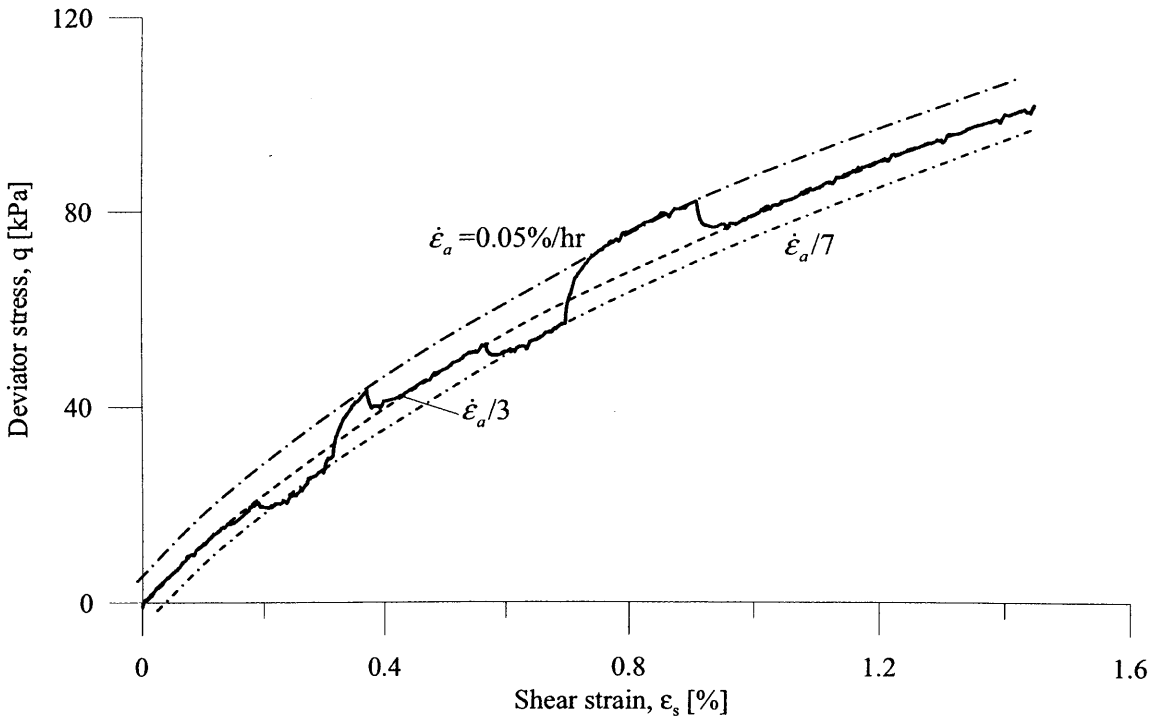

Figure 5-5 Effect of step changes in axial strain rate on drained stress-strain shearing path of NC reconstituted London Clay at low stresses (S2LCrA2)

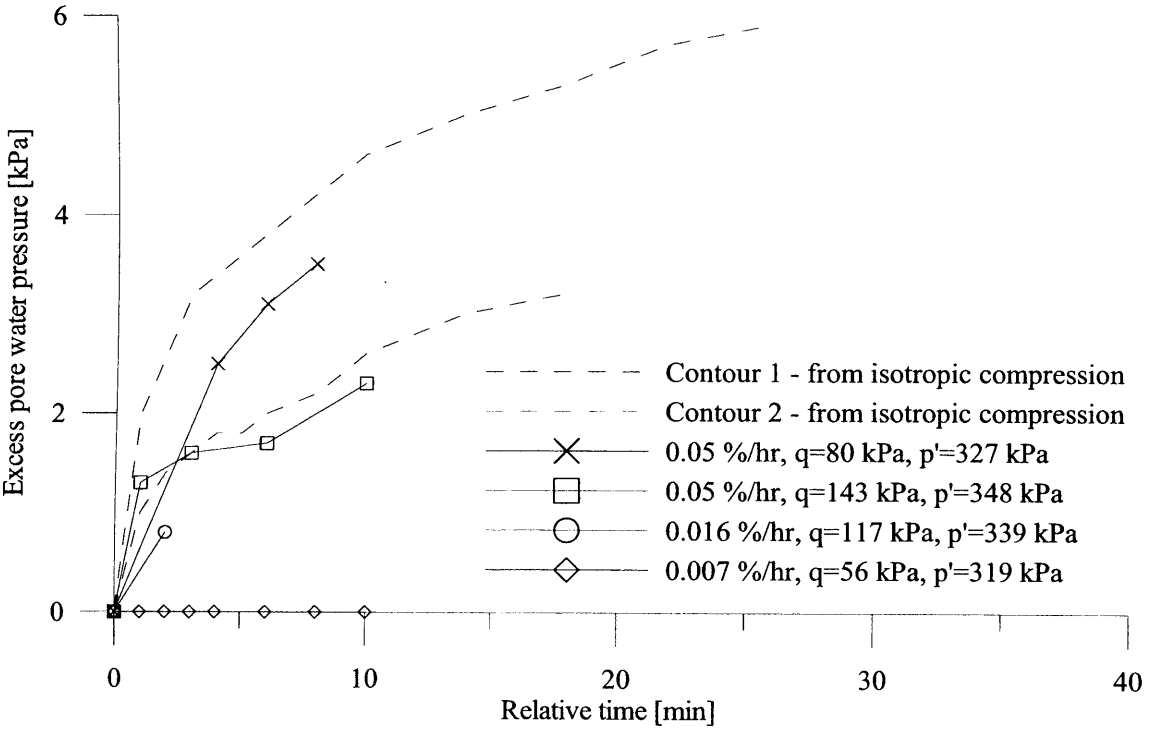

Figure 5-6 Build-up of excess pore water pressure during drained triaxial compression of NC reconstituted London Clay (S2LCrA2)

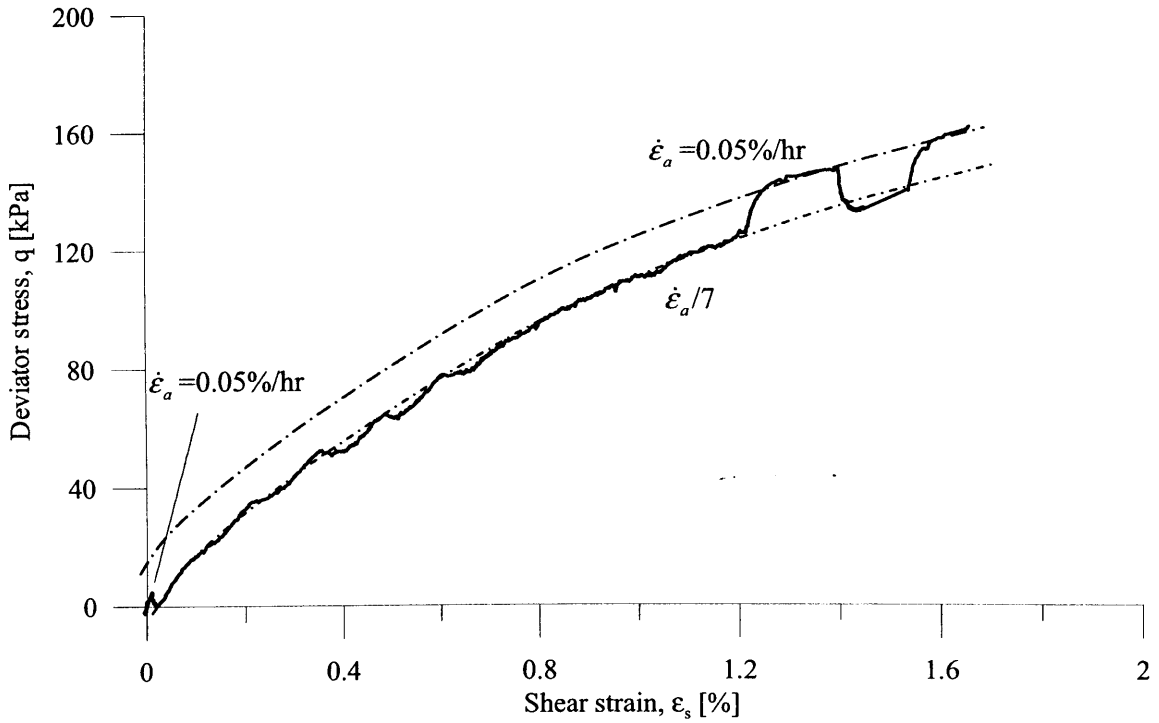

Figure 5-7 Effect of step changes in axial strain rate on drained stress-strain shearing path of NC reconstituted London Clay at intermediate stresses (S1LCrA3)

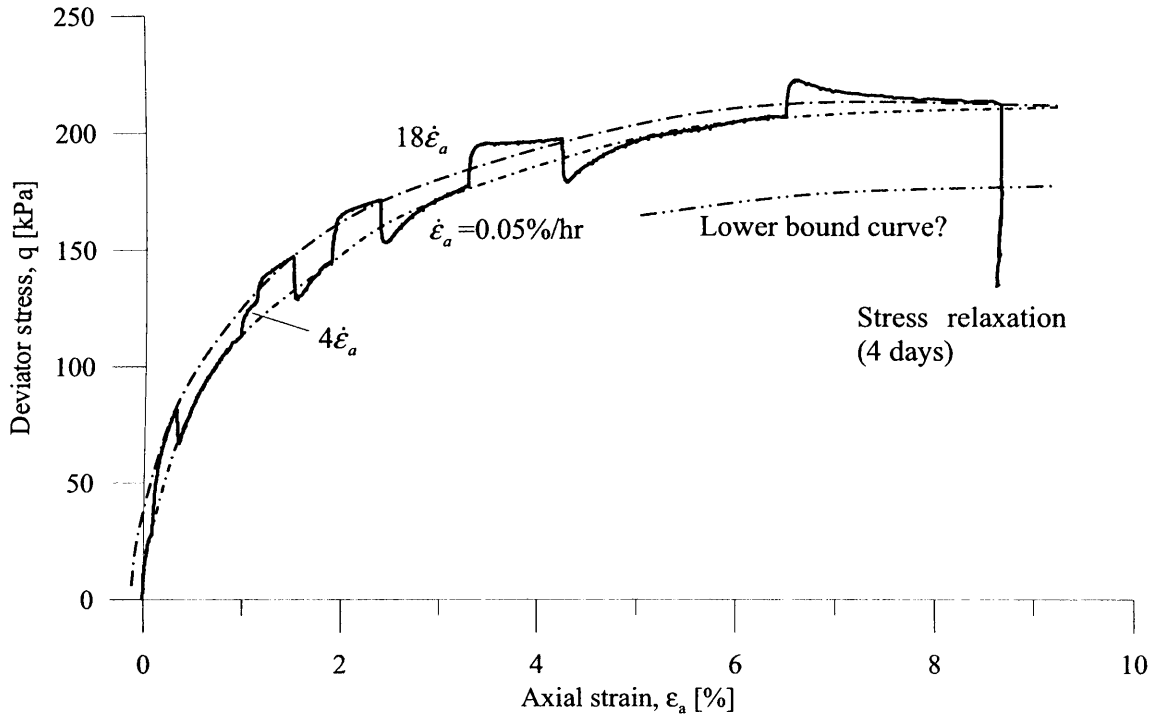

Figure 5-8 Illustrating the persistent effect of step changes in axial strain rate on undrained stress-strain shearing path of NC reconstituted London Clay (S1LCrA2)

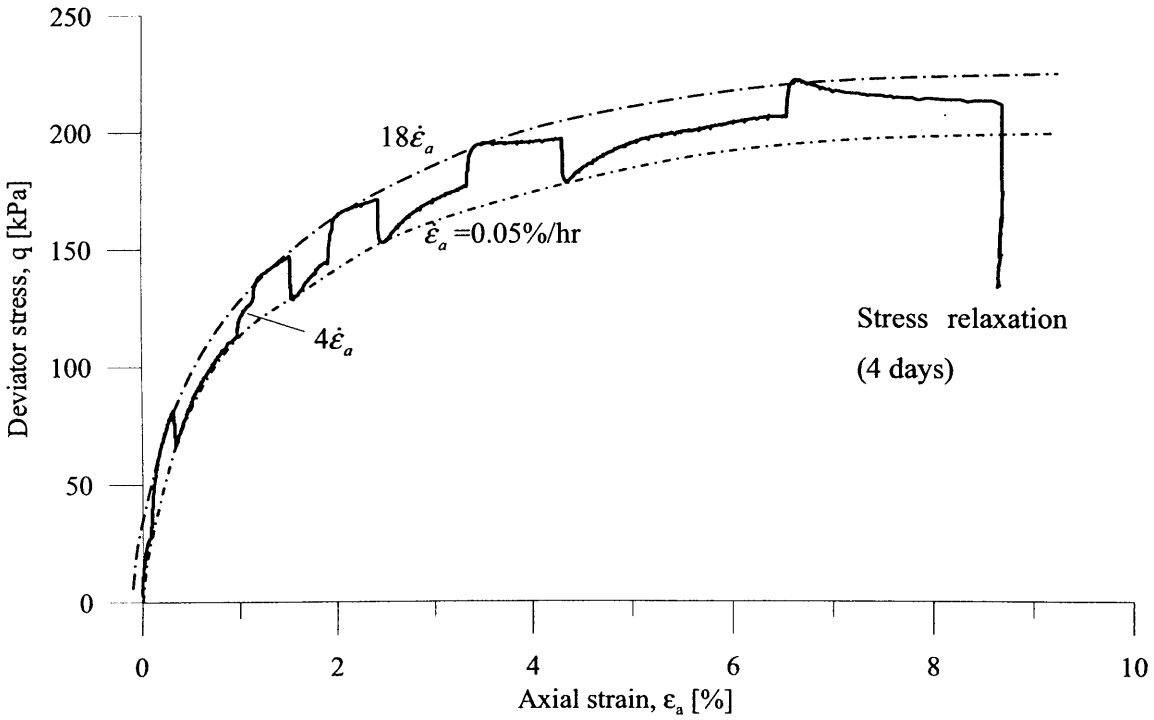

Figure 5-9 Illustrating the temporary effect of step changes in axial strain rate on undrained stress-strain shearing path of NC reconstituted London Clay (S1LCrA2)

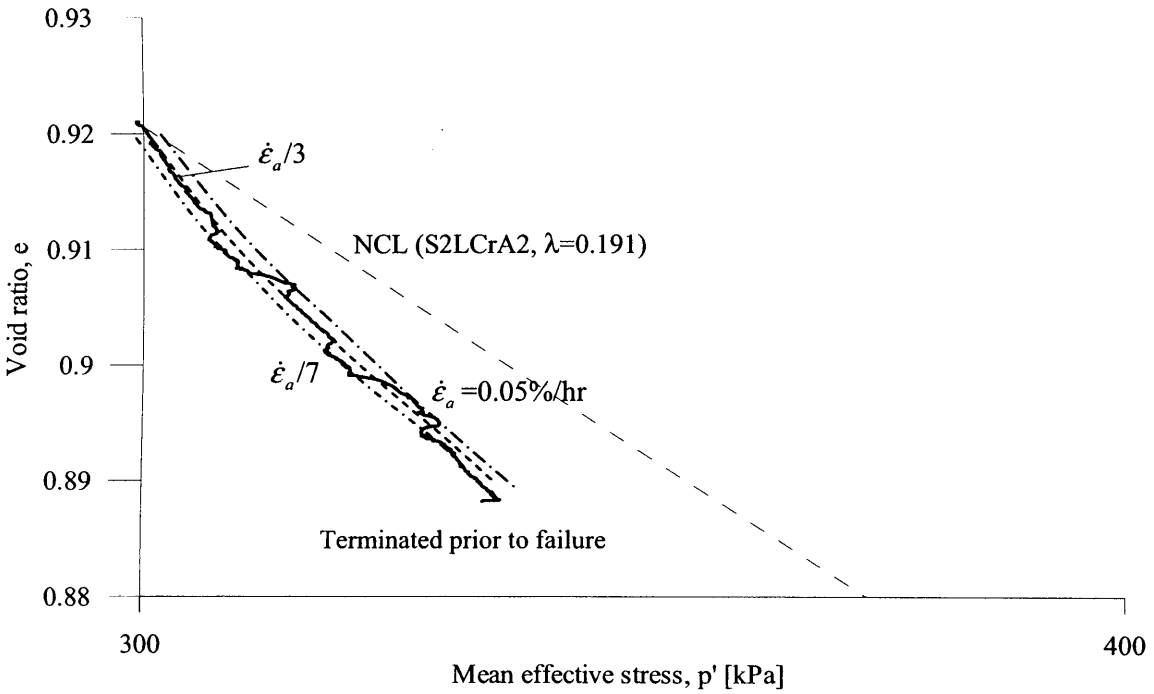

Figure 5-10 Effect of step changes in axial strain rate on drained compression path of NC reconstituted London Clay at low stresses during shearing (S2LCrA2) – semi log scale

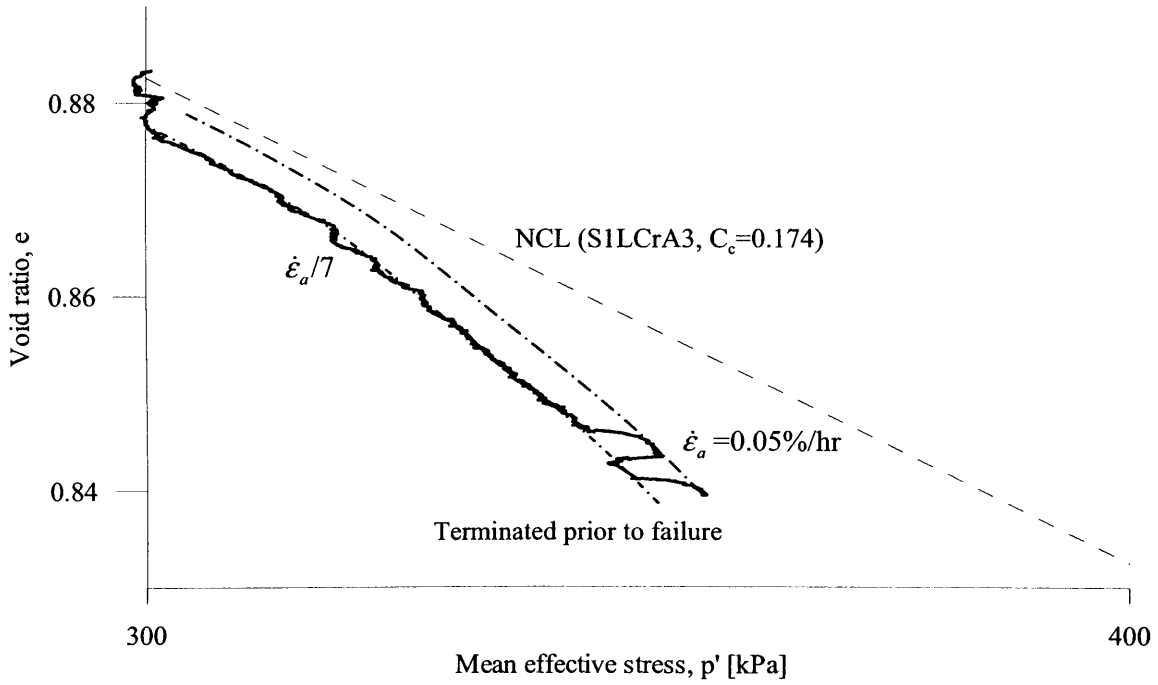

Figure 5-11 Effect of step changes in axial strain rate on drained compression path of NC reconstituted London Clay at intermediate stresses during shearing (S1LCrA3) – semi log scale

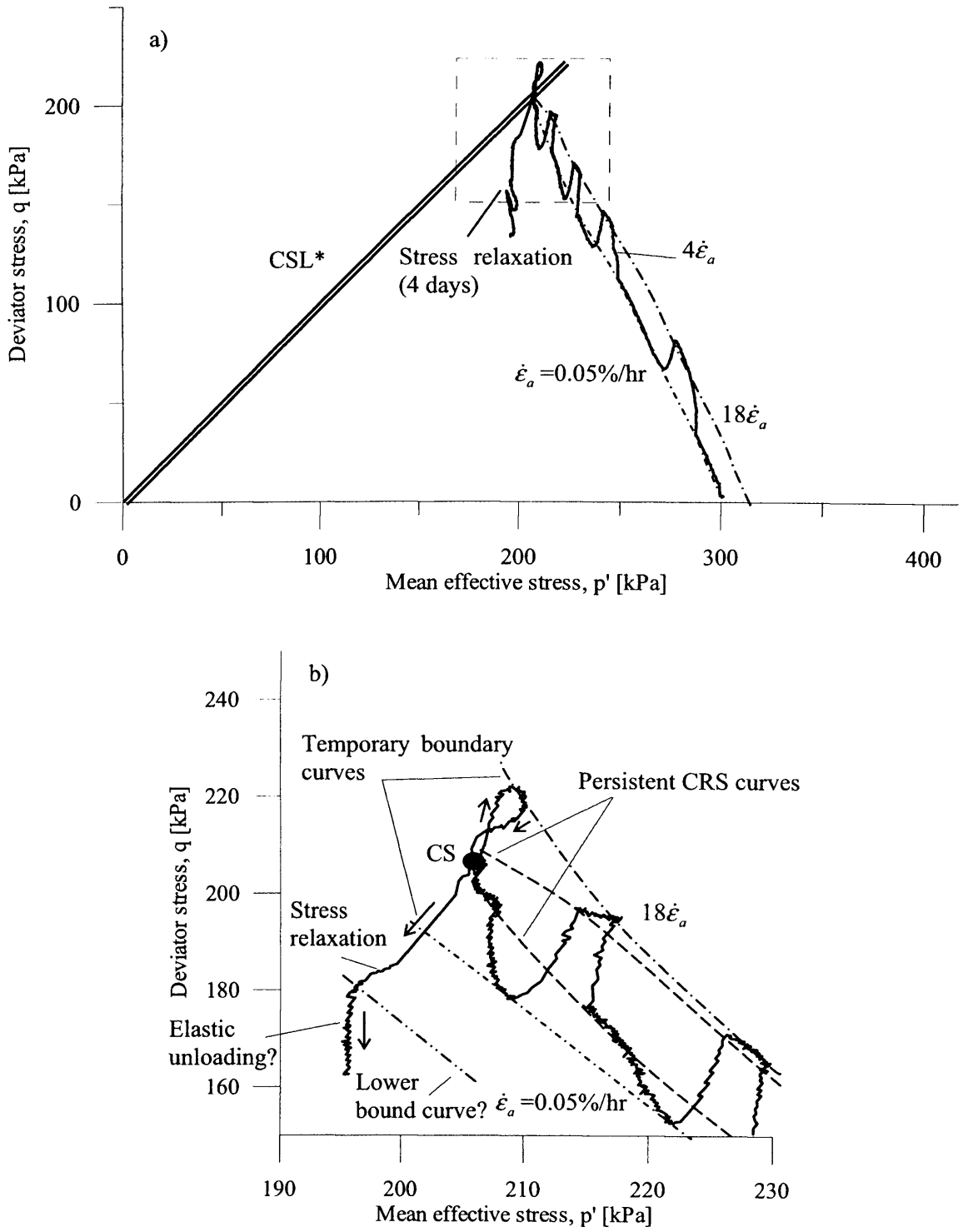

Figure 5-12 Effect of step changes in axial strain rate on undrained stress path of NC reconstituted London Clay (S1LCrA2)

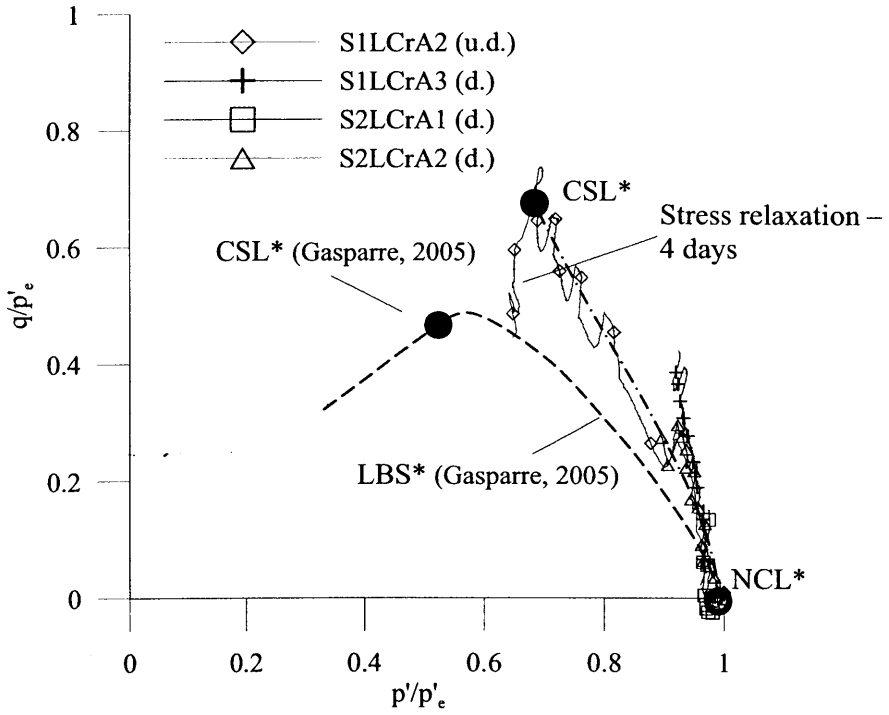

Figure 5-13 Effect of step changes in axial strain rate on normalised stress paths of NC reconstituted London Clay

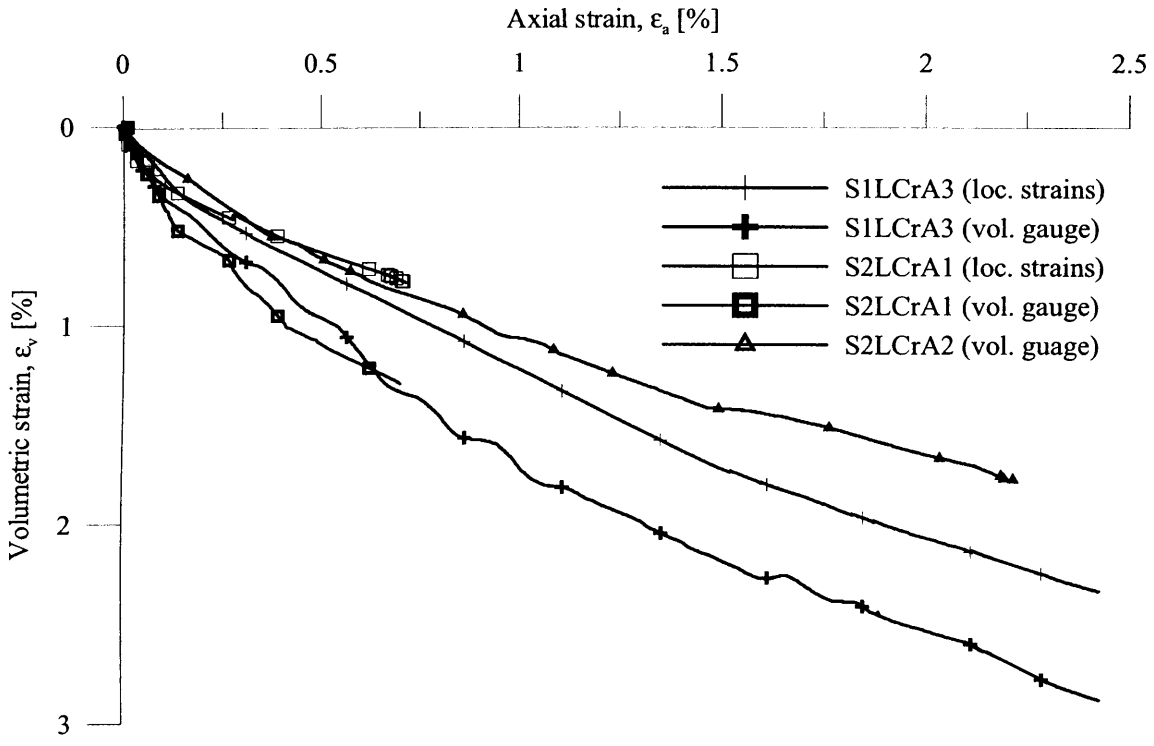

Figure 5-14 Effect of step changes in axial strain rate on the evolution of volumetric strains during drained shearing of NC reconstituted London Clay

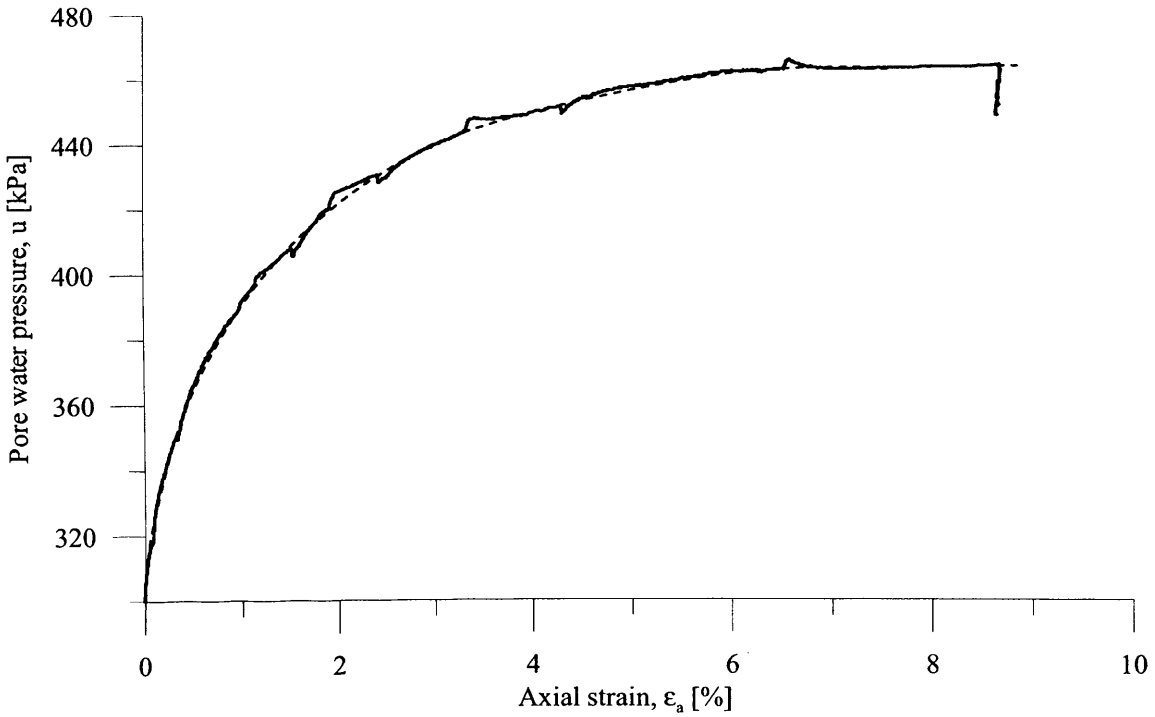

Figure 5-15 Effect of step changes in axial strain rate on the accumulation of pore water pressures during undrained shearing of NC reconstituted London Clay (S1LCrA2)

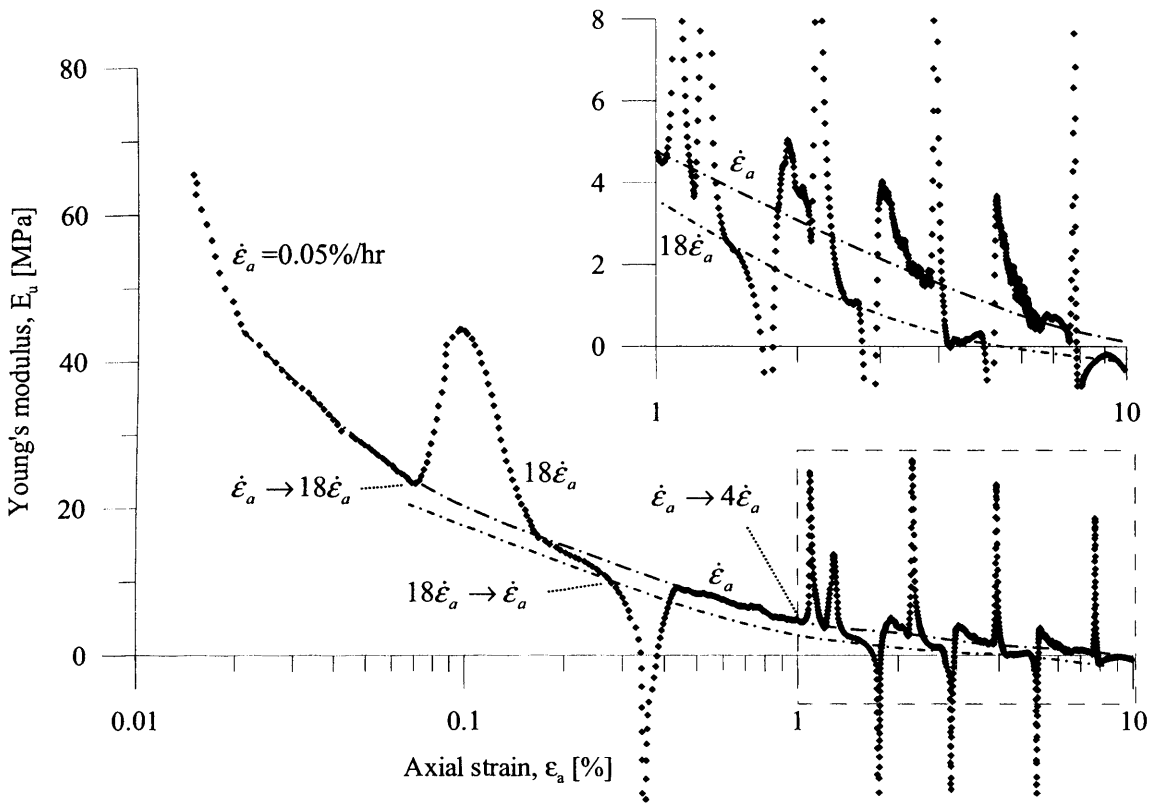

Figure 5-16 Effect of step changes in axial strain rate on the small to large strain stiffness during undrained shearing of NC reconstituted London Clay (S1LCrA2)

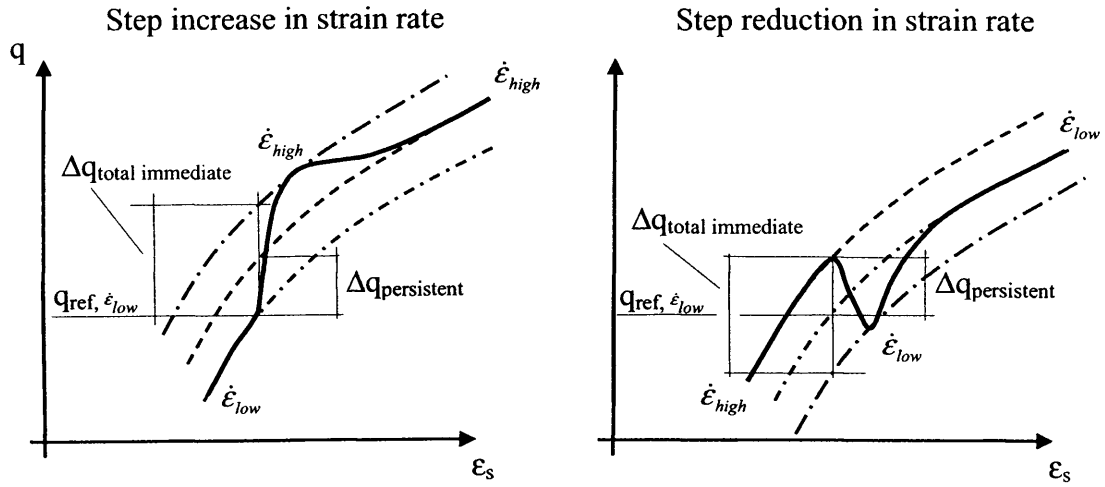

Figure 5-17 Definition of stress jump due to step changes in axial (and shear) strain rate in triaxial compression

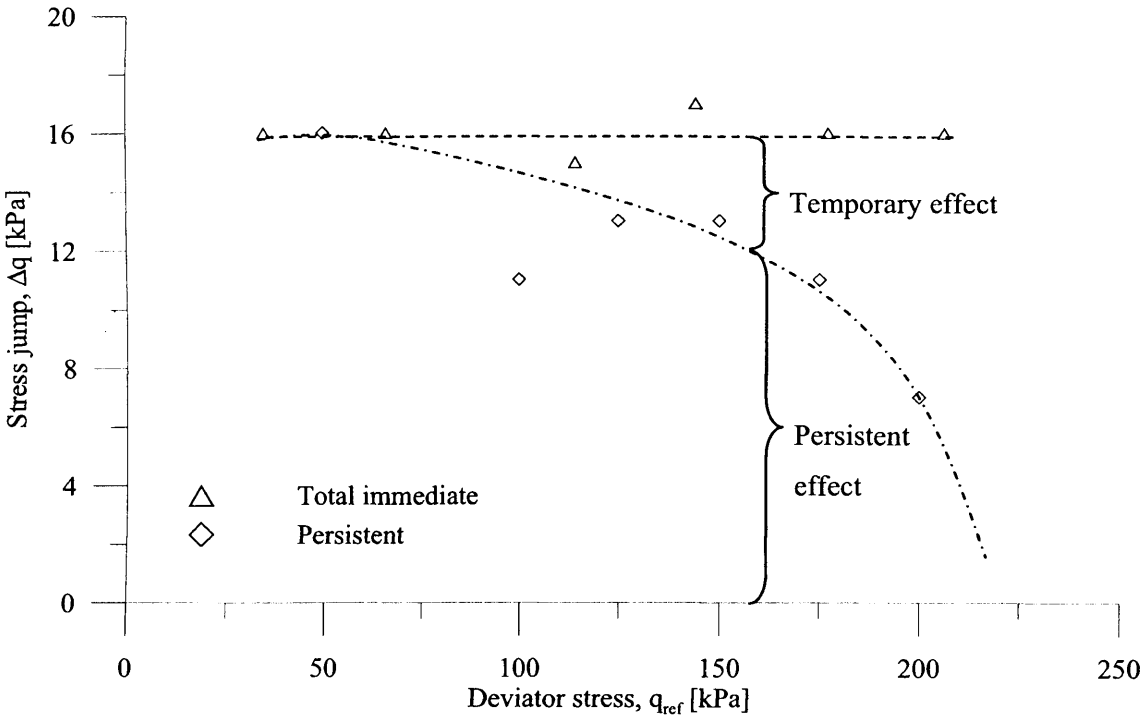

Figure 5-18 Influence of stress level on the viscous stress jump during undrained shearing of NC reconstituted London Clay for an absolute axial strain rate change of 18x (S1LCrA2)

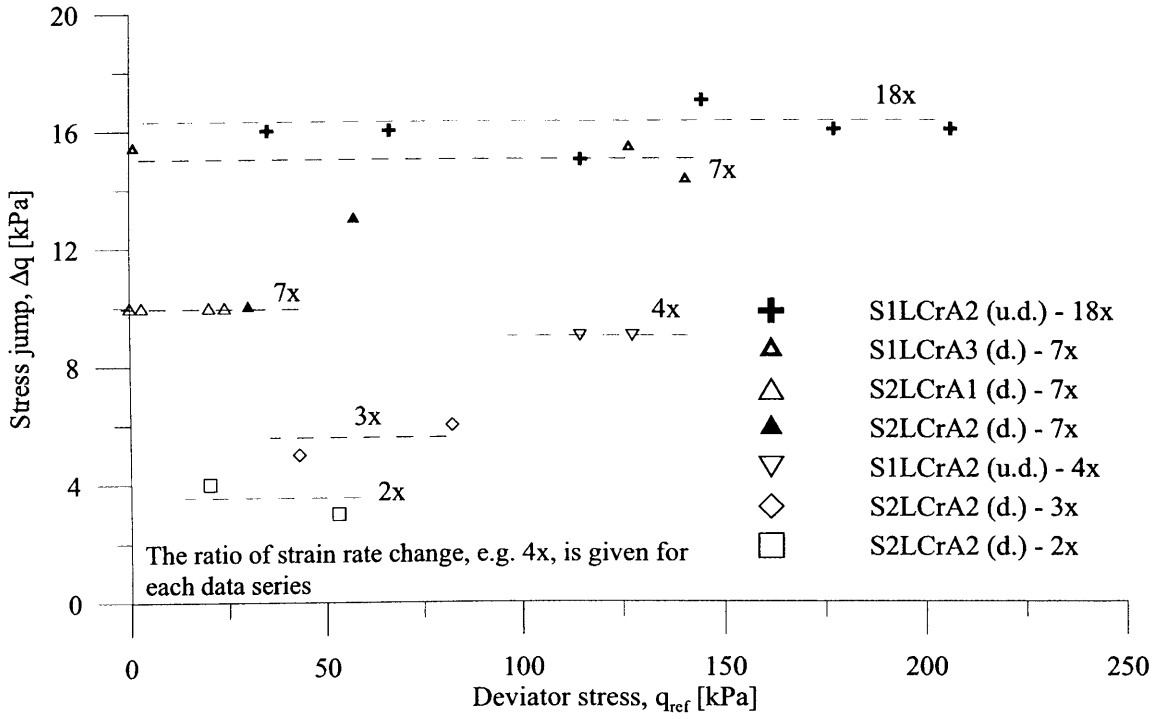

Figure 5-19 Influence of axial strain rate change and stress level on the total immediate viscous stress jump during shearing of NC reconstituted London Clay

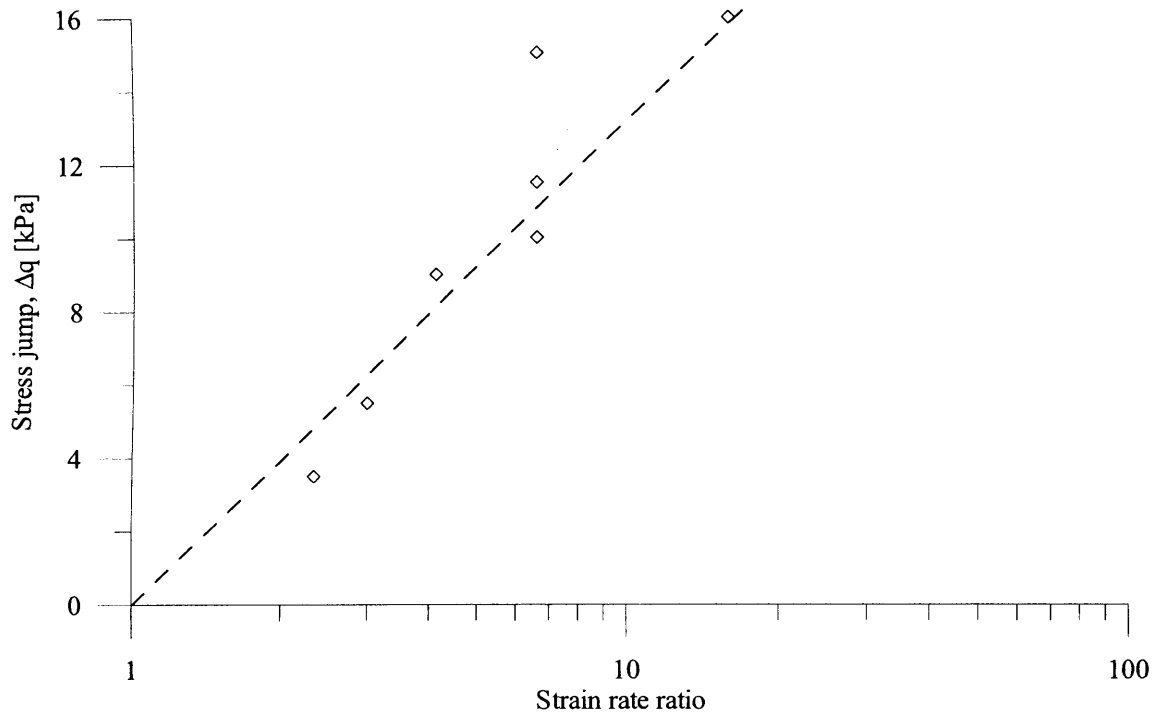

Figure 5-20 Relationship between ratio of axial strain rate change and the total immediate viscous stress jump during shearing of NC reconstituted London Clay

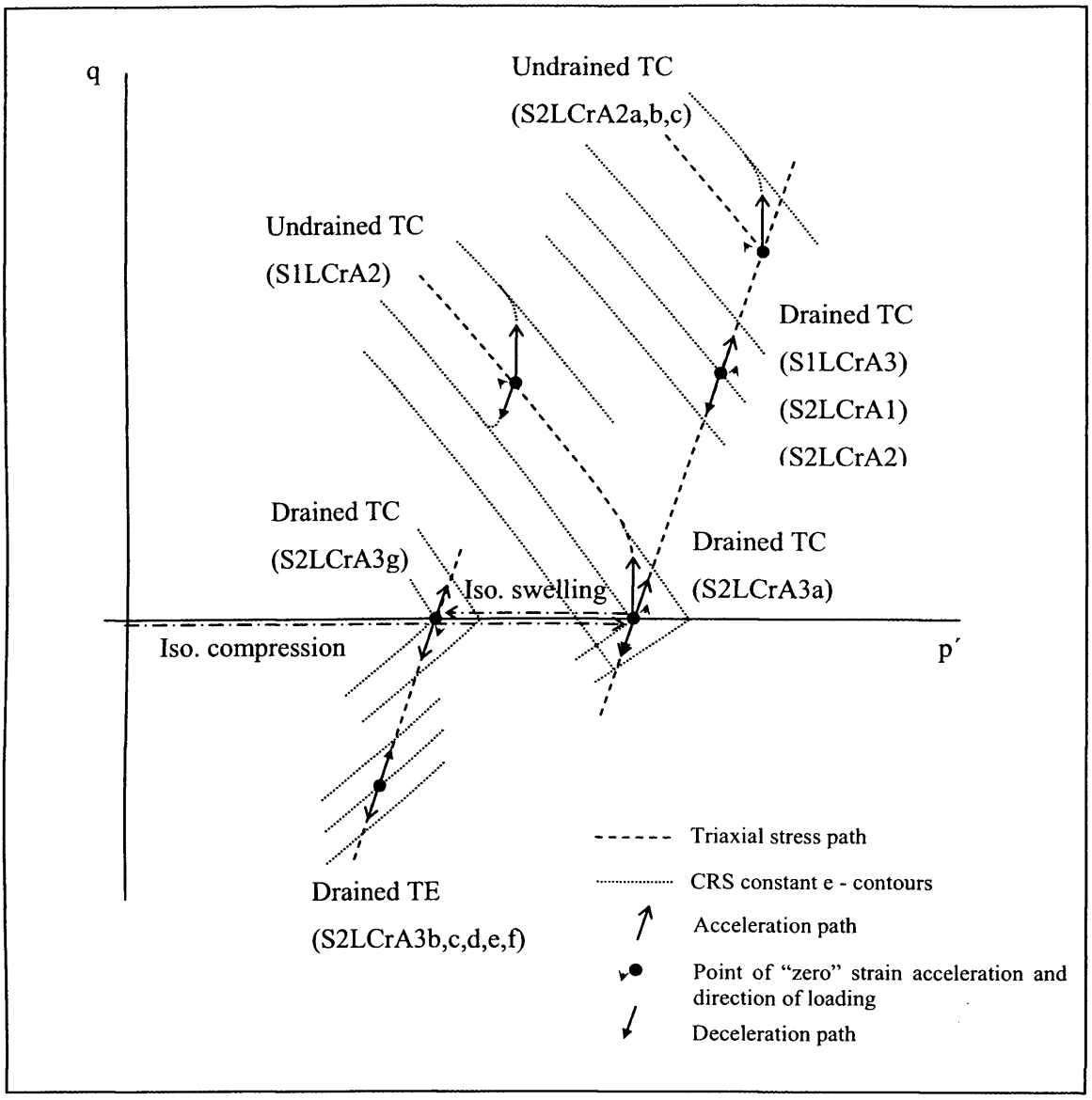

Figure 5-21 Schematic diagram illustrating the general test procedures used in the investigation of strain acceleration in reconstituted London Clay

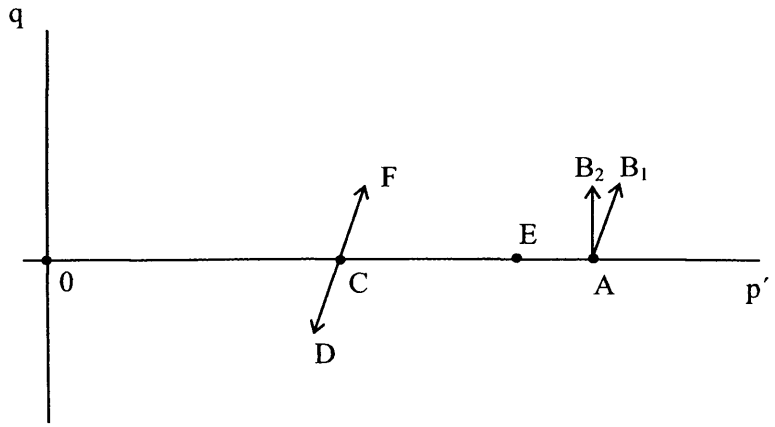

Sample	Description of test path		Stress path
All	Isotropic compression	-	0→A
S2LCrA2	Undrained TC	Acceleration	A→B_2→A
S1LCrA3	Drained TC	Deceleration	A→B_1→A
S2LCrA1	Drained TC	Deceleration	A→B_1→A
S2LCrA2	Drained TC	No acceleration	A→B_1→A
S2LCrA3a	Drained TC	Acceleration	A→B_1→A
S2LCrA3a-b	Isotropic swelling	-	A→C
S2LCrA3b	Drained TE	No acceleration	C →D→C
S2LCrA3c	Drained TE	No acceleration	C →D
S2LCrA3d	Drained TE	Acceleration	D→C
S2LCrA3d-e	Isotropic compression-swelling	-	C→E→C
S2LCrA3e	Drained TE	No acceleration	C →D→C
S2LCrA3f	Drained TE	Acceleration	C →D→C
S2LCrA3g	Drained TC	Acceleration	C →F

Figure 5-22 Schematic diagram illustrating the test procedures for investigating the influence of strain acceleration at isotropic stress state in reconstituted London Clay

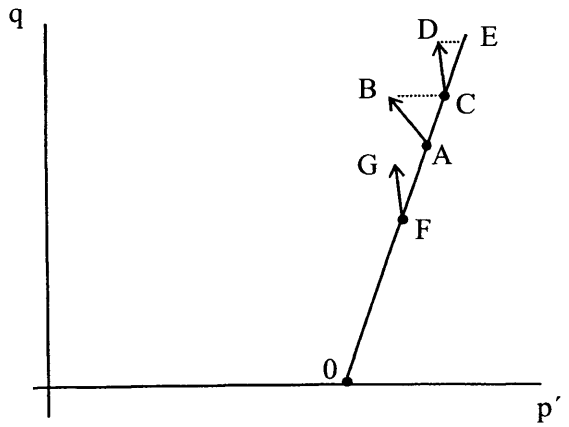

Sample	Description of test path		Stress path
S2LCrA2	Drained TC	-	0→A
S2LCrA2a	Undrained TC	No acceleration	A→B
S2LCrA2a-b	Drained TC	-	B→C
S2LCrA2b	Undrained TC	Acceleration	C→D
S2LCrA2b-c	Drained stress relaxation	-	D→E→F
S2LCrA2c	Undrained TC	Acceleration	F→G

Figure 5-23 Schematic diagram illustrating the test procedures for investigating the influence of strain acceleration at large strains with a change in drainage conditions in reconstituted London Clay

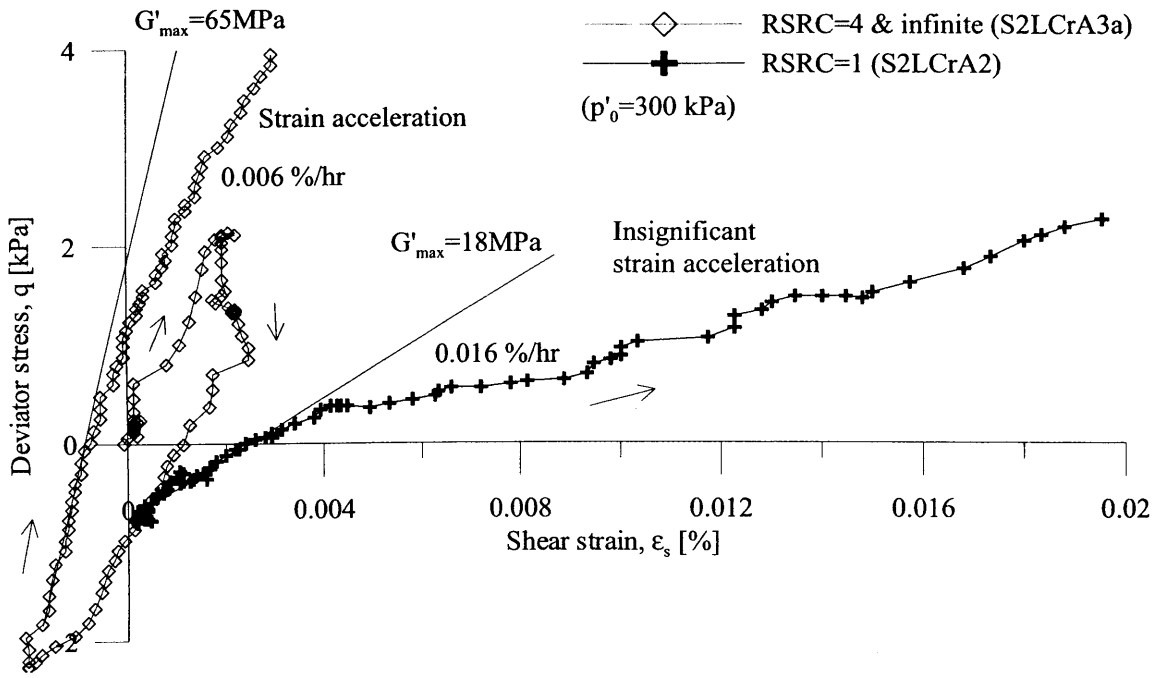

Figure 5-24 Influence of shear strain acceleration after isotropic compression on stress-strain path in drained triaxial compression of reconstituted London Clay - comparison

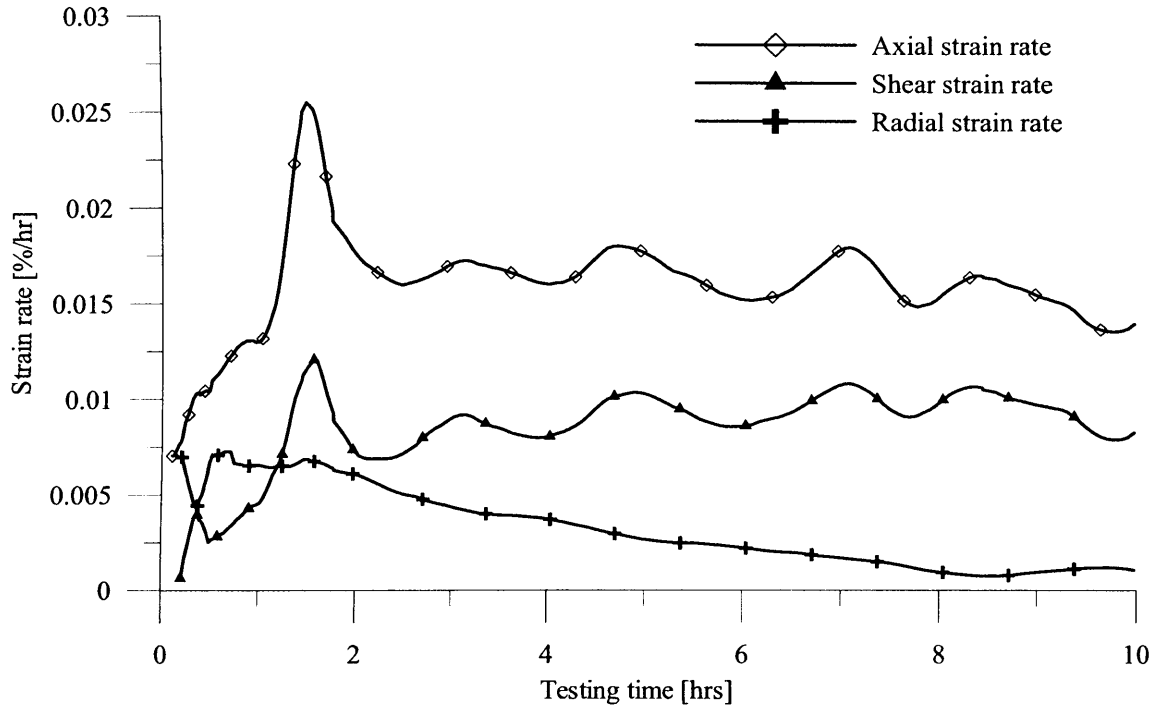

Figure 5-25 Initial variation of strain rates in drained triaxial compression of reconstituted London Clay after isotropic compression (initial RSRC=1, S2LCrA2)

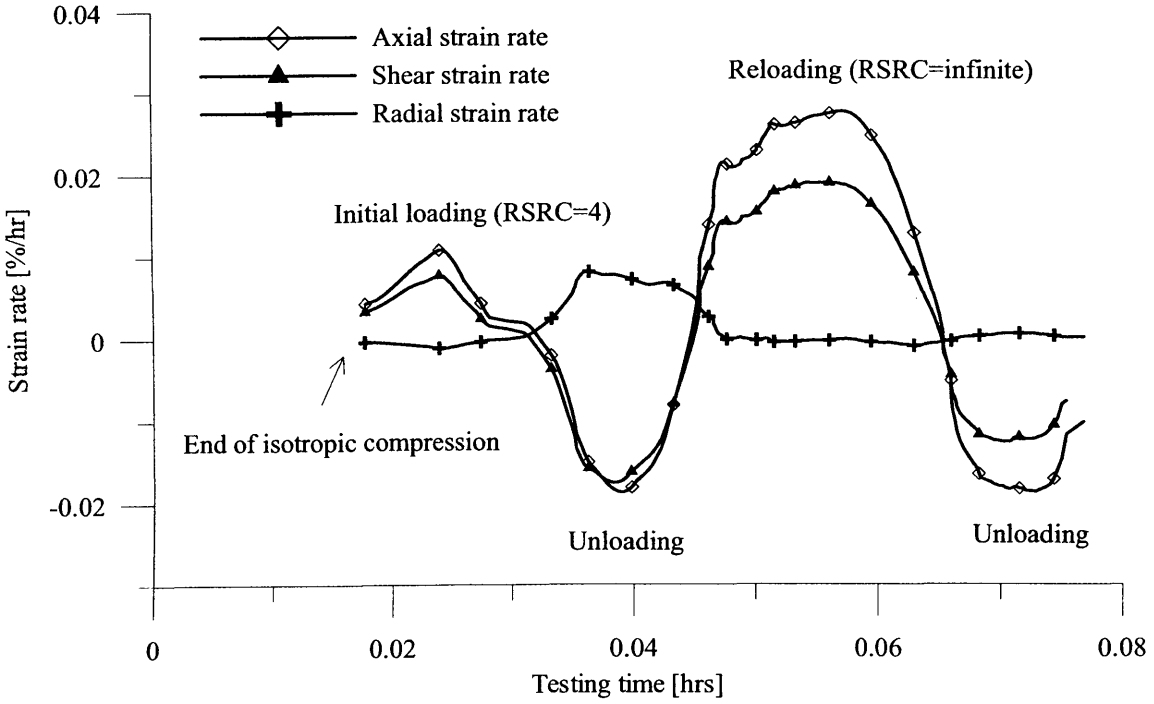

Figure 5-26 Variation of strain rates in drained triaxial compression of reconstituted London Clay with unload-reload cycle after isotropic compression (S2LCrA3a)

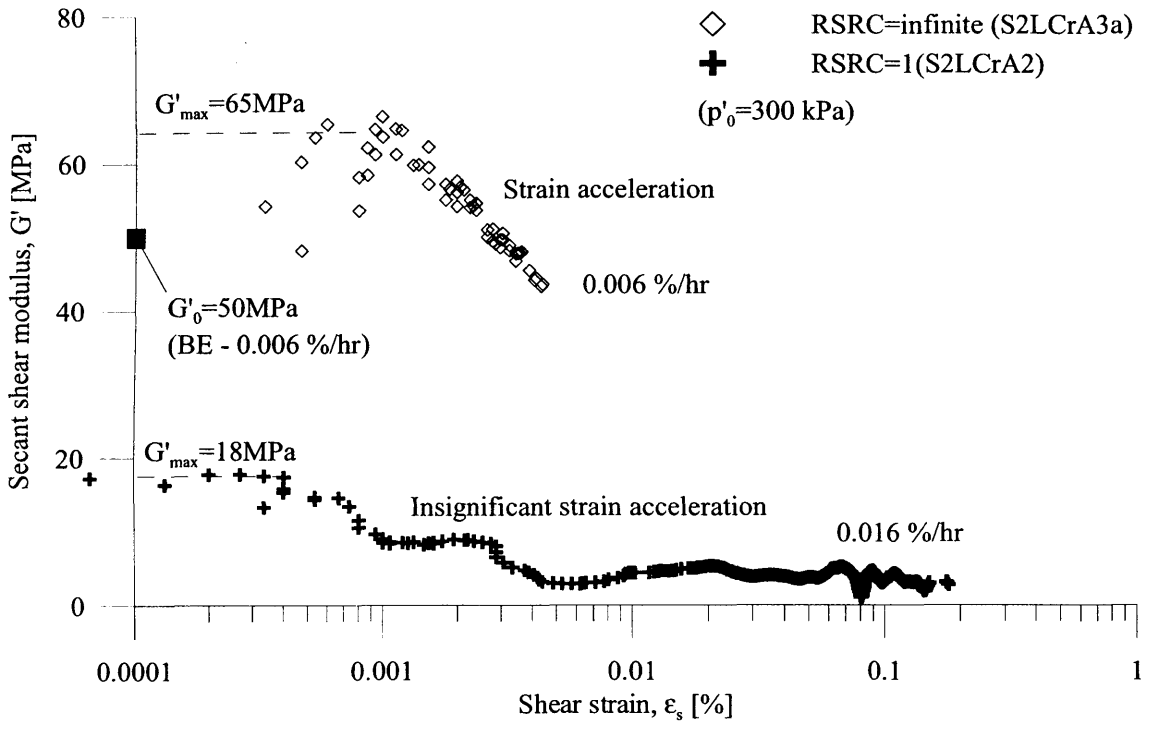

Figure 5-27 Influence of shear strain acceleration after isotropic compression on shear stiffness in drained triaxial compression of reconstituted London Clay - comparison

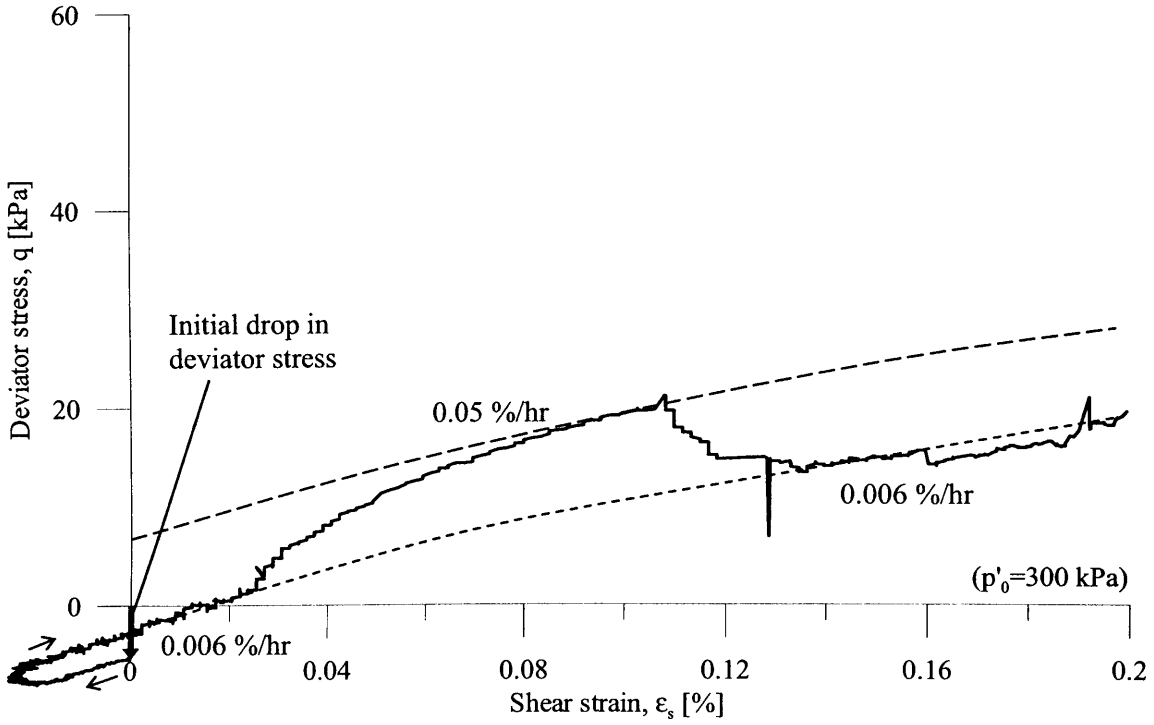

Figure 5-28 Effect of axial strain deceleration after isotropic compression on stress-strain path in drained triaxial compression of reconstituted London Clay (initial RSRC=1/10, S2LCrA1)

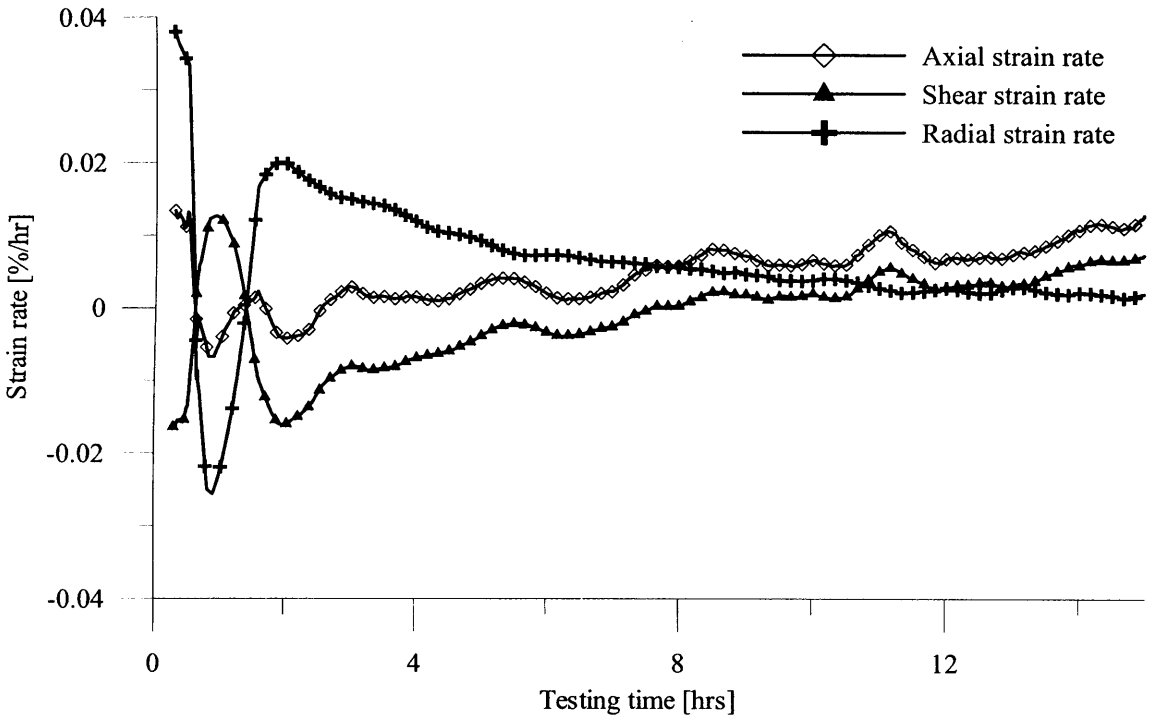

Figure 5-29 Initial variation of strain rates in drained triaxial compression of reconstituted London Clay after isotropic compression (initial RSRC=1/10, S2LCrA1)

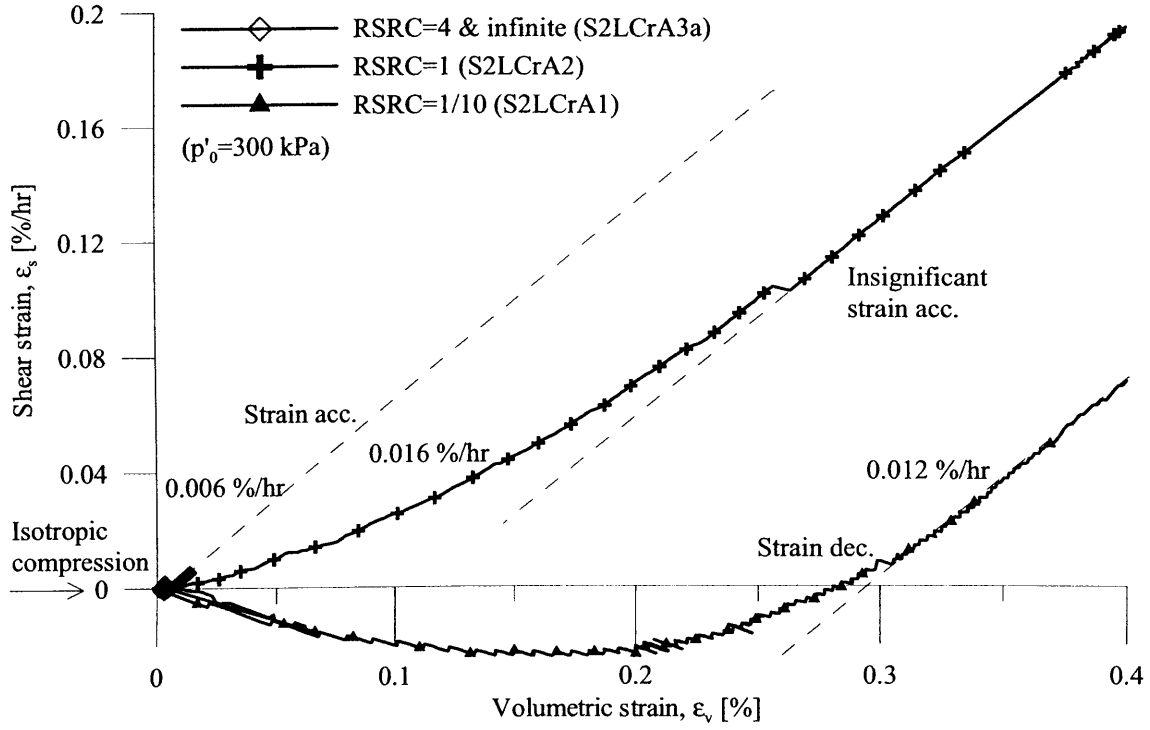

Figure 5-30 Influence of shear strain acceleration after isotropic compression on strain path in drained triaxial compression of reconstituted London Clay - comparison

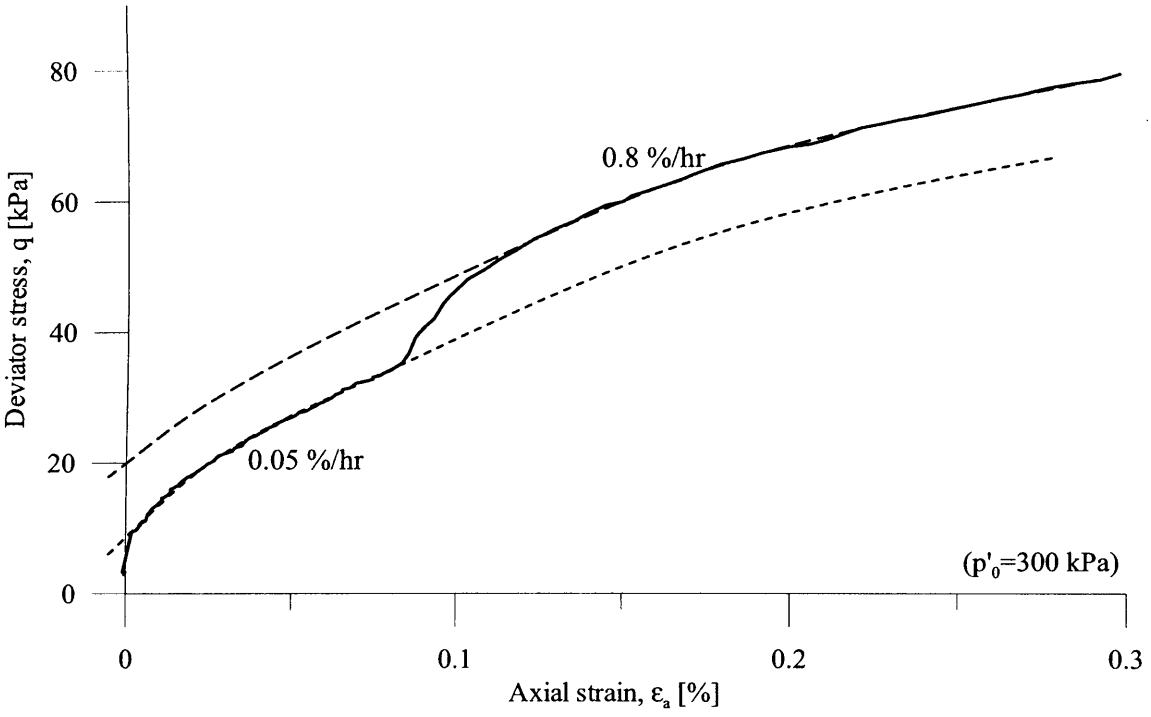

Figure 5-31 Effect of axial strain acceleration after isotropic compression on stress-strain path in undrained triaxial compression of reconstituted London Clay (initial RSRC=4, S1LCrA2)

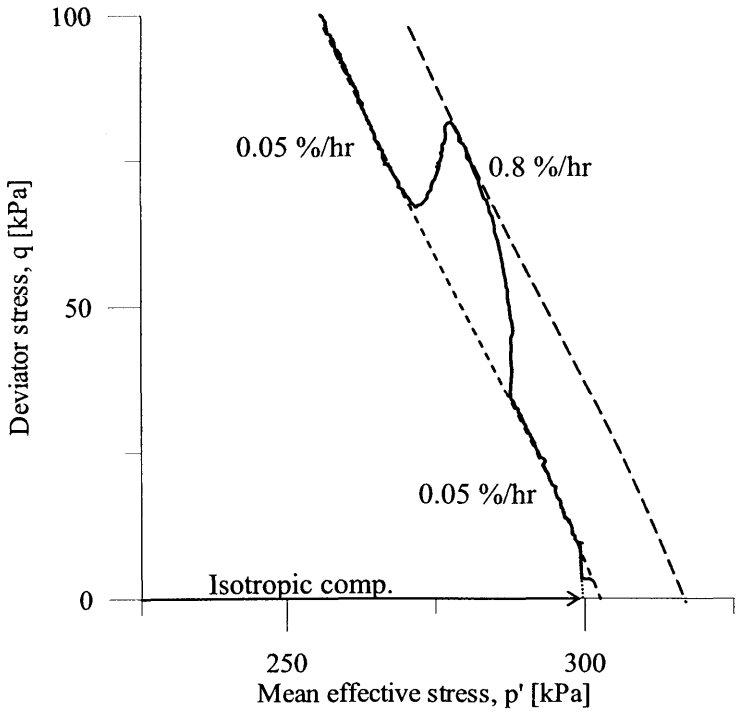

Figure 5-32 Effect of axial strain acceleration after isotropic compression on stress path in undrained triaxial compression of reconstituted London Clay (initial RSRC=4, S1LCrA2)

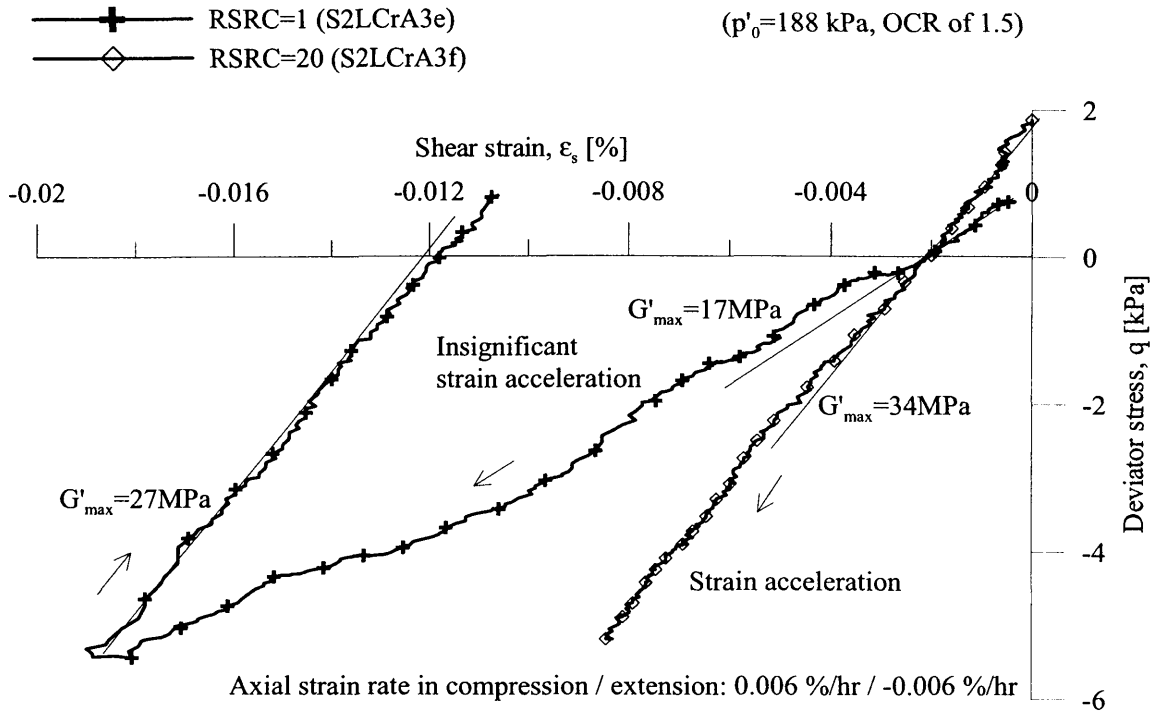

Figure 5-33 Influence of shear strain acceleration after isotropic swelling on shear stiffness in drained triaxial extension of reconstituted London Clay - comparison

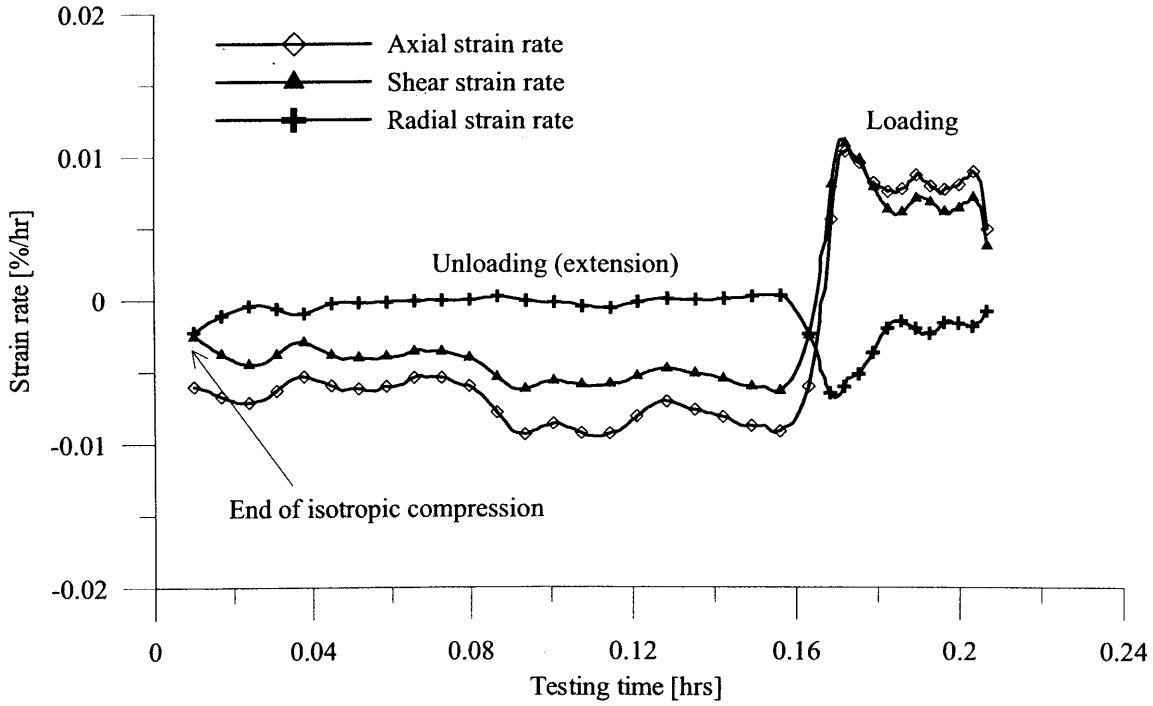

Figure 5-34 Initial variation of strain rates in drained triaxial extension of reconstituted London Clay after isotropic swelling (initial RSRC=1, S2LCrA3e)

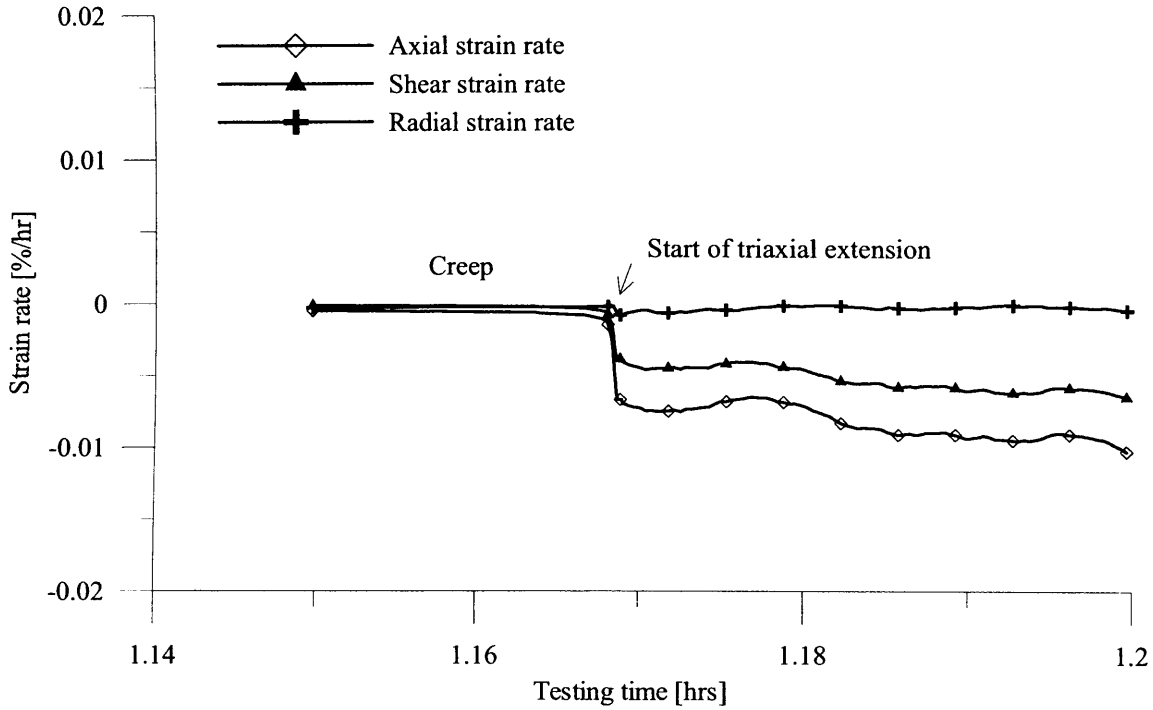

Figure 5-35 Initial variation of strain rates in drained triaxial extension of reconstituted London Clay after creep at isotropic stress state (initial RSRC=20, S2LCrA3f)

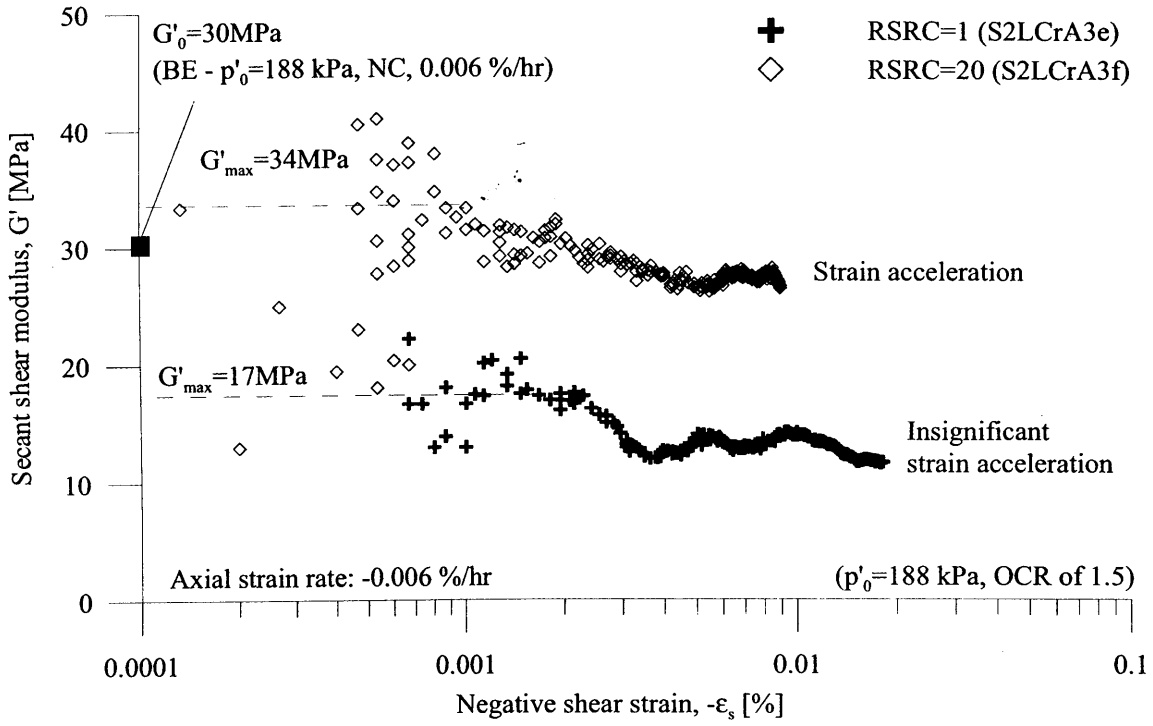

Figure 5-36 Influence of shear strain acceleration after isotropic swelling on shear stiffness in drained triaxial extension of reconstituted London Clay - comparison

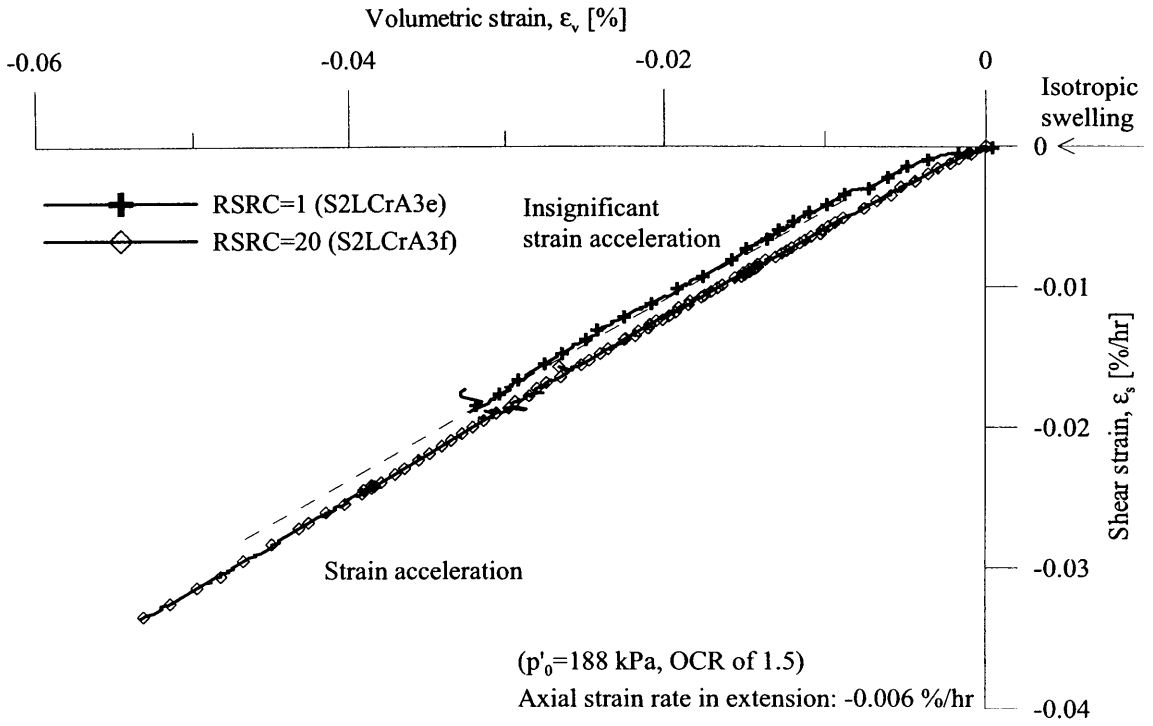

Figure 5-37 Influence of shear strain acceleration after isotropic swelling on strain path in drained triaxial extension of reconstituted London Clay - comparison

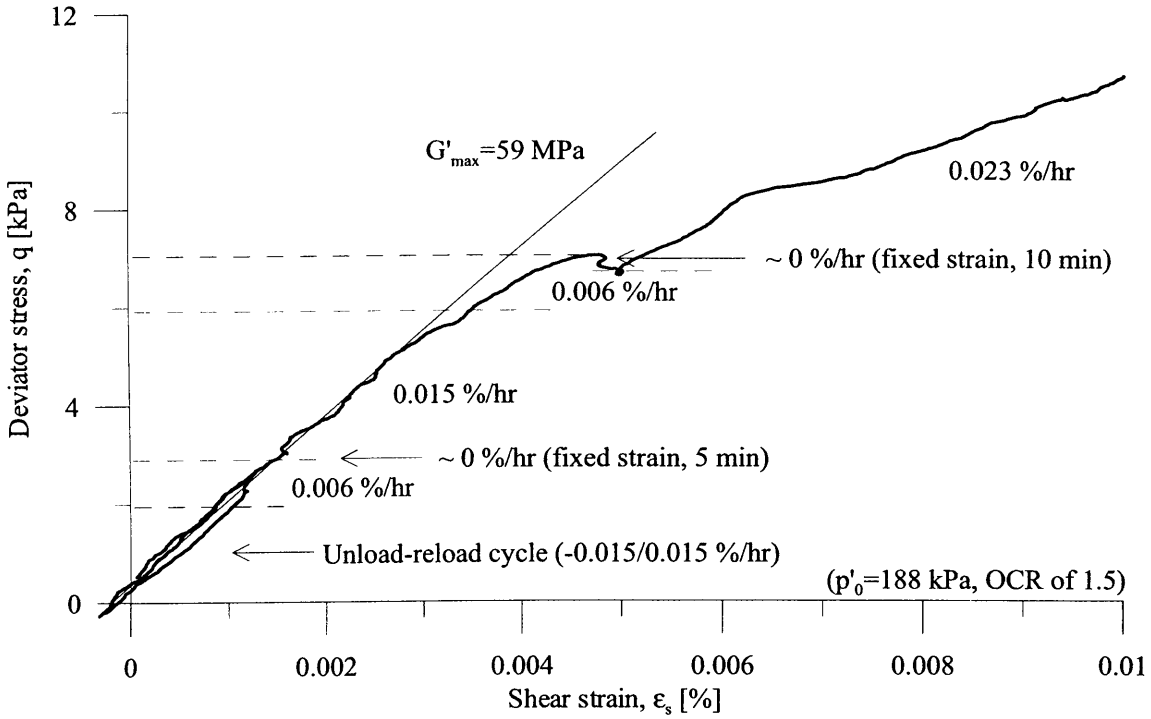

Figure 5-38 Influence of shear strain acceleration at small strains on the stress-strain path in drained triaxial compression of reconstituted London Clay (initial RSRC=75, S2LCrA3g)

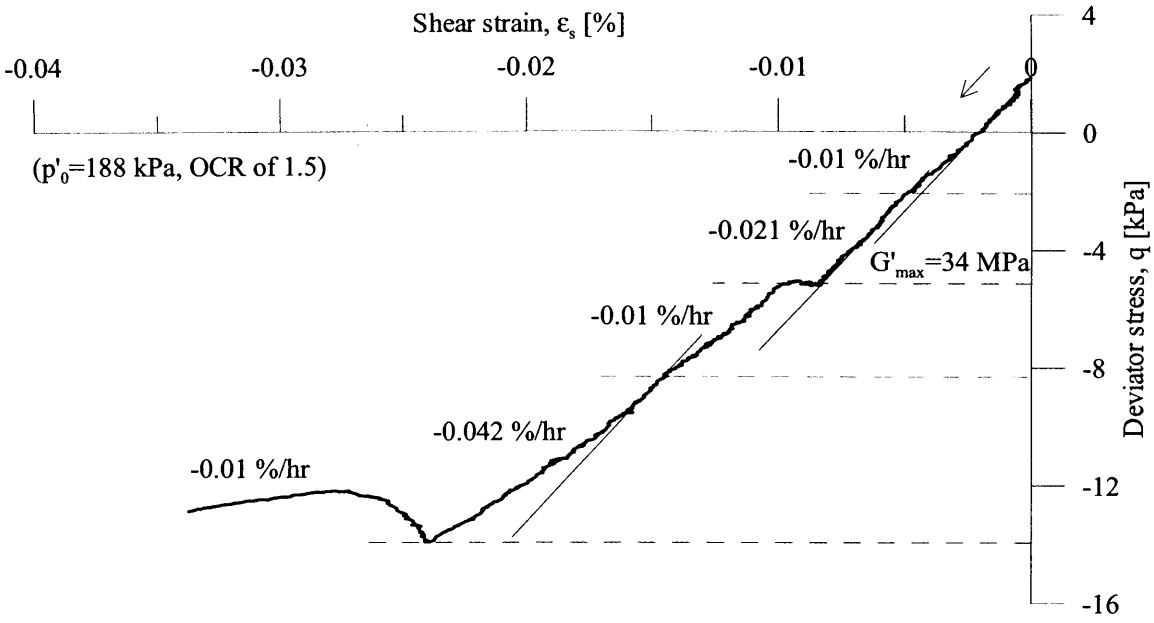

Figure 5-39 Influence of shear strain acceleration at small strains on the stress-strain path in drained triaxial extension of reconstituted London Clay (initial RSRC=20, S2LCrA3f)

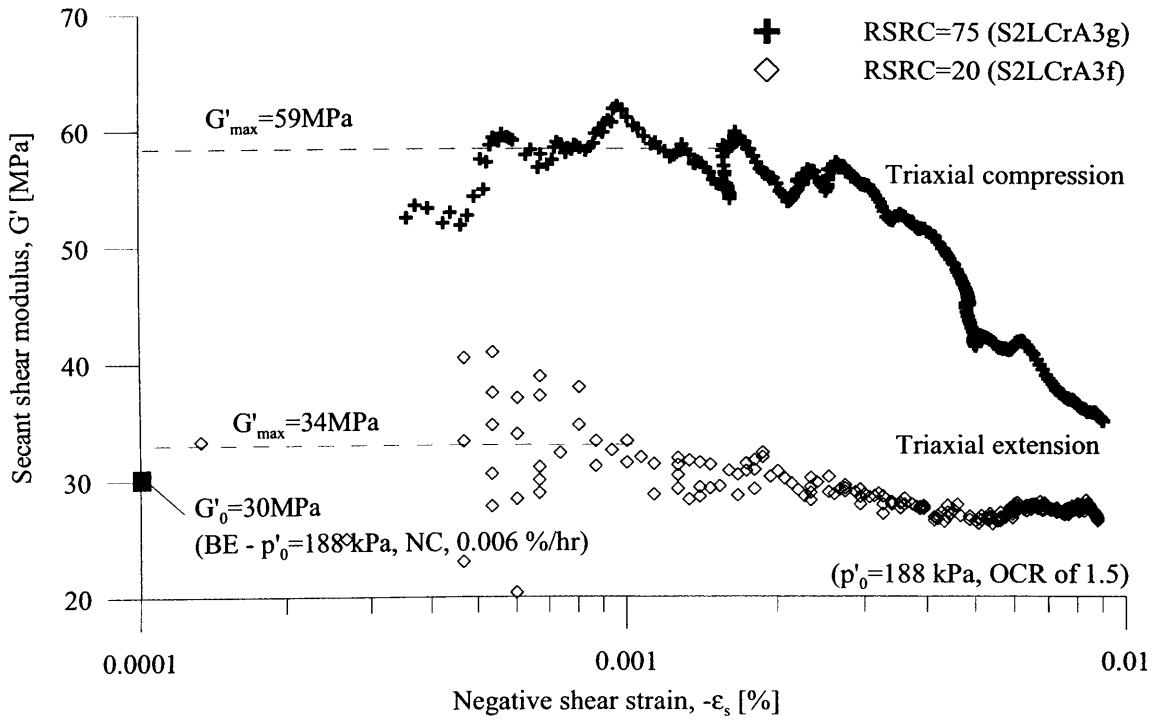

Figure 5-40 Influence of shear strain acceleration at small strains on secant shear stiffness in drained triaxial compression and extension of reconstituted London Clay

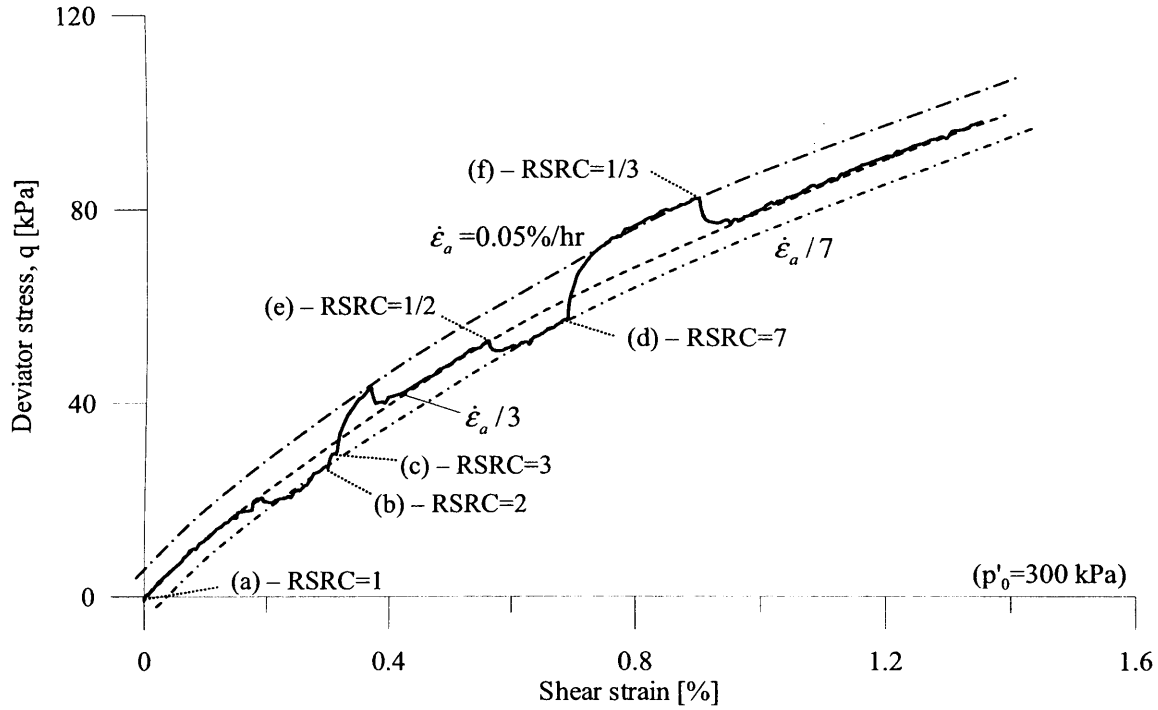

Figure 5-41 Influence of shear strain acceleration at large strains on the stress-strain path in drained triaxial compression of reconstituted London Clay (S2LCrA2)

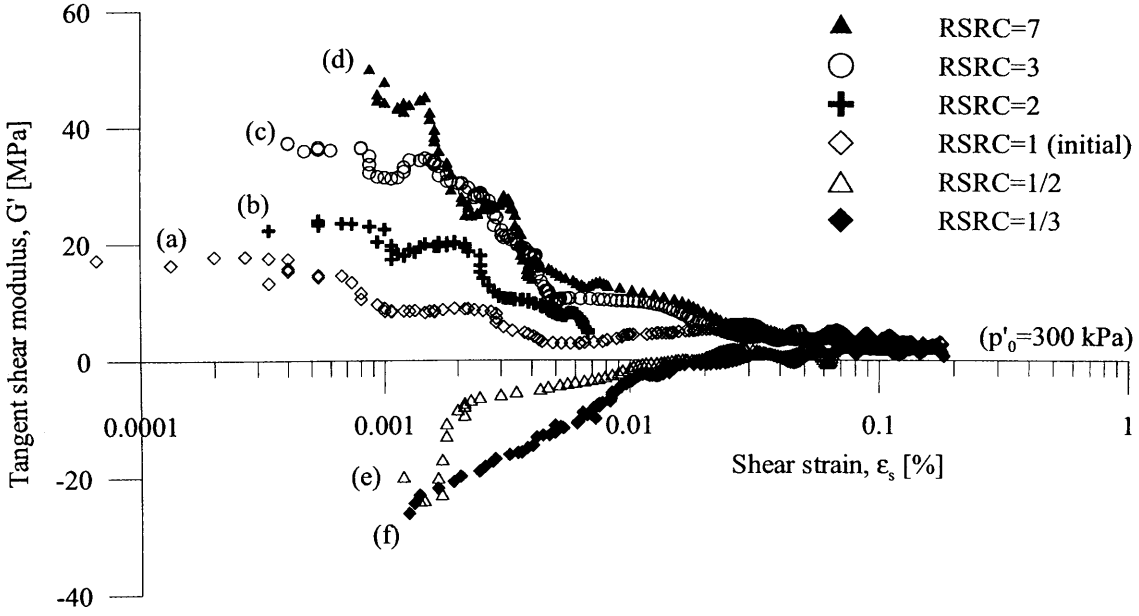

Figure 5-42 Influence of shear strain acceleration at large strains on the shear stiffness in drained triaxial compression of reconstituted London Clay (S2LCrA2)

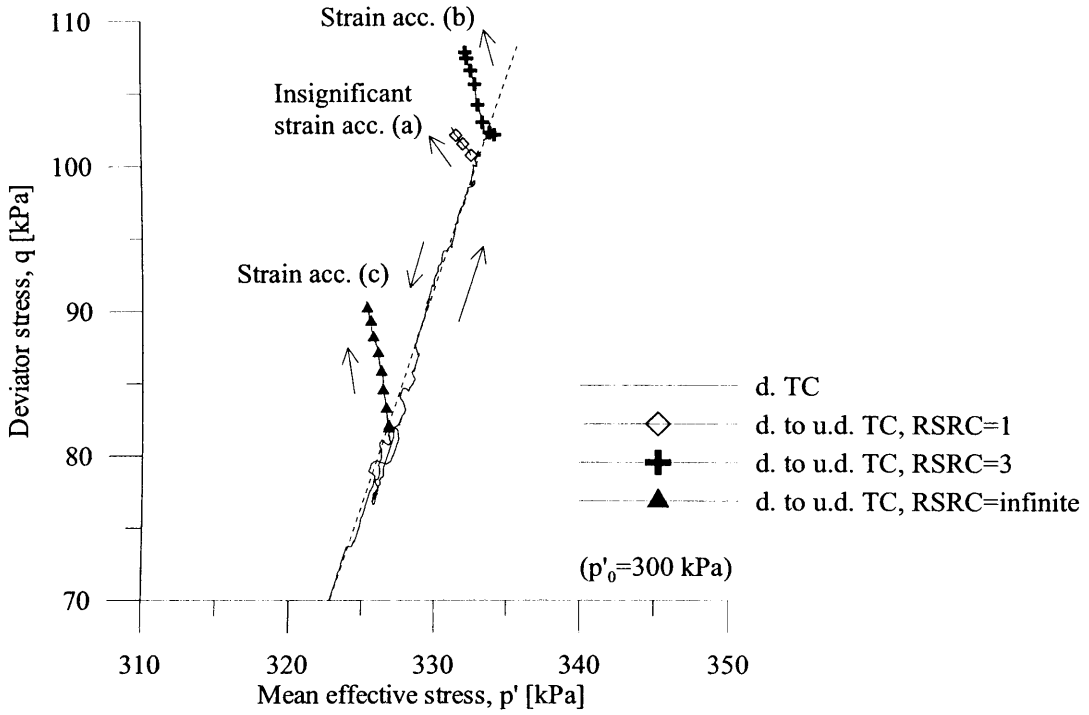

Figure 5-43 Influence of axial strain acceleration at large strains on the stress path when changing from drained to undrained triaxial compression of reconstituted London Clay (S2LCrA2a-c)

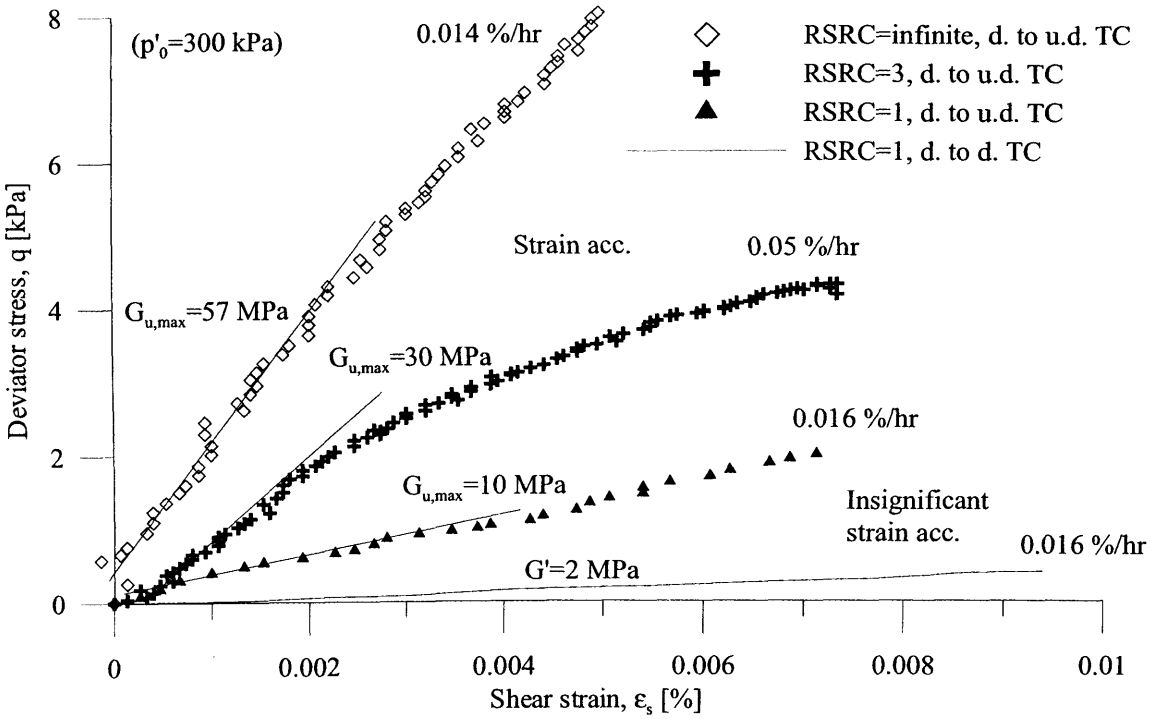

Figure 5-44 Influence of axial strain acceleration at large strains on the stress-strain path when changing from drained to undrained triaxial compression of reconstituted London Clay (S2LCrA2a-c)

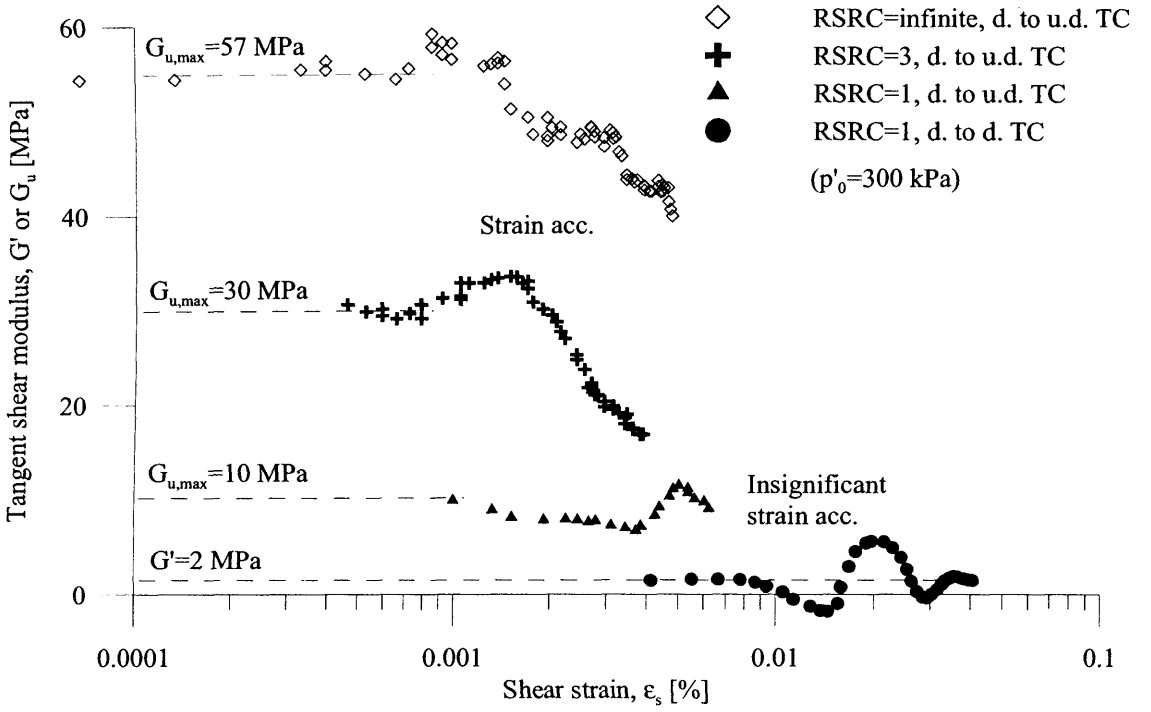

Figure 5-45 Influence of axial strain acceleration at large strains on the shear stiffness when changing from drained to undrained triaxial compression of reconstituted London Clay (S2LCrA2a-c)

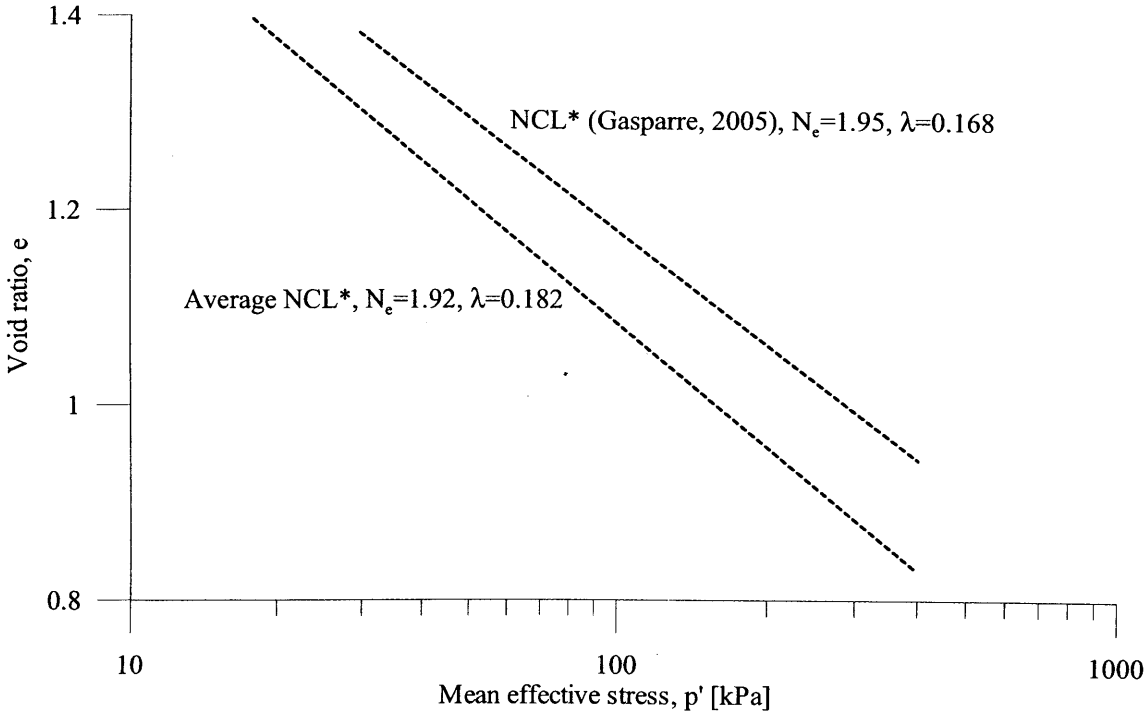

Figure 5-46 Comparison of the NCL* of reconstituted London Clay with data from literature

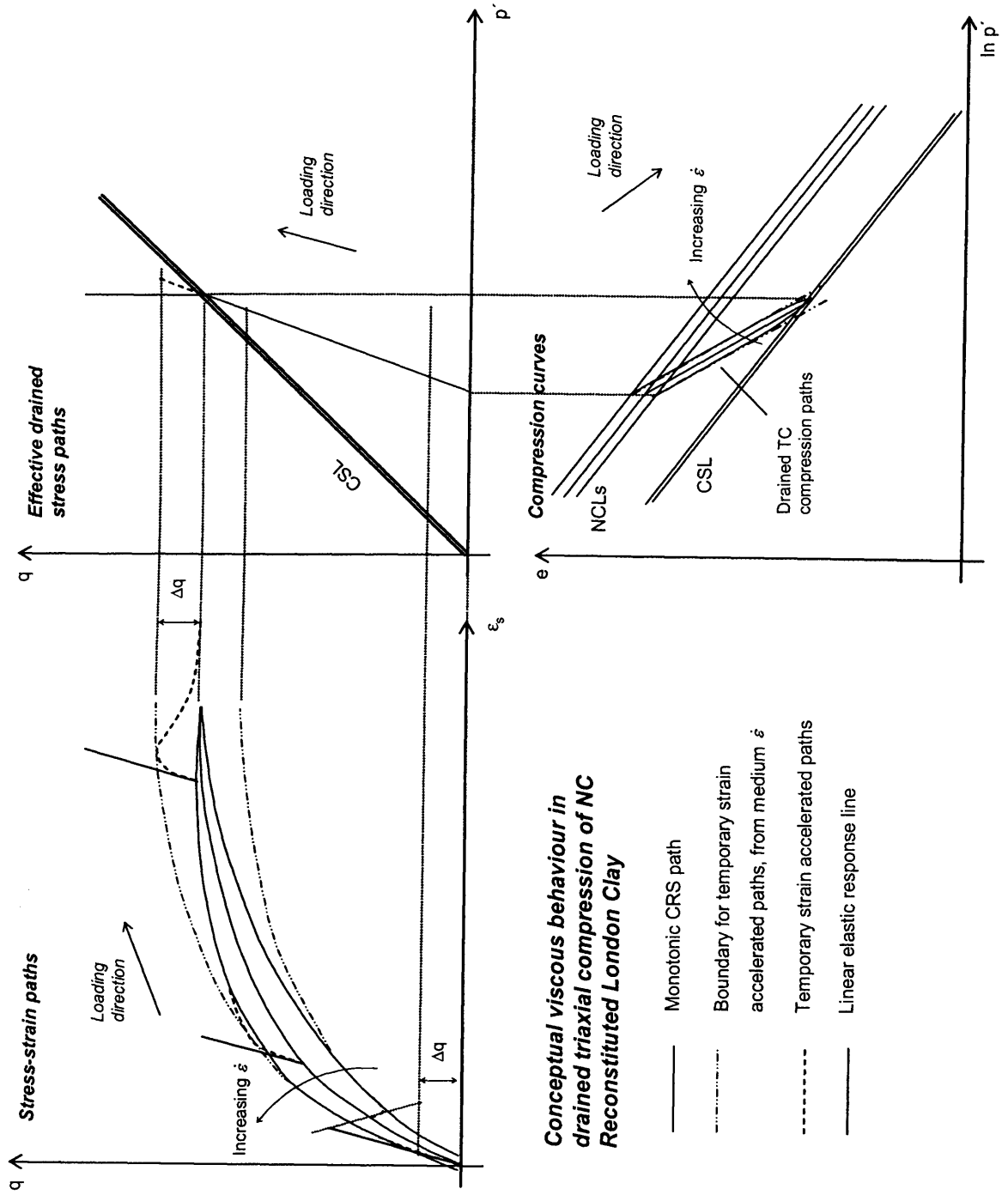

Figure 5-47 Schematic diagram of the viscous behaviour of reconstituted London Clay in drained triaxial compression – conceptual behaviour

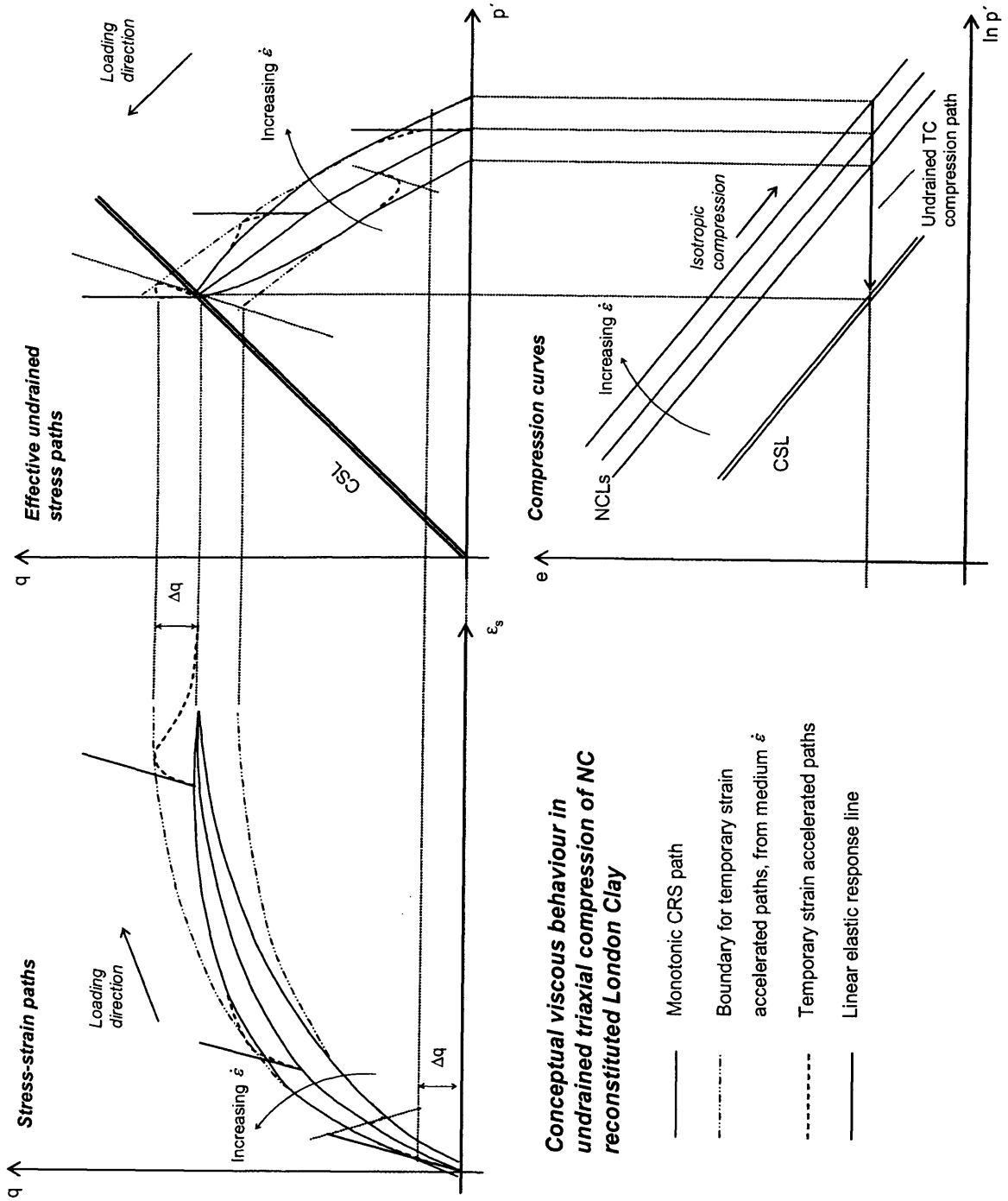

Figure 5-48 Schematic diagram of the viscous behaviour of reconstituted London Clay in undrained triaxial compression – conceptual behaviour

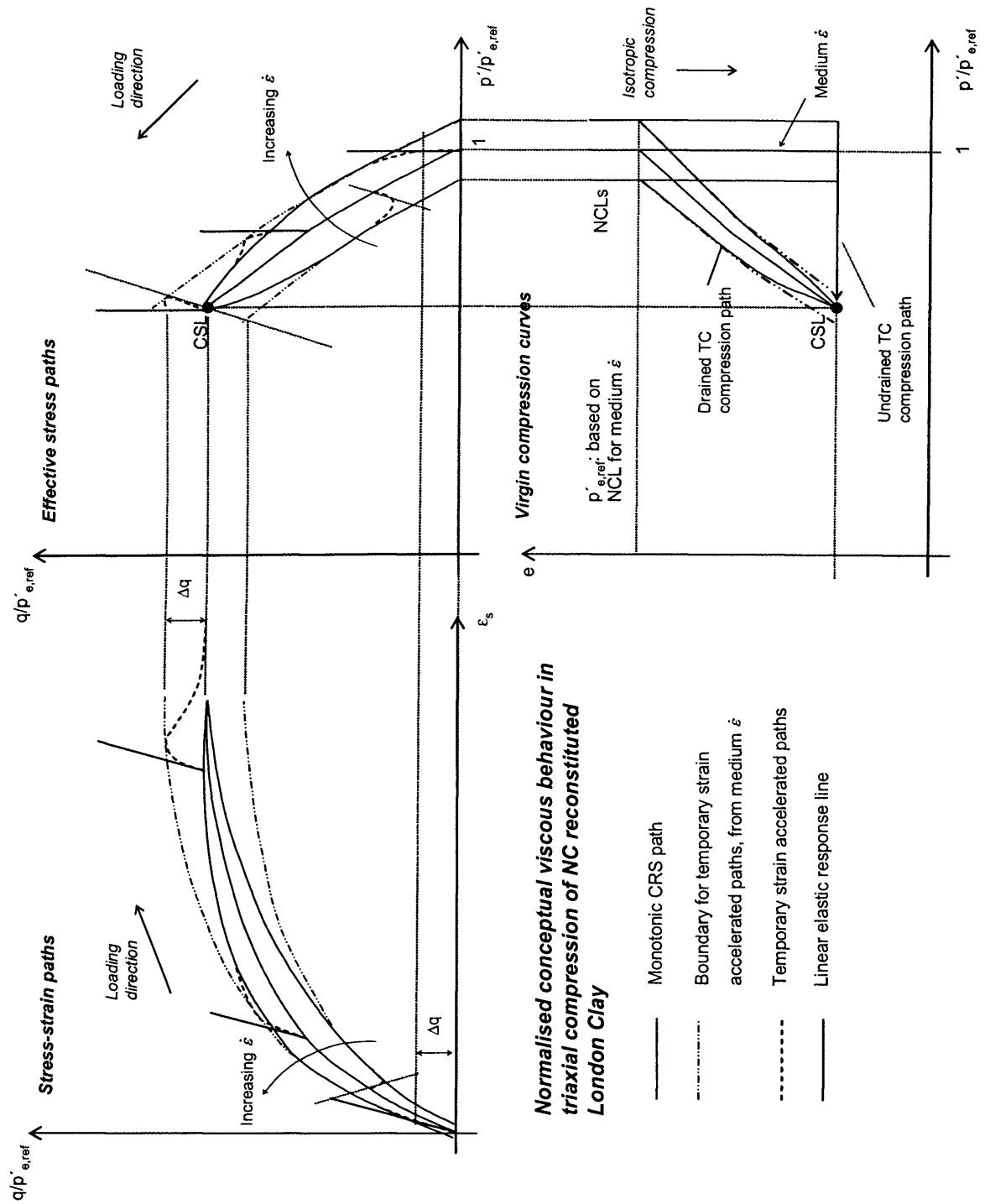

Figure 5-49 Schematic diagram of the normalised viscous behaviour of reconstituted London Clay in triaxial compression – conceptual behaviour

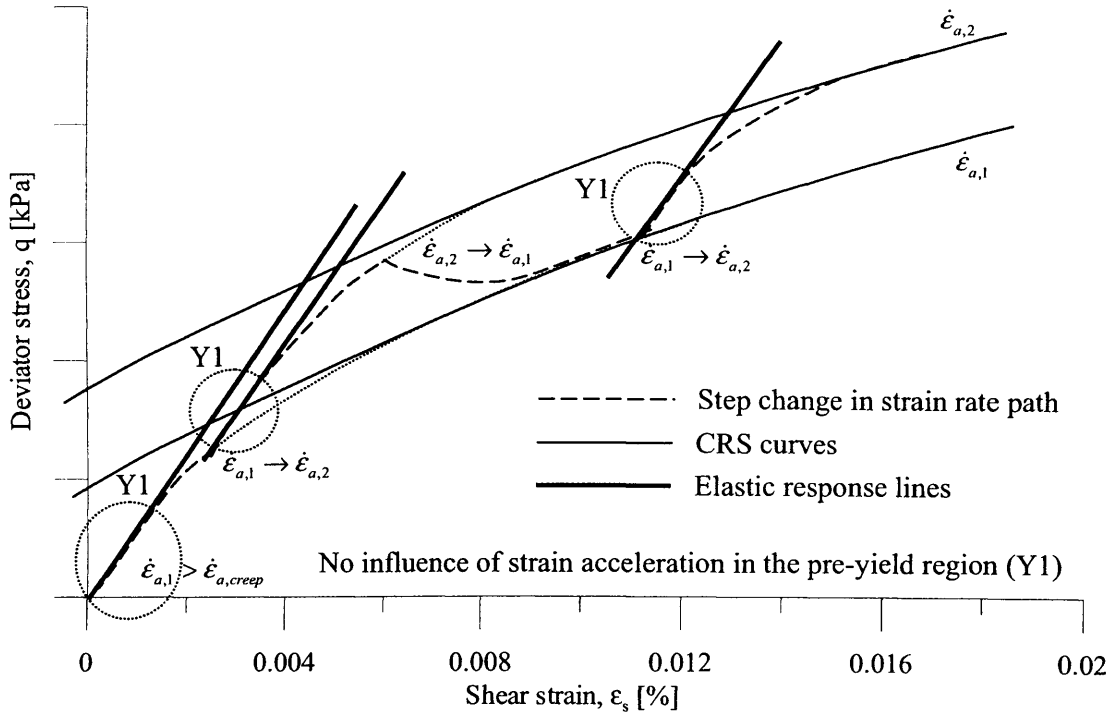

Figure 5-50 Schematic diagram of the influence of strain rate and strain acceleration on the stress-strain path in the pre-yield and small strain post-yield regions – conceptual behaviour

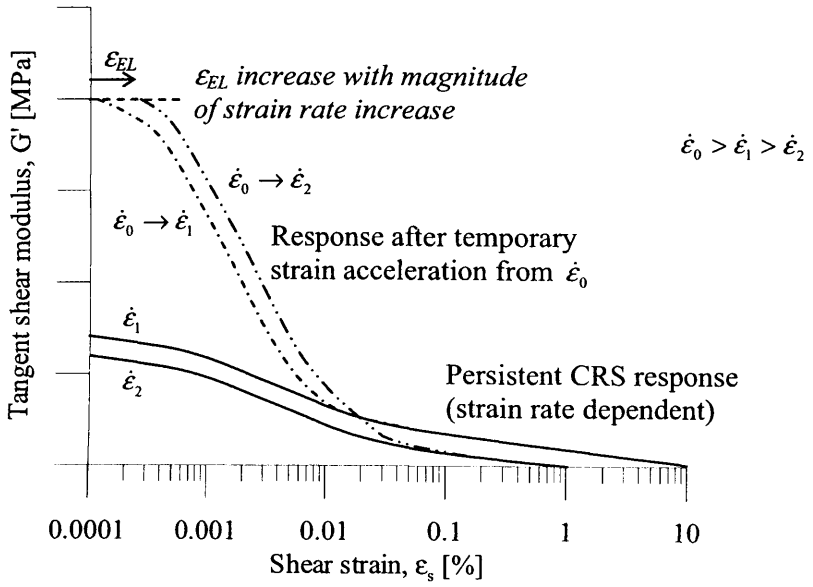

Figure 5-51 Schematic diagram of the influence of strain rate and strain acceleration on the stiffness degradation curve in triaxial compression of reconstituted London Clay – conceptual behaviour

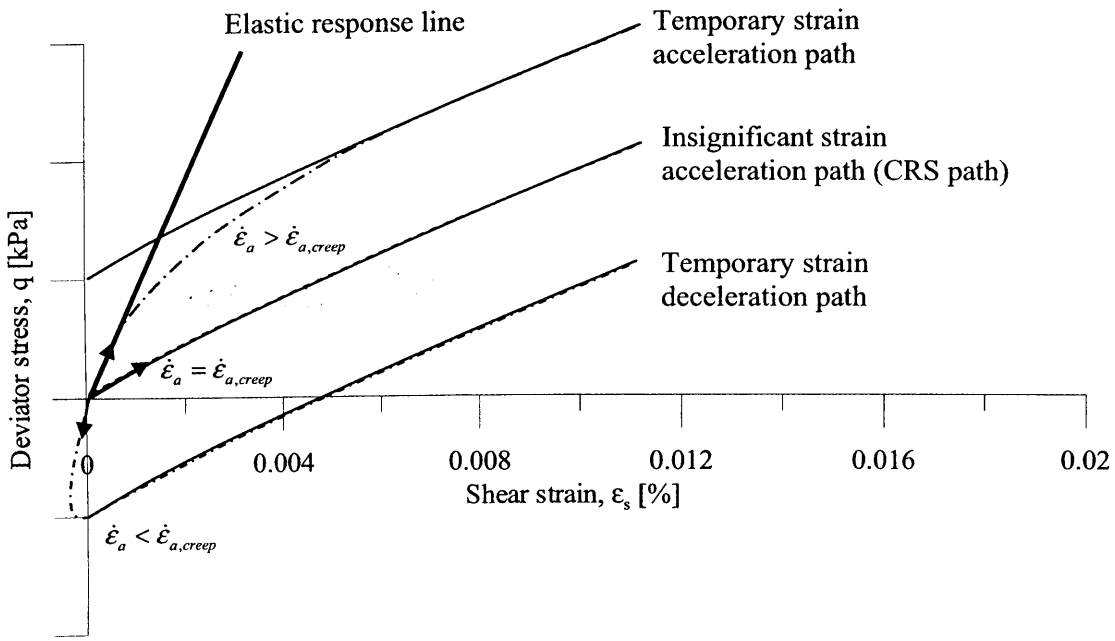

Figure 5-52 Schematic diagram of the influence of strain acceleration on the initial shearing path from isotropic stress state – conceptual behaviour

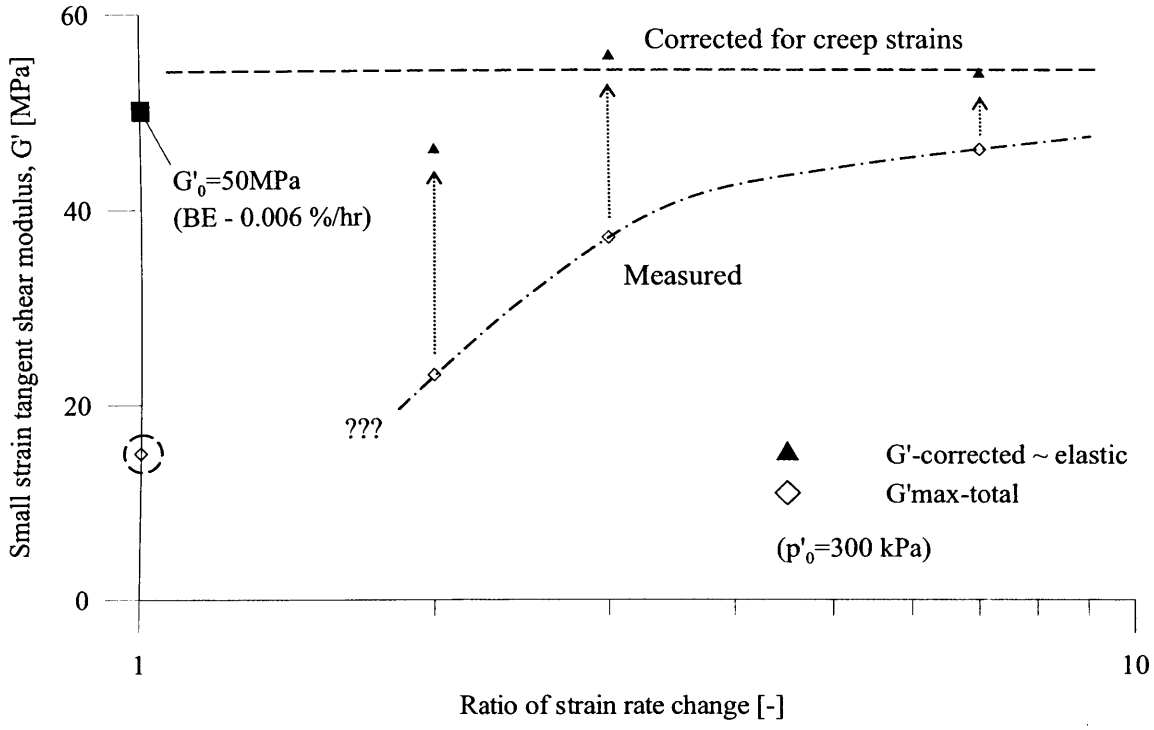

Figure 5-53 Influence of ratio of strain rate change on the small strain shear stiffness in drained triaxial compression of reconstituted London Clay (S2LCrA2)

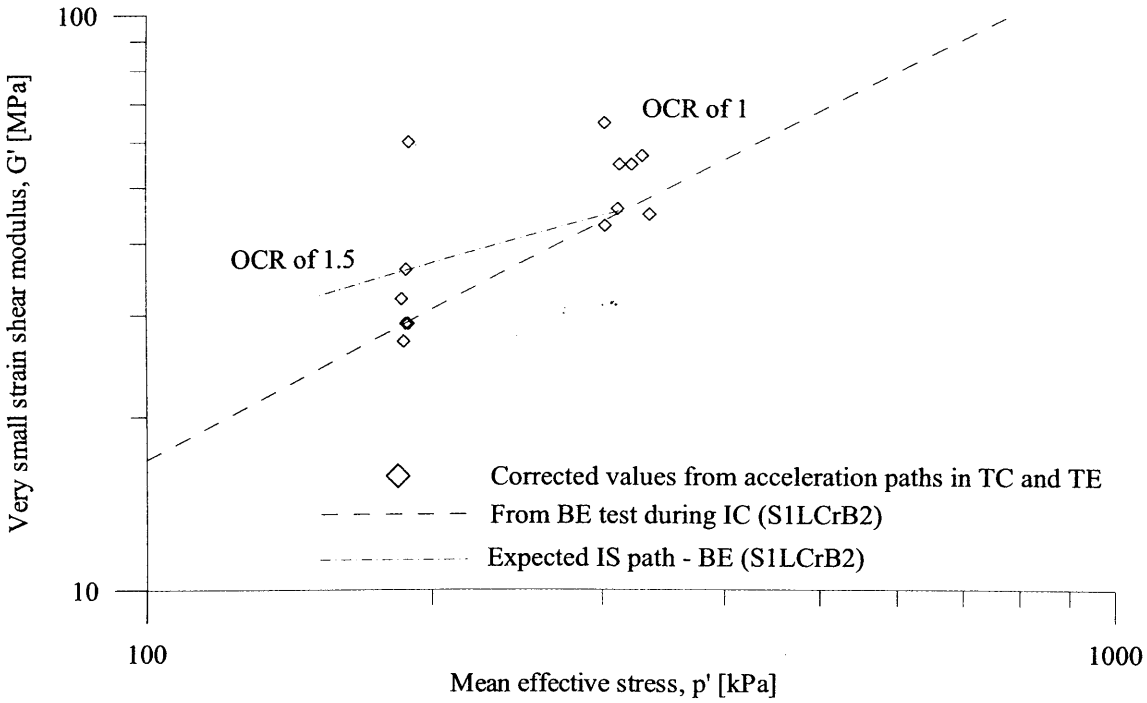

Figure 5-54 Comparing values of G'_0 corrected for creep strains in triaxial compression and extension with values of G'_0 determined from dynamic bender element tests during isotropic compression of reconstituted London Clay

CHAPTER 6 COUPLING OF AGEING AND VISCOUS EFFECTS IN TWO CLAYS

6.1 INTRODUCTION

This chapter describes part of the experimental research work, focusing on two complementary series of monotonic triaxial compression tests; one series of tests on artificially cemented kaolin and another series of tests on overconsolidated reconstituted and naturally structured specimens of London Clay. These tests were carried out to investigate the influence of structure, both natural and artificial, on the monotonic stress-strain behaviour and viscous behaviour of the tested clays. Section 6.2 reports on the influence of cementation and curing time on the monotonic behaviour of cement-mixed kaolin and the coupling of curing and viscous effects, while Section 6.3 reports on the observed influence of structure on the viscous behaviour of London Clay. The findings are finally discussed and compared to previous research in Section 6.4. Details of the geomaterials, testing equipment, general testing procedures and data analysis were given in Chapter 3.

6.2 COUPLING OF CURING AND VISCOUS EFFECTS IN CEMENT-MIXED KAOLIN DURING DRAINED TRIAXIAL COMPRESSION

6.2.1 Purpose and overview of study

This section reports on the observed influence of artificial cementation and total accumulated curing time on the monotonic behaviour of cement-mixed kaolin in drained shearing. The coupling of viscous and ageing (curing) effects and how they vary with the applied rate of strain and total curing time are investigated. The behaviour of artificially cemented kaolin has been compared to that of pure kaolin reported in the literature to establish the influence of artificial cementation on the monotonic behaviour of kaolin. The tests on cement-mixed kaolin were performed in the period 18th to 29th September 2003 in the Koseki laboratory at the Institute of Industrial Science, University of Tokyo, and details of the conducted triaxial tests have been summarised in Table 6-1.

6.2.2 Special testing procedures

In the following a brief description of the testing procedures is given. For clarity the procedures are also illustrated in Figure 6-1. A more detailed description of sample preparation and setup has been given in Section 3.4.4.

All the tested samples of cement-mixed kaolin were generally prepared by pre-compacting a dry mixture of kaolin clay powder and 3 % (by weight) Rapid Hardening Portland (RPH) cement. Subsequently, the samples were setup in the IIS type triaxial cell, isotropically compressed under dry conditions to a stress state of p'=100 kPa and finally saturated at this

state, apart from sample S0cmk, which was sheared dry to a deviator stress of q=100 kPa before saturation. Measured B-values and initial void ratios after saturation at the start of shearing are given in Table 6-1. It should be noted that due to the used method of sample preparation and saturation the obtained degree of saturation was expected to be somewhat less than one, which was also indicated by the measured B-values. Generally, after saturation, the samples were sheared to failure under fully drained conditions in triaxial compression. Hydration and curing of the cement was assumed to have initiated at the point of saturation. The curing time at a given state has therefore in the following been calculated as the total accumulated curing time from start of saturation, including time taken during testing. Any setting time of the cement has been ignored. To investigate the influence of accumulated curing time six samples (S2-5cmk & S9cmk) were sheared to the same stress state of q=210 kPa, at which point each sample experienced a prolonged constant effective stress creep period between 2 and 9 days. After the creep stage the samples were sheared to failure. A few supplementary tests were carried out to investigate the influence of stress state during curing. Two samples (S0cmk & S6cmk) were cured for one day during drained creep at lower (q=100 kPa) and higher (q=390 kPa) shear stress levels respectively. To investigate the coupled influence of axial strain rate and accumulated curing time, three additional samples (S7-8cmk & S10cmk) were sheared at three different constant rates of strain. The nominal axial strain rates were; 0.08 %/hr, 0.60 %/hr and 2.6 %/hr. In the majority of the tests small unload-reload cycles with a strain amplitude of about $\Delta\varepsilon_a$=0.02 % were performed to determine the small strain secant Young's modulus. Furthermore, as way to characterise the viscous behaviour, many of the samples were subjected to step changes in the axial strain rate during shearing. The nominal axial strain rate was generally varied step-wise between 0.08 %/hr, 0.60 %/hr and 2.6 %/hr, which gave ratios of axial strain rate changes of 1/8x, 1/4x, 4x, 8x and 33x.

6.2.3 Influence of artificial cementation and total curing time on the monotonic behaviour of cement-mixed kaolin in drained triaxial compression

a Influence of artificial cementation and curing time on monotonic behaviour

Figure 6-2 shows the influence of cementation and curing time on the monotonic stress-strain behaviour of cement-mixed kaolin. The plot compares the stress-strain behaviour of two cement-mixed samples (S5cmk and S7cmk) sheared at the same rate of strain from an initial isotropic stress state. Both samples followed the same initial shearing path. At q=210 kPa however, sample S5cmk experienced a drained creep period of 9 days (referred to as d. creep – 9 days in the figures) before continuing shearing, while sample S7cmk continued shearing without experiencing a period of rest (referred to as d. creep – 0 days in the figures). For comparison the stress-strain curve for a sample of pure kaolin is shown as well. The sample of pure kaolin (data from Komoto, 2004) was saturated at a stress state of p'=117 kPa and q=50 kPa before shearing along the same drained stress paths as the two samples of cement-

mixed kaolin. The equivalent axial strains that would have been experienced when sheared to q=50 kPa under saturated conditions have been estimated and used as the starting point of the stress-strain curve. Figure 6-3 and Figure 6-4 show the stiffness response after creep and volumetric response respectively for the two samples of cement-mixed kaolin.

Pure kaolin generally shows a ductile stress-strain behaviour, typical of an insensitive normally consolidated clay. The two samples of cement-mixed kaolin illustrate that as a result of adding just 3 % cement to the saturated kaolin a significant increase in both the stiffness and the peak strength is experienced. When sheared relatively quickly at early curing time the stress-strain behaviour of cement-mixed kaolin still appear to be predominantly ductile (S7cmk), showing strain-hardening to high strains. In contrast after a prolonged creep stage at fixed deviator stress, the initial response when shearing is resumed is seen to be very stiff (S5cmk). The subsequent stress-strain path clearly overshoots the original extrapolated path and reaches a significantly higher peak stress as a result of the created cement bonds at inter-particle contacts. It is furthermore observed that as the total curing time to failure increases distinct brittle behaviour develops with significant strain-softening experienced after reaching the peak strength at around 4 % axial strain. This is most likely caused by the breakage of the created cement bonds at large strains. With further straining in the post-peak region sample S5cmk appeared to reach a steady state with little change in volume and deviator stress (apparent critical state), while sample S7cmk continued to show strain hardening and contracting volumetric behaviour beyond an axial strain of 5 %, attributed to the significant curing effects still persisting.

b Influence of total curing time on peak strength and critical state strength

Figure 6-5 shows the influence of total curing time on the peak strength and critical state strength of cement-mixed kaolin. The plotted data have been obtained from all of the performed tests (in a few cases by means of extrapolation) on samples which have been cured at different stress states and experienced different loading histories. Note that in the figure for each of the tests the primary curing deviator stress level is shown in brackets. Interestingly, the post-peak critical state strength does not seem to be affected by ageing, and is unique for the soil mixture. In contrast the peak strength initially increases rapidly over the first day, to reach an apparent plateau of maximum strength. An average critical state strength of around 380 kPa (ϕ'_{cs}=40 degrees) is determined, which is significantly lower than the plateau of peak strength at around q=560 kPa (ϕ'_{peak}=47 degrees). This highlights the brittle nature of the samples for curing times greater than one day, the drop in strength being a result of the breakage of cement bonds at large strains. Both the critical state strength and peak strength of cement-mixed kaolin are seen to be significantly greater than the strength of pure kaolin, estimated to be around 130 kPa (ϕ'_{cs}=23 degrees) from the illustrated test in Figure 6-2. This highlights the positive effect of cement on the strength envelope and also indicates that cement-mixed kaolin after curing is

likely to be intrinsically different to pure kaolin. It has not been possible to confirm from the tests whether at low curing times the peak strength of cement-mixed kaolin approaches the peak strength of pure kaolin.

A few tests, marked by an arrow in Figure 6-5, experienced a rapid unload-reload cycle to a nearly isotropic stress state after curing at constant effective stress state (drained creep). These tests clearly show reduced peak strengths compared to the general trend, which is believed to be a result of the additional breakage of created cement bonds caused by the significant unloading event and the associated straining. It is also noted from the comparison of peak strengths for samples cured at different deviator stress levels (curing deviator stress shown in brackets in Figure 6-5) that the curing stress state appears to have had insignificant influence on the strength development.

c Influence of total curing time on monotonic stress-strain relationship

To investigate the general influence of total curing time on the stress-strain relationship, post-yield stress-strain points from all the performed tests on cement-mixed kaolin have been extracted for total curing times varying between 0.125-9.5 days. These are plotted in Figure 6-6 and stress-strain contours for fixed total curing times have been drawn. It can be seen from the plot that unique stress-strain relationships are found for different total curing times, not only the peak strength but the whole stress-strain curve is seen to evolve with total curing time during the first day of curing. For curing times greater than about 0.75-1 day however, the stress-strain relationship is seemingly unaffected by changes in curing time as further increase in curing time beyond this period of time does not appear to result in higher mobilised strength at given strain level. The figure also highlights that the threshold for ductile stress-strain behaviour is about 0.375-0.5 days of total curing time, at which point the peak strength equals the critical state strength. For total curing times greater than about 0.5 days the stress-strain behaviour is brittle showing significant strain softening after reaching a peak at around 4 % axial strain.

d Influence of total curing time on failure strain and shear banding

In Figure 6-7 the axial strain measured at the peak stress in all of the performed tests on cement-mixed kaolin has been plotted against the total curing time at failure. The plot shows that for curing times greater than about one day the peak stress is consistently reached at about 4 % axial strain, while at early curing times, where the stress-strain behaviour is predominantly strain hardening, failure occurs at much greater strains (test S1 is an exception for unknown reasons). Interestingly, it has been observed that samples S6cmk, S7cmk and S8cmk, which reached 4 % axial strain in less than a day, all developed multiple shearbands, while all other samples with curing times greater than one day showed only a single shear-plane post peak. It is hypothesized that for samples sheared quickly, the rate at which bonds are created in the failure zone will exceed the rate at which they are broken by the shearing action. It is possible that the dilation in the shear band will result in water being drawn in and the hydration of the cement

and strength development will therefore be greater in the shear band than in the remainder of the sample. As a result the first shearband, which develop around 4 % axial strain, regains strength and the failure plane is forced to relocate, requiring additional straining. On the other hand, in samples which have been cured for more than a day prior to reaching failure the curing rate is slow and these samples therefore fail on the first created shear plane at around 4 % axial strain.

The relationship between the recorded stress-strain behaviour and the observed shear banding for sample S6cmk is shown in Figure 6-8 as an example. The sample was sheared immediately after saturation at isotropic stress state and relatively quickly reached about 3.7 % axial strain. The irregular appearance of the curve is due to the changes in axial strain rate during shearing. As can be seen from the stress-strain curve in Figure 6-8a, an apparent peak stress at q=390 kPa (i.e. apparent failure) is reached around 3.0 % axial strain at which point straining continued with minor increase in the deviator stress (i.e. stiffness is almost zero). At the apparent peak state the sample was left to rest for 24 hours (drained creep) after which shearing resumed. Despite the high stress ratio, acceleration of strains and creep rupture did not occur during the period of rest. When resuming loading after the creep stage the initial stress-strain response is seen to be very stiff and with only further small straining a definite failure stress is reached at a stress level significantly higher than the initial apparent peak stress. Correspondingly, the sample was seen to develop two distinct shear planes, as shown by the photo in Figure 6-8b. Interestingly, an apparent peak plateau, located much lower than the final peak stress, was also observed in the constant rate of strain tests on sample S7cmk at around 4 % axial strain (Figure 6-2).

e Influence of total curing time on small strain stiffness

For the range of tests investigated the small strain secant Young's modulus E′ was derived from small unload-reload cycles of about $\Delta\varepsilon_a$=0.02 % at different stress states and different total curing times. Figure 6-9 shows the stiffness data plotted against the mean effective stress level p' at the start of each unload-reload cycle. The values of total curing time are given next to each data point. Viggiani & Atkinson (1995) showed that the very small strain shear modulus G'_0 of normally consolidated clays is dependent on the mean effective stress p' by the following relation;

$$G'_0 = A\left(\frac{p'}{p'_r}\right)^n \tag{6.1}$$

Where p'_r is a reference pressure used to make the expression dimensionally consistent, while the material parameters A and n are positive constants. The effective elastic Young's modulus E'_0 can be related to the elastic shear modulus G'_0 using Poisson's ratio ν';

$$E'_0 = 2(1+\nu')G'_0 \tag{6.2}$$

In Figure 6-9 it was assumed as a rough approximation that small strain secant Young's modulus of cement-mixed kaolin would be related to mean effective stress in a similar way, and

the relationship proposed by Viggiani & Atkinson (1995) was plotted, using a value of 0.2 for Poisson's ratio and coefficients A=1964 and n=0.653 determined for pure kaolin by Viggiani & Atkinson (1995) using a reference pressure p'_r=1 kPa. This first approximation, which can be assumed to correspond to the relationship for a total curing time of zero, plots as a straight line in lnE'-lnp' plot. The data points for short periods of curing (0.1 to 0.8 hour) plot close to the reference line based on Viggiani & Atkinson (1995). This shows that the first approximation is not as unreasonable as might have been expected. Data points for longer total curing times plot above the reference line, the further away from that line the longer the total curing time. Figure 6-10 shows the same data points normalised for stress with respect to the reference line. There is a clear linear increase in Young's modulus with the logarithm of total curing time. This suggests that there is a unique relationship between mean effective stress, total curing time and very small strain stiffness for normally consolidated cemented clays. However, unlike the previously shown relationship between curing time and peak strength or the entire stress-strain curve, the increase in small strain stiffness with curing time does not appear to cease after the first day of curing.

6.2.4 Coupled effect of strain rate and curing time on the monotonic behaviour of cement-mixed kaolin in drained triaxial compression

Figure 6-11 shows the influence of applied axial strain rate on the stress-strain response of cement-mixed kaolin specimens (S7cmk, S8cmk and S10cmk) in drained triaxial shearing from isotropically consolidated states. The three samples were initially sheared at an axial strain rate of 0.6 %/hr up to 0.2 % axial strain. At this point samples S8cmk and S10cmk experienced a sudden change in strain rate, while sample S7cmk continued shearing at the original rate of strain. The axial strain rate of sample S8cmk was reduced by a factor of 8 to about 0.08 %/hr, while sample S10cmk experienced an increase in axial strain rate by a factor of 4 to about 2.6 %/hr. Subsequently the samples were sheared to failure at the new constant rates of strain. The sudden change in strain rate at 0.2 % axial strain for samples S8cmk and S10cmk is seen to be associated with a significant change in stiffness, which persists until failure (Figure 6-12). Unlike typically seen behaviour of natural soils in drained tests the soil mixture reached higher strengths when tested at slower strain rates. It can also be observed that the behaviour gradually changes from being ductile to being brittle. This can be attributed to the large strain behaviour being driven by the curing effect rather than the viscous response of the soil structure; hence as the axial strain rate reduces the sample experiences an associated increase in curing time over a given strain interval and the stiffness and mobilised strength therefore increase as a result of the additional created cement bonds at inter-particle contacts.

A unique relationship between curing time and the stress-strain response was previously suggested from Figure 6-6. However, this relationship did not consider the influence of strain rate. To investigate further the coupled effect of strain rate and curing time, Figure 6-13 and

Figure 6-14 compare the stress-strain paths of different samples subjected to different strain histories. In Figure 6-13 the constant rate of strain path of sample S7cmk is compared to the stress-strain response of sample S6cmk, which was subjected to a more complex strain history with several changes in axial strain rate during shearing. Both samples were sheared from isotropically consolidated states. The stress-strain response of sample S6cmk to changes in axial strain rate is seen to be affected by both strain rate effects and curing effects. The immediate response to strain rate changes is dominated by the strain rate effect (viscous effect), hence an increase in axial strain rate is seen to give an immediate positive jump in deviator stress. With further straining however the response is rapidly overshadowed by the curing effect. As a result, with further straining the stiffness is seen to reduce and the stress-strain path moves below the extrapolated path given by the original rate of strain, similarly to what was observed in Figure 6-11 for different constant rates of strain. Interestingly, Figure 6-13 shows that despite completely different strain histories samples S6cmk and S7cmk reach the same stress state after shearing to the same strain level (~2.3 % axial strain) in the same total time (t = 270 min) when the shearing rates are the same (0.6 %/hr). This suggests that not only is the relationship between curing time and the stress-strain response unique, there appears to be a unique post yield stress-strain-strain rate-curing time relationship which is independent of strain history. The meeting of the two curves could have been a coincidence, but similar trend is observed when comparing samples S6cmk and S9cmk in Figure 6-14. Since the samples were cured at different stress states this again appears to indicate that the curing stress state or density state only has minor influence on the strength development. In the following the influence of cementation and curing on the viscous effects i.e. response to step-changes in strain rate in cement-mixed kaolin will be investigated.

6.2.5 Influence of artificial cementation on the viscous behaviour of kaolin in drained triaxial compression

By comparing the observed viscous behaviour of cement-mixed kaolin with the viscous behaviour of pure kaolin reported in the literature (Section 2.3.2a) the influence of artificial cementation on the viscous behaviour of kaolin can be established. It was shown above that at curing times shorter than 1-2 days the progressive curing of the cement significantly affected the stress-strain behaviour of cement-mixed kaolin, while at accumulated curing times longer than 1-2 days further curing was observed to only have minor effect on the stress-strain shearing behaviour. As a result it will be shown in the following that at short accumulated curing times the persistent effects of strain rate changes are overshadowed by the curing effect and only the immediate effects of strain rate changes can therefore be observed. At longer accumulated curing times on the other hand both persistent and temporary viscous effects are more easily observed and the complete viscous behaviour of the soil-mixture can therefore be characterised.

a Effect of step-wise change in strain rate on the stress-strain shearing path of artificially cemented kaolin

Figure 6-15 shows an example of the influence of step changes in the axial strain rate on the stress-strain curve of cemented kaolin at short curing time and low stress level. In the test a sample of cement-mixed kaolin (S9cmk) was sheared immediately after saturation at an isotropic stress state with step changes in the axial strain rate by a factor of 4. It is seen from the plot that the immediate effect of a axial strain rate increase is a significant increase in the deviator stress and vice versa a significant reduction in the deviator stress is seen after a strain rate reduction. This behaviour is consistent with the expected immediate viscous response of the soil structure as reported for London Clay. With continued straining however the soil-mixture shows a behaviour which is not typical of natural soils. The post yield persistent stress-strain path after an increase in the axial strain rate is seen to have a significant lower gradient (i.e. stiffness) than the gradient of the stress-strain path extrapolated for the original lower axial strain rate. As a result, the stress-strain path for the higher strain rate is seen to move below the stress-strain path for the slower strain rate. This atypical behaviour is due to the high rate of curing at short accumulated curing times. As the strain rate reduces the curing time at given strain level increases. This results in an increase in the stiffness at given strain level and hence the stress-strain path moves upwards. The curing effects therefore clearly overshadow the persistent effects of strain rate changes at short accumulated curing times, and it is therefore not possible to conclude at short accumulated curing times whether cement-mixed kaolin shows isotach or non-isotach viscous characteristics.

At long accumulated curing times, longer than about 1-2 days, the curing effects are on the other hand found to be negligible. This is exemplified in Figure 6-16. The plot shows the effect of axial strain rate changes on the final part of the stress-strain shearing path for sample S9cmk after 2 days of drained creep (i.e. curing) at a high deviator stress of q=210 kPa. The initial part of the stress-strain path at short curing times was described above. In contrast to the described behaviour at short accumulated curing times, at long accumulated curing times and large strains temporarily stress overshooting or undershooting of the persistent paths are observed after a step increase or a step reduction in the axial strain rate. As straining continues at a constant strain rate after the step change in strain rate, the stress-strain paths appear to approach a unique strain rate independent stress-strain curve. Hence, at large strains close to the peak state the viscous behaviour shows pure TESRA characteristics dominated by temporary effects, while the persistent effects of strain rate changes are insignificant.

From the performed tests it has not been possible to establish whether persistent effects of strain rate changes are significant at small strains and low stresses, since in all tests the curing effect overshadowed the persistent effects of strain rate changes at small strains. Nevertheless the viscous effect can be quantified over the full strain range by the total immediate stress jump, by assuming a minor influence of curing in the time period immediately before and after the

change in strain rate. As explained previously, the total immediate stress jump is the combined stress jump from persistent and temporary effects (defined in Figure 5-17). The total immediate stress jumps in deviator stress have been extracted from all the performed tests and plotted in Figure 6-17 against the reference deviator stress. Generally, the (total) axial strain rate was varied between three different rates of axial strain during shearing, which gave ratios of axial strain rate change of 1/8x, 1/4x,3x, 4x, 8x and 33x. The plotted data show a consistent increase in the stress jump with increasing stress level and increasing ratio of axial strain rate change. It can also be seen that a reduction in axial strain rate results in a negative stress jump with an absolute magnitude equal to or near the magnitude of the positive stress jump experienced when increasing the axial strain rate by the same ratio. For a given change in axial strain rate the jump in deviator stress is found to be, as a good approximation, proportional to the sum of the initial deviator stress and a constant value, q_0 of about 100 kPa. This results in linear lines with a common negative intercept (q=-100 kPa) on the x-axis and gradients that are influenced by the ratio of change in axial strain rate. However, results from the highest ratio of strain rate change (33x) at low stress levels are found to deviate a bit from this relationship, showing slightly higher stress jumps at low stress level. Since, the confining pressure used in the tests was kept at 100 kPa, it is suggested that the stress jump is better related to the magnitude of the vertical effective stress rather than the deviator stress, which is in agreement with findings by e.g. Tatsuoka et al. (2003) in triaxial tests on a wide range of non-cemented soils incl. sands, gravels and soft and stiff clays. Figure 6-18 shows the stress jump in the vertical effective stress, which equals the stress jump in deviator stress, plotted against the reference vertical effective stress level. As a result all the data points in Figure 6-17 have been shifted by 100kPa on the x-axis and now all the linear relationships are seen to intersect the origin. This appears to indicate that the viscous effect is a unique function of the principal effective stress. From Figure 6-19 it is shown that the ratio of stress change over stress level is more or less proportional to the logarithm of the ratio of strain rate change. The proportionality constant given as:

$$\beta = \frac{\frac{\Delta\sigma'_v}{\sigma'_v}}{\log\frac{\dot{\varepsilon}_{a,after}}{\dot{\varepsilon}_{a,before}}} \tag{6.3}$$

has a value of β=0.047, i.e. the vertical effective stress increase is about 5% per log cycle increase in the axial strain rate. The proportionality constant differs from the rate-sensitivity coefficient defined by Tatsuoka et al. (2003) (Equation 2.16) in that they defined the rate-sensitivity coefficient in terms of change in the plastic shear strain rate rather than the change in total axial strain rate as suggested here. However, since the radial strain rate in the performed tests was minor and the total strain rate approximately equals the plastic strain rate in the post yield region, the two different expressions will give similar results. It is seen that for cement-mixed kaolin the viscous stress jump in triaxial compression tests for any change in strain rate at

any stress level up until peak can be determined approximately by just one parameter. Based on the results, it appears that the accumulated curing time only has a minor influence on the viscous effect. It is uncertain what happens with the viscous effect post peak.

Interestingly, the plot in Figure 6-17 suggests that even at the start of shearing at q=0 kPa, there will be a significant influence of strain rate changes on the stress-strain path. Similar indications were also made in tests on reconstituted and intact natural samples of London Clay and the significance of this has been discussed in Sections 5.4.3 and 5.4.4.

b Influence of artificial cementation on the viscous behaviour of kaolin

This observed viscous behaviour of cement-mixed kaolin cured for 2 days is clearly in contrast to the Isotach viscous behaviour of pure kaolin, which has been reported in the literature over the full strain range until peak state (Tatsuoka et al., 2002). It can be deducted that artificial cementation has a significant effect on the viscous behaviour of kaolin. The tests suggest that the TESRA type viscous behaviour of artificially cemented kaolin at large strains close to the peak state may be a result of the presence of strong cementation in the soil mixture or the breakdown thereof. In Section 6.4.4c the findings are compared to the observed behaviour of other artificially cemented soils reported in the literature and the possible cause of the observed behaviour is discussed further in Section 6.4.5 by considering the influence of microstructure.

6.3 INFLUENCE OF STRUCTURE ON THE VISCOUS BEHAVIOUR OF LONDON CLAY IN TRIAXIAL COMPRESSION

6.3.1 Purpose and overview of study

Two triaxial tests were carried out on intact specimens of London Clay with the main purpose to characterise the influence of natural structure on the viscous behaviour and compare with the previously reported behaviour of the NC reconstituted London Clay (Section 5.2). Intact London Clay is heavily overconsolidated as a result of significant erosion events after deposition and moreover naturally structured from both sedimentation processes and post-sedimentation processes such as ageing. Therefore, an additional test on a sample of overconsolidated reconstituted London Clay was carried out to isolate the effect of mechanical overconsolidated on the viscous behaviour. The tests on intact and reconstituted overconsolidated specimens of London Clay were carried out in the period 4th May 2004 to 13th July 2005 in the geotechnical research laboratory at UCL. Details of the conducted triaxial tests have been summarised in Table 6-2.

6.3.2 Special testing procedures

In the following a brief description of the testing procedures is given. A more detailed description of sample preparation and setup is given in Section 3.4.3.

Two samples of intact heavily overconsolidated natural London Clay (S1LC and S2LC) were prepared by careful hand-trimming of the rotary cores. The rotary cores were obtained from the same depth in succession (13.95m-15.45m below ground level within the geological $B_{2(b)}$-sub-unit, Gasparre, 2005) and could therefore be assumed to be of similar nature. Additionally, a single overconsolidated reconstituted London Clay sample S2LCrA5(OC) was prepared from the second batch of reconstituted London Clay (refer to Section 3.4.3b) by means of preconsolidation. The reconstituted sample was preconsolidated in a consolidometer under a maximum vertical stress of about 1500 kPa, which is somewhat less than the assumed overburden pressure of around 2000 kPa for the intact sample of London Clay (refer to Section 3.2.3) . The three samples of London Clay used in this study were tested in (UCL) Triaxial cell no. 1, which utilised highly accurate miniature LVDTs for local axial and radial strain measurements. Following saturation in the triaxial cell the samples were subjected to isotropic compression. Similarly to the test method followed for the normally consolidated reconstituted samples, the samples were recompressed to a mean effective stress of approximately 300 kPa, corresponding to an overconsolidation ratio (OCR), defined as the ratio of the actual maximum preconsolidation pressure p'_c (equal to the overburden pressure for the intact sample) over the current mean effective stress p', of about 5 for the intact samples and an OCR of about 4 for the OC reconstituted sample (assuming a K_0 value of 0.64). Since the main interest concerned the shearing behaviour, the OC reconstituted and intact samples were rapidly compressed to

minimize the testing time. This meant that excess pore water pressures accumulated during isotropic compression, and the samples were hence allowed to rest for up to 6 days before commencement of shearing in order to allow the excess pore water pressures to dissipate. Measured *B*-values after saturation and initial void ratios at the start of shearing are given in Table 6-2. The high stiffness of the samples generally meant that the measured *B*-values were found to be lower than 1, and the listed values are therefore not necessarily indicative of a poor degree of saturation (Head, 1998). Apart from the first test on sample S1LC, which was compressed and sheared with a backpressure of 150 kPa, the backpressure was generally maintained at 300 kPa during compression and shearing. The samples were sheared in triaxial compression with step changes in the axial strain rate from the initial isotropic stress state of p'=300 kPa in order to characterise the viscous behaviour. The intact sample S2LC was sheared under nominal drained conditions, while the intact sample S1LC and OC reconstituted sample S2LCrA5(OC) were sheared undrained. Both undrained tests were taken to large strains beyond failure, while the more time consuming drained test (S2LC) experienced technical problems and was terminated prior to reaching the peak strength at around 2.7 % shear strain. Following shearing to large strains the OC reconstituted sample (S2LCrA5(OC)) was unloaded with step changes in the axial strain rate. The nominal axial strain rate was varied between 0.05 %/hr, 0.2 %/hr and 0.8 %/hr by a factor of up to 16 for sample S1LC, between 0.007 %/hr and 0.05 %/hr by a factor of up to 7 for sample S2LC and between 0.007 %/hr, 0.05 %/hr and 0.5 %/hr by a factor of up to 70 in testing on sample S2LCrA5(OC). Similarly to the tests on normally consolidated reconstituted samples the strain rates were chosen to allow full dissipation of pore pressures under drained conditions and full equalisation of pore water pressure under undrained conditions. In addition to the step-wise change in strain rate during shearing a limited number of small strain amplitude unload-reload cycles were performed in all three tests at different stress levels in order to get a feel of the magnitude of the elastic shear stiffness.

6.3.3 Influence of natural structure on the monotonic and viscous behaviour of London Clay in drained and undrained triaxial compression

The two tests on intact natural London Clay samples were carried out with step changes in the axial strain rate to characterise the viscous behaviour; more specifically to investigate the influence of strain rate on the stress-strain shearing path, stress path, volumetric strains in drained tests and accumulation of pore water pressures under undrained conditions. By comparing the viscous behaviours of normally consolidated reconstituted London Clay, reported previously in Section 5.2, and intact natural London Clay, the influence of the natural structure on the viscous behaviour of London Clay can be demonstrated. The results from the tests on samples S1LC and S2LC presented in the following show that similar trends are obtained in drained and undrained shearing over the tested strain range. However, before looking at the

influence of strain rate changes on the stress-strain behaviour, the influence of the natural structure of monotonic behaviour of the intact London Clay is described briefly in below.

a Influence of natural structure on the monotonic behaviour of London Clay

Generally, the observed monotonic behaviour of intact London Clay is typical of that of a one-dimensionally heavily overconsolidated structured clay. Figure 6-20 and Figure 6-21 show the undrained and drained stress-strain shearing paths of intact London Clay samples S1LC and S2LC respectively. From Figure 6-20 the monotonic stress-strain behaviour of intact natural London Clay is seen to be very brittle; after reaching a peak stress of approximately 500 kPa at around 2.9% shear strain, the deviator stress is seen to drop quite significantly to a value around 350 kPa at large strains. The brittle behaviour can primarily be attributed to the breakdown of natural structure such as bonding and cementation at peak state in addition to the partial alignment of particles on the shear plane at large strains. It should be noted that because of the development of a single plane shearband at peak state both the deviator stress and local strain measurements will be in slight error in the post peak region. As mentioned in Section 3.5.3c, the post peak deviator stress may be slightly underestimated, as no area corrections have been made for the single plane shearband. Nevertheless, the associated errors are believed to be of minor significance over the tested strain range and both the pre-peak and post-peak behaviour are characterised well in the figure. The corresponding undrained and drained shear stiffness degradation curves for samples S1LC and S2LC are shown in Figure 6-22 and Figure 6-23 respectively. A clear linear elastic range cannot be observed at very small strains due to a significant scatter in the results, however a maximum shear stiffness G'_0 in the region of 90 MPa to 110 MPa is indicated. The momentarily high stiffness jumps observed in the post-yield region at large shear strains result from the step increases in axial strain rate and the performed small unload-reload cycles and it is seen that the maximum values of these compare well with the initial high stiffness at very small strains. For step reductions in axial strain rate a comparable momentarily reduction in shear stiffness to negative values is experienced, however these data points have not been plotted.

Figure 6-24 shows the undrained stress path in a plot of q against p' for sample S1LC and the corresponding accumulation of pore water pressure with axial strain is shown in Figure 6-25. Unfortunately, errors occurred in the pore pressure readings and the stress path can only be shown up to a deviator stress of about 400 kPa. In Figure 6-24 the approximate location of the intrinsic critical state line (CSL*) is also shown, which was determined from the previously described tests on specimens of normally consolidated reconstituted London Clay. From the plot it is observed that the stress path of the intact London Clay initially moves to the left, as the sample tries to contract further under increasing stresses. Then the sample is seen to reach gross yield (Y_3) at a deviator stress around 330 kPa, at which point the dilative nature of the heavily overconsolidated sample starts to take effect. This results in a reversal of the stress path, as the pore water pressure starts to reduce with continued straining. The initial contractive and final

dilative nature of the intact London Clay is also shown from the evolution of volumetric strains during drained shearing of sample S2LC, which have been plotted in Figure 6-26. The stress path plot for sample S1LC furthermore clearly illustrates how the presence of natural structure enables the stress path for the intact clay to move notably above the CSL*. Intact London Clay will therefore have a significantly greater peak angle of shearing resistance (not possible to determine exact value) than the value determined for the reconstituted London Clay. To aid in the comparison, the stress paths for the intact samples have been normalised with respect to the equivalent preconsolidation pressure, p'_e determined from the average intrinsic isotropic normal compression line, NCL* given by Equation 5.1 for the current void ratio to remove effects of void ratio changes during drained shearing (Hvorslev, 1937). The normalised stress paths have been plotted in Figure 6-27. In the plot the stress paths for both samples of intact London Clay are seen to move well outside the intrinsic peak strength envelope (Hvorslev surface) given by (Gasparre, 2005), which illustrates the significant influence of natural structure on the peak strength envelope. Similar results for intact samples of London Clay were also obtained by (Gasparre, 2005).

b Effect of step-wise change in strain rate on the stress-strain behaviour of intact London Clay

In the two tests on specimens of intact London Clay the axial strain rate was changed step-wise to characterise the viscous behaviour. From both tests the viscous behaviour is generally observed to have distinct Isotach characteristics with persistent effects of strain rate changes on the stress-strain path, as seen in Figure 6-20 and Figure 6-21. Independently of strain history there appear to be a unique stress-strain curve for a given rate of (plastic) strain. Isotach characteristics are seen under both drained and undrained conditions and moreover appear at both small and large strains in the pre- and post-peak regions. The immediate response of intact London Clay to a step increase in the axial strain rate is observed to be very stiff and nearly elastic, followed by gradual yield. With continued straining the stress-strain path then approaches the persistent curve given by the new higher rate of strain without any signs of overshooting, which is the main characteristic of Isotach viscous behaviour. The influence of step-wise changes in the axial strain rate on the small to large strain stiffness degradation curve is shown in Figure 6-22 and Figure 6-23 for undrained and drained shearing respectively. Least scatter in the results was obtained for undrained shearing of sample S1LC, as shown in Figure 6-22. From the plot it can be observed that the persistent effects of strain rate changes on the shear stiffness appear to be negligible at large strains. On the other hand, as shown more clearly from Figure 6-23, immediately after step increases in the axial strain rate the stiffness is seen to increase significantly towards the initial elastic value. The stiffness derived from small strain amplitude unload-reload cycles at large strains is similarly seen to reach maximum values, which appear to correspond quite well with the initial high (very) small strain shear modulus.

The viscous behaviour in both drained and undrained shearing has been quantified in Figure 6-28. For isotach viscous behaviour the total immediate stress jump (defined in Figure 5-17) equals the persistent stress jump, since temporary effects of strain rate changes are non existent. In Figure 6-28 the absolute persistent stress jump in deviator stress is plotted against the reference deviator stress level for both positive and negative step changes in the axial strain rate. Results have been obtained and plotted for ratios of axial strain rate changes of 4 and 16 times during undrained shearing (sample S1LC) and for a ratio of axial strain rate change of 7 times in drained shearing (sample S2LC). Results obtained from the post-peak region in undrained shearing are also included on the figure. It can be observed that for a given ratio of strain rate change the stress jump increases consistently with stress level towards the peak state. The drained test on sample S2LC indicates an exponential increase in the stress jump with increasing stress level, while results from the undrained test on sample S1LC indicate approximate linear relationships over the limited stress intervals. In the pre-peak region the stress jump at given deviator stress increases consistently with increases in the ratio of strain rate change and the results from the drained and the undrained tests are seen to compare well. In undrained shearing the stress jump is found to more or less double as the ratio of axial strain rate change is increased from 4 to 16 times. Hence, in agreement with the findings for the reconstituted samples of London Clay (Section 5.2.4e) and findings made in previous research e.g. Tatsuoka et al. (2003) it is suggested that the stress jump at given deviator stress level increases linearly with increases in the logarithm of the ratio of axial strain rate change (can be realised by considering that $\ln\left(\frac{\dot{\varepsilon}_{a,after}}{\dot{\varepsilon}_{a,before}}\right)=\ln(16)=\ln(4^2)=2\cdot\ln(4)$). The influence of stress level on the stress jump for intact London Clay is however in marked contrast to the stress level independency shown for reconstituted London Clay (Figure 5-19) and the linear relationship observed between stress jump and stress level in artificially cemented kaolin (Figure 6-17). From the results in Figure 6-28 it also seen that in the post peak region the stress jump reduces rapidly with reducing stress level as the sample approaches an assumed critical state. It can be deducted that the peak strength is significantly affected by the strain rate, while on the other hand the critical state strength at large strains seems to be much less affected or possibly not affected at all.

Visible persistent effects of strain rate changes are also observed on the undrained stress path and the accumulated pore water pressure response, as shown in Figure 6-24 and Figure 6-25 respectively. The pore water pressure at a given strain level is found to increase with an increase in the axial strain rate, which somehow contradicts the expected behaviour. Since, the behaviour is contractive over the initial part of the tested strain range, higher pore water pressures could have been expected to develop at reducing strain rates, because at given strain level more time would have been allowed for positive volumetric creep strains to develop, which would have been compensated by an increase in the pore water pressure. The strain rate

dependency of the pore water pressure will shift the stress path to the left with increasing strain rates. This however is not clearly observed, as it is overshadowed by the strain rate dependency of the deviator stress, which results in a significant upwards shift in the stress path with increasing strain rates (Figure 6-24). For this reason the stress path appears to move to the right with increasing strain rates during the initial contractive behaviour and then at gross yield it shifts over and subsequently appears to move to the left with increasing strain rates when the behaviour is dominantly dilative. It can be deducted that the strain rate dependency of the deviator stress is a controlling factor, which means that the mobilised effective strength also increases with increasing strain rates. Interestingly, in contrast to the observed influence of strain rate on the accumulation of pore water pressure in the undrained test, the evolution of volumetric strains against shear strains in the drained test is indicated to be independent of strain rate and strain rate changes, as shown in Figure 6-26.

c Influence of natural structure on the viscous behaviour of London Clay

The heavily overconsolidated nature of intact London Clay and the presence of natural structure is seen to have affected the monotonic behaviour of the intact soil quite dramatically; the size of the yield and strength envelopes are noticeably increased, which allows the structured soil to move outside the SBS* given by the reconstituted material and moreover the stress-strain behaviour is characterised by being distinctly brittle in contrast to the ductile behaviour of the NC reconstituted London Clay. However, not only does the natural structure affect the monotonic behaviour it is also seen to have significant effect on the viscous behaviour of London Clay. Similarities and differences in the viscous behaviours of intact and NC reconstituted London Clay have been summarised in Table 6-3. The Isotach viscous characteristics of intact London Clay clearly contrasts the previously reported viscous behaviour of NC reconstituted London Clay (Section 5.2), which was characterised by Isotach behaviour at smaller strains and increasing temporary effects of strain rate changes at larger strains towards failure. For the intact London Clay persistent effects of strain rate changes were observed on both the peak strength envelope and the pore water pressure in undrained tests, while the shear stiffness and volumetric strains against shear strain in drained tests appeared to be independent of the applied strain rate. This was in marked contrast to the observed strain rate dependent shear stiffness and strain rate independent critical state strength envelope and pore water pressure response in the tests on specimens of NC reconstituted London Clay. Nevertheless, both intact and NC reconstituted samples showed similar strain rate independent behaviour with regards to the volumetric response against shear strain, which seem to indicate that the (axial) strain rate and strain rate changes affect the volumetric strain and shear strain equally. A general feature that could also be observed in the tests was the immediate very stiff response followed by gradual yield after step increases in the strain rate. Despite differences in the variation of the combined persistent and temporary viscous stress jump with stress level, samples of intact and reconstituted London Clay are generally characterised by a linear

relationship between the viscous stress jump and the logarithm of the ratio of strain rate change at given stress level.

Based on the comparison between intact and NC reconstituted London Clay samples it was not possible to deduct whether the observed differences in viscous behaviours could be attributed solely to the presence of natural structure, such as bonding and cementation in the intact soil, or if the heavily overconsolidated nature of the intact samples could have had an influence too. In order to clarify this, the viscous behaviour of a single overconsolidated sample of reconstituted London Clay was subsequently investigated. The findings from this test are reported in the following, which makes it possible to identify and separate the influences of natural structure and mechanical overconsolidation on the viscous behaviour of London Clay.

6.3.4 Influence of mechanical overconsolidation on the monotonic and viscous behaviour of London Clay in undrained triaxial compression

a Influence of mechanical overconsolidation on the monotonic behaviour of London Clay

Generally, the observed monotonic behaviour of OC reconstituted London Clay is typical of that of an isotropically heavily over consolidated non-structured clay. The isotropic recompression curve to p'=300 kPa of the OC reconstituted sample is shown in Figure 6-29 along side the intrinsic normal compression line (NCL*) determined from the previous reported isotropic compression tests on reconstituted samples of London Clay. The recompression path is initially seen to be very stiff, followed by gradual yielding as it approaches the NCL*. A clear point of yielding cannot be observed. It should be noted that the compression curve is expected to be somewhat in error because of the accumulation of non-recorded pore water pressures during the rapid compression, which is also indicated by the significant change in void ratio during the final resting period. The indicated final state after dissipation of excess pore water pressures can however be assumed to be correct. From Table 6-2 the final void ratio after recompression of the OC reconstituted sample is seen to correspond quite well with the void ratios obtained at the end of recompression for the intact samples of London Clay. This confirms that the preconsolidation pressure used to preconsolidate the reconstituted sample is of similar magnitude to the maximum pressure experienced in situ by the intact soil.

The stress-strain curve obtained from the subsequent undrained shearing is shown in Figure 6-30. From the plot the behaviour is seen to be predominantly strain hardening with only a slight tendency of reducing strength after reaching an apparent peak strength of approximately q=300 kPa at around 5% shear strain. It should be noted that the sample showed sign of bulging during shearing and the development of a shear band was not observed. The associated shear stiffness degradation curve for sample S2LCrA5(OC) is shown in Figure 6-31. A clear linear elastic range cannot be observed at very small strains due to a significant scatter in the results, however a maximum shear stiffness $G_{u,0}$ in the region of 40 to 60 MPa is indicated, which is lower than expected, as similar values were found for NC reconstituted samples of London Clay.

Part of the significant difference in the values of $G_{u,0}$ for samples of OC reconstituted and intact OC London Clay can be explained by the presence of structure in the intact soil, since the initial void ratio-stress states are similar. Figure 6-32 shows the undrained stress path in a plot of q against p' and the corresponding accumulation of pore water pressure with shear strain is shown in Figure 6-33. In Figure 6-32a the approximate location of the intrinsic critical state line (CSL*) is also shown, which was determined from the previously described tests on specimens of normally consolidated reconstituted London Clay. The heavily overconsolidated nature of the sample is clearly expressed in these plots. As the sample initially tries to contract further under increasing stresses the pore water pressure rapidly increases and as a result the stress path moves to the left. At a shear strain of around 1.5 % and deviator stress of about 160 kPa the sample is seen to reach gross yield (Y_3) at which point the dilative nature of the heavily overconsolidated sample starts to take effect, similarly to what was observed for the intact OC samples. As the pore water pressure begins to reduce with continued straining the stress path then reverses and subsequently moves to the right until the sample reaches failure close to the CSL*. At large strains the pore water pressure appears to stabilise, indicating a critical state is reached. The maximum rate of dilation can be assumed to correspond to the point of maximum rate of pore water pressure reduction. As seen from Figure 6-33 this occurs at a shear strain of about 5 %, which agree well with the peak strain. Generally, both the proximity of the peak state to the CSL* and the strain hardening behaviour indicate the lack of structure in the OC reconstituted sample in contrast to the intact OC samples. In order to compare the monotonic stress path of the OC reconstituted sample with the NC reconstituted behaviour the stress path was normalised with respect to an equivalent pressure p'_e on the average isotropic NCL* determined from Equation 5.1 to remove the effect of void ratio. The normalised stress path shown in Figure 6-34 agrees well with the intrinsic state boundary surface determined by (Gasparre, 2005). However there are some discrepancies between the critical state indicated by the NC reconstituted samples and the OC reconstituted samples from this study, which may be due to a true critical state not being reached in either of the tests and/or due to errors in the determination of the void ratio.

b Effect of step-wise change in strain rate on the stress-strain behaviour of OC reconstituted London Clay

In the test on OC reconstituted London Clay the axial strain rate was changed step-wise between three different rates to characterise the viscous behaviour. As will be reported in the following the viscous behaviour of OC reconstituted London Clay is in some respects similar to the viscous behaviour of intact London Clay and in other respects similar to the viscous behaviour of NC reconstituted London Clay. Similarities and differences in the viscous behaviours of intact, NC reconstituted and OC reconstituted London Clay have been summarised in Table 6-3. The undrained stress-strain curve is shown in Figure 6-30a alongside the extrapolated persistent curves for the three applied rates of strain, as shown with stippled lines. Figure 6-30b on the

other hand illustrates the stress-strain boundary curves for the temporary effects for the highest and lowest rates of applied strain. It is observed from the figures that OC reconstituted London Clay shows isotach viscous characteristics up to a shear strain of about 1%. Beyond this strain level increasing temporary effects of strain rate changes are observed to occur towards failure, as seen from the over- and undershooting of the persistent curves in Figure 6-30a. The effects of strain rate changes on the stress-strain curve are hence very similar for OC and NC reconstituted samples of London Clay. As has been generally observed in the previous tests, the immediate response of step increases in the axial strain rate is found to be very stiff and nearly elastic, followed by gradual yield. Both the temporary boundary curves and the persistent paths are seen to separate towards the peak state, while there are some indication that the persistent paths may approach each other in the post peak region as the strength reduces towards a critical state. Nevertheless, the peak strength is clearly influenced by strain rate, a phenomenon which was also seen for the intact samples. If it is assumed that a critical state was reached at the end of the test, as was indicated by the stabilisation of the pore water pressure response, it appears that the critical state strength may be independent of strain rate, similarly to what was shown in the test on NC reconstituted London Clay. As seen from the stiffness degradation curve in Figure 6-31, after each step increase in axial strain rate the stiffness experiences a significant temporary increase, which then reduces rapidly with further straining. Due to a large scatter in the data it is however not clear if there are any persistent effects of strain rate changes on the intermediate and large strain shear stiffness.

The viscous behaviour in undrained shearing of the OC reconstituted sample has been quantified in Figure 6-35 by the total immediate and persistent viscous jump in the deviator stress respectively (defined in Figure 5-17). In the plot the absolute values of the viscous stress jump have been plotted against the reference deviator stress level for both positive and negative step changes in the axial strain rate. Data have been plotted for a ratio of strain change of 70 times during shearing. At low stress level the total immediate and the persistent stress jumps are of similar magnitude, since the viscous behaviour has Isotach characteristics with only minor temporary effects of strain rate changes. At higher stress levels the temporary effects increase, while the persistent effect appear to be unaffected by stress level for a given ratio of strain rate change until peak strength. No data has been obtained after peak strength, but the stress-strain curves do indicate a reduction in the persistent stress jump towards the critical state. A consistent increase in the total immediate stress jump with stress level is indicated, unlike what was seen for NC reconstituted London Clay (Figure 5-19). The total immediate stress jumps for different ratios of strain rate change, have been determined from the test on OC reconstituted London Clay and plotted against stress level in Figure 6-36. In the plot the stress jump is seen to increase consistently with increasing ratios of strain rate change. For a ratio of axial strain rate change of 7 times an approximate linear increase in the stress jump with increasing stress level is observed, while for higher ratios of strain rate change simple linear relationships do not fit the

data well. The observed stress level dependency of the stress jump is found to be similar to that observed in intact samples of London Clay in the pre-peak region, but clearly contrasts the stress level independency shown in reconstituted London Clay. From Figure 6-36 the stress jump is found to more or less double as the ratio of axial strain rate change is increased from between 7 and 10 times to 70 times. This again suggests that the stress jump at given deviator stress level increases linearly with increases in the logarithm of the ratio of axial strain rate change (can be realised by considering that $\ln\left(\frac{\dot{\varepsilon}_{a,after}}{\dot{\varepsilon}_{a,before}}\right) = \ln(70) \approx \ln(8^2) = 2 \cdot \ln(8)$), as also found in NC reconstituted and OC intact London Clay.

Temporary and persistent effects of strain rate changes are also observed on the undrained stress path and the accumulated pore water pressure response, as shown in Figure 6-32 and Figure 6-33 respectively. The pore water pressure at a given strain initially shows a sharp increase with an increase in the axial strain rate; in the contractive range this increase appear to be persistent, similar to the intact London Clay behaviour, while in the dilative range much of the increase appears to be only temporary, as was seen for NC reconstituted London Clay. At large strains the persistent pore water pressure response is indicated to be unaffected by the axial strain rate. As discussed for the intact samples, in contrast to the findings, the pore water pressure would have been expected to be higher for the slowest rate of strain in the contractive range and lower in the dilative range. It is not clear why this is not observed, but is possible that the stiff behaviour of the soil in the initial contractive range does not allow significant plastic creep strains to develop and the pore water pressure response is then primarily controlled by the elastic response of the soil structure. From the stress path plot it can be seen that the strain rate dependency of the pore water pressure is overshadowed by the strain rate dependency of the deviator stress, which results in a significant upwards shift in the stress path with increasing strain rates. For this reason the stress path appears to move to the right with increasing axial strain rates during the initial contractive behaviour and then at gross yield it shifts over and subsequently appears to move to the left with increasing axial strain rates when the behaviour is dominantly dilative, similarly to the observed behaviour of intact OC London Clay. It can be deducted that there is an increase in the effective mobilised strength with increasing strain rates at given strain level, as has also been generally observed in test on both NC reconstituted and intact OC London Clay.

c Separating the influences of natural structure and mechanical overconsolidation on the viscous behaviour of London Clay

The influence of strain rate changes on the stress-strain behaviours of NC reconstituted, OC reconstituted and intact OC London Clay have been reported in Sections 5.2, 6.3.4 and 6.3.3 respectively. It can be concluded that the viscous characteristics of London Clay are significantly affected by the presence of natural structure from post-sedimentation processes

like bonding and cementation, while mechanical overconsolidation appears only to have limited influence on the viscous stress-strain characteristics. The performed tests show that when the natural structure is removed by reconstitution the viscous behaviour changes from Isotach to combined Isotach and TESRA type behaviour that is characterised by increasing temporary effects of strain rate changes towards failure. Generally, it was found that upon step increases in the axial strain rate an initial stiff response is observed, which is followed by gradual yield. Moreover, independently of the degree of structure and overconsolidation the total immediate stress jump at a given deviator stress level increases linearly with increases in the logarithm of the ratio of strain rate change. Figure 6-37 compares the influence of stress level and ratio of strain rate change on the total immediate deviatoric stress jump experienced by the reconstituted and undisturbed London Clay samples. For the OC samples, both undisturbed and reconstituted, the stress jump was seen to increase consistently with increasing stress level, while in contrast for the NC sample the stress jump remained constant for a given ratio of strain rate change independently of stress level. Strain rate effects, when quantified by the total immediate stress jump after changes in strain rate, are seen to be noticeably lower in the OC reconstituted clay than in the NC reconstituted clay and in the OC undisturbed clay, when comparing results for similar ratios of strain rate change.

The strain rate dependency of the pore water pressure response in the initial contractive range observed for both OC reconstituted and intact OC samples may be related to the stiff nature of the samples, as mentioned above, and as such is therefore not directly related to the viscous behaviour of the soil. In contrast both OC reconstituted and NC reconstituted samples indicate that the persistent pore water pressure response is not significantly affected by the applied rate of strain in the post gross yield region, at which point significant plastic strains develop. From the tests it can generally be concluded that the peak strength envelope is affected significantly by strain rate in addition to the significant affect of structure, while the critical state appears to be independent of strain rate. It is not possible to conclude if the critical state will be affected by structure. However it seems unlikely that all of the natural structure will break down with shearing and some effects of structure may therefore remain at a critical state.

6.4 DISCUSSION

6.4.1 Consistency and reliability of presented results

a Tests on OC reconstituted and undisturbed London Clay

Despite the fact that measurements of pore water pressure were not taken during drained shearing of the intact London Clay specimen S2LC, it was assumed that the test was conducted fully drained with insignificant build-up of excess pore water pressures. Similarly full equalisation of pore water pressures was assumed in undrained shearing of samples S1LC and S2LCrA5(OC). This was based on the findings in Section 5.2.4 that insignificant excess pore water pressures accumulated in the drained triaxial compression tests on reconstituted specimens of London Clay under the maximum axial strain rate of 0.05 %/hr. Additionally, significantly higher consolidation rates would be expected in the specimens of OC reconstituted and undisturbed London Clay, since these behave stiffer than the specimens of NC reconstituted London Clay. The consistent nature of the measured pore water response in undrained tests and volumetric response in drained tests at strain rates varying by up to several orders of magnitude also supports the assumptions. The tests performed to investigate time effects in London Clay were long, generally weeks, up to 3 months in some cases, and complex. These factors increased the risk of failure of the system during testing and meant that the tests could not be repeated to check consistency of the obtained results. Nevertheless, the two tested samples of undisturbed London Clay, one drained and the other undrained, appeared to show consistent monotonic and isotach viscous behaviour.

b Tests on cement-mixed kaolin

The consistency of the sample preparation can be deducted from Table 6-1, in which the initial void ratio for samples saturated at an isotropic pressure of 100kPa is seen to range between 1.14 and 1.30, with a mean of 1.25. Apart from sample 2, which recorded the highest initial density (e= 1.14), all other samples deviate by a maximum of 4% from the average value of initial void ratio, which is satisfying. Despite differences in strain (loading) histories, consistent general monotonic behaviour was shown by the tested samples and good consistency in the data was indicated from the deduced trends such as the influence of curing time on strength, stiffness and failure strain. Inconsistencies were however seen in the peak strength and stiffness development of samples S2-4cmk after drained creep, which as mentioned previously could be attributed to destructuration caused by significant unloading.

Most samples were sheared with no measurements of pore water pressure, since top and bottom were both used as drainage boundaries to minimize the build-up of excess pore water pressure in the samples at high rates of straining. However, to investigate if full drainage was generally achieved, sample S6cmk was sheared allowing only bottom drainage, while pore water pressure measurements were taken from the top of the sample. It was found that at

shearing rates of 0.6 %/hr and slower, the build-up of excess pore water pressures was minor, while excess pore water pressures gradually developed at low mean effective stresses when the sample was sheared at the fastest rate of 2.6 %/hr. At higher mean effective stresses, the sample behaved stiffer, consolidation rates increased, and the measurements showed that excess pore water pressures did not develop even at the fastest rate of shearing. Based on this, it can generally be assumed that the samples have been sheared fully drained. The only exception may be during the constant high rate shearing of sample S8cmk, where significant excess pore pressures may have developed, but these were not recorded.

6.4.2 Influence of artificial structure and curing effect on the monotonic behaviour of cement-mixed kaolin compared with behaviour observed in the literature

a Influence of artificial cementation on the monotonic stress-strain response of cement-mixed kaolin

The artificially structured kaolin tested in this study is characterised by very high strength and stiffness compared to pure kaolin, and shows distinct brittle behaviour in triaxial compression when cured for more than one day. This highlights that the meta-stable characteristics of naturally structured clays as observed in triaxial compression can be reproduced by means of artificial cementation. In cement-mixed kaolin the high strength and stiffness, when compared to pure kaolin, can be attributed to the strong inter-particle bonds formed as a result of hydration of the added cement, while the brittle nature of samples cured more than one day can primarily be associated with the breakage of the created cement bonds in a narrow shear zone (as suggested by the formation of a slip plane at peak strength). The breakage of cement bonds in the shearband is likely to create an aggregated fabric of strongly bonded clusters of clay in this zone, which could explain why the critical state angle of shearing resistance of cured cement-mixed kaolin is still significantly higher than the value seen for pure kaolin. Since, the hydration of the cement cannot be reversed, and the strong cement bonds are not likely to be completely removed by the process of reconstitution, cured cement-mixed kaolin will be intrinsically different to pure kaolin. It can therefore be argued that a comparison between the two materials would be somewhat meaningless; it would be like comparing clay with soft rock or gravel. Nevertheless, if the comparison is performed in time domain (i.e. curing time), pure kaolin makes a good reference for cured cement-mixed kaolin, since the behaviour of cement-mixed kaolin at "zero" curing time is expected to be similar to that of pure kaolin because the quantity of added cement is minor. The assumed reference line in Figure 6-9 for pure kaolin after (Viggiani & Atkinson, 1995) can therefore be justified.

b Strength and stiffness development due to curing effects in cement-mixed kaolin

The curing of the cement in cement-mixed kaolin can be taken to represent ageing that would occur in natural clay during its geological history, but at a much faster rate so that it can be more

easily observed in the laboratory. It should be noted, however, that since cementation is just one aspect of the ageing that occurs in natural clays, the observed strength development in cement-mixed kaolin with curing time may not represent well the strength development measured in natural soils over a geological time scale. In the study, kaolin was mixed with Rapid Hardening Portland (RHP) cement, which under normal circumstances has a setting time of minimum 75 minutes and reaches about 50% of its 28-day strength in 2 days (Tennis, 1998). Hence, if water is readily available the cement will hydrate very rapidly in the first days and slowly increase in strength thereafter, as shown in Figure 6-38. Since the strength development with time in cement-mixed kaolin is primarily governed by the hydration of cement and associated creation of cement bonds between particles, it was therefore expected to show similar trend to that observed for RHP cement on its own. In contrast to expectations, this was however not found in the study, as the tests appeared to indicate a maximum peak strength plateau after about 1 day of total curing time (Figure 6-5). The observed behaviour is also in contrast to the findings by Komoto (2004), reported previously in the literature review, who indicated the drained peak strength of cement-mixed kaolin to gradually increase with curing time up to at least 45 days of curing (Figure 2.48). Other studies reported in the literature on cement-mixed clays and granular soils have generally found a logarithmic linear increase in strength with curing time (e.g. Horpibulsuk et al., 2003, Kongsukprasert & Tatsuoka 2003a, Lohani et al., 2003). It is possible that a different trend would have emerged from the results in this study, if data had been obtained for samples of cement-mixed kaolin sheared after longer curing times or if some samples had not been disturbed by unloading. The small strain stiffness of cement-mixed kaolin was in contrast to the peak strength envelope found to show the expected logarithmic linear increase with curing time, which may indicate that the small strain stiffness in cemented soils generally is less affected by disturbance than the strength.

In this study on cement-mixed kaolin it was noted from the comparison of peak strengths for samples cured at different deviator stress levels that the curing stress state (and loading history) appeared to have had insignificant influence on the strength development. This is in agreement with findings by Komoto (2004) who carried out similar tests on cement-mixed kaolin and the findings by e.g. Rotta et al. (2003) in tests on an artificially cemented sand, which showed the incremental yield stress in isotropic compression not to be influenced by the curing isotropic confining stress. However, other studies have in contrast found clear evidence of an influence of curing stress (loading history) state on the strength development of cement-mixed soils, e.g. Kongsukprasert & Tatsuoka (2003) in tests on cement-mixed Chiba gravel.

6.4.3 Coupled effect of viscosity and ageing in naturally and artificially structured clays

a Coupled effect of viscosity and curing in cement-mixed soils

It was found in this study that the coupling between viscous and curing effects in cement-mixed kaolin depends on several factors, including; total accumulated curing time, considered interval

of strain rates, and time or strain level after the last significant change in strain rate. The performed triaxial compression tests on cement-mixed kaolin show that curing effects dominate the persistent stress-strain response at early curing times, resulting in viscous effects being completely overshadowed. As the curing time increases the curing effects rapidly decrease and at curing times greater than about one day curing effects are minor, at which point viscous effects are seen to dominate the behaviour. Independently of curing time, however, the immediate response of strain rate changes appears to be primarily controlled by viscous effects and the viscous characteristics of cement-mixed kaolin could therefore be quantified in Section 6.2.5a by considering the immediate stress jump in deviator stress. Similar coupling between curing and viscous effects have been reported in other artificially cemented soils (e.g. cemented gravel, Kongsukprasert & Tatsuoka, 2003 and cemented kaolin, Komoto, 2004).

b Coupled effect of viscosity and ageing in natural clays

The cement-mixed kaolin is a representation of natural soils but with an accelerated ageing rate. In natural structured soils the rate of ageing is very slow, so that at strain rates of the order of those usually applied in the laboratory, viscous effects will dominate the behaviour. Ageing effects may only be observed if the strain rates imposed are very slow, as indicated for example in 1D compression tests on Batiscan clay (Leroueil et al., 1985) or in 1D compression tests on artificially sedimented Jonquière clay (Leroueil et al., 1996), where positive ageing effects were observed on the yield envelope for volumetric strain rates (=axial strain rates) in the order of 0.0061 %/hr and 0.036 %/hr respectively. Yet, even at axial strain rates in the order of 0.0061 %/hr or below some natural clays may still not show any significant ageing effects, as found in this study on reconstituted and undisturbed London Clay and reported in the literature for other clays (Leroueil et al., 1996). The study on London Clay, in both reconstituted and undisturbed states, shows that viscous effects dominate the behaviour at standard strain rates. In the performed triaxial compression tests, no ageing effects were observed under axial strain rates as low as 0.007 %/hr. This agrees well with the previous observations made in Section 4.3.3, where a sample of reconstituted London Clay similarly did not indicate any significant effects of ageing on the yield envelope when resuming CRS one-dimensional compression after drained creep for about one month, even though this was associated with a reduction in the axial strain rate to around 0.0002 %/hr. The bender element test described in Chapter 4 also suggested that ageing effects on the elastic shear stiffness were minor for drained creep periods up to one month, as the measured increase in elastic shear stiffness could be attributed solely to strain rate effects. An apparent lack of significant ageing effects in intact London Clay was also reported by Yimsiri (2001), as one might have expected for an undisturbed sample of stiff natural clay. Despite the lack of observed ageing effect in laboratory time, the comparison between intact and reconstituted London Clay indicates that London Clay has developed a significant degree of meta-stable structure during its geological history. Considering the monotonic behaviour only, it is however not certain whether this can be attributed to fabric-related sedimentation structure or

if it is rather a result of environmental ageing effects such as changes in pore water chemistry or gradual addition of cementing agents from external sources.

c Characteristic strain rate

The cement-mixed kaolin is a representation of natural soils but with an accelerated ageing rate. In natural structured soils the rate of ageing is very slow, and at strain rates of the order of those usually applied in the laboratory, viscous effects will dominate the behaviour. Ageing effects will only be observed if the strain rates imposed are very slow, (e.g. $\dot{\varepsilon}_v = 1.00 \cdot 10^{-7}$ s^{-1} = 0.036 %/hr for artificially sedimented Jonquière clay Leroueil et al., 1996, as shown in Figure 2-57). It is suggested that at a given time after hydration there must be a point (characteristic strain rate) at which the behaviour of cement-mixed kaolin changes from being dominated by cementation (curing) effects to being predominantly viscous, as illustrated in Figure 6-39a. The net cementation effect can be defined as the strength increase per unit time due to development of cement bonds, subtracting any destruction caused by straining, while the viscous effect can be defined as the strength increase per unit change in strain rate. At strain rates lower than the characteristic value, bonds are allowed to develop faster than they are being destroyed by the compression or shearing action and hence the cementation effects will dominate the observed stress-strain behaviour (Figure 6-39b). While for applied strain rates above the characteristic rate, new bonds are continuously destroyed by the straining, resulting in the net cementation effect being zero and the stress-strain relationship being dominated by the viscous effects. It should be noted that the characteristic strain rate is highly dependent on the magnitude of the cementation effects, i.e. the rate at which the strength increase per unit time due to curing. Since the cementation (curing) effect is seen to reduce rapidly with time after initial hydration in the artificially cemented kaolin, a comparable reduction in the characteristic strain rate can therefore be expected with time. Similar coupling between ageing effects and viscous effects may be expected in active natural clays, which have been subjected to recent disturbance. Inactive clays and undisturbed natural clays, which have been aged over a geological time scale, will in contrast be likely to have a characteristic strain rate which is extremely low and the strength development in these clays will primarily be affected by changes in the surrounding environment rather than anything else.

6.4.4 Influence of structure on the viscous behaviour of kaolin and London Clay compared with findings from the literature

a Influence of mechanical overconsolidation on the viscous behaviour of clays

The comparison between the viscous behaviours of NC reconstituted and OC reconstituted London Clay indicated that mechanical overconsolidation had only little effect on the viscous behaviour of London Clay in reconstituted state. This suggests that the mechanical overconsolidation experienced by London Clay, as a result of significant erosion events during

its geological history, similarly will not influence the viscous behaviour of the tested intact samples. As reported previously in the literature review in Section 2.3.2b, comparable findings were made for stiff Fukakusa clay (Oka et al., 2003), for which undrained triaxial compression tests on normally consolidated and overconsolidated reconstituted samples showed little effect of overconsolidation on the viscous behaviour. The viscous behaviour of Fukakusa clay in both NC and OC reconstituted states could be characterised by Isotach behaviour at low stresses and increasing TESRA behaviour towards the failure state, like what has been generally seen for reconstituted London Clay in this study (Table 2-1). The samples of both NC and OC reconstituted Fukakusa clay, however, showed significant persistent effects of axial strain rate changes even at 20 % axial strain in the post peak region, while the tests on NC and OC reconstituted London Clay both indicated minor persistent effects at large strains near the assumed critical state. Oka and co-authors nevertheless suggested that the intrinsic CSL was independent of the applied axial strain rate, signifying that the observed rate dependency of the large strain critical strength was caused by a rate dependent pore water pressure response rather than an influence of strain rate on the effective critical state angle of shearing resistance.

b Influence of natural structure on the viscous behaviour of clays

The performed tests on London Clay in this study showed that the viscous characteristics of London Clay were significantly affected by the presence of natural structure, while mechanical overconsolidation appeared only to have limited influence on the viscous stress-strain characteristics. The elements of the natural structure which do not result from the processes of mechanical overconsolidation can therefore be said to cause the radical alterations of the viscous characteristics seen between intact natural London Clay and the reconstituted counterpart. If it is considered that mechanical overconsolidation typically results in a break down of the sedimentation structure in heavily overconsolidated clays (Skempton & Northey, 1952) then it can be assumed that in London Clay the natural structure is attributed primarily to post-sedimentation processes such as ageing. It has been outside the scope of the performed tests to investigate in more detail to what degree different elements of the natural structure would influence and contribute to the viscous behaviour of the intact natural London Clay.

In the literature review it became clear that several conflicting findings have been made concerning the influence of ageing and structure on the magnitude of the viscous strain rate effect in clays. One study reported a reduction in the viscous effect with an increase in structure and geological age of a Pleistocene clay (Komoto et al., 2003), another study appeared to argue the opposite by showing an increase in the strain rate effects with an increase in the meta-stability index of various clays (Soga & Mitchell, 1996), while a third study on Canadian clays concluded that the influence of natural structure and geological age on the viscous effects were minor (Leroueil et al., 1996). Part of the reason for these conflicting findings may to some extent be due to different methods used to quantify the strain rate effects, while the collapse of meta-stable soils with shearing may explain the increase in strain rate effects with increasing

meta-stability. In this study, the results gave no clear correlation between the level of structure and the magnitude of the strain rate effects. At high stress levels the intact natural samples of London Clay appeared to show higher strain rate effects than the reconstituted samples, while at low stress levels the results were ambiguous (Figure 6-37).

c Influence of artificial cementation on the viscous behaviour of clays and other soils

The performed tests on cement-mixed kaolin in this study suggest that the presence of artificial cementation or the breakdown thereof influences the viscous behaviour of kaolin notably. The viscous behaviour of pure kaolin without cement has in the literature been reported to show distinct Isotach characteristics (Table 2-2). In contrast, the viscous behaviour of cement-mixed kaolin after curing was shown to be of the TESRA type at high stress levels near the failure state. For weakly cemented soils the breakdown of the cement between particles can be expected to accelerate as the strains tend to localise on a shear plane near the failure state. It therefore seems likely that the breakdown of cement somehow is linked to the observed change in the viscous behaviour. This notion is supported by previous studies on the influence of a relatively small quantity of cement on the monotonic behaviour of various soils including sands, gravels and clays. For example, as reported in the literature review, in triaxial compression tests on cement-mixed Chiba gravel (Kongsukprasert & Tatsuoka, 2003) the viscous behaviour was observed to be Isotach in the pre-peak stress range. Yet, close to failure the viscous behaviour suddenly changed to show distinct TESRA characteristics with continued straining in the post-peak region. Tests on non-cemented Chiba gravel have in contrast shown viscous behaviour which can be characterised as General TESRA in both the pre-peak and post-peak region (Tatsuoka et al., 2000). It is therefore suggested that cemented gravel shows TESRA type viscous behaviour as a result of the breakdown of the cementation, while in the pre-peak region before any breakage of cementation takes place, the cementation between the particles results in Isotach viscous characteristics. Despite indications that the magnitude of the viscous effects may be influenced by the level of natural structure, as explained above, reported studies in the literature on both cement-mixed kaolin (Komoto, 2004) and cement-mixed gravel (Kongsukprasert & Tatsuoka, 2003) appear to indicate that the viscous effects do not change with curing time.

6.4.5 General viscous behaviour of soils

a Influence of strain rate on the yield and strength envelopes of clays

The performed tests in this study on cement-mixed kaolin and intact and reconstituted London Clay generally confirm that the stress-strain behaviour of clays is significantly rate dependent. The tests on London Clay agreed, in many respects, well with findings reported in the literature for other clays, while in a few respects discrepancies were found. Generally, the rate dependency of the yield envelope was confirmed along with indications that the critical state

line in stress space is independent of axial strain rate. However, the tests on London Clay also tended to indicate that the critical state line in *e-q-p'* space is unique, while the peak strength envelope for intact London Clay was found to be notably strain rate dependent. The conceptual viscous behaviour of NC reconstituted, OC reconstituted and OC intact London Clay are compared and illustrated in Figure 6-40. The figure also illustrates the observed influence of axial strain rate and step changes in axial strain rate on the normalised state boundary surface. The observed behaviour of London Clay is found to contrast with many reported studies in the literature, which indicate that both the peak strength envelope and the critical state line are independent of axial strain rate. In these cases the observed reduction in undrained strength or large strain critical state strength of both NC and OC clays with reducing strain rate is therefore explained purely by creep driven pore pressure changes (Leroueil & Marques, 1996; Soga & Mitchell, 1996; Vaid & Campanella, 1977).

b Factors influencing the general viscous behaviour of soils

Generally, the viscous behaviour of soils in response to strain rate changes can be classified either as Isotach, TESRA or intermediate behaviour termed General TESRA (Tatsuoka et al., 2000). Isotach behaviour is characterised by persistent effects of strain rate changes, while with TESRA behaviour the effects of strain rate changes are purely temporary. Intermediate behaviour characterised by a combination of persistent and temporary effects of strain rate changes have been termed General TESRA. Generally, published data show that clays are most likely to show Isotach viscous behaviour, while unbounded granular soils like sands and gravels typically show dominantly TESRA type viscous characteristics. Furthermore, clays generally show greater strain rate dependency, which results in greater creep deformation than seen in granular soils. However, as highlighted by published studies the viscous behaviour of different soils is not only a simple function of the particle size, it appears to be influenced by many other factors including: particle shape (large particles only), grading characteristics, inter-particle bonding, strain level and inter-particle contact point as listed in Table 2-6 after Tatsuoka (2006). Hence, for soils in general and even just for clays the issue of viscous behaviour appears to be very complex.

The performed tests on cement-mixed kaolin and London Clay in this study confirm that the viscous behaviour of clays is significantly influenced by structure such as artificial cementation or natural structure resulting from e.g. ageing processes. These findings complement well existing studies, which primarily have concentrated on the important influence of artificial cementation on the viscous behaviour of gravels and sands. It generally appears that strong inter-particle bonding such as the cementation and bonding present in soft rocks, artificially cemented soils and undisturbed stiff clays, like intact London Clay will result in Isotach characteristics (Table 2-3), while unbounded materials like sands and gravels predominantly show TESRA behaviour (Table 2-2). Interestingly, soft normally consolidated reconstituted clays, like pure kaolin clay (Tatsuoka et al., 2002) and undisturbed soft natural

clays, for example Winnipeg clay and Belfast clay (Graham et al., 1983) generally also show distinct Isotach characteristics (Table 2-3). Since these clays cannot be said to be strongly bonded, the viscous characteristics is most likely governed by the small particle size.

The influence of strain level on the viscous behaviour during shearing has been emphasized in several previous studies. The effect of strain level is probably most evident in reported tests on artificially cemented soils, where the viscous behaviour in the pre-peak region is Isotach due to the strong cementation, while in the post-peak region the viscous behaviour changes to being predominantly of the TESRA type. The TESRA behaviour can be assumed to be a result of the localization of strains at large strains and the associated significant breakdown of the cementation along the shear plane, as suggested by the tests on cement-mixed kaolin in this study. Interestingly, both artificially cemented granular soils and artificially cemented clays, like kaolin, show TESRA type viscous behaviour in the post-peak region (Table 2-2). Since non-cemented pure kaolin has been found to show distinct Isotach viscous characteristics, this suggests that the viscous behaviour of cemented clays in the post-peak region is governed by the aggregated nature of the fabric along the shear plane, which was created as a result of partial breakage of the strong inter-particle cementation. In this study the influence of strain level was furthermore highlighted by the observed change in viscous behaviour of reconstituted London Clay during shearing from seemingly Isotach behaviour at small and intermediate strains (<1% axial strain) to increasing TESRA behaviour with increasing strains towards the failure state. This behaviour was found to be consistent with the viscous behaviour of other reconstituted stiff natural clays reported in the literature (Table 2-2). The viscous behaviour of reconstituted natural clays is however not as simple to explain as for artificially cemented soils, where the observed change in viscous behaviour can be linked to a specific micro-mechanical event, i.e. significant breakage of the inter-particle cementation. As reconstitution of the natural clays is thought to have removed all of the natural structure, further significant breakdown of inter-particle bonding with shearing is not likely to take place. This can therefore not explain the observed behaviour. The explanation for the observed behaviour is complex and may possibly be found in the fabric of the reconstituted clays, which will be related to the mineralogy. If the fabric changes significantly as a result of shearing, the viscous behaviour can be expected to change as well.

The effects of artificial cementing on the strain rate sensitivity of kaolin were seen to be different to the influence of natural structure on the strain rate sensitivity of London Clay. The findings therefore suggest that the difference in strain rate effects in the intact and reconstituted London Clay cannot be simply associated to cementing. This is in agreement with the evidence shown on micrographs by Gasparre, 2005 that the structure in the natural London Clay is not due to bonding but predominantly due to fabric.

c Analogy to solid and fluid mechanics

In the following a simple analogy will be made to solid and fluid mechanics, in an attempt to explain the viscous behaviour of soils in general by relating the observed viscous characteristics to micro-mechanical behaviours.

In idealised worlds solid mechanics is governed by frictional behaviour, while fluid mechanics is governed by flow behaviour. Frictional behaviour is usually considered at a macroscopic scale, while fluid mechanics is considered at a microscopic scale. For frictional behaviour, the frictional resistance between two surfaces in contact is independent of the rate of relative displacement. If a force equal to the frictional resistance is applied, then the relative rate of displacement will be constant. While if a force greater than the frictional resistance is applied then the relative displacement will accelerate in proportion to the extra force applied. For flow behaviour on the other hand, the viscous resistance to flow increases consistently with an increase in the relative rate of displacement, while an acceleration of the displacement requires no extra force. The idealised concepts of solid mechanics and fluid mechanics are illustrated in Figure 6-41. From the described behaviour, the analogy between soil behaviour and solid and fluid mechanics is striking. With these simple concepts in mind it can be deducted that a pure frictional material will show behaviour which closely resembles the TESRA type viscous behaviour in soils, where the steady state shearing resistance is independent of strain rate and a temporary acceleration of deformation will give rise to a temporary increase in shear resistance. On the other hand the flow behaviour closely resembles the Isotach viscous behaviour in soils, which is characterised by a unique relationship between the shearing resistance and the shearing rate. A combined effect of flow and frictional behaviour can then be linked to what we observe as combined Isotach and TESRA viscous behaviour in soils (General TESRA type viscous behaviour). The concept of Isotach and TESRA viscous behaviour is illustrated in Figure 6-42. Despite being very idealised the above concept shows that analogy to solid and fluid mechanics may partially explain the observed viscous behaviour of soils at a macro-scale.

d A new proposed hypothesis explaining the general viscous behaviour of soils

It is proposed that the viscous behaviour of soils is dependent on the continuum or particulate nature of the microstructure of the soil. Unbounded granular soils are generally characterised by a particulate microstructure made up of stiff particles. This in turn gives granular soils a frictional nature and these therefore predominantly exhibit TESRA type viscous behaviour. The observed temporary increase in the shearing resistance after a step change in strain rate is a result of the temporary acceleration of strains. In terms of micro-mechanics the temporary effect may be explained by the idea that upon a step increase in strain rate the entire soil structure will initially act as continuum, which gives rise to the nearly elastic response. With further straining, however, the particulate soil yields due to localized slips at particle contacts. As a consequence stress columns gradually collapse, and the shearing resistance is seen to drop under a constant

rate of strain. In contrast, soft non-structured clays will act as a (slow) flowing continuum at both small and large strains. In soft clays the process of deformation generally encompasses the entire volume of soil and as a consequence the effect of strain rate changes is seen to be persistent, i.e. Isotach viscous characteristics. In particulate soils the localization of strains due to slippage can be expected to be greater when the particles are rounder, uniformly graded and less crushable. Granular soils with these characteristics will therefore show predominant TESRA viscous behaviour, as suggested by Tatsuoka (2006) in Table 2.6. In contrast, granular soils with particles that are more angular, well graded and more crushable, will have processes of deformation which encompasses more of the soil body, primarily because of an increase in the number of contact points. As found by Tatsuoka (2006) these soils can in turn be expected to show viscous behaviour characterised by a combination of persistent and temporary effects of strain rate changes (Table 2.6). Strongly bonded soils such as soft rocks, structured clays and artificially cemented soils of both granular and clayey nature have a structure which acts as a stiff continuum. These soils therefore show Isotach viscous behaviour, as long as the inter-particle bonds remain wholly intact. As demonstrated in tests on artificially cemented soils, when the inter-particle cementation breaks down as a result of large straining, the soil mixture consequently show particulate viscous behaviour, which may be explained by the aggregated nature of the fabric in the shear zone. Reconstituted stiff clays that show Isotach behaviour at small strains and increasingly dominating TESRA behaviour towards failure, illustrate complex behaviour, which is not easily explained without further research into clay mineralogy and fabric studies. One suggestion, plausible or implausible, which could explain the observed behaviour of reconstituted London Clay, considers that London Clay is made up of a mixture of different clay minerals (predominantly illite and to lesser extend kaolinite and smectite), which during preconsolidation would generate inter-particle bonds with different bond strengths. Upon shearing, the soil initially acts as a continuum. However, at large strains the weak bonds break down first, while the most active clay particles remain bonded together. This in turn results in an aggregated fabric with particulate frictional behaviour.

Because the post yield process of deformation in soft clays occurs in the entire volume of soil rather than being localized at inter-particle contact points as is the case in stiff granular soils, soft clays generally show quantitatively higher viscous effect compared to granular soils. Moreover strongly bonded clays would be expected to show quantitatively lower viscous effect than non-structured clays because strong inter-particle bonding would restrict the movement of the entire volume of soil. Weakly bonded, low density natural soft clays characterised by high meta-stability could on the other hand be expected to demonstrate significant deformation as a result of the collapse of card-house like fabric, and these may therefore show quantitatively higher viscous effect than the their reconstituted non-structured counterparts at a given stress level. At comparable void ratios the soft non-structured clays would however be expected to show quantitatively higher viscous effect than their intact meta-stable counterparts.

This chapter concludes the experimental work. The following chapter examines the possibility for implementing the proposed conceptual viscous behaviour of reconstituted and intact London Clay into an existing advanced constitutive model.

6.5 TABLES AND FIGURES FOR CHAPTER 6

Table 6-1 Overview of SRS and CRS CiD triaxial compression tests on cement-mixed kaolin

Test no.	Type	Nominal axial strain rates $\dot{\varepsilon}_a$ = 0.6 %/hr	Creep state p'/q [kPa]	Creep time [days]	B-value after saturation	Void ratio after saturation
S9cmk	SRS	$\dot{\varepsilon}_a, 4\dot{\varepsilon}_a$	170/210	2	0.69	1.30
S4cmk	SRS	$1/8\dot{\varepsilon}_a, \dot{\varepsilon}_a, 4\dot{\varepsilon}_a$	170/210	2	0.70	1.30
S3cmk	SRS	$1/8\dot{\varepsilon}_a, \dot{\varepsilon}_a, 4\dot{\varepsilon}_a$	170/210	3	0.77	1.23
S2cmk	SRS	$1/8\dot{\varepsilon}_a, \dot{\varepsilon}_a, 4\dot{\varepsilon}_a$	170/210	6	0.75	1.14
S5cmk	SRS	$\dot{\varepsilon}_a$	170/210	9	0.67	1.28
S0cmk	SRS	$1/8\dot{\varepsilon}_a, \dot{\varepsilon}_a, 4\dot{\varepsilon}_a$	133/100	1	0.58	1.18
S6cmk	SRS	$1/8\dot{\varepsilon}_a, \dot{\varepsilon}_a, 4\dot{\varepsilon}_a$	230/390	1	0.67	1.26
S1cmk	SRS	$1/8\dot{\varepsilon}_a, \dot{\varepsilon}_a, 4\dot{\varepsilon}_a$	-	-	0.67	1.28
S8cmk	CRS	$4\dot{\varepsilon}_a$	-	-	-	1.22
S7cmk	CRS	$\dot{\varepsilon}_a$	-	-	0.71	1.26
S10cmk	CRS	$1/8\dot{\varepsilon}_a$	-	-	0.69	1.26

Table 6-2 Overview of additional SRS triaxial compression tests on London Clay

Test no.	Type	Nominal axial strain rates $\dot{\varepsilon}_a$ = 0.05 %/hr	B-value after saturation	e_i	p'_e * [kPa]	$G_{u,0}$ or G'_0 [MPa]
S1LC	CiU	$\dot{\varepsilon}_a, 4\dot{\varepsilon}_a, 16\dot{\varepsilon}_a$	0.946	0.70[$]	815	80-100
S2LC	CiD	$\dot{\varepsilon}_a/7, \dot{\varepsilon}_a$	0.84	0.72[#]	745[i]	80-100
S2LCrA5 (OC)	CiU	$\dot{\varepsilon}_a/7, \dot{\varepsilon}_a, 10\dot{\varepsilon}_a$	0.96	0.75[#]	621	40-60

[$] based on initial water content and volumetric deformation calculated from local strain measurements
[#] based on initial dimensions and volumetric deformation calculated from volume gauge measurements
[i] initial value after recompression/at start of shearing
* p'_e: equivalent preconsolidation pressure determined from the average intrinsic isotropic NCL* given by Equation 5.1 for the current void ratio

Table 6-3 Summary of observed viscous behaviour of London Clay in reconstituted and intact states

	OC intact	**NC reconstituted**	**OC reconstituted**
Monotonic behaviour	Very brittle	Ductile	Slightly brittle
Viscous behaviour - small strains	Isotach		
Viscous behaviour - larger strains	Isotach	Non-isotach	Non-isotach
Persistent stress jump for given ratio of axial strain rate change until peak	Increases with increasing stress level	Reduces with increasing stress level	Constant?
Temporary stress jump for given ratio of axial strain rate change until peak	None	Increases with increasing stress level	Increases with increasing stress level
Total immediate stress jump for given ratio of axial strain rate change until peak	Increases with increasing stress level	Constant	Increases with increasing stress level
Immediate stiffness response to axial strain rate increases	Very stiff		
Strain rate dependency of:....			
Peak strength envelope / State boundary surface	Dependent	N/A	Dependent
Critical state line	?	Independent	Independent
Shear stiffness against shear strain	Independent?	Dependent	?
Pore water pressure (u.d.) against shear strain	Dependent	Independent	(In)dependent
Volumetric strain (d.) against shear strain	Independent	Independent	?

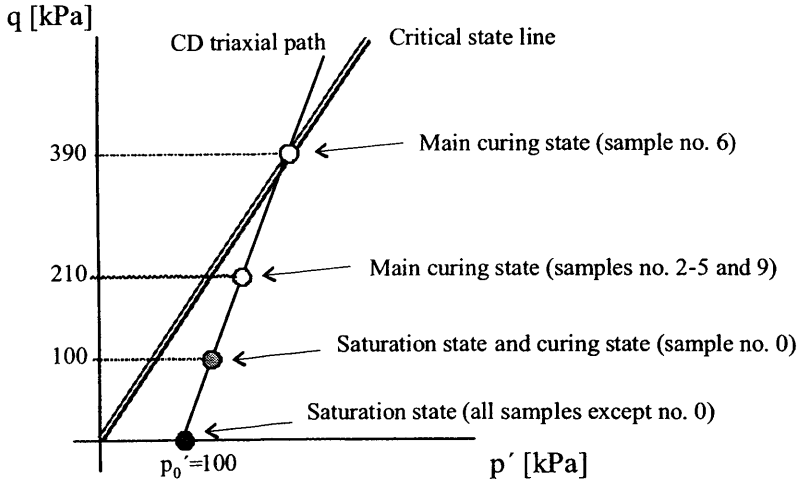

Figure 6-1 Illustration of testing procedures followed for the investigation on cement-mixed kaolin

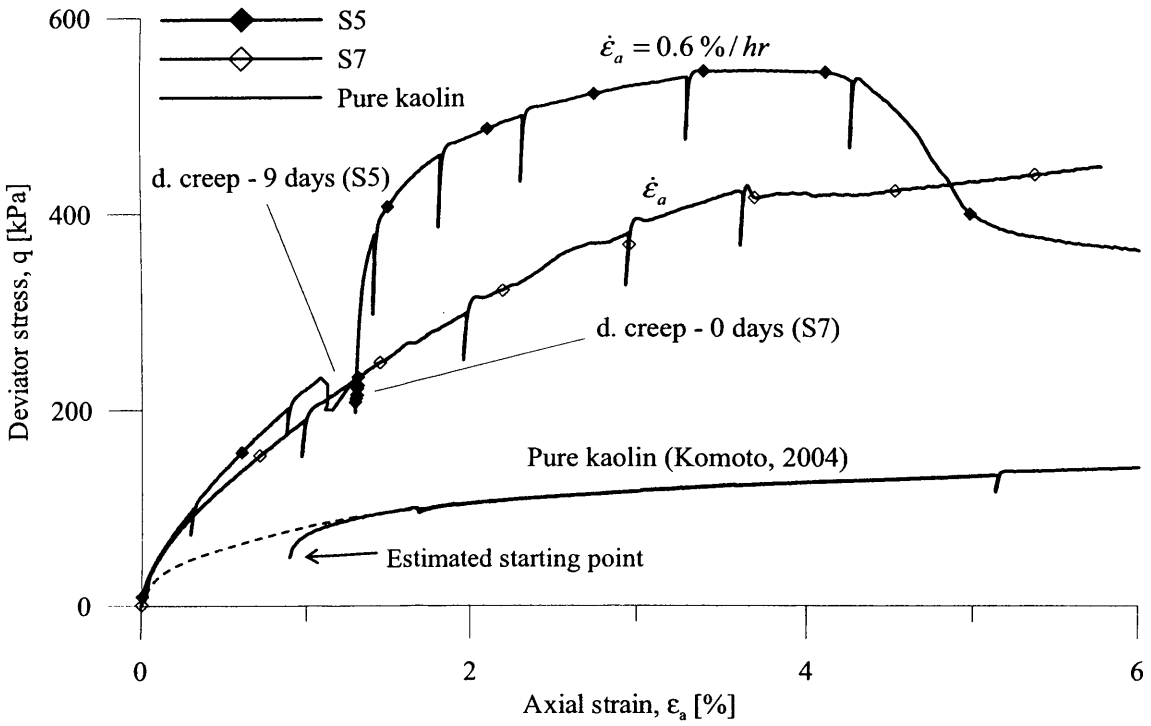

Figure 6-2 Influence of cement and curing time on stress-strain behaviour in cement-mixed kaolin

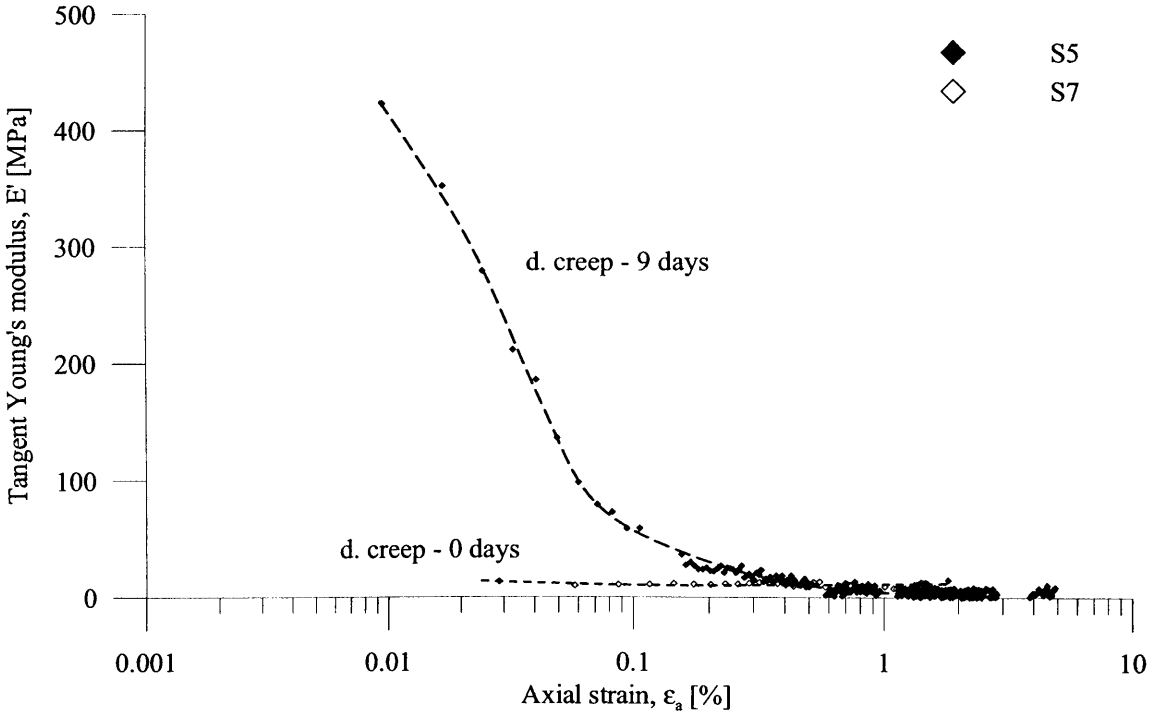

Figure 6-3 Influence of curing during drained creep on stiffness response after creep stage at q=210 kPa in cement-mixed kaolin

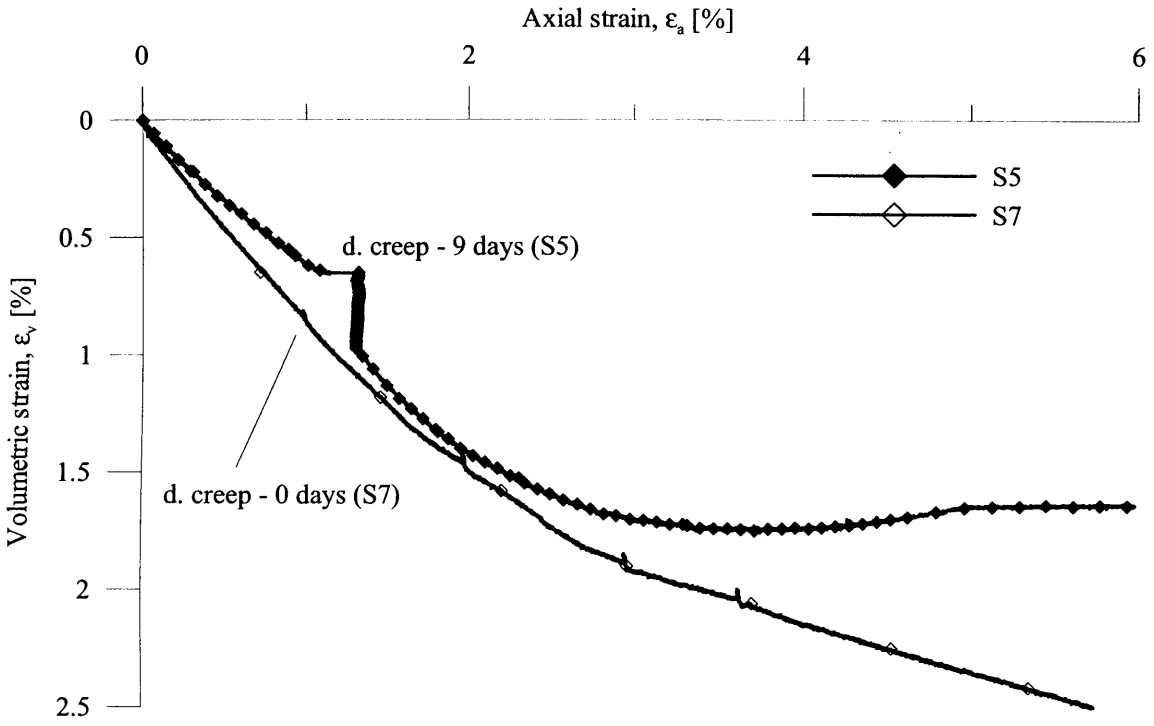

Figure 6-4 Influence of curing during drained creep at q=210 kPa on volumetric response in cement-mixed kaolin

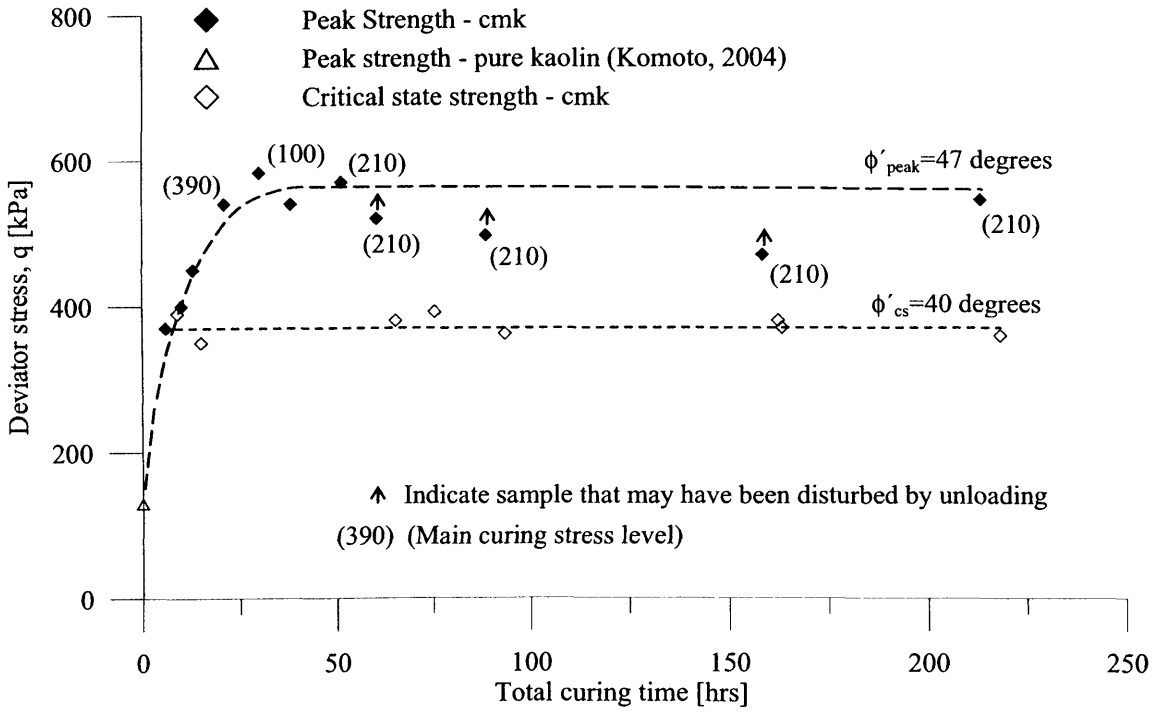

Figure 6-5 Effect of total curing time on peak and critical state strengths in cement-mixed kaolin

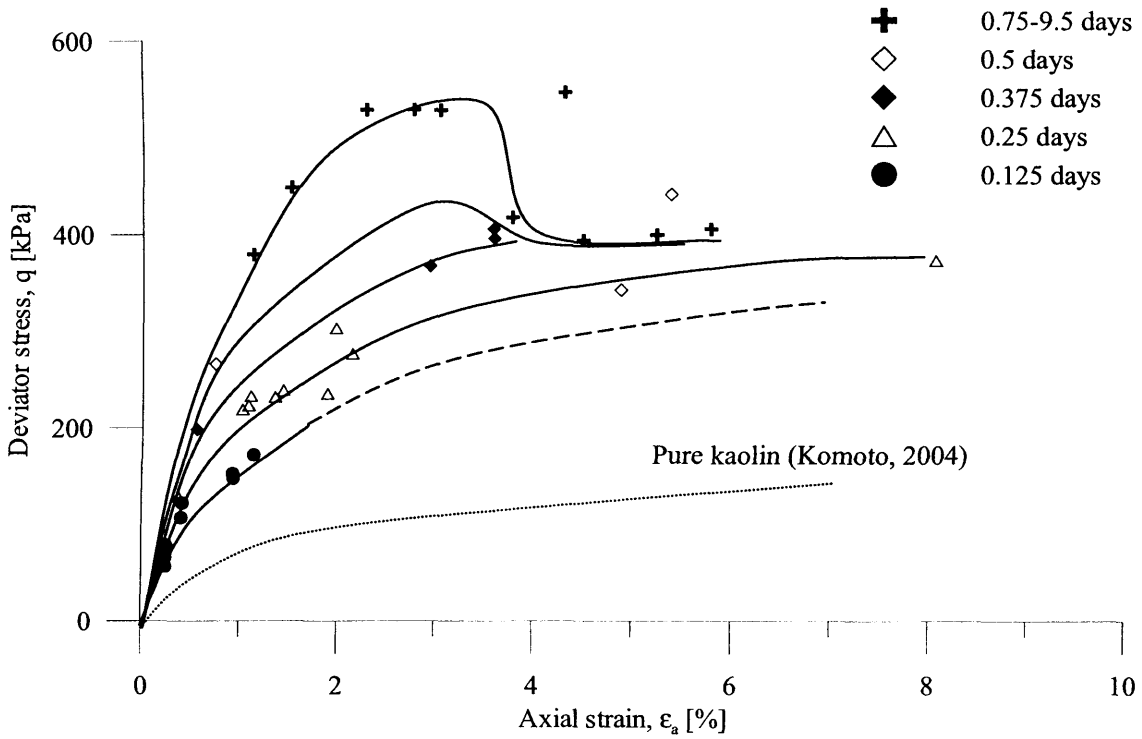

Figure 6-6 Effect of total curing time on stress-strain response in cement-mixed kaolin

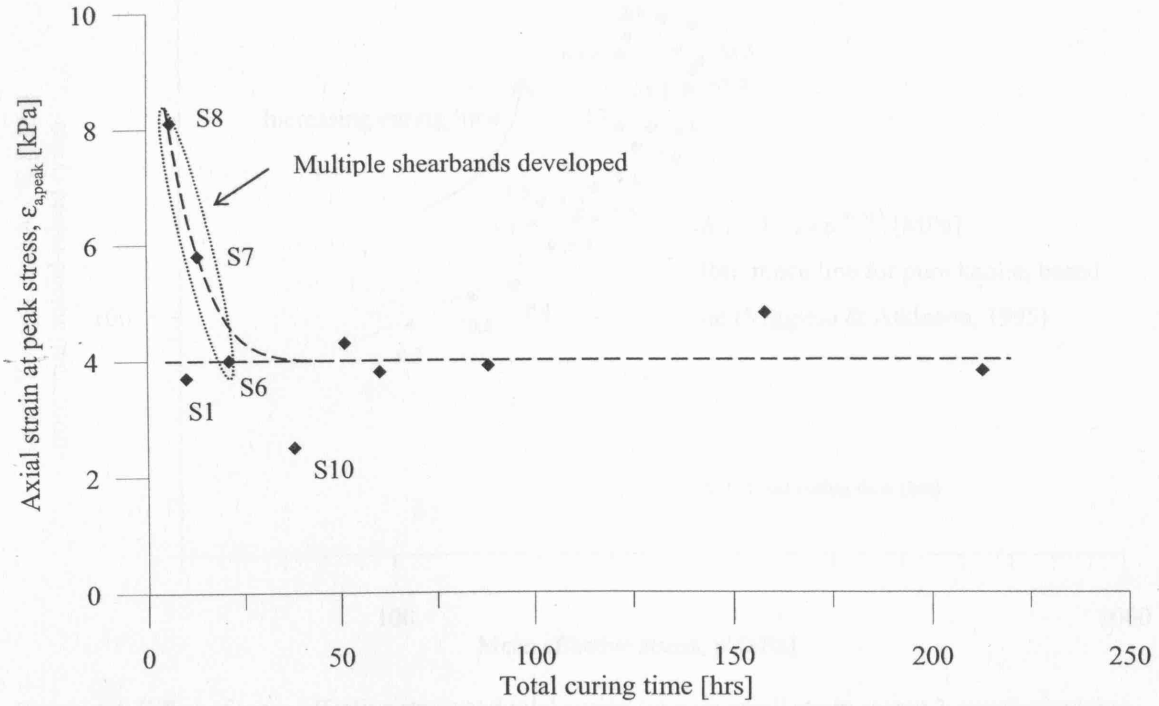

Figure 6-7 Effect of total curing time on failure strain in cement-mixed kaolin

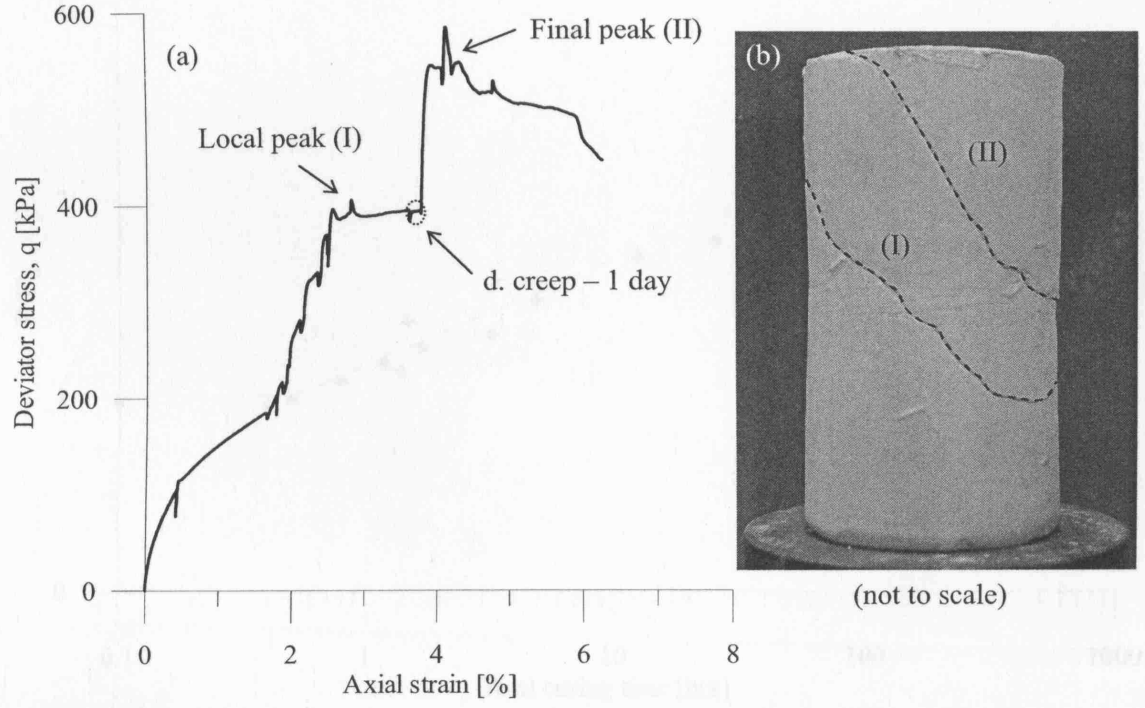

Figure 6-8 Illustrating the development of multiple shearbands at low curing time in cement-mixed kaolin (S6cmk) (a) stress-strain curve, (b) photo of shearbands in specimen

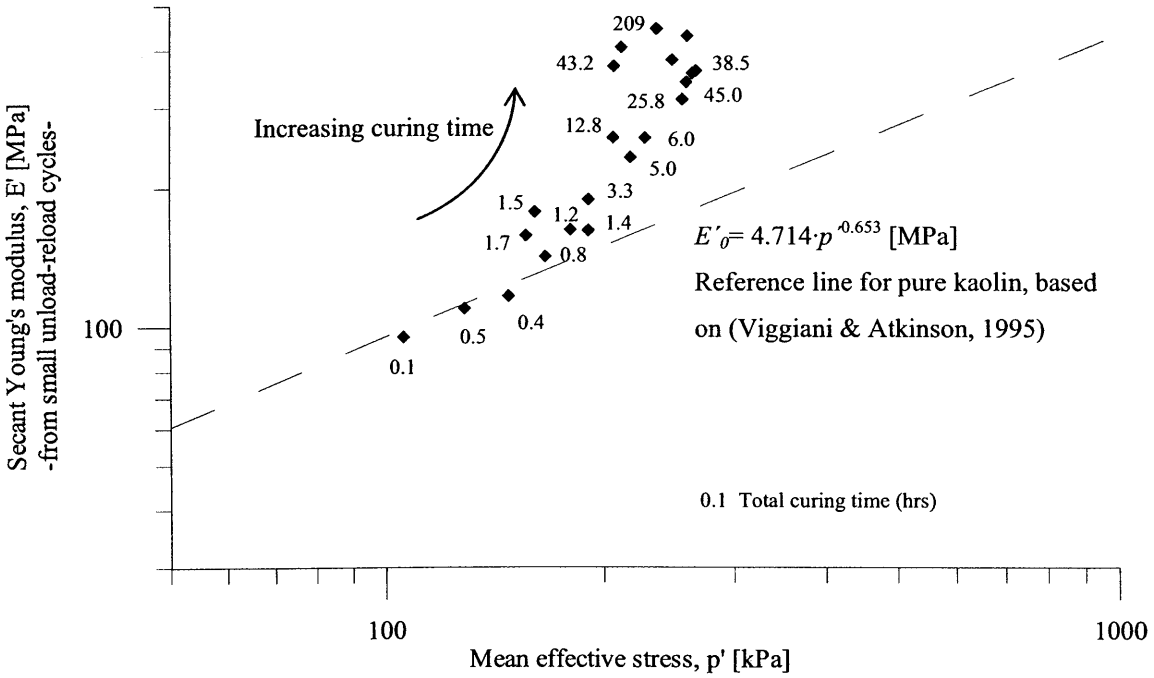

Figure 6-9 Effect of mean effective stress and total curing time on small strain secant Young's modulus in cement-mixed kaolin

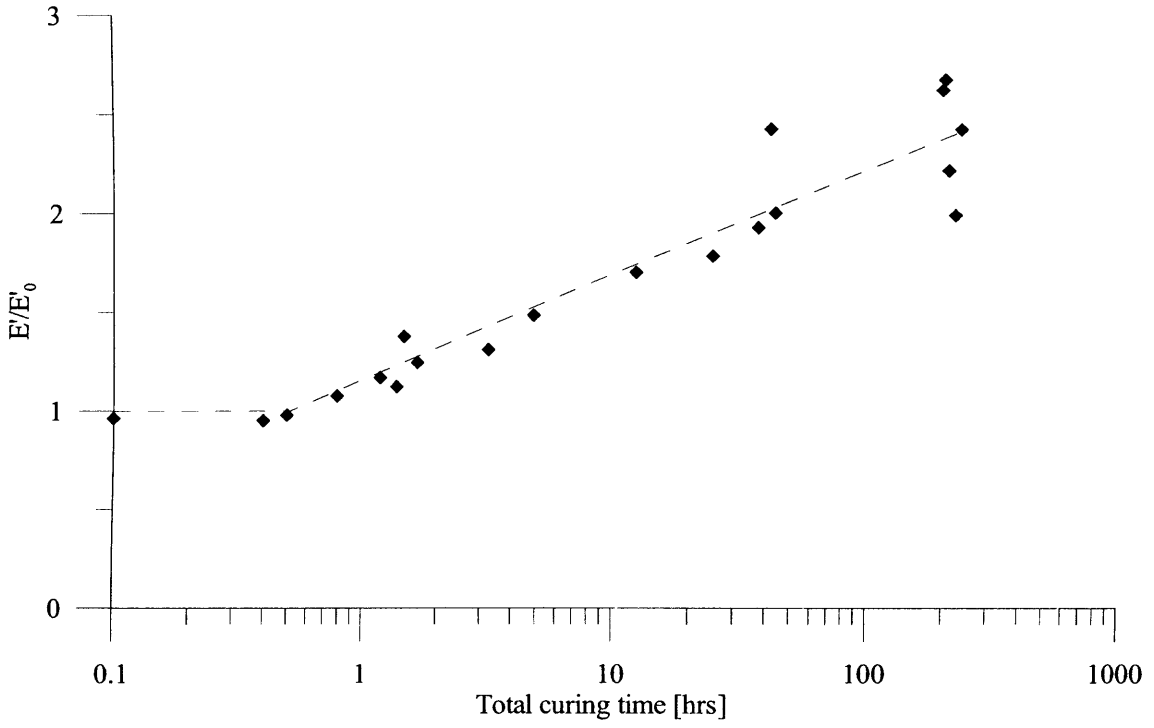

Figure 6-10 Effect of total curing time on normalised small strain secant Young's modulus in cement-mixed kaolin

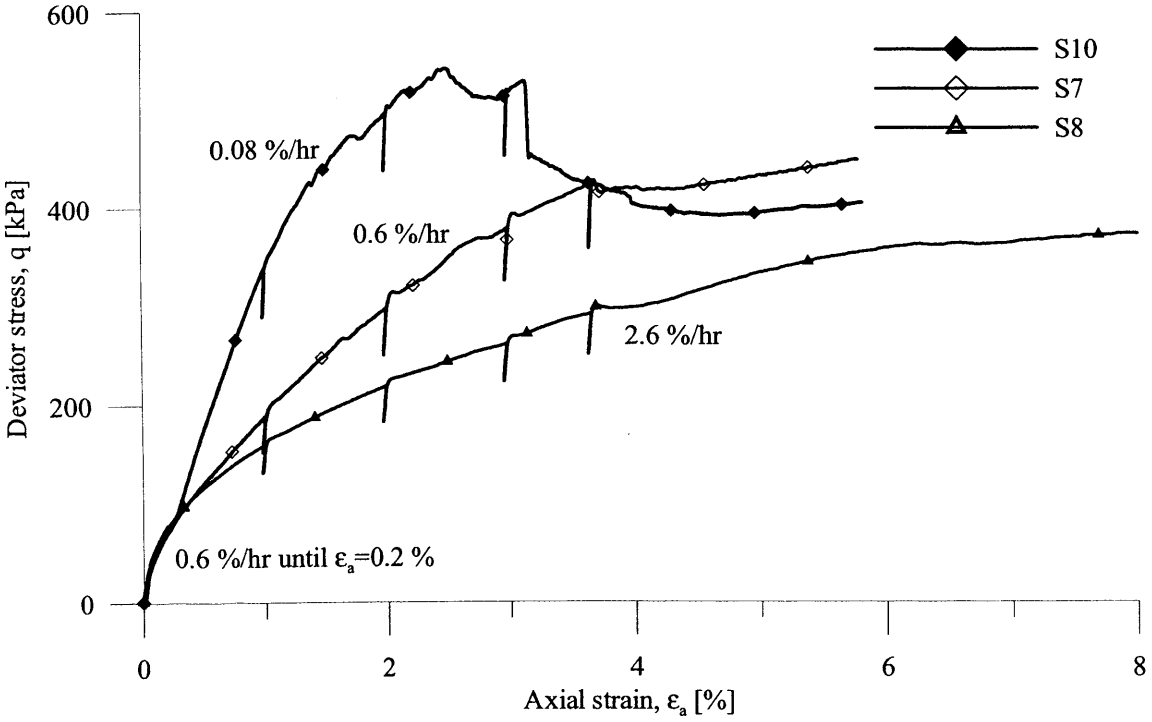

Figure 6-11 Coupled effect of axial strain rate and curing time on the stress-strain relationship in cement-mixed kaolin

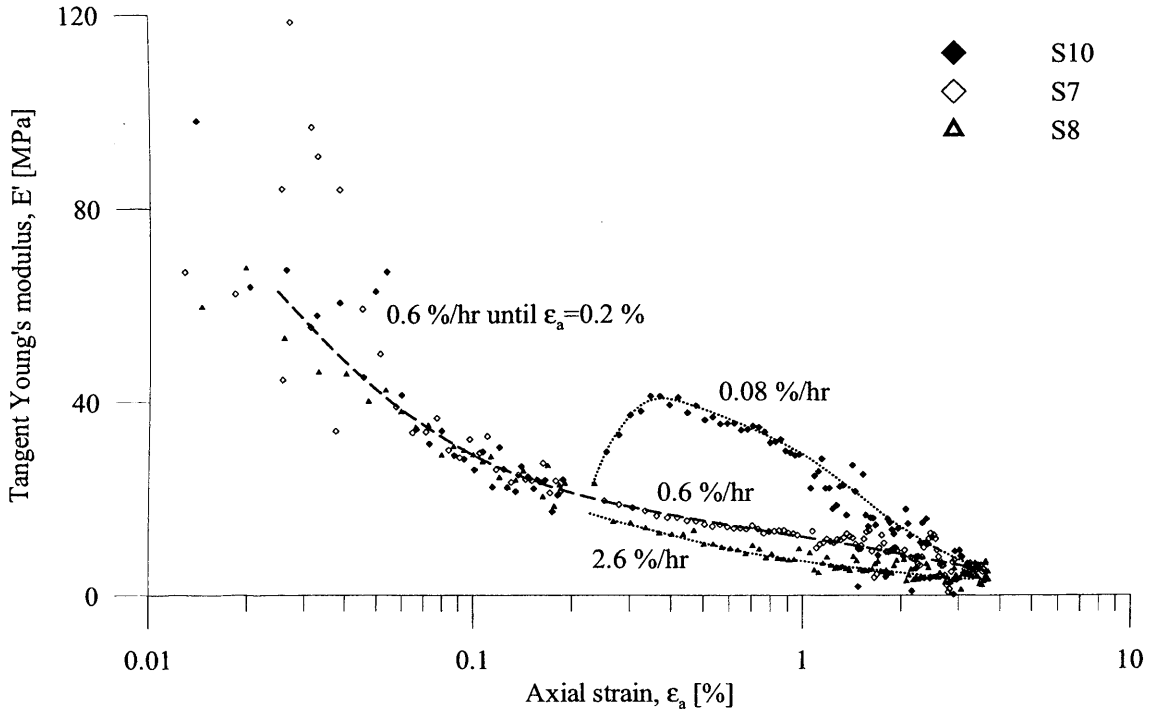

Figure 6-12 Coupled effect of axial strain rate and curing time on the tangent Young's modulus in cement-mixed kaolin

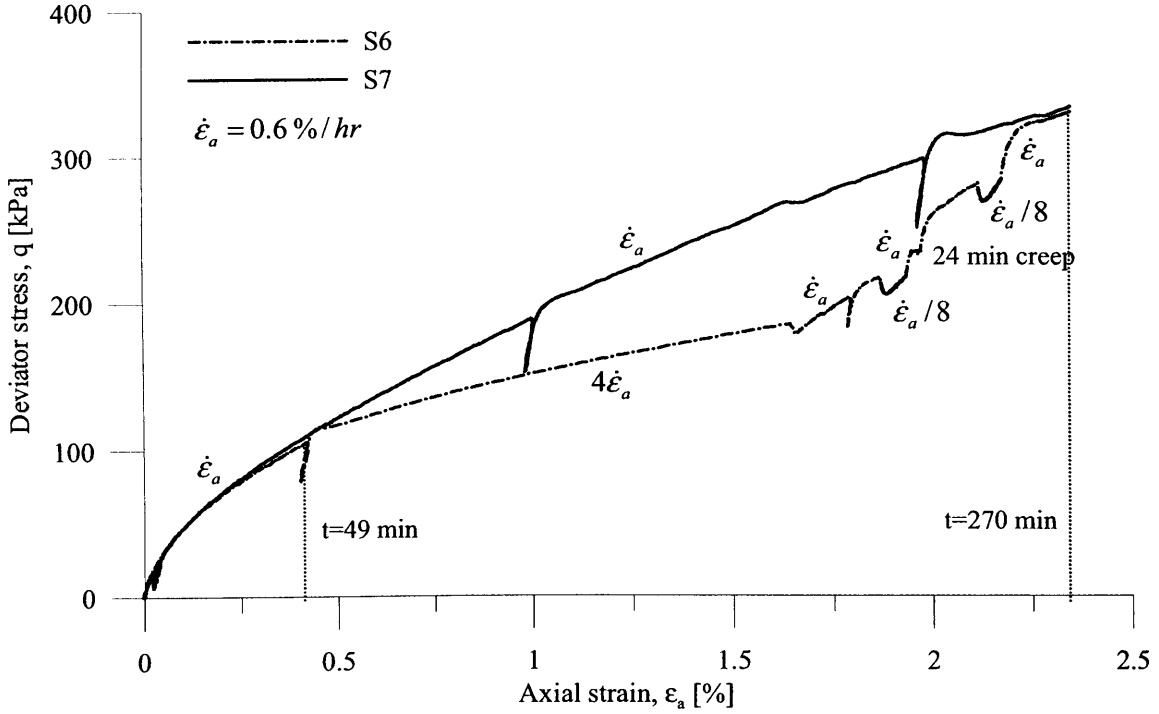

Figure 6-13 Effect of axial strain rate and curing time on stress-strain response in cement-mixed kaolin

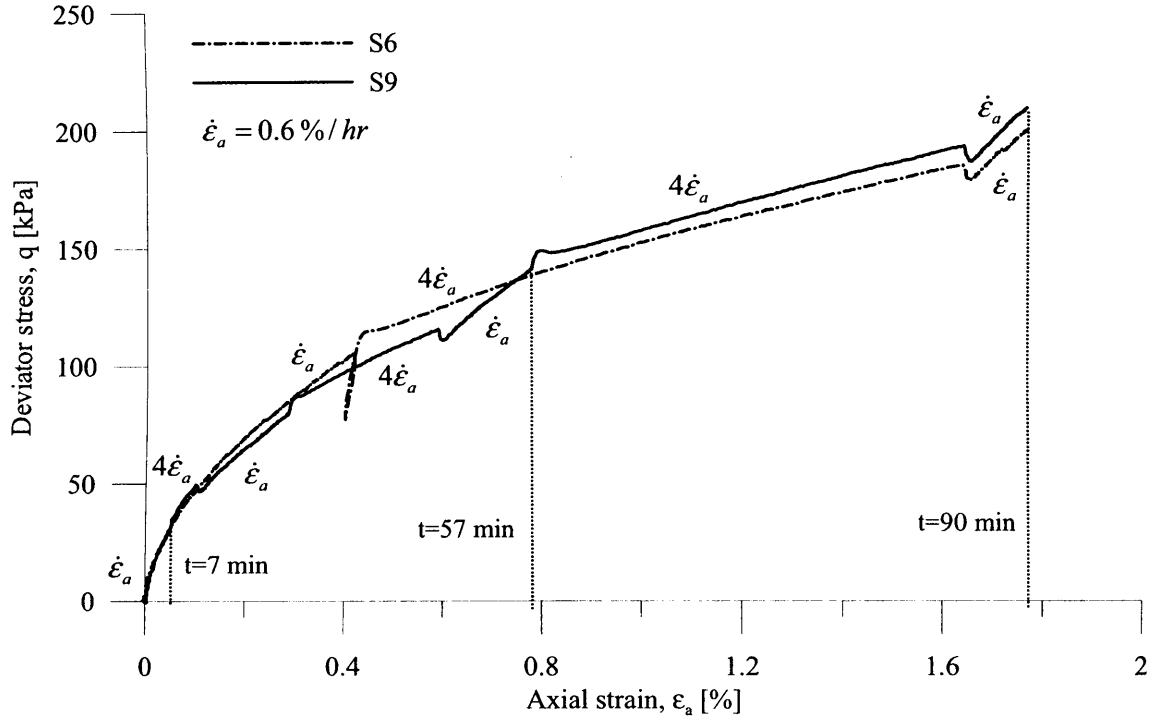

Figure 6-14 Effect of axial strain rate and curing time on stress-strain response in cement-mixed kaolin

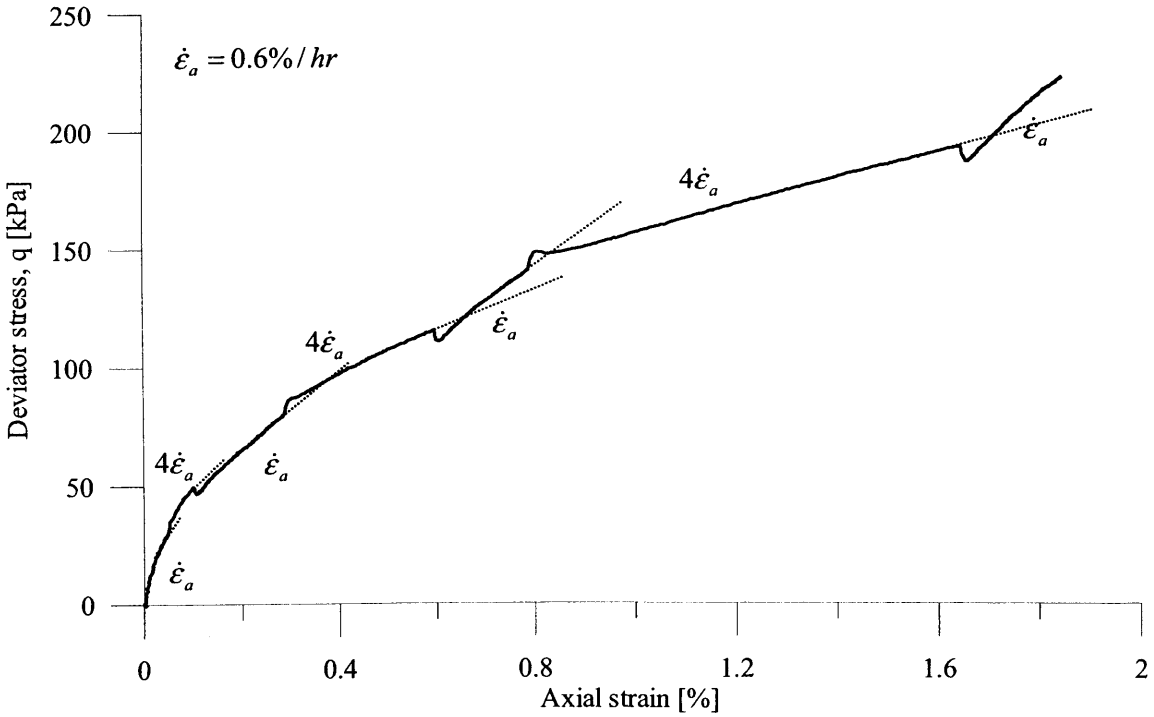

Figure 6-15 Coupled effect of axial strain rate and curing time on the drained stress-strain shearing path of cement-mixed kaolin at early curing time (S9cmk)

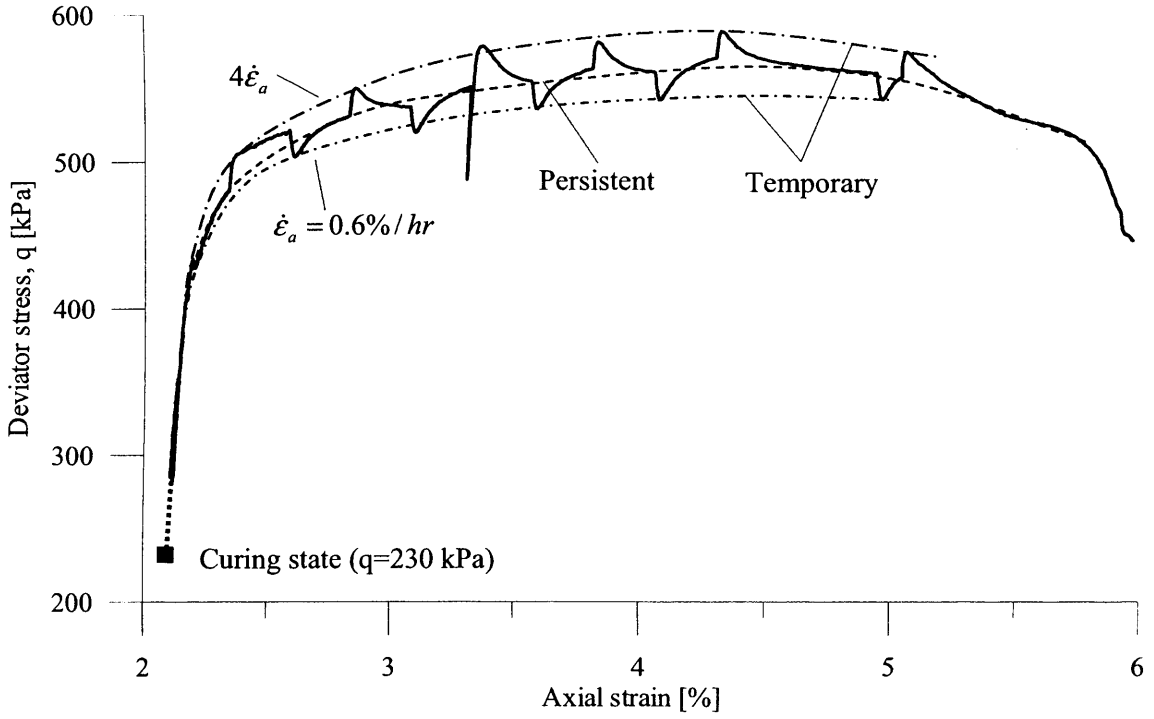

Figure 6-16 Temporary and persistent effects of step-wise change in axial strain rate on the drained stress-strain shearing path of cement-mixed kaolin after 2 days of curing at high deviator stress (S9cmk)

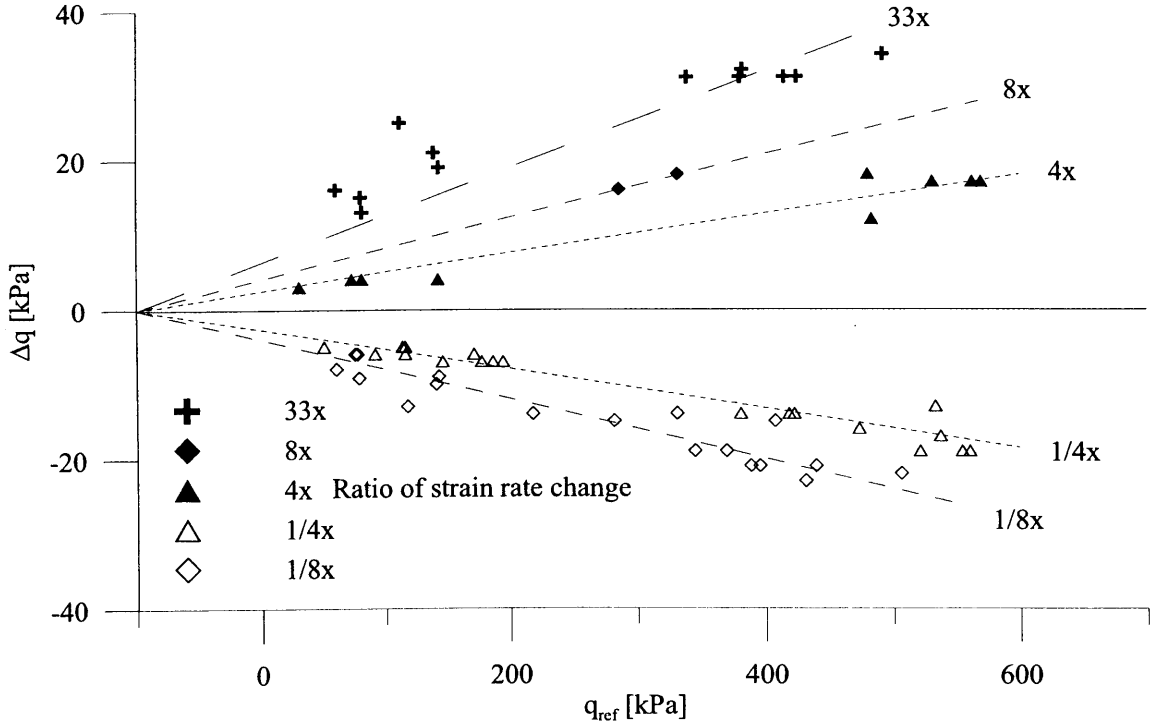

Figure 6-17 Influence of axial strain rate change and deviator stress level on the immediate viscous stress jump during shearing of cement-mixed kaolin

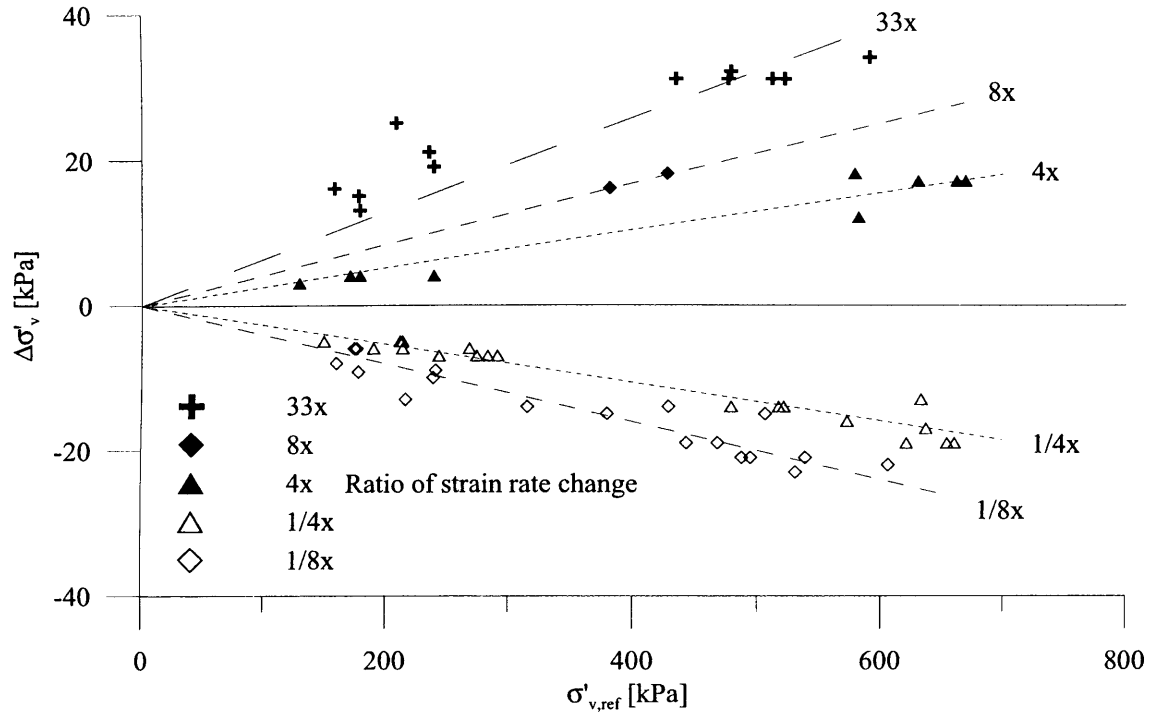

Figure 6-18 Influence of axial strain rate change and vertical effective stress level on the immediate viscous stress jump during shearing of cement-mixed kaolin

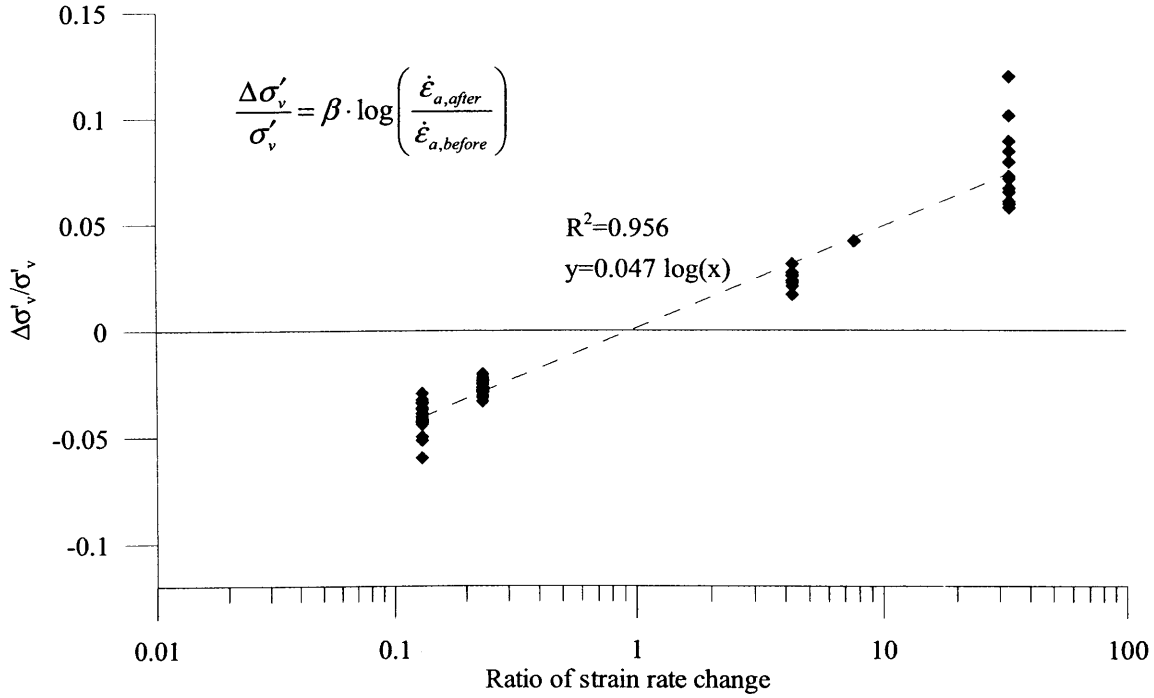

Figure 6-19 Relationship between stress change normalised for current stress level and ratio of axial strain rate change during shearing of cement-mixed kaolin

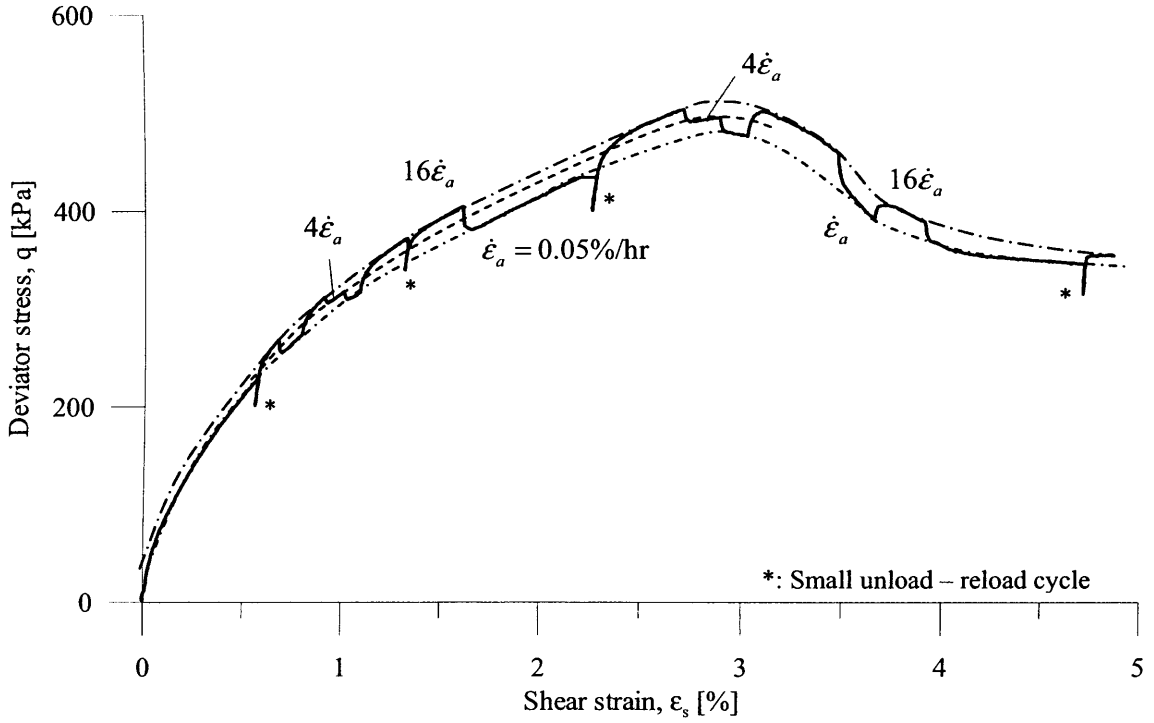

Figure 6-20 Effect of step-wise change in axial strain rate on the undrained stress-strain shearing path of OC intact London Clay (S1LC)

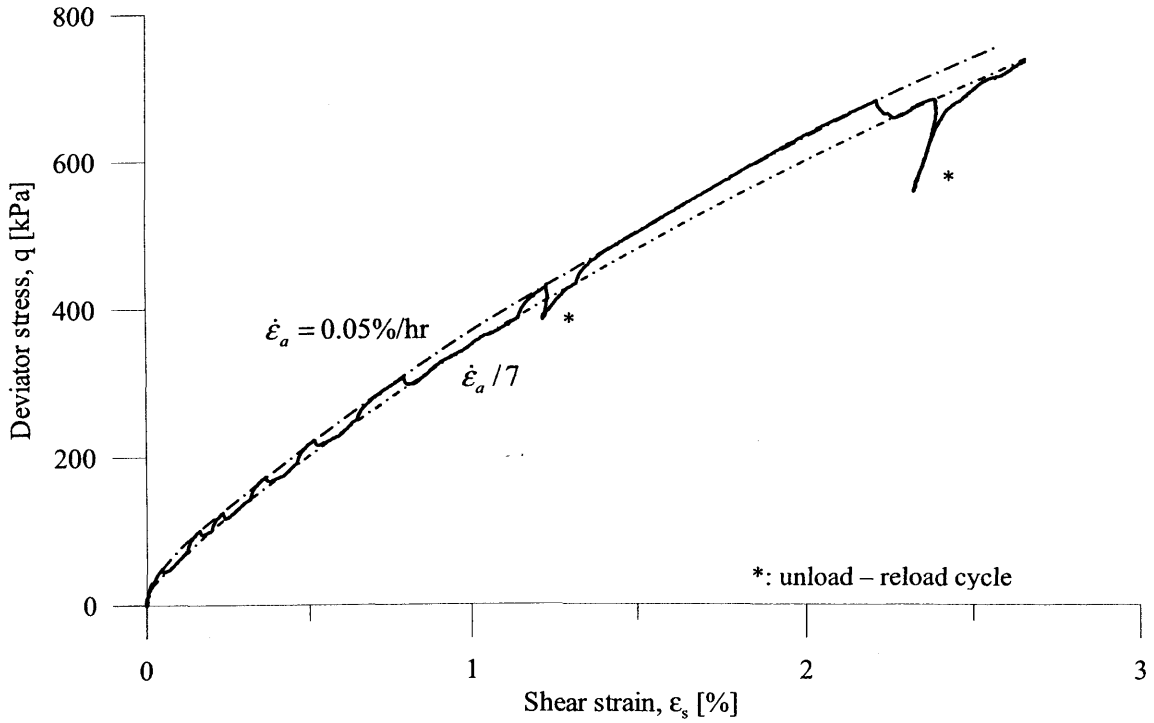

Figure 6-21 Effect of step-wise change in axial strain rate on the drained stress-strain shearing path of OC intact London Clay (S2LC)

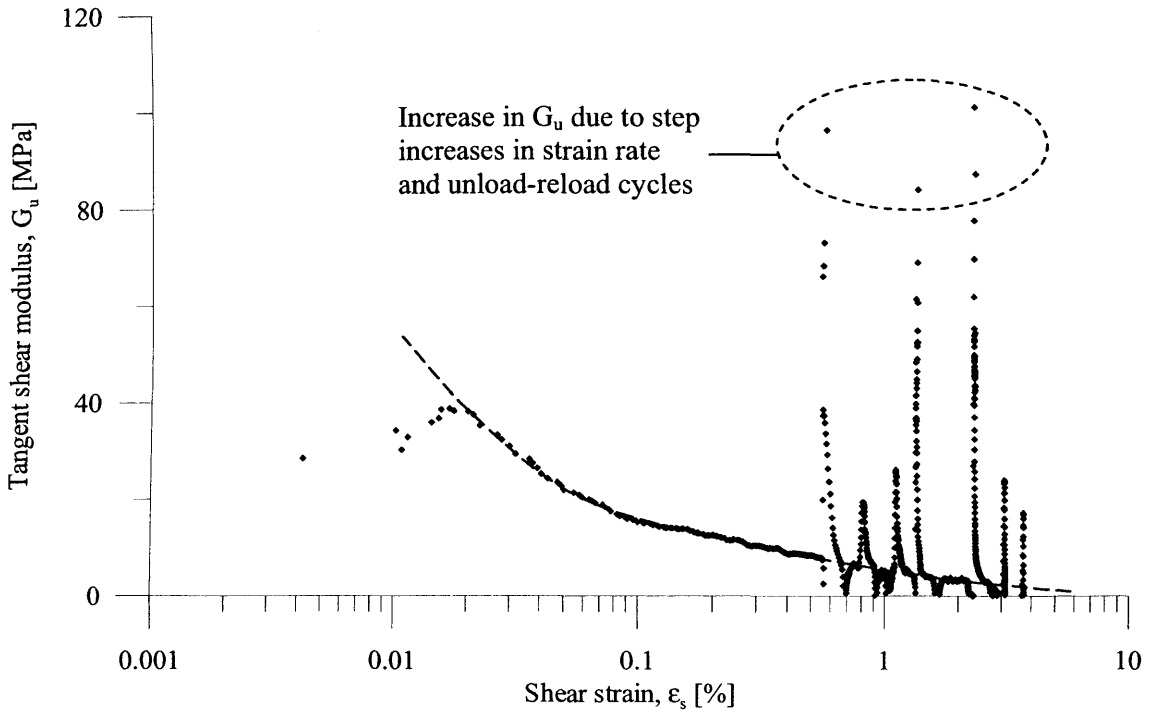

Figure 6-22 Effect of step-wise change in axial strain rate on the small to large strain stiffness during undrained shearing of OC intact London Clay (S1LC)

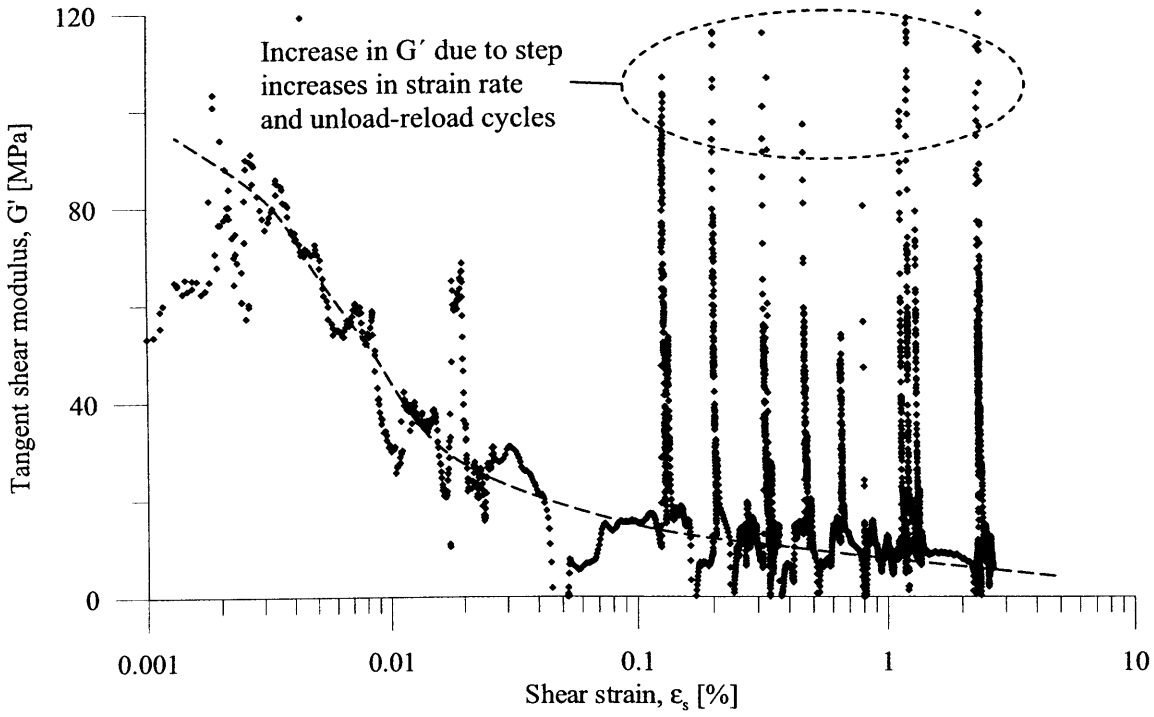

Figure 6-23 Effect of step-wise change in axial strain rate on the small to large strain stiffness during drained shearing of OC intact London Clay (S2LC)

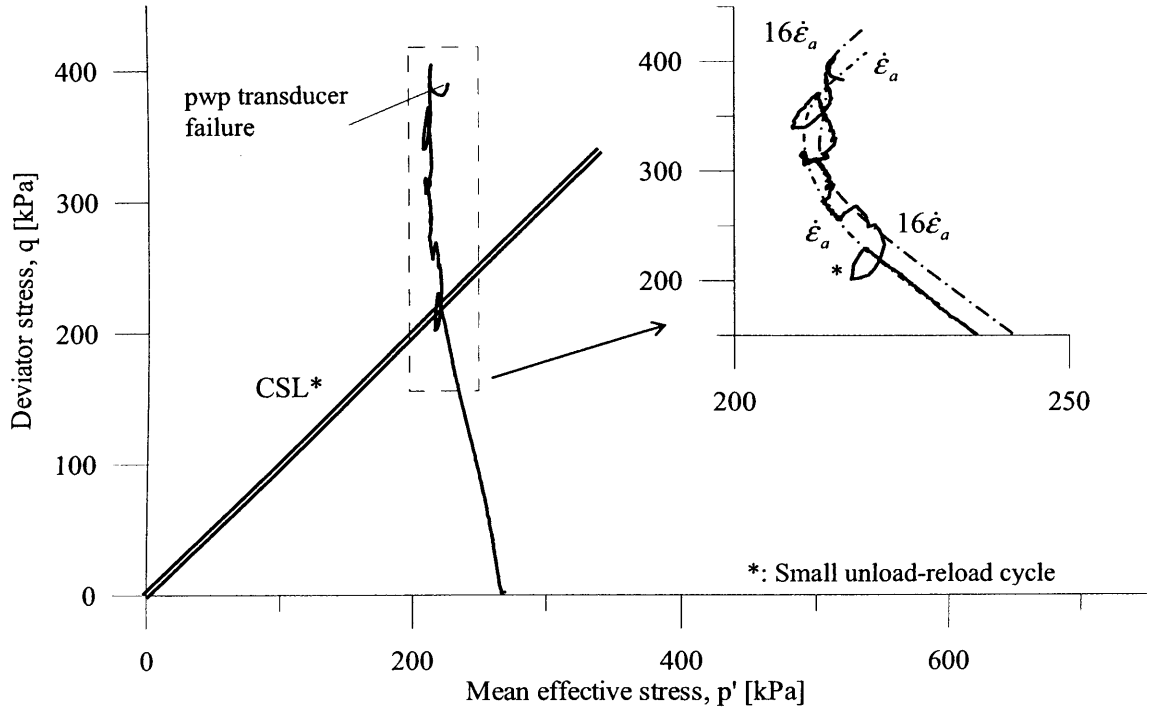

Figure 6-24 Effect of step-wise change in axial strain rate on the undrained stress path of OC intact London Clay (S1LC)

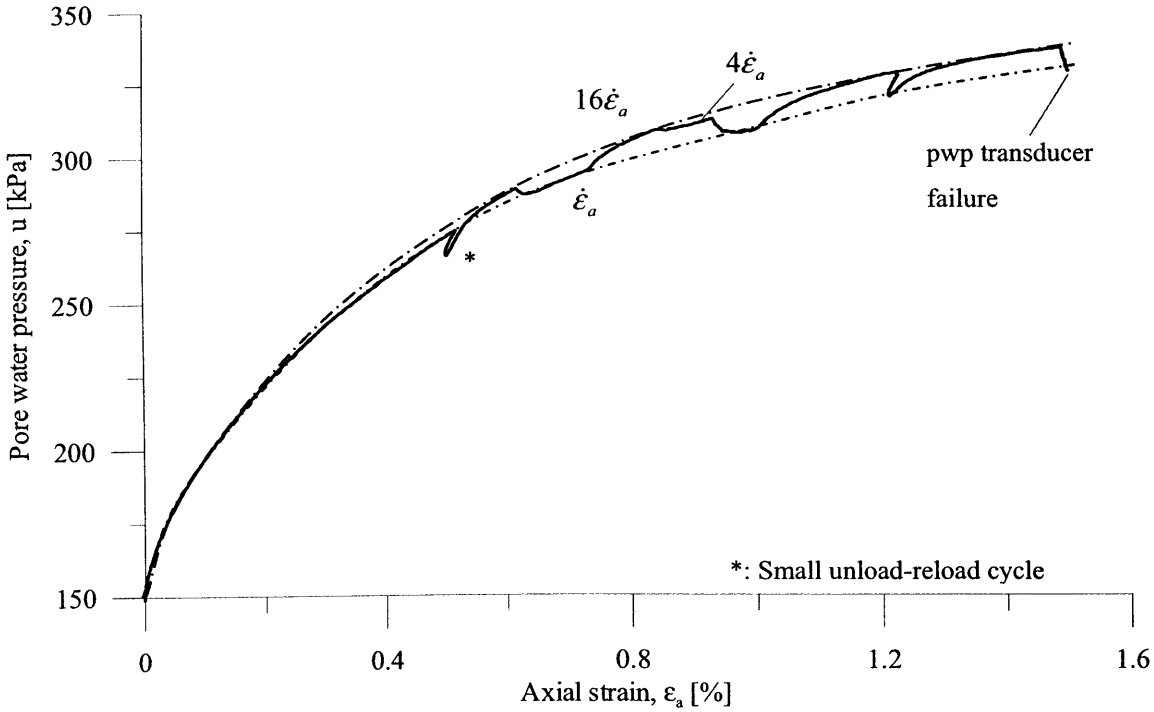

Figure 6-25 Effect of axial strain rate on the accumulation of pore water pressures during undrained shearing of OC intact London Clay (S1LC)

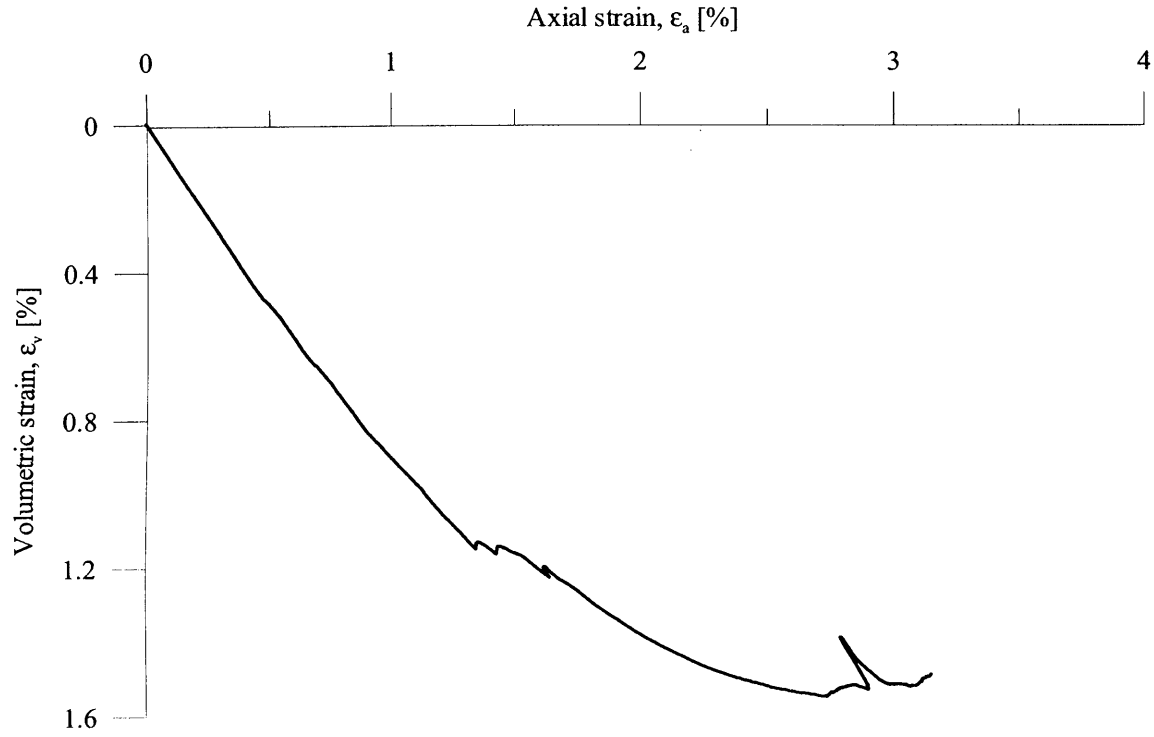

Figure 6-26 Effect of axial strain rate on the evolution of volumetric strains during drained shearing of OC intact London Clay (S2LC)

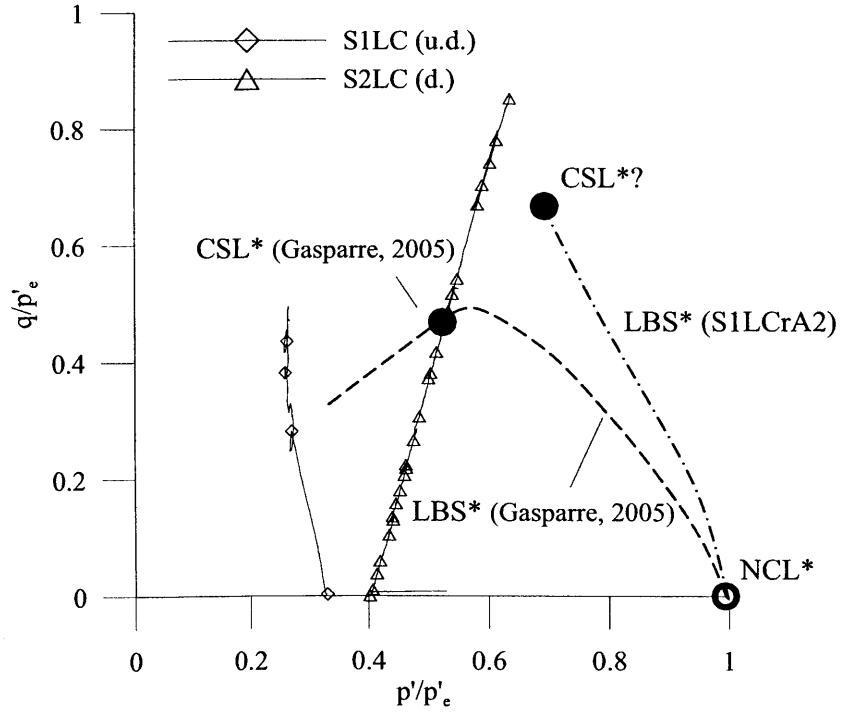

Figure 6-27 Effect of step-wise change in axial strain rate on normalised stress paths of OC intact London Clay

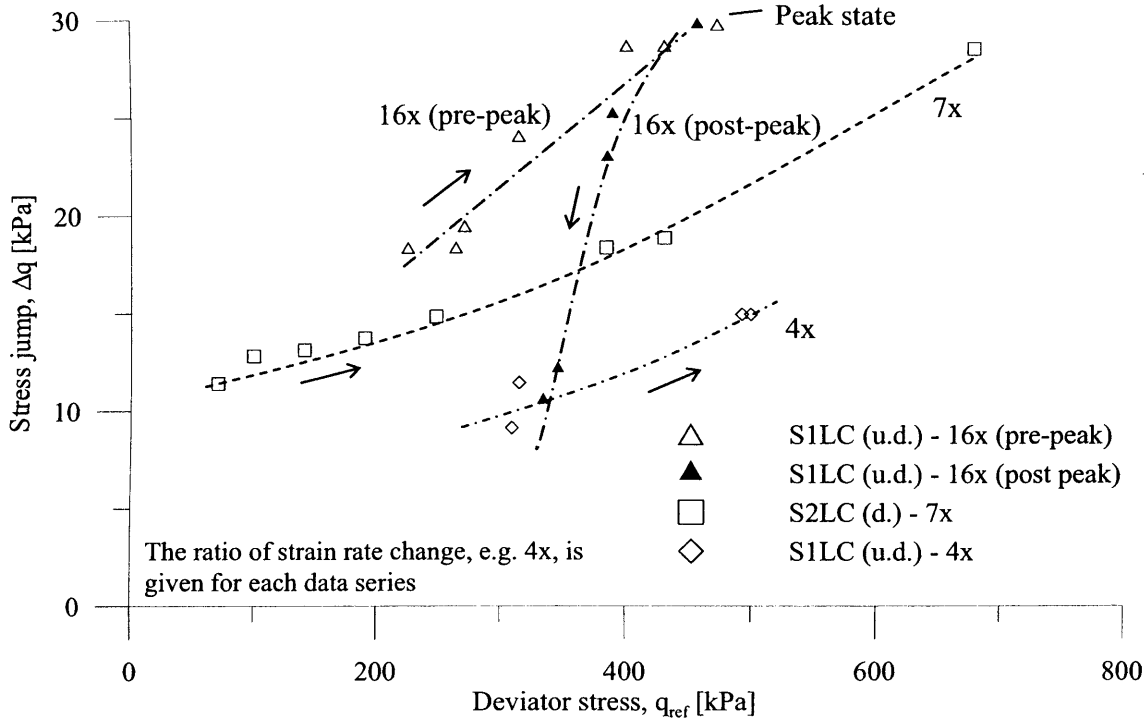

Figure 6-28 Influence of axial strain rate change and stress level on the persistent viscous stress jump during shearing of OC intact London Clay

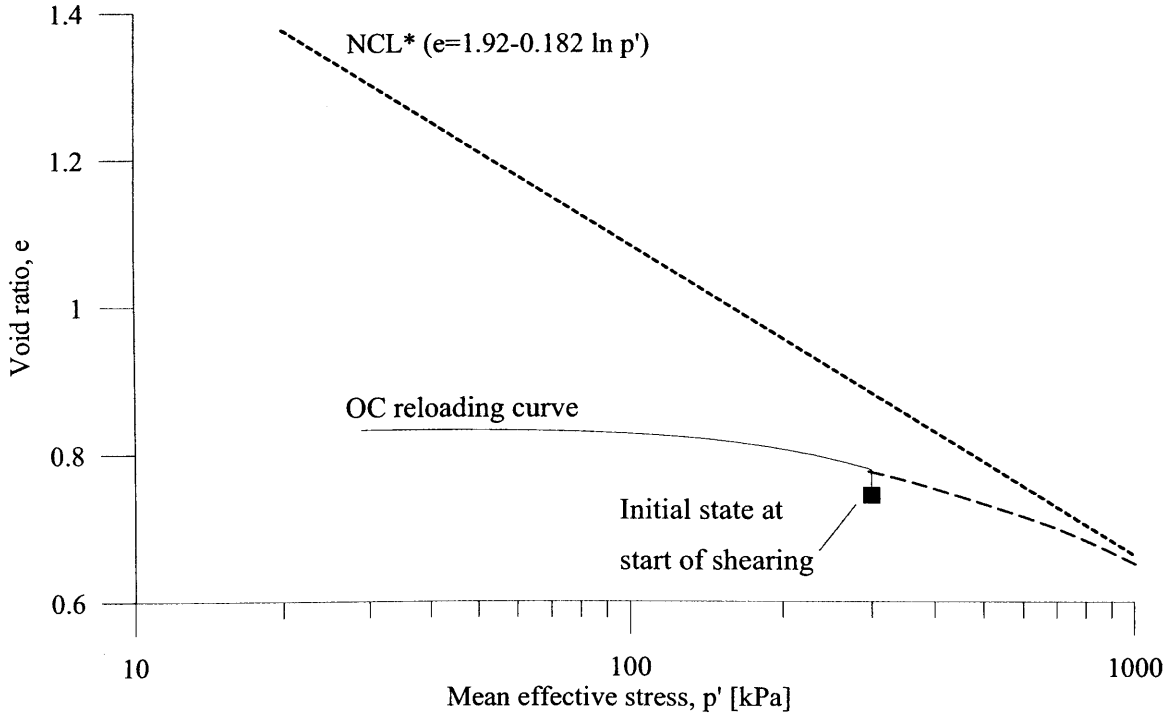

Figure 6-29 Isotropic reloading curve for OC reconstituted London Clay

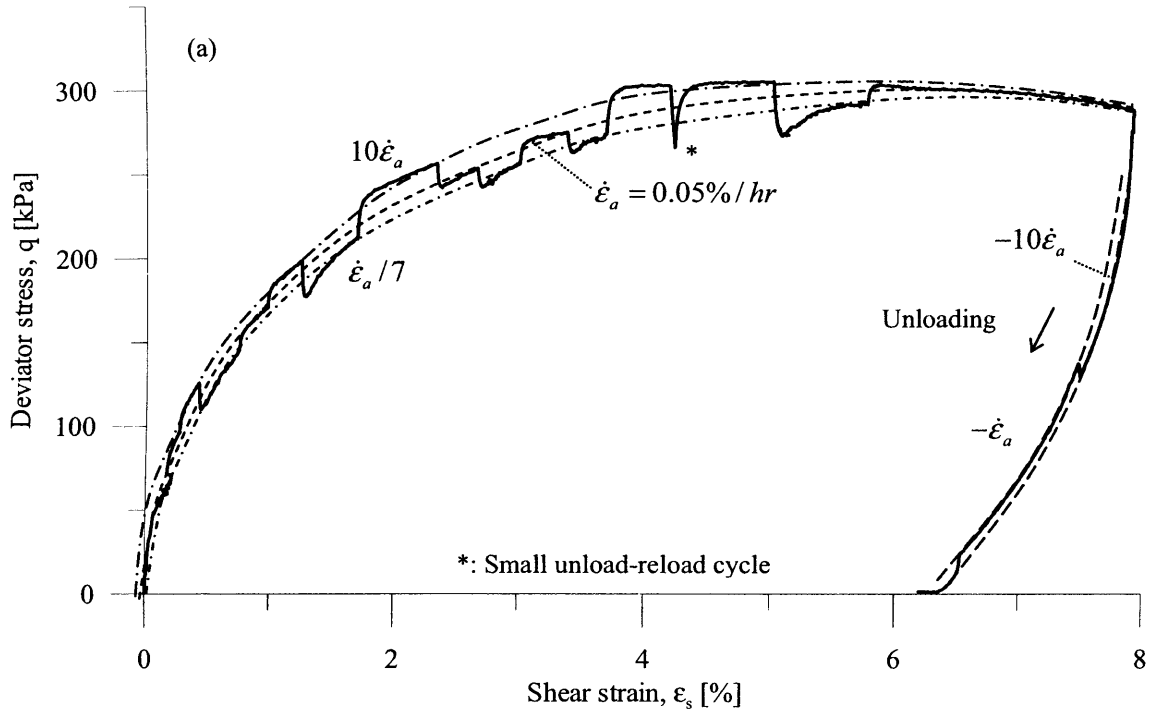

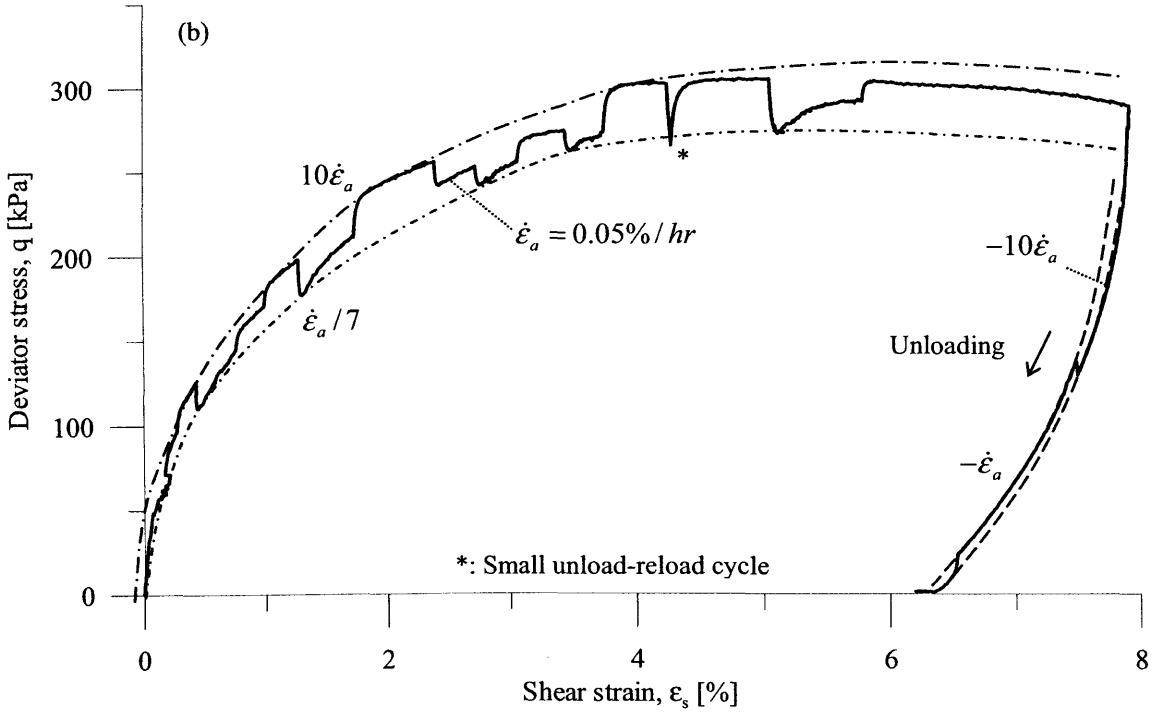

Figure 6-30 Illustrating the effects of step-wise change in axial strain rate on the undrained stress-strain shearing path of OC reconstituted London Clay (S2LCrA5(OC)), (a) persistent effects and (b) boundary curves for the temporary effects

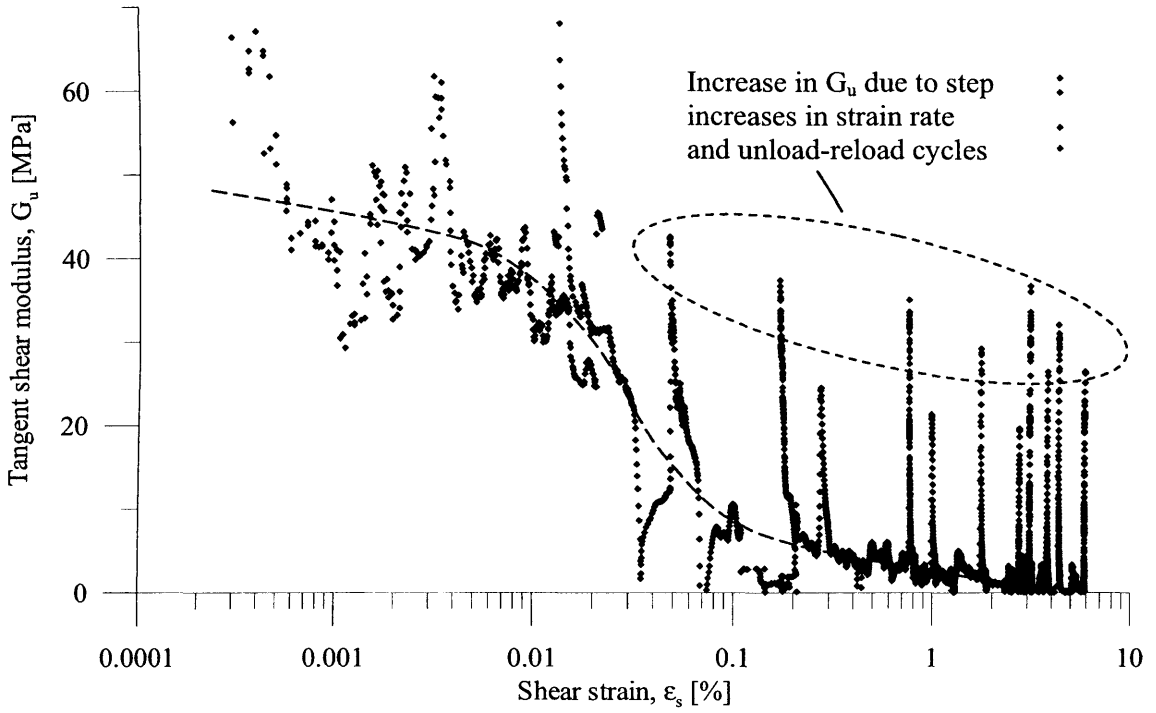

Figure 6-31 Effect of step-wise change in axial strain rate on the small to large strain stiffness during undrained shearing of OC reconstituted London Clay (S2LCrA5(OC))

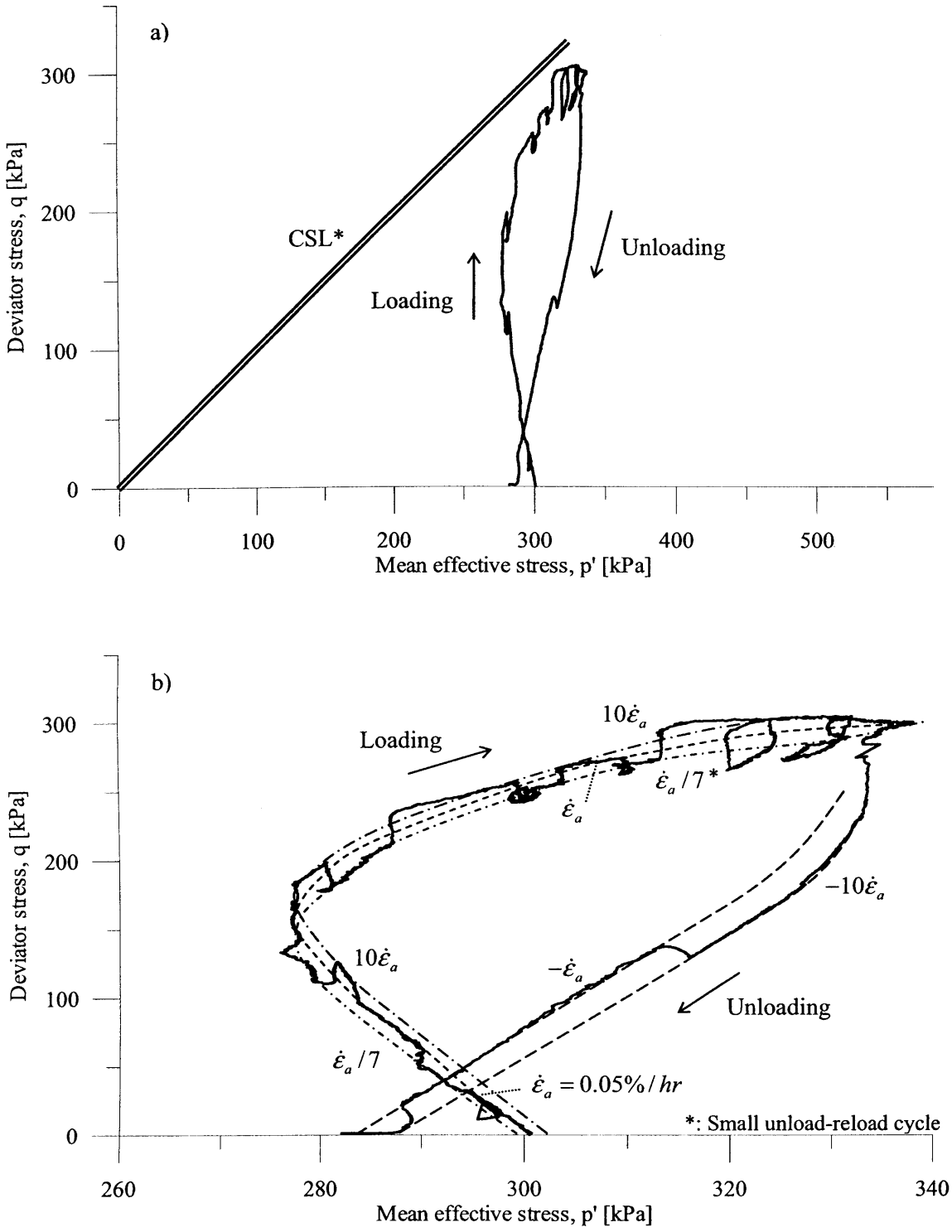

Figure 6-32 Effect of step-wise change in axial strain rate on the undrained stress path of OC reconstituted London Clay (S2LCrA5(OC))

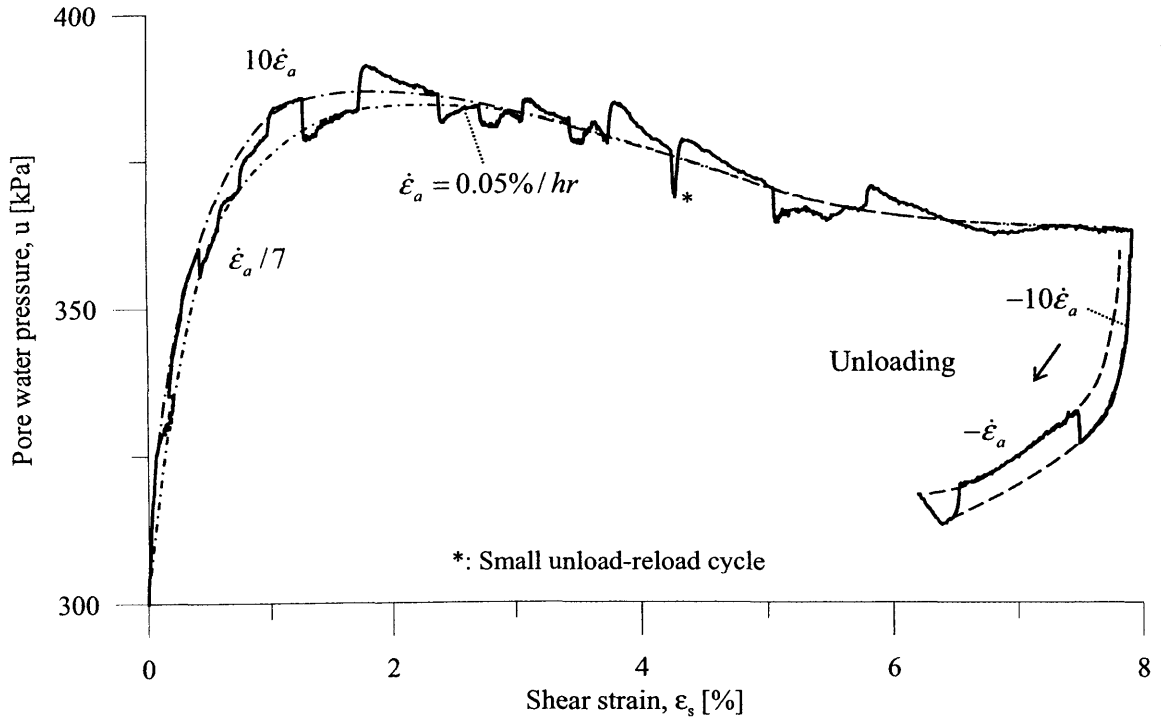

Figure 6-33 Effect of axial strain rate on the accumulation of pore water pressures during undrained shearing of OC reconstituted London Clay (S2LCrA5(OC))

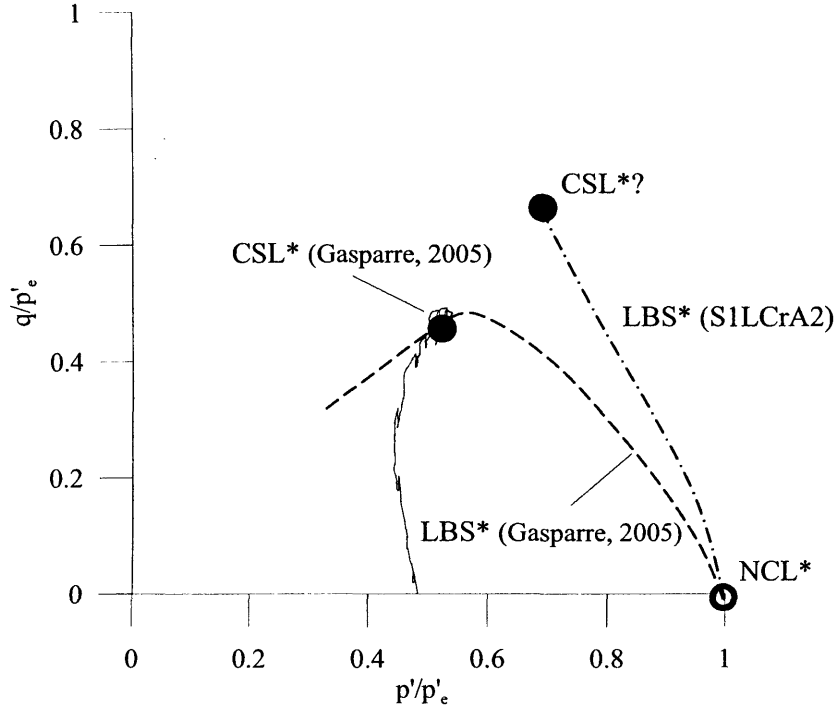

Figure 6-34 Effect of step-wise change in axial strain rate on normalised stress paths of OC reconstituted London Clay (S2LCrA5(OC))

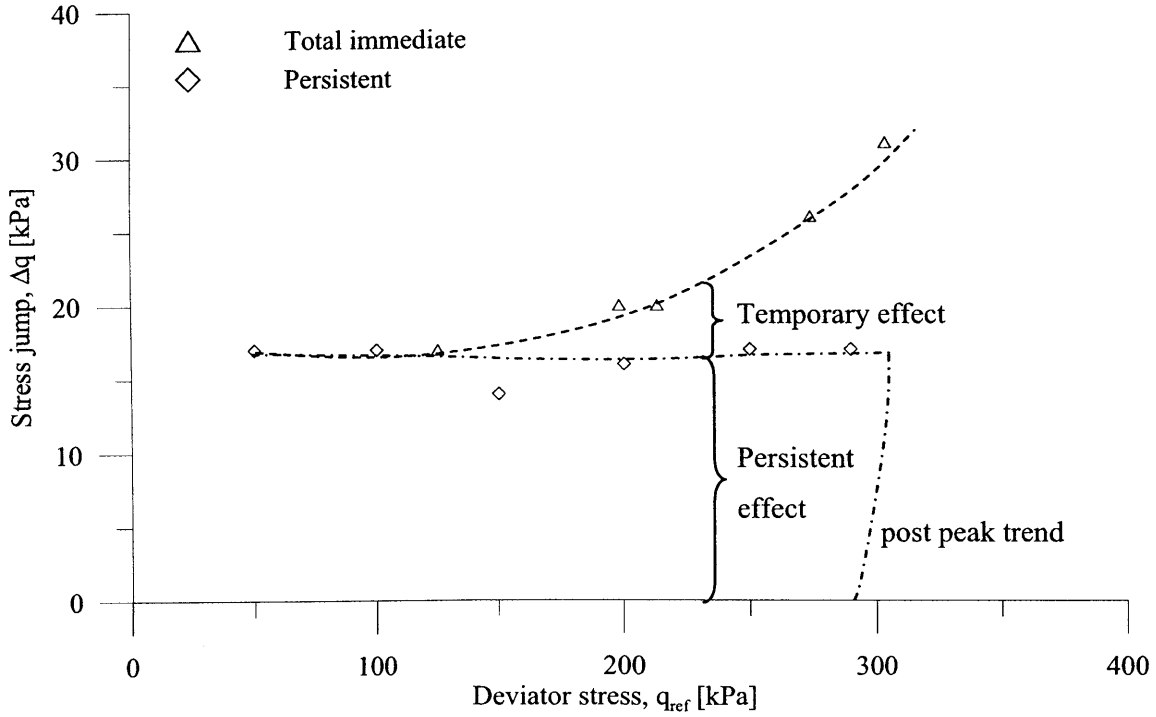

Figure 6-35 Influence of stress level on the viscous stress jump during undrained shearing of OC reconstituted London Clay for a axial strain rate change of 70x (S2LCrA5(OC))

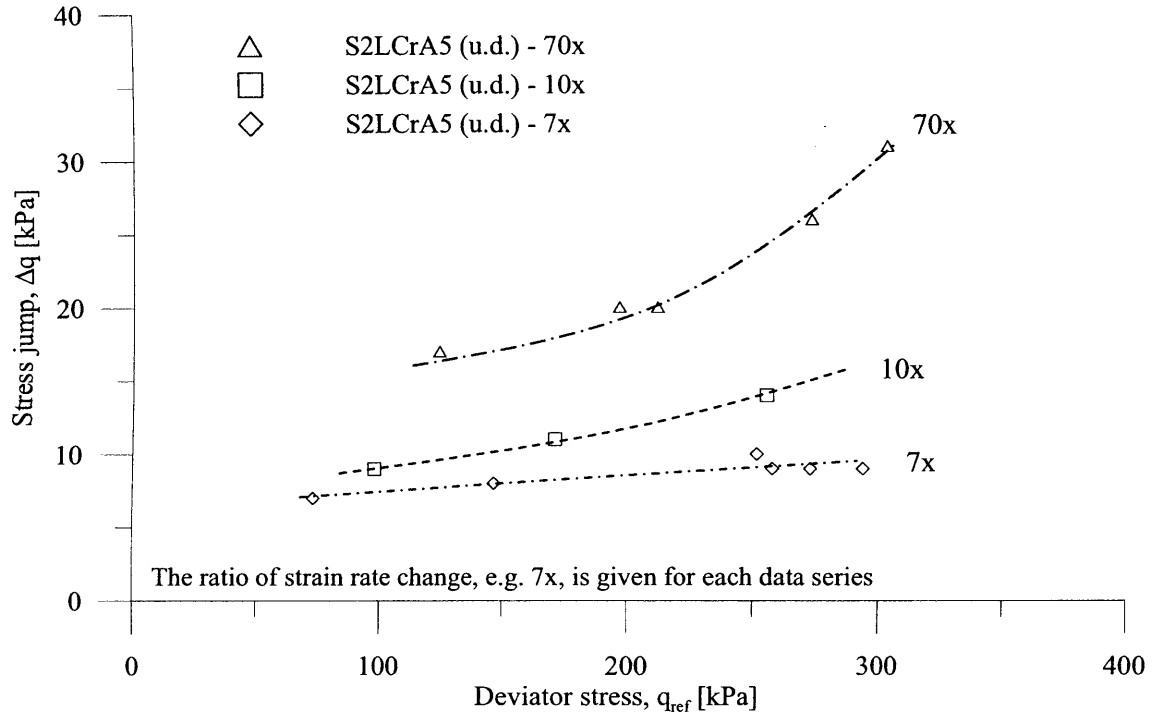

Figure 6-36 Influence of axial strain rate change and stress level on the total immediate viscous stress jump during shearing of OC reconstituted London Clay (S2LCrA5(OC))

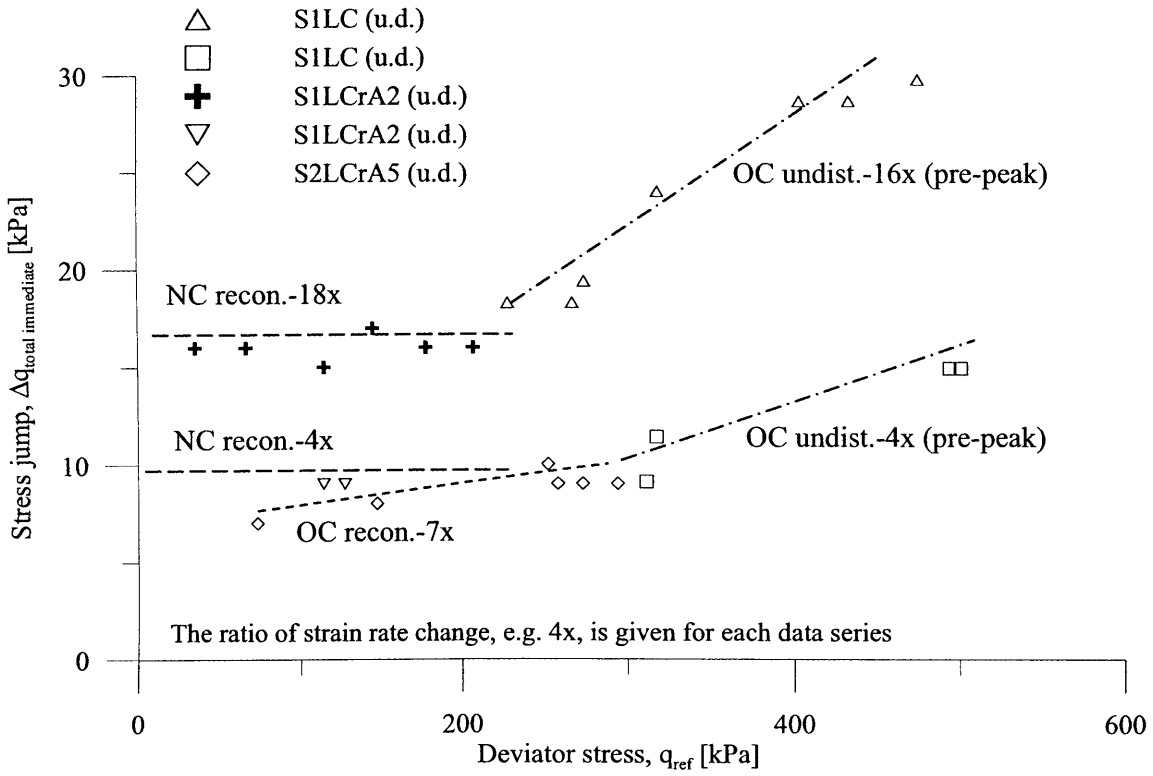

Figure 6-37 Comparing the influence of axial strain rate change and stress level on the total immediate viscous stress jump during shearing of London Clay

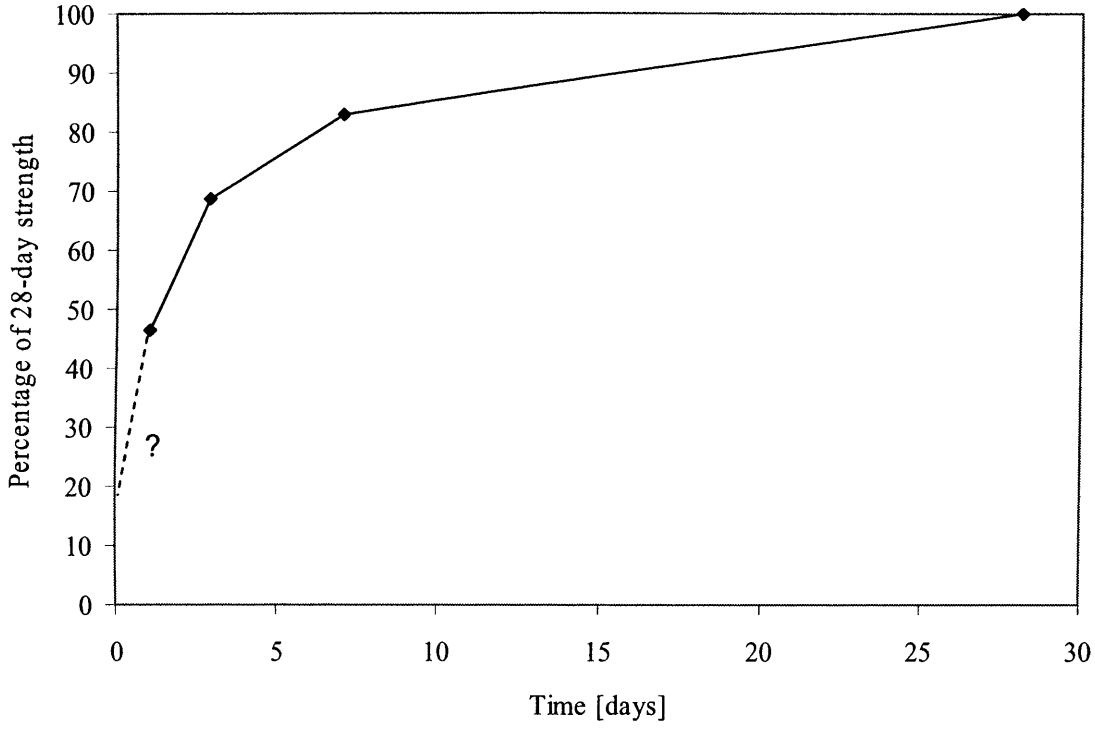

Figure 6-38 Schematic illustration of compressive strength increase of RHP cement, data points from (Tennis, 1998)

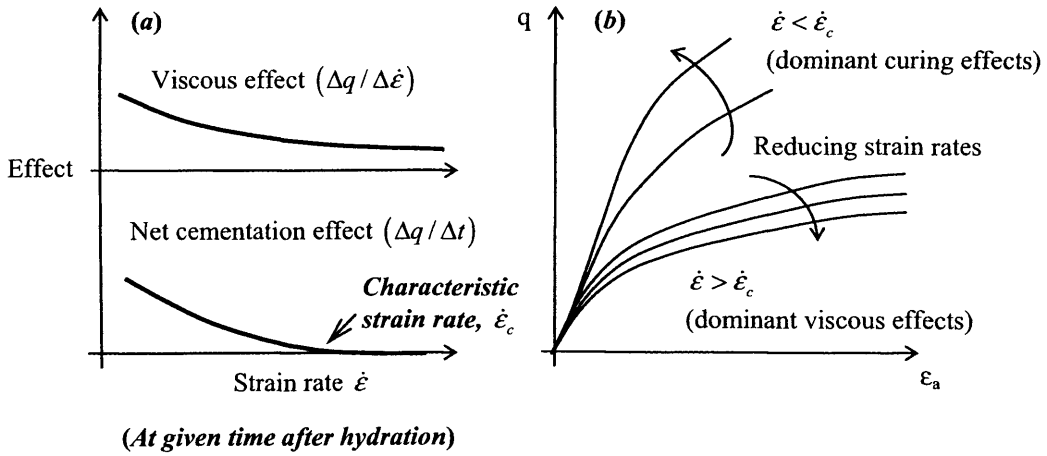

Figure 6-39 Coupled effect of strain rate and curing time (characteristic strain rate)

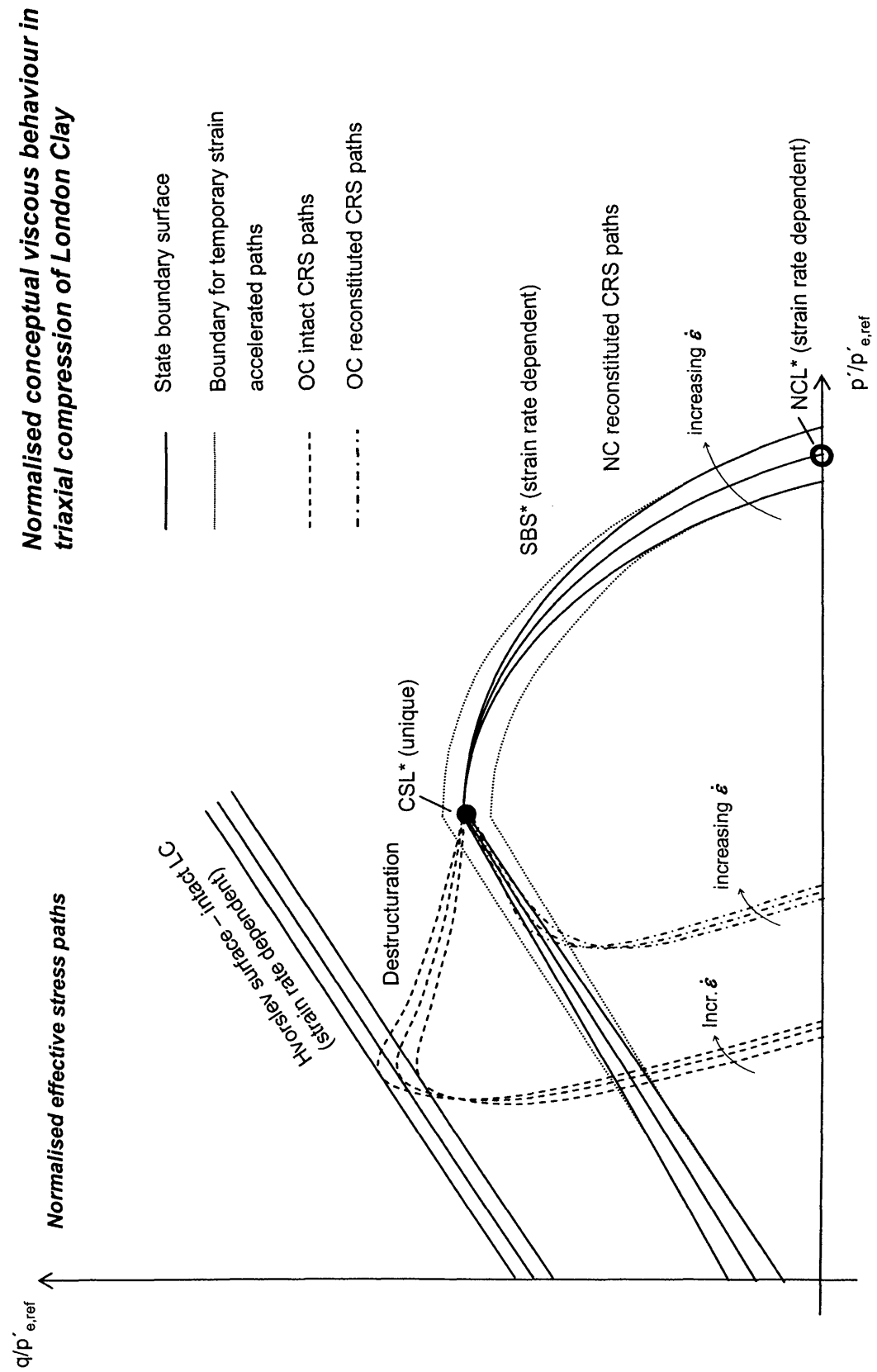

Figure 6-40 General normalised viscous behaviour of London Clay in triaxial compression – illustration of conceptual behaviour

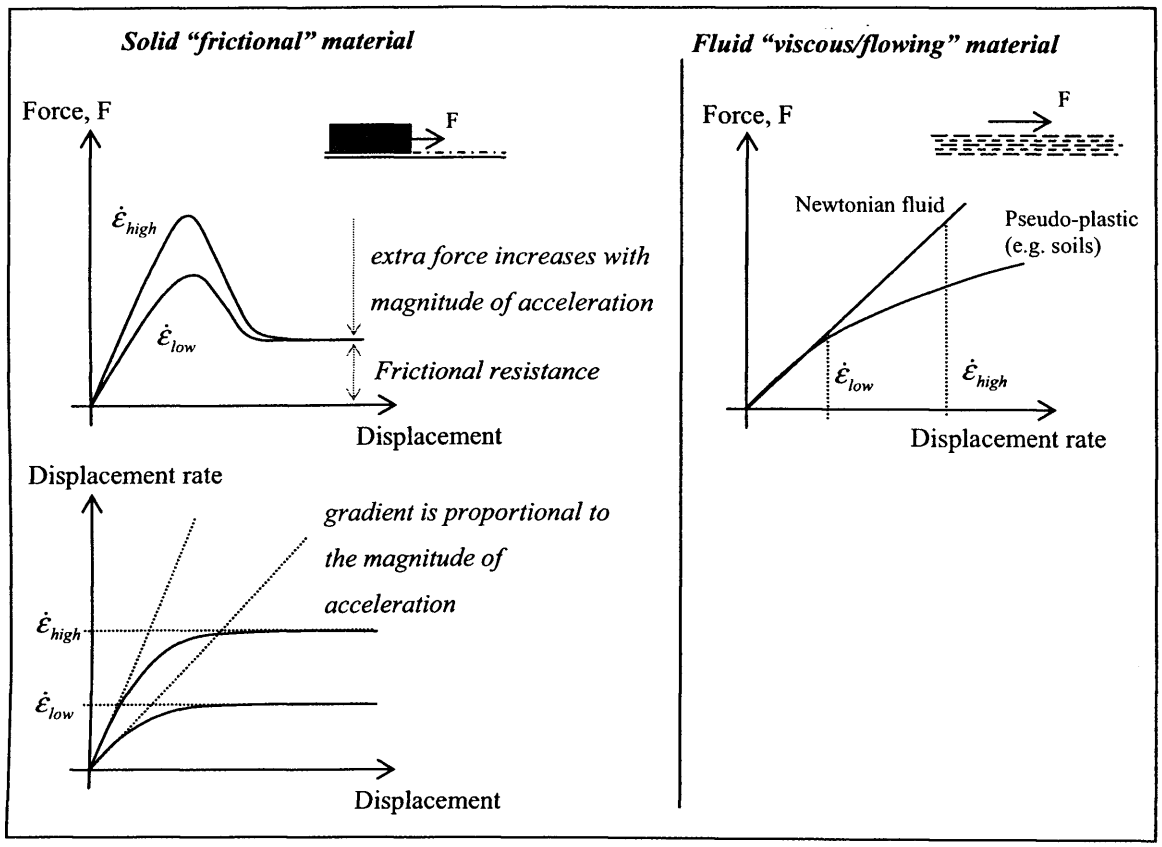

Figure 6-41 Idealised concepts of solid and fluid mechanics

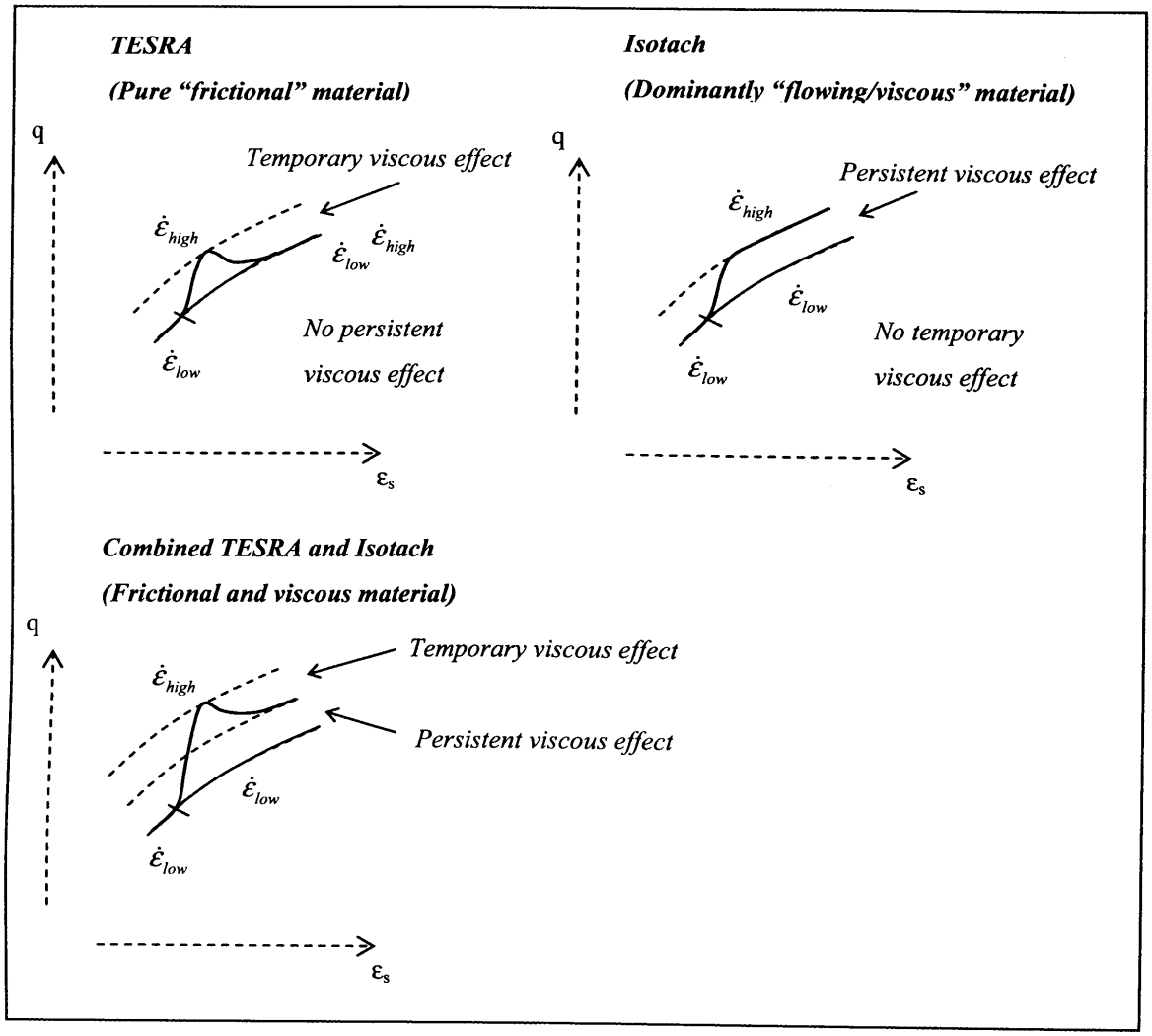

Figure 6-42 Concept of viscous behaviour of soils

CHAPTER 7 CONSTITUTIVE MODELLING

7.1 MODIFICATION OF AN EXISTING ADVANCED CONSTITUTIVE MODEL

The conceptual viscous behaviour of reconstituted and undisturbed London Clay derived from the test results in this study and presented in Chapters 5 and 6, has been used as a basis to extend an existing advanced constitutive model for clays to include viscous effects. This chapter presents the outcome of a simple study that was carried out to investigate the possibilities of implementing viscous behaviour into the existing BRICK constitutive model of soil behaviour. The most significant results of this study are the introduction of a limited number of new parameters and a proposed set of relatively simple modifications to the existing model, which will extend its capabilities to include the simulation of general observed viscous behaviour in soils. It has however been outside the scope of this research to implement the proposed modifications. Nevertheless, this is planned in future work carried out in collaboration with Dr. Simpson and Arup Geotechnics.

In Section 7.1.1 below, the original BRICK model of soil behaviour is briefly described along with a description of recent relevant extensions proposed and implemented by other researchers. The modifications proposed in this study are described in the subsequent sections.

7.1.1 The BRICK soil model

a Description of soil model

The advanced BRICK soil model, described in detail by Simpson (1992a); Simpson (1992b), was developed to better predict ground movements encountered around typical engineering structures, such as deep basement excavations, by taking account of the highly non-linear elasto-plastic behaviour of soils. BRICK can be classified as a multiple kinematic yield surface model formulated within the conventional Cam Clay critical state framework (Schofield & Wroth, 1968). A novel feature of the constitutive model is that the soil behaviour is modelled in strain plane rather than the traditional stress plane. Within strain plane the model is based on an analogue of a man pulling a number of bricks via strings of various lengths. The man represents the current point in strain plane of the soil element while each brick represents a proportion of the soil. The movement of the man then represents the total strain of the soil element, the weighted movement of the bricks represents the plastic strain and the difference between the two is the elastic strain, as illustrated in Figure 7-1. It is assumed that only the elastic strains give rise to stress changes. If all the strings initially are slack and the soil element is subjected to a small strain increment, the man initially moves without moving the bricks, i.e. the total strain is fully elastic and the stiffness corresponds to the maximum stiffness. Then as the slack on the shortest string is taken up, the corresponding brick starts to follow the movement of the man,

resulting in limited plastic straining, i.e. yield. If the man continues in the same direction, the remaining bricks on the longer strings will be engaged one after the other, and a greater proportion of the soil can be said to yield. Each string can therefore be taken to represent the size of the kinematic yield surface for a given proportion of the soil. As the yield surfaces are gradually engaged the plastic strain gradually occupies an increasing proportion of the total strain and the stiffness reduces correspondingly.

b Details of soil model

Non-linear behaviour is simulated in the model by an idealised S-shaped stiffness degradation curve, which is specified using a finite number of strings with different lengths in terms of shear strain and a corresponding reduction in relative tangent shear modulus G_t/G_{max}. Figure 7-2 shows the standard stiffness degradation specified by Simpson (1992b) for London Clay for use in the BRICK model. The number of used strings is 10 and the string lengths vary between 0.0083 % and 8 % in terms of shear strain. This means that the soil behaviour is linear elastic until a shear strain of 0.0083 % and the shear stiffness reaches a minimum at a shear strain of 8 %. Generally, the deviator stress is controlled by the stiffness degradation curve and the shear strain level. However, in order to achieve a realistic angle of shearing resistance for different stress paths a modified Drucker-Pracker strength envelope was incorporated into the model at a later stage to control the failure state (Oasys Ltd., 2001). Post-yield, the virgin compression and swelling behaviours are described by two constants λ and κ, and pre-yield, the elastic behaviour (initial stage of swelling or recompression) is specified by the constant ι, as illustrated in Figure 7-3.

c Capabilities of soil model

The BRICK soil model, which is able to perform analyses of soil behaviour under both plain strain and axi-symmetric conditions, has been implemented into the Oasys SAFE finite element program. The original parameters for the model were obtained from tests on reconstituted London Clay, which the model was validated against (Simpson, 1992). The validation highlighted that the model is able to simulate many fundamental aspect of soil behaviour, including features such as:

- Non-linear elasto-plastic soil behaviour with high linear elastic shear stiffness at very small strains and gradual stiffness degradation in the small to large strain post-yield region.
- Kinematic hardening.
- Effect of recent stress history, as found by Atkinson et al. (1990), i.e. the small strain stiffness increase with an increase in the angle of rotation between the approach stress path and the outgoing loading path. It was discussed in Section 5.4.5 that this behaviour is most likely due to viscous effects in the soil.
- Stress-induced anisotropy.

- Influence of state and effect of mechanical overconsolidation on the elastic shear stiffness.
- Fully drained or fully undrained soil behaviour.

As with all advanced soil models, despite the advanced capabilities of the BRICK soil model, many important features of soil behaviour, some of which have been highlighted in this study, still remain to be addressed. These features mainly concern time-dependent aspects of soil behaviour such as:

- Consolidation as a result of dissipation of excess pore water pressures.
- Viscous behaviour (e.g. creep, stress relaxation, strain rate effects, strain acceleration).
- Inherent ageing effect (e.g. thixotropy, bonding, cementation) and environmental ageing effect (e.g. weathering, leaching).

Or aspects related to the micro-structure of the soil, e.g.:

- Inherent anisotropy.
- Effect of both stable (fabric) and unstable (bonding and cementation) components of soil structure, including the destructuration of unstable structure with plastic straining.
- Accurate prediction of dilative behaviour in heavily overconsolidated soils, such as undisturbed London Clay.

d Extensions to the BRICK model implemented by other researchers

In recent years a few studies have proposed simple modifications to the BRICK model in order to extend its capabilities.

The BRICK-S extension developed by Vukandin (2004) enables the model to simulate typically observed characteristics of structured soils by introducing eight additional parameters; two "structure" parameters describe the influence of stable and unstable structure on the distance between the intrinsic and structured normal compression lines of the reconstituted and structured soil in terms of volumetric strain, another two parameters describe the effect of stable and unstable structure on the stiffness degradation curve, while the final four parameters are used to describe the rate of destructuration of the unstable structure with plastic volumetric and shear strains. Similar to the original BRICK model, volumetric behaviour in strain softening soils is not predicted well by the BRICK-S model.

The BRICK on Ice model developed by den Hann (2001) introduces the effects of viscous behaviour by giving each of the bricks individual creep rates, whilst keeping the string lengths constant. This simple modification, which uses only one additional parameter to describe the creep behaviour, enables the model to simulate typical observed viscous effects in one-dimensional compression such as; creep, stress relaxation, creep strain reversal after a prolonged resting period following unloading, unique stress-strain-strain rate relationships in virgin compression and initial stiff response upon reloading at the original strain rate after a rest period. However, as a result of the simplicity of the model, unrealistic behaviour may be

predicted. For example the model does not predict parallel virgin compression lines for different strain rates. Moreover since the string lengths are independent of strain rate changes, the state does not remain on the yield surface during stress relaxation. As a result the initial response upon reloading is always stiffer than before, even if the strain rate is not increased. This may not be realistic.

Aiming to simulate creep effects, Kanapathipillai (1996) investigated if a manual modification of the string lengths in the original BRICK model could improve the surface settlement predictions for tunnel excavations in stiff overconsolidated London Clay. The study was prompted when the initial prediction of the settlement trough for the excavation of the Heathrow Express Trial Tunnel was significantly different to the observed surface settlements (Simpson, 1999). Creep or ageing after the significant geological unloading history of the London Clay was thought to be one of the causes for the discrepancy. To simulate the effects of time-related plastic creep swelling after the geological unloading history in London Clay, the string lengths in BRICK were reduced by an arbitrary amount (half of original lengths) while maintaining fixed vertical stress (overburden pressure) and rigid lateral boundaries. To maintain equilibrium, vertical creep then took place and the soil experienced a reduction in lateral stress and a corresponding reduction in the value of K_0. Subsequently, at the beginning of the recent stress history cycle, the string lengths were restored to their original lengths to simulate the increase in strain rate at the start of tunnel excavation. This in turn moved the current state inside the yield surfaces and gave rise to an initial stiff response. As a result of the stiffer behaviour of the surrounding soil, the finite element analysis was found to predict a greater and more accurate concentration of the settlements along the centre line of the tunnel, where the greatest disturbance (stress relaxation) had occurred.

It was hence indicated by Kanapathipillai (1996) that creep effects may be simulated in the BRICK model by modifying the string lengths (i.e. yield surfaces) temporarily. In this study this idea has been taken a step further by formulating a direct relationship between the string lengths and the governing factors, which could be either creep time or strain rate. To simulate viscous effects it was deemed most appropriate to use the strain rate as the governing factor rather than time, which would be more appropriate for controlling ageing effects, as highlighted in the literature review and findings from the experimental study. As explained above the bricks on ice concept proposed by den Hann (2001), is particularly good for simulating creep behaviour in both compression and swelling, however the model does not predict the strain rate dependent behaviour well. Hence, rather than adopting bricks with individual creep rates it was believed to be more appropriate to make the string lengths a function of strain rate in order to simulate common aspects of viscous behaviour of soils, such as unique constant rate of strain curves, influence of step-changes in strain rate, creep and stress relaxation. The proposed modifications to the BRICK model are described in the following sections.

7.1.2 Introducing strain rate dependent string lengths in the BRICK soil model to simulate isotach viscous behaviour

A simple modification to the BRICK model is proposed, enabling the model to simulate the conceptual pre-peak isotach viscous behaviour of undisturbed London Clay described previously in Section 6.3.3 and illustrated in Figure 6.40. As highlighted in the literature review (Section 2.3.2a) the model will also be applicable to a range of other soils that exhibit isotach viscous behaviour, including soft clays, other stiff undisturbed natural clays, soft rocks and strongly cemented soils in the pre-peak region. Building on the previous work by Kanapathipillai (1996) it is suggested to introduce strain rate dependent string lengths in the model. As explained in the following, this relatively simple modification allows the model to simulate viscous soil behaviour of the isotach type, which can be characterised by unique stress-strain-strain rate relationships.

a Influence of strain rate dependent string lengths on predicted soil behaviour

If the analogue of the man pulling bricks (Figure 7-1) is considered again, the only difference now is that the man and each individual brick at any given time are moving at individual rates, while the length of each string connecting them will increase with increases in (plastic) strain rate of the corresponding brick. If the man is moving at a constant rate, elastic strains increase gradually and as an increasing number of bricks starts to move the behaviour becomes increasingly plastic. The stress level therefore increases and the stiffness reduces as prescribed by the idealised stiffness degradation curve for given constant strain rate and string lengths.

Now let's consider the situation where the movement of the man is suddenly brought to a halt, the equivalent of a stress relaxation stage with fixed total strain. For a small period of time after the event, the movements of the bricks are unaffected by the halt of the man. The bricks, i.e. plastic strain, will therefore continue their movements towards the man at their original rate. As a result the elastic strain and thereby the stress level reduce. To achieve the reduction in stress level at constant total strain the current area under the stiffness degradation curve G_t vs. ε_s, which is equal to stress level, must reduce correspondingly, as illustrated in Figure 7-4. This however is only possible if the string lengths reduce and therefore as given by the proposed relationship the plastic strain rate will reduce as well. Subsequently as the period of fixed total strain progresses, the bricks gradually move closer to the man at an ever decreasing rate of strain (as controlled by the strain rate dependency of the string lengths) and the stress level reduces correspondingly. If after the rest period the man starts to move again at the original strain rate, the strings will increase back to their original lengths. As a result the strings will initially all be slack and the initial response of the soil will be very stiff. With further straining the stiffness will reduce back to what it would have been if the straining of the soil had continued at a constant rate and at this point the state of the soil will also return to the unique stiffness-strain curve given by the current rate of (plastic) strain.

Figure 7-5 illustrates the influence of creep and subsequent reloading at the original strain rate on the stress-strain path and stiffness degradation curve. In contrast to stress relaxation, during creep the stress level and hence the elastic strain are both fixed. As a result the increase in total strain (movement of the man) equals the increase in plastic strain (movement of bricks) and to maintain a constant area under the stiffness degradation curve (i.e. constant stress level) with increasing plastic strain, the string lengths and hence plastic strain rate gradually reduce with time. When loading is initiated at the original strain rate, the strings increase back to their original lengths. As a result, the current state is momentarily inside all of the kinematic yield surfaces and an initial stiff response is seen followed by gradual yield towards the original stress-strain curve with further straining.

Generally, if strain rate-dependent string lengths are introduced in BRICK, the model will be able to predict a unique stress-plastic strain-plastic strain rate relationship with "parallel" constant rate of strain curves. For a step increase in strain rate, independently of the previous strain or stress history, the model will predict an initial stiff response followed by yield towards a higher lying stress-strain curve, similarly to what can be seen after a rest period. If on the other hand the soil experiences a step reduction in strain rate the string lengths will reduce and the current state will be momentarily outside the previously engaged yield surfaces in non permitted strain space. As a consequence the stress level will be forced to reduce until the state returns to the lower lying stress-strain curve. During creep and stress relaxation in the post yield region, the state stays on the engaged yield surfaces and the subsequent yield stress upon loading is dependent on strain rate, which is realistic. Additionally, during creep under constant deviator stress the elastic to plastic ratio is seen to decrease, which may lead to creep rupture at high deviator stresses. The modified BRICK model may also be able to predict realistic CRS curves in unloading and reloading and negative creep strains after significant unloading, if the strain rate dependency of the string lengths considers this. The model however will be limited to pre-peak soil behaviour and it cannot predict eventual long term reversal of creep strains back to positive after unloading events, as found by e.g. den Hann (2001). In order to achieve this, the strain rate of the bricks should be governed by a creep function, rather than be controlled by the rate dependency of the string lengths, but here a more general model is aimed for. It should furthermore be noted that because the final strength is governed by the modified Drucker-Pracker strength envelope, the strain rate dependency of the string lengths is not enough to achieve a realistic strain rate dependency of the peak strength. Hence, the size of the strength envelope should be a function of the strain rate as well.

b Proposed relationship between strain rate and string lengths

The isotach viscous behaviour of soils can be characterised and quantified in a number of ways, among others from the strain rate dependency of the soil strength, strain rate dependency of the entire stress-strain curve or from the creep behaviour at given stress levels. For the purpose of simplification, it is possible to use the strain rate dependency of the peak strength, e.g. as

reported in the literature from undrained triaxial tests on clays. The relative increase in undrained peak strength, $\frac{\Delta q_{u,peak}}{q_{u,peak}}$ is usually indicated to be proportional to the logarithm of the ratio of strain rate change $\ln\left(\frac{\dot{\varepsilon}}{\dot{\varepsilon}_r}\right)$ (Tatsuoka et al., 2000). Since the undrained strength, $q_{u,peak}$ is more or less proportional to the weighted string lengths, the influence of the absolute plastic strain rate $|\dot{\varepsilon}|$ on the length of each individual string SL can be expressed as;

$$SL = SL_r\left(1+\beta\cdot\ln\left(\frac{|\dot{\varepsilon}|}{\dot{\varepsilon}_r}\right)\right) \tag{7.1}$$

Where SL_r is the string length that define the reference curve at the reference strain rate $\dot{\varepsilon}_r$, and β is a material constant determining the viscous property of the material, similarly to that used by Tatsuoka et al. (1999). If all the string lengths are modified by the same ratio, then the stress level at any given strain will be proportional to $\ln\left(\frac{\dot{\varepsilon}}{\dot{\varepsilon}_r}\right)$, which is in agreement with findings by e.g. Tatsuoka et al. (2000) in tests on clays. Even at the start of shearing a change in strain rate will result in an increase in string lengths. The linear elastic range ε_{EL}, which correspond to the length of the shortest string, will therefore increase with an increase in strain rate whilst the value of the elastic shear stiffness will remain unaffected (Figure 7-7), which is in agreement with the findings by e.g. Shibuya et al. (1996).

A drawback of Equation (7.1) is that it does not incorporate an upper or lower limit to the given relationship. If this is not kept in mind it could lead to significant errors in the predicted behaviour. For example, for very long term creep phenomena it could predict unrealistic large creep strains or predict unrealistic high or low peak strengths for strain rates significantly greater or smaller than the range of strain rates used to calibrate the model. A simple way of incorporating a lower bound limit to the stress strain curves, would be to modify Equation (7.1) as follows;

$$SL = SL_r\left(1+\beta\cdot\ln\left(\frac{|\dot{\varepsilon}|}{\dot{\varepsilon}_r}+1\right)\right) \tag{7.2}$$

The string lengths now rapidly approach the lower limit, SL_r as the strain rate $\dot{\varepsilon}$ reduces beyond the reference strain rate $\dot{\varepsilon}_r$. While for changes in strain rates above the value of $\dot{\varepsilon}_r$ the string lengths changes in proportion to $\ln\left(\frac{|\dot{\varepsilon}|}{\dot{\varepsilon}_r}\right)$. The relationships between strain rate and string lengths given by Equations (7.1) and (7.2) are shown in Figure 7-6, while a schematic diagram of the predicted isotach type viscous behaviour is illustrated in Figure 7-7. The creep behaviour predicted by Equation (7.2) for strain rate above $\dot{\varepsilon}_r$ is illustrated in Figure 7-8. At low stress levels, the minimal curvature of the stress-strain curves means that the stress-strain curves are

approximately at equidistance in both stress (y-axis) and strain (x-axis) directions for log cycles of strain rate. The predicted creep behaviour will therefore here, to a good approximation, conform to the commonly suggested relationships; $\Delta\varepsilon \propto \Delta \ln \dot{\varepsilon}$ and $\Delta\varepsilon \propto \Delta \ln t$. At higher stress levels however, the curvature of the stress-strain curves increases significantly and the creep behaviour will therefore not fit the usual suggested relationships.

The study on London Clay highlighted that the relationship between volumetric strain and shear strain is independent of the applied strain rate. It was furthermore suggested in the study on London Clay that the expansion of a single state boundary surface with increasing strain rate could govern the yield behaviour both in isotropic compression with insignificant shear straining and in undrained triaxial compression with insignificant volumetric straining. If this idea is extended to the proposed BRICK model, it is suggested that the string lengths are a function of the vectorial plastic strain rate $\dot{\varepsilon}$, given by;

$$\dot{\varepsilon} = \sqrt{(\dot{\varepsilon}_v)^2 + (\dot{\varepsilon}_s)^2} \tag{7.3}$$

Where $\dot{\varepsilon}_v$ and $\dot{\varepsilon}_s$ are the plastic volumetric and shear strain rates respectively. It should be noted that to model the shearing behaviour correctly, the idealised shear stiffness degradation curve should be specified in terms of shear strain. Hence, it is only the shear strain component of each brick position, which will affect the degradation of the shear stiffness. The volumetric strain rate on the other hand should affect the location of the volumetric compression curve ε_v vs. p′ both during isotropic and one-dimensional compression and during shearing. With an increase in strain rate the normal compression line is typically seen to shift upwards, thereby enabling the soil to sustain a higher void ratio at given stress level. In the BRICK model the location of the volumetric compression curve is however not affected by the string lengths. For example for isotropic compression the normal compression line is specified by a constant gradient λ and an initial state in terms of volumetric strain $\varepsilon_{v,0}$ and mean stress. To simulate the observed influence of strain rate on the compression behaviour, it is therefore suggested that the initial volumetric state $\varepsilon_{v,0}$ is a function of the volumetric strain rate, as given by the following relationship;

$$\varepsilon_{v0} = \varepsilon_{v0,r}\left(1 + \beta^* \cdot \ln\left(\frac{|\dot{\varepsilon}_v|}{\dot{\varepsilon}_{v,r}} + 1\right)\right) \tag{7.4}$$

As for the string lengths, Equation (7.4) predicts a lower bound NCL, given by the initial reference volumetric state $\varepsilon_{v0,r}$, when the volumetric strain rate reduces below the reference rate $\dot{\varepsilon}_{v,r}$, whilst for volumetric strain rates greater than the reference rate, the NCL shifts upwards (in terms of volumetric strain) in proportion to $\ln\left(\frac{|\dot{\varepsilon}_v|}{\dot{\varepsilon}_{v,r}}\right)$, as illustrated in Figure 7-9.

The yield stress in one-dimensional compression is typically found to show similar magnitude of strain rate dependency as the strain rate dependency of the undrained strength in triaxial

compression (Soga & Mitchell, 1996). The viscous material constant β^* in Equation (7.4), which quantifies the viscous effect on the void ratio in one-dimensional compression, will therefore be approximately equal to the sum of the gradient λ and the material constant β from Equation (7.2), which on the other hand quantifies the viscous effect on the undrained strength.

7.1.3 Introducing temporarily extendable string lengths in the BRICK soil model to simulate general viscous behaviour

As explained above, the proposed introduction of strain rate dependent string lengths will enable the BRICK model to simulate commonly seen isotach viscous behaviour in soils. It has however been highlighted from both the literature review and findings in this study that many soils do not conform to the simple isotach concept characterised by a unique relationship between stress, plastic strain and its rate. Temporary effects of strain rate changes e.g. as seen from the temporary overshooting of the persistent CRS curves upon step increases in strain rate, have been observed in various soils, including granular soils, reconstituted stiff natural clays and weakly cemented soils. In this study the pure TESRA type behaviour was observed in cemented kaolin close to the peak state, while in reconstituted London Clay the temporary effects of strain rate changes became more pronounced with straining towards the failure state. In order to simulate this type of viscous behaviour, further measures need to be taken. It is therefore proposed to further extend the BRICK model by introducing temporarily extendable string lengths upon strain rate changes in addition to the strain rate dependency proposed above. This will enable the model to simulate general viscous behaviour, which covers a wider range of soils. Upon a significant strain rate change the string lengths will change as prescribed above by Equation (7.2). Then as straining subsequently progresses at constant rate of strain, the string lengths will gradually reduce to given values as a function of the strain.

Pure TESRA type viscous behaviour, which is characterised by a single unique persistent CRS stress-strain curve independently of the rate of strain, is typically seen for clean sands (Tatsuoka et al., 2000). To simulate this type of behaviour it is proposed that after strain rate changes, independently of the magnitude of strain rate, the string lengths gradually change back to a set of reference lengths; the reference string lengths being those which define the unique CRS stress-strain curve. Based on suggestions by Simpson (2005), it is proposed to modify the relationship between string lengths and strain rate given by Equation (7.1) as follows;

$$SL = SL_r \left(1 + \beta \cdot \ln \left(\frac{|\dot{\varepsilon}|}{\dot{\varepsilon}_n} \right) \right) \tag{7.5}$$

Where the neutral strain rate $\dot{\varepsilon}_n$, in contrast to the reference strain rate $\dot{\varepsilon}_r$ used in Equation (7.1), changes with increasing strain ε towards the imposed strain rate $\dot{\varepsilon}$, at a rate which can be assumed to be a function of $[\dot{\varepsilon} - \dot{\varepsilon}_n]$ and take the form;

$$\frac{d\dot{\varepsilon}_n}{d\varepsilon} = A[\dot{\varepsilon} - \dot{\varepsilon}_n] \tag{7.6}$$

The variation in the neutral strain rate $\dot{\varepsilon}_n$ and the ratio of the applied strain rate to neutral strain rate $\frac{|\dot{\varepsilon}|}{\dot{\varepsilon}_n}$ with strain after a step change in strain rate are illustrated in Figure 7-10. As given by Equation (7.5) the variation in the string lengths with strain will be similar to the variation in $\frac{|\dot{\varepsilon}|}{\dot{\varepsilon}_n}$. This means that the string lengths change towards the reference lengths at a rate which reduces with increasing strain after a step change in strain rate, which is in agreement with what has been indicated from the performed tests on reconstituted NC London Clay. The variable A controls the rate at which the size of the yield surfaces changes with further straining and hence if A is a constant the rate of change will be independent of the initial level of strain or stress. This is agreement with findings by Tatsuoka et al. (2002) for pure TESRA type viscous behaviour of clean sands. Now, considered the situation where the soil has been sheared at a constant rate of strain for a while, at a rate corresponding to the neutral strain rate. In this situation $\frac{|\dot{\varepsilon}|}{\dot{\varepsilon}_n} = 1$, straining therefore takes place on the strain rate independent stress-strain curve defined by the reference string lengths SL_r. Then if the strain rate is suddenly increased to $\dot{\varepsilon} > \dot{\varepsilon}_n$, $\frac{|\dot{\varepsilon}|}{\dot{\varepsilon}_n}$ will be greater than one, as $\dot{\varepsilon}_n$ initially remains at the original rate, and the string lengths will be increased in proportion to $\frac{|\dot{\varepsilon}|}{\dot{\varepsilon}_n}$. This moves the state momentarily inside all of the yield surfaces and the subsequent response will be elastic. As a result, the stress-strain path overshoots the unique stress-strain curve. With further straining however, $\dot{\varepsilon}_n$ gradually approaches the applied strain rate $\dot{\varepsilon}$ and the string lengths correspondingly reduce back towards their reference values. When $\frac{|\dot{\varepsilon}|}{\dot{\varepsilon}_n} = 1$ again the stress-strain path will rejoin the unique curve. It should be noted that due to the formulation of Equation (7.5), the string lengths have no theoretical lower limit to step reductions in strain rate. The gradual change in the neutral strain rate towards the current strain rate will however tend to limit the reduction in string lengths during creep and stress relaxation. A schematic diagram of the predicted pure TESRA type viscous behaviour is illustrated in Figure 7-11. It should be noted that the plotted stress-strain paths for step-changes in strain rate have been derived by assuming that the state always lies on the CRS path given by the current $\frac{|\dot{\varepsilon}|}{\dot{\varepsilon}_n}$. This is in fact not correct, as the state actually gradually

approaches the CRS path given by the current $\frac{|\dot{\varepsilon}|}{\dot{\varepsilon}_n}$ with straining. The actual predicted viscous behaviour will therefore be slightly different to the illustrated behaviour.

General TESRA type viscous behaviour, which can be characterised by increasing temporary effects of strain rate changes with straining towards failure, is typically seen for reconstituted stiff natural clays, as reported in the literature review and observed in this study on reconstituted London Clay. This type of viscous behaviour can be simulated if the rate of change in the neutral strain rate is considered to increase with strain level ε. Hence, instead of A being a constant in Equation (7.6), A should be a function of strain, i.e.;

$$\frac{d\dot{\varepsilon}_n}{d\varepsilon} = A(\varepsilon)[\dot{\varepsilon} - \dot{\varepsilon}_n] \tag{7.7}$$

The parameter $A(\varepsilon)$ could take the form;

$$A(\varepsilon) = A_f \cdot \left[1 - e^{-\frac{1}{c}\varepsilon}\right] \tag{7.8}$$

Where A_f and c are material positive constants, so as to achieve a lower bound value of $A(\varepsilon) = 0$ at $\varepsilon = 0$ increasing towards an upper bound value $A(\varepsilon) = A_f$ for $\varepsilon \to \infty$, as illustrated in Figure 7-10. Hence at the start of shearing the neutral strain rate changes very little and the behaviour therefore resembles the isotach type behaviour. With increasing straining $A(\varepsilon)$ increases and the temporary effects of strain rate changes become more pronounced. When $A(\varepsilon)$ reaches the maximum value A_f it remains constant and the viscous behaviour is equivalent to the pure TESRA type behaviour, previously described by Equation (7.6). Depending on the value of the constant c, the behaviour may be similar to that of the pure TESRA type behaviour at the failure state, as seen for reconstituted London Clay, or persistent effects of strain rate changes may still remain, as seen in the literature for e.g. reconstituted Valericca clay or reconstituted Fujinomori clay (Tatsuoka et al., 2000). A schematic diagram of the predicted General TESRA type behaviour is shown in Figure 7-12. As mentioned above, the plotted stress-strain paths for step-changes in strain rate have been derived by assuming that the state always lies on the CRS path given by the current $\frac{|\dot{\varepsilon}|}{\dot{\varepsilon}_n}$. This means that the actual predicted viscous behaviour will be slightly different to the illustrated behaviour. As for simulation of pure TESRA behaviour the string lengths have no theoretical lower limit to step reductions in strain rate. The gradual change in the neutral strain rate towards the current strain rate will however tend to limit the reduction in string lengths during creep and stress relaxation, particularly at large strains.

If the constant c in Equation (7.8) is given a value close to zero (e.g $c = 10^{-5}$), then $A(\varepsilon) = A_f$ for any strain increment above zero, meaning that Equation (7.7) and Equation (7.6)

will be equal and both will simulate pure TESRA behaviour in conjunction with Equation (7.5), as illustrated in Figure 7-10. If on the other hand the constant A_f is given a value of zero or the constant c is given a very large value (e.g. c=10^6), then the neutral strain rate does not change with straining and Equation (7.5) now simulates isotach viscous behaviour similarly to Equation (7.2). From the above description, is it seen that simple isotach behaviour can be implemented into the BRICK model by introducing only one new additional parameters in addition to the introduction of a time parameter, which enables the calculation of strain rates. One additional parameter is needed to simulate pure TESRA behaviour and an extra parameter is required to simulate general TESRA behaviour. It should be noted that the proposed equations for the variation of string lengths with strain rate and initial level of strain are all subject to validation against test data after implementation into the BRICK model. This is mainly because the advanced nature of the BRICK model has made the prediction of the simulated behaviour difficult. The simulated behaviour may therefore be somewhat different to the expected. As stated previously, it has been outside the scope of this research project to implement the proposed modifications to the BRICK model, and simulation of the viscous behaviour is therefore not yet possible.

7.2 FIGURES FOR CHAPTER 7

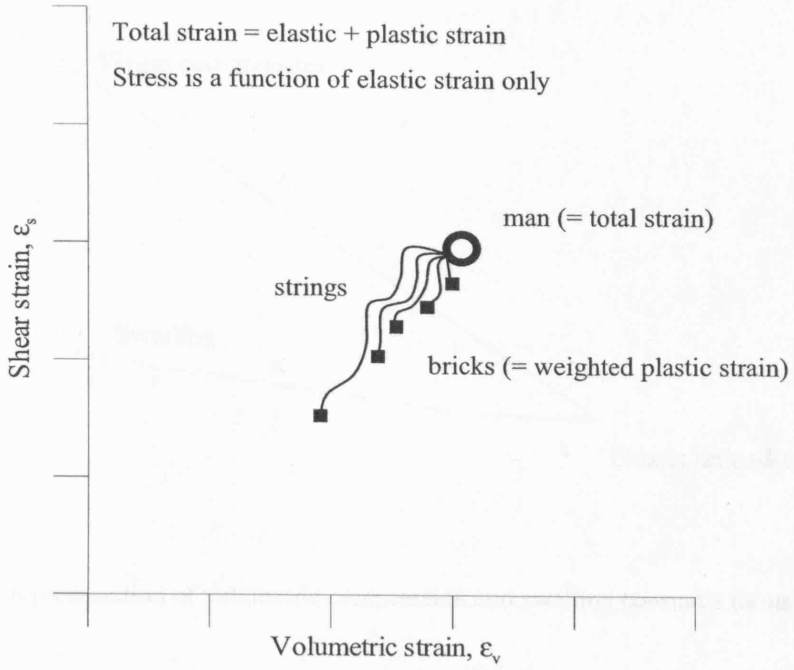

Figure 7-1 The multiple kinematic yield surface BRICK soil model – analogue of a man pulling bricks in strain plane

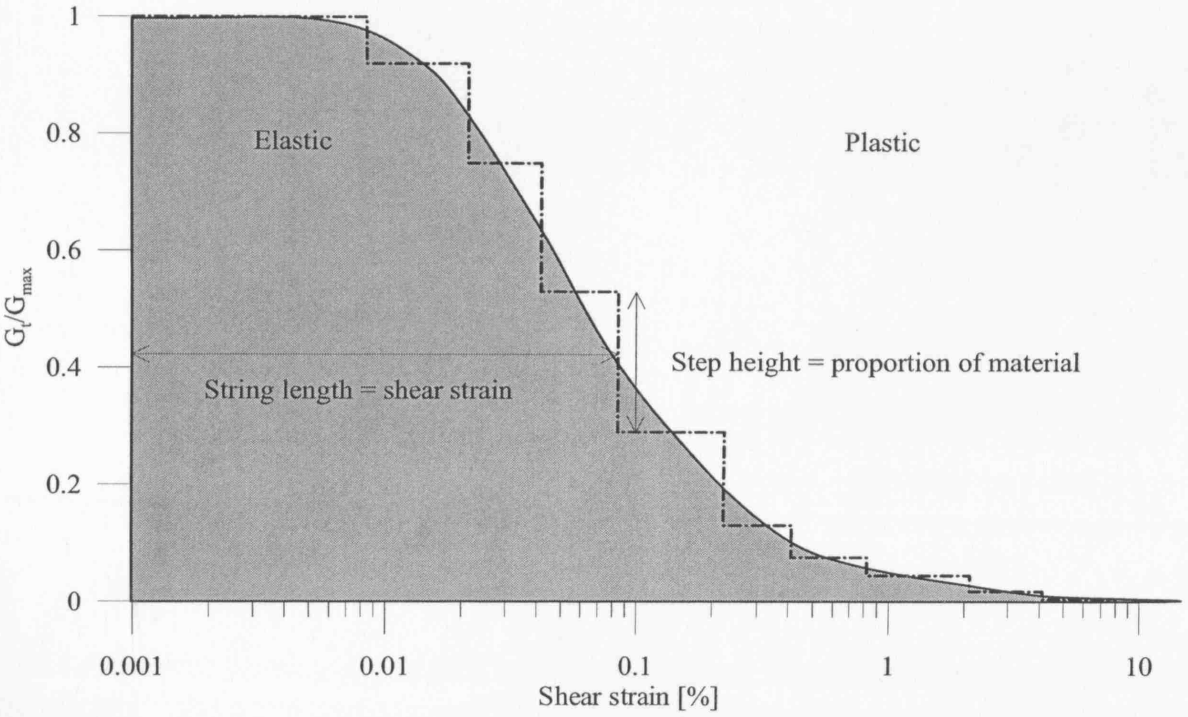

Figure 7-2 Idealised S-shaped stiffness degradation curve using Rankine parameters for London Clay after significant strain reversal

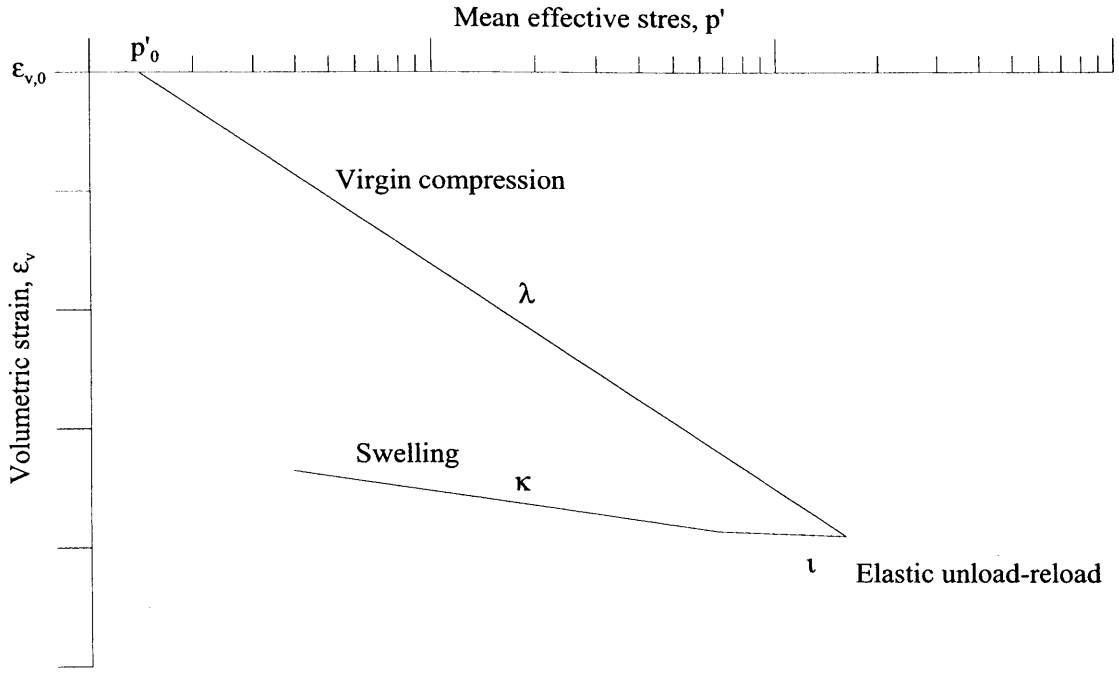

Figure 7-3 Schematic representation of volumetric compression and swelling constants for use in the BRICK soil model

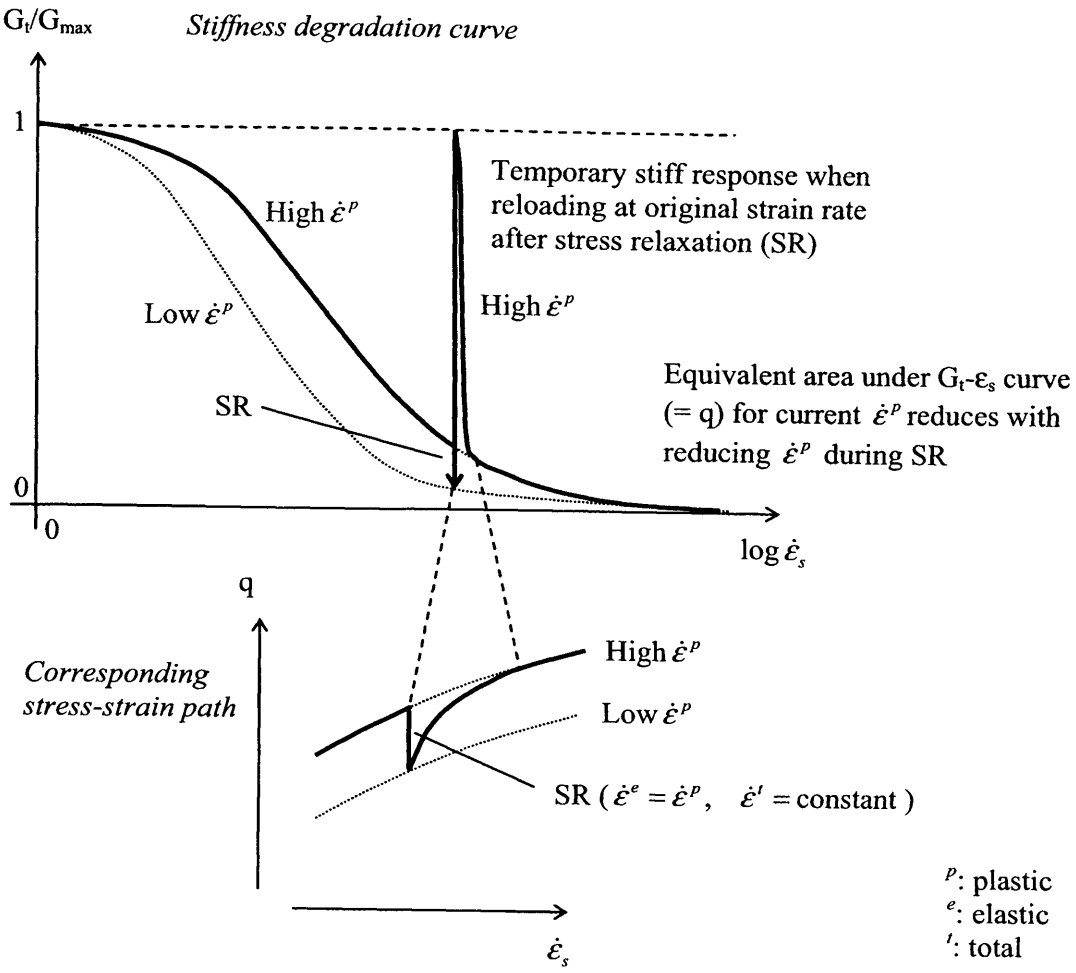

Figure 7-4 Schematic diagram of stiffness response and stress-strain paths followed during and after stress relaxation when reloading at original strain rate that would be predicted using the modified BRICK model

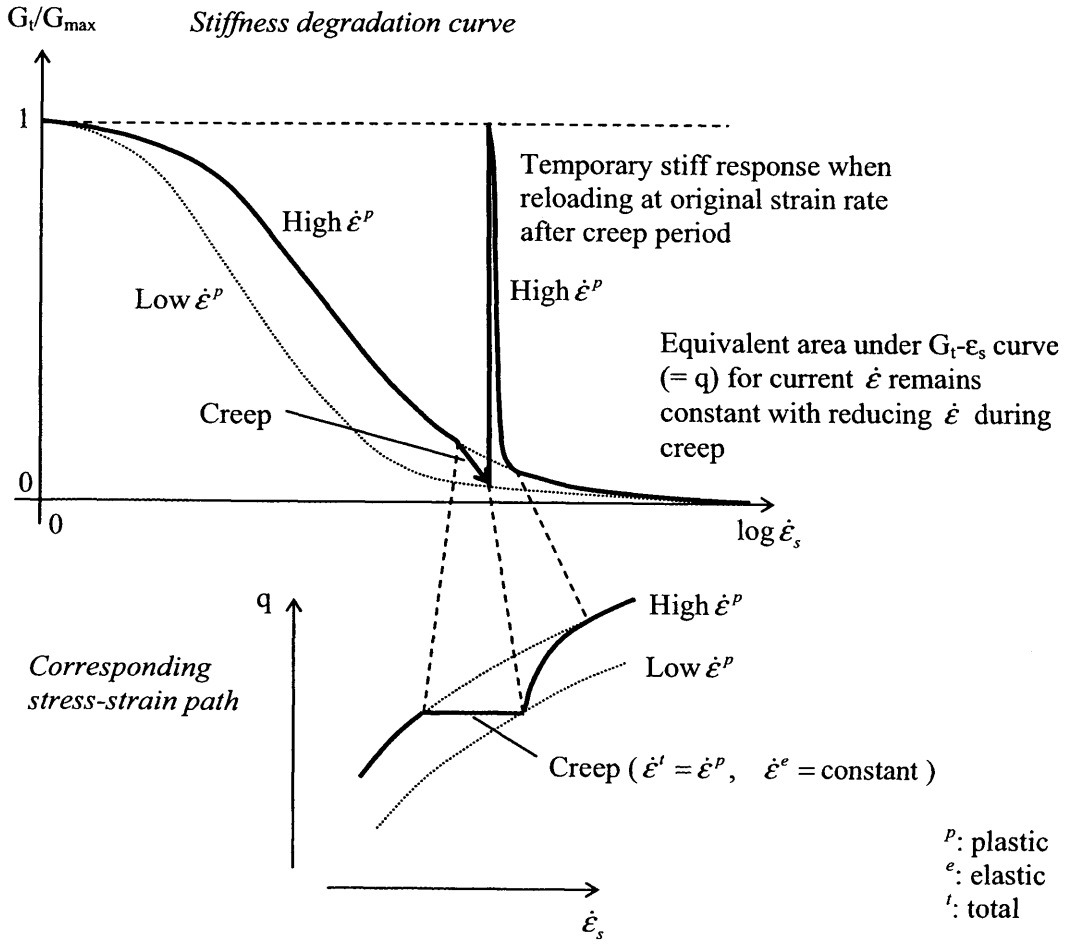

Figure 7-5 Schematic diagram of stiffness response and stress-strain paths followed during and after creep when reloading at original strain rate that would be predicted using the modified BRICK model

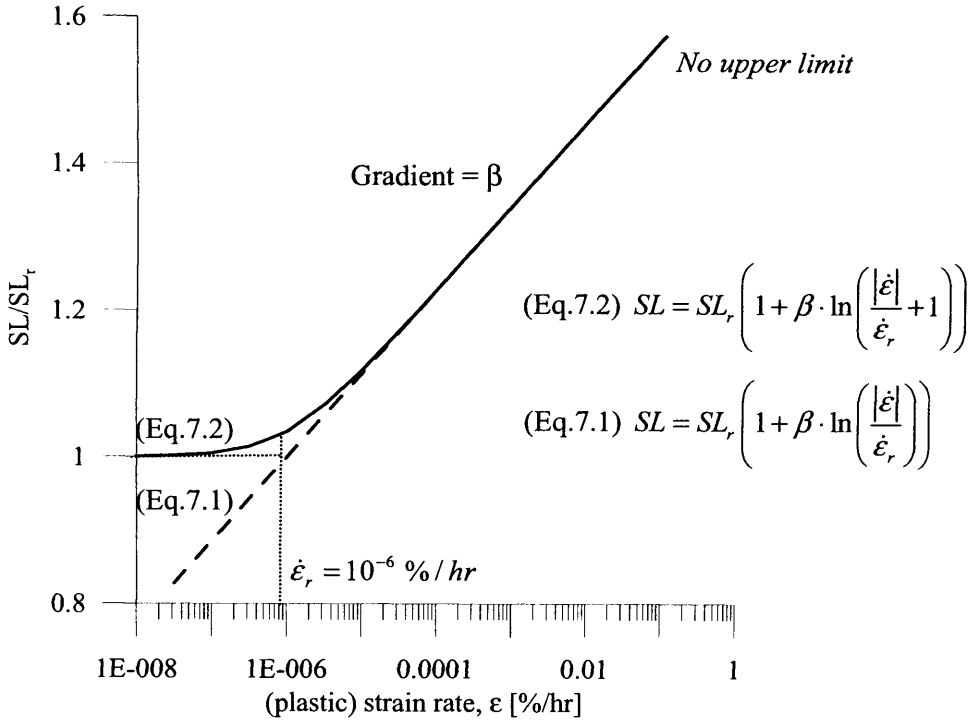

Figure 7-6 Illustration of the proposed variation of string lengths with plastic strain rate

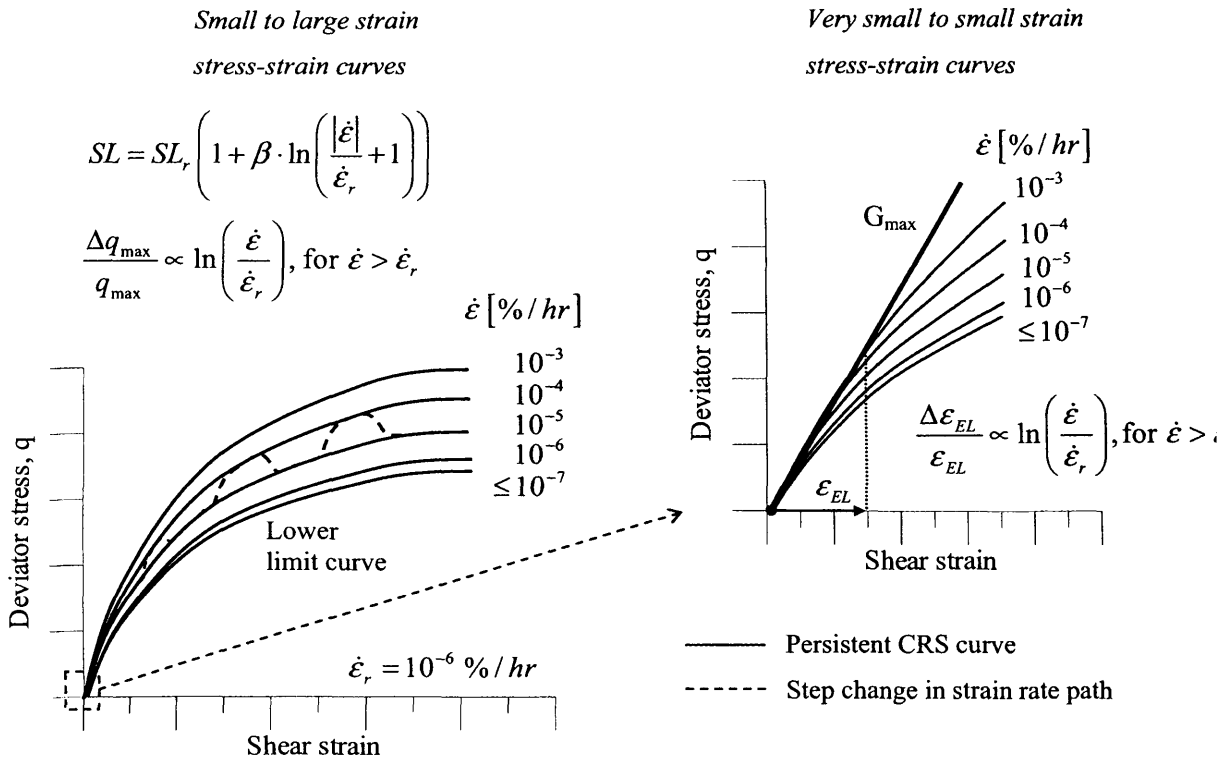

Figure 7-7 Schematic diagram of isotach stress-strain curves with lower limit string lengths that would be predicted using the modified BRICK model

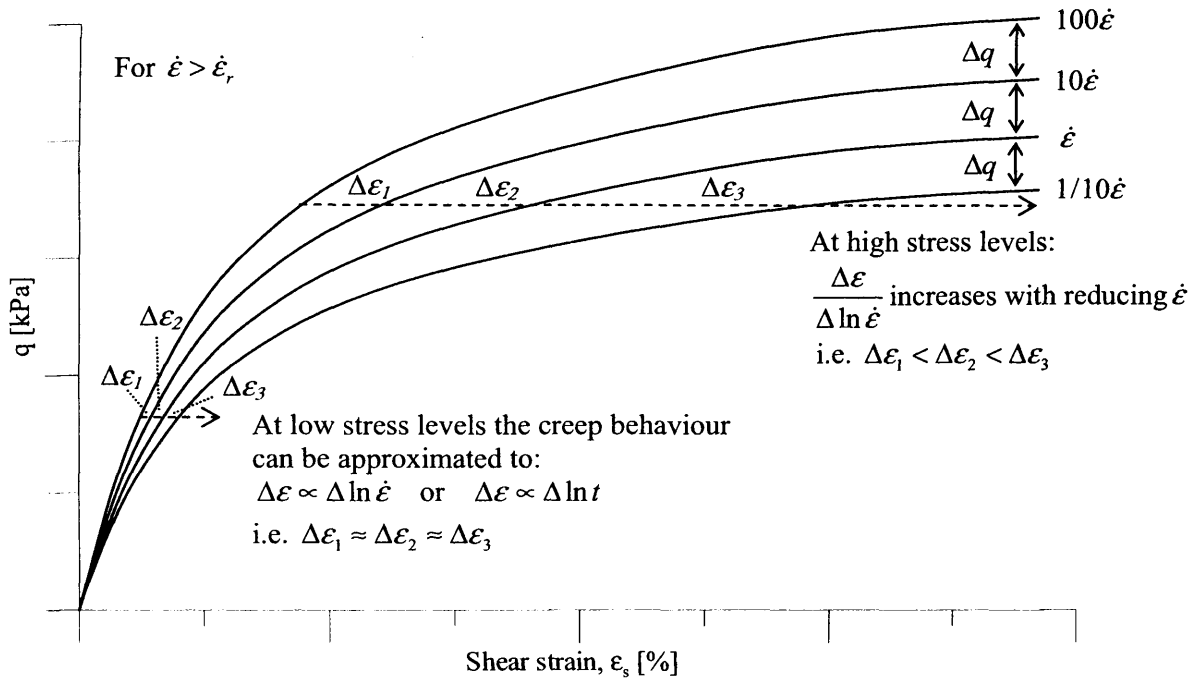

Figure 7-8 Schematic diagram explaining creep behaviour for isotach type viscous behaviour that would be predicted using the modified BRICK model

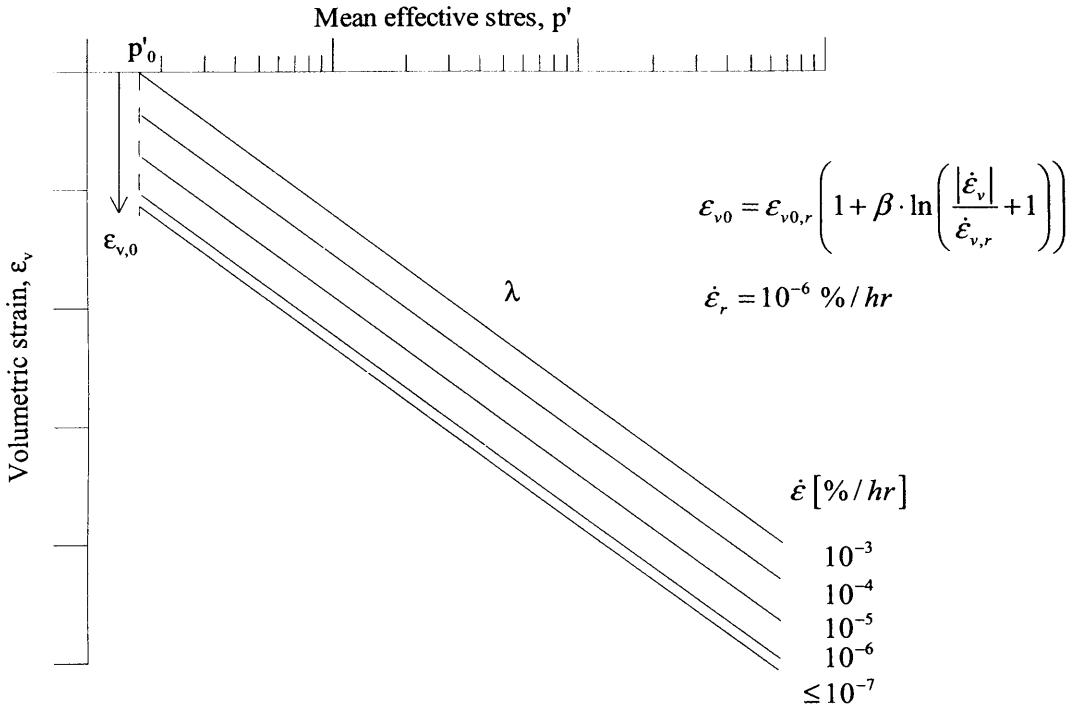

Figure 7-9 Schematic diagram of isotach isotropic compression curves with lower limit initial volumetric strain that would be predicted using the modified BRICK model

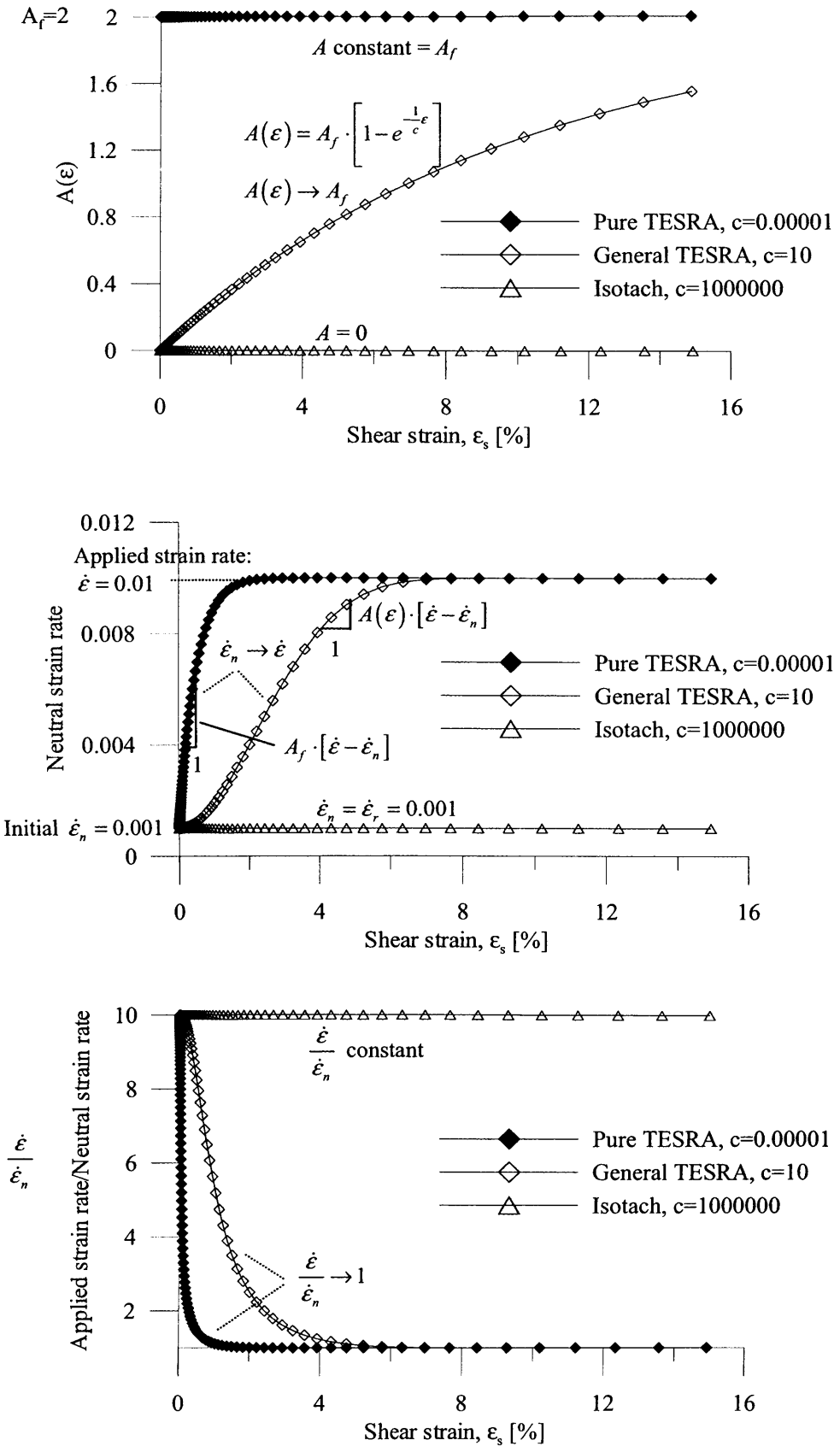

Figure 7-10 Illustrating the interrelationships and variations of parameters for the modified BRICK model

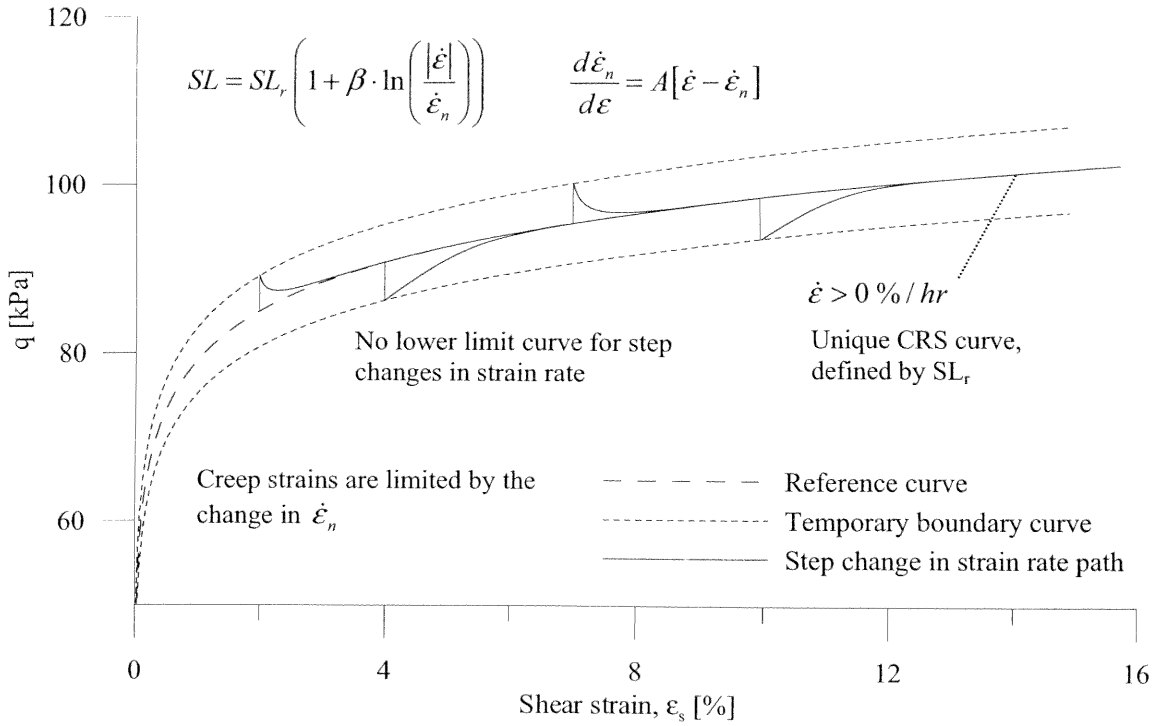

Figure 7-11 Schematic diagram of Pure TESRA type viscous behaviour that would be predicted using the modified BRICK model

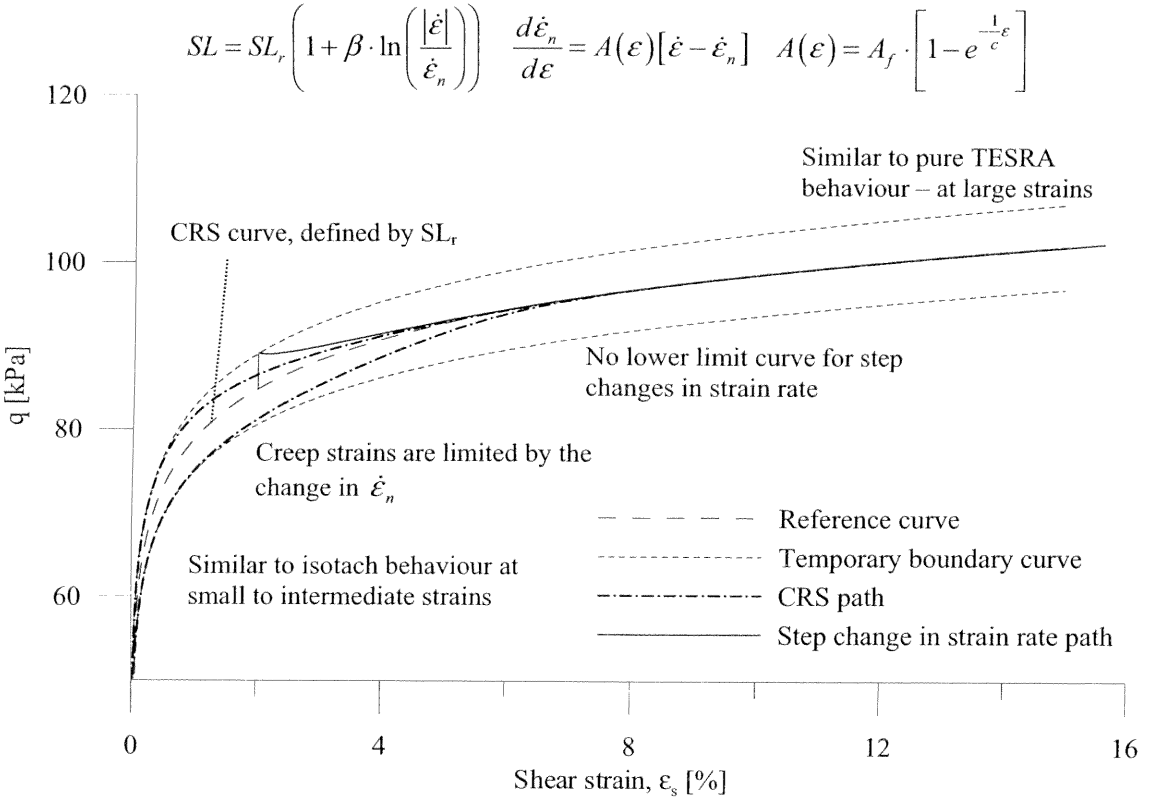

Figure 7-12 Schematic diagram of General TESRA type viscous behaviour that would be predicted using the modified BRICK model

CHAPTER 8 CONCLUSIONS

8.1 SUMMARY AND CONCLUSIONS

To serve as a reminder, the key objectives of the research work, as formulated in the introduction, were:

- To achieve a better understanding of the time-dependent behaviour of clays, particularly stiff natural clays, through critical review of literature and a program of laboratory testing. With emphasis on examining the effects of viscosity and ageing, the laboratory testing would add to the existing database of results and address important "grey areas" highlighted from the literature review.
- To develop a framework of conceptual time-dependent behaviour of clays on the basis of the first objective with the underlying intention to characterise parameters that could eventually be used in a model for natural clays.

To address the key objectives a series of advanced triaxial and oedometer tests were conducted in this research project. On the basis of the literature review and the findings from these tests, a framework for the conceptual time-dependent behaviour of natural clays was formulated. A preliminary study was carried out examining the implementation of the conceptual framework into an existing advanced constitutive model. The findings and conclusions of the literature review, experimental work and numerical work are summarised in the following.

8.1.1 Elastic shear stiffness and its relation to global strain rate and ageing

The study, presented in Chapter 4, comprised a series of monotonic one-dimensional and isotropic compression tests, which were carried out to investigate the influence of global strain rate (measured at the sample boundaries) and ageing (i.e. time) on the elastic shear stiffness. Reconstituted samples of kaolin and London Clay were tested under one-dimensional deformation conditions in an advanced modified oedometer apparatus and under isotropic stress conditions in an advanced triaxial apparatus. The oedometer cell and the triaxial cell had both been fitted with in-house made bender elements in the top cap and base pedestal to enable dynamic shear wave velocity measurements and determination of the elastic shear modulus, G_0 in the vertical direction.

a Determination of a suitable method of interpretation of the bender element test results

A review of testing techniques, for shear wave velocity determination from bender element tests, revealed that there is no standard objective method of interpretation currently being used by researchers. Several methods of interpretation have been suggested in previous research, with particular regards to determining the travel time of the shear wave propagating through the sample. In this study three methods of determination of the travel time were compared; the two

time-domain methods; first arrival time and peak to peak correlation, and additionally the phase-delay method in frequency domain. The influences of several factors were also investigated, including: the number of transmitted pulses (single pulse, multiple pulses, semi continues signal and continuous signals) and the frequency of the transmitted signal. The method of correlation between characteristic peaks or troughs at the resonant frequency using a continuous signal was deemed the most suitable because of its reliability and simplicity. This method was therefore used to obtain the presented results in this study. The high consistency of the presented results further emphasised the reliability of the chosen method of interpretation.

b Effect of strain rate and creep time on the elastic shear stiffness in one-dimensional and isotropic compression tests on kaolin and reconstituted London Clay

One-dimensional and isotropic compression tests were performed with either step changes in strain rate, step changes in stress rate or step loading of the two clays. In addition prolonged periods of creep and stress relaxation up to one month in duration were introduced at different stages, and the elastic shear modulus was determined from bender element tests at intervals during compression. The performed tests investigated the effect of global strain rate, ageing, creep, stress relaxation and excess pore water dissipation on the compression behaviour and the elastic shear modulus. Several interesting and possibly controversial findings were made in the study. Important conclusions drawn from the results include (where nothing else is mentioned, these conclusions refer to the isotropic compression behaviour only):

- The most reliable results were obtained from the isotropic compression tests, where the complete stress state was known and the bender elements worked the best.
- Generally, in agreement with findings in the literature the normal compression line in one-dimensional and isotropic compression was found to be strain rate dependent.
- In contrast to expectations, however, the elastic shear modulus determined from bender element tests, was also found to be highly dependent on the applied global axial strain rate.
- Unique linear relationships were found between void ratio e, the logarithm of stress level (σ'_v in one-dimensional compression or p' in isotropic compression) and the logarithm of elastic shear stiffness G_0, which clearly highlighted that the rate dependency of the elastic shear modulus could not be explained by changes in the state of the soil.
- By normalising the current G_0 with respect to a reference G_0 predicted from the current mean effective stress at a reference strain rate, the effect of stress state (and indirectly void ratio as well) was removed and the influence of ageing and strain rate could be observed. A unique linear relationship was found between the normalised elastic shear stiffness and the logarithm of the axial strain rate for data obtained both from gradual reductions in strain rate during creep and for step reductions in strain rate. The proportionality constant, which quantifies the rate dependency of the normalised G_0,

was termed the global rate coefficient α_0 and expressed as:

$$\alpha_0 = -\frac{\Delta\left(G_0 / G_{0(p',\dot{\varepsilon}_{a,ref})}\right)}{\Delta \log \dot{\varepsilon}_a} \quad \text{(refer to Equation 4.7).}$$

For both reconstituted kaolin and reconstituted London Clay the value of α_0 was around 0.12, i.e. the elastic shear stiffness increased by around 12% per log cycle reduction in strain rate.

- The findings generally suggest that the changes in the elastic shear stiffness observed during pore water dissipation, creep, stress relaxation and as a results of strain rate changes in the short-term one-dimensional and isotropic compression of the tested clays can be attributed to the combined effects of changes in state and changes in the plastic strain rate rather than time-dependent ageing effects. Ageing effects on the elastic shear modulus in reconstituted kaolin and reconstituted London Clay was therefore indicated to be negligible in short-term periods up to one month. These findings clearly contrast conclusions drawn in past studies, where researchers typically attribute the observed extraordinary increase in the elastic shear stiffness determined from dynamic testing during creep to structuration effects, even for an inactive clay like kaolin (Lohani et al., 2001; Anderson & Stoke, 1978).
- It is suggested that the general relationship between elastic shear stiffness and mean effective stress, proposed by (Viggiani & Atkinson, 1995) for normally consolidated reconstituted clays, can be modified to consider the influence of strain rate as well:

$$\frac{G_0}{p_r} = A_{\dot{\varepsilon}_{a,ref}} \left(\frac{p'}{p_r}\right)^n R_{\alpha_0} \quad \text{(refer to Equation 4.5).}$$

Where the rate parameter R_{α_0} is a function of the global rate coefficient α_0 and the applied strain rate.

- The commonly used coefficient, N_G, which quantifies the increase in G_0 with time during stages of fixed effective stress creep, is found to be somewhat subjective. Therefore, based on the above findings, a modification of N_G is proposed, in order to quantify the increase in G_0 with time in a more objective manner. The new creep time coefficient N_G^*, is given as:

$$N_G^* = \frac{\Delta\left(G_0 / G_{0(p',\dot{\varepsilon}_{ref})}\right)}{\Delta \log t} \quad \text{(refer to Equation 4.9)}$$

For reconstituted kaolin and reconstituted London Clay the obtained values of N_G were typically 8%-11%, while the corresponding values of N_G^* were slightly higher at around 10%-13% for reference strain rates in the order of 0.07-0.1 %/hr.

- Conveniently N_G^* can be related to the global rate coefficient α_0 and the creep coefficient $m = \frac{\Delta \log \dot{\varepsilon}_a}{\Delta \log t}$ (Singh & Mitchell, 1968) in the following manner:

  $N_G^* = \alpha_0 \cdot m$ (refer to Equation 4.10)

  The obtained results in this study support this relationship, however since the data are limited, more data are needed to verify the validity of the proposed simple relationship.

8.1.2 Viscous behaviour of reconstituted London Clay

The study, presented in Chapter 5, comprised a series of monotonic isotropically consolidated drained and undrained triaxial compression and extension tests on specimens of normally consolidated reconstituted London Clay, which were carried out to investigate the viscous behaviour of a natural stiff clay in its reconstituted state. Detailed aspects of viscous behaviour such as the response to step changes in the strain rate, strain acceleration and constant strain rate were examined in both the pre-yield and post-yield regions. Several interesting and possibly controversial findings were made in the study. The most important findings and conclusions drawn from the results were:

- Reconstituted London Clay has an isotach response to isotropic compression and shearing at low strain levels, but at higher strain levels, towards peak strength, strain rate effects become increasingly temporary. This behaviour was observed in both drained and undrained tests and it is similar to previously reported behaviour of other reconstituted stiff clays and rather similar to the observed behaviour of most weakly cemented soils.
- The undrained peak and critical state strengths of reconstituted NC London Clay were found to be independent of the applied rate of strain. Yet, at failure significant temporary effects of strain rate changes were still observed.
- The steady state pore water pressure response and the relationship between volumetric strain and axial strain were both found to be independent of the applied strain rate. This highlights that the observed strain rate dependency of the stress path in undrained shearing in the pre-peak region cannot be explained by creep driven changes in the pore water pressure response, as otherwise suggested in previous research on different clays.
- The total immediate stress jump upon step changes in strain rate is found to increase consistently with increasing ratios of strain rate change, while for a given ratio of strain rate change the total immediate stress jump appears to be constant with stress level. A linear relationship between the stress jump and the logarithm of ratio of strain rate change is suggested. The independency on stress level is in contrast to the observed behaviour of other clays reported in the literature, which typically are reported to show a proportional relationship between the stress jump and the initial stress level.

- The results indicated that the extrapolated persistent CRS paths generally maintain a separation in both the stress-strain plot and in stress plane at the start of shearing. This suggests that the yield envelope is significantly affected by the applied strain rate even at very small shear strains, which is consistent with the observed strain rate dependency of the intrinsic isotropic NCL. Hence, the findings generally suggest that the strain rate dependency of a single state boundary surface can describe the viscous behaviour observed in both isotropic compression and shearing in agreement with previous research on the general creep behaviour of clays.
- Another interesting finding highlighted from the results, is the indication that only the persistent CRS path corresponding to an axial strain rate equal to the final axial creep rate remaining after isotropic compression (or extension), will intersect the origin.
- If the very small strain stiffness was corrected for creep strains it was found that acceleration of strains in the post yield region in triaxial compression would give rise to an elastic response of the soil similarly to the elastic response seen at very small strains at the start of shearing.
- The performed tests further revealed that, in contrast to predictions from the concept of recent stress history, it is possible to have a significant rotation of both the stress path and the strain path without observing an associated increase in the shear stiffness, and vice versa; it is also possible to observe a high stiffness response without having an associated significant rotation of the stress path or strain path. It all comes down to whether or not the soil experiences an acceleration of (plastic) strains.
- Based on the findings it can be hypothesized that the initial elastic stiffness response (linear or not) observed in most standard triaxial tests on non-cemented clays is a result of significant strain acceleration only, while the subsequent degradation of stiffness is governed by the transition from a state of acceleration to a steady state with constant rate of straining. Therefore, it seems that a better understanding of soil behaviour and more reliable design parameters can be achieved by considering relevant stress-strain relationships for the expected variation in strain rates rather than the associated stiffness degradation curve(s).
- In order to better represent and model the observed rate-dependent soil behaviour a modified concept of kinematic yield surfaces is proposed, where the size of the yield surfaces are dependent on the applied strain rate and a temporary expansion of the yield surfaces occurs as a result of strain acceleration. A detailed examination of the implementation of this concept into an existing advanced constitutive model was discussed further in Chapter 7.

Part of the findings from this study have also been presented in a paper entitled "Stiffness revised: Influence of strain acceleration on stiffness of clay in the small strain region"

(Sorensen, 2005), which won the *British Geotechnical Association iYGEC paper contest 2005.*

8.1.3 Influence of natural and artificial structure on the viscous behaviour of London Clay and cement-mixed kaolin

Results from a series of laboratory tests on London Clay and artificially cemented kaolin were presented and used to develop a preliminary framework for the time-dependent behaviour of soils, applicable to stiff clays and other soils. In the same way that the natural structure of clays has been shown to influence their monotonic behaviour, it is shown that it can also alter their response to changes in strain rate (i.e. viscous behaviour). The relative influence of mechanical overconsolidation and natural structure (arising from sedimentation and post-sedimentation processes such as ageing) on the time-dependent behaviour of London Clay was investigated in triaxial compression tests. The study was carried out in two steps, comparing first the behaviours of normally consolidated reconstituted and undisturbed natural samples of London Clay subjected to step-wise changes in strain rate, then comparing these with the behaviour of a sample of overconsolidated reconstituted London Clay. Effects of cementing on strain rate sensitivity were investigated in triaxial compression of artificially cemented kaolin. The following findings were made:

- The data obtained for the strain rate dependent behaviour of London Clay show results that fit well with the existing data base for different soils.
- Overconsolidation does not seem to affect the strain rate dependent behaviour of reconstituted London Clay, which is consistent with other published data on stiff clays.
- Undisturbed London Clay shows an isotach behaviour both pre- and post- peak during shearing. This is similar to the behaviour of soft rocks, soft clays and other undisturbed stiff natural clays.
- Cemented kaolin shows pure temporary effects of strain rate changes during shearing in the peak and post-peak region. This is similar to the behaviour of granular soils and other cemented soils post-peak.

From the above findings the following conclusions were drawn:

- Intact and reconstituted overconsolidated samples show different behaviours, highlighting that it is the elements of the natural structure resulting from post-sedimentation processes other than mechanical overconsolidation that influence the time-dependent behaviour of London Clay.
- The effects of artificial cementing on the strain rate sensitivity of kaolin were seen to be different to the influence of natural structure on the strain rate sensitivity of London Clay. The findings therefore suggest that the difference in strain rate effects in the intact and reconstituted London Clay cannot be simply associated to cementing. This is in

agreement with the evidence shown in literature that the structure in the natural London Clay is not due to bonding but predominantly due to fabric.

- A preliminary framework is proposed, where the time-dependent behaviour of soil depends on its particulate or continuum nature. It could be suggested that soils behaving like a continuum, either because their particles are bonded together through "flexible" forces (for example electrical and chemical forces in young normally consolidated clays like normally consolidated samples of pure kaolin) or because the fabric is strongly bonded (for example soft rocks or maybe undisturbed London Clay), have an isotach behaviour, while in soils behaving like granular (particulate) materials, for example sands or "broken" cemented kaolin, strain rate effects are only temporary.
- It can be imagined that in a particulate material the deformation is more localised at inter-particle contact points, while in a continuum the behaviour may be associated with the deformation of the entire volume of soil. This could explain why clays, which can be characterised by predominant continuum behaviour, generally show significantly greater viscous effect than granular soils, which are particulate in nature.

The findings from this study have also been presented in a paper entitled "Influence of structure on the time-dependent behaviour of a stiff sedimentary clay" *(Sorensen et al., 2007)*, which has been submitted for publishing in the forthcoming *Géotechnique Symposium in Print 2007: "Stiff sedimentary clays - Genesis and engineering behaviour"*.

8.1.4 Coupling of curing and viscous effects in cement mixed kaolin

A series of short term isotropically consolidated drained triaxial compression tests was conducted to investigate the influence of cementation, total curing time and strain rate on the stress-strain behaviour of cement-mixed kaolin. Based on the findings the following conclusions were drawn:

- The results suggest that the behaviour of cement-mixed kaolin can be described by a unique stress-plastic strain-time relationship independently of strain (curing) history.
- In the initial stages of curing, when the curing rate is fast the behaviour is dominated by ageing effects rather than viscous effects.
- In cement-mixed kaolin there appears to be a plateau for peak strength achieved after about one day of curing, which defines an upper bound strength. Further tests are however needed to confirm this trend. As the cement-mixed soil approaches the upper bound peak strength its behaviour changes from being ductile to being brittle. The post-peak critical state strength is on the contrary seen to be constant with curing.
- Curing also seems to affect the small strain stiffness of cement-mixed kaolin. The small strain stiffness normalised with respect to the assumed influence of effective stress shows a linear increase with the logarithm of total curing time. Hence the results

suggest that there might be a unique stiffness-stress-time relationship for natural structured clays.

- The cement-mixed kaolin is a representation of natural soils but with an accelerated ageing rate. In natural structured soils the rate of ageing is very slow, and at strain rates of the order of those usually applied in the laboratory, viscous effects will dominate the behaviour. It is suggested that at a given time there must be a point (characteristic strain rate) at which the behaviour of cement-mixed kaolin changes from being dominated by cementation effect to being predominantly viscous. Similar coupling between ageing effects and viscous effects may be expected in natural clays, which have been subjected to recent disturbance. Undisturbed natural clays on the other hand, which have been aged over a geological time scale are likely to have a characteristic strain rate, which is extremely low and primarily affected by changes in the surrounding environment rather than anything else.

The findings from this study have also been presented in a paper entitled "Coupling of ageing and viscous effects in an artificially structured clay" (Sorensen et al., 2006), which has been submitted for publishing in the forthcoming *Proceedings for the Geotechnical Symposium in Roma 2006: "Soil Stress-Strain Behavior: Measurement, Modeling and Analysis"*.

8.1.5 Implementing viscous effects into the BRICK model of soil behaviour

The general observed viscous behaviour of clays reported in the literature and the conceptual viscous behaviour of reconstituted and undisturbed London Clay, as derived from the findings in this research project and presented previously in Chapters 5 and 6, has been used as basis for the further development of an existing advanced constitutive model to include the observed viscous behaviour. As described in Chapter 7, a preliminary study was carried out to investigate the possibilities of implementing viscous behaviour into the non-linear elasto-plastic BRICK constitutive model of soil behaviour (Simpson, 1992). The BRICK model, which can be classified as a multiple kinematic yield surface model formulated within the conventional Cam Clay critical state framework, is based on an analogue of a man pulling a number of bricks on strings of various lengths in strain plane; the movement of the man represents total strain of the soil element, the weighted movement of the bricks represents plastic strain and the difference between the two is the elastic strain. The string lengths can therefore be said to represent the individual sizes of the kinematic yield surfaces. When a string becomes fully extended the sample engages another yield surface and as result the behaviour becomes increasingly plastic. Despite the advanced capabilities of the BRICK model, it is in its current version not able to simulate important aspects of soil behaviour relating to time and rate effects. This is therefore found to be one of the key areas in which the model can be improved. The outcome of the study includes the introduction of a limited number of new parameters and a proposed set of relatively simple modifications to the BRICK model, which will extend its capabilities to include the

simulation of general observed viscous behaviour of soils. As stated in the introduction in Chapter 1, it has however been outside the scope of this research to implement the proposed modifications. The following conclusions were drawn from the study:

- It is proposed to simulate general viscous type behaviour using the BRICK model by introducing two new features in the model: firstly, strain rate dependent string lengths and secondly, temporarily extendable string lengths upon strain rate changes. This would be equivalent to making the sizes of the yield surfaces dependent on the applied strain rate and introducing a temporary expansion of the yield surfaces as a result of strain acceleration.
- It is argued that simple isotach type viscous behaviour can be simulated successfully by having strain rate dependent string lengths, while temporary effects of strain rate changes as observed for pure TESRA behaviour and general TESRA behaviour can be accounted for by a temporary extension or retraction of the string lengths.
- The modified model will be applicable to a range of soils including granular soils, soft clays, stiff undisturbed natural clays, soft rocks and strongly cemented soils in the pre-peak region.
- The study shows that and general TESRA behaviour, which encompasses both simple isotach behaviour and pure TESRA behaviour, can be implemented into the BRICK model by introducing only three new parameters in addition to the introduction of a time parameter, which enables the calculation of strain rates.

8.2 SUGGESTIONS FOR FURTHER RESEARCH

The experimental work in this study has added significant data to the existing data base of time-dependent behaviour of clays. In the view of the findings and discussion thereof, the following recommendations, for further research on the time-dependent behaviour of clays, are made:

- Coupling of ageing and viscous effects in natural clays: The study on reconstituted London Clay showed insignificant ageing effects for creep periods up to one month. Longer resting periods, possibly up to several years, will therefore be required to observe significant ageing effects in this clay. The extremely low strain rate required to observe ageing effects during constant rate of shearing, will on the other hand make this impractical to perform. To investigate the coupling of ageing and viscous effects in short-term laboratory tests on natural clays, tests could be performed on a highly active clay, such as an organic soft clay tested at low pressures.
- Long-term curing effects in artificially cemented kaolin: The performed tests on artificially cemented kaolin only investigated the influence of curing times up to 9 days. Uncertainty in the strength development after the first day of curing was highlighted, so in order to clear this up, additional tests need be carried out to investigate the strength and stiffness development to longer curing times.
- Influence of sedimentation structure on the viscous behaviour of London Clay: The influence of structure arising from post-sedimentation processes such as ageing and overconsolidation on the viscous behaviour of London Clay has been investigated in this study. To complement these findings it would be of interest to examine the influence of sedimentation structure as well. This could be part of a more detailed study of the influence of fabric and micro-structure on the viscous behaviour of soils.
- Influence of strain acceleration on the stress-strain behaviour of stiff clays: Significant and consistent strain acceleration effects on the shear stiffness were observed in the performed tests on reconstituted London Clay. It would be of interest to examine if similar influence of strain acceleration can be observed in intact London Clay or other stiff natural clays, where the creep strain rate will be much slower.
- Long-term drained tests: The stability of the testing equipment needs to be improved in order to characterise the complete pre- and post failure viscous behaviour of London Clay in drained conditions, as this require long testing time (several months) due to the slow applied strain rates.
- Viscous behaviour in unloaded conditions and in triaxial extension: To build a more general framework of viscous behaviour of clays, further tests need to be carried out to examine in more detail the influence of step changes in strain rate on the stress-strain behaviour during unloading and in triaxial extension to failure.

- Influence of strain rate and step changes in strain rate on the elastic shear modulus determined from dynamic testing during shearing and unloaded conditions: These tests should be carried out to complement the findings in one-dimensional and isotropic virgin compression.
- Finally, it would be of essential value to implement the proposed modifications to the BRICK model of soil behaviour. This is therefore planned in future work carried out in collaboration with Arup Geotechnics. Because of the complex nature of the advanced BRICK model, only after implementation and calibration of the new model against actual data can it be revealed if the proposed modifications will result in a satisfactory simulation of general viscous behaviour of soils. The proposed framework for the viscous behaviour of soils could also be applied to other existing advanced soil models. The question of coupling between structure and rate effects needs addressing in order to implement the above framework into existing models for structured soils such as the S3-SKH model (Baudet & Stallebrass, 2004) or the BRICK-S model (Vukandin, 2004).

REFERENCES

Abbiss, C. P. (1981). Shear wave measurements of the elasticity of the ground. *Géotechnique* **31**, No. 2, 94-104.

Acosta-Martinez, H. E., Tatsuoka, F., & Li, J.-Z. (2003). Viscosity in one-dimensional deformation of clay and considerations for its modelling. *Proc. 38th Japan National Conf. Geotech. Engng, JGS, Akita.*

Akai, K., Adachi, T., & Ando, N. (1975). Existence of a unique stress-strain-time relation of clays. *Soils and Foundations* **15**, No. 1, 1-16.

Allam, M. M. & Sridharan, A. (1979). The influence of aging on the shear strength behaviour of two fine-grained soils. *Canadian Geotechnical Journal* **16**, 391-397.

Allman, M. A. & Atkinson, J. H. (1992). Mechanical properties of reconstituted Bothkennar soil. *Géotechnique* **42**, No. 2, 289-301.

Almeida, M. S. S. & Marques, M. E. S. (2003). The behaviour of Sarapui soft clay. *Characterisation and Engineering Properties of Natural Soils*, Tan et al., ed., Swets & Zeitlinger, Lisse, 477-501.

Anderson, D. G. & Stoke, K. H. I. (1978). Shear modulus: a time-dependent soil property. *Dynamic Geotechnical Testing, ASTM* **STP 654**.

Arroyo, M., Muir Wood, D., & Greening, P. D. (2003). Source near-field effect and pulse tests in soil samples. *Géotechnique* **53**, No. 3, 337-345.

Atkinson, J. H. (2000). Non-linear soil stiffness in routine design. *Géotechnique* **50**, No. 5, 487-508.

Atkinson, J. H., Richardson, D., & Robinson, P. J. (1987). Compression and extension of K0 normally consolidated kaolin clay. *J.Geotech.Engng, ASCE* **113**, No. 12, 1468-1482.

Atkinson, J. H., Richardson, D., & Stallebrass, S. E. (1990). Effect of stress history on the stiffness of overconsolidated soil. *Géotechnique* **40**, No. 4, 531-540.

Baldi, G., Hight, D. W., & Thomas, G. E. (1986). Reevaluation of conventional triaxial test methods. *ASTM.Special Technical Publication* **STP 977**, 219-263.

Baudet, B. & Stallebrass, S. (2004). A constitutive model for structured clays. *Géotechnique* **54**, No. 4, 269-278.

Bishop, A. W. (1966). The strength of soils as engineering materials. *Milestones in Soil Mechanics*, Thomas Telford Ltd, 131-172.

Bishop, A. W. & Wesley, L. D. (1975). A hydraulic triaxial apparatus for controlled stress path testing. *Géotechnique* **25**, No. 4, 657-670.

Bjerrum, L. (1967). Engineering geology of Norwegian normally-consolidated marine clays as related to settlements of buildings. *Milestones in Soil Mechanics*, Thomas Telford Ltd, 173-211.

Braja, M. D. (1985). *Advanced soil mechanics*, International student edn. McGraw-Hill Book Co, Singapore.

Burgers, J. M. & Scott Blair, G. W. (1948). Report on the principles of rheological nomenclature. *Joint Commitee on Rheology of the International Council of Scientific Unions. Proc. Int. Rheol. Cong, Amsterdam.*

Burland, J. B. (1990). On the compressibility and shear strength of natural clays (Rankine Lecture 1990). *Géotechnique* **40**, No. 3, 329-378.

Clayton, C. R. I. (2004). *Comment on stiffness degradation curves.*
Ref Type: Personal Communication.

Clayton, C. R. I. & Heymann, G. (2001). Stiffness of geomaterials at very small strains. *Géotechnique* **51**, No. 3, 245-255.

Clayton, C. R. I. & Khatrush, S. A. (1986). A new device for measuring local axial strain on triaxial specimen. *Géotechnique* **36**, No. 4, 593-597.

Coop, M. R. (2004).
Ref Type: Personal Communication.

Coop, M. R., Atkinson, J. H., & Taylor, R. N. (1995). Strength and stiffness of structured and unstructured soils. *11th European Conf. Soil Mech. Fndn Engng.*

Cotecchia, F. & Chandler, R. J. (2000). A general framework for the mechanical behavior of clays. *Géotechnique* **50**, No. 4, 431-447.

Cuccovillo, T. & Coop, M. R. (1997). The measurement of local axial strains in traixial tests using LVDTs. *Géotechnique* **47**, No. 1, 167-171.

den Hann, E. J. (2001). *Bricks on ice.* GeoDelft Eureka project nr. 511200.

den Hann, E. J. & van den Berg, P. (2001). *Evaluation of creep models for soft soils.* CO-710203/21.

Di Benedetto, H., Tatsuoka, F., & Ishihara, M. (2002). Time-dependent shear deformation characteristics of sand and their constitutive modelling. *Soils and Foundations* **42**, No. 2, 1-22.

Dyvik, R. & Madshus, C. (1985). Laboratory measurements of Gmax using bender elements. *Proc of the ASCE Annual Convention: Advantages in the area of testing soils under cyclic conditions.*, 185-196.

Feda, J. (1992). *Creep of soils and related phenomena.* Elsevier Science Publishers B.V., Amsterdam.

Gasparre, A. (2005). *Advanced laboratory investigation of London Clay.* PhD thesis, Imperial College of Science Technology and Medicine, University of London.

Graham, J., Crooks, J. H. A., & Bell, A. L. (1983). Time effects on the stress-strain behaviour of natural soft clays. *Géotechnique* **33**, No. 3, 327-340.

Greening, P. D., Nash, D. F. T., Benahmed, N., Ferreira, C., & Viana da Fonseca, A. (2003). Comparison of shear wave velocity measurements in different materials using time and frequency domain techniques. *Proc. 3rd Int. Symp. Deformation Characteristics of Geomaterials, IS Lyon*, 381-386.

Hardin, B. O. & Black, W. L. (1969). Closure to 'Vibration modulus of normally consolidated clay'. *J.Soil Mech.Fndns Div., ASCE* **95**, No. 6, 1531-1537.

Head, K. H. (1998). *Manual of soil laboratory testing* John Wiley & Sons Ltd., Chichester.

Hight, D. W., Böese, R., Clayton, C. R. I., & Smith, P. R. (1992). Disturbance of the Bothkennar clay prior to laboratory testing. *Géotechnique* **42**, No. 2, 199-217.

Horpibulsuk, S., Miura, N., & Nagaraj, T. S. (2003). Assessment of strength development in cement-admixed high water content clays with Abrams' law as a basis. *Géotechnique* **53**, No. 4, 439-444.

Houlsby, G. T. & Wroth, C. P. (1991). The variation of shear modulus of a clay with pressure and overconsolidation ratio. *Soils and Foundations* **18**, No. 3, 138-143.

Hvorslev, M. J. (1937). Uber die Festigkeitseirgenschaften Gestorter Bindiger Boden. *Ingeniorvidenskabelige Skrifter* **A**, No. 45.

Jardine, R. J. (1985). *Investigation of pile-soil behaviour with special reference to the foundations of offshore structures.* PhD thesis, University of London.

Jardine, R. J. (1992). Some observations on the kinematic nature of soil stiffness. *Soils and Foundations* **29**, No. 3, 436-447.

Jardine, R. J. (1994). One perspective of the pre-failure deformation characteristics of some geomaterials. *Proc. Int. Symp. Pre-Failure Deformation Characteristics of Geomaterials, IS Hokkaido.*

Jotisankasa, A. (2003). *Radial strain belt design.*
Ref Type: Personal Communication.

Jovicic, V. & Coop, M. R. (1998). The measurement of stiffness anisotropy in clays with bender element tests in the triaxial apparatus. *ASTM Geotechnical Testing Journal* **21**, No. 1, 3-10.

Jovicic, V., Coop, M. R., & Simic, M. (1996). Objective criteria for determining G_{max} from bender element tests. *Géotechnique* **46**, No. 2, 357-362.

Kanapathipillai, A. (1996). *Review of the BRICK model of soil behaviour.* MSc thesis, Imperial College, London.

Komoto, N. (2004). *Experimental study on ageing effect using cement-mixed clay.* MSc thesis, University of Tokyo (in Japanese).

Komoto, N., Tatsuoka, F., & Nishi, T. (2003). Viscous stress-strain properties of undisturbed Pleistocene clay and its constitutive modelling. *Proc. 3rd Int. Symp. Deformation Characteristics of Geomaterials, IS Lyon*, 579-587.

Kongsukprasert, L. (2003). *Time effects on the strength and deformation characteristics of cement-mixed gravel.* PhD thesis, Univeristy of Tokyo.

Kongsukprasert, L. & Tatsuoka, F. (2003a). Ageing effects developed during creep loading and during extremely slow straining of cement-mixed gravel. *Proc. 38th Japan National Conf. Geotech. Engng, JGS, Akita.*

Kongsukprasert, L. & Tatsuoka, F. (2003b). Viscous effects coupled with ageing effects on the stress-strain behaviour of cement-mixed gravel. *Proc. 3rd Int. Symp. Deformation Characteristics of Geomaterials, IS Lyon*, 569-577.

Lacerda, W. A. & Houston, W. N. (1973). Stress relaxation in soils. *Proc. 8th Int. Conf. Soil Mech. Fndn Engng, Moscow.*, 221-227.

Leroueil, S., Kabbaj, M., Tavenas, F., & Bouchard, R. (1985). Stress-strain-strain rate relationship for the compressibility of sensitive natural clays. *Géotechnique* **35**, No. 2, 159-180.

Leroueil, S. & Marques, M. E. S. (1996). Importance of strain rate and temperature effects in geotechnical engineering. *ASCE Geotechnical Special Publication* **61**, 1-60.

Leroueil, S., Perret, D., & Locat, J. (1996). Strain rate and structuring effects on the compressibility of a young clay. *ASCE Geotechnical Special Publication* **61**, 137-150.

Leroueil, S. & Vaughan, P. R. (1990). The general and congruent effects of structure in natural soils and weak rocks. *Géotechnique* **40**, No. 3, 467-488.

Li, J.-Z., Tatsuoka, F., Nishi, T., & Komoto, N. (2003). Viscous stress-strain behaviour of clay under unloaded conditions. *Proc. 3rd Int. Symp. Deformation Characteristics of Geomaterials, IS Lyon.*

Lings, M. L. & Greening, P. D. (2001). A novel bender/extender element for soil testing. *Géotechnique* **51**, No. 8, 713-717.

Lo Presti, D. C. F., Jamoilkowski, M., Pallara, O., & Cavallaro, A. (1996). Rate and creep effect on the stiffness of soils. *ASCE Geotechnical Special Publication* **61**, 166-180.

Lo Presti, D. C. F., Jamoilkowski, M., Pallara, O., & Tordella, M. L. (1999). Assessment of sample disturbance in the laboratory. *Proc. 2nd Int. Symp. Pre-failure Deformation Characteristics of Geomaterials, IS Torino* **1**, 11-18.

Locat, J., Tanaka, H., Tan, T. S., Dasari, G. R., & Lee, H. (2003). Natural soils: geotechnical behaviour and geological knowledge. *Characterisation and Engineering Properties of Natural Soils*, Tan et al., ed., Swets & Zeitlinger, Lisse, 3-28.

Lohani, T. N., Imai, G., Tani, K., & Shibuya, S. (2001). G_{max} of fine-grained soils at wide void ratio range, focussing on the time-dependent behavior. *Soils and Foundations* **41**, No. 5, 87-102.

Lohani, T. N., Kongsukprasert, L., & Tatsuoka, F. (2003). Ageing effects on strength and stiffness of cement-mixed gravel from triaxial compression tests. *Proc. 38th Japan National Conf. Geotech. Engng, JGS, Akita.*

Marshall, C. E. (1975). *The physical chemistry and mineralogy of soils* Robert E. Krieger Publishing Company, New York.

Matešic, L. & Vucetic, M. (2003). Strain-rate effect on soil secant shear modulus at small cyclic strains. *J.Geotech.Geoenv.Engng, ASCE* **129**, No. No. 6, 536-549.

Mesri, G. & Castro, A. (1987). Cα/Cc concept and K_0 during secondary compression. *J.Geotech.Engng, ASCE* **113**, No. 3, 230-247.

Mitchell, J. K. (1960). Fundamental aspects of thixotropy in soils. *J.Soil Mech.Fndns Div., ASCE* **83**, No. 3, 19-52.

Mitchell, J. K. (1976). *Fundamentals of soil behaviour* John Wiley & Sons, Inc., London.

Mitchell, J. K., Baxter, C. D. P., & Soga, K. (1997). Time effects on the stress-deformation behaviour of soils. *Proc. of Professor Sakuro Murayama Memorial Symp., Kyoto University*, 1-64.

Morgan Electro Ceramics. Piezoelectric ceramics properties & applications. http://www.morgan-electroceramics.com/pzbook.html. 2003.
Ref Type: Electronic Citation

Morris, G. (2003). *Chemistry of kaolinite particles.*
Ref Type: Personal Communication.

Mukabi, J. N. & Tatsuoka, F. (1999). Effects of stress path and ageing in recosolidation on derformation characteristic of stiff clays. *Proc. 2nd Int. Symp. Pre-failure Deformation Characteristics of Geomaterials, IS Torino* **1**, 131-140.

Oasys Ltd. (2001). *Manual for BRICK 17 - GEO suite for windows.*

Oka, F., Kodaka, T., Kimoto, S., Ishigaki, S., & Tsuji, C. (2003). Step-changed strain rate effect on the stress-strain relations of clay and a constitutive modelling. *Soils and Foundations* **43**, No. 4, 189-202.

Perrin, R. M. S. (1971). *The clay mineralogy of British sediments* Mineralogical society, London.

Rammah, K. I., Val, D. V., & Puzrin, A. M. (2004). Effect of ageing on small-strain stiffness of overconsolidated clays. *Géotechnique* **54**, No. 5, 319-322.

Rampello, S., Viggiani, G., & Amorosi, A. (1997). Small-strain stiffness of reconstituted clay compressed along constant triaxial effective stress ratio paths. *Géotechnique* **47**, No. 3, 475-489.

Richardson, A. M. & Whitman, R. V. (1963). Effect of strain rate upon undrained shear resistance of a saturated remoulded fat clay. *Géotechnique* **13**, No. 3, 310-324.

Rio, J. (2005). *Movement of bender elements in air.*
Ref Type: Personal Communication.

Rotta, G. V., Consoli, N. C., Prietto, P. D. M., Coop, M. R., & Graham, J. (2003). Isotropic yielding in an artificially cemented soil cured under stress. *Géotechnique* **53**, No. 5, 493-501.

Santagata, M., Germaine, J. T., & Ladd, C. C. (2005). Factors affecting the intitial stiffness of cohesive soils. *J.Geotech.Geoenv.Engng, ASCE* **131**, No. 4, 430-441.

Santucci de Magistris, F., Sato, T., & Koseki, J. (1998). Effects of strain rate and ageing on small strain behaviour of compacted silty sand. *The Geotechnics of Hard Soil - Soft Rocks, Proc. 2rd Int. Symp. Hard Soils and Soft Rocks, Napoli.*, 843-854.

Schofield, A. N. & Wroth, C. P. (1968). *Critical state soil mechanics* McGraw-Hill, London.

Shibuya, S. (2000). Assessing structure of aged natural sedimentary clays. *Soils and Foundations* **40**, No. 3, 1-16.

Shibuya, S., Mitachi, T., Hosomi, A., & Hwang, S. C. (1996). Strain rate effects on stress-strain behaviour of clay as observed in monotonic and cyclic triaxial tests. *Measuring and Modeling Time Dependent Soil Behaviour, Geotechnical Special Publication, ASCE Washington Convention '96*, 214-227.

Shirley, D. J. & Hampton, L. D. (1977). Shear-wave measurements in laboratory sediments. *Journal of Acoustic Society of America* **63**, No. 2, 607-613.

Simpson, B. (1992a). Development and application of a new soil model for prediction of ground movements. *Wroth Memorial Symp.*, Oxford.

Simpson, B. (1992b). Retaining structures: displacement and design. 32nd Rankine Lecture. *Géotechnique* **42**, No. 4.

Simpson, B. (1999). Engineering needs. *Proc. 2nd Int. Symp. Pre-failure Deformation Characteristics of Geomaterials, IS Torino .*

Simpson, B. (2002). *BRICK soil model.*
Ref Type: Presentation.

Simpson, B. (2005). *Concept of neutral stress-strain curve.*
Ref Type: Personal Communication.

Singh, A. & Mitchell, J. K. (1968). General stress-strain-time function for soils. *J.Soil Mech.Fndns Div., ASCE* **94**, No. 1, 21-46.

Skempton, A. W. (1954). The pore pressure coefficients A and B. *Géotechnique* **4**, No. 4.

Skempton, A. W. & Henkel, D. J. (1957).(1957). Tests on London Clay from Deep Borings at Paddington, Victoria and the South Bank. *Proc. 4th Int. Conf. Soil Mech. Fndn Engng, London* **1**, 100-106.

Skempton, A. W. & Northey, R. D. (1952). The sensitivity of clays. *Géotechnique* **3**, No.1, 30-53.

Smith, P. R. (1992). *The behaviour of natural high compressibility clay with special reference to construction on soft ground.* PhD thesis, Imperial College of Science, Technology and Medicine.

Smith, P. R., Jardine, R. J., & Hight, D. W. (1992). The yielding of Bothkennar clay. *Géotechnique* **42**, No. 2, 257-274.

Soga, K. & Mitchell, J. K. (1996). Rate-dependent deformation of structured natural clays. *ASCE Geotechnical Special Publication no.61* 243-257.

Sorensen, K. (2005). Stiffness revised: Influence of strain acceleration on stiffness of clay in the small strain region. *BGA iYGEC Paper Competition* (winning paper).

Sorensen, K., Baudet, B., & Simpson, B. (2007). Influence of structure on the time-dependent behaviour of a stiff sedimentary clay. *"Stiff sedimentary clays - Genesis and engineering behaviour".Géotechnique Symposium in print* (paper submitted).

Sorensen, K., Baudet, B., & Tatsuoka, F. (2006). Coupling of ageing and viscous effects in an artificially structured clay. *Soil Stress-Strain Behavior: Measurement, Modeling and Analysis. Proceeding of the Geotechnical Symposium in Roma 2006.*

Sugai, D., Tatsuoka, F., & Uchimura, T. (2003). Effects of ageing and viscosity on the stress-strain beahviour of a cement-mixed soft clay. *Proc. 3rd Int. Symp. Deformation Characteristics of Geomaterials, IS Lyon.*

Tanaka, H., Ritoh, F., & Omukai, N. (2003). Geotechnical properties of clay deposits of the Osaka Basin. *Characterisation and Engineering Properties of Natural Soils*, Tan et al., ed., Swets & Zeitlinger, Lisse, 455-474.

Tang, Y. X. & Tsuchida, T. (1999). The development of shear strength for sedimentary soft clay with respect to aging effect. *Soils and Foundations* **39**, No. 6, 13-24.

Tatsuoka, F. (2003a). *Comments received on "Brief report on ageing".*
Ref Type: Personal Communication.

Tatsuoka, F. (2003b). Effects of viscous properties and ageing on the stress-strain behaviour of geomaterials. *ASCE Geotechnical Special Publication* **143**, 1-60.

Tatsuoka, F. (2003c). *Study visit to Japan.*
Ref Type: Personal Communication.

Tatsuoka, F. (2006). Keynote lecture: Inelastic deformation characteristics of geomaterials and their simulation. *Soil Stress-Strain Behavior: Measurement, Modeling and Analysis. Proceeding of the Geotechnical Symposium in Roma 2006.*

Tatsuoka, F., Di Benedetto, H., & Nishi, T. (2003). A framework for modelling of the time effects on the stress-strain behaviour of geomaterials. *Proc. 3rd Int. Symp. Deformation Characteristics of Geomaterials, IS Lyon.*

Tatsuoka, F., Enomoto, T., & Kiyota, T. (2005). Viscous property of geomaterial in drained shear. *ASCE Geotechnical Special Publication* **?**.

Tatsuoka, F., Ishihara, M., Di Benedetto, H., & Kuwano, R. (2002). Time-dependent shear deformation characteristics of geomaterials and their simulation. *Soils and Foundations* **42**, No. 2, 103-129.

Tatsuoka, F., Jardine, R. J., Lo Presti, D. C. F., Di Benedetto, H., & Kodaka, T. (1999). Theme lecture: Characterising the pre-failure deformation properties of geomaterials. *Proc. 14th Int. Conf. Soil Mech. Fndn. Engng.*

Tatsuoka, F., Santucci de Magistris, F., Hayano, K., Koseki, J., & Momoya, Y. (2000). Some new aspects of time effects on the stress-strain behaviour of stiff geomaterials. *The Geotechnics of Hard Soil - Soft Rocks, Proc. 2rd Int. Symp. Hard Soils and Soft Rocks, Napoli*, 1285-1371.

Tatsuoka, F., Uchimura, T., Hayano, K., Koseki, J., Di Benedetto, H., & Siddiquee, M. S. A. (2001). Time-dependent deformation characteristics of stiff geomaterials in engineering practice. *Proc. 2nd Int. Symp. Pre-failure Deformation Characteristics of Geomaterials, IS Torino*, 1161-1250.

Tavenas, F. & Leroueil, S. (1977). Effects of stresses and time on yielding of clays. *9th Int. Conf. Soil Mech. Fndn Engng*, Tokyo. 1, 319-326.

Tavenas, F., Leroueil, S., La Rochelle, P., & Roy, M. (1978). Creep behaviour of an undisturbed lightly overconsolidated clay. *Canadian Geotechnical Journal* **15**, No. 3, 402-423.

Tennis, P. D. (1998). Portland Cement Characteristics - 1998. *Concrete technology today, Portland Cement Association.*

Terzaghi, K. (1944). Ends and means in soil mechanics. *Engineering Journal (Canada)* **27**, 608.

Vaid, Y. P. & Campanella, R. G. (1977). Time-dependent behaviour of undisturbed clay. *J.Geotech.Div., ASCE* **103**, No. GT 7, 693-709.

Vaid, Y. P., Robertson, P. K., & Campanella, R. G. (1979). Strain rate behaviour of Saint-Jean-Vianney clay. *Canadian Geotechnical Journal* No. 16, 34-42.

Viggiani, G. & Atkinson, J. H. (1995a). Interpretation of bender element tests. *Géotechnique* **45**, No. 1, 149-154.

Viggiani, G. & Atkinson, J. H. (1995b). Stiffness of fine-grained soil at very small strains. *Géotechnique* **45**, No. 2, 249-265.

Vucetic, M. & Tabata, K. (2003). Effect of average straining rate on shear modulus at small cyclic strains. *Proc. 3rd Int. Symp. Deformation Characteristics of Geomaterials, IS Lyon.*

Vukandin, V. (2004). *BRICKS - Constitutive model for hard soils and soft rocks.*
Ref Type: Presentation.

Yimsiri, S. (2001). *Pre-failure deformation characteristics of soils: anisotropy and soil fabric.* PhD thesis, University of Cambridge.

Zreik, D. A., Germaine, J. T., & Ladd, C. C. (1998a). Effect of aging and stress history on the undrained strength of ultra-weak cohesive soils. *Soils and Foundations* **39**, No. 4, 31-39.

Zreik, D. A., Germaine, J. T., & Ladd, C. C. (1998b). Failure envelope of cohesive soils in the ultra-low stress range. *Soils and Foundations* **38**, No. 2, 201-210.